
Electronic Thesis and Dissertation Repository

4-23-2015 12:00 AM

Design, Synthesis, and Reactivity of Bimetallic Complexes of Dimethylplatinum(II) Containing Ditopic Ligands

Matthew S. McCready
The University of Western Ontario

Supervisor
Dr. Richard J. Puddephatt
The University of Western Ontario

Graduate Program in Chemistry
A thesis submitted in partial fulfillment of the requirements for the degree in Doctor of Philosophy
© Matthew S. McCready 2015

Follow this and additional works at: <https://ir.lib.uwo.ca/etd>

 Part of the [Inorganic Chemistry Commons](#), [Materials Chemistry Commons](#), [Medicinal-Pharmaceutical Chemistry Commons](#), and the [Organic Chemistry Commons](#)

Recommended Citation

McCready, Matthew S., "Design, Synthesis, and Reactivity of Bimetallic Complexes of Dimethylplatinum(II) Containing Ditopic Ligands" (2015). *Electronic Thesis and Dissertation Repository*. 2757.
<https://ir.lib.uwo.ca/etd/2757>

This Dissertation/Thesis is brought to you for free and open access by Scholarship@Western. It has been accepted for inclusion in Electronic Thesis and Dissertation Repository by an authorized administrator of Scholarship@Western. For more information, please contact wlsadmin@uwo.ca.

DESIGN, SYNTHESIS, AND REACTIVITY OF BIMETALLIC COMPLEXES OF
DIMETHYLPLATINUM(II) CONTAINING DITOPIC LIGANDS

by

Matthew S. McCready

Department of Chemistry

A thesis submitted in partial fulfillment
of the requirements for the degree of
Doctor of Philosophy

The School of Graduate and Postdoctoral Studies
The University of Western Ontario
London, Ontario, Canada
March 2015

© Matthew S. McCready 2015

ABSTRACT

This thesis describes a study of monometallic and bimetallic dimethylplatinum(II) complexes containing ditopic nitrogen donor ligands. This work details the design and synthesis of side-to-side and cofacial arranged ligands and their respective coordination chemistry. The study of the synthesis, characterization and reaction mechanisms of the various dimethylplatinum(II) complexes is outlined in detail with special emphasis focused on the reactivity of the complexes towards oxidative addition.

The ditopic ligand 6-dppd, 1,4-di(2-pyridyl)-5,6,7,8,9,10-hexahydrocycloocta[d]pyridazine, was observed to coordinate only a single equivalent of a platinum(II) center. The inability to coordinate a second equivalent, even through an assisted bridging atom, is presumed to be due to a steric clash between the free pyridyl group and the cyclooctyl backbone. In attempts to make heterobimetallic complexes of 6-dppd, the complex $[\text{PtMe}_2(6\text{-dppd})]$ was observed to react preferentially with mercuric halides by oxidative addition rather than coordination of the mercuric salt in the second coordination site giving complexes $[\text{PtXMe}_2(\text{HgX})(6\text{-dppd})]$ where $\text{X} = \text{Br}, \text{Cl}, \text{OAc}$. This indicates that the platinum center is actually a better nucleophile than the free pyridyl nitrogen atom. The oxidative addition of solvent dichloromethane was also observed showing the enhanced reactivity of $[\text{PtMe}_2(6\text{-dppd})]$. Finally, $[\text{PtMe}_2(6\text{-dppd})]$ was treated with DCl at low temperature to give the deuteridoplatinum(IV) complex. The deuteridoplatinum(IV) complex reductively eliminates methane in solution and extensive H/D exchange occurs into the CH_4 product at low temperature indicating very easy reversibility of the exchange between hydridomethylplatinum(IV) and methaneplatinum(II) complexes.

The abstraction of a chloride ligand from $[\text{PtClMe}(6\text{-dppd})]$ led to the formation of a complex dimer structure *endo,endo*- $[\text{Pt}_2\text{Me}_2(\mu_2\text{-}\kappa^3\text{-}6\text{-dppd})_2][\text{OTf}]_2$. This process allowed for the formation of a bimetallic platinum(II) complex which retained the initial stereochemistry. The protonolysis of $[\text{PtMe}_2(6\text{-dppd})]$ with one equivalent of HOTf led to the generation of methane gas and the concomitant formation of both *endo,endo*- $[\text{Pt}_2\text{Me}_2(\mu_2\text{-}\kappa^3\text{-}6\text{-dppd})_2][\text{OTf}]_2$ and *exo,exo*- $[\text{Pt}_2\text{Me}_2(\mu_2\text{-}\kappa^3\text{-}6\text{-dppd})_2][\text{OTf}]_2$. The structures of the *exo* isomeric clamshell dimers appeared much less sterically hindered in the solid state and were observed experimentally and computationally to be the thermodynamically preferred

isomers. The mechanism, selectivity and reversibility of this isomerism process was explored in detail.

The reactions of [PtMe₂(6-dppd)] with alkyl bromides RCH₂Br, which possess hydrogen bonding functionality, result in the formation of stable organoplatinum(IV) complexes capable of forming supramolecular structure via hydrogen bonding. Both intra and inter molecular hydrogen bonding is observed in the formation of supramolecular architectures which self-assemble in the solid state through additional π -stacking and weak secondary interactions.

The new anthracene derived ditopic ligands, **bpad** = N¹,N⁸-bis(pyridin-2-ylmethylene)anthracene-1,8-diamine and **adpa** = (N,N)-4,4'-(anthracene-1,8-diylbis(ethyne-2,1-diyl))-bis(N-(pyridin-2-ylmethylene)aniline) were prepared, characterized and used to coordinate dimethylplatinum(II) centers giving cofacial bimetallic complexes of dimethylplatinum(II). [Pt₂Me₄(bpad)] was shown to degrade over time in solution through a proposed metalation event involving the anthracene backbone. The oxidative addition of a variety of substrates was performed using [Pt₂Me₄(adpa)] giving stable diplatinum(IV) complexes as characterized by ¹H NMR spectroscopy. The new xanthene derived ditopic ligands, **ppxda** = 2,7-di-*tert*-butyl-9,9-dimethyl-N⁴,N⁵-bis(4-(pyridin-2-ylmethyleneamino)phenyl)-xanthene-4,5-dicarboxamide and **pmxda** = 2,7-di-*tert*-butyl-9,9-dimethyl-bis(pyridine-2-ylmethylene)-9H-xanthene-4,5-diamine were prepared, characterized and used to ligate two equivalents of a dimethylplatinum(II) center. Diplatinum complexes of both ligands were shown to easily undergo oxidative addition to give the corresponding diplatinum(IV) complexes which adopt the *anti* orientation. The *syn* alignment of metal centers was accessible through the abstraction of halides ligands and incorporation of bridging groups as is the case for the pyrazine bridged bimetallic platinum complex [Pt₂Me₆(C₄H₄N₂)(pmxda)][OSO₂CF₃]₂.

KEYWORDS

Platinum complexes, ditopic ligands, bimetallic complexes, oxidative addition, reductive elimination, isomeric platinum(II) complexes, supramolecular chemistry, hydrogen bonding, xanthenes, anthracene, NMR spectroscopy, X-ray Crystallography, H-D exchange

CO-AUTHORSHIP STATEMENT

The following thesis contains materials from previously published and submitted works, as well as works in preparation co-authored by Dr. Fenbao Zhang, Dr. Anwar Abo-Amer and Dr. Richard J. Puddephatt.

ACKNOWLEDGMENTS

First of all I would like to express my utmost gratitude to my supervisor, Dr. Richard J. Puddephatt. His patient approach to graduate research, coupled with his vast knowledge of the field makes him an excellent supervisor. He has constantly encouraged me through this process and if not for his leadership and guidance none of this thesis would have been possible.

I would also like to take this opportunity to thank the excellent research staff here at Western University for their help and assistance throughout my time here. Specifically I would like to thank Dr. Mathew Willans for his assistance with NMR Spectroscopy as well as his stimulating soccer dialogue. I would also like to acknowledge Doug Hairsine for his help with all mass spectrometry in this thesis. Further gratitude is extended to the team of Dr. Paul Boyle, Dr. Benjamin Cooper, Dr. Guerman Popov and Mrs. Aneta Borecki who provided valuable expertise in single crystal X-ray crystallography over my time here.

I would also like to thank Dr. Nick Payne for his valuable advice in X-ray crystallography and Dr. John Corrigan for his assistance and contributions along the way.

I developed many strong friendships throughout this process with graduate students and staff which helped make the journey more enjoyable. Specifically; Dr. Muhieddine Safa, Dr. Mohammad Afifi, Dr. Nasser Nasser, Mr. Shawn Robinson and Mr. Kyle Pellarin kept me level in the lab. Along with Mr. Will Humenny; Shawn, Kyle and myself have made a friendship that will hopefully last a lifetime.

Last but certainly not least I would like to thank the people who least understand why or what I did but constantly had my back and supported me along the way. My family; Barry, Cathy and Sean have provided a lot of emotional support and validation along the way which pulled me through the tougher times. My friends Tyler Plant, Clarke Campbell, Patrick Gruggen, Mike Steffler and so many more stayed with me this entire voyage and I look forward to returning the favour as our lives progress. I couldn't have done this without all of you.

TABLE OF CONTENTS

Abstract.....	ii
Keywords.....	iii
Co-Authorship Statement.....	iv
Acknowledgments.....	v
Table of Contents.....	vi
List of Tables.....	x
List of Figures.....	xiv
Abbreviations.....	xxiv
Dedication.....	xxvii
CHAPTER 1 – General Introduction	1
1.1 The Use of Platinum in Organometallic Chemistry	2
1.2 Oxidative Addition.....	5
1.2.1 Three-Center Concerted Mechanism	6
1.2.2 Bimolecular S _N 2 Mechanism.....	8
1.2.3 Radical Non-chain Mechanism.....	10
1.2.4 The Radical Chain Mechanism.....	11
1.3 Reductive Elimination.....	13
1.4 The Activation of Inert Bonds.....	15
1.5 Bimetallic Complexes and Ditopic Ligand Design.....	21
1.6 Supramolecular Chemistry.....	25
1.7 A Description of the Thesis.....	29
1.8 References	31
CHAPTER 2 - Synthesis and Reactivity of a Potentially Bimetallic Platinum(II) Complex Based on a 3,6-dipyridylpyridazine Ligand Design.....	40
2.1 Introduction	41

2.2	Ligand Synthesis	44
2.3	Synthesis of platinum(II) complexes of 6-dppd	46
2.4	Efforts Towards the Synthesis of a Bimetallic Complex of 6-dppd.....	51
2.4.1	Attempting to synthesize a diplatinum complex of 6-dppd	51
2.4.2	Efforts towards a heterobimetallic complex of 6-dppd.....	53
2.5	Reactivity of Complex 2 towards Oxidative Addition.....	61
2.5.1	Reactions of [PtMe ₂ (6-dppd)] with Halogens, X ₂ (X = Br, I)	61
2.5.2	Reactions of [PtMe ₂ (6-dppd)] with Benzylic Halides	70
2.5.3	Reaction of [PtMe ₂ (6-dppd)] with dichloromethane	74
2.5.4	Reaction of [PtMe ₂ (6-dppd)] with DCl.....	80
2.6	Conclusions	83
2.7	Experimental	85
2.8	References	104
CHAPTER 3 - Self-assembly of Isomeric Clamshell Dimers of Platinum(II).....		109
3.1	Introduction	110
3.2	Synthesis of the clamshell dimers	113
3.2.1	Synthesis of <i>endo,endo</i> -[Pt ₂ Me ₂ (μ ₂ -κ ³ -6-dppd) ₂](OTf) ₂	113
3.2.2	Synthesis of <i>exo,exo</i> -[Pt ₂ Me ₂ (μ ₂ -κ ³ -6-dppd) ₂](OTf) ₂	117
3.3	Studies of the Mechanism and Selectivity	125
3.4	Reversibility of Formation of the Clamshell Dimers	138
3.5	Conclusions	143
3.6	Experimental	145
3.7	References	156

CHAPTER 4 - Supramolecular Organoplatinum(IV) Chemistry: Complexes with a Pendent Hydrogen Bond Acceptor	160
4.1 Introduction	161
4.2 Reaction of 2 with Carboxylic Acid Derivatives	165
4.3 Reaction of Complex 2 with an alcohol as a hydrogen bond donor.....	183
4.4 Reaction of Complex 2 with boronic acid derivatives as hydrogen bond donors	187
4.5 Conclusions	197
4.6 Experimental	199
4.7 References	212
CHAPTER 5 - Design, Synthesis and Reactivity of Bimetallic Platinum(II) Complexes Based on Ditopic Ligand Designs.....	218
5.1 Introduction	219
5.2 Ligand Synthesis	222
5.3 Synthesis of a dimethylplatinum(II) complex of bpad.....	224
5.4 Reactivity of complex 26 towards oxidative addition.....	229
5.5 Ligand Synthesis	234
5.6 Synthesis of a dimethylplatinum(II) complex of adpa	236
5.7 Reactivity of Complex 29 towards Oxidative Addition.....	238
5.8 Ligand Synthesis	243
5.9 Synthesis of a bimetallic dimethylplatinum(II) complex of ppxda.....	246
5.10 Reactivity of Complex 33 Towards Oxidative Addition.....	247
5.11 Ligand Synthesis	266
5.12 Synthesis of a bimetallic dimethylplatinum(II) complex of pmxda.....	269
5.13 Reactivity of Complex 40 Towards Oxidative Addition.....	270
5.14 Conclusions	291
5.15 Experimental:	295

5.16	References	316
CHAPTER 6 – General Conclusions.....		320
6.1	General Conclusions.....	321
6.2	Future Work	327
CURRICULUM VITAE.....		328

LIST OF TABLES

Table	Description	Page
1.1	Properties of Hydrogen Bonds	27
2.1	Bond lengths [\AA] and angles [$^{\circ}$] for $[\text{PtClMe}(6\text{-dppd})]$, 1	48
2.2	Bond lengths [\AA] and angles [$^{\circ}$] for $[\text{PtMe}_2(6\text{-dppd})]$, 2	51
2.3	Bond lengths [\AA] and angles [$^{\circ}$] for $[\text{PtClMe}_2(\text{HgCl})(6\text{-dppd})]$, 3	58
2.4	Bond lengths [\AA] and angles [$^{\circ}$] for $[\text{PtBrMe}_2(\text{HgBr})(6\text{-dppd})]$, 4	58
2.5	Bond lengths [\AA] and angles [$^{\circ}$] for $[\text{PtIme}_3(6\text{-dppd})]$, 8	68
2.6	Bond lengths [\AA] and angles [$^{\circ}$] for $[\text{PtI}_3\text{Me}(6\text{-dppd})]$, 9	69
2.7	Bond lengths [\AA] and angles [$^{\circ}$] for $[\text{PtBrMe}_2(\text{CH}_2\text{C}_6\text{H}_5)(6\text{-dppd})]$, 10	72
2.8	Bond lengths [\AA] and angles [$^{\circ}$] for $[\text{PtBrMe}_2(\text{CH}_2\text{C}_6\text{H}_4\text{CH}_2\text{Br})(6\text{-dppd})]$, 11	73
2.9	Selected NMR data [δ ppm, J in Hz], for the dichloromethane adducts (see scheme 2.12 for labelling system)	76
2.10	Bond lengths [\AA] and angles [$^{\circ}$] for $[\text{PtClMe}_2(\text{CH}_2\text{Cl})(6\text{-dppd})]$, 12a	79
2.11	Crystallographic data for $[\text{C}_{20}\text{H}_{20}\text{N}_4]$, 6-dppd	94
2.12	Crystallographic data for $[\text{PtClMe}(6\text{-dppd})]$, 1	95

2.13	Crystallographic data for [PtMe ₂ (6-dppd)], 2	96
2.14	Crystallographic data for [PtClMe ₂ (HgCl)(6-dppd)], 3	97
2.15	Crystallographic data for [PtBrMe ₂ (HgBr)(6-dppd)], 4	98
2.16	Crystallographic data for [PtIme ₃ (6-dppd)], 8	99
2.17	Crystallographic data for [PtI ₃ Me(6-dppd)], 9	100
2.18	Crystallographic data for [PtBrMe ₂ (CH ₂ C ₆ H ₅)(6-dppd)], 10	101
2.19	Crystallographic data for [PtBrMe ₂ (CH ₂ C ₆ H ₄ CH ₂ Br)(6-dppd)], 11	102
2.20	Crystallographic data for [PtClMe ₂ (CH ₂ Cl)(6-dppd)], 12a	103
3.1	Bond lengths [Å] and angles [°] for <i>endo,endo</i> -[Pt ₂ Me ₂ (μ ₂ -κ ³ -6-dppd) ₂](OTf) ₂ , 13a	117
3.2	Bond lengths [Å] and angles [°] for <i>exo,exo</i> -[Pt ₂ Me ₂ (μ ₂ -κ ³ -6-dppd) ₂](OTf) ₂ •2(C ₃ H ₆ O)•(H ₂ O), 13b •2(C ₃ H ₆ O)•(H ₂ O)	121
3.3	Bond lengths [Å] and angles [°] for <i>exo,exo</i> -[Pt ₂ Me ₂ (μ ₂ -κ ³ -6-dppd) ₂](OTf) ₂ •2(C ₃ H ₆ O), 13b •2(C ₃ H ₆ O)	122
3.4	Bond lengths [Å] and angles [°] for <i>exo,exo</i> -[Pt ₂ Me ₂ (μ ₂ -κ ³ -6-dppd) ₂](OTf) ₂ •CH ₂ Cl ₂ , 13b •CH ₂ Cl ₂	123
3.5	Selected parameters for comparison of 13b •2(C ₃ H ₆ O)•(H ₂ O), 13b •2(C ₃ H ₆ O), and 13b •CH ₂ Cl ₂	124
3.6	Bond lengths [Å] and angles [°] for <i>exo</i> -[PtMe(PPh ₃)(6-dppd)](OTf), 16b	142
3.7	Crystallographic data for <i>endo,endo</i> -[Pt ₂ Me ₂ (μ ₂ -κ ³ -6-dppd) ₂](OTf) ₂ , 13a	151

3.8	Crystallographic data for <i>exo,exo</i> -[Pt ₂ Me ₂ (μ ₂ -κ ³ -6-dppd) ₂](OTf) ₂ •2(C ₃ H ₆ O)•(H ₂ O), 13b •2(C ₃ H ₆ O)•(H ₂ O)	152
3.9	Crystallographic data for <i>exo,exo</i> -[Pt ₂ Me ₂ (μ ₂ -κ ³ -6-dppd) ₂](OTf) ₂ •2(C ₃ H ₆ O), 13b •2(C ₃ H ₆ O)	153
3.10	Crystallographic data for <i>exo,exo</i> -[Pt ₂ Me ₂ (μ ₂ -κ ³ -6-dppd) ₂](OTf) ₂ •CH ₂ Cl ₂ , 13b •CH ₂ Cl ₂	154
3.11	Crystallographic data for <i>exo</i> -[PtMe(PPh ₃)(6-dppd)](OTf), 16b	155
4.1	Bond lengths [Å] and angles [°] for [PtBrMe ₂ (CH ₂ -4-(C ₆ H ₄ CO ₂ H)(6-dppd)], 17	168
4.2	Bond lengths [Å] and angles [°] for [PtBrMe ₂ (CH ₂ -4-(C ₆ H ₄ CH ₂ CO ₂ H)(6-dppd)], 18	171
4.3	Bond lengths [Å] and angles [°] for [PtBrMe ₂ (CH ₂ CO ₂ H)(6-dppd)], 19a	178
4.4	Bond lengths [Å] and angles [°] for [PtBrMe(6-dppd)], 21	182
4.5	Bond lengths [Å] and angles [°] for [PtBrMe ₂ (CH ₂ -2-(C ₆ H ₄ -CH ₂ OH)(6-dppd)], 22	186
4.6	Bond lengths [Å] and angles [°] for [PtBrMe ₂ (CH ₂ -3-C ₆ H ₄ -B(OH) ₂)(6-dppd)], 24	191
4.7	Bond lengths [Å] and angles [°] for [PtBrMe ₂ (CH ₂ -2-C ₆ H ₄ -B(OH) ₂)(6-dppd)], 25	196
4.8	Crystallographic data for [PtBrMe ₂ (CH ₂ -C ₆ H ₄ -CO ₂ H)(6-dppd)], 17	205

4.9	Crystallographic data for [PtBrMe ₂ (CH ₂ -C ₆ H ₄ -CH ₂ CO ₂ H)(6-dppd)], 18	206
4.10	Crystallographic data for [PtBrMe ₂ (CH ₂ CO ₂ H)(6-dppd)], 19a	207
4.11	Crystallographic data for [PtBrMe(6-dppd)], 21	208
4.12	Crystallographic data for [PtBrMe ₂ (CH ₂ -2-C ₆ H ₄ -CH ₂ OH)(6-dppd)], 22	209
4.13	Crystallographic data for [PtBrMe ₂ (CH ₂ -3-C ₆ H ₄ -B(OH) ₂)(6-dppd)], 24	210
4.14	Crystallographic data for [PtBrMe ₂ (CH ₂ -2-C ₆ H ₄ -B(OH) ₂)(6-dppd)], 25	211
5.1	Bond lengths [Å] and angles [°] for [Pt ₂ I ₂ Me ₆ (ppxda)], 34b	255
5.2	Bond lengths [Å] and angles [°] for [Pt ₂ I ₂ Me ₆ (pmxda)], 41	277
5.3	Crystallographic data for [Pt ₂ I ₂ Me ₆ (ppxda)], 34b	315
5.4	Crystallographic data for [Pt ₂ I ₂ Me ₆ (pmxda)], 41	316

LIST OF FIGURES

Figure	Description	Page
1.1	A sampling of the variety of the geometries for platinum complexes.	4
1.2	Schematic of the two electron (a) and one electron (b) oxidative addition processes.	6
1.3	Schematic of the three-center concerted mechanism of oxidative addition	7
1.4	Example of a <i>cis</i> three-center concerted oxidative addition of an aryl C-H bond in modern synthesis	8
1.5	Schematic of the bimolecular S _N 2 oxidative addition	9
1.6	The S _N 2 oxidative addition of I ₂ at [PtMe ₂ (bipy)] yielding both <i>trans</i> and <i>cis</i> products	10
1.7	Schematic for the radical non-chain mechanism of oxidative addition	11
1.8	Schematic of the radical chain mechanism of one electron oxidative addition	12
1.9	The oxidative addition of CH ₂ Cl ₂ at [PtMe ₂ (bipy)] via the radical chain mechanism	12
1.10	Schematic of the reductive elimination reaction	13
1.11	The inhibition of reductive elimination by a rigid <i>trans</i> chelating ligand	14

1.12	Reductive elimination of ethane from a five coordinate cationic platinum(IV) complex after initial solvent ligand loss	15
1.13	The Shilov system, X = Cl, OAc	17
1.14	Idealized catalytic conversion of methane to methanol	18
1.15	The aerobic oxidation of a dimethylplatinum(II) complex by methanol	19
1.16	The Catalytica process for oxidation of methane to methyl bisulfate	20
1.17	The insertion of oxygen into a Pd-H bond and Pt-H bond	21
1.18	Bimetallic complex capable of the catalytic generation of H ₂ from water	22
1.19	Typical structural architectures for bimetallic complexes	23
1.20	Example of a bimetallic nickel complex undergoing a cooperative bond forming between CO and biphenyl to give fluorenone	24
1.21	Reductive coupling of CO ₂ to oxalate using the cooperative effect of a dinuclear copper(I) complex	25
1.22	Description of a generic hydrogen bond and denotation of its measured parameters	27
1.23	Synthetic strategy using the oxidative addition reaction to access organoplatinum(IV) complexes for supramolecular chemistry	29

2.1	Various ligands (A-F) which are potential candidates for the preparation of multimetallic complexes and 2 , the dimethylplatinum(II) complex of D	42
2.2	¹ H NMR spectrum of 6-dppd in CDCl ₃	45
2.3	Molecular structure of 6-dppd , with an atomic numbering scheme	45
2.4	¹ H NMR spectrum of [PtClMe(6-dppd)], 1 in CD ₂ Cl ₂	46
2.5	Molecular structure of complex 1 , with an atomic numbering scheme	47
2.6	¹ H NMR spectrum of complex 2 in CDCl ₃	50
2.7	Molecular structure of complex 2 , with an atomic numbering scheme	50
2.8	¹ H NMR spectrum of complex 3 , [PtClMe ₂ (HgCl)(6-dppd)] in CDCl ₃	56
2.9	Molecular structure of complex 3 , with an atomic numbering scheme	57
2.10	Molecular structure of complex 4 , with an atomic numbering scheme	57
2.11	Views of the structures of (a) 3 and (b) 4 showing the loosely associated dimers formed by secondary bonding between adjacent HgX units	59
2.12	¹ H NMR spectrum of complex 5a/5b in acetone- <i>d</i> ₆	60
2.13	¹ H NMR spectrum of complex 6 in CDCl ₃	62

2.14	^1H NMR spectrum of the methylplatinum region for the oxidative addition of iodine at complex 2 in CDCl_3	62
2.15	^1H NMR spectrum of complex 8 in acetone- d_6	64
2.16	^1H NMR spectrum of complex 9 in CDCl_3	65
2.17	Molecular structure of complex 8 , with an atomic numbering scheme	68
2.18	Molecular structure of complex 9 , with an atomic numbering scheme	69
2.19	Molecular structure of complex 10 , with an atomic numbering scheme	72
2.20	Molecular structure of complex 11 , with an atomic numbering scheme	73
2.21	^1H NMR spectrum of the methyl and methylene regions for complexes 12a , 12b and 12c in acetone- d_6	75
2.22	Time series ^1H NMR spectra of the oxidative addition of methylene-chloride- d_2 at complex 2	77
2.23	A view of the structure of complex 12a	78
2.24	^1H NMR spectrum of the reductively eliminated isotopomers of methane	81
3.1	Isomers formed by self-assembly	111
3.2	Isomeric diplatinum(II) complexes	112
3.3	^1H NMR spectrum of complex 13a in acetone- d_6	114

3.4	Molecular structure of complex 13a with an atomic numbering scheme	116
3.5	¹ H NMR spectrum of complex 13b in CD ₂ Cl ₂	118
3.6	Molecular structure of complex 13b •2(C ₃ H ₆ O)•(H ₂ O) with an atomic numbering scheme	121
3.7	Molecular structure of complex 13b •2(C ₃ H ₆ O) with an atomic numbering scheme	122
3.8	Molecular structure of complex 13b •CH ₂ Cl ₂ with an atomic numbering scheme	123
3.9	Comparison of the solvent inclusions and α angles of the three analogous clamshell structures of 13b	125
3.10	Variable temperature ¹ H NMR spectra of the protonolysis of complex 2 yielding 14a/14b on route to the formation of complex 13b .	127
3.11	Variable temperature ¹ H NMR spectra of the protonolysis of complex 2 yielding 15a/15b , the acetonitrile adducts of 14a/14b	129
3.12	Calculated structures and relative energies for the isomers of the model complex [PtMe(NCMe)(dppd)] ⁺	132
3.13	¹ H NMR spectra monitoring the formation of complexes 15a/15b and the concurrent isomerization to 13b	133
3.14	Calculated structures and relative energies for the models of the dimer complexes 13a and 13b	135

3.15	¹ H NMR spectra monitoring the protonolysis of complex 2 yielding complexes 13a and 13b and the subsequent isomerization from 13a to 13b over 6 days	136
3.16	¹ H NMR spectrum of complex 16b in acetone- <i>d</i> ₆	140
3.17	³¹ P{ ¹ H} NMR spectrum of 16b in acetone- <i>d</i> ₆	140
3.18	Calculated structures and relative energies for the isomers of the model complex [PtMe(PPh ₃)(dppd)] ⁺	141
3.19	Molecular structure of complex 16b	142
4.1	Various ligands derived on 2,2'-bipyridine used for crystal engineering and supramolecular organometallic chemistry	162
4.2	Ligands and platinum(II) complexes possessing hydrogen bond acceptor atoms built into the ligand backbone	164
4.3	¹ H NMR spectrum of complex 17 in acetone- <i>d</i> ₆	167
4.4	Molecular structure of complex 17 with an atomic numbering scheme	168
4.5	A view of the supramolecular polymeric structure of 17	169
4.6	¹ H NMR spectrum of complex 18 in CD ₂ Cl ₂	170
4.7	Molecular structure of complex 18 with an atomic numbering scheme	171
4.8	A view of the supramolecular polymeric structure of 18	172
4.9	¹ H NMR spectrum of the methylplatinum region for the oxidative addition of bromoacetic acid at complex 2 giving 19a , 19b , and 19c	174

4.10	Methylplatinum regions of the ^1H NMR spectra monitoring the formation and isomerization between complexes 19a , 19b , and 19c over time	177
4.11	Molecular structure of complex 19a with an atomic numbering scheme	178
4.12	A view of the supramolecular dimer structure of 19a	179
4.13	^1H NMR spectrum of the reaction between 2 and 3-bromopropionic acid in CD_2Cl_2	180
4.14	Molecular structure of complex 21 with an atomic numbering scheme	182
4.15	^1H NMR spectrum of complex 22 in CD_2Cl_2	185
4.16	Molecular structure of complex 22 with an atomic numbering scheme	186
4.17	^1H NMR spectrum of complex 23 in acetone- d_6	189
4.18	^1H NMR spectrum of complex 24 in acetone- d_6	190
4.19	Molecular structure of complex 24 with an atomic numbering scheme	191
4.20	A view of the supramolecular polymer structure of 24	192
4.21	^1H NMR spectrum of complex 25 in acetone- d_6	194
4.22	Molecular structure of complex 25 with an atomic numbering scheme	195
4.23	A view of the supramolecular dimer structure of 25	196

5.1	Examples of ditopic ligands which allow for cooperative effects in bimetallic complexes	220
5.2	Bimetallic complexes based on a xanthene ligand scaffold	221
5.3	^1H NMR spectrum of the ligand bpad in CDCl_3	224
5.4	^1H NMR spectrum of the complex 26 in acetone- d_6	226
5.5	^1H NMR spectra of 26 in toluene- d_8 acquired over a period of 18 hours while heating	228
5.6	^1H NMR spectrum of the complex 27 in dms- d_6	231
5.7	^1H NMR spectrum of the ligand adpa in CDCl_3	236
5.8	^1H NMR spectrum of the complex 29 in CDCl_3	238
5.9	^1H NMR spectrum of the complex 30 in CDCl_3	240
5.10	^1H NMR spectrum of the complex 32 in acetone- d_6	242
5.11	^1H NMR spectrum of the ligand ppxda in CDCl_3	245
5.12	^1H NMR spectrum of the complex 33 in acetone- d_6	247
5.13	^1H NMR spectrum of the product mixture from the oxidative addition of MeI at 33	250
5.14	Time series ^1H NMR spectra of the isomerization between isomers of 34	251
5.15	Molecular structure of complex 34b , with an atomic numbering scheme	253
5.16	Molecular structure of complex 34b depicting the puckering of the xanthene backbone	253

5.17	^1H NMR spectrum of the complex 34b in acetone- d_6	255
5.18	^1H NMR spectrum of a potentially bromide-bridged diplatinum complex, 37 .	260
5.19	Variable temperature ^1H NMR spectra of complex 38a/38b	263
5.20	^1H NMR spectrum of the complex 39 in acetone- d_6	265
5.21	^1H NMR spectrum of the ligand pmxda in CD_2Cl_2	268
5.22	Possible rotational conformations of pmxda	268
5.23	^1H NMR spectrum of the complex 40 in acetone- d_6	270
5.24	^1H NMR spectrum of the complex 41 acquired at 298K in acetone- d_6	272
5.25	Variable temperature NMR spectra of 41 in CD_2Cl_2	274
5.26	Molecular structure of complex 41 with an atomic numbering scheme	275
5.27	^1H NMR spectrum of the complex 42 in CD_2Cl_2	278
5.28	Molecular structure of complex 42 with an atomic numbering scheme	279
5.29	^1H NMR spectrum of the complex 43 in CD_2Cl_2	281
5.30	^1H NMR spectrum of a potentially bromide-bridged diplatinum complex, 46	284
5.31	^1H NMR spectrum of the complex 47 in acetone- d_6	285
5.32	^1H NMR spectrum of the pyrazine bridged diplatinum(IV) complex 48 in CD_2Cl_2	288

5.33	Molecular structure of 48 with an atomic numbering scheme	288
5.34	^1H NMR spectrum of the complex 49 in acetone- d_6	290

ABBREVIATIONS

a, b, c, α , β , γ = unit cell parameters

Å = Ångstrom = 10^{-8} meters

adpa = (N,N)-4,4'-(anthracene-1,8-diylbis(ethyne-2,1-diyl))-bis(N-(pyridin-2-ylmethylene)aniline)

Anal Calc'd = analysis calculated

amu = atomic mass unit

ar = aryl

bipy = 2,2'-bipyridyl

bpad = N¹,N⁸-bis(pyridin-2-ylmethylene)anthracene-1,8-diamine

br. = broad

dppe = diphenylphosphinoethane

6-dppd = 1,4-di(2-pyridyl)-5,6,7,8,9,10-hexahydrocycloocta[d]pyridazine

^tBu = tertiary-butyl

°C = degrees Celsius

δ = chemical shift

Δ = with heat

d = doublet

dd = doublet of doublets

dt = doublet of triplets

ESI-MS = Electrospray Ionization Mass Spectrometry

Eq. = equation

equiv. = equivalent

fac = facial

g = gram

ΔG = free energy activation

hr = hour

h = Planck's constant

$h\nu$ = electromagnetic radiation

Hz = hertz

J = coupling constant

$^xJ(AB)$ = coupling constant between nuclei A and B through X number of bonds

J = Joule

K = degrees Kelvin

L = ligand

L-L/N-N = bidentate diimine ligand

MS = mass spectrometry

m = meta/multiplet depending on context

Me = methyl

MHz = megahertz

min = minutes

mL = millilitre

mmol = millimole

MW = molecular weight in g/mol

M = molarity or metal center dependent on context

mol = mole

nm = nanometer

NMR = nuclear magnetic resonance

N_A = Avogadro's number

ν = frequency

o = ortho

p = para

ppm = parts per million

Ph = phenyl

pmxda = 2,7-di-*tert*-butyl-9,9-dimethyl-bis(pyridine-2-ylmethylene)-9H-xanthene-4,5-diamine

ppxda = 2,7-di-*tert*-butyl-9,9-dimethyl- N^4, N^5 -bis(4-(pyridin-2-ylmethyleneamino)phenyl)-xanthene-4,5-dicarboxamide

Py = pyridyl

q = quartet

R = ideal gas constant or alkyl/aryl group dependent on context

s = singlet

S_N2 = bimolecular nucleophilic substitution reaction

t = triplet

T = temperature

T_C = coalescence temperature

tert = tertiary

μ = indicates bridging

VT-NMR = variable temperature-NMR (1H unless stated otherwise)

X = halogen (unless stated otherwise)

Z = number of formula units

- *To my family and friends* -

CHAPTER 1

General Introduction

1.1 The Use of Platinum in Organometallic Chemistry

Platinum has been systematically studied for over 250 years and has enabled many significant advances in the area of transition metal chemistry to be realized [1,2]. Specifically, the study of platinum and its reactivity can be attributed for much of the progress in the field of coordination chemistry [3]. This is due in part to the tendency of platinum to undergo ligand substitution following the principles of the *trans* effect; whereby a ligand coordinating to platinum facilitates the substitution of the ligand positioned *trans* to itself [4-6]. Along with platinum aiding in the establishment of the *trans* effect, which is kinetic in nature, the chemistry of platinum also contributed to the determination of the thermodynamic component of ligand substitution, the *trans* influence. The *trans* influence is exemplified by a change in the ground state thermodynamic properties of a complex due to ligand substitution and commonly manifests through the analysis of coupling constants in NMR spectroscopy or through the lengthening of metal-ligand bond distances in X-ray crystallography [4-8]. Through the study of varying the ligands of a platinum complex, trends in both the *trans* effect and *trans* influence have been established. The use of platinum in the study of these ligand effects is desirable due to its tendency to undergo ligand substitution with retention of stereochemistry. This tendency also allows for the design and synthesis of highly specified coordination complexes as well as specific isomeric complexes of platinum [9-16]. The predictable ligand substitution and the inert nature of platinum complexes to *cis-trans* isomerization makes these complexes highly useful in medicine, and as such there is a wide array of platinum containing pharmaceuticals [5,6,17].

Along with its significance to coordination chemistry, the use of platinum has given rise to the discovery of a very significant field of chemistry; organometallic chemistry [3]. Organometallic chemistry is defined as the chemistry of compounds possessing at least one chemical bond between a metal center and a carbon atom [6], and was pioneered by the discovery of the first organometallic compound by W.C. Zeise in 1827 [18]. Zeise's salt, or $\text{K}[\text{Pt}(\text{C}_2\text{H}_4)\text{Cl}_3] \cdot \text{H}_2\text{O}$, was discovered as yellow needle-like crystals after refluxing PtCl_4 in ethanol followed by the addition of KCl . This was the first of a long line of significant organoplatinum complexes to be discovered including

the first metal-carbonyl compound, $[\text{PtCl}_2(\text{CO})_2]$ by Schützenberger [19], one of the first alkyl transition-metal compounds, $[(\text{PtMe}_3\text{I})_4]$ by Pope, [20], and a biologically active antitumour chemotherapeutic agent *cis*-platin, *cis*- $[\text{PtCl}_2(\text{NH}_3)_2]$ [17,20,21]. The intrigue in the use of platinum for organometallic chemistry is due in large part to its versatility which is provided by the presence of many oxidation states of the element. Commonly, platinum is observed to exist in three oxidation states, 0, +II, and +IV [22]. The presence of a two-electron separation between common oxidation states lends platinum an excellent metal center to facilitate oxidative addition and reductive elimination reactions which formally involve two electron donation between the ligands and the metal center, and *vice versa* [5]. These reaction pathways play a critical role in a bulk of the chemistry involving platinum and are vital to the completion of the work outlined in this thesis. Oxidation states of +I and +III have been reported in which the platinum centers adopt dimeric structures involving metal-metal bonds [22]. Higher oxidation states of usually +V and +VI have also been observed. However, they are very rare and limited to a few platinum compounds containing fluoride ligands [4]. Even negative oxidation states of platinum have been observed in the case of cluster complexes with carbonyl ligands [1,4,23].

Along with the variety of oxidation states that platinum can be observed in, its versatility further extends to the differing geometries it can adopt. Platinum(0) complexes adopt varying geometries dependent upon the type and quantity of the ligand ranging from a tetrahedral geometry as is observed for $[\text{Pt}(\text{PPh}_3)_4]$, (a) in figure 1.1 [24], or linear as in the complex $[\text{Pt}(\text{PPh}'\text{Bu}_2)_2]$, [25] (b) figure 1.1. Square planar complexes such as $[\text{PtMe}_2(\text{bipy})]$, (c) figure 1.1, are typically observed in the case of platinum complexes in oxidation state of II, whereas standard geometry for platinum(IV) complexes such as $[\text{PtI}_2\text{Me}_2(\text{bipy})]$, is octahedral, (d) figure 1.1.

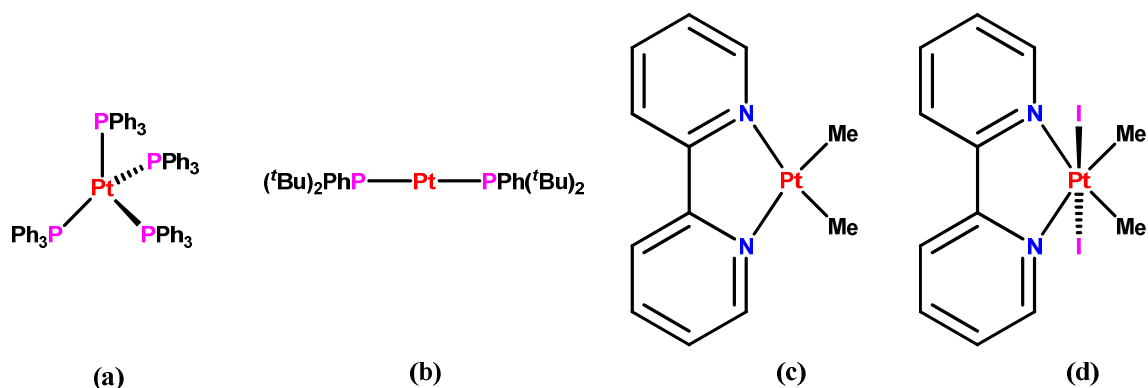


Figure 1.1. A sampling of the variety of the geometries for platinum complexes

The use of platinum in organometallic chemistry also provides for some additional spectroscopic benefits. Platinum has three major isotopes, ^{194}Pt , ^{195}Pt and ^{196}Pt ; each with a relatively equal natural abundance [23,26,27]. These isotopes provide rather diagnostic isotope patterns when analyzing complexes via mass spectrometry which can help the chemist quickly identify masses which could contain platinum atoms. In addition to this, ^{195}Pt is an NMR active nucleus possessing a spin of $I = \frac{1}{2}$. As it is found in a natural abundance of 33.7%, ^{195}Pt can therefore be utilized with relative ease for ^{195}Pt NMR spectroscopy. The real value when studying organometallic complexes of platinum through NMR spectroscopy is the fact that ^{195}Pt will give rise to satellites on ^1H resonances through a ^{195}Pt - ^1H coupling interaction [23,26,27]. These coupling values will allow for the determination of the oxidation state of the metal and the strength of the ligands at the metal center through the application of the *trans* influence. It also provides a spectroscopic probe which can help one determine what may be occurring in complex reactions.

Due to the relative kinetic inertness of platinum, with respect to its lighter congeners, it is often utilized to model complex organometallic reactions [1,4,5]. This practice is especially observed when it comes to analyzing and designing pathways for catalysis. Nickel and palladium both possess a huge potential and are widely used in catalysis. However, these metals tend to react too rapidly to elucidate the respective mechanisms. The fact that the third row metals such as platinum often react much slower than their congeners makes them better candidates to aid in the elucidation of the

mechanistic pathways [1,4,5,28]. By coupling with slower reactivity allowing for the detection of reaction intermediates, with the NMR spectroscopic handle, platinum is highly utile in outlining the pathways of catalytic processes. Considering the aforementioned traits, it becomes evident why platinum has and will always play a critical role in organometallic chemistry.

1.2 Oxidative Addition

The oxidative addition reaction is of pivotal importance to organometallic chemistry. It is observed at the heart of most catalytic pathways and is a key step in most synthetic reactions in late transition metal chemistry [5]. The oxidative addition reaction involves the oxidation of metal center through the addition of a substrate A-B at the metal center, which increases both the formal oxidation state of the metal center and the coordination number by two units. In turn the reaction leads to the formation of two new bonds M-A and M-B [5,7,29]. It is typical to observe oxidative addition reactions in which two electrons are involved in the oxidation of a single metal center, figure 1.2a, although examples of one electron pathways are known, figure 1.2b. In a two electron pathway, the metal center increases its formal oxidation state by two units as a result of donating two electrons from the metal d orbitals to the substrate. This in turn leads to an increase in the coordination number by two units. Two electron oxidative addition is most prevalent in transition metal complexes with 16 electrons or fewer although examples of oxidative additions at 18 electron complexes are known. This is because the reaction requires that the metal center be coordinatively unsaturated leaving a vacant site at the metal center for the ligand to coordinate [5]. Platinum commonly undergoes the two electron oxidation pathway as platinum(II) complexes possess 16 electrons and adopt a square planar geometry leaving two vacant coordination sites for the substrates to bond to the metal center. This in turn gives 18 electron platinum(IV) complexes that adopt octahedral geometry and are relatively stable. The one electron pathway on the other hand, involves two distinct metal centers each donating a single electron. This in turn leads to an increase in oxidation state by 1 and coordination number by 1 at each metal center. This type of oxidative addition pathway typically leads to the formation of metal-metal bonds.

The nucleophilicity of platinum(II) is greatly enhanced through the use of diimine nitrogen donor ligands which increase the reactivity of the square planar complex as well as stabilizing the resultant octahedral platinum(IV) complex [7,29]. As there are a variety of substrates that can be involved in the oxidative addition reaction, there are several pathways by which the oxidative addition can occur. These are highlighted in the following sections.

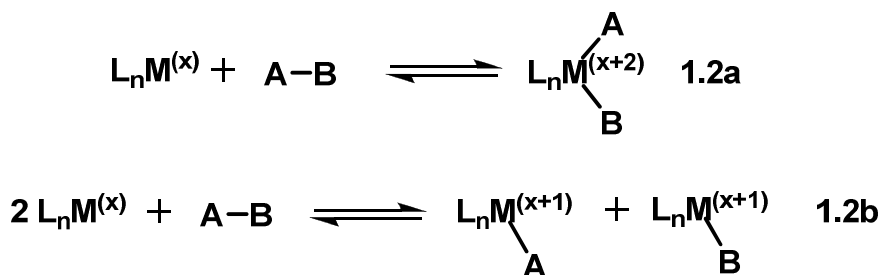


Figure 1.2. Schematic of the two electron (a) and one electron (b) oxidative addition processes.

1.2.1 Three-Center Concerted Mechanism

The three-center concerted mechanism of oxidative addition is typically observed in the case where the substrates involved have little to no net dipole. These essentially non-polar molecules, such as H₂, alkanes (R-H), arenes (Ar-H), and silanes (R₃Si-H), are what would be considered Class A substrates for oxidative additions [7,30]. These substrates are often challenging to activate under standard conditions due mainly to the thermodynamic stability they possess. Typically the activation of the substrate, in this case R-H, first involves the formation of a weakly associated σ-complex in which the R-H σ bond of the substrate acts as a two electron donor to the metal center. This intermediate then undergoes the oxidation step through the strong back donation from the metal into a vacant σ* orbital of the substrate. This leads to the cleavage of the R-H bond and concomitant formation of two new bonds, M-H and M-R. The nature of this three-centered concerted mechanism leads to a mutually *cis* geometry of the ligands at the metal center [7,30,31]. This mechanism is outlined in figure 1.3. This mechanism requires that there be a vacant coordination site present and as such can also be defined as an associative substitution reaction.

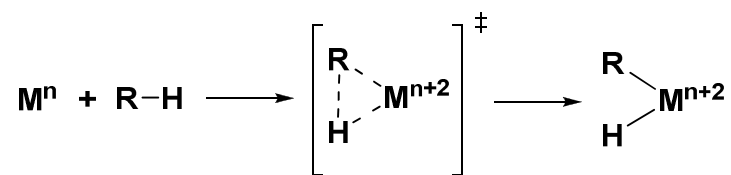


Figure 1.3. Schematic of the three-center concerted mechanism of oxidative addition.

This type of oxidative addition is commonly observed in the activation of aryl C-H bonds through a metalation event [32-36]. Through knowledgeable and appropriate design, aryl C-H bonds can be activated through the three-center concerted mechanism to yield metallated products. These types of reactions are critical for cross-coupling catalysis and can be performed selectively through the use of directing and mediating groups. Consider the case in figure 1.4 as an example, where the work by Dixon *et al.* shows that the incorporation of saturated nitrogen containing heterocycles within benzylic substrates act as sufficient directing groups to promote aryl C-H bond activations [37]. These C-H bond activations then follow the *cis* concerted oxidative addition pathway selectively in the *ortho* position. This *ortho* metalation then allows for the functionalization of the arene through a subsequent cross coupling step followed by a reductive elimination event [37].

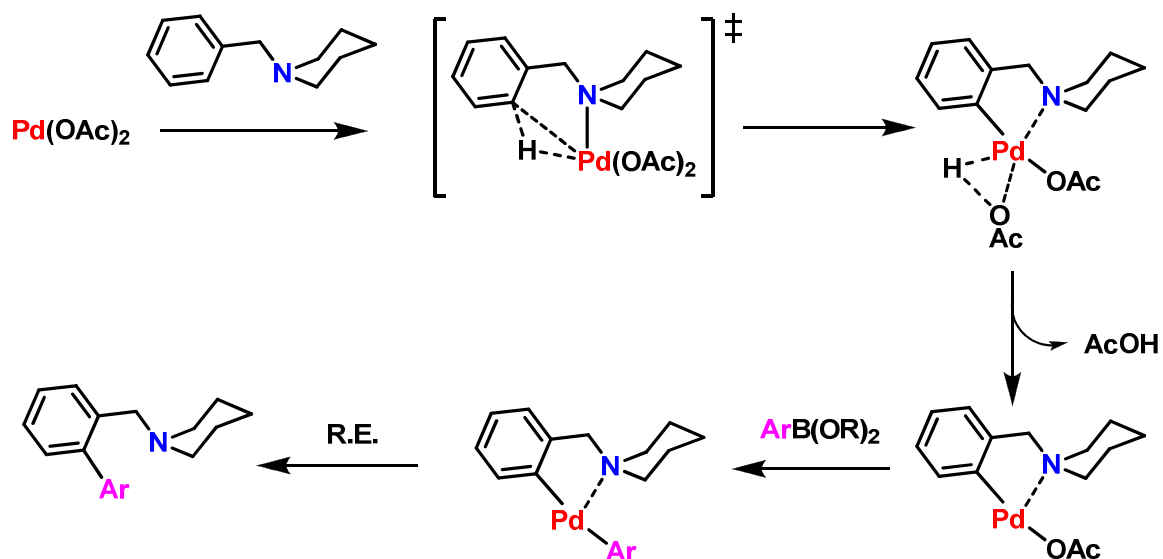


Figure 1.4. Example of a *cis* three-center concerted oxidative addition of an aryl C-H bond in modern synthesis.

1.2.2 Bimolecular S_N2 Mechanism

The bimolecular S_N2 mechanism is observed for electrophilic substrates which appreciable dipole moments such as alkyl halides [29]. It is this net dipole within the substrate that renders it susceptible to nucleophilic attack by the metal center, and initially forms a five coordinate geometry around the metal center, figure 1.5. The nucleophilic attack by the metal center on the substrate occurs at the least electronegative atom of the A-B bond, severing the bond and temporarily forming a five coordinate cationic intermediate [5-8]. The formation of this cationic intermediate has been supported through low temperature ¹H NMR studies of model complexes [PtMe₂(bipy)] and [PtPh₂(bipy)], whereby these intermediate complexes are observed in strong polar solvents at -80°C. The cationic intermediate is often stabilized by the coordination of a solvent molecule as is the case for the oxidative addition of methyl iodide at [PtMe₂(bipy)] to give the complex [PtMe₃(S)(bipy)]⁺ I⁻, where “S” represents a solvent molecule [38-40]. The significant *trans* effect of the methyl ligand *trans* to the solvent molecule and the increased Lewis basicity of the free anion eventually lead to the loss of the solvent molecule and subsequent coordination of the anionic ligand. After the

coordination of the anionic ligand, the now coordinatively saturated metal center typically exhibits an overall *trans* configuration of the added substrate. This mechanism of oxidative addition exhibits all of the common characteristics of an S_N2 reaction as observed in organic chemistry. The reaction kinetics are second order in nature, and the rate of the reaction is greatly accelerated in the presence of polar solvents [29]. The classical reactivity patterns of S_N2 chemistry hold true where by the reactivity follows Me > primary > secondary > tertiary; and in terms of leaving groups, I > Br > Cl > F. Inversion of stereochemistry is also observed in the case of the substrate possessing a chiral carbon atom as is exemplified in figure 1.5 [8].

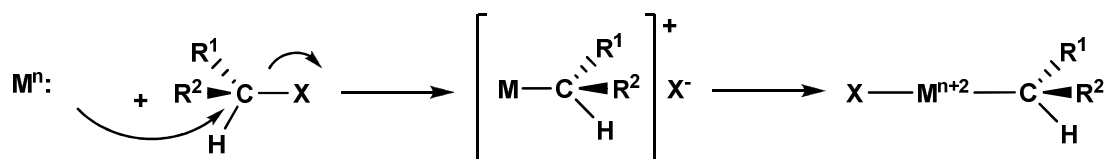


Figure 1.5. Schematic of the bimolecular S_N2 oxidative addition.

The bimolecular S_N2 pathway is observed for the oxidative addition of halogens, however not always are *trans* addition products observed. As a consequence of the five coordinate cationic complexes being stereochemically non-rigid, rearrangements at this stage could lead to the formation of a product of apparent *cis* oxidative addition. It is also possible that an equilibration between the *trans* and *cis* addition products could occur if the thermodynamics would allow, as is the case for the oxidative addition of iodine at [PtMe₂(bipy)] as shown in figure 1.6 [38-40].

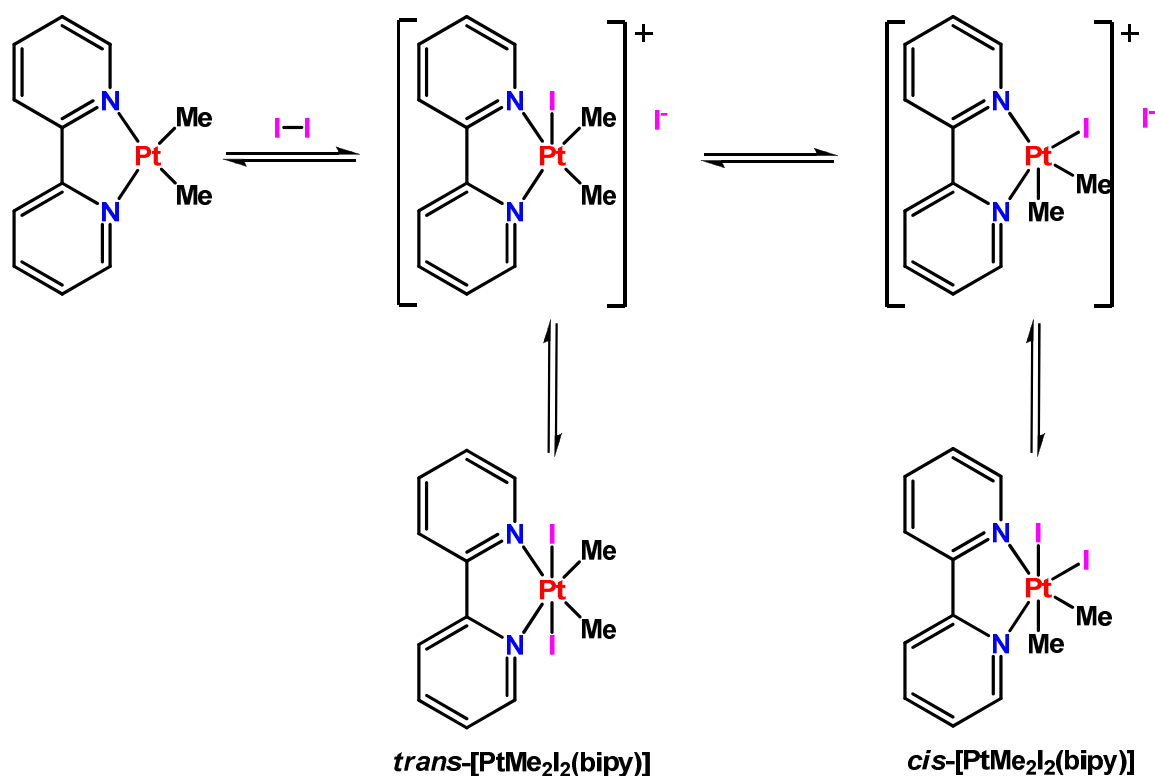


Figure 1.6. The S_N2 oxidative addition of I_2 at $[PtMe_2(bipy)]$ yielding both *trans* and *cis* products.

1.2.3 Radical Non-chain Mechanism

The radical non-chain mechanism is an example of a one electron oxidative addition pathway which is depicted in figure 1.7 [29, 41, 42]. These reactions are often complex and occur between metal center and an alkyl halide. The oxidative addition of the alkyl halide at the metal center often leads to a mixture of products [43]. In this mechanism, the coordination of the alkyl halide, (R-X), at the metal center is followed by the subsequent transfer of an electron from the metal center to the R-X substrate. This electron transfer leads to the formation of a solvent-caged radical pair. Once this radical pair has been formed, there are two directions the reaction may take. The first pathway would be the collapse of the radical pair leading to the formation of the oxidative addition product. This product of oxidative addition is similar to that of the S_N2 oxidative addition pathway although rather than inversion of stereochemistry of R, a racemic mixture is often obtained. The second pathway would be the escape of the free radical $R\cdot$

which could go on to perform more radical chemistry leading to the formation of unwanted byproducts. This reaction pathway follows standard principles of radical chemistry, such that the alkyl halides give the more stable radicals typically react faster as they are simpler to form [29].

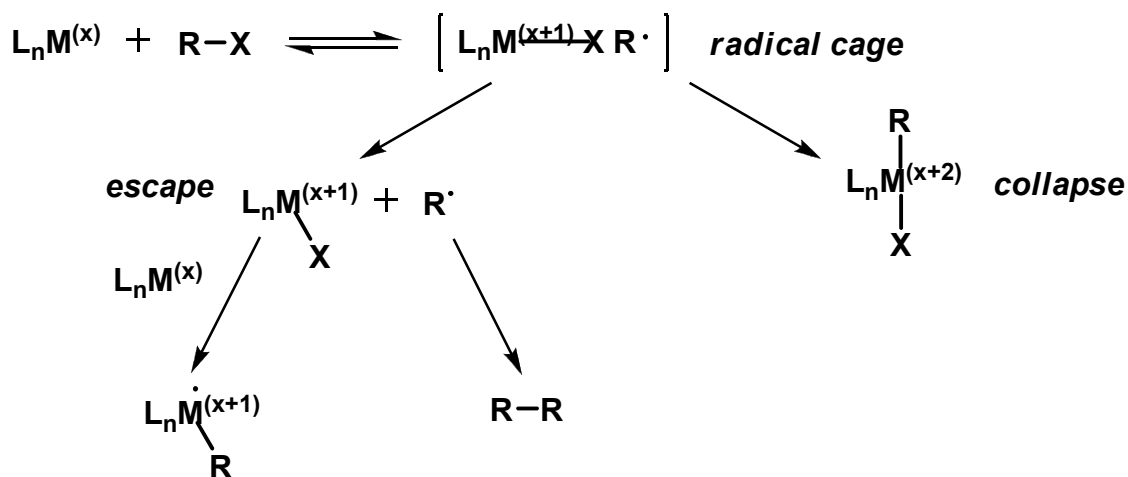


Figure 1.7. Schematic for the radical non-chain mechanism of oxidative addition.

1.2.4 The Radical Chain Mechanism

A second single electron oxidative addition pathway is often observed in the oxidative addition of alkyl halides at a metal center [41-43]. Unlike the non-chain mechanism, the chain mechanism requires a radical initiator to facilitate the reaction, however this initiator could arise from the escape process of the non-chain mechanism. The mechanism as outlined in figure 1.8, follows typical radical chemistry steps such as initiation, propagation and termination [42]. The oxidative addition again involves a coordinatively unsaturated metal center and an alkyl halide substrate.

It has been shown both experimentally and theoretically by Puddephatt *et al.*, that dimethylplatinum(II) complexes with diimine nitrogen ligands can oxidatively add solvent dichloromethane and chloroform via the radical chain mechanism as is shown in figure 1.9, [44]. These reactions have been shown to be accelerated by photolysis as well as inhibited by radical scavengers. The reaction after initiation is facilitated by the abstraction of a chlorine atom from the solvent dichloromethane and the propagation will continue until the reaction is terminated most likely by the formation of side products.

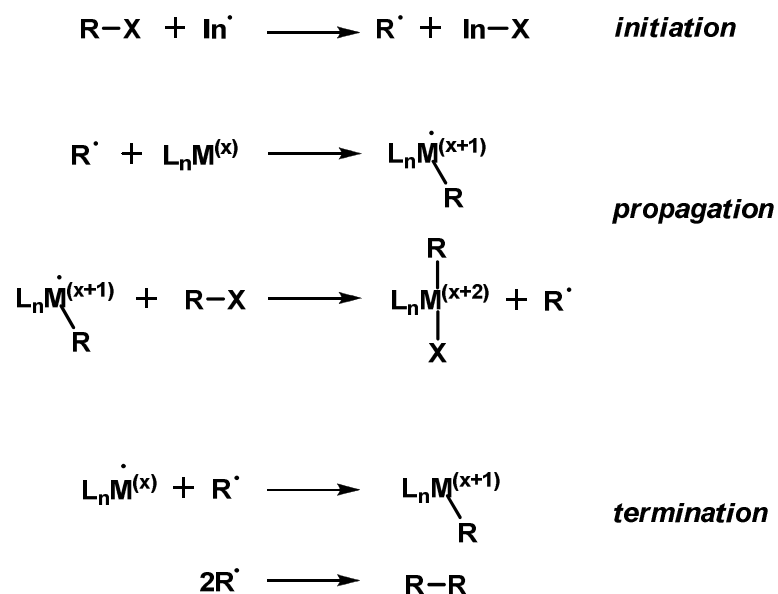


Figure 1.8. Schematic of the radical chain mechanism of one electron oxidative addition.

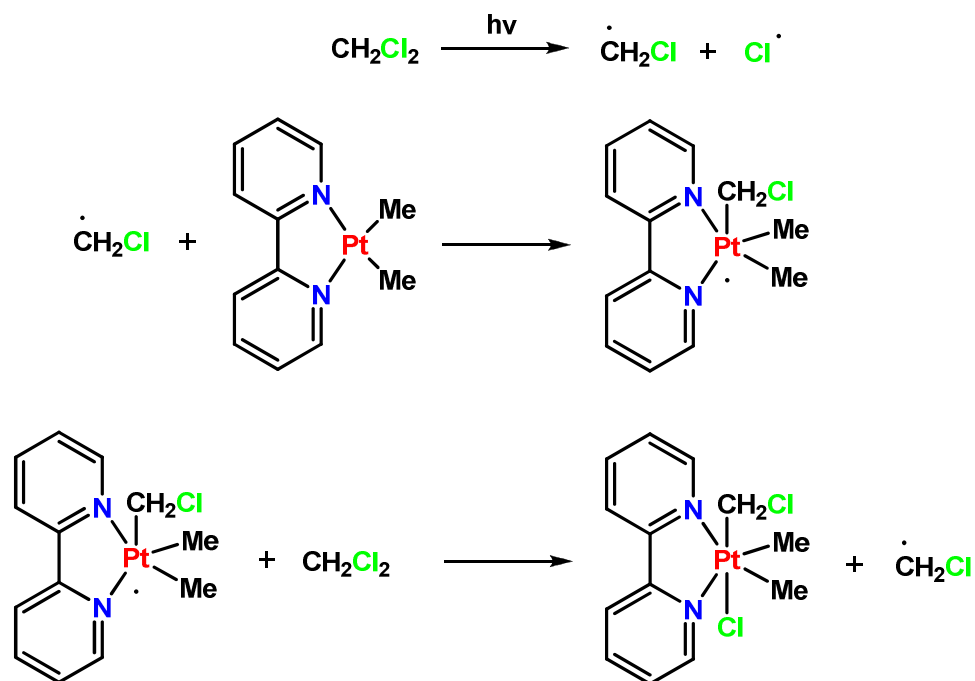


Figure 1.9. The oxidative addition of CH₂Cl₂ at [PtMe₂(bipy)] via the radical chain mechanism.

1.3 Reductive Elimination

The reductive elimination reaction is the reverse process to oxidative addition and is of significant interest due in part to its role in forming bonds between carbon atoms and other elements, [6,7,23]. Figure 1.10 depicts the variety of pathways by which reductive elimination can occur. Typically the reductive elimination reaction is reserved for transition metal complexes which are formally electron deficient and of high oxidation states and as such is readily observed for d^6 platinum(IV) complexes. In mononuclear metallic species' the process lowers the coordination number of the metal center by two while also decreasing the oxidation state of the metal by two, figure 1.10a. In the case of a bimetallic reductive elimination, figure 1.10b, the coordination number and oxidation state of each metal center is reduced by one [7,23].

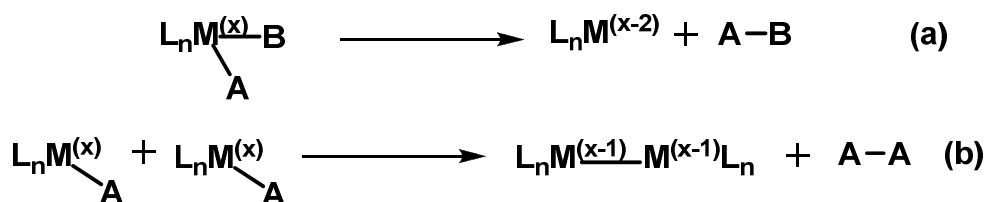


Figure 1.10. Schematic of the reductive elimination reaction. (a) represents a monometallic reductive elimination reaction and (b) represents a co-operative bimetallic reductive elimination reaction.

In order for the concerted reductive elimination reaction to operate, the ligands which are to be lost must be in a mutually *cis* arrangement [6,7,23]. This requires that ligands *trans* to one another must first undergo a *trans-to-cis* isomerization prior to the reductive elimination event [7]. The reductive elimination at a metal center can be effected by the incorporation of sterically rigid ligands which do not allow for *trans-to-cis* isomerization as is shown in figure 1.11, [45]. Once the ligands are oriented in a mutually *cis* manner, the reductive elimination of the product can be facilitated by a three-center concerted mechanism.

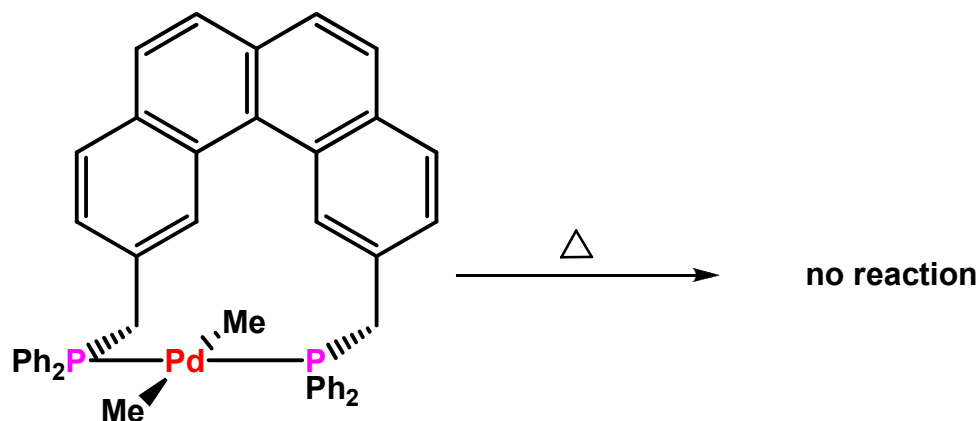


Figure 1.11. The inhibition of reductive elimination by a rigid *trans* chelating ligand.

The rate of the reductive elimination reaction is markedly enhanced by electronic factors as well as steric factors [46]. By incorporating ligands which are predominantly electron withdrawing in nature, one can increase the rate of reductive elimination. In that effect, reductive elimination often requires initial ligand loss to form a five-coordinate cationic intermediate which then can undergo reductive elimination prior to coordination of the initial ligand [47,48]. This process was best described by Goldberg *et al.* when they observed that the reductive elimination of ethane from the complex [PtMe₃I(dppe)] required that the iodide ligand first become uncoordinated at the metal center. The loss of a ligand can become difficult when chelating ligands are utilized. In the case of tetramethylplatinum(IV) complexes, the reductive elimination of ethane is inhibited by the use of chelating ligands such as dppe or bipy [49]. However by replacing these chelating ligands with monodentate ligands the reductive elimination of ethane is observed for tetramethylplatinum(IV) complexes. This supports that the five coordinate cationic intermediate greatly enhances the rate of reductive elimination. This vacant coordination site allows for ligand migration and is determined to be a low energy barrier for the reaction as is reported by Mayer *et al* [50]. Their investigation outlined that by imparting steric bulk in the ligand backbone the rate of solvent ligand loss would increase leading to a faster rate of reductive elimination, figure 1.12. The reductive elimination reaction plays a critical role in bond forming reactions and as such is a pivotal part of cross coupling strategies. This reaction has allowed the synthetic chemist to access a

plethora of substituted arenes, alkynes and alkanes and in turn has simplified many synthetic protocols.

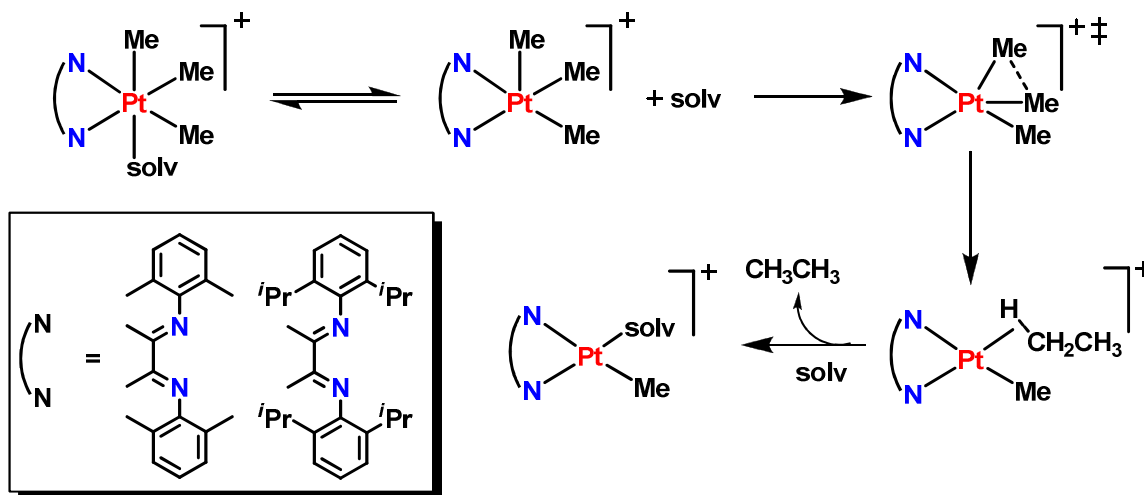


Figure 1.12. Reductive elimination of ethane from a five coordinate cationic platinum(IV) complex after initial solvent ligand loss.

1.4 The Activation of Inert Bonds

It is well established that alkanes are major components of natural gas and petroleum and as such have a major impact on today's society. Despite their importance, the development of practical processes to convert these alkanes into even more valuable compounds has been lacking to date. There is an obvious potential for the selective transformation of the C-H bonds in alkanes to other functional groups such as alcohols, ethers, or acids; however the relative inertness of these C-H bonds makes their functionalization a challenge [47,51-54]. It would be advantageous to develop methods to functionalize highly abundant alkanes into more commonly utilized commodity organic chemicals for both industrial and practical applications. However, general lack of reactivity in alkanes renders them underutilized as chemical feedstocks. The inert nature of the C-H bond in alkanes stems from the relatively strong and localized nature of their bonds and their lacking of vacant low energy orbitals that could participate in chemical reactions, unlike their olefinic counterparts [55,56]. The development of the

chemistry surrounding the functionalization of alkanes would have a distinct impact on the utilization of methane and in turn impact our earth's environment and climate. By developing a method to harness the potential of methane and functionalize it to methanol for example would significantly improve the overall utilization of methane [55-58]. The challenge that faces chemists is in how to exploit the potential of these alkanes. The use of transition metal complexes to facilitate the activation of alkanes presents an excellent opportunity to harness their full potential, and as such there has been a considerable increase in these research efforts. To this end there have been numerous examples of the successful activation of C-H bonds in alkanes by transition metal complexes [59-60]. The use of transition metals to activate C-H bonds allows for the use of relatively mild reaction conditions while often imparting high selectivity in the functionalization. Another considerably advantage of the use of transition metals is the application of catalytic processes to affect these transformations. Of note, platinum(II) complexes and their chemistry have been vital to the progression of this field. The first example of platinum(II) being utilized to activate alkanes dates back to 1969 when Shilov and coworkers reported the functionalization of C-H bonds in alkanes to produce the corresponding alcohols [47,48,51-55,58-61]. The Shilov system, as depicted in figure 1.13, presented a manner by which alkanes could be functionalized under mild conditions and were carried out in aqueous solutions in the presence of air. The major drawback that limited this systems utility was the use of a stoichiometric platinum(IV) oxidant [62,63].

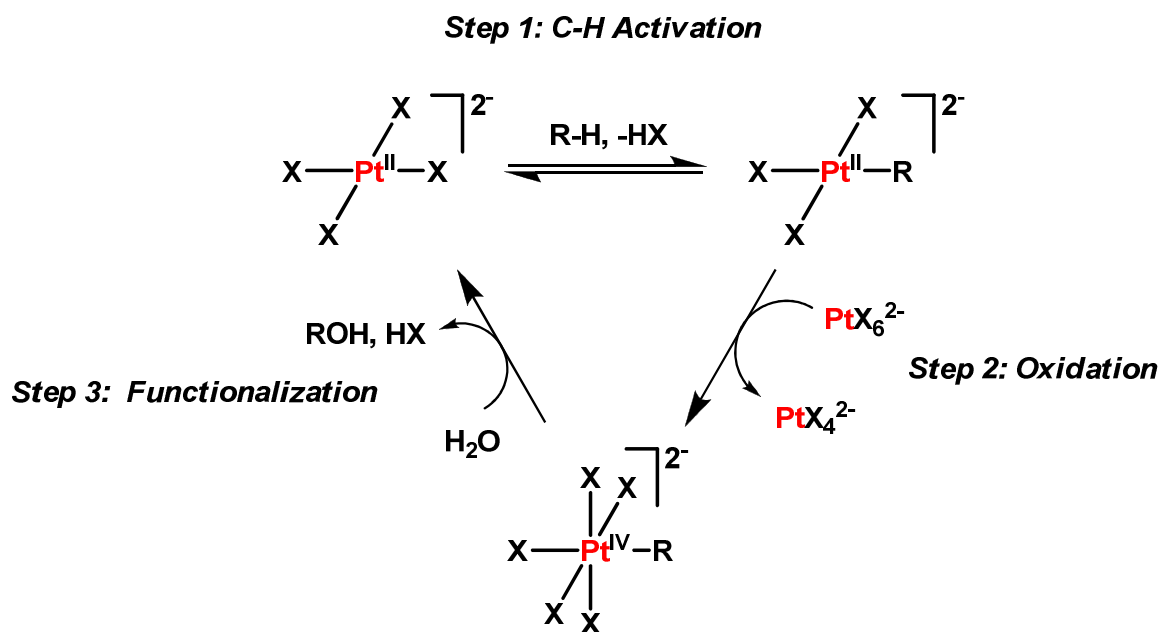


Figure 1.13. The Shilov system, X = Cl, OAc.

The Shilov system functions as a three part process. In the initial stage, an electrophilic displacement of a proton in the alkane substrate by platinum(II) occurs which in turn generates an alkylplatinum(II) complex, step 1 in figure 1.13. This is then followed by the oxidation of the alkylplatinum(II) complex to its corresponding alkylplatinum(IV) complex by $[PtCl_6]^{2-}$, step 2 in figure 1.13. After oxidation, the alkylplatinum(IV) complex is attacked by water leading to the cleavage of the platinum-carbon bond and subsequent formation of corresponding alcohol and regeneration of platinum(II) complex, step 3 in figure 1.13. This proposed mechanism is widely accepted and many independent research groups have evaluated and explored each step of the process [55,61-63].

In a manner similar to that of the Shilov system, the first step in a proposed idealized catalytic conversion of methane to methanol would involve the coordination of methane gas to a platinum(II) precursor, figure 1.14, [62]. This initial coordination would involve the displacement of a weakly coordinating solvent molecule which under aqueous conditions would be water. The coordination of methane would occur through the formation of an initial sigma complex of methane at platinum(II). This sigma complex has been supported through the evaluation of the protonolysis of

methylplatinum(II) complexes. This reaction is the reverse process of the activation of an alkane and as such would share an intermediate complex. Through the characterization of alkyl(hydrido)platinum(IV) complexes and their H/D exchange reactions, the initial coordination of a sigma methane complex has been accepted as a viable initial step in the activation of the C-H bond in methane [59, 64-66]. Once the sigma methane complex is formed, **A** in figure 1.14, a three-centered concerted oxidative addition reaction can occur to activate the C-H bond in methane and afford the corresponding methyl(hydrido)platinum(IV) species, **B**. A reductive elimination event, proton loss, would then need to occur in order to generate a methylplatinum(II) complex, **C**. The second major step of the reaction would be the oxidation of the methylplatinum(II) complex **C** in the presence of water and dioxygen to give **D**, the methyl(dihydroxy)platinum(IV) complex. The final step would be a reductive elimination of methanol from **D** leaving the initial platinum(II) catalyst ready to turn the cycle again [64-72].

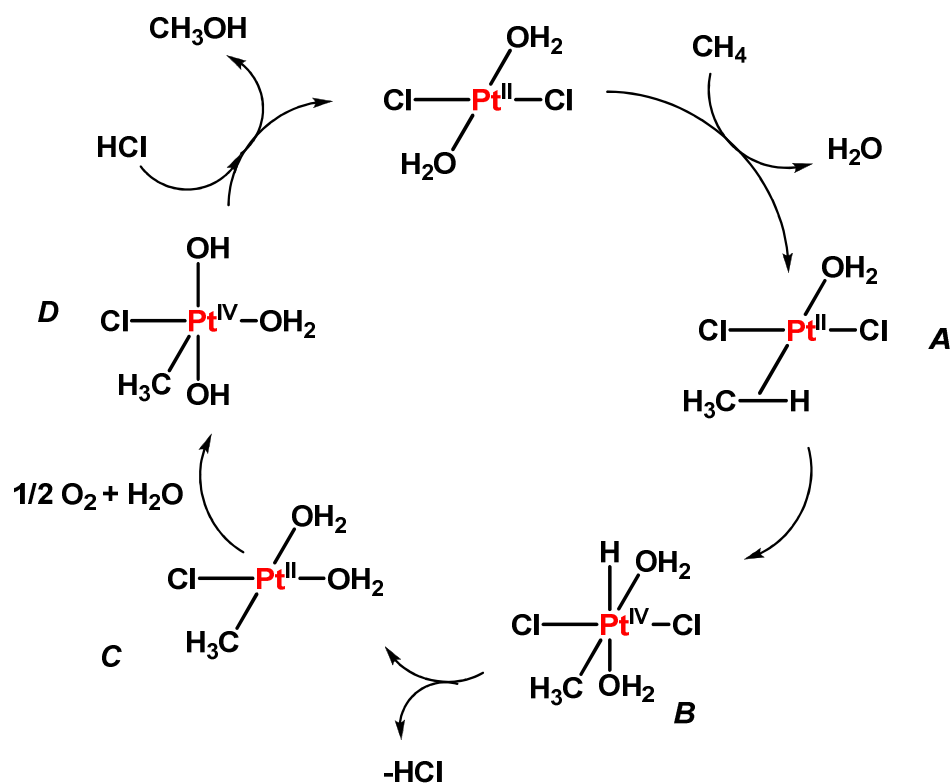


Figure 1.14. Idealized catalytic conversion of methane to methanol.

The Shilov system, as initially proposed, utilized a platinum(IV) oxidant which is highly undesirable due to its inherent high cost [62]. The ideal oxidant for this process would be the cheaper and more abundant dioxygen, O₂ [73,74]. The use of O₂ as an oxidant was investigated in the pioneering work of Puddephatt and coworkers where a dimethylplatinum(II) complex was found to be oxidized by alcohols or water to give the resultant dimethylplatinum(IV) alkoxides, figure 1.15 [75]. Later, the research group of Bercaw followed up these results and determined that the oxidation of the dimethylplatinum(II) complexes was indeed facilitated by O₂ [76]. This observation coupled with the ability of platinum(II) complexes to activate C-H bonds holds promise for the development of a complex that can both activate C-H bonds and catalyze their oxidation to alcohols by the use of oxygen as an oxidant. It is with that motivation that continuous efforts to develop the ideal process for the oxidation of alkanes to alcohols and other functionalized derivatives are being explored.

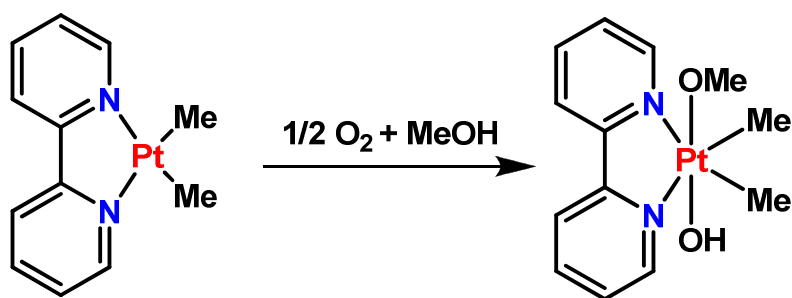


Figure 1.15. The aerobic oxidation of a dimethylplatinum(II) complex by methanol.

The Catalytica process, figure 1.16, developed by Periana *et. al.* illustrates another manner by which methane can be functionalized [57]. In this method, a platinum(II) complex is used to catalyze the oxidation of methane using sulfuric acid as an oxidant, to give methyl bisulfate. This process marks a significant advancement as the organometallic complex used is stable under the reaction conditions and also the product is obtained with a high degree of selectivity. The drawback to this process is that the product methyl bisulfate would need to be converted to a more useful compound in a second process and therefore the Catalytica process is likely not of economic value.

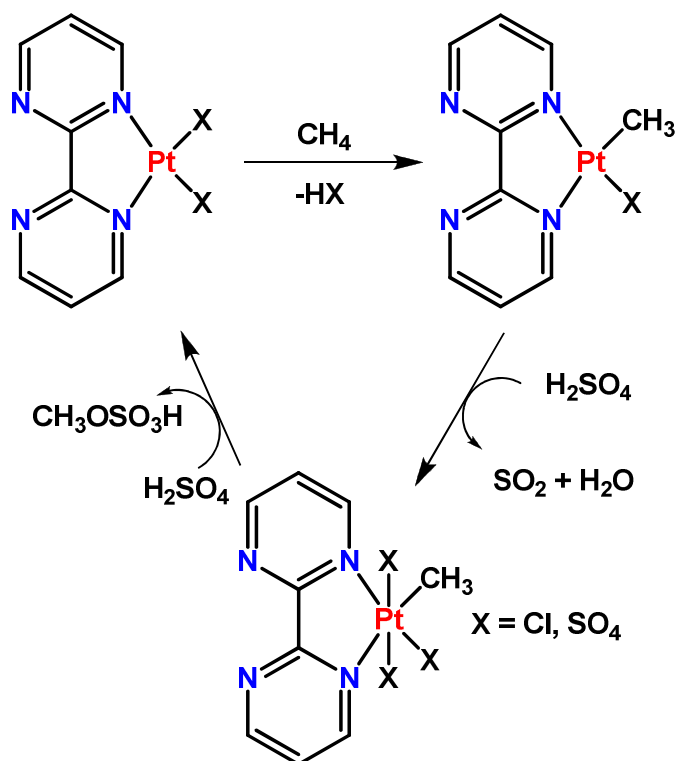


Figure 1.16. The Catalytic process for oxidation of methane to methyl bisulfate.

More recently, there has been an extensive focus on the use of dioxygen as an inexpensive, benign and readily available oxidant to be used for oxidations on a large scale. Of note electron rich late transition metal centers can react with molecular oxygen and under the proper conditions cleave the oxygen-oxygen bond [77-79]. There have been numerous reports of molecular oxygen reacting with palladium(II) hydride complexes to give the corresponding Pd-OOH moiety. These reactions are in fact formal insertions of molecular oxygen into a palladium hydride bond. The example in figure 1.17a shows how the reaction of a stoichiometric equivalent of oxygen leads to the formation of the resultant oxygen inserted complex. Computational studies support the findings of the Goldberg research group that the insertion occurs as a result of initial hydrogen atom abstraction leading to an $\cdot\text{OOH}$ radical which rapidly combines with the palladium center to form the product. In an analogous manner, Goldberg and coworkers also discovered that molecular oxygen would insert into a methylplatinum bond to give the Pt-OOMe complex [80-84]. The rate of this reaction was greatly enhanced by the presence of light indicating that it likely proceeded via a radical chain mechanism.

Insertion of oxygen into a platinum(IV) hydride bond was also reported, figure 1.17b, giving a resultant Pt-OOH complex. All of these oxygen insertion events hold promise for the ability to oxidize alkane derivatives to the corresponding alcohol derivatives but require a further understanding of the mechanism by which they operate [77, 85-87]. Elucidation of this mechanism will better allow for the development of catalytic processes which can exploit the use of dioxygen as an environmentally benign and cheap oxidant.

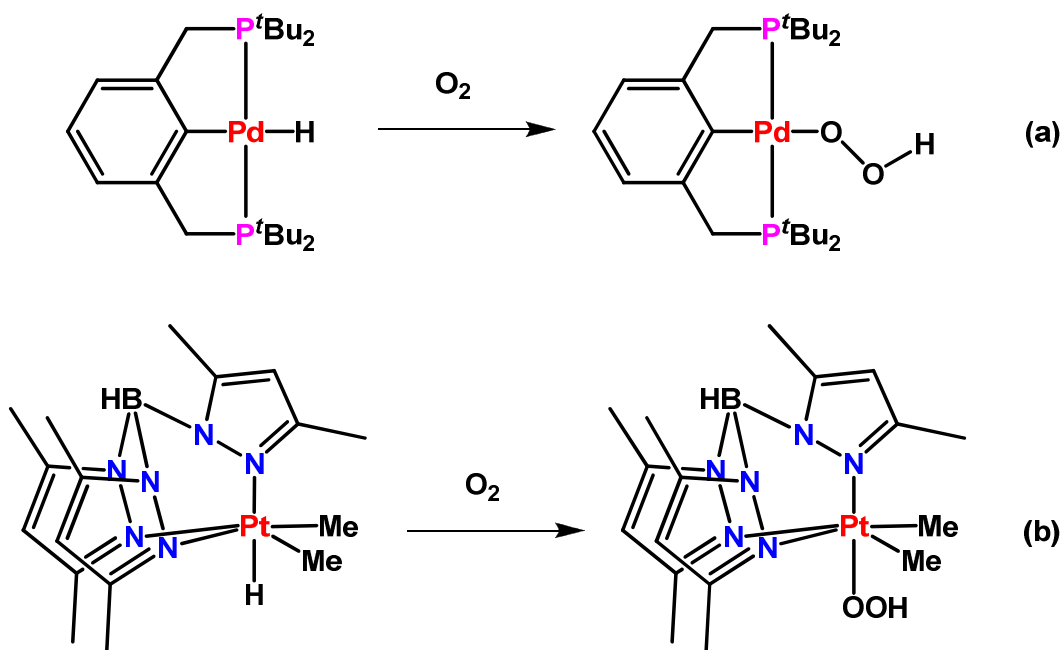


Figure 1.17. The insertion of oxygen into a Pd-H bond (a), and a Pt-H bond (b).

1.5 Bimetallic Complexes and Ditopic Ligand Design

The rational design and synthesis of bimetallic complexes is of significant interest to many different areas of chemistry. Originally motivated by biology, the preparation of bimetallic complexes allowed scientists to explore the coordination environments of various metal centers at biologically active sites [88-90]. Although their importance to biology is well documented, bimetallic complexes also have significant benefit to the

fields of catalysis, activation of organic and inorganic molecules, solar energy harvesting and general coordination chemistry [91]. It is with this motivation that the design of polytopic ligands has garnered significant interest. With regards to bimetallic complexes, the requirement is that the ligand be ditopic, meaning the ligand functions as a receptor possessing two remote binding sites to coordinate metal centers. By effectively designing ligands capable of complexing multiple metal centers, the synergistic effects of these metals can be realized [92-94]. For example, the heterobimetallic complex depicted in figure 1.18 is capable of producing hydrogen catalytically from water upon visible light irradiation [95,96].

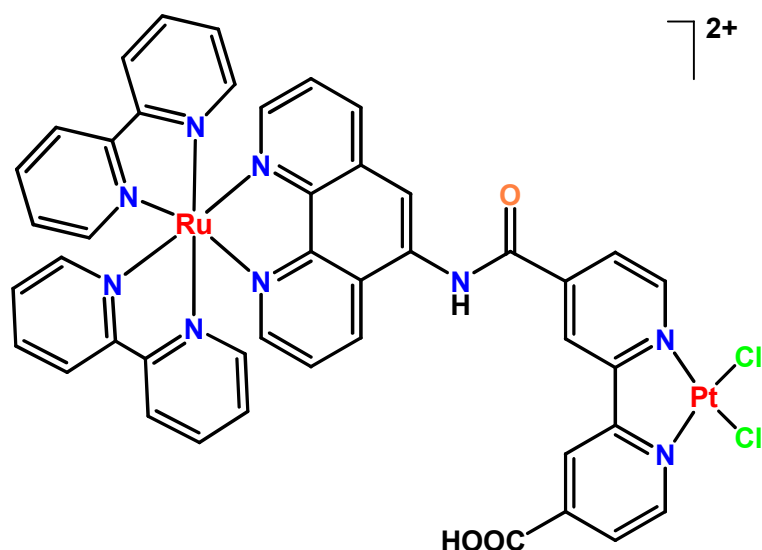


Figure 1.18. Bimetallic complex capable of the catalytic generation of H₂ from water.

The rational and intelligent design of the coordinating ligand becomes of paramount importance when attempting to illicit a cooperative effect by complexing two distinct metal centers within a close proximity [97,98]. Simple yet elegant strategies to prepare ditopic ligands often surround the use of Schiff base condensations between aldehydes and amines or the formation of amides by amines and carboxylic acid derivatives. This often allows for the morphology of the coordination site to be tailored to effectively ligate the metal center. This can be altered through the use of varying degrees of denticity, although bidentate and tridentate ligands are most common, as well

as through altering the chelate size. Coupling these variations with the wide variety of donor atoms one can employ, (N, P, O, S, C being the most common), a specifically tailored ligand can be created with specificity for desired metal centers [90]. The ligand should also be capable of holding the metal centers within a 5 Å distance to maximize the cooperative effect, [91,99]. By utilizing these principles and applying organic synthetic strategies one can allow for the modification of the flexibility or rigidity of the backbone, the electron withdrawing or donating nature of any functional groups, and the incorporation of extended conjugated aromatic systems. Independent of the nature of the backbone, ditopic ligands typically possess four common structural motifs with respect to the orientation of the metal centers. Figure 1.19 depicts these motifs for model complexes. The side-by-side orientation involves a ligand which maintains a coplanar arrangement of the metal centers allowing for the formation of a metal-metal bond between the two metal centers. In the absence of a metal-metal bond or bridging group between the metal centers, the complex is referred to as a face-to-face bimetallic complex. Halogen bridged dimers represent an additional structural conformation for bimetallic complexes and often involve two bridging halide groups. A final bimetallic structure commonly observed is the A-frame structural motif which involves a more bent and flexible backbone and a bridging ligand between the adjacent metal centers [91].

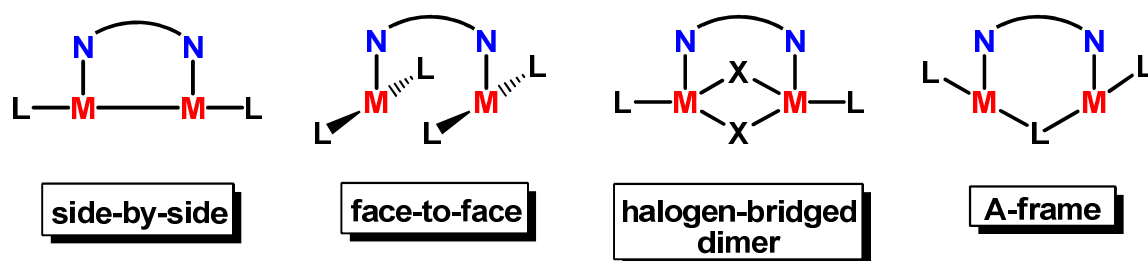


Figure 1.19. Typical structural architectures for bimetallic complexes.

The ligand design is critical in accessing useful bimetallic complexes. However these bimetallic complexes are only useful if their cooperative activity is greater than that of the individual metal centers [100]. An additional major benefit would be if the bimetallic complex allows one to access new chemistry that the monometallic complexes could not. This cooperative reactivity is exemplified in the case of cooperative bond

forming reactions and cooperative substrate activation as the incorporation of two metal centers imparts reactivity that monometallic complexes could not access [101-103]. Although there are several examples of cooperative bond forming reactions, the work by Agapie and coworkers exemplifies this well [104-108]. They have designed a dinuclear Ni(I) dimeric complex based on a terphenylphosphane ligand system which performs C-C bond formation reactions between bis(orthometallated) biphenyls and CO, figure 1.20. Both nickel centers work cooperatively undergoing oxidation and reduction reactions to lead to the formation of fluorenones. The bimetallic complex in this case shows versatility in the electronic state of the metal-metal bond to facilitate the bond forming reactions. By developing a method to regenerate the active dinickel species, this process could easily be applied catalytically [106-109].

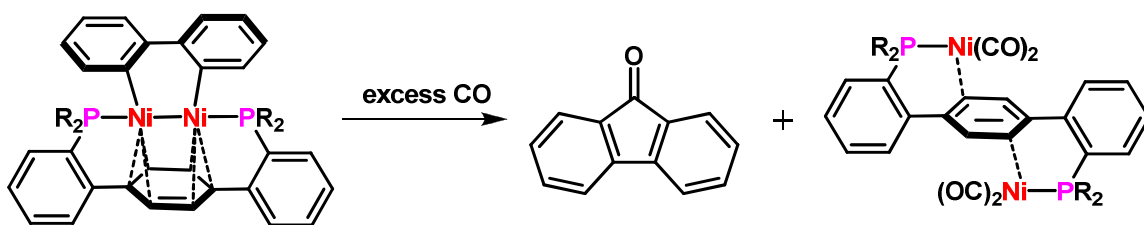


Figure 1.20. Example of a bimetallic nickel complex undergoing a cooperative bond forming between CO and biphenyl to give fluorenone.

Bouwman *et. al.* have developed a dinuclear copper(I) complex where the metal centers are bridged by a disulfide linker [110]. This bimetallic complex has been shown to reductively couple CO₂ to form oxalate with high selectivity, figure 1.21. This system was also shown to be able to be applied catalytically through electrocatalytically regenerating the active dinuclear copper complex.

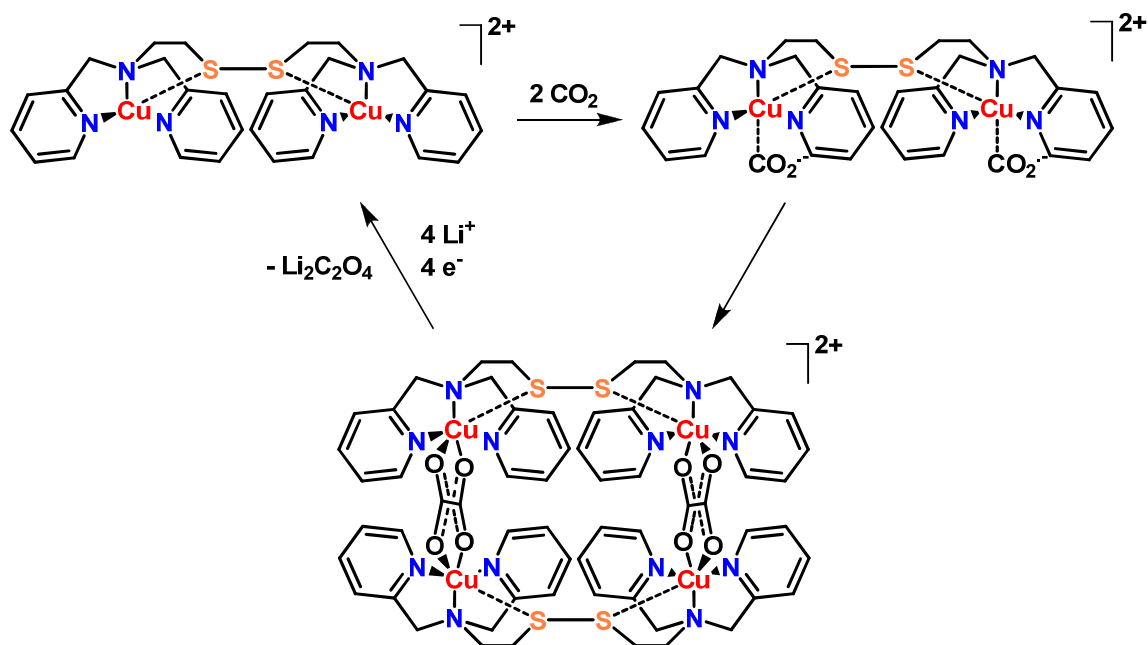


Figure 1.21. Reductive coupling of CO₂ to oxalate using the cooperative effect of a dinuclear copper(I) complex.

These brief examples illustrate the power that the rational design and synthesis of ditopic ligands and their resultant bimetallic complexes could impart on cooperative catalysis and substrate activation. It is with that motivation that this thesis describes the synthesis of ditopic ligands and the reactivity of the corresponding dimethylplatinum(II) complexes.

1.6 Supramolecular Chemistry

The concept of supramolecular chemistry and its ability to be utilized in the rational design of highly complex architectures has garnered significant attention and developed rapidly in recent years. It involves the use of relatively weak non-covalent interactions between molecules to design highly ordered and often highly specified intermolecular architectures [111]. These can range from simple dimeric structures, to highly ordered polymers, structures capable of encapsulating substrates, and even clusters capable of catalyzing reactions. Since the notion of supramolecular chemistry was

initially introduced in 1978 by Lehn, it has been refined to consist primarily of the chemistry surrounding non-covalent bonds [112-114]. As such a bulk of the interest surrounds the use of hydrogen bonds, van der Waals interactions, anion or cation – π interactions and π - π stacking interactions.

By designing molecules which possess groups capable of intermolecular interactions, one can access a range of supramolecular structures. A common strategy is to incorporate hydrogen bond donors and acceptors into the molecular frameworks. By doing so, these monomeric building blocks can associate to give higher order structures such as helices or other polymers. These polymeric structures in turn often offer different properties than their monomeric precursors and are coined functional molecular materials. The hydrogen bond is a rather unique type of electrostatic interaction in that it involves the sharing of a proton between a donor and acceptor group [111]. As defined, a hydrogen bond exists between a donor functional group A-H, and an acceptor functional group B as depicted in figure 1.22 [113]. These interactions are only considered to be hydrogen bonds if there is both evidence of bond formation as well as the bond being formed must involve the hydrogen atom initially bound to A. This often requires an electronegative character in both A and B leading to the electron pairs in each sharing the proton which often bridges the two atoms [115]. Typical hydrogen bond donor groups amines, carboxylic acids, alcohols, thiols and amides; whereas typical acceptor groups are often carbonyls, alcohols, amines, imines and even halogen atoms [112-114]. As there is a variety of groups capable of hydrogen bonding interactions, the strength of the interaction will also vary. A typical range associated with hydrogen bonding interactions is 14 – 40 kcal/mol for a strong hydrogen bond and < 4 kcal/mol for a weak hydrogen bond [116,117]. A quick summary of the bond lengths, angles and energies for a variety of hydrogen bonding interactions is summarized in table 1.1

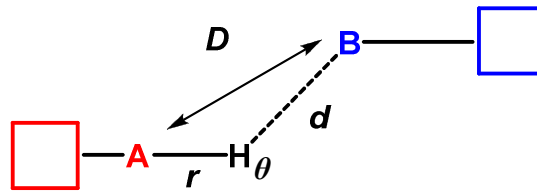


Figure 1.22. Depiction of a generic hydrogen bond and denotation of its measured parameters. r the measured bond distance of the A-H bond; D the donor acceptor distance, d the acceptor-hydrogen (B-H) distance, θ the hydrogen bond angle.

Table 1.1. Properties of hydrogen bonds.

	Strong	Moderate	Weak
Hydrogen bond interaction type	Predominantly covalent	Covalent / electrostatic	Predominantly electrostatic
Donor-Hydrogen vs. Acceptor Hydrogen Bond Lengths	A - H \approx B - H	A...H > B...H	A...H \gg B...H
Acceptor-Hydrogen Bond Length (Å) (d)	1.2 – 1.5	1.5 – 2.2	2.2 – 3.4
Donor-Acceptor distance (Å) (D)	2.2 – 2.5	2.5 – 3.2	3.2 – 4.0
Bond Angle (°) (θ)	175 – 180	130 - 180	90 – 180
Bond Energy (kcal/mol)	14.0 – 40.0	4.0 – 15.0	< 4.0
Example	Carboxylic Acids	Alcohols	Donor – π interactions

By employing these intermolecular interactions in a logical way, monomer units can self-assemble into higher order structures. Self-assembly involves the use of these interactions, such as hydrogen bonding or π -stacking, to form an organized structure from a previously disordered system without external direction [118]. As such, these supramolecular structures formed through self-assembly occur spontaneously and due to the relatively weak nature of some of the interactions can even occur reversibly. This reversibility allows for self-sorting and error correction in supramolecular chemistry that is not abundantly observed in molecular chemistry. This in turn often allows for the targeted synthesis of isomeric supramolecular species with high selectivity [118,119].

Of particular interest, organometallic complexes have allowed for significant contributions to be made in the field of supramolecular chemistry [120-124]. These contributions were made in spite of the fact that many metal-carbon bonds are susceptible to protonolysis by typically employed hydrogen bonding groups such as NH and OH donors. Organometallic complexes are capable of incorporating functionality for supramolecular interactions in a variety of ways. Work from the Puddephatt group centered around organoplatinum complexes specifically, has shown that these functional groups can be embedded in the initial ligand design resulting in an organoplatinum(II) complex with the ability to undergo supramolecular interactions. They have also shown that oxidative addition provides an effective route to install hydrogen bonding functionality into an organoplatinum(IV) species, by tailoring the substrate used for oxidative addition. This oxidative addition strategy, figure 1.23, has become highly useful and as a result numerous organometallic supramolecular structures have been prepared ranging from dimers to highly specified polymers [124-129].

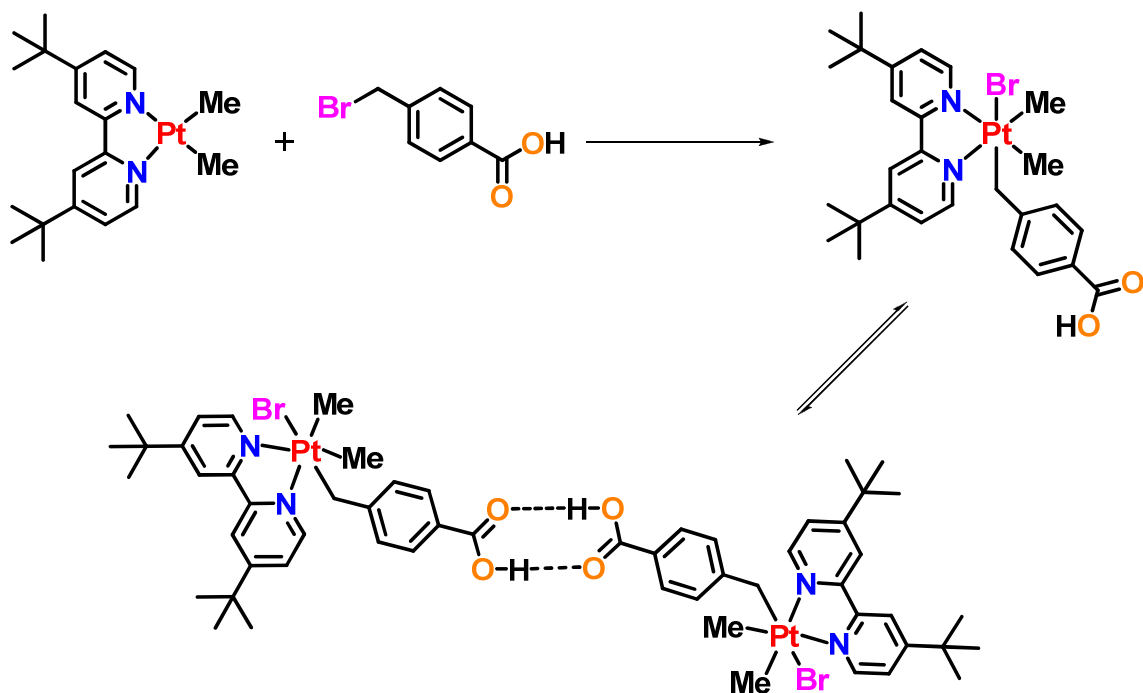


Figure 1.23. Synthetic strategy using the oxidative addition reaction to access organoplatinum(IV) complexes for supramolecular chemistry.

1.7 A Description of the Thesis

This thesis describes the synthesis, reactivity and spectroscopic analysis of dimethylplatinum(II) complexes containing ditopic bidentate nitrogen donor ligands. The synthesis and challenges faced in the preparation and design of these ligands and their abilities to form bimetallic complexes is outlined. The reactivity of bimetallic complexes towards the oxidative addition reaction is also investigated. Challenges faced in the design of the ligand with respect to rigidity and solubility are also outlined.

Chapter 2 outlines the design of a ditopic ligand which held potential to form side-to-side bimetallic dimethylplatinum(II) complexes. Numerous attempts to make homo and heterobimetallic complexes are outlined. The ligand, (6-dppd) or 1,4-di(2-pyridyl)-5,6,7,8,9,10-hexahydrocycloocta[d]pyridazine, was shown to only give monometallic complexes. The reactivity of the monometallic complex [PtMe₂(6-dppd)]

was then investigated via the oxidative addition of a variety of organic and inorganic substrates. $[\text{PtMe}_2(6\text{-dppd})]$ was observed to form metal-metal bonds when mercuric halides or pseudohalides were introduced. A reaction between solvent molecules and $[\text{PtMe}_2(6\text{-dppd})]$ was also outlined. The propensity of $[\text{PtMe}_2(6\text{-dppd})]$ to perform C-H activation chemistry was also explored. The mechanisms of these reactions are discussed and the corresponding products are evaluated.

Chapter 3 deals with the self-assembly of platinum(II) complexes of the ligand 6-dppd in solution to give isomeric clam shell complexes. Two different isomers of these complexes are prepared selectively and in a logical manner. The mechanism and reversibility of the formation of these isomeric complexes is explored and detailed in depth. The complexes are characterized fully and a synthetic protocol for the preparation of isomeric organometallic clamshell complexes is outlined.

Chapter 4 further elaborates on the utility of the complex $[\text{PtMe}_2(6\text{-dppd})]$ as it highlights the supramolecular architectures it can form via the oxidative addition of a variety of organic substrates. The possession of a pendent hydrogen bond acceptor in the ligand backbone allows for a variety of structures to be formed ranging from monomers, to hydrogen bonded dimers and polymers. These structures are clearly elucidated using single crystal X-ray crystallography.

Chapter 5 in this thesis highlights the design and synthesis of four different ligands based on the premise of a cofacial arrangement of the metal centers. Two ligands utilizing an anthracene scaffold and two ligands using a xanthene based scaffold are prepared and their ability to form bimetallic platinum(II) complexes is investigated. The reactivity of these complexes is studied using a variety of substrates. The ability of the platinum(II) complexes to form stable diplatinum(IV) species is studied primarily by ^1H NMR spectroscopy. The cooperativity of the metal centers is probed by making bridged diplatinum complexes and by reacting the diplatinum(II) complexes with bifunctional substrates.

Chapter 6 in this thesis provides a summary of the work and gives some general conclusions. Future work and considerations are also provided here.

1.8 References

1. Hartley, F.R. "*Chemistry of the Platinum Group Metals Recent Developments*," Elsevier Publishers, Amsterdam, **1991**.
2. Cotton, S.A. "*Chemistry of Precious Metals*", Blackie Academic and Professional, New York, **1997**.
3. McDonald, D. "*A History of Platinum*", Johnson Matthey & Co. Ltd, London, **1960**.
4. Wilkinson, G.; Stone, F.G.A; Abel, E.W. "*Comprehensive Organometallic Chemistry*", Vol. 6, Pergamon Press, Oxford, **1982**.
5. Shriver, D.F.; Atkins, P.; Langford, C.H. "*Inorganic Chemistry*", 4th Ed., W.H. Freeman and Company, New York, **1994**.
6. Spessard, G.O.; Miessler, G. "*Organometallic Chemistry*", 2nd Ed., Oxford University Press, New York, **2010**.
7. Crabtree, R.H. "*The Organometallic Chemistry of the Transition Metals*", 5th Ed., John Wiley and Sons Inc., Toronto, **2009**.
8. Collman, J.P.; Hegedus, L.S.; Norton, J.R.; Finke, R.A. "*Principles and Applications of Organotransition Metal Chemistry*", 2nd Ed., University Science Books, Mill Valley, **1987**.
9. Chernyaev, I.I. *Ann. Inst. Platine SSSR*. **1926**, 4, 261.
10. Grinberg, A.A. *Ann. Inst. Platine SSSR*. **1927**, 5, 109.
11. Langford, C.H.; Gray, H.B. "Ligand Substitution Processes." Wiley, New York, 1965.
12. Jain, V.K.; Jain, L. *Coord. Chem. Rev.* **2005**, 249, 3075.
13. Nedelec, N.; Rochon, F.D. *Inorg. Chem.* **2001**, 40, 5236.
14. Matsumoto, K.; Moriyama, H.; Suzuki, K. *Inorg. Chem.* **1990**, 29, 2096.

15. Chatt, J.; Hart, F.A. *J. Chem. Soc.* **1960**, 2807.
16. Reedijk, J. *Proc. Natl. Acad. U.S.A.* **2003**, *100*, 3611.
17. Rosenburg, B.; van Camp, L.; Krigas, T. *Nature* **1965**, *205*, 698.
18. Zeise, W.C. *Ann. Phys.* **1827**, *9*, 932.
19. Schutzenberger, M.P. *Annalen.* **1868**, *15*, 100.
20. Yamamoto, A. “*Organotransition Metal Chemistry*”, John Wiley and Sons, Toronto, **1986**.
21. Rosenburg, B.; van Camp, L.; Trosko, J.E.; Mansour, V.H. *Nature.* **1969**, *222*, 385
22. Belluco, U. “*Organometallic and Coordination Chemistry of Platinum*”, Academic Press, London, **1974**.
23. Cotton, F.A.; Wilkinson, G.; Murillo, C.A.; Bochmann, M. “*Advanced Inorganic Chemistry*”, 6th Ed. John Wiley and Sons, Toronto, **1999**.
24. Inglis, T.; Kilner, M. *Nature.* **1972**, *239*, 13.
25. Shriver, D.F. *Inorg. Synth.* **2009**, *19*, 106.
26. Pregosin, P. *Annual Reports on NMR Spectroscopy.* **1986**, *17*, 285.
27. Still, B.M.; Kumar, P.G.; Aldrich-Wright, J.R.; Price, W.S. *Chem. Soc. Rev.* **2007**, *36*, 665.
28. Hartley, F.R. “*The Chemistry of Platinum and Palladium*”, Applied Science Publishers, London, **1973**.
29. Rendina, M.L.; Puddephatt, R.J. *Chem. Rev.* **1997**, *97*, 1735.
30. Hartwig, J.F. “*Organotransition Metal Chemistry*”, University Science Books, Sausalito, **2010**.

31. Crabtree, R.H. *Angew. Chem. Int. Ed.* **1993**, 32, 789.
32. Anderson, C.M. Puddephatt, R.J.; Ferguson, G.; Lough, A. *J. Chem. Soc. Chem. Commun.* **1989**, 1927.
33. Anderson, C.M.; Crespo, M.; Jennings, M.C.; Lough, A.; Ferguson, G.; Puddephatt R.J. *Organometallics.* **1991**, 10, 2672.
34. Puddephatt, R.J. *Coord. Chem. Rev.* **2001**, 157.
35. Jia, C.; Kitamura, T.; Fujiwara, Y. *Acc. Chem. Res.* **2001**, 34, 633.
36. Wencel-Delord, J.; Glorius, F. *Nature Chem.* **2013**, 5, 369.
37. Tan, P.W.; Haughey, M.; Dixon, D.J. *Chem. Commun.* **2015**, doi: 10.1039/c5cc00410a
38. Jawad, J.K.; Puddephatt, R.J. *J. Chem. Soc.; Dalton Trans.* **1977**, 1466.
39. Ferguson, G.; Monaghan, P.K.; Parvez, M.; Puddephatt, R.J. *Organometallics.* **1985**, 4, 1669.
40. Nabavizadeh, S. M.; Amini, H.; Rashidi, M.; Pellarin, K. R.; McCready, M. S.; Cooper, B. F. T.; Puddephatt, R. J. *J. Organomet. Chem.* **2012**, 713, 60–67.
41. Volger, A.; Kunkely, H. *Angew. Chem. Int. Ed.* **1982**, 21, 209.
42. Hill, R.H.; Puddephatt, R.J. *J. Am. Chem. Soc.* **1985**, 107, 1218.
43. Peloso, A. *J. Chem. Soc.; Dalton Trans.* **1976**, 1466.
44. Abo-Amer, A.; McCready, M.S.; Zhang, F.; Puddephatt, R.J. *Can. J. Chem.*, **2012**, 90, 1, 46.
45. Gillie, A.; Stille, J.K. *J. Am. Chem. Soc.* **1980**, 102, 4933.
46. Hall, P.W.; Puddephatt, R.J.; Tipper, C.F.H. *J. Organomet. Chem.* **1975**, 84, 407.

47. Fekl, U.; Kaminsky, W.; Goldberg, K.I. *J. Am. Chem. Soc.* **2001**, *123*, 6423.
48. Fekl, U.; Goldberg, K.I. *Adv. Inorg. Chem.* **2003**, *54*, 259.
49. Hill, G.S.; Vittal, J.J.; Puddephatt, R.J. *Organometallics.* **1997**, *16*, 1209.
50. Lanci, M.P.; Remy, M.S.; Lao, D.B.; Sanford, M.S.; Mayer, J.M. *Organometallics.* **2011**, *30*, 3704.
51. Labinger, J.A.; Bercaw, J.E. *Nature.* **2002**, *417*, 507.
52. Williams, T.J.; Caffyn, A.J.; Hazari, N.; Oblad, P.F.; Labinger, J.A.; Bercaw, J.E. *J. Am. Chem. Soc.* **2008**, *130*, 2418.
53. Waltz, K.M.; Hartwig, J.F. *J. Am. Chem. Soc.* **2000**, *122*, 11358.
54. Chen, H.Y.; Schlecht, S.; Semple, T.C.; Hartwig, J.F. *Science.* **2000**, *287*, 1995.
55. Stahl, S.S.; Labinger, J.A.; Bercaw, J.E. *Angew. Chem. Int. Ed.* **1998**, *37*, 2180.
56. Shilov, A.E.; Shul'pin, G.B. *Chem. Rev.* **1997**, *97*, 2879.
57. Periana, R.A.; Jaube, D.J.; Gamble, S.; Taube, H.; Satoh, T.; Fujii, H. *Science.* **1998**, *280*, 560.
58. Gol'dshleger, N.F.; Es'kova, N.F.; Shilov, A.E.; Shteinman, A.A. *Zh. Fiz. Khim.* **1972**, *46*, 1353.
59. Zhong, H.A.; Labinger, J.A.; Bercaw, J.E. *J. Am. Chem. Soc.* **2002**, *124*, 1378.
60. Arndtsen, B.A.; Bergman, R.G.; Mobley, T.A.; Peterson, T.H. *Acc. Chem. Res.* **1995**, *28*, 154.
61. Stahl, S.S.; Labinger, J.A.; Bercaw, J.E. *J. Am. Chem. Soc.* **1996**, *118*, 5961.
62. Lersch, M.; Tilset, M. *Chem. Rev.* **2005**, *105*, 2471.

63. Shilov, A.E. "Activation of Saturated Hydrocarbons by Transition Metal Complexes", D. Reidal Publishing, Dordrecht, **1984**.
64. Holtcamp, M.W.; Henling, L.M.; Day, M.W.; Labinger, J.A.; Bercaw, J.E. *Inorg. Chim. Acta.* **1998**, 270, 467.
65. Holtcamp, M.W.; Labinger, J.A.; Bercaw, J.E. *J. Am. Chem. Soc.* **1997**, 119, 848.
66. Johansson, L.; Ryan, O.B.; Tilset, M. *J. Am. Chem. Soc.* **1999**, 121, 1974.
67. Prokopchuk, E.M.; Puddephatt, R.J. *Organometallics.* **2003**, 22, 787.
68. Wik, B.J.; Lersch, M.; Tilset, M. *J. Am. Chem. Soc.* **2002**, 124, 12116.
69. Zhang, F.; Jennings, M.C.; Puddephatt, R.J. *Organometallics.* **2004**, 23, 1396.
70. Hill, G.S.; Rendina, L.M.; Puddephatt, R.J. *Organometallics.* **1995**, 14, 4966.
71. Hill, G.S.; Puddephatt, R.J. *J. Am. Chem. Soc.* **1996**, 118, 6875.
72. Jenkins, H.A.; Yap, G.S.; Puddephatt, R.J. *Organometallics*, **1997**, 16, 1946.
73. Vedernikov, A.N. *Chem. Commun.* **2009**, 4871.
74. Rostovtsev, V.V.; Henling, L.M.; Labinger, J.A.; Bercaw, J.E. *Inorg. Chem.* **2002**, 41, 3608.
75. Monaghan, P.K.; Puddephatt, R.J. *Organometallics.* **1984**, 3, 444.
76. Rostovtsev, V.V.; Labinger, J.A.; Bercaw, J.E. *Organometallics.* **1998**, 17, 4530.
77. Grice, K.A.; Goldberg, K.I. *Organometallics*, **2009**, 28, 953.
78. Taylor, R.; Law, D.; Sunley, G.; White, A.; Britovsek, G. *Angew. Chem. Int. Ed.* **2009**, 48, 5900.
79. Scheuermann, M.L.; Goldberg, K.I. *Chem. Eur. J.* **2014**, 20, 14556.

80. Denney, M.C.; Smythe, N.A.; Cetto, K.L.; Kemp, R.A.; Goldberg, K.I. *J. Am. Chem. Soc.* **2006**, *128*, 2508.
81. Keith, J.M.; Muller, R.P.; Kemp, R.A.; Goldberg, K.I.; Goddard, W.A.; Oxgaard, J. *Inorg. Chem.* **2006**, *45*, 9631.
82. Lansing, R.B.; Goldberg, K.I.; Kemp, R.A. *Dalton Trans.* **2011**, *40*, 8950.
83. Konnick, M.M.; Stahl, S.S. *J. Am. Chem. Soc.* **2008**, *130*, 5753.
84. Konnick, M.M.; Gandhi, B.A.; Guzei, I.A.; Stahl, S.S. *Angew. Chem. Int. Ed.* **2006**, *118*, 2970.
85. Prokopchuk, E.M.; Puddephatt, R.J. *Can. J. Chem.* **2003**, *81*, 476.
86. Wenzel, T.T. *Stud. Surf. Sci. Catal.* **1991**, *66*, 545.
87. Look, J.L.; Wick, D.D.; Mayer, J.M.; Goldberg, K.I. *Inorg. Chem.* **2009**, *48*, 1356.
88. Wilkinson, M.J.; van Leeuwen, P.W.N.M.; Reek, J.N.H. *Org. Biomol. Chem.* **2005**, *3*, 2371.
89. Kirby, A.J. *Angew. Chem. Int. Ed.* **1996**, *35*, 707.
90. Kharisov, B.I.; Martinez, P.E.; Jimenez-Perez, V.M.; Kharissova, O.V.; Martinez, B.N.; Perez, N. *J. Coord. Chem.* **2010**, *63*, 1.
91. Lopez-Valbuena, J.M.; Escudero-Adan, E.C.; Benet-Buchholz, J.; Freixa, Z.; van Leeuwen, P.V.N.M. *Dalton Trans.* **2010**, *39*, 8560.
92. Jedrzejak, M.J.; Setlow, P. *Chem. Rev.* **2001**, *101*, 607.
93. Weng, Z.Q.; Teo, S.; Liu, Z.P.; Hor, T.S.A. *Organometallics.* **2007**, *26*, 2950.
94. Fenton, D.E. *Chem. Soc. Rev.* **1999**, *28*, 159.

95. Ozawa, H.; Haga, M.; Sakai, K. *J. Am. Chem. Soc.* **2006**, 4926.
96. Inagaki, A.; Akita, M. *Coord. Chem. Rev.* **2010**, 254, 1220.
97. Bosnich, B. *Inorg. Chem.* **1999**, 38, 2554.
98. Rowlands, G.J. *Tetrahedron.* **2001**, 57, 1865.
99. Van de Vlugt, J.I. *Eur. J. Inorg. Chem.* **2012**, 363.
100. Adams, R.D.; Cotton, F.A. "Catalysis by Di and Polynuclear Metal Cluster Complexes", Wiley-VCH, New York, **1998**.
101. Kember, M.R.; Buchard, A.; Williams, C.K. *Chem. Commun.* **2011**, 47, 141.
102. Breinbauer, R.; Jacobsen, E.N. *Angew. Chem. Int. Ed.* **2000**, 39, 3640.
103. Fafard, C.M.; Adhikari, D.; Foxman, B.M.; Mindiola, D.J.; Ozerov, O.V. *J. Am. Chem. Soc.* **2007**, 129, 10318.
104. Christmann, U.; Vilar, R.; White, A.J.P.; Williams, D.J. *Chem. Commun.* **2004**, 1294.
105. Christmann, U.; Pantazis, D.A.; Benet-Buchholz, J.; McGrady, J.E.; Maseras, F.; Villar, R. *J. Am. Chem. Soc.* **2006**, 128, 6376.
106. Velian, A.; Lin, S.; Miller, A.J.M.; Day, M.W.; Agapie, T. *J. Am. Chem. Soc.* **2010**, 132, 6296.
107. Lin, S.; Day, M.W.; Agapie, T. *J. Am. Chem. Soc.* **2011**, 133, 3828.
108. Chao, S.T.; Lara, N.C.; Lin, S.; Day, M.W.; Agapie, T. *Angew. Chem. Int. Ed.* **2011**, 50, 7529.
109. Kanady, J.S.; Tsui, E.Y.; Day, M.W.; Agapie, T. *Science.* **2011**, 333, 733.

110. Angamuthu, R.; Byers, P.; Lutz, M.; Spek, A.L.; Bouwman, E. *Science*. **2010**, 327, 313.
111. Lindoy, L.F.; Atkinson, I.M. “*Self-Assembly in Supramolecular Systems*”, **2000**.
112. Lehn, J-M. *Pure Appl. Chem.* **1978**, 50, 871.
113. Lehn, J-M. “*Supramolecular Chemistry: Concepts and Perspectives*”, VCH, Weinheim, **1995**.
114. Steed, J.W.; Atwood, J.L. “*Supramolecular Chemistry*”, John Wiley and Sons, Toronto, **2000**.
115. Pimentel, G.C.; McClellan, A.L. “*The Hydrogen Bond*”, Freeman, San Francisco, **1960**.
116. Jeffrey, G.A. “*An Introduction to Hydrogen Bonding*”, Oxford University Press, New York, **1997**.
117. Atwood, J.L.; Steed, J.W. “*Encyclopedia of Supramolecular Chemistry*”, Marcel Dekker, New York, **2004**.
118. Au, R.H.W.; Jennings, M.C.; Puddephatt, R.J. *Organometallics*. **2009**, 28, 3734.
119. McCreedy, M.S.; Puddephatt, R.J. *Dalton Trans.*, **2012**, 41: 12378-12385.
120. Braga, D.; Grepioni, F.; Desiraju, G. *J. Organomet. Chem.* **1997**, 548, 33.
121. Zhang, F.; Jennings, M.C.; Puddephatt, R.J. *Chem. Commun.* **2007**, 1496.
122. Au, R.H.W.; Jennings, M.C.; Puddephatt R.J. *Organometallics*. **2009**, 28, 3754.
123. Au, R.H.W.; Jennings, M.C.; Puddephatt R.J. *Organometallics*. **2009**, 28, 5052.
124. Fraser, C.S.A.; Eisler, D.J.; Jennings, M.C.; Puddephatt, R.J. *Chem. Commun.* **2002**, 1224.

125. Zhang, F.; Kirby, C.W.; Hairsine, D.W.; Jennings, M.C.; Puddephatt R.J. *J. Am. Chem. Soc.* **2005**, *127*, 14196.
126. Safa, M.A.; Abo-Amer, A.; Borecki, A.; Cooper, B.F.T.; Puddephatt, R.J. *Organometallics*. **2012**, *31*, 2675.
127. Abo-Amer, A.; Boyle, P.D.; Puddephatt, R.J. *J. Organomet. Chem.* **2014**, *770*, 79.
128. Abo-Amer, A.; Puddephatt, R.J. *J. Inorg. Organomet. Polym.* **2014**, *24*, 114.
129. Safa, M.A.; Puddephatt, R.J. *J. Organomet. Chem.* **2013**, *724*, 7.

CHAPTER 2

Synthesis and Reactivity of a Potentially Bimetallic Platinum(II) Complex Based on a 3,6-dipyridylpyridazine Ligand Design

A version of this chapter has been published: a) Abo-Amer, A.; McCready, M.S.; Zhang, F.; Puddephatt, R.J. *Can. J. Chem.*, **2012**, 90, 1, 46-54. b) McCready, M.S.; Puddephatt, R.J. *Organometallics*. **2015**, doi: 10.1021/om501023r

2.1 Introduction

The design and synthesis of multinuclear transition metal complexes has garnered significant interest due in part to their ability to catalyze complex reactions [1-14] and mimic biological enzymes [15-21]. To that end, there is an ever present need to synthesize ligands which are not only capable of complexing multiple metal centers, but also hold these metal centers in close proximity to encourage beneficial intermetallic interactions. These ligands should possess multiple nitrogen donor atom sites, such as those depicted in figure 2.1, and be designed in a manner that allows metal centers to be held in adjacent positions without the aid of a metal-metal bond [22]. Ghedini and co-workers have shown that ligands based on a 3,6-bis(2'-pyridyl)pyridazine scaffold, **A** in figure 2.1, are excellent candidates for the formation of bimetallic complexes [23,24]. This was further supported by the syntheses of dinuclear palladium complexes based on a similar scaffold by Inoue and co-workers, **B** and **C** in figure 1 [25]. This specific ligand design holds the metal centers in adjacent positions in a fixed manner, providing the potential for these metal centers to work in cooperation. These tetradentate nitrogen-donor ligands also offer the ability to introduce various functionality to the backbone through the use of Diels-Alder type chemistry. This allows for the ability to tune both sterics and electronics of the pyridazine ring which could alter the chemistry observed at the metal centers, as well as the ability of the ligand to coordinate multiple metal centers. The group of Schroder *et al.* have taken advantage of this ability by employing these 3,6-diaryl-1,2,4,5-tetrazines to establish ligand motifs that possess multiple nitrogen donor sites through the use of the "inverse electron demand" Diels-Alder reaction, **E** and **F** [26]. These ligand motifs allow for the establishment of multimetallic complexes which can be utilized in the design of higher nuclearity compounds, molecular grids and polymeric compounds.

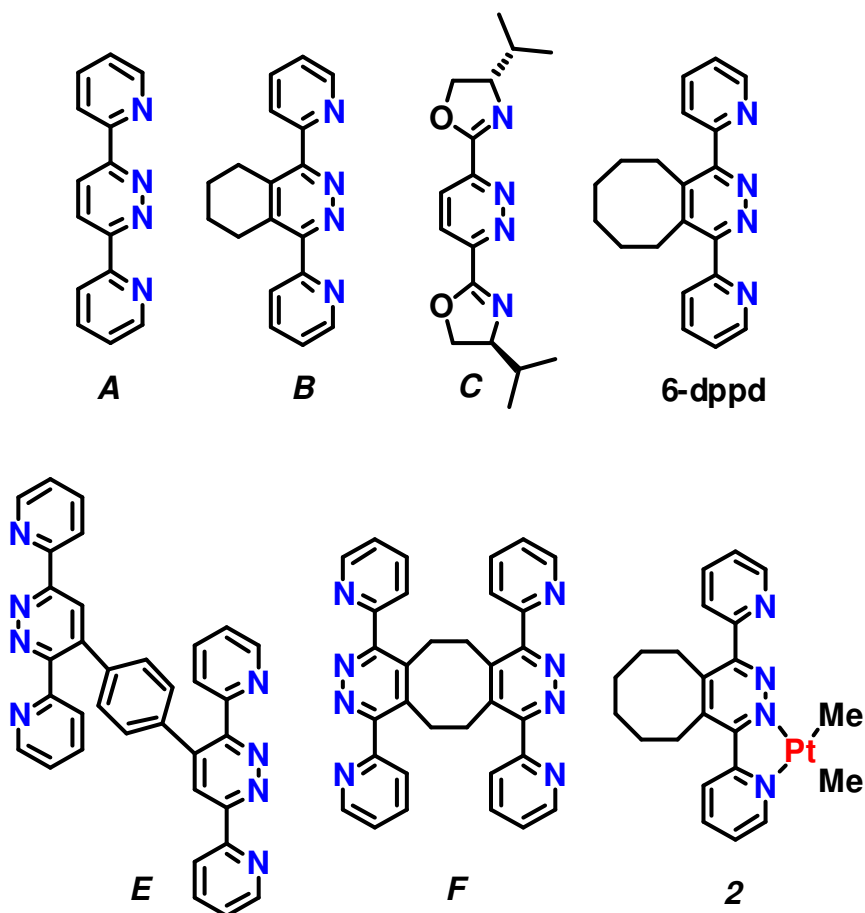


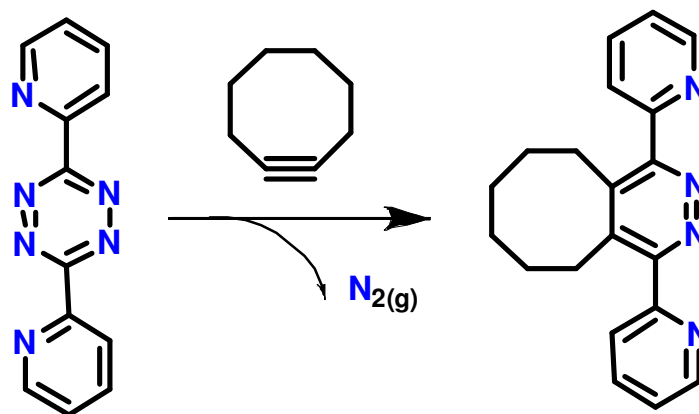
Figure 2.1. Various ligands (A-F) which are potential candidates for the preparation of multimetallic complexes and **2**, the dimethylplatinum(II) complex of **6-dppd**.

It has been well established that dimethylplatinum(II) complexes possessing nitrogen donor ligands are highly reactive towards the oxidative addition of a variety of substrates [27-41]. For example, alkyl halides have been shown to oxidatively add to dimethylplatinum(II) complexes in a *trans* manner resulting in the corresponding organoplatinum(IV) products and, when the substrates are selected rationally, can elicit varying supramolecular chemistry [42-45] or, as is shown recently, some interesting photochemistry [46]. By designing a ligand system which can accommodate two platinum centers, the previously established and observed reactivity of these organoplatinum compounds could be harnessed and it could become possible to activate and functionalize substrates in a cooperative manner. This concept would lend itself specifically useful for the functionalization of typically inert substrates such as alkanes. This would occur through the activation of a C-H bond at one platinum center followed by functionalization in cooperation with the second platinum center.

This chapter describes the reactivity and chemistry of platinum(II) complexes of the ligand **6-dppd**, 1,4-di(2-pyridyl)-5,6,7,8,9,10-hexahydrocycloocta[d]pyridazine, **D** in figure 2.1. This ligand appeared to have potential for the coordination of two metal centers in adjacent positions and as such garnered our interest in its use for bimetallic cooperative catalysis. Although the goal was to coordinate two dimethylplatinum(II) metal centers in the adjacent coordination sites, this proved to be unattainable. The monoplatinum derivative of the ligand, [PtMe₂(6-dppd)] complex **2** in figure 2.1, was formed as a stable product and demonstrated enhanced reactivity towards oxidative addition chemistry. This allowed for the synthesis of heterobimetallic complexes of **6-dppd** through the oxidative addition of mercuric halides and carboxylates. Various other oxidative addition reactions, including the oxidative addition of a solvent molecule, as well as a C-H activation experiment were performed. These reactions allowed for the understanding of the reactivity profile of complex **2** and are reported in this chapter.

2.2 Ligand Synthesis

The ligand **6-dppd**, 1,4-di(2-pyridyl)-5,6,7,8,9,10-hexahydrocycloocta[d]pyridazine, was synthesized by the Diels-Alder addition of cyclooctyne to 3,6-di(2-pyridyl)-1,2,4,5-tetrazine, as outlined in scheme 2.1. The pungent smelling cyclooctyne was synthesized following the procedure established by Verkrujisse and Brandsma [47], in which *cis*-cyclooctene is first brominated and subsequently dehydrobrominated twice to yield cyclooctyne. Then following the procedure outlined by Sauer [48], a dichloromethane solution of the yellow cyclooctyne liquid is added dropwise to a bright pink dichloromethane solution of 3,6-di(2-pyridyl)-1,2,4,5-tetrazine until a yellow colour persists. Reducing the volume of the solution *in vacuo*, yields a yellow residue which is subsequently recrystallized with hexane and stored at 5°C overnight. After 16hrs, off-white crystals of **6-dppd** were produced in good yield, which were then characterized by ¹H, (figure 2.2), and ¹³C NMR as well as ESI-MS and single crystal X-ray crystallography. The solid state structure is shown in figure 2.3.



Scheme 2.1. The synthesis of ligand, **6-dppd**.

It becomes evident upon examination of the structure of **6-dppd** that the cyclooctene ring imposes a large steric constraint to the ligand system. This steric hindrance leads to the pyridyl rings being skewed by 55° relative to the pyridazine ring in order to reduce the steric congestion. As outlined in previous research by Ghedini [23], the 3,6-di-(2-pyridyl)pyridazine ligand exhibits exceptional donor ability and has been shown to enhance the reactivity of the corresponding dimethylplatinum(II) complex [24].

The drawback is that the complexes suffer from poor solubility in most common organic solvents. The introduction of the cyclooctene ring, although it introduces significant steric constraint on the system, provides enhanced solubility, which allows the ligand to be utilized and characterized more effectively than its parent systems [49].

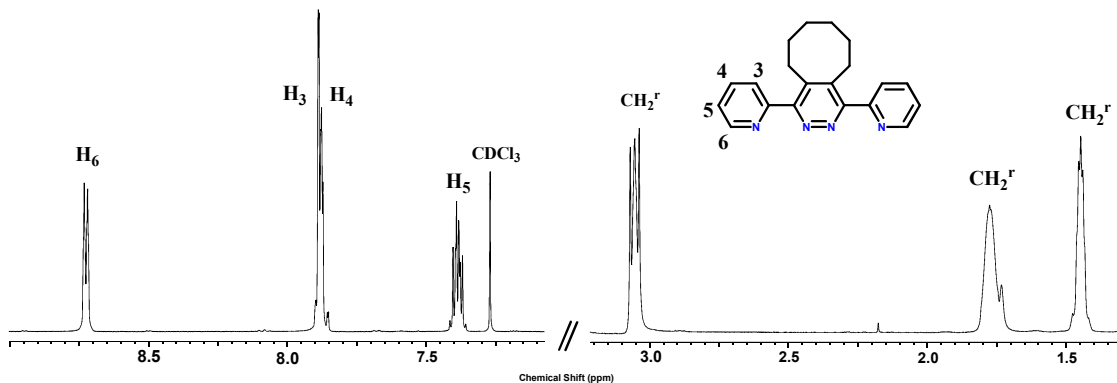


Figure 2.2. ^1H NMR spectrum of **6-dppd** in CDCl_3 . Pyridyl proton resonances labelled according to included figure. CH_2^r indicates the resonances arising due to the protons of the cyclooctyl ring.

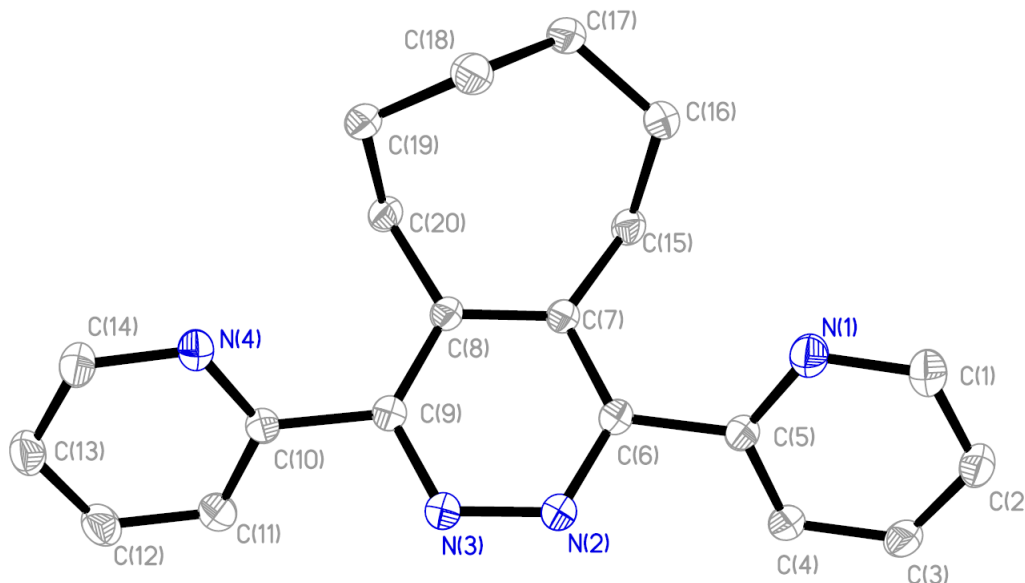
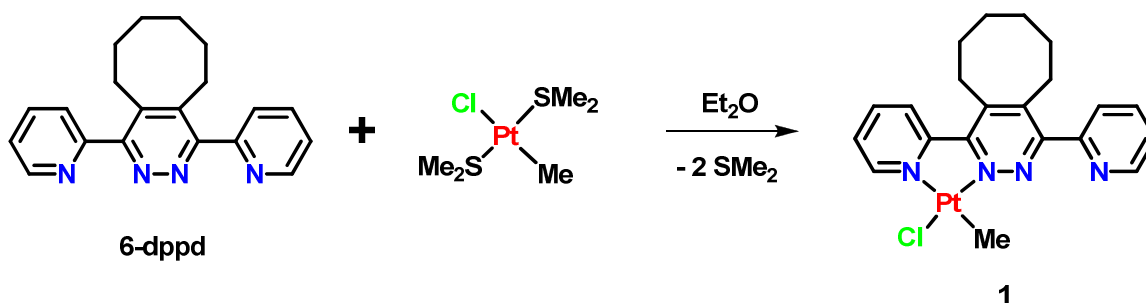


Figure 2.3. Molecular structure of **6-dppd**, with an atomic labeling scheme.

2.3 Synthesis of platinum(II) complexes of 6-dppd

Complex **1**, [PtClMe(6-dppd)] was synthesized by the addition of *trans*-[PtClMe(SMe₂)₂] to **6-dppd**. The complex *trans*-[PtClMe(SMe₂)₂] was synthesized according to the literature [50], of which a diethyl ether solution was added in a 1:1 stoichiometric ratio to a diethyl ether solution of **6-dppd** in order to afford a high yield of the orange powdered monomethylplatinum(II) complex [PtClMe(6-dppd)], **1**. This synthesis is outlined in scheme 2.2. The ¹H NMR spectrum of complex **1**, figure 2.4, contained a single methylplatinum resonance at 1.36 ppm and ²J(PtH) = 80 Hz, and eight aromatic resonances. Thus the ¹H NMR spectrum provided evidence for the formation of complex **1**.



Scheme 2.2. Synthesis of complex **1**, [PtClMe(6-dppd)].

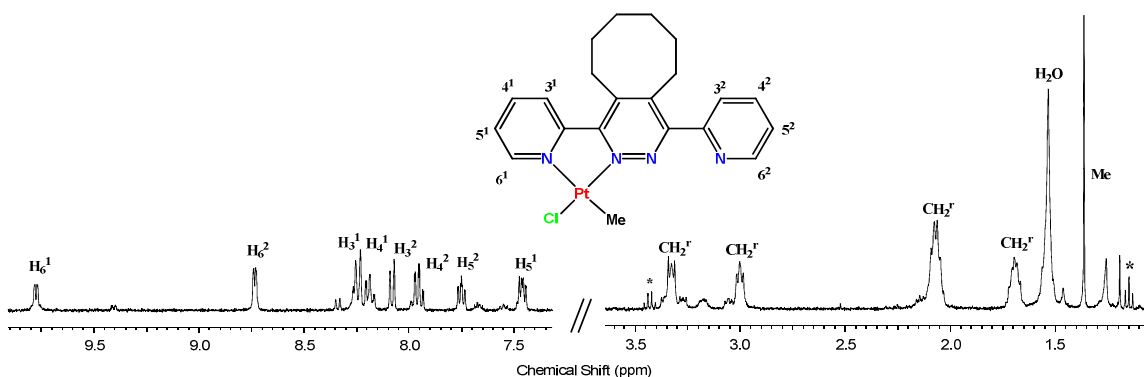


Figure 2.4. ¹H NMR spectrum of [PtClMe(6-dppd)], **1**, in CD₂Cl₂. Pyridyl resonances labelled according to conventional assignment, CH₂^r indicates protons of the cyclooctyl ring, * represents residual diethyl ether.

Crystals suitable for single crystal X-ray crystallographic analysis were grown from the slow vapour diffusion of pentane into an acetone solution of complex **1**. Figure 2.5 depicts the solid state structure of complex **1**. It is important to note that the platinum(II) compound shows preference to the square planar orientation in which the methyl group is directed inward. This is also confirmed through the use of ^1H - ^1H NOESY NMR spectroscopy. The preference is presumed to be due to the unfavourable interaction of the bulkier chloride ligand with the dangling pyridyl group. Twisting of the dangling pyridyl group is observed leading to a 54° skew from planarity relative to the pyridazine ring.

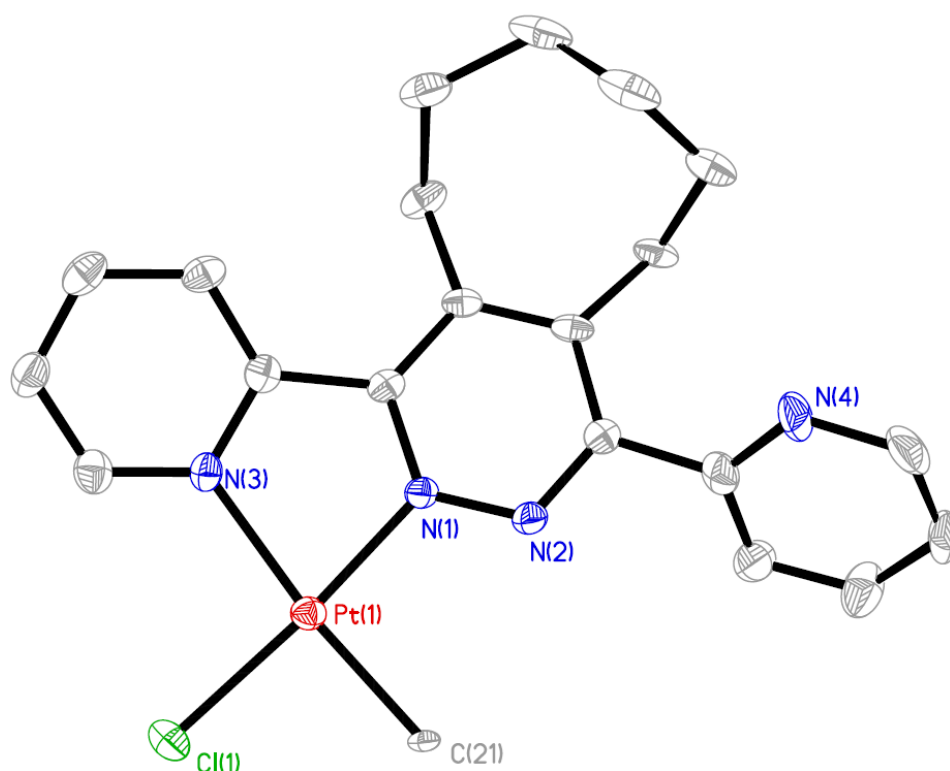
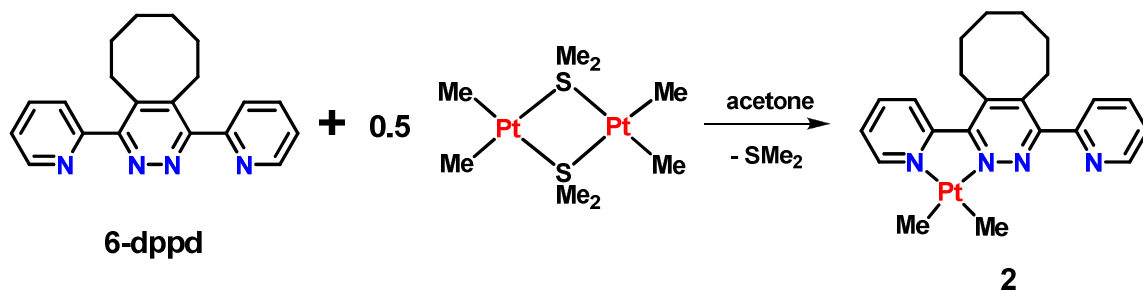


Figure 2.5. Molecular structure of complex **1**, with an atomic numbering scheme (hydrogen atoms omitted for clarity).

Table 2.1: Bond lengths [Å] and angles [°] for [PtClMe(6-dppd)], 1

Pt(1)-N(3)	2.095(5)	Pt(1)-N(1)	1.988(5)
Pt(1)-Cl(1)	2.3099(16)	Pt(1)-C(21)	2.062(5)
N(3)-Pt(1)-N(1)	79.0(2)	Cl(1)-Pt(1)-C(21)	89.93(16)
N(3)-Pt(1)-Cl(1)	96.56(15)	N(1)-Pt(1)-C(21)	94.5(2)
N(3)-Pt(1)-C(21)	173.5(2)	N(1)-Pt(1)-Cl(1)	174.28(15)
N(3)-C(11)-C(10)-N(1)	15.1(7)	N(2)-C(1)-C(16)-N(4)	126.4(6)

Complex **2**, [PtMe₂(6-dppd)] was prepared by the addition of an acetone solution of **6-dppd** to a dry toluene solution of a dimethylplatinum(II) precursor complex, [Pt₂Me₄(μ-SMe₂)₂], as depicted in scheme 2.3 [50, 51]. A deep scarlet red powder of complex **2** precipitated out of solution after 18hrs of cooling at 5°C. Complex **2** was isolated by vacuum filtration in good yield and then washed with pentane. Scarlet red crystals suitable for single crystal X-ray crystallographic analysis were grown by the slow diffusion of pentane into an acetone solution of complex **2**.

**Scheme 2.3.** Synthesis of complex **2**, [PtMe₂(6-dppd)].

^1H NMR spectroscopic analysis provided evidence for the formation of complex **2** through the presence of eight distinct signals in the aromatic region of the spectrum, as can be seen in figure 2.6. Further evidence for the coordination of the dimethylplatinum(II) center was provided by the presence of ^{195}Pt satellites on the *ortho*-hydrogen, H_6 , of the pyridyl ring with a coupling constant of $^3J(\text{PtH}) = 18$ Hz. The unsymmetrical nature of the complex leads to the presence of two distinct methyl platinum resonances. ^1H - ^1H NOESY NMR analysis allows for the absolute assignment of these methyl groups, as the outward directed methyl group possesses a through space interaction with the *ortho*-hydrogen of the pyridyl group. This lead to the assignment of the methyl group furthest upfield at 1.26 ppm being the inward directed methyl group, Me_A , with a $^2J(\text{PtH})$ value of 84 Hz; and the furthest downfield at 1.46 ppm being the outward directed methyl group, Me_B with a $^2J(\text{PtH})$ value of 88 Hz. Further downfield, from 1.54ppm to 3.27ppm, five signals were observed due to the methylene protons of the cyclooctene ring and are labeled in figure 2.6.

The single crystal X-ray structure determination supported the formation of complex **2**. The structure of this square planar dimethylplatinum(II) complex, figure 2.7 provides insight into the inability of complex **2** to ligate a second dimethylplatinum(II) center. The vacant coordination site of complex **2** is sterically crowded by a methyl group of the coordinated platinum center. This steric hindrance prevents the facile coordination of a second dimethylplatinum group. In addition to this, there is a rotation of the dangling pyridyl group of the **6-dppd** backbone with an N4-C13-C4-N3 torsion angle of 42° . This is likely occurring to decrease the steric interaction of pyridyl ring with the cyclooctyl backbone.

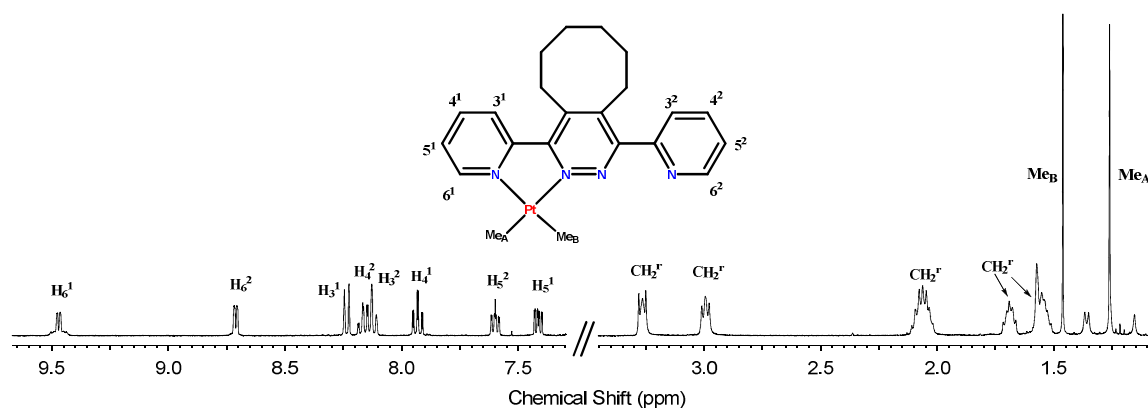


Figure 2.6. ^1H NMR spectrum of complex **2** in CDCl_3 . Pyridyl resonances labelled according to conventional assignment. CH_2^r indicates resonances resulting from the protons of the cyclooctyl ring.

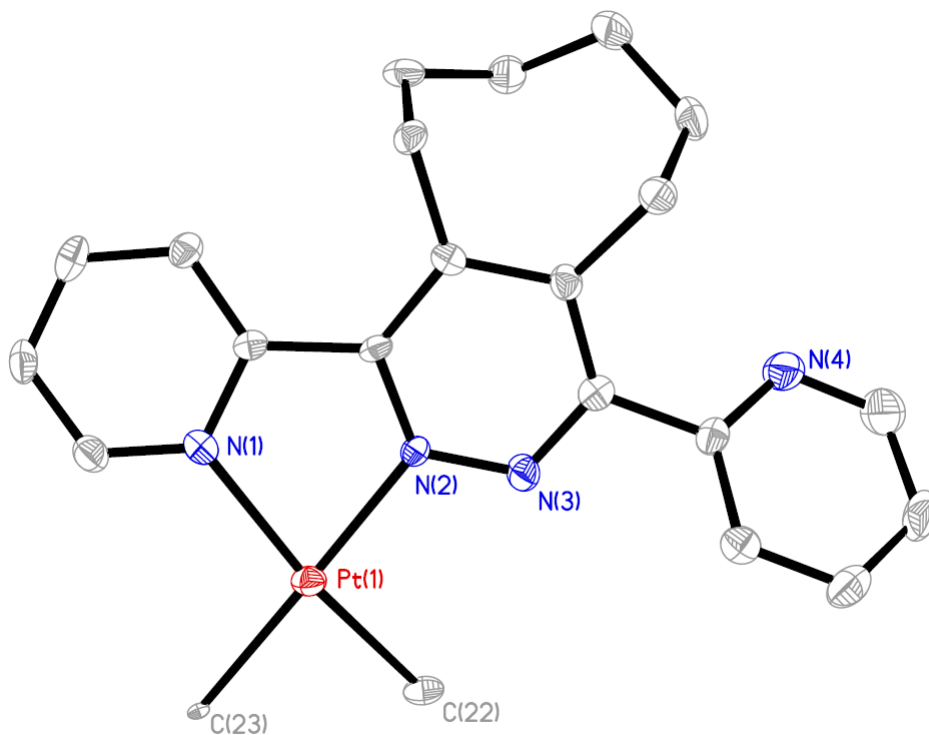


Figure 2.7. Molecular structure of complex **2**, with an atomic numbering scheme (hydrogen atoms excluded for clarity).

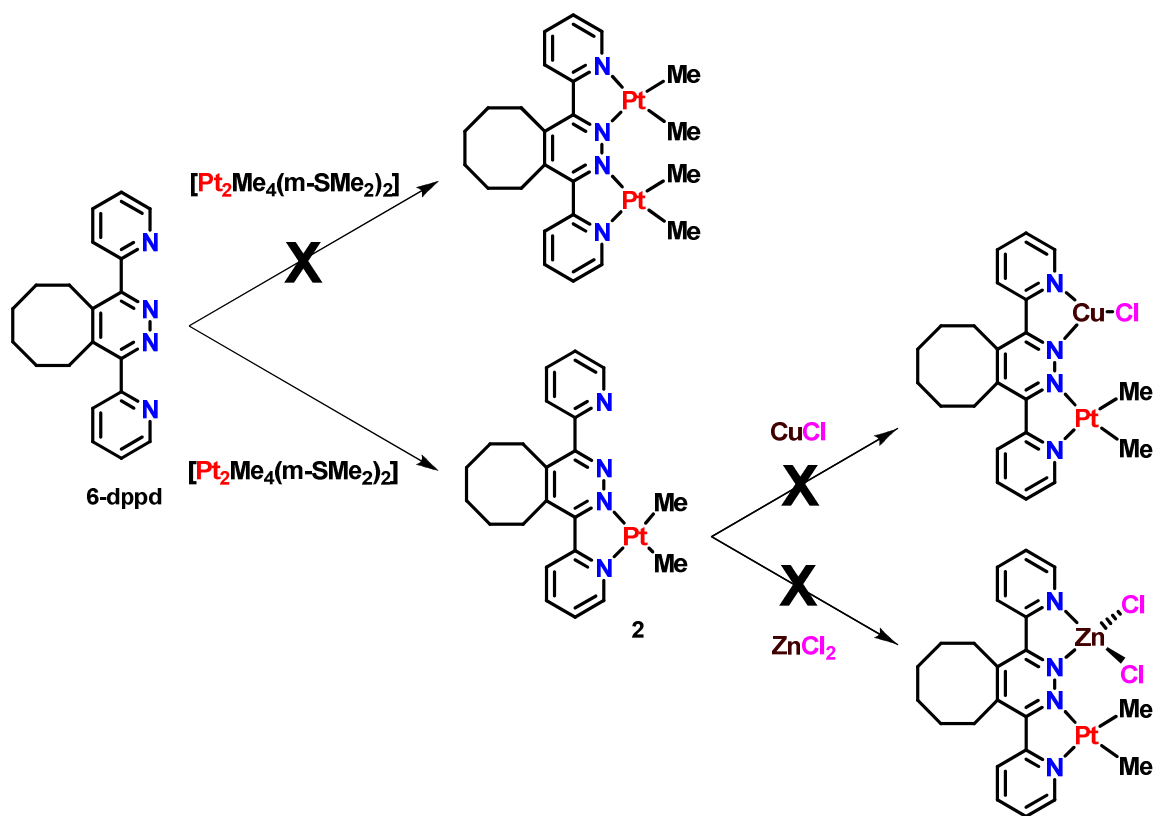
Table 2.2: Bond lengths [Å] and angles [°] for [PtMe₂(6-dppd)], 2

Pt(1)-N(1)	2.105(5)	Pt(1)-N(2)	2.060(5)
Pt(1)-C(22)	2.307(5)	Pt(1)-C(23)	2.082(5)
N(1)-Pt(1)-N(2)	76.58(18)	C(22)-Pt(1)-C(23)	84.9(2)
N(2)-Pt(1)-C(22)	96.9(2)	N(1)-Pt(1)-C(23)	101.95(19)
N(1)-Pt(1)-C(22)	172.0(2)	N(2)-Pt(1)-C(23)	176.34(18)
N(1)-C(1)-C(2)-N(2)	12.8(7)	N(3)-C(4)-C(13)-N(4)	138.5(5)

2.4 Efforts Towards the Synthesis of a Bimetallic Complex of 6-dppd

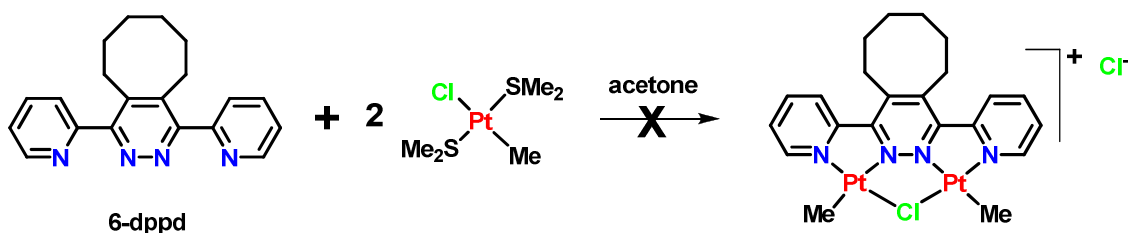
2.4.1 Attempting to synthesize a diplatinum complex of 6-dppd

It was believed that the use of 6-dppd as a ligand should allow for the formation of a variety of bimetallic complexes due to the incorporation of two distinct sites for chelation of a metal center. Being such, the ligand was treated with two equivalents of a dimethylplatinum(II) center as shown in scheme 2.4. Rather than the diplatinum product [Pt₂Me₄(6-dppd)], the monoplatinum product [PtMe₂(6-dppd)], complex **2**, was observed even upon heating at 60°C.



Scheme 2.4. Synthetic efforts towards the synthesis of a bimetallic complex of **6-dppd**.

This monoplatinum product, **2** is proposed to be formed preferentially over the diplatinum product due to the unfavourable rotation of the non-coordinated 2-pyridyl group to effectively relieve some steric constraint within the molecule [52]. As another avenue to attain a diplatinum complex of **6-dppd**, we opined that, by reacting two equivalents of *trans*- $[PtClMe(SMe_2)_2]$ simultaneously with an equivalent of **6-dppd**, a bimetallic platinum complex possessing a bridging chloride ligand would be obtained, scheme 2.5. This reaction, even upon heating to $60^\circ C$, did not yield the formation of the bridged chloride diplatinated complex, rather again producing complex **1**.

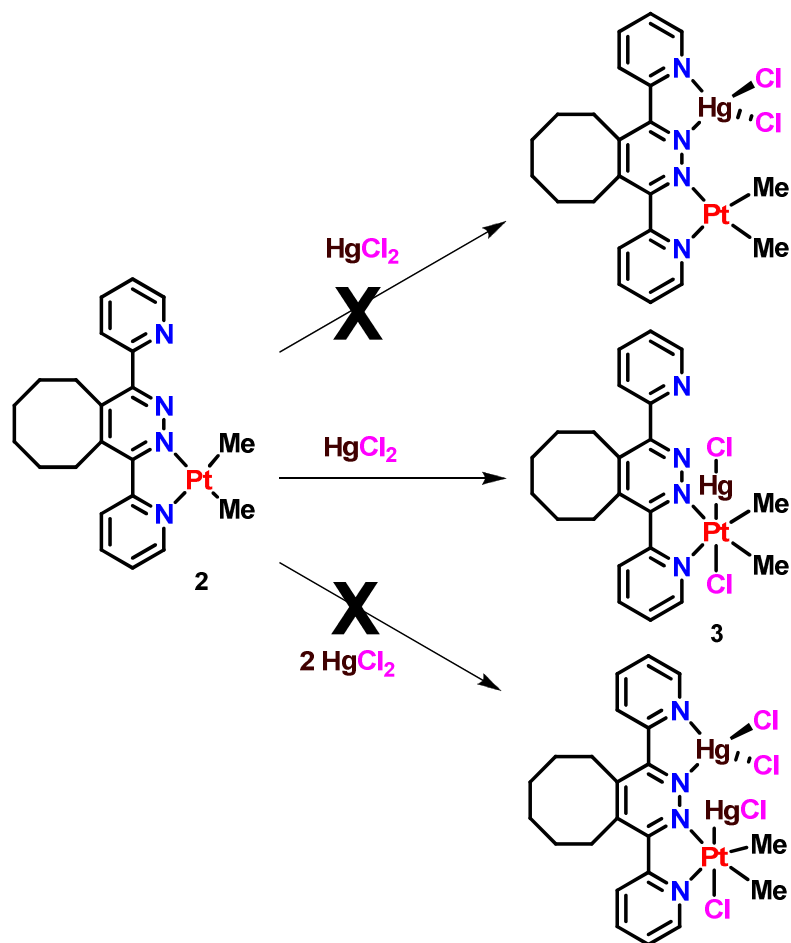


Scheme 2.5. Attempted synthesis of a diplatinum complex of **6-dppd** incorporating a bridged chloride ligand.

2.4.2 Efforts towards a heterobimetallic complex of **6-dppd**

The inability to accommodate two metal centers of square planar geometry such as dimethylplatinum(II) units due to steric effects led us to evaluate the ability of complex **2** to ligate metal centers of alternative geometry. To this end, complex **2** was treated with one equivalent of CuCl, ZnCl₂ or HgCl₂ to examine if the coordination of metal centers of alternative geometry was indeed possible. As is further illustrated in scheme 2.4, **2** was unable to incorporate a second metal center in the cases of CuCl and ZnCl₂, even though these metals adopt a geometry which should reduce the steric clash between metal centers. It is believed that the inability of **2** to ligate the second metal center is again due to the rotation of the non-coordinated 2-pyridyl group away from the pyridazine nitrogen atom.

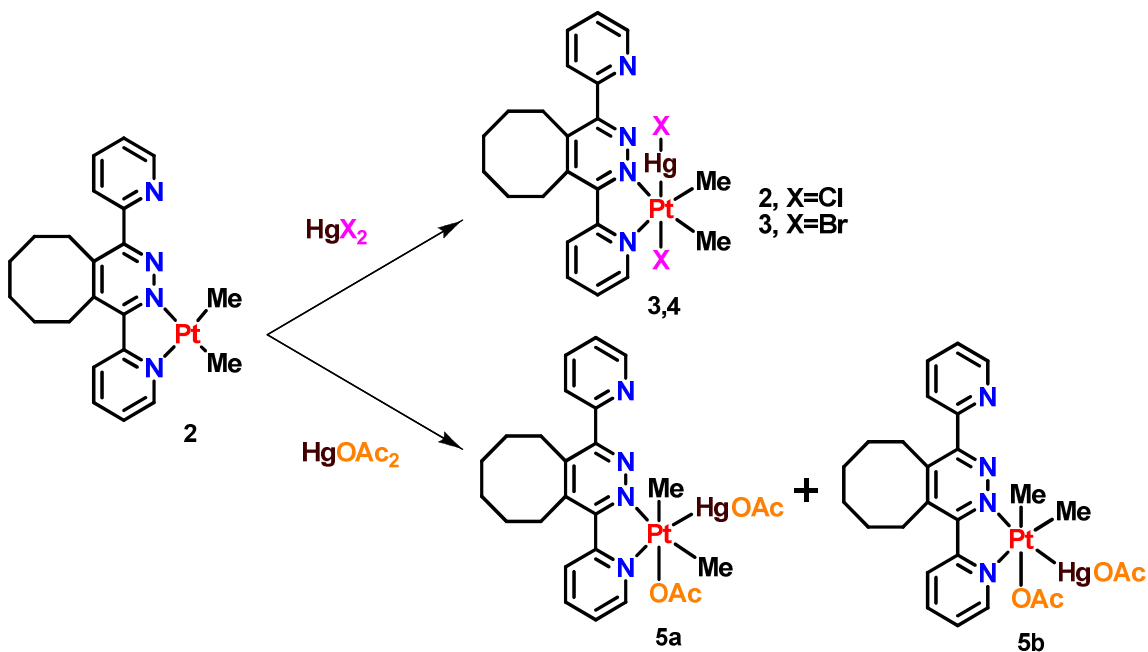
However, when complex **2** was treated with an equivalent of HgCl₂, the originally red acetone solution of complex **2** gradually changed to a yellow solution. Through ¹H NMR spectroscopy it was concluded that, rather than forming the bimetallic platinum(II)-mercury(II) compound [PtMe₂(HgCl₂)(6-dppd)], it was the platinum(IV) complex, [PtClMe₂(HgCl)(6-dppd)], **3**, that was formed via the oxidative addition of HgCl₂, scheme 2.6. This reaction was not without precedent, but does however indicate that the oxidative addition of the mercuric halides occurs preferentially over the coordination of the mercuric halide by the non-coordinated nitrogen donor atoms [53-55]. If a second equivalent of mercuric chloride was added to a solution of the completely oxidized platinum(IV) compound, again no reaction was observed indicating that the second potential coordinating site remains non-coordinating in these cases.



Scheme 2.6. The reaction of **2** with 1 or 2 equivalents of HgCl_2 .

Due to the observation of the oxidative addition of mercuric chlorides at **2** yielding the heterobimetallic complex **3**, similar reactions were performed using mercuric bromide and mercuric acetate. The oxidative addition of mercuric halides and mercuric acetate at **2**, as shown in scheme 2.7, results in the formation of platinum(IV) compounds which possess a Pt-Hg metal-metal bond. The reaction of equimolar amounts of HgCl_2 with **2** afforded a yellow solid, $[\text{PtClMe}_2(\text{HgCl})(6\text{-dppd})]$ complex **3**, which was characterized by ^1H NMR spectroscopy, figure 2.8. Two methylplatinum resonances were observed each possessing both platinum-195 and mercury-199 satellites, $\delta = 1.72$ ppm, $^2J_{\text{PtH}} = 64$ Hz, $^3J_{\text{HgH}} = 6$ Hz and $\delta = 1.99$ ppm, $^2J_{\text{PtH}} = 64$ Hz, $^3J_{\text{HgH}} = 8$ Hz. These coupling constant and chemical shift values are indicative of the formation of a platinum(IV) species via oxidative addition of the HgCl_2 in a *trans* manner, and are consistent with previously reported mercury containing platinum(IV) compounds [53,55].

The observation of long range couplings ${}^3J(\text{HgPtMe}) = 6\text{--}8\text{ Hz}$ provides evidence for Pt-Hg bonding as opposed to a donor-acceptor interaction.



Scheme 2.7. The oxidative addition of mercuric halides and mercuric acetate to yield the corresponding mercury(II)-platinum(IV) species via *trans* or *cis* addition.

In a similar manner to the preparation of **3**, $[\text{PtMe}_2\text{Br}(\text{HgBr})(6\text{-dppd})]$ complex **4** was prepared via the *trans* oxidative addition of HgBr_2 . Again two methylplatinum resonances were observed at $\delta = 1.62\text{ ppm}$ and $\delta = 1.99\text{ ppm}$, with coupling values of $[{}^2J_{\text{PtH}} = 64\text{ Hz}, {}^3J_{\text{HgH}} = 7\text{ Hz}]$ and $[{}^2J_{\text{PtH}} = 64\text{ Hz}, {}^3J_{\text{HgH}} = 7\text{ Hz}]$, respectively. These values are quite similar to those of **3** as is expected.

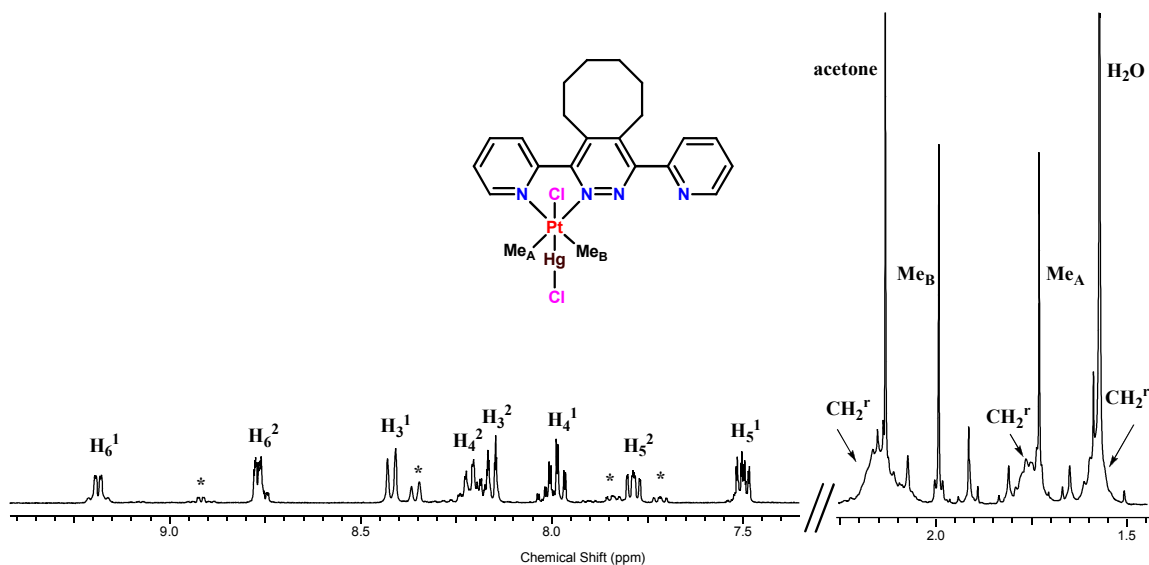


Figure 2.8. ^1H NMR spectrum of complex **3**, $[\text{PtClMe}_2(\text{HgCl})(6\text{-dppd})]$, in CDCl_3 . Pyridyl resonances labelled following the conventional labelling scheme. CH_2^r represents the resonances due to the protons of the cyclooctyl ring. * represents trace amounts of unreacted starting material **2**.

Single crystals suitable for X-ray crystallographic analysis were grown for both complexes **3** and **4**, and their solid state structures are depicted in figure 2.9 and 2.10 respectively. The *trans* geometry was observed supporting the proposed *trans* oxidative addition of the mercuric halides at the platinum center. The Pt-Hg bond distances observed for **3** and **4** were 2.536(2) Å and 2.544(1) Å, respectively. These values are similar to previously observed values of Pt-Hg bonds [53,55] and are slightly shorter than the sum of the radii of Pt and Hg (2.63 Å) [56]. These Pt-Hg bond lengths being shorter than the sum of the radii of Pt and Hg support the formation of covalent bonds between the two metal centers rather than a donor-acceptor bond. The Pt-X bond distances were determined to be 2.433(2) Å when X = Cl, and 2.558(1) Å when X = Br. These bond distances are slightly longer than the sum of the covalent radii (Pt-Cl = 2.37 Å and Pt-Br = 2.52 Å) [56,57], which is likely due to the *trans*-influence of mercury. The Pt-Hg-X bond angles deviate slightly from linearity in each case, (**3** = 174.8(3)° and **4** = 171.9(3)°). Both complexes **3** and **4** are observed to exist as loosely associated dimers in the solid state as is depicted in figure 2.11. These dimers are weakly associated through

intermolecular secondary bonding between adjacent molecules with intermolecular Hg(1)...X(1A)-Hg(1A) contacts of 3.523(2) Å and 3.375(1) Å for **3** and **4** respectively [58].

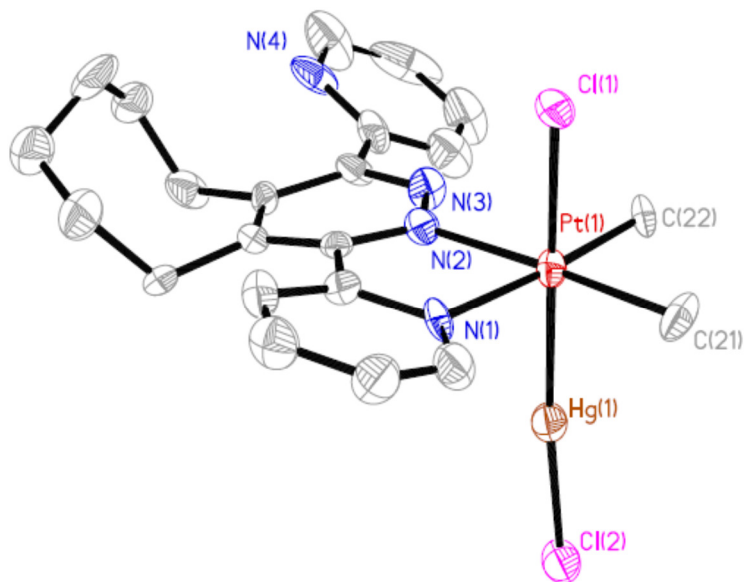


Figure 2.9. Molecular structure of complex **3**, with an atomic numbering scheme (hydrogen atoms excluded for clarity).

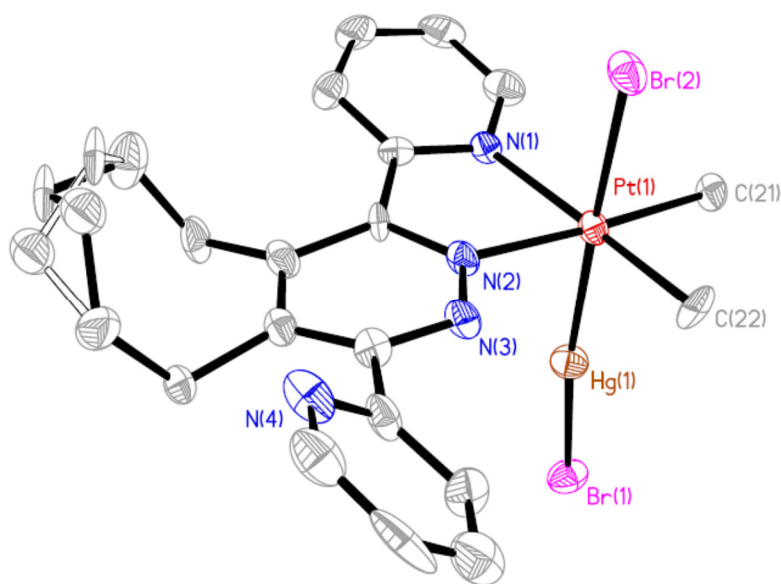


Figure 2.10. Molecular structure of complex **4**, with an atomic numbering scheme (hydrogen atoms excluded for clarity).

Table 2.3: Bond lengths [Å] and angles [°] for [PtClMe₂(HgCl)(6-dppd)], 3

Pt(1)-N(1)	2.143(9)	Pt(1)-N(2)	2.127(9)
Pt(1)-C(21)	2.071(11)	Pt(1)-C(22)	2.071(11)
Pt(1)-Cl(1)	2.433(3)	Pt(1)-Hg(1)	2.5358(10)
Hg(1)-Cl(2)	2.395(3)		
N(1)-Pt(1)-N(2)	76.2(3)	C(21)-Pt(1)-C(22)	85.7(5)
N(2)-Pt(1)-C(22)	99.0(4)	N(1)-Pt(1)-C(21)	99.1(4)
N(1)-Pt(1)-C(22)	175.2(4)	N(2)-Pt(1)-C(21)	175.3(4)
C(21)-Pt(1)-Cl(1)	90.7(4)	C(22)-Pt(1)-Cl(1)	91.1(4)
N(1)-Pt(1)-Cl(1)	89.2(3)	N(2)-Pt(1)-Cl(1)	88.0(3)
C(21)-Pt(1)-Hg(1)	88.8(4)	C(22)-Pt(1)-Hg(1)	88.9(4)
N(1)-Pt(1)-Hg(1)	92.1(3)	N(2)-Pt(1)-Hg(1)	91.3(3)
Cl(1)-Pt(1)-Hg(1)	179.47(7)	Cl(2)-Hg(1)-Pt(1)	174.85(8)
N(1)-C(5)-C(6)-N(2)	13.1(14)	N(3)-C(9)-C(10)-N(4)	149.9(11)

Table 2.4: Bond lengths [Å] and angles [°] for [PtBrMe₂(HgBr)(6-dppd)], 4

Pt(1)-N(1)	2.142(7)	Pt(1)-N(2)	2.116(7)
Pt(1)-C(21)	2.154(8)	Pt(1)-C(22)	2.058(8)
Pt(1)-Br(2)	2.5575(15)	Pt(1)-Hg(1)	2.5439(11)
Hg(1)-Br(1)	2.5234(15)		
N(1)-Pt(1)-N(2)	75.4(3)	C(21)-Pt(1)-C(22)	85.2(4)
N(2)-Pt(1)-C(22)	99.2(3)	N(1)-Pt(1)-C(21)	100.2(3)
N(1)-Pt(1)-C(22)	173.5(3)	N(2)-Pt(1)-C(21)	175.6(3)
C(21)-Pt(1)-Br(2)	90.3(23)	C(22)-Pt(1)-Br(2)	89.1(3)
N(1)-Pt(1)-Br(2)	87.2(2)	N(2)-Pt(1)-Br(2)	89.6(2)
C(21)-Pt(1)-Hg(1)	86.1(3)	C(22)-Pt(1)-Hg(1)	91.7(3)
N(1)-Pt(1)-Hg(1)	92.3(2)	N(2)-Pt(1)-Hg(1)	93.9(2)
Br(2)-Pt(1)-Hg(1)	176.29(3)	Br(1)-Hg(1)-Pt(1)	171.94(3)
N(1)-C(5)-C(6)-N(2)	10.8(13)	N(3)-C(9)-C(10)-N(4)	138.4(10)

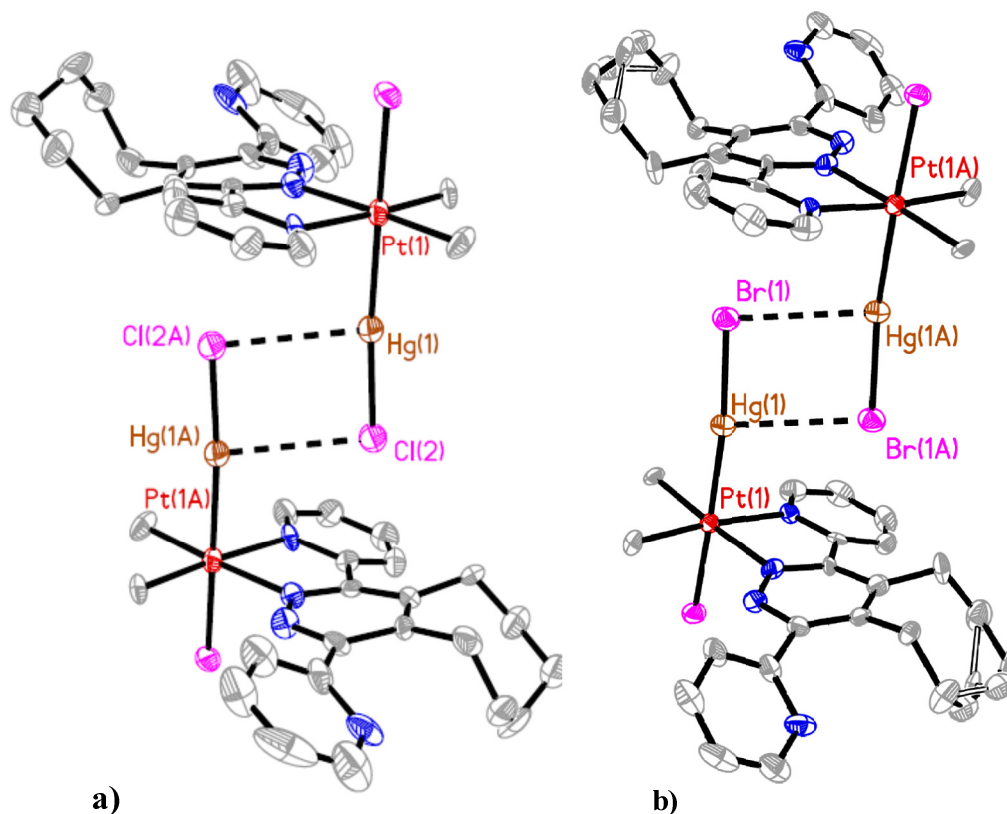


Figure 2.11. Views of the structures of (a) **3** and (b) **4** showing the loosely associated dimers formed by secondary bonding between adjacent HgX units.

The reaction of mercuric carboxylates with platinum(II) compounds has been shown previously to occur via *trans* oxidative addition with subsequent *trans-cis* isomerization occurring to yield a *cis* addition product [54,55]. To explore this, an equimolar amount of mercuric acetate, $\text{Hg}(\text{O}_2\text{CCH}_3)_2$, was added with stirring to an acetone solution of complex **2**. After stirring at room temperature for 15 minutes, the original deep red colour of **2**, dissipated and the solution became a pale yellow colour. Removing the solvent *in vacuo* yielded a bright yellow solid. The resultant solid was analyzed by ^1H NMR spectroscopy, and four distinct methylplatinum resonances were observed, figure 2.12. This is logical due to the lack of symmetry in complex **5** yielding two possible *cis* isomers depending whether the equatorial methyl group was proximal, **5a**, or distal, **5b**, to the *ortho* proton of the coordinated pyridyl ring. The methylplatinum resonances appeared slightly more upfield than is observed for the methyl groups of complex **3** and **4** at $\delta = 0.81$ and 1.53 ppm with respective $^2J(\text{PtH})$ coupling constants of 72 Hz and 63 Hz for complex **5a** and $\delta = 0.88$ and 1.30 ppm with respective $^2J(\text{PtH})$

coupling constants of 72 Hz and 64 Hz. These values of the coupling constants are diagnostic of platinum(IV) complexes which indicates that an oxidative addition reaction must have occurred. These coupling constants also give evidence for the expected *cis*-oxidative addition product. The Pt-Me resonance with the larger $^2J(\text{PtH})$ value, (73 Hz), is assigned *trans* to oxygen and the Pt-Me resonance with the smaller $^2J(\text{PtH})$ value, (64 Hz), is assigned *trans* to nitrogen on the basis of the higher *trans* influence of nitrogen compared to oxygen. A small long range coupling is also observed at the most upfield methylplatinum resonance, $^3J(\text{HgPtH}) = 14$ Hz, which indicates the presence of a platinum-mercury bond. These results indicate the final platinum(IV) species possesses an octahedral geometry with the acetate and mercuric acetate ligands in *cis* positions relative to one another as depicted in scheme 2.7. Integration of comparative peaks indicates that **5a** is formed with a slight preference over **5b** at a ratio of 3:2. Unfortunately single crystals suitable for X-ray diffraction analysis could not be grown for **5** and therefore this assignment could not be confirmed in the solid state.

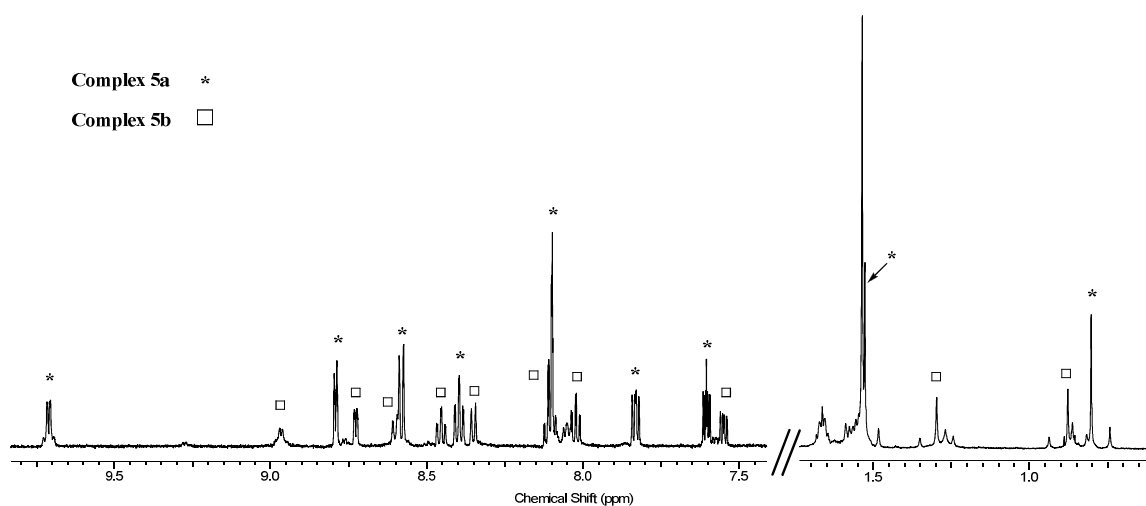
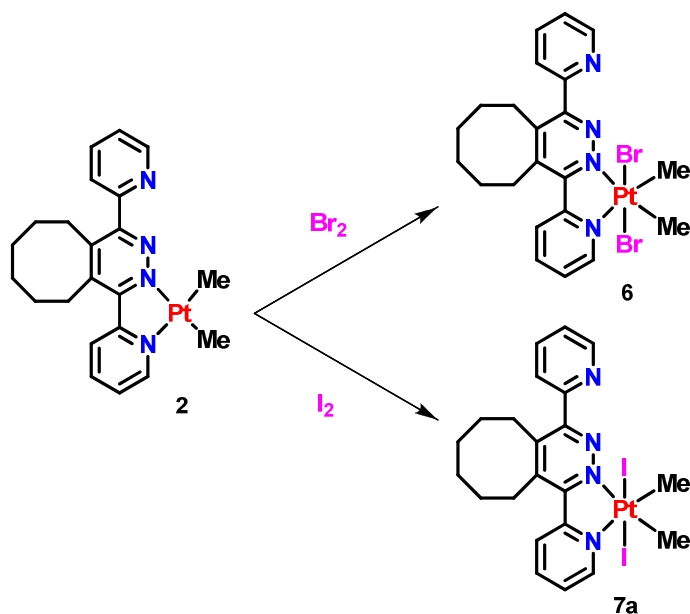


Figure 2.12. ^1H NMR spectrum of complex **5a/5b** in acetone- d_6 .

2.5 Reactivity of Complex 2 towards Oxidative Addition

2.5.1 Reactions of [PtMe₂(6-dppd)] with Halogens, X₂ (X = Br, I)

The reaction of bromine or iodine with complex **2** occurred by *trans* oxidative addition as depicted in scheme 2.8. The ¹H NMR spectrum of complex **6**, [PtBr₂Me₂(6-dppd)], figure 2.13, contained two methylplatinum resonances at δ = 2.12ppm and δ = 2.43ppm each possessing ¹⁹⁵Pt satellites with ²J(PtH) = 71Hz. These chemical shifts and coupling constants are diagnostic of methyl groups being *trans* to nitrogen, thus indicating that the bromine indeed added in a *trans* manner in the axial positions, which is consistent with the literature [59,60]. Eight proton resonances in the aromatic region further suggests that a single unsymmetrical product was produced and no evidence for any isomerization to *cis* products is observed.



Scheme 2.8. Oxidative addition of bromine and iodine at **2**.

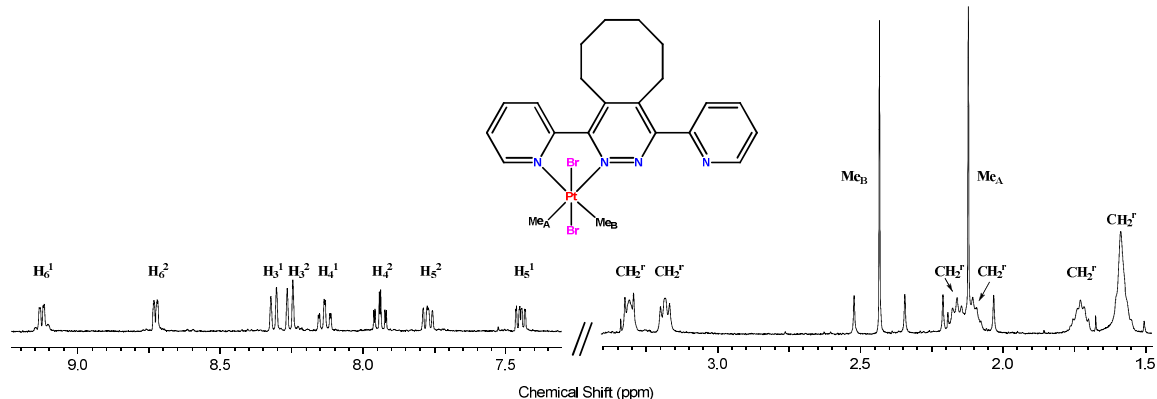


Figure 2.13. ^1H NMR spectrum of complex **6** in CDCl_3 . Standard labelling applies. CH_2^r refers to protons of cyclooctyl ring.

In a somewhat similar fashion, iodine was shown to initially react with complex **2** yielding primarily the *trans* oxidative addition product $[\text{PtI}_2\text{Me}_2(6\text{-dppd})]$, complex **7a**, although a complex mixture of products resulting in ten distinct methylplatinum resonances was observed in the ^1H NMR spectrum as depicted in figure 2.14.

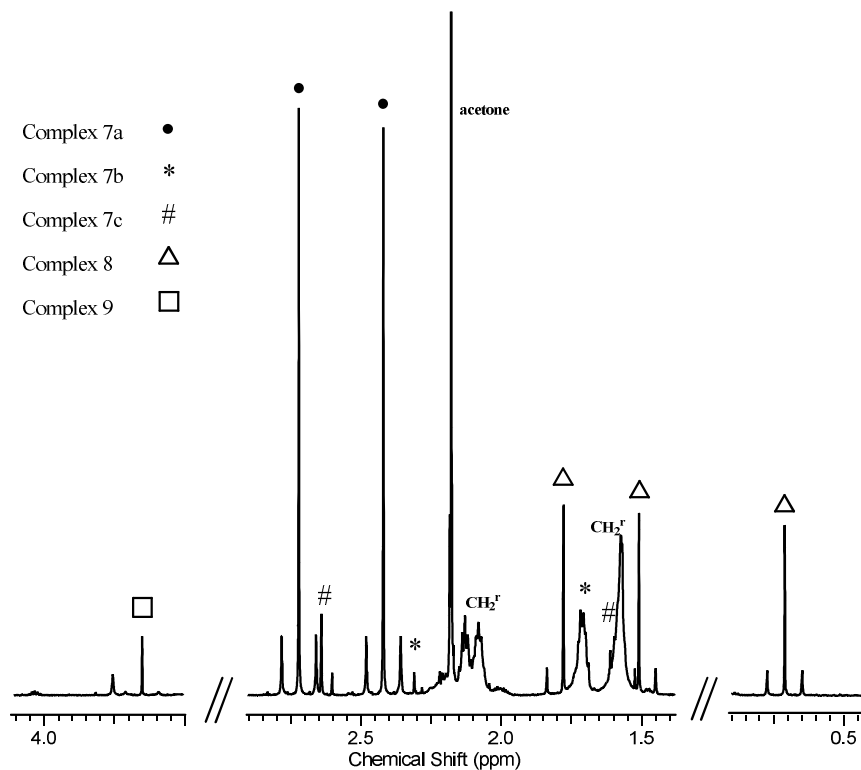


Figure 2.14. ^1H NMR spectrum of the methylplatinum region for the oxidative addition of iodine at complex **2** in CDCl_3 .

Complex **7a** was characterized as the major product in the mixture and was observed to produce methylplatinum resonances at $\delta = 2.41\text{ppm}$ and 2.72ppm each with ${}^2J(\text{PtH}) = 74\text{ Hz}$ and equal integration values. The chemical shift and coupling constants suggest that these resonances are those of the product of *trans* addition of iodine, complex **7a**. These results are consistent with the literature where it has been established that the addition of iodine at dimethylplatinum(II) complexes proceeds via the polar $\text{S}_{\text{N}}2$ mechanism of oxidative addition yielding the *trans* oxidative addition product [61-63]. Two additional minor complexes were also observed in the ${}^1\text{H}$ NMR spectrum which are proposed to be the products of an isomerization of **7a** to its two *cis* isomers **7b** and **7c**, as outlined in scheme 2.10. These products are characterized through their methylplatinum resonances at 1.61 ppm and 2.26 ppm with coupling constants of ${}^2J(\text{PtH}) = 74\text{ Hz}$ and ${}^2J(\text{PtH}) = 68\text{ Hz}$ respectively for **7b** and 1.71 ppm and 2.55 ppm with coupling constants of ${}^2J(\text{PtH}) = 74\text{ Hz}$ and ${}^2J(\text{PtH}) = 68\text{ Hz}$ respectively for **7c**. The chemical shifts and coupling constants of the most upfield resonances are diagnostic of methyl groups being *trans* to iodide as iodide has a lower *trans* influence relative to the nitrogen of the pyridyl ring. Ultimate assignment of the *cis* isomers **7b** and **7c** was determined through the use of ${}^1\text{H}$ - ${}^1\text{H}$ NOESY 2D NMR. This spectrum displayed a correlation between the methylplatinum resonance of **7b** at 2.26 ppm with the *ortho* proton resonance of the coordinated pyridyl ring. This enabled the assignment of isomer **7b** to be the *cis* isomer with the *exo* methyl group and *endo* iodide. The remaining four methylplatinum resonances therefore did not arise due to any isomers of complex **7** and could only be described as the products of side reactions. It was postulated that the products of the side reactions could be $[\text{PtI}\text{Me}_3(6\text{-dppd})]$ **8**, and $[\text{PtI}_3\text{Me}(6\text{-dppd})]$ **9** based on the resonances remaining in the methylplatinum region of the ${}^1\text{H}$ NMR spectrum. Three methylplatinum resonances of equal integration were observed at 0.82 ppm , 1.42 ppm and 1.71 ppm with coupling constants of 76 Hz , 70 Hz and 70 Hz respectively. The chemical shifts and coupling constants support that the most upfield resonance was attributed to the axial methyl group *trans* to iodine and the more downfield resonances attributed to the equatorial methyl groups *trans* to nitrogen. The assignment of complex **8** being a by-product in the oxidative addition of iodine at **2** was confirmed by independently preparing **8** via the oxidative addition of MeI to complex **2**. The ${}^1\text{H}$ NMR

spectrum of complex **8**, figure 2.15, produced via the addition of methyl iodide exhibited methylplatinum resonances of identical chemical shift and coupling constant to that observed in the complex mixture produced in the oxidative addition of iodine at **2**.

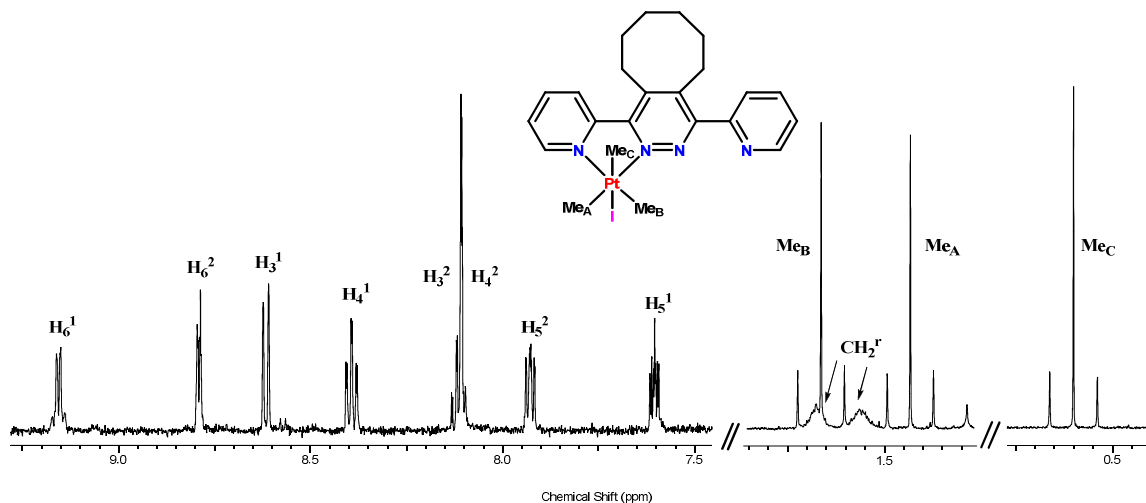
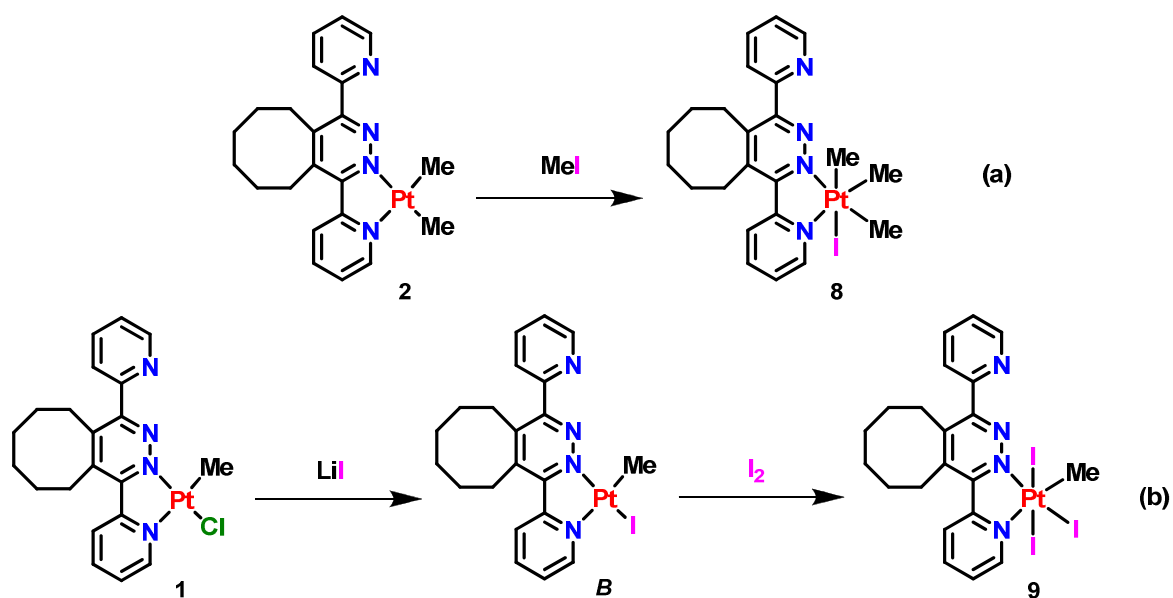


Figure 2.15. ^1H NMR spectrum of complex **8**, $[\text{PtIme}_3(6\text{-dppd})]$ in acetone- d_6 . Conventional labelling schemes for pyridyl rings are used. CH_2^r is used to indicate proton resonances of the cyclooctyl ring.

In order to explain the formation of complex **8** in the mixture, we opine that the remaining unassigned methylplatinum resonance at 3.65 ppm with a coupling constant of 70 Hz must arise due to the formation of complex **9**, $[\text{PtI}_3\text{Me}(6\text{-dppd})]$. To prove this, complex **9** needed to be synthesized and characterized for comparison, scheme 2.9. Complex **9** was synthesized by first performing an anion exchange reaction between LiI and $[\text{PtClIme}(6\text{-dppd})]$, complex **1**. The resulting product, $[\text{PtIme}(6\text{-dppd})]$, complex **B**, was then characterized by ^1H NMR, yielding a single methylplatinum resonance at $\delta = 1.71$ ppm and $^2J(\text{PtH}) = 78$ Hz which is typical of a platinum(II) compound. To a dichloromethane solution of this product, was added a stoichiometric amount of iodine. This product, $[\text{PtI}_3\text{Me}(6\text{-dppd})]$ complex **9**, was characterized by ^1H NMR spectroscopy and as predicted, the methylplatinum resonance was observed at $\delta = 3.65$ ppm with $^2J(\text{PtH}) = 70$ Hz directly corresponding to the remaining unassigned signal of the ^1H NMR spectrum of the product mixture.



Scheme 2.9: a) The preparation of **8**, *fac*-[PtI Me₃(6-dppd)], and b) The preparation of **9**, *mer*-[PtI₃ Me(6-dppd)].

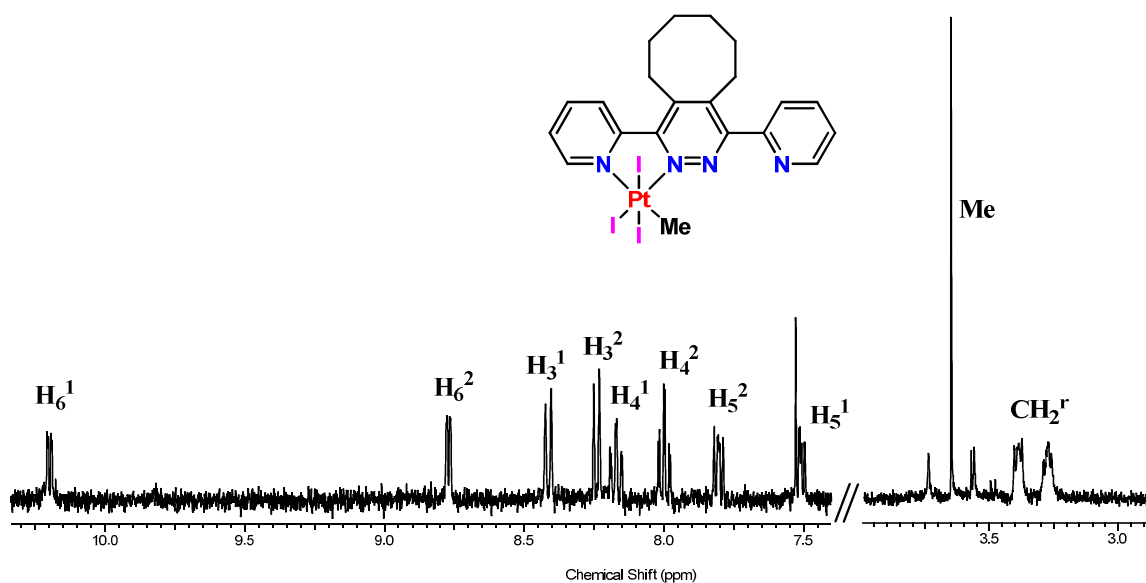
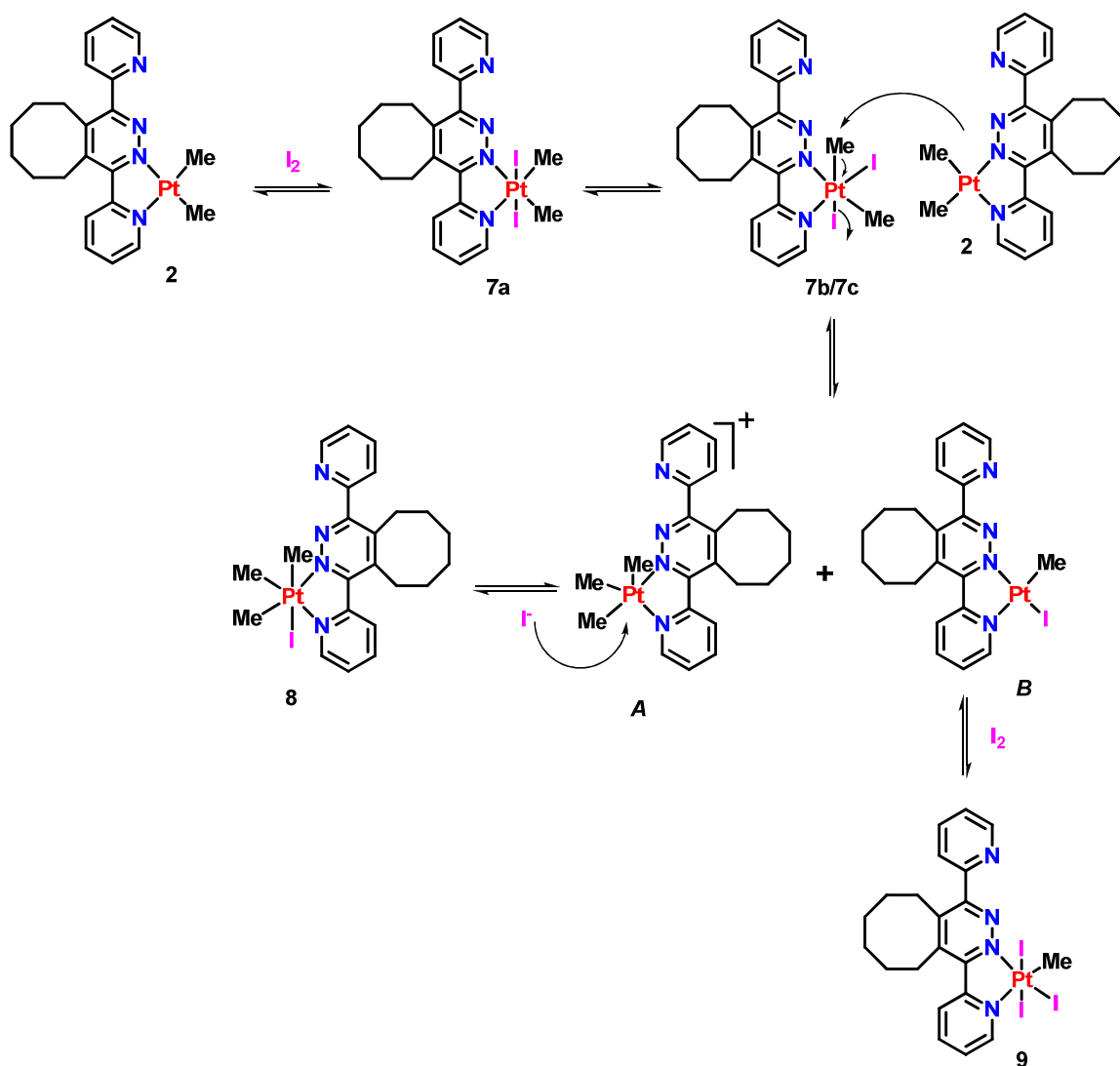


Figure 2.16. ¹H NMR spectrum of complex **9**, [PtI₃ Me(6-dppd)] in CDCl₃. Conventional labelling schemes are utilized for pyridyl rings. CH₂^r represents the protons of the cyclooctyl ring.

Scheme 2.10 illustrates the proposed mechanism by which the byproducts **8** and **9** are produced. After **7a** isomerizes to form **7b** and **7c**, we propose that a molecule of complex **2** reacts with **7b/7c** by abstracting a methyl group from **7b/7c**, affording intermediates **A** and **B**. The trimethylplatinum intermediate **A** can then coordinate the free iodide produced in the previous step yielding complex **8**. The iodomethylplatinum(II) intermediate **B** can then oxidatively add an equivalent of iodine yielding the triiodomethylplatinum(IV) complex **9**.



Scheme 2.10. Proposed mechanism for the formation of **7a**, **7b**, **7c**, **8** and **9** during the addition of iodine to **2**.

The structures of complexes **8**, and **9** were confirmed by single crystal X-ray diffraction analysis, through the independent synthesis of these complexes via scheme 2.9a and 2.9b respectively. The structure of complex **8** is shown in figure 2.17, and confirms that it is formed by the oxidative addition of methyl iodide. The methyl groups therefore adopt a *fac* geometry at platinum with the equatorial methyl groups having a bond distance of Pt(1)-C(1) = 2.050(7) Å and Pt(1)-C(2) = 2.092(7) Å, due to the differing donor ability of the pyridyl and pyridazine rings; and the axial methyl group having a bond distance of Pt(1)-C(3) = 2.058(8) Å. It is noted that in the structure of **8**, the coordinated 2-pyridyl group is twisted out of the plane of the pyridazine ring by 16° representing a balance between ideal planar geometry and steric hindrance. The free 2-pyridyl group is rotated 53° away from the plane of the pyridazine ring which is consistent with previously reported findings [52,64]. Similarly complex **9**, as depicted in figure 2.18, is confirmed by its solid state structure to be the result of *trans* oxidative addition of iodine to [PtIme(6-dppd)] or **B** from scheme 2.9b. In this case the three iodide substituents adopt a meridional geometry at the platinum center, with equatorial bond distance of Pt(1)-I(3) = 2.595(6)Å, and axial bond distances Pt(1)-I(1) = 2.657(6)Å and Pt(1)-I(2) = 2.649(6)Å. The coordinated 2-pyridyl group deviates again from planarity by 18° to accommodate steric demand, while the free 2-pyridyl group exhibits a 45° twist relative to the pyridazine ring.

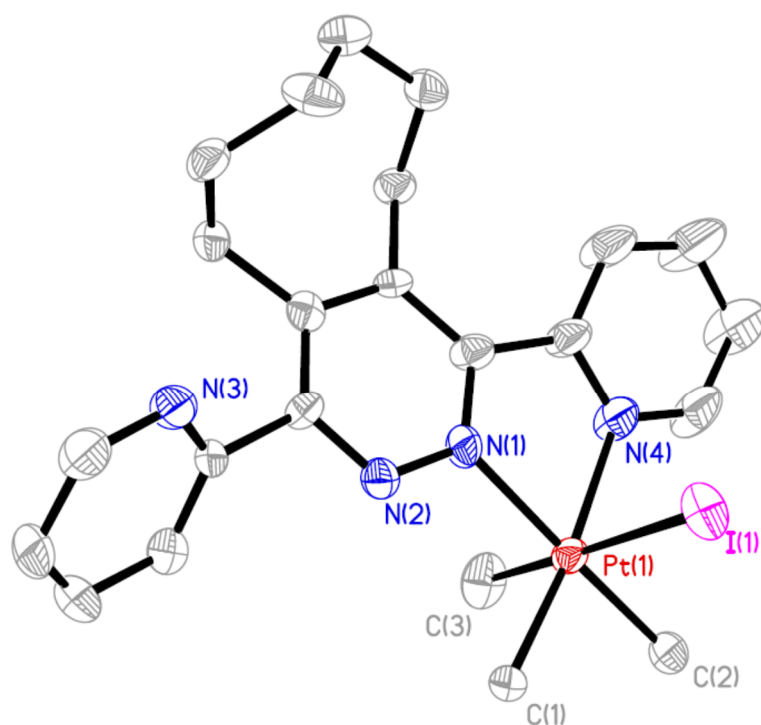


Figure 2.17. Molecular structure of complex **8**, (hydrogen atoms excluded for clarity).

Table 2.5: Bond lengths [Å] and angles [°] for [Pt(Me)₃(6-dppd)], **8**

Pt(1)-N(1)	2.127(6)	Pt(1)-N(4)	2.150(6)
Pt(1)-C(1)	2.050(7)	Pt(1)-C(2)	2.092(7)
Pt(1)-C(3)	2.058(8)	Pt(1)-I(1)	2.7564(7)
N(1)-Pt(1)-N(4)	75.2(2)	C(1)-Pt(1)-C(2)	86.3(3)
N(4)-Pt(1)-C(3)	91.2(3)	N(4)-Pt(1)-C(2)	101.0(3)
N(4)-Pt(1)-C(1)	172.7(3)	N(1)-Pt(1)-C(2)	174.8(3)
C(1)-Pt(1)-I(1)	93.5(2)	C(2)-Pt(1)-I(1)	93.8(2)
N(1)-Pt(1)-C(1)	97.5(3)	N(1)-Pt(1)-C(3)	90.9(3)
C(1)-Pt(1)-C(3)	89.1(3)	C(2)-Pt(1)-C(3)	85.6(3)
N(1)-Pt(1)-I(1)	89.48(17)	N(4)-Pt(1)-I(1)	86.27(19)
C(3)-Pt(1)-I(1)	177.3(2)		
N(1)-C(18)-C(19)-N(4)	16.2(11)	N(2)-C(4)-C(5)-N(3)	127.6(7)

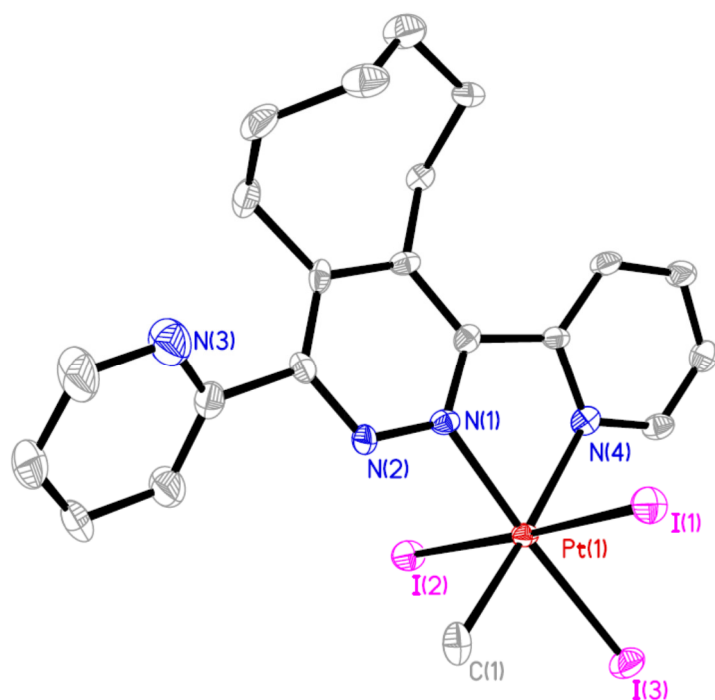


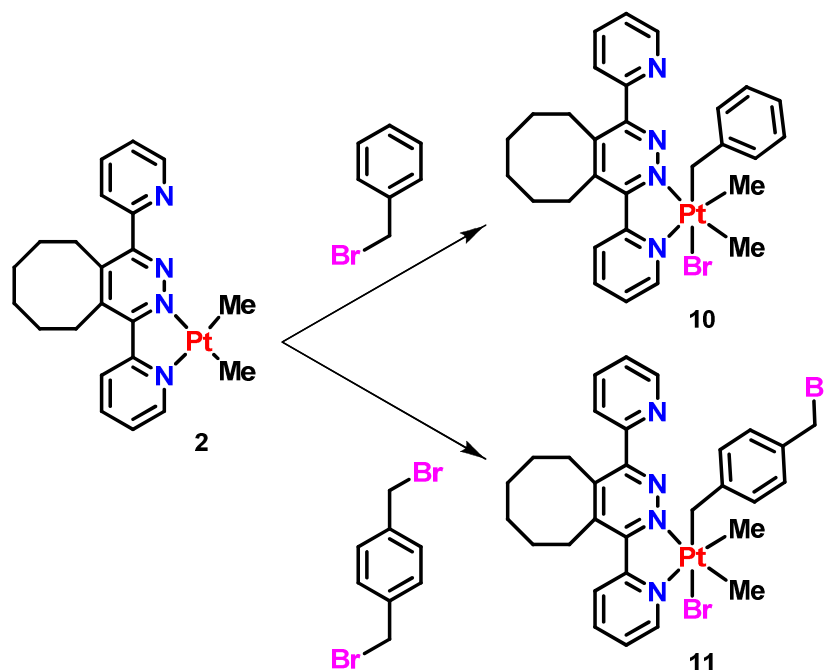
Figure 2.18. Molecular structure of complex **9**, (hydrogen atoms excluded for clarity).

Table 2.6: Bond lengths [Å] and angles [°] for [PtI₃Me(6-dppd)], **9**

Pt(1)-N(1)	2.065(5)	Pt(1)-N(4)	2.164(6)
Pt(1)-C(1)	2.087(7)	Pt(1)-I(3)	2.5953(6)
Pt(1)-I(1)	2.6569(6)	Pt(1)-I(2)	2.6495(6)
N(1)-Pt(1)-N(4)	76.7(2)	C(1)-Pt(1)-I(3)	86.6(2)
N(4)-Pt(1)-I(1)	87.74(15)	N(4)-Pt(1)-I(2)	91.527(18)
N(4)-Pt(1)-C(1)	174.2(3)	N(1)-Pt(1)-I(3)	175.23(16)
C(1)-Pt(1)-I(1)	89.6(2)	I(3)-Pt(1)-I(1)	91.930(18)
N(1)-Pt(1)-C(1)	98.1(3)	N(1)-Pt(1)-I(2)	87.64(15)
C(1)-Pt(1)-I(2)	89.7(2)	N(1)-Pt(1)-I(1)	88.99(15)
N(4)-Pt(1)-I(3)	98.67(15)	N(4)-Pt(1)-I(2)	92.65(15)
I(2)-Pt(1)-I(1)	176.422(19)		
N(1)-C(4)-C(5)-N(4)	17.6(8)	N(2)-C(2)-C(16)-N(3)	135.5(7)

2.5.2 Reactions of [PtMe₂(6-dppd)] with Benzylic Halides

The oxidative addition reactions of some compounds possessing carbon-halogen bonds to complex **2** are illustrated in scheme 2.11. Benzyl bromide has been observed to react with dimethylplatinum(II) complexes to give products that result from *trans* oxidative addition [65]. The reaction of benzyl bromide with **2** occurred rapidly to afford [PtBrMe₂(CH₂C₆H₅)(6-dppd)], **10**, as a yellow solid. This complex was readily characterized by its ¹H NMR spectrum which contained two methylplatinum resonances at $\delta = 1.38$ ppm, $^2J_{\text{PtH}} = 70$ Hz and $\delta = 1.62$ ppm, $^2J_{\text{PtH}} = 71$ Hz, corresponding to the two methyl groups being oriented *trans* to the nitrogen donor atoms. In addition, two doublet resonances were observed at $\delta = 3.10$ and $\delta = 3.11$ ppm which possessed Pt-195 satellites. This AB doublet resonance represents the inequivalent protons that reside on the CH₂ bridge of the benzyl ligand, the more upfield doublet having a coupling constant value $^2J_{\text{PtH}} = 94$ Hz and the more downfield resonance a value of $^2J_{\text{PtH}} = 81$ Hz. The proposed *trans* geometry of **10** was confirmed by single crystal X-ray diffraction analysis and the solid state structure of the complex is depicted in figure 2.19. As can be observed in the solid state structure, the benzyl group orients itself directly above the pyridazine ring at an interplanar distance of 3.444 Å. This interplanar distance is consistent with similar complexes in the literature, [52], and occurs due to favourable π - π interactions between the aromatic groups. Again, as is observed for **8** and **9**, the non-coordinating 2-pyridyl group deviates from planarity by 47° to alleviate unfavourable steric strain.



Scheme 2.11. Oxidative addition of carbon-halogen bonds to yield complexes **10** and **11**.

In a manner similar to the one employed for the synthesis of **10**, equimolar amounts of complex **2** and α,α' -dibromo-*p*-xylene were allowed to stir in solution, yielding the formation of a yellow solid. This solid, complex **11**, was readily characterized through ^1H NMR spectroscopy as the *trans* oxidative addition product, $[\text{PtBrMe}_2(p\text{-CH}_2\text{C}_6\text{H}_4\text{CH}_2\text{Br})(6\text{-dppd})]$. The observation of two methylplatinum resonances $\delta = 1.43$ ppm, $^2J_{\text{PtH}} = 70$ Hz and $\delta = 1.70$ ppm, $^2J_{\text{PtH}} = 70$ Hz is consistent with that of a product in which both methyl groups are oriented *trans* to the nitrogen donor atoms of the **6-dppd** ligand. Similar to complex **10**, an AB doublet is observed at $\delta = 2.83$ ppm and $\delta = 3.01$ ppm with $^2J_{\text{PtH}} = 94$ Hz and $^2J_{\text{PtH}} = 89$ Hz respectively, indicating that the xylene ligand is coordinated at platinum. Single crystals of complex **11** were grown as a chloroform solvate and confirm the proposed *trans* oxidative addition geometry, figure 2.20. Unlike complex **10**, complex **11** exhibits much less effect of the π - π interactions between the pyridazine and benzyl rings, with an interplanar distance of 3.878 Å. In complex **11** the non-coordinating 2-pyridyl group again deviates from planarity with respect to the pyridazine ring by 53° to alleviate the unfavourable steric congestion.

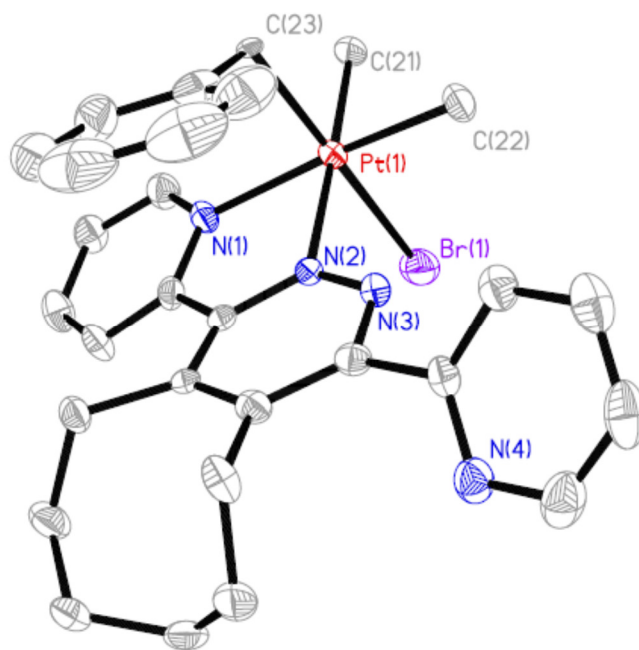


Figure 2.19. The solid state structure of complex **10**, (hydrogen atoms excluded for clarity).

Table 2.7: Bond lengths [Å] and angles [°] for [PtBrMe₂(CH₂C₆H₅)(6-dppd)], **10**

Pt(1)-N(1)	2.155(4)	Pt(1)-N(2)	2.131(4)
Pt(1)-C(21)	2.078(5)	Pt(1)-C(22)	2.045(5)
Pt(1)-Br(1)	2.5861(6)	Pt(1)-C(23)	2.159(4)
N(1)-Pt(1)-N(2)	75.84(15)	C(21)-Pt(1)-C(22)	85.3(2)
N(2)-Pt(1)-C(22)	96.98(18)	N(2)-Pt(1)-C(23)	93.98(15)
N(2)-Pt(1)-C(21)	177.55(17)	N(1)-Pt(1)-C(22)	172.74(18)
C(21)-Pt(1)-C(23)	86.83(18)	C(22)-Pt(1)-C(23)	90.1(2)
N(1)-Pt(1)-C(21)	101.87(17)	N(1)-Pt(1)-C(23)	89.27(16)
N(2)-Pt(1)-Br(1)	88.97(10)	C(22)-Pt(1)-Br(1)	91.91(16)
N(1)-Pt(1)-Br(1)	89.10(11)	C(21)-Pt(1)-Br(1)	90.13(15)
C(23)-Pt(1)-Br(1)	176.18(12)	Pt(1)-C(23)-C(24)	113.8(3)
N(1)-C(5)-C(6)-N(2)	14.3(6)	N(3)-C(9)-C(10)-N(4)	132.6(5)

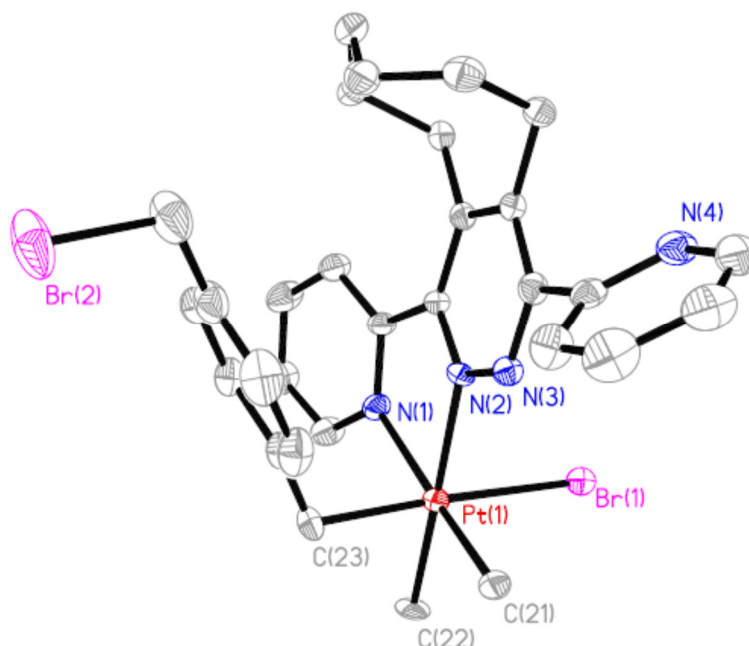


Figure 2.20. The solid state structure of complex **11**, (hydrogen atoms excluded for clarity).

Table 2.8: Bond lengths [Å] and angles [°] for [PtBrMe₂(CH₂C₆H₄CH₂Br)(6-dppd)], **11**

Pt(1)-N(1)	2.144(4)	Pt(1)-N(2)	2.144(4)
Pt(1)-C(21)	2.054(5)	Pt(1)-C(22)	2.086(4)
Pt(1)-Br(1)	2.6003(6)	Pt(1)-C(23)	2.1031(5)
N(1)-Pt(1)-N(2)	75.16(15)	C(21)-Pt(1)-C(22)	87.5(2)
N(2)-Pt(1)-C(21)	98.19(18)	N(2)-Pt(1)-C(23)	95.91(18)
N(2)-Pt(1)-C(22)	173.75(17)	N(1)-Pt(1)-C(21)	172.534(18)
C(21)-Pt(1)-C(23)	88.9(2)	C(22)-Pt(1)-C(23)	86.8(2)
N(1)-Pt(1)-C(22)	99.32(18)	N(1)-Pt(1)-C(23)	88.39(19)
N(2)-Pt(1)-Br(1)	87.74(11)	C(22)-Pt(1)-Br(1)	89.56(15)
N(1)-Pt(1)-Br(1)	92.17(12)	C(21)-Pt(1)-Br(1)	90.95(15)
C(23)-Pt(1)-Br(1)	176.33(15)	Pt(1)-C(23)-C(24)	113.6(3)
N(1)-C(1)-C(6)-N(2)	10.7(6)	N(3)-C(9)-C(10)-N(4)	126.9(5)

2.5.3 Reaction of [PtMe₂(6-dppd)] with dichloromethane

In an attempt to prepare crystals of complex **2** for single crystal X-ray diffraction, complex **2** was dissolved in the minimum volume of dichloromethane and pentane was allowed to migrate into the vial slowly over time. After 3 days, the originally red solution became a yellow colour and small yellow crystals had begun to form on the sides of the vial. To investigate what was occurring, a sample of complex **2** was again dissolved in dichloromethane in a round-bottomed flask and allowed to stir overnight. After removing the solvent *in vacuo* and washing the yellow product with pentane, ¹H NMR spectra were acquired of the product. The ¹H NMR spectrum of the yellow solid in acetone-*d*₆ gave evidence for a mixture of products as could be concluded from the presence of six distinct methylplatinum resonances, figure 2.21. Integration of these resonances indicated that there were three independent species present in the solution. Each of the three species present possessed two distinct methylplatinum resonances of equivalent integration, which is consistent with the asymmetry of the dimethylplatinum(II) precursor complex **2**. ²J(PtH) coupling constants of the methylplatinum signals ranged from 70 – 74 Hz which is diagnostic of these resonances arising due to different platinum(IV) species. The coupling constant values being comparable to other platinum(IV) species provided evidence for the oxidative addition of a dichloromethane solvent molecule at the platinum(II) complex **2**. The three different products observed in the ¹H NMR spectrum, (figure 2.21), would therefore arise due to the presence of three distinct isomers. The major product appeared to be that of the *trans* oxidative addition of dichloromethane, **12a**, which would be followed by *trans-cis* isomerization to yield the two possible *cis* isomers, **12b/12c**, as depicted in scheme 2.12. The major isomer, **12a**, was readily identified by the presence of two methylplatinum resonances of equivalent integration values at 1.26 ppm (Me_A) and 1.41 ppm (Me_B), with coupling constant values of 70 Hz which is diagnostic of a methyl group being *trans* to the nitrogen atoms of **6-dppd**, as these nitrogen atoms possess a lower *trans* influence.

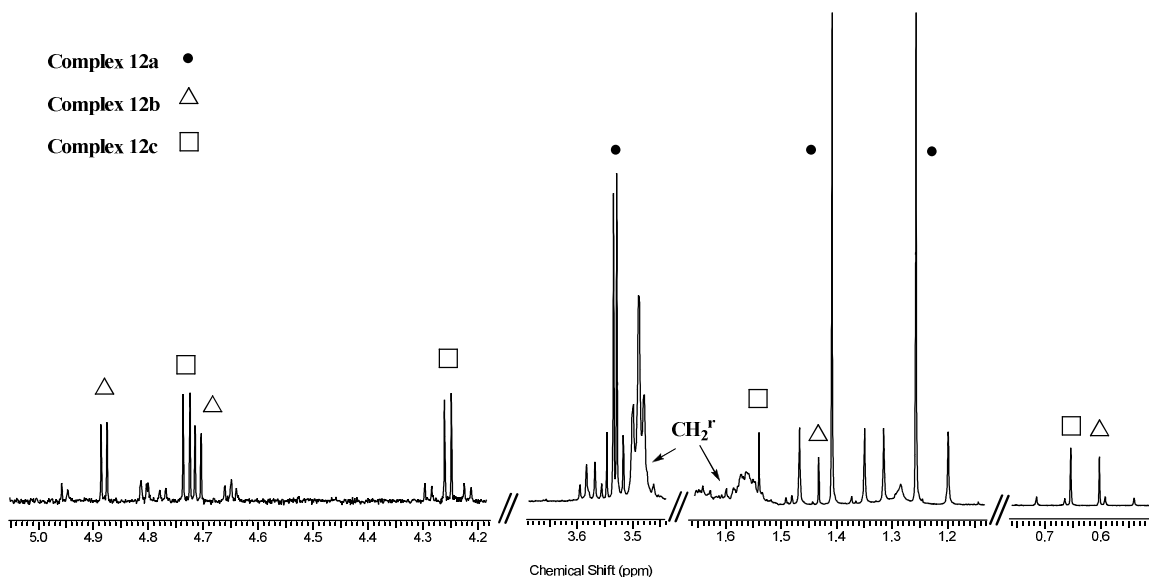
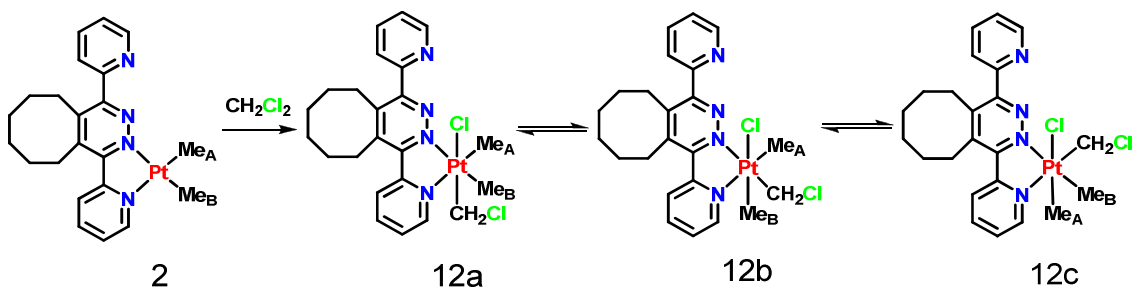


Figure 2.21. ^1H NMR spectrum of the methyl and methylene region for complexes **12a**, **12b**, and **12c** in acetone- d_6 . The aromatic region is omitted for clarity. CH_2^r is used to indicate the resonances arising from the protons of cyclooctyl ring in complex **12a**.

The remaining four methylplatinum resonances could be attributed to their specific *cis* isomers through the use of ^1H - ^1H gCOSY and NOESY NMR experiments. These experiments allowed for the determination of whether the methyl group of **12c** or the chloromethyl group of **12b** were adjacent to the *ortho* proton of the coordinated pyridyl ring of the ligand. Utilizing these spectra, the ultimate assignment of all isomers of **12** was possible and the values are summarized in table 2.9.



Scheme 2.12. Oxidative addition of CH_2Cl_2 to complex **2** and the subsequent isomerization.

Table 2.9: Selected NMR data [δ ppm, J in Hz] for the dichloromethane adducts (see scheme 2.12 for labelling system).

Complex	$\delta(\text{Me}^a)$	$^2J(\text{PtH})$	$\delta(\text{Me}^b)$	$^2J(\text{PtH})$	$\delta(\text{Me}^c)$	$^2J(\text{PtH})$	$\delta(\text{CH}_2\text{Cl})$	$^2J(\text{PtH})$
12a	1.26	70	1.41	70			3.53	48
							3.54	58
12b	1.44	70			0.61	74	4.72	78
							4.89	86
12c			1.55	70	0.66	74	4.26	44
							4.74	92

The reaction was further investigated through the analysis of the slow reaction of complex **2** with solvent CD_2Cl_2 , figure 2.22. This reaction was observed to produce a mixture of **12a:12b:12c** in the ratio 3:2:1 after two hours reaction but 5:1:1 after 48 hours, as determined through monitoring the reaction by ^1H NMR. In this case, the oxidative addition is slow and was only about 20% complete after two hours but complete after 24 hours. From this analysis it was concluded that the rate of isomerization is competitive with the rate of oxidative addition. It was also observed that complex **12b** is formed in a higher proportion early in the reaction and is therefore considered to be the kinetically preferred product.

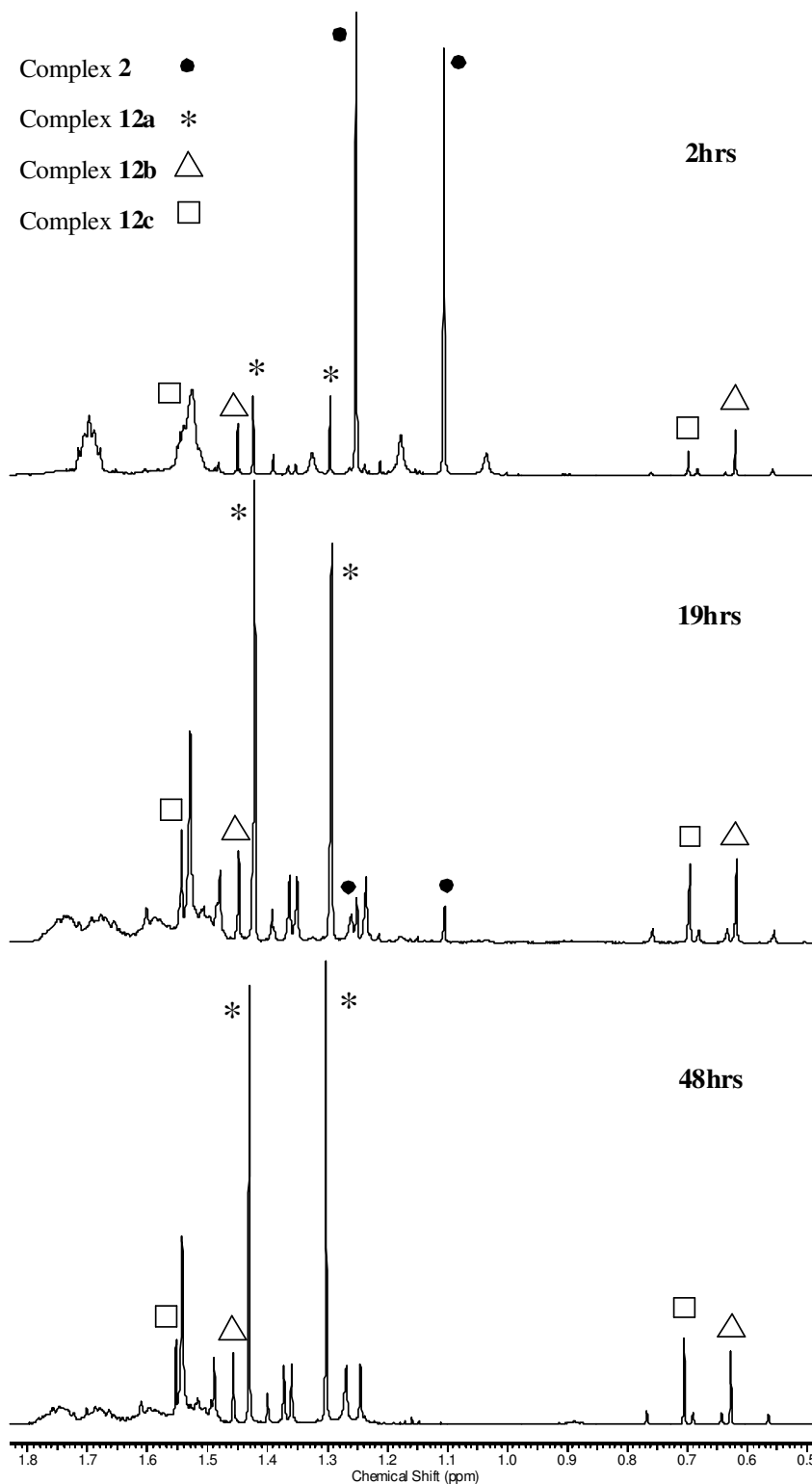


Figure 2.22. Time series ^1H NMR spectrum of the oxidative addition of methylene chloride- d_2 at complex **2**.

Figure 2.23 shows the structure of complex **12a**. The chlorine atom of the chloromethyl group lies above the nitrogen atom of the coordinated pyridyl group, with torsion angle $N4-Pt1-C21-Cl1 = 5^\circ$ and bond angle $Pt1-C21-Cl1 = 116.2(4)^\circ$. Again it can be observed that the presence of the cyclooctene ring imposes steric hindrance in overall conformation of complex **12a**, resulting in the pyridyl and pyridazine rings being skewed by 17° to reduce the steric congestion. The vacant pyridyl group also exhibits skewing relative to the pyridazine ring by 49° to presumably reduce the steric hindrance.

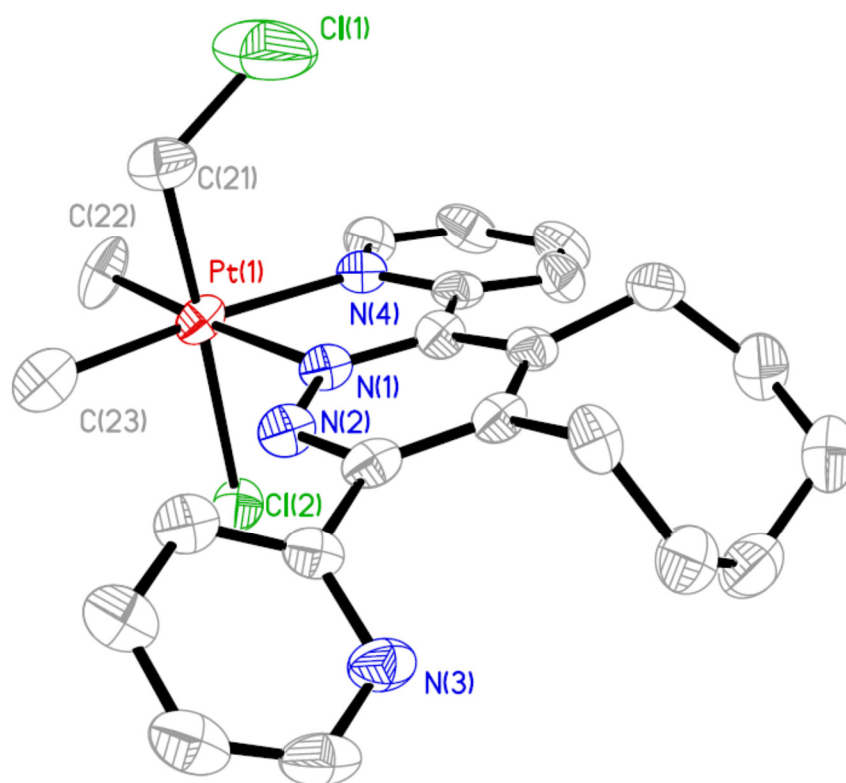
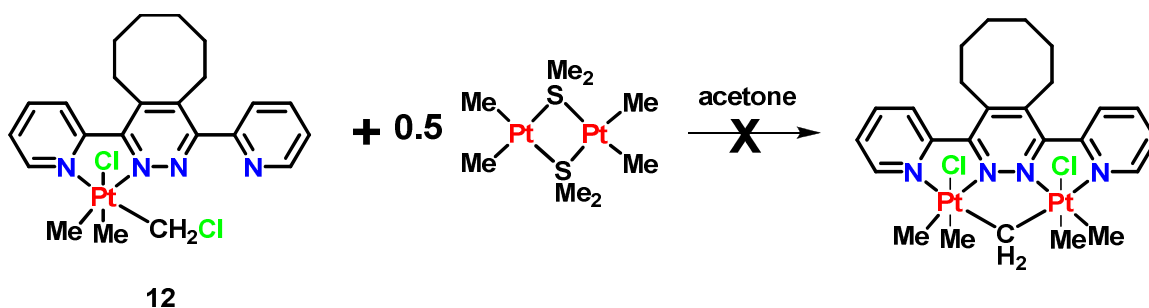


Figure 2.23. A view of the structure of complex **12a**, (hydrogen atoms excluded for clarity).

**Table 2.10: Bond lengths [Å] and angles [°] for [PtClMe₂(CH₂Cl)(6-dppd)],
12a**

Pt(1)-N(1)	2.136(5)	Pt(1)-N(4)	2.133(6)
Pt(1)-C(22)	2.046(7)	Pt(1)-C(23)	2.052(8)
Pt(1)-Cl(2)	2.4371(18)	Pt(1)-C(21)	2.027(8)
N(1)-Pt(1)-N(4)	75.0(2)	C(22)-Pt(1)-C(23)	85.6(2)
N(4)-Pt(1)-C(22)	99.5(3)	N(1)-Pt(1)-C(23)	99.9(3)
N(4)-Pt(1)-C(23)	174.4(3)	N(1)-Pt(1)-C(22)	174.5(3)
C(21)-Pt(1)-C(23)	85.4(3)	C(21)-Pt(1)-C(22)	89.5(3)
N(1)-Pt(1)-C(21)	91.3(3)	N(4)-Pt(1)-C(21)	97.0(3)
N(4)-Pt(1)-Cl(2)	86.33(15)	C(22)-Pt(1)-Cl(2)	93.1(2)
N(1)-Pt(1)-Cl(2)	86.60(15)	C(23)-Pt(1)-Cl(2)	91.0(2)
C(21)-Pt(1)-Cl(2)	175.4(2)	Pt(1)-C(21)-Cl(1)	116.2(4)
N(1)-C(15)-C(16)-N(4)	10.0(8)	N(2)-C(1)-C(2)-N(3)	132.2(7)

The formation of **12** provided a potential opportunity to access a diplatinum complex of **6-dppd**. It was opined that the presence of the chloromethyl ligand attached to the platinum center could allow for an additional oxidative addition reaction across the CH₂-Cl bond which may then allow for the second platinum center to coordinate in the vacant coordination site as depicted in scheme 2.13. To that end, an acetone solution of **12** was added to an acetone solution of an equivalent of [Pt₂Me₄(μ-SMe₂)₂] and stirred for 4 hours. After working up the reaction mixture, no evidence for coordination of a second platinum center was observed. To ensure that the reactivity of the chloromethyl group was not the issue, the correspond bromomethyl and iodomethyl complexes were generated and tested through their *in situ* generation by stirring **2** in an acetone solution of dibromomethane or diiodomethane and then adding an equivalent of [Pt₂Me₄(μ-SMe₂)₂]. Again the incorporation of a second platinum center was not observed.



Scheme 2.13. The attempted synthesis of a diplatinated complex of **6-dppd** through the use of a bridging methylene approach.

2.5.4 Reaction of [PtMe₂(6-dppd)] with DCl

It has been previously established that hydrogen/deuterium exchange reactions in hydridomethylplatinum(IV) complexes occur in a reversible manner to yield methane or its isotopomers as a product of reductive elimination [66,67]. In an effort to evaluate the capability for complex **2** to undergo C-H bond activation, a deuteriolysis experiment utilizing DCl was performed. DCl was generated *in situ* via the addition of acetyl chloride to a mixture of methanol-*d*₄ and methylene chloride-*d*₂. Complex **2** was then added to the solution containing DCl at -40°C and the protonolysis reaction was then subsequently monitored through a variable temperature ¹H NMR experiment. Immediately upon mixing evidence for the addition of D⁺ was observed in the ¹H NMR spectrum through the incorporation of deuterium into methane. This observed methane is the product resultant from the reductive elimination event which would follow the formation of a platinum(IV) hydride species. Even though this hydridomethylplatinum(IV) species was not directly detected in the ¹H NMR spectrum, the observation of deuterium incorporation into the reductively eliminated methane indirectly supports this species being formed. The reaction of DCl with complex **2** led to the formation of all of the observable isotopomers of methane, CH_nD_{4-n}, as depicted in figure 2.24, and presumably also produced CD₄ which would not be observed in the ¹H NMR spectrum. The observation of all isotopomers of methane would indicate that there is a relatively rapid equilibration between the methyl(hydrido)platinum(IV) and methane-platinum(II) complexes prior to the loss of methane. Scheme 2.14 depicts this reaction

pathway but shows only the reactions leading as far as CH_2D_2 . It is apparent that repetition can lead to formation of all isotopomers of $\text{CH}_{4-n}\text{D}_n$. Complex **2** demonstrates the ability to activate C-H bonds under these acidic conditions and also exhibits the propensity to incorporate deuterium into the methylplatinum and methane products at low temperatures. Although the hydridomethylplatinum(IV) complex was not observed to be stable and as such may not lend itself useful for the direct activation and functionalization of C-H bonds, this experiment indicated that complex **2** has the ability to undergo facile reversibility between hydridomethylplatinum(IV) and (methane)platinum(II) complexes. The ability to activate C-H bonds even if the resultant hydridomethylplatinum(IV) complex is unstable, indicates that **2** may lend itself useful for other forms of catalysis as is observed by similar platinum complexes [68].

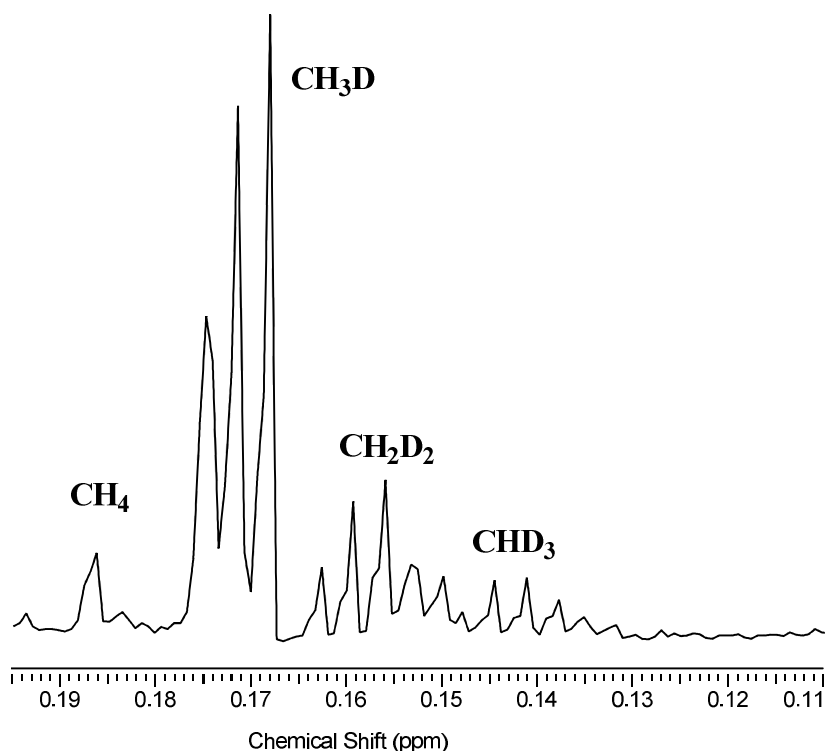
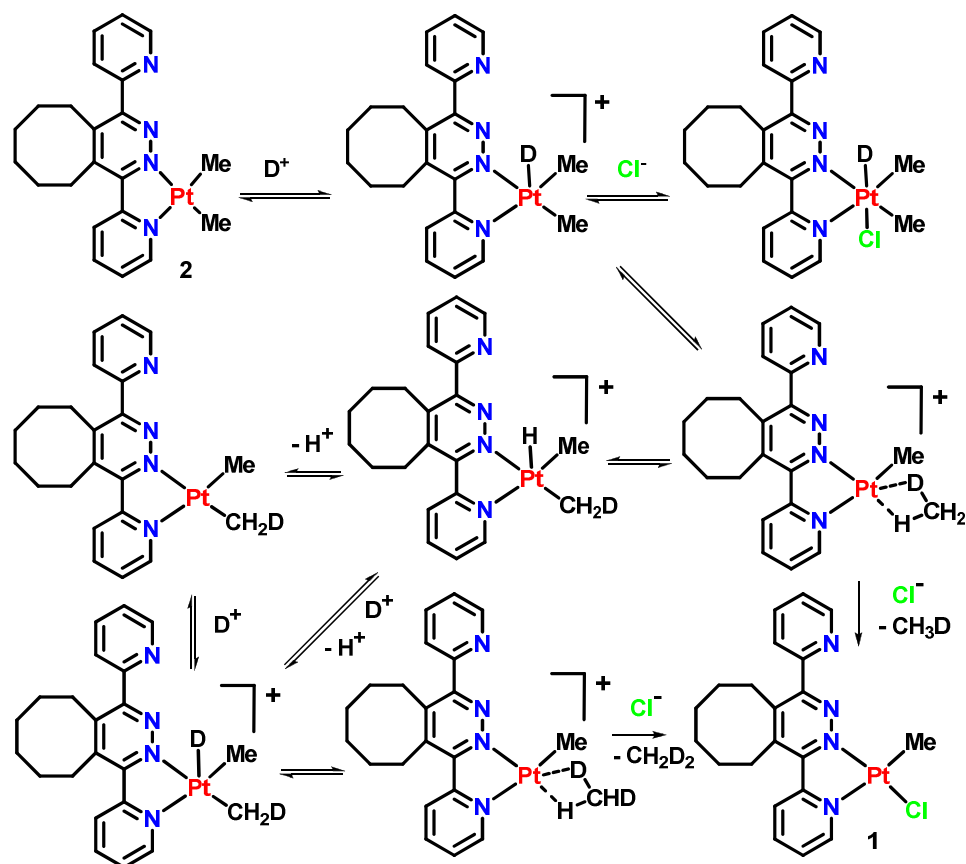


Figure 2.24. ^1H NMR spectrum of the reductively eliminated isotopomers of methane, $\text{CH}_n\text{D}_{4-n}$, from the protonolysis of complex **2** with DCl.



Scheme 2.14. Protonolysis of complex **2** with DCl and the subsequent reductive elimination of the various isotopomers of methane.

2.6 Conclusions

The reaction of the ligand **6-dppd** with the platinum precursor *trans*-[PtClMe(SMe₂)₂] in diethyl ether proceeded in a facile manner at room temperature forming the resultant monoplatinum chloromethylplatinum(II) complex, [PtClMe(6-dppd)], complex **1**. Complex **1** proved to be incapable of incorporating an additional chloromethylplatinum(II) center through the formation of a bridging chloride. A similar reaction between the ligand **6-dppd** and [Pt₂Me₄(μ-SMe₂)₂] again resulted in the formation of the monoplatinated complex [PtMe₂(6-dppd)], complex **2**. Both complexes **1** and **2** are stable for long periods of time at room temperature and resist oxidation under atmospheric conditions. Complex **2** proved to be incapable of coordinating an additional metal center in its potentially vacant coordination site independent of the geometry or size of the metal center. This is presumably due to the steric crowding imposed by the *endo* directed methyl group in complex **2** along with the presence of the cyclooctyl ring, which in turn leads to a rotation of the free 2-pyridyl group away from the pyridazine nitrogen atom. This in turn renders the potential second coordination site unable to ligate additional metal centers. Despite the inability to coordinate additional metal centers, **2** shows high reactivity towards a variety of substrates as illustrated by the formation of various organoplatinum(IV) derivatives. Notably, the oxidative addition of mercuric halides resulted in platinum(IV) complexes which possess metal-metal bonds. These mercuric halides were observed to oxidatively add in a *trans* manner whereas mercuric carboxylates tended to add in a *cis* manner at the platinum center. These resultant platinum(IV) complexes were also shown to have some interesting secondary interactions between two adjacent equivalents of the molecule forming dimeric species with secondary mercury halide bonding.

Complex **2** reacted with bromine via oxidative addition easily at room temperature to afford the corresponding platinum(IV) complex via *trans* oxidative addition. The oxidative addition reaction between iodine and complex **2** proved to be much more complicated. Although the oxidative addition reaction proceeded in a *trans* manner resulting in complex **7a**, an easy equilibrium between *cis* and *trans* isomers is observed leading to the formation of **7b** and **7c** in solution. Complexes **7b/7c** were

observed to react in solution with complex **2** via abstraction of the axial methyl ligand concomitant with the loss of an iodide ligand yielding two intermediate complexes, $[\text{PtMe}_3(6\text{-dppd})]^+ \mathbf{A}$, and $[\text{PtIME}(6\text{-dppd})] \mathbf{B}$. The free iodide anion then coordinates to the trimethylplatinum complex yielding complex **8** *fac*- $[\text{PtIME}_3(6\text{-dppd})]$, the identity of which was proven by independent synthesis through the oxidative addition of methyl iodide in a *trans* manner at complex **2**. Intermediate **B**, then reacts with an equivalent of iodine via oxidative addition in a *trans* manner yielding complex **9**, *mer*- $[\text{PtI}_3\text{Me}(6\text{-dppd})]$. Again, the identity of complex **9** was proven through independent synthesis.

Complex **2** reacted with benzylbromide derivatives to yield the corresponding platinum(IV) derivatives via *trans* oxidative addition. These complexes exhibited π - π interactions between the benzyl fragment and the aromatic pyridazine ring of the ligand, which helped to stabilize the resulting structures.

Complex **2** reacts with a dichloromethane solvent molecule via oxidative addition to yield the corresponding complex $[\text{PtClMe}_2(\text{CH}_2\text{Cl})(6\text{-dppd})]$. This reaction lead to the formation of 3 isomers, 1 *trans* and 2 *cis*, and it was found that the rate of oxidative addition was comparable to the rate of isomerisation. This reaction proceed over the course of 72 hours but the rate of the reaction could be increased through photolytic activation. It is likely that the oxidative addition of dichloromethane to complex **2** proceeds via the free radical chain mechanism.

Finally complex **2** exhibited the ability to incorporate deuterium into reductively eliminated methane after being subjected to deuteriolysis via CH bond activation events. This was observed through the reaction of DCl with **2** yielding $[\text{PtClDMe}_2(6\text{-dppd})]$ at low temperatures and subsequent reductive elimination of methane. The H/D exchange was evident due to the formation of all possible isotopomers of methane. These results demonstrate the ability of this relatively simple system to undergo C-H bond activation events.

2.7 Experimental

Reagents and General Procedures. All reactions were carried out in an inert atmosphere of dry nitrogen using standard Schlenk techniques, unless otherwise specified. All solvents used for air and moisture sensitive materials were purified using an Innovative Technology Inc. *PURE SOLV* solvent purification system (SPS). The complexes *cis/trans*-[PtCl₂(SMe₂)₂] and [Pt₂Me₄(μ-SMe₂)₂] were prepared from K₂[PtCl₄] according to the literature [50]. NMR spectra were recorded at ambient temperature, unless otherwise noted (ca. 25°C), on Varian Mercury 400 or Varian Inova 400 or 600 spectrometers. ¹H chemical shifts are reported relative to TMS (¹H). Complete assignment of each compound was aided by the use of ¹H-¹H NOESY, ¹H-¹³C{¹H}-HSQC and ¹H-¹H gCOSY experiments. The standard labeling schemes for pyridyl rings are utilized when labeling signals in NMR spectroscopic analysis. Elemental analyses were performed by either Guelph Chemical Laboratories or Laboratoire d'Analyse Élémentaire de l'Université de Montréal. Mass spectrometric analysis was carried out using an electrospray PE-Sciex Mass Spectrometer (ESI-MS) coupled with a TOF detector.

X-ray Crystallography. A suitable crystal of each compound was coated in Paratone oil and mounted on a glass fiber loop. X-ray data for compounds **1**, **2**, **3**, **4**, **8**, **9**, **10** and **12** were collected at 150K with ω and ϕ scans on a Bruker Smart Apex II diffractometer using graphite-monochromated MoK α radiation ($\lambda = 0.71073 \text{ \AA}$) and Bruker SMART software [69]. Unit cell parameters were calculated and refined from the full data set. Cell refinement and data reduction were performed using the Bruker APEX2 and SAINT programs respectively [70]. Reflections were scaled and corrected for absorption effects using SADABS [71]. X-ray data for compounds **6-dppd** and **11** were collected at 150K with ω and ϕ scans on a Nonius Kappa-CCD diffractometer using graphite-monochromated MoK α radiation ($\lambda = 0.71073 \text{ \AA}$) and COLLECT software [72]. Unit cell parameters were calculated and refined from the full data set. Cell refinement and data reduction were performed using the DENZO-SMN software programs [73]. Reflections were scaled and corrected for absorption effects using DENZO-SMN [73]. All structures were solved by either Patterson or direct methods with SHELXS [74] and refined by full-

matrix least-squares techniques against F^2 using SHELXL [75]. All non-hydrogen atoms were refined anisotropically. The hydrogen atoms were placed in calculated positions and refined using the riding model.

[1,4-di(2-pyridyl)-5,6,7,8,9,10-hexahydrocycloocta[d]pyridazine], (6-dppd). The procedure of Brandsma and Verkruijsse² was employed with slight modifications in the distillation procedures in order to synthesize cyclooctyne. Fractional distillation was used to fully separate the cyclooctyne from the by-products and starting materials. The pungent smelling cyclooctyne was also stored in a cool dark place under nitrogen until further use. The final product, 6-dppd, was synthesized using the procedure by Sauer et al.³ as a template but some modifications were made. First the yellow cyclooctyne solution was dissolved in dichloromethane. 0.635g of 3,6-di-2-pyridyl-1,2,4,5-tetrazine was then dissolved in minimal dichloromethane and stirred vigorously. To this solution, the cyclooctyne was added, slowly titrating until the pink colour of the tetrazine no longer persists. The evolution of N₂ gas is observed by the presence of bubbles which provides a visual handle for the completion of the reaction. The dichloromethane solvent was then removed in a water pump vacuum affording a pale yellow residue which was subsequently recrystallized from hexanes producing pale yellow crystals of 6-dppd in 86% yield. **¹H NMR in CDCl₃:** δ 1.45 (m, 4H, 2 x CH₂), 1.78 (m, 4H, 2 x CH₂), 3.05 (m, 4H, 2 x CH₂), 7.39 (m, 2H, 2 x CH), 7.88 (m, 2H, 2 x CH), 7.89 (m, 2H, 2 x CH), 8.73 (dt, 2H, 2 x CH). **¹³C NMR in CDCl₃:** δ 26.0 (CH₂), 27.2 (CH₂), 30.8 (CH₂), 123.2 (CH), 125.6 (CH), 137.1 (CH), 141.9 (C), 148.7 (CH), 157.3 (C), 159.4 (C). **Elemental Analysis:** Anal. Calcd. C₂₀H₂₀N₄(%): C, 75.92; H, 6.37; N, 17.71. Found: C, 75.79; H, 6.64; N, 17.83. **ESI-MS(TOF):** [C₂₀H₂₀N₄]⁺ Calculated = 316.169 g/mol; Determined Precise Mass = 316.168 g/mol.

[PtClMe(6-dppd)], complex 1. *trans*-[PtClMe(SMe₂)₂] was prepared as outlined in the literature by Hill et al. A solution of *trans*-[PtClMe(SMe₂)₂] in ether, (0.010g, 0.027 mmol) was added with stirring to an equimolar solution of **6-dppd** in ether, (0.008g, 0.027 mmol). An immediate colour change was observed as a bright orange precipitate formed in the reaction flask. After letting the reaction stir for 30mins, the solvent was decanted, the product washed with ether (3 x 5mL) and then dried under high vacuum.

Yield 82%. Crystals of the product were grown by dissolving the orange powdered solid in dichloromethane and allowing excess pentane to migrate into the vial. **¹H NMR in CD₂Cl₂**: δ 1.36 (s, 3H, ²J(PtH) = 80 Hz, CH₃), 1.56 (m, 2H, CH₂), 1.70 (m, 2H, CH₂), 2.07 (m, 4H, 2 x CH₂), 3.00 (t, 2H, CH₂), 3.33 (t, 2H, CH₂), 7.46 (m, 1H, H₅²), 7.75 (t, 1H, H₅¹), 7.96 (t, 1H, H₄²), 8.08 (t, 1H, H₄¹), 8.20 (d, 1H, H₃¹), 8.23 (d, 1H, H₃²), 8.73 (d, 1H, H₆²), 9.77 (d, 1H, ³J(Pt-H₆¹) = 21 Hz, H₆¹). **¹³C NMR in CDCl₃**: δ -11.15 (s, CH₃, Pt-CH₃), 26.09 (s, cyclic CH₂), 26.74 (s, cyclic CH₂), 28.01 (s, cyclic CH₂), 28.12 (s, cyclic CH₂), 29.83 (s, cyclic CH₂), 30.70 (s, cyclic CH₂), 124.29 (s, aromatic C), 125.89 (s, aromatic C), 125.94 (s, aromatic C), 127.32 (s, aromatic C), 131.67 (s, aromatic C), 136.51 (s, aromatic C), 137.19 (s, aromatic C), 137.36 (s, aromatic C), 137.77 (s, aromatic C), 146.28 (s, aromatic C), 146.79 (s, aromatic C), 148.54 (s, aromatic C), 150.89 (s, aromatic C), 154.64 (s, aromatic C). **Elemental Analysis**: Anal. Calc'd. [C₂₁H₂₃N₄ClPt]•0.25(CH₂Cl₂) (%): C, 43.76; H, 4.06; N, 9.61. Found: C, 43.75; H, 3.97; N, 9.57.

[PtMe₂(6-dppd)], complex 2. [Pt₂Me₄(μ-SMe₂)₂] (0.5 g, 0.869 mmol) dissolved in toluene was added to a stirring solution of 6-dppd, (0.55g, 1.74 mmol), in diethyl ether. Upon mixing the two components an immediate colour change was observed and the complex began to precipitate out of the now deep scarlet red solution. After 16hrs of the reaction mixture being cooled to 5°C, the remaining solvent was carefully decanted off and the product was then washed with diethyl ether, (3 x 5mL) and pentane (3 x 5mL) before being dried under high vacuum. This afforded an air and temperature stable deep scarlet red powder in an 84% yield. Red needle-shaped crystals, suitable to be studied by X-ray crystallography, were grown by dissolving the red powdered solid in acetone and layering it with excess pentane in an NMR tube. **¹H NMR in CDCl₃**: δ 1.26 (s, 3H, ²J(PtH)=84 Hz, Me_A), 1.46 (s, 3H, ²J(PtH)=88 Hz, Me_B), 1.54 (m, 2H, CH₂^D), 1.69 (m, 2H, CH₂^C), 2.06 (m, 4H, 2 x CH₂^{B,E}), 2.99 (t, 2H, CH₂^A), 3.27 (t, 2H, CH₂^F), 7.41 (m, 1H, H₅²), 7.60 (t, 1H, H₅¹), 7.93 (t, 1H, H₄²), 8.15 (t, 1H, H₄¹), 8.18 (d, 1H, H₃¹), 8.24 (d, 1H, H₃²), 8.71 (d, 1H, H₆²), 9.48 (d, 1H, ³J(Pt-H₆¹)=21 Hz, H₆¹). **Elemental Analysis**: Anal. Calc'd. [C₂₂H₂₆N₄Pt]•0.25(C₃H₆O) (%): C, 49.14; H, 4.98; N, 10.08. Found: C, 49.43; H, 4.58; N, 10.33.

[PtClMe₂(HgCl)(6-dppd)] complex 3. To a suspension of complex **2** in acetone, (0.150g, 0.277 mmol) was added an acetone solution of HgCl₂ (0.075g, 0.277 mmol). An immediate colour change from deep red to yellow was observed. After 30 minutes of stirring the remaining solvent was removed under reduced pressure and the resultant yellow residue recrystallized from pentane. The yellow solid was then collected by Hirsch filtration and washed with pentane (3 x 5mL). Yield 87%. **¹H NMR in acetone-*d*₆** for [PtClMe₂(HgCl)(6-dppd)]: δ = 1.55 [m, 2H, CH₂], 1.72 [s, 3H, ²J(Pt-H)=64 Hz; ³J(HgPtH)=6 Hz, CH₃], 1.75 [m, 2H, CH₂], 1.99 [s, 3H, ²J(Pt-H)= 64Hz, ³J(HgPtH)= 8 Hz, CH₃], 2.15 [m, 2H, CH₂], 3.09-3.20 [m, 4H, 2 x CH₂], 3.32 [m, 2H, CH₂], 7.49 [dd, 1H, ³J(HH)=5 Hz, ³J(HH)=8 Hz, H₅¹], 7.77 [dd, 1H, ³J(HH)=6 Hz, ³J(HH)=8 Hz, H₅], 7.97 [dd, 1H, ³J(HH)=8 Hz, ³J(HH)=8 Hz, H₄¹], 8.15 [d, 1H, ³J(HH)=8 Hz, H₃¹], 8.19 [d, 1H, ³J(HH)=8 Hz, ³J(HH)=8 Hz H₄], 8.41 [d, 1H, ³J(HH)=8 Hz, H₃], 8.76 [d, 1H, ³J(HH)=5 Hz, H₆¹], 9.17 [d, 1H, ³J(HH)=6 Hz, ⁴J(PtH)=21 Hz, H₆]. **Elemental Analysis:** Anal. Calc'd for C₂₂H₂₆Cl₂N₄HgPt•1.25(C₅H₁₂)(%): C, 37.57; H, 4.58; N, 6.20. Found: C, 37.61; H, 4.30; N, 6.43.

[PtBrMe₂(HgBr)(6-dppd)] complex 4. Complex **2** was prepared in an analogous manner to complex **3** but utilizing an equimolar amount of HgBr₂, (0.100g, 0.277mmol). Yield 91%. **¹H NMR in acetone-*d*₆**: δ = 1.58 [m, 2H, CH₂], 1.63 [s, 3H, ²J(Pt-H)=64Hz; ³J(HgPtH)=7Hz, CH₃], 1.70 [m, 2H, CH₂], 1.92 [s, 3H, ²J(Pt-H)=64Hz, ³J(HgPtH)=7Hz, CH₃], 2.10 – 2.20 [m, 4H, 2 x CH₂], 3.22 [m, 2H, CH₂], 3.48 [m, 2H, CH₂], 7.62 [m, 1H, H₅¹], 7.95 [t, 1H, H₅], 8.13 [d, 1H, H₃¹], 8.42 [td, 1H, H₄¹], 8.46 [t, 1H, H₄], 8.67 [d, 1H, H₃¹], 8.81 [d, 1H, H₆¹], 9.35 [d, 1H, ⁴J(PtH)=22Hz, H₆]. **Elemental Analysis:** Anal. Calc'd for C₂₂H₂₆Br₂N₄HgPt•0.5(C₃H₆O)(%): C, 30.32; H, 3.14; N, 6.02. Found: C, 30.08; H, 2.81; N, 6.03.

[PtMe₂OAc(HgOAc)(6-dppd)] complex 5a/5b. To a suspension of complex **2** in acetone, (0.150g, 0.277 mmol) was added an acetone solution of Hg(OAc)₂ (0.088g, 0.277 mmol). An immediate colour change from deep red to yellow was observed. After 30 minutes of stirring the remaining solvent was removed under reduced pressure and the resultant yellow residue recrystallized from pentane. The yellow solid was then collected by Hirsch filtration and washed with pentane (3 x 5mL). Yield 90%. **¹H NMR in**

acetone-*d*₆ for 5a: 0.81 [s, 3H, $^2J(\text{PtH})=72\text{Hz}$, CH₃], 1.53 [s, 3H, $^2J(\text{Pt-H})=63\text{Hz}$; $^3J(\text{HgPtH})=14\text{Hz}$, CH₃], 1.54 [s, 3H, CH₃], 1.59 [m, 2H, CH₂], 1.69 [m, 2H, CH₂], 2.05 – 2.12 [m, 4H, 2 x CH₂], 3.30 [m, 2H, CH₂], 3.52 [m, 2H, CH₂], 7.60 [m, 1H, H₅¹], 7.83 [t, 1H, H₅], 8.10 [td, 1H, H₄¹], 8.11 [td, 1H, H₄], 8.40 [d, 1H, H₃], 8.57 [d, 1H, H₃¹], 8.79 [d, 1H, H₆¹], 9.71 [d, 1H, H₆]. **5b:** 0.88 [s, 3H, $^2J(\text{Pt-H})=72\text{Hz}$, $^3J(\text{HgPtH})=14\text{Hz}$, CH₃], 1.30 [s, 3H, $^2J(\text{Pt-H})=64\text{Hz}$, CH₃], 1.54 [s, 3H, CH₃], 1.59 [m, 2H, CH₂], 1.69 [m, 2H, CH₂], 2.05 – 2.12 [m, 4H, 2 x CH₂], 3.30 [m, 2H, CH₂], 3.52 [m, 2H, CH₂], 7.55 [m, 1H, H₅¹], 8.02 [t, 1H, H₅], 8.09 [td, 1H, H₄¹], 8.34 [td, 1H, H₄], 8.46 [d, 1H, H₃], 8.62 [d, 1H, H₃¹], 8.72 [d, 1H, H₆¹], 8.97 [d, 1H, H₆].

[PtBr₂Me₂(6-dppd)], complex 6. To a solution of complex **2** in acetone, (0.010g, 0.018 mmol) is added 0.018 mmol of Br₂ whilst stirring. Immediately the reaction mixture became a bright yellow colour. After 30mins the volume of solvent was reduced to ~1mL and pentane was added to precipitate out a yellow powder. This solid product was then washed with pentane (3 x 2mL) and dried on high vacuum. Yield 89%. **¹H NMR in CDCl₃:** δ = 2.12 [s, 3H, $^2J(\text{PtH})=71\text{Hz}$, CH₃], [s, 3H, $^2J(\text{PtH})=71\text{Hz}$, CH₃], 1.58 [m, 2H, CH₂], 1.72 [m, 2H, CH₂], 2.10 [m, 4H, 2 x CH₂], 3.18 [t, 2H, CH₂], 3.31 [t, 2H, CH₂], 7.45 [m, 1H, H₅¹], 7.78 [t, 1H, H₅], 7.94 [t, 1H, H₄¹], 8.14 [t, 1H, H₄], 8.26 [d, 1H, H₃], 8.32 [d, 1H, H₃¹], 8.73 [d, 1H, H₆¹], 9.12 [d, 1H, H₆]. **Elemental Analysis:** Anal. Calc'd for C₂₂H₂₆Br₂N₄Pt(%): C, 37.67; H, 3.74; N, 7.99. Found: C, 37.02; H, 3.58; N, 7.79.

[PtI₂Me₂(6-dppd)], complex 7 (7a, 7b, 7c). Complex **7** was synthesized similarly to complex **6**, but using an equimolar amount of I₂ (0.0047g, 0.0184 mmol). The reddish brown solid was formed in an 89% yield. **¹H NMR analysis** indicated that there was a mixture of three complexes of complex **7**, as well as traces of complexes **8** and **9**. **¹H NMR in CDCl₃:** **(7a)** δ = 2.41 [s, 3H, $^2J(\text{PtH})=72\text{Hz}$, CH₃], 2.72 [s, 3H, $^2J(\text{Pt-H})=73\text{Hz}$, CH₃], 1.57 [m, 2H, CH₂], 1.71 [m, 2H, CH₂], 2.14 [m, 4H, 2 x CH₂], 3.20 [m, 2H, CH₂], 3.31 [m, 2H, CH₂], 7.45 [t, 1H, $^3J(\text{H}_5^1\text{H}_6^1)=5\text{Hz}$; $^3J(\text{H}_4^1\text{H}_5^1)=8\text{Hz}$, H₅¹], 7.74 [t, 1H, $^3J(\text{H}_5\text{H}_6)=7\text{Hz}$; $^3J(\text{H}_4\text{H}_5)=8\text{Hz}$, H₅], 7.95 [td, 1H, $^3J(\text{H}_3^1\text{H}_4^1)=8\text{Hz}$; $^3J(\text{H}_4^1\text{H}_5^1)=8\text{Hz}$, H₄¹], 8.12 [td, 1H, $^3J(\text{H}_3\text{H}_4)=8\text{Hz}$, $^3J(\text{H}_4\text{H}_5)=8\text{Hz}$, H₄], 8.24 [d, 1H, $^3J(\text{H}_3^1\text{H}_4^1)=8\text{Hz}$, H₃¹], 8.32 [d, 1H, $^3J(\text{H}_3\text{H}_4)=8\text{Hz}$, H₃], 8.73 [d, 1H, $^3J(\text{H}_5^1\text{H}_6^1)=5\text{Hz}$, H₆¹], 9.18 [d, 1H, $^3J(\text{H}_5\text{H}_6)=7\text{Hz}$, $^2J(\text{PtH}_6)=20\text{Hz}$, H₆]. **(7b)** δ 1.71 [s, 3H, $^2J(\text{PtH})=72\text{Hz}$, CH₃], 2.26 [s,

3H, $^2J(\text{PtH})=68\text{Hz}$, CH₃], 1.50 – 3.50 (6 x CH₂, 12H unresolvable), 7.40 – 10.25 (8H, 8 x CH on pyridyl groups unresolvable). (**7c**) δ 1.61 [s, 3H, $^2J(\text{PtH})=72\text{Hz}$, CH₃], 2.55 [s, 3H, $^2J(\text{PtH})=68\text{Hz}$, CH₃], 1.50 – 3.50 (6 x CH₂, 12H unresolvable), 7.40 – 10.25 (8H, 8 x CH on pyridyl groups unresolvable). **Elemental Analysis:** Anal. Calc'd for C₂₂H₂₆I₂N₄Pt•1.5(I₂)(%): C, 26.68; H, 3.08; N, 5.19. Found: C, 26.48; H, 2.65; N, 5.46.

[PtMe₃(6-dppd)], complex 8. To a solution of complex **2** in acetone, (0.010g, 0.0184 mmol) is added 0.0184 mmol of MeI whilst stirring. Immediately the reaction mixture became a bright yellow colour. After the solvent was removed under reduced pressure, the orange-red product was washed with pentane (3 x 2mL) and dried on high vacuum. Yield 93%. **¹H NMR in acetone-*d*₆:** δ = 0.60 [s, 3H, $^2J(\text{PtH})=73\text{Hz}$, CH₃], 1.43 [s, 3H, $^2J(\text{PtH})=71\text{Hz}$, CH₃], 1.66 [s, 3H, $^2J(\text{PtH})=72\text{Hz}$, CH₃], 1.56 [m, 2H, CH₂], 1.69 [m, 2H, CH₂], 2.13 [m, 2H, CH₂], 3.17 [m, 2H, CH₂], 3.30 [m, 2H, CH₂], 3.48 [m, 2H, CH₂], 7.61 [t, 1H, $^3J(\text{H}_5^1\text{H}_6^1)=5\text{Hz}$; $^3J(\text{H}_4^1\text{H}_5^1)=8\text{Hz}$ H₅¹], 7.94 [t, 1H, $^3J(\text{H}_5\text{H}_6)=6\text{Hz}$; $^3J(\text{H}_4\text{H}_5)=8\text{Hz}$ H₅], 8.11 [d, 1H, $^3J(\text{H}_3^1\text{H}_4^1)=7\text{Hz}$, H₃¹], 8.15 [td, 1H, $^3J(\text{H}_3^1\text{H}_4^1)=7\text{Hz}$; $^3J(\text{H}_4^1\text{H}_5^1)=8\text{Hz}$, H₄¹], 8.40 [td, 1H, $^3J(\text{H}_3\text{H}_4)=8\text{Hz}$, $^3J(\text{H}_4\text{H}_5)=8\text{Hz}$, H₄], 8.62 [d, 1H, $^3J(\text{H}_3\text{H}_4)=8\text{Hz}$, H₃], 8.80 [d, 1H, $^3J(\text{H}_5^1\text{H}_6^1)=5\text{Hz}$, H₆¹], 9.16 [d, 1H, $^3J(\text{H}_5\text{H}_6)=6\text{Hz}$; $^3J(\text{PtH}_6)=20\text{Hz}$, H₆]. **Elemental Analysis:** Anal. Calc'd for C₂₃H₂₉I₂N₄Pt(%): C, 40.42; H, 4.28; N, 8.20. Found: C, 40.65; H, 4.40; N, 7.98.

[PtMe(6-dppd)], complex B. A solution of complex **1** in acetone, (0.020g, 0.0178 mmol) is added to a slight excess of LiI (0.005g) dissolved in acetone and allowed to react while stirring for 20 hours. The solvent was then removed *in vacuo* yielding an orange solid which is subsequently washed with pentane (3 x 3mL) and dried on high vacuum. Yield 78%. **¹H NMR in CDCl₃:** δ = 1.71 [s, 3H, $^2J(\text{PtH})=78\text{Hz}$, CH₃], 1.55 [m, 2H, CH₂], 1.72 [m, 2H, CH₂], 2.06 – 2.12 [m, 4H, 2 x CH₂], 3.04 [t, 2H, CH₂], 3.33 [t, 2H, CH₂], 7.45 [m, 1H, $^3J(\text{H}_5^1\text{H}_6^1)=4\text{Hz}$; $^3J(\text{H}_4^1\text{H}_5^1)=8\text{Hz}$, H₅¹], 7.67 [t, 1H, $^3J(\text{H}_5\text{H}_6)=6\text{Hz}$; $^3J(\text{H}_4\text{H}_5)=8\text{Hz}$, H₅], 7.95 [td, 1H, $^3J(\text{H}_3^1\text{H}_4^1)=8\text{Hz}$; $^3J(\text{H}_4^1\text{H}_5^1)=8\text{Hz}$, H₄¹], 8.13 [td, 1H, $J(\text{H}_3\text{H}_4)=8\text{Hz}$; $^3J(\text{H}_4\text{H}_5)=8\text{Hz}$, H₄³], 8.17 [d, 1H, $^3J(\text{H}_3^1\text{H}_4^1)=8\text{Hz}$, H₃¹], 8.19 [d, 1H, $^3J(\text{H}_3\text{H}_4)=8\text{Hz}$, H₃], 8.73 [d, 1H, $^3J(\text{H}_5^1\text{H}_6^1)=4\text{Hz}$, H₆¹], 10.32 [d, 1H, $^3J(\text{H}_5\text{H}_6)=5\text{Hz}$; $^3J(\text{PtH}_6) = 19\text{Hz}$, H₆].

[PtI₃Me(6-dppd)], complex 9. To a dichloromethane solution of complex **B** (0.010g, 0.0153 mmol) is added one equivalent, (0.0039g, 0.0153 mmol) of I₂. The reaction mixture is left to stir for 8 hours prior to the solvent being removed under reduced pressure. The purple-black residue was dissolved in minimal dichloromethane and layered with ~2mL of pentane. Precipitation of a deep purple solid was observed after 4 hours at 5°C. The solid was collected via Hirsch filtration and washed with pentane (2 x 2mL) and dried. Yield 73%. **¹H NMR in CDCl₃:** δ = 1.58 [m, 2H, CH₂], 1.72 [m, 2H, CH₂], 2.14 – 2.20 [m, 4H, 2 x CH₂], 3.28 [t, 2H, CH₂], 3.39 [t, 2H, CH₂], 3.65 [s, 3H, ²J(PtH)=71Hz, CH₃], 7.51 [m, 1H, ³J(H₅¹H₆¹)=4Hz; ³J(H₄¹H₅¹)=8Hz, H₅¹], 7.82 [t, 1H, ³J(H₅H₆)=6Hz; ³J(H₄H₅)=8Hz, H₅], 8.02 [td, 1H, ³J(H₃¹H₄¹)=8Hz; ³J(H₄¹H₅¹)=8Hz, H₄¹], 8.19 [td, 1H, ³J(H₃H₄)=8Hz; ³J(H₄H₅)=8Hz, H₄], 8.25 [d, 1H, ³J(H₃¹H₄¹)=8Hz, H₃¹], 8.41 [d, 1H, ³J(H₃H₄)=8Hz, H₃], 8.78 [d, 1H, ³J(H₅¹H₆¹)=4Hz, H₆¹], 10.20 [d, 1H, ³J(H₅H₆)=5Hz; ³J(PtH₆) = 19Hz, H₆]. **Elemental Analysis:** Anal. Calc'd for C₂₁H₂₃I₃N₄Pt•2(I₂)(%): C, 20.28; H, 2.01; N, 4.30. Found: C, 20.19; H, 1.94; N, 4.55.

[PtBrMe₂(p-CH₂C₆H₅)(6-dppd)], complex 10. To an acetone solution of complex **2** (0.010g, 0.0184 mmol) is added one equivalent, (2.19μL, 0.0184 mmol) of benzyl bromide. The reaction mixture is left to stir for 24 hours prior to the solvent being removed under reduced pressure, affording a yellow powdered solid. The yellow powder was dissolved in minimal acetone and layered with ~2mL of pentane. Precipitation of a yellow solid was observed after 30mins at room temperature. The solid was collected via Hirsch filtration and washed with pentane (2 x 2mL) and dried. Yield 81%. **¹H NMR in acetone-d₆:** δ = 1.38 [s, 3H, , ²J(PtH)=70Hz, CH₃], 1.62 [s, 3H, ²J(PtH)=71Hz, CH₃], 1.40 – 3.25 (12H, 6 x CH₂ on ring unresolvable); 3.10 [d, 1H, ²J(H_AH_B)=6Hz, ²J(PtH)=45Hz], 3.11 [d, 1H, ²J(H_AH_B)=6Hz, ²J(PtH)=45Hz], 6.31 [d, 1H, ³J(H_BH_C)=8Hz], 6.50 [t, 2H, ³J(H_BH_C)=8Hz, ³J(H_BH_A)=8Hz], 6.72 [d, 2H, ³J(H_AH_B)=8Hz, ⁴J(PtH)=20Hz], 7.74 [m, 1H, ³J(H₅¹H₆¹)=4Hz; ³J(H₄¹H₅¹)=7Hz, H₅¹], 7.93 [m, 1H, ³J(H₅H₆)=6Hz; ³J(H₄H₅)=7Hz, H₅], 8.00 [t, 1H, ³J(H₄¹H₅¹)=7Hz, ³J(H₃¹H₄¹)=8Hz, H₄¹], 8.11 [t, 1H, ³J(H₄H₅)=7Hz, ³J(H₃H₄)=8Hz, H₄], 8.18 [d, 1H, ³J(H₃¹H₄¹)=8Hz, H₃¹], 8.29 [d, 1H, ³J(H₃H₄)=8Hz, H₃], 8.72 [d, 1H, ³J(H₅¹H₆¹)=4Hz, H₆¹], 9.13 [d, 1H, ³J(H₅H₆)=5Hz; ³J(PtH₆) = 22Hz, H₆]. **Elemental Analysis:** Anal.

Calc'd for C₂₉H₃₃Br₁N₄Pt•H₂O(%): C, 47.67; H, 4.83; N, 7.67. Found: C, 47.34; H, 4.56; N, 7.13.

[PtBrMe₂(p-CH₂C₆H₄CH₂Br)(6-dppd)], complex 11. To an acetone solution of complex 2 (0.010g, 0.0184 mmol) is added one equivalent, (0.0049g, 0.0184 mmol) of p- α,α' -dibromoxylene. The reaction mixture is left to stir for 24 hours prior to the solvent being removed under reduced pressure, affording a yellow powdered solid. The yellow powder was dissolved in minimal acetone and layered with ~2mL of pentane.

Precipitation of a yellow solid was observed after 30mins at room temperature. The solid was collected via Hirsch filtration and washed with pentane (2 x 2mL) and dried. Yield 88%. **¹H NMR in CDCl₃:** δ = 1.43 [s, 3H, ²J(PtH)=70Hz, CH₃], 1.70 [s, 3H, ²J(PtH)=70Hz, CH₃], 1.40 – 3.25 (12H, 6 x CH₂ on ring unresolvable); 2.73 [d, 1H, ²J(H_CH_D)=6Hz], 2.83 [d, 1H, ²J(H_CH_D)=6Hz], 3.00 [d, 1H, ²J(H_AH_B)=6Hz, ²J(PtH)=45Hz], 3.01 [d, 1H, ²J(H_AH_B)=6Hz, ²J(PtH)=45Hz], 6.17 [d, 2H, ³J(H_EH_F)=8Hz, ⁴J(PtH_E)=19Hz], 6.48 [d, 2H, ³J(H_EH_F)=8Hz], 7.37 [m, 1H, ³J(H₅¹H₆¹)=4Hz; ³J(H₄¹H₅¹)=8Hz, H₅¹], 7.43 [m, 1H, ³J(H₅H₆)=6Hz; ³J(H₄H₅)=8Hz, H₅], 7.85 [m, 2H, H₄/H₄¹], 7.90 [d, 1H, ³J(H₃¹H₄¹)=8Hz, H₃¹], 8.13 [d, 1H, ³J(H₃H₄)=8Hz, H₃], 8.64 [d, 1H, ³J(H₅¹H₆¹)=4Hz, H₆¹], 8.75 [d, 1H, ³J(H₅H₆)=5Hz; ³J(PtH₆) = 18Hz, H₆].

Elemental Analysis: Anal. Calc'd for C₃₀H₃₄Br₂N₄Pt(%): C, 44.73; H, 4.25; N, 6.96. Found: C, 44.61; H, 4.52; N, 7.09.

[PtClMe₂(CH₂Cl)(6-dppd)], complex 12 (12a, 12b, 12c). A solution of [PtMe₂(6-dppd)] (25 mg, 0.046mmol) in methylene chloride (5mL) was allowed to stand overnight. The solvent was then removed under vacuum, and washed with pentane (2 x 5mL). The resultant yellow solid was recrystallized from acetone/pentane: yield 84%. Crystals were prepared by dissolving [PtClMe₂(CH₂Cl)(6-dppd)] in minimal acetone and allowing for the slow migration of pentane into the solution. Yielded translucent yellow block-like crystals with approximate dimensions of 0.02 mm x 0.02 mm x 0.04 mm. **¹H NMR in acetone-d₆:** 12a: 1.26 (s, 3H, ²J(PtH) = 70Hz, Pt-Me_A trans to N); 1.41 (s, 3H, ²J(PtH) = 70Hz, Pt-Me_B trans to N); 1.54 – 1.75 (m, 4H, 2 x CH₂ on ring); 2.01 (m, 2H, CH₂ on ring); 2.13 (m, 2H, CH₂ on ring); 3.25 (m, 2H, CH₂ on ring); 3.49 (m, 2H, CH₂ on ring); 3.53 (d, 1H, ²J(H^aH^b) = 7Hz, ²J(PtH^b) = 48Hz, Pt-CH^aH^bCl); 3.54 (d, 1H, ²J(H^aH^b) =

7Hz, $^2J(\text{PtH}^a) = 58\text{Hz}$, Pt-CH^aH^bCl); 7.61 (m, 1H, H₅¹); 7.95 (t, 1H, H₅); 8.11 (m, 2H, H₃²/H₄²); 8.41 (t, 1H, H₄¹); 8.60 (d, 1H, H₃¹); 8.79 (d, 1H, H₆¹); 9.06 (d, 1H, H₆, $^3J(\text{PtH}) = 19\text{Hz}$). **12b**: 0.61 (s, 3H, $^2J(\text{PtH}) = 74\text{Hz}$, Pt-Me_B trans to Cl); 1.44 (s, 3H, $^2J(\text{PtH}) = 70\text{Hz}$, Pt-Me_A trans to N); 1.55 – 3.50 (12H, 6 x CH₂ on ring unresolvable); 4.72 (d, 1H, $^2J(\text{H}^a\text{H}^b) = 6\text{Hz}$, $^2J(\text{PtH}) = 78\text{Hz}$); 4.89 (d, 1H, $^2J(\text{H}^a\text{H}^b) = 6\text{Hz}$, $^2J(\text{PtH}) = 86\text{Hz}$); 7.55 – 9.55 (8H, 8 x CH on pyridyl groups unresolvable). **12c**: 0.66 (s, 3H, $^2J(\text{PtH}) = 74\text{Hz}$, Pt-Me_A trans to Cl); 1.55 (s, 3H, $^2J(\text{PtH}) = 70\text{Hz}$, Pt-Me_B trans to N); 1.55 – 3.50 (12H, 6 x CH₂ on ring unresolvable); 4.26 (d, 1H, $^2J(\text{H}^a\text{H}^b) = 8\text{Hz}$, $^2J(\text{PtH}) = 44\text{Hz}$); 4.74 (d, 1H, $^2J(\text{H}^a\text{H}^b) = 8\text{Hz}$, $^2J(\text{PtH}) = 92\text{Hz}$); 7.55 – 9.55 (8H, 8 x CH on pyridyl groups unresolvable). **Elemental Analysis**: Anal. Calc'd for C₂₃H₂₈Cl₂N₄Pt(%): C, 44.10; H, 4.50; N, 8.94. Found: C, 43.83; H, 4.58; N, 8.67.

General procedure for deuteriolysis experiment.

An NMR tube is charged with 0.010g, (0.0184mmol), of complex **2** dissolved in a 50:50 mixture of methanol-*d*₄ and dichloromethane-*d*₂. DCl was then generated *in situ* through the addition of acetyl chloride to the NMR tube. After briefly mixing the sample various spectra were attained at temperature increments from -40°C to +20°C.

Table 2.11: Crystallographic data for [C₂₀H₂₀N₄], **6-dppd**.

C₂₀H₂₀N₄	
Empirical Formula	C ₂₀ H ₂₀ N ₄
Formula Weight	316.40
Wavelength	0.71073 Å
Crystal System	Triclinic
Space Group	P -1
Unit Cell Dimensions	a = 7.0827(14) Å α = 97.29(3)° b = 7.2540(15) Å β = 98.24(3)° c = 16.885(3) Å γ = 100.83(3)°
Volume	832.7(3) Å ³
Z	2
Density (calculated)	1.262 Mg/m ³
Absorption Coefficient (μ)	0.077 mm ⁻¹
Crystal Size	0.45 x 0.45 x 0.08 mm ³
Refinement Method	Full-matrix least-squares on F ²
Goodness of fit on F ²	1.030
Final R indices [I>2σ(I)]	R1 = 0.0606, wR2 = 0.1493
R indices (all data)	R1 = 0.1225, wR2 = 0.1787

Table 2.12: Crystallographic data for [PtClMe(6-dppd)], 1.**[PtClMe(6-dppd)]**

Empirical Formula	C ₂₁ H ₂₃ ClN ₄ Pt
Formula Weight	561.96
Wavelength	0.71073 Å
Crystal System	Monoclinic
Space Group	P 2 ₁ /c
Unit Cell Dimensions	a = 18.164(4) Å α = 90° b = 12.904(3) Å β = 93.249(7)° c = 8.2595(16) Å γ = 90(3)°
Volume	1932.8(7) Å ³
Z	4
Density (calculated)	1.931 Mg/m ³
Absorption Coefficient (μ)	7.411 mm ⁻¹
Crystal Size	0.04 x 0.04 x 0.02 mm ³
Refinement Method	Full-matrix least-squares on F ²
Goodness of fit on F ²	1.049
Final R indices [I > 2σ(I)]	R1 = 0.0352, wR2 = 0.0425
R indices (all data)	R1 = 0.0727, wR2 = 0.0501

Table 2.13: Crystallographic data for [PtMe₂(6-dppd)], **2**.**[PtMe₂(6-dppd)]**

Empirical Formula	C ₂₂ H ₂₆ N ₄ Pt
Formula Weight	541.56
Wavelength	0.71073 Å
Crystal System	Monoclinic
Space Group	P 2 ₁ /c
Unit Cell Dimensions	a = 12.4230(15) Å α = 90° b = 18.826(2) Å β = 105.068(4)° c = 8.6433(10) Å γ = 90(3)°
Volume	1951.9(4) Å ³
Z	4
Density (calculated)	1.843 Mg/m ³
Absorption Coefficient (μ)	7.203 mm ⁻¹
Crystal Size	0.04 x 0.02 x 0.01 mm ³
Refinement Method	Full-matrix least-squares on F ²
Goodness of fit on F ²	1.034
Final R indices [I > 2σ(I)]	R1 = 0.0389, wR2 = 0.0512
R indices (all data)	R1 = 0.0809, wR2 = 0.0585

Table 2.14: Crystallographic data for [PtClMe₂(HgCl)(6-dppd)], **3**.**[PtClMe₂(HgCl)(6-dppd)]**

Empirical Formula	C ₂₂ H ₂₆ Cl ₂ HgN ₄ Pt
Formula Weight	813.05
Wavelength	0.71073 Å
Crystal System	Triclinic
Space Group	P -1
Unit Cell Dimensions	a = 9.7210(19) Å α = 87.53(3)° b = 10.796(2) Å β = 72.28(3)° c = 10.581(3) Å γ = 81.62(3)°
Volume	1541.0(5) Å ³
Z	2
Density (calculated)	1.752 Mg/m ³
Absorption Coefficient (μ)	9.695 mm ⁻¹
Crystal Size	0.16 x 0.14 x 0.14 mm ³
Refinement Method	Full-matrix least-squares on F ²
Goodness of fit on F ²	1.117
Final R indices [I > 2σ(I)]	R1 = 0.0488, wR2 = 0.1657
R indices (all data)	R1 = 0.0736, wR2 = 0.1798

Table 2.15: Crystallographic data for [PtBrMe₂(HgBr)(6-dppd)], **4**.**[PtBrMe₂(HgBr)(6-dppd)] • 2 CHCl₃**

Empirical Formula	C ₂₄ H ₂₈ Br ₂ Cl ₆ HgN ₄ Pt
Formula Weight	1140.70
Wavelength	0.71073 Å
Crystal System	Triclinic
Space Group	P -1
Unit Cell Dimensions	a = 9.931(2) Å α = 83.75(3)° b = 10.646(2) Å β = 78.27(3)° c = 15.848(3) Å γ = 83.91(3)°
Volume	1624.8(6) Å ³
Z	2
Density (calculated)	2.332 Mg/m ³
Absorption Coefficient (μ)	11.994 mm ⁻¹
Crystal Size	0.21 x 0.13 x 0.11 mm ³
Refinement Method	Full-matrix least-squares on F ²
Goodness of fit on F ²	1.252
Final R indices [I>2σ(I)]	R1 = 0.0530, wR2 = 0.1342
R indices (all data)	R1 = 0.0867, wR2 = 0.1659

Table 2.16: Crystallographic data for [PtMe₃(6-dppd)], **8**.**[PtMe₃(6-dppd)]**

Empirical Formula	C ₂₃ H ₂₉ IN ₄ Pt
Formula Weight	683.49
Wavelength	0.71073 Å
Crystal System	Orthorhombic
Space Group	P bca
Unit Cell Dimensions	a = 17.296(2) Å α = 90° b = 12.4255(14) Å β = 90° c = 22.067(3) Å γ = 90°
Volume	4742.3(10) Å ³
Z	8
Density (calculated)	1.915 Mg/m ³
Absorption Coefficient (μ)	7.235 mm ⁻¹
Crystal Size	0.04 x 0.02 x 0.02 mm ³
Refinement Method	Full-matrix least-squares on F ²
Goodness of fit on F ²	1.003
Final R indices [I > 2σ(I)]	R1 = 0.0364, wR2 = 0.0603
R indices (all data)	R1 = 0.0860, wR2 = 0.0737

Table 2.17: Crystallographic data for [PtI₃Me(6-dppd)], **9**.**[PtI₃Me(6-dppd)] • CHCl₃**

Empirical Formula	C ₂₂ H ₂₄ Cl ₃ I ₃ N ₄ Pt
Formula Weight	1026.59
Wavelength	0.71073 Å
Crystal System	Monoclinic
Space Group	P 2 ₁ /c
Unit Cell Dimensions	a = 15.6434(8) Å α = 90° b = 8.8024(4) Å β = 97.130(2)° c = 21.5436(10) Å γ = 90°
Volume	2943.6(2) Å ³
Z	4
Density (calculated)	2.316 Mg/m ³
Absorption Coefficient (μ)	8.204 mm ⁻¹
Crystal Size	0.06 x 0.04 x 0.01 mm ³
Refinement Method	Full-matrix least-squares on F ²
Goodness of fit on F ²	1.019
Final R indices [I > 2σ(I)]	R1 = 0.0364, wR2 = 0.0613
R indices (all data)	R1 = 0.0780, wR2 = 0.0883

Table 2.18: Crystallographic data for [PtBrMe₂(CH₂C₆H₅)(6-dppd)], **10.****[PtBrMe₂(CH₂C₆H₅)(6-dppd)]**

Empirical Formula	C ₂₉ H ₃₃ BrN ₄ Pt
Formula Weight	712.59
Wavelength	0.71073 Å
Crystal System	Monoclinic
Space Group	P 2 ₁ /c
Unit Cell Dimensions	a = 8.8073(3) Å α = 90° b = 18.8399(5) Å β = 90.543(2)° c = 15.8807(4) Å γ = 90°
Volume	2634.95(13) Å ³
Z	4
Density (calculated)	1.796 Mg/m ³
Absorption Coefficient (μ)	6.867 mm ⁻¹
Crystal Size	0.08 x 0.07 x 0.03 mm ³
Refinement Method	Full-matrix least-squares on F ²
Goodness of fit on F ²	1.037
Final R indices [I > 2σ(I)]	R1 = 0.0345, wR2 = 0.0658
R indices (all data)	R1 = 0.0506, wR2 = 0.0701

Table 2.19: Crystallographic data for [PtBrMe₂(CH₂C₆H₄CH₂Br)(6-dppd)], **11**.**[PtBrMe₂(CH₂C₆H₄CH₂Br)(6-dppd)] • CHCl₃**

Empirical Formula	C ₃₀ H ₃₄ Br ₂ Cl ₃ N ₄ Pt
Formula Weight	911.87
Wavelength	0.71073 Å
Crystal System	Triclinic
Space Group	P -1
Unit Cell Dimensions	a = 8.8801(18) Å α = 88.68(3)° b = 14.409(3) Å β = 81.33(3)° c = 15.019(3) Å γ = 73.04(3)°
Volume	1816.7(6) Å ³
Z	3
Density (calculated)	2.500 Mg/m ³
Absorption Coefficient (μ)	9.458 mm ⁻¹
Crystal Size	0.23 x 0.21 x 0.13 mm ³
Refinement Method	Full-matrix least-squares on F ²
Goodness of fit on F ²	1.078
Final R indices [I > 2σ(I)]	R1 = 0.0361, wR2 = 0.0989
R indices (all data)	R1 = 0.0412, wR2 = 0.1013

Table 2.20: Crystallographic data for [PtClMe₂(CH₂Cl)(6-dppd)], **12a**.**[PtClMe₂(CH₂Cl)(6-dppd)]**

Empirical Formula	C ₂₃ H ₂₈ Cl ₂ N ₄ Pt
Formula Weight	626.48
Wavelength	0.71073 Å
Crystal System	Monoclinic
Space Group	P 2 ₁ /n
Unit Cell Dimensions	a = 8.0978(6) Å α = 90° b = 20.7047(16) Å β = 98.960(2)° c = 13.9170(11) Å γ = 90°
Volume	2304.9(3) Å ³
Z	4
Density (calculated)	1.805 Mg/m ³
Absorption Coefficient (μ)	6.337 mm ⁻¹
Crystal Size	0.04 x 0.04 x 0.02 mm ³
Refinement Method	Full-matrix least-squares on F ²
Goodness of fit on F ²	1.070
Final R indices [I > 2σ(I)]	R1 = 0.0449, wR2 = 0.0804
R indices (all data)	R1 = 0.0808, wR2 = 0.0907

2.8 References

1. Choy, S. W. S.; Page, M. J.; Bhadbhade, M.; Messerle, B. A. *Organometallics* **2013**, *32*, 4726–4729.
2. Ho, J. H. H.; Choy, S. W. S.; Macgregor, S. A.; Messerle, B. A. *Organometallics* **2011**, *30*, 5978–5984.
3. Radlauer, M.; Day, M. W.; Agapie, T. *Organometallics* **2012**, *31*, 2231–2243.
4. Salata, M. R.; Marks, T. J. *Macromolecules* **2009**, *42*, 1920–1933.
5. Liao, B.-S.; Liu, S.-T. *J. Org. Chem.* **2012**, *77*, 6653–6656.
6. Liao, B.-S.; Liu, S.-T. *Catal. Commun.* **2013**, *32*, 28–31.
7. Deprez, N. R.; Sanford, M. S. *J. Am. Chem. Soc.* **2009**, *131*, 11234–11241.
8. Chuang, G. J.; Wang, W.; Lee, E.; Ritter, T. *J. Am. Chem. Soc.* **2011**, *133*, 1760–1762.
9. Powers, D. C.; Xiao, D. Y.; Geibel, M. A. L.; Ritter, T. *J. Am. Chem. Soc.* **2010**, *132*, 14530–14536.
10. Powers, D. C.; Ritter, T. *Nature Chem.* **2009**, *1*, 302–309.
11. Hernández-Gil, J.; Ferrer, S.; Castiñeiras, A.; Liu-González, M.; Lloret, F.; Ribes, A.; Coga, L.; Bernecker, A.; Mareque-Rivas, J. C. *Inorg. Chem.* **2013**. (ASAP).
12. Champouret, Y. D. M.; Fawcett, J.; Nodes, W. J.; Singh, K.; Solan, G. A. *Inorg. Chem.* **2006**, *45*, 9890–9900.
13. Bratko, I.; Gómez, M. *Dalton Trans.* **2013**, *42*, 10664–10681.
14. Kong, S.; Song, K.; Liang, T.; Guo, C.-Y.; Sun, W.-H.; Redshaw, C. *Dalton Trans.* **2013**, *42*, 9176–9187.
15. Yuan, H.; Yoo, W.-J.; Miyamura, H.; Kobayashi, S. *J. Am. Chem. Soc.* **2012**, *134*, 13970–13973.
16. Wöckel, S.; Galezowska, J.; Dechert, S.; Meyer, F. *Inorg. Chem.* **2012**, *51*, 2486–2493.
17. Smith, S. J.; Peralta, R. A.; Jovito, R.; Horn, A.; Bortoluzzi, A. J.; Noble, C. J.; Hanson, G. R.; Stranger, R.; Jayaratne, V.; Bortolotto, T.; Razzera, G. *Inorg. Chem.* **2012**, *51*, 2065–2078.

18. Almaraz, E.; de Paula, Q. a; Liu, Q.; Reibenspies, J. H.; Darensbourg, M. Y.; Farrell, N. P. *J. Am. Chem. Soc.* **2008**, *130*, 6272–6280.
19. Jaime, E.; Weston, J. *Eur. J. Inorg. Chem.* **2006**, *2006*, 793–801.
20. Bauer-Siebenlist, B.; Dechert, S.; Meyer, F. *Chemistry* **2005**, *11*, 5343–5352.
21. Linck, R. C.; Spahn, C. W.; Rauchfuss, T. B.; Wilson, S. R. *J. Am. Chem. Soc.* **2003**, *125*, 8700–8701.
22. Manotti Lanfredi, A. M.; Tiripicchio, A.; Ugozzoli, F.; Ghedini, M; Neve, F. *J. Chem. Soc. Dalton Trans.* **1988**, 651.
23. Ghedini, M.; Longeri, M.; Neve, F. *Inorg. Chim. Acta.* **1987**, *132*, 223.
24. Ghedini, M.; Neve, F.; Longeri, M.; Bruno, M.C. *Inorg. Chim. Acta.* **1988**, *149*, 131.
25. Tsukada, N.; Sato, T.; Mori, H.; Sugawara, S.; Kabuto, C.; Miyano, S.; Inoue, Y. *J. Organomet. Chem.* **2001**, *627*, 121-126.
26. Thébault, F.; Blake, A.J.; Wilson, C.; Champness, N.R.; Schröder, M. *New J. Chem.* **2006**, *30*, 1498-1508.
27. Monaghan, P. K.; Puddephatt, R. J. *Organometallics* **1984**, *3*, 444–449.
28. Monaghan, P. K.; Puddephatt, R. J. *Dalt. Trans.* **1988**, *1*, 595–599.
29. Rendina, L. M.; Puddephatt, R. J. *Chem. Rev.* **1997**, *97*, 1735–1754.
30. Rostovtsev, V. V; Henling, L. M.; Labinger, J. A; Bercaw, J. E. *Inorg. Chem.* **2002**, *41*, 3608–3619.
31. Zhang, F.; Broczkowski, M. E.; Jennings, M. C.; Puddephatt, R. J. *Can. J. Chem.* **2005**, *83*, 595–605.
32. Bonnington, K. J.; Jennings, M. C.; Puddephatt, R. J. *Organometallics* **2008**, *27*, 6521–6530.
33. McKeown, B. a; Gonzalez, H. E.; Friedfeld, M. R.; Gunnoe, T. B.; Cundari, T. R.; Sabat, M. *J. Am. Chem. Soc.* **2011**, *133*, 19131–19152.
34. Hoseini, S. J.; Nasrabadi, H.; Nabavizadeh, S. M.; Rashidi, M.; Puddephatt, R. J. *Organometallics* **2012**, *31*, 2357–2366.
35. Pellarin, K. R.; McCready, M. S.; Sutherland, T. I.; Puddephatt, R. J. *Organometallics* **2012**, *31*, 8291–8300.

36. Pellarin, K. R.; McCready, M. S.; Puddephatt, R. J. *Organometallics* **2012**, *31*, 6388–6394.
37. Calvet, T.; Crespo, M.; Font-Bardía, M.; Jansat, S.; Martínez, M. *Organometallics* **2012**, *31*, 4367–4373.
38. Momeni, B. Z.; Rashidi, M.; Jafari, M. M.; Patrick, B. O.; Abd-El-Aziz, A. S. *J. Organomet. Chem.* **2012**, *700*, 83–92.
39. Pellarin, K. R.; McCready, M. S.; Puddephatt, R. J. *Dalton Trans.* **2013**, *42*, 10444–10453.
40. Pellarin, K. R.; Puddephatt, R. J. *Organometallics* **2013**, *32*, 3604–3610.
41. Safa, M.; Puddephatt, R. J. *J. Organomet. Chem.* **2013**, *724*, 7–16.
42. Fraser, C. S.; Jenkins, H.; Jennings, M. C.; Puddephatt, R. J. *Organometallics* **2000**, *19*, 1635–1642.
43. Safa, M. A.; Abo-Amer, A.; Borecki, A.; Cooper, B. F. T.; Puddephatt, R. J. *Organometallics* **2012**, *31*, 2675–2681.
44. Au, R. H. W.; Fraser, C. S. a.; Eisler, D. J.; Jennings, M. C.; Puddephatt, R. J. *Organometallics* **2009**, *28*, 1719–1729.
45. Abo-Amer, A.; Puddephatt, R.J. *J. Inorg. Organomet. Polym.* **2014**, *24*, 114–120.
46. Moustafa, M. E.; McCready, M. S.; Puddephatt, R. J. *Organometallics* **2013**, *32*, 2552–2557.
47. Brandsma, L.; Verkruijsse, H.D. *Synthesis.* **1978**, *4*, 290.
48. Sauer, J.; Heldmann, D.K.; Hetzenegger, J.; Krauthan, J.; Sichert, H.; Schuster, J. *Eur. J. Org. Chem.* **1998**, *12*, 2885–2896.
49. El-Qisairi, A.K; Qaseer, H.A.; Zaghal, M.H.; Kana'n, S.; Atfah, M.A. *J. Coord. Chem.* **2007**, *60*, 1165–1171.
50. Hill, G.; Irwin, M. J.; Levy, C. J.; Rendina, L. M.; Puddephatt, R. J. *Inorg. Synth.* **1998**, *32*, 149–153.
51. Monaghan, P.K.; Puddephatt, R.J. *Organometallics.* **1984**, *3*, 444–449.
52. McCready, M. S.; Puddephatt, R. J. *Dalton Trans.* **2012**, *41*, 12378–12385.

53. Janzen, M.C.; Jennings, M.C.; Puddephatt, R.J. *Inorg. Chem.* **2001**, *40*, 1728-1729.
54. Kuyper, J. *Inorg. Chem.* **1978**, *17*, 99–101.
55. Janzen, M.C.; Jennings, M.C.; Puddephatt, R.J. *Inorg. Chim. Acta.* **2005**, *358*, 1614-1622.
56. Bandoli, G.; Caputo, P.A.; Intini, F.P.; Sivo, M.F.; Natile, G. *J. Amer. Chem. Soc.* **1997**, *119*, 10370.
57. Cotton, F.A.; Wilkinson, G. *Advanced Inorganic Chemistry*, sixth ed., New York, 1999.
58. Haiduc, I.; Edelman, F.T. *Supramolecular Organometallic Chemistry*, Wiley-VCH, New York, 1999.
59. Werner, M.; Wagner, C.; Steinborn, D. *J. Organomet. Chem.* **2009**, *694*, 190–198.
60. Safa, M.; Jennings, M. C.; Puddephatt, R. J. *Organometallics* **2012**, *31*, 3539–3550.
61. Nabavizadeh, S. M.; Amini, H.; Rashidi, M.; Pellarin, K. R.; McCready, M. S.; Cooper, B. F. T.; Puddephatt, R. J. *J. Organomet. Chem.* **2012**, *713*, 60–67.
62. Yahav, A.; Goldberg, I.; Vigalok, A. *Organometallics* **2005**, *24*, 5654–5659.
63. Beek, J. A. M. Van; Koten, I. G. Van; Smeets, J.; Spek, A. L. *J. Am. Chem. Soc.* **1986**, *108*, 5010–5011.
64. Abo-amer, A.; McCready, M. S.; Zhang, F.; Puddephatt, R. J. *Can. J. Chem.* **2012**, *54*, 46–54.
65. Aseman, M. D.; Rashidi, M.; Nabavizadeh, S. M.; Puddephatt, R. J. *Organometallics* **2013**, *32*, 2593–2598.
66. Zhang, F.; Prokopchuk, E.M.; Broczkowski, M.E.; Jennings, M.C.; Puddephatt, R.J. *Organometallics.* **2006**, *25*, 1583-1591.
67. Zhang, F.; Jennings, M. C.; Puddephatt, R. J. *Organometallics* **2004**, *23*, 1396–1404.
68. Periana, R.A.; Taube, D.J.; Gamble, S.; Taube, H.; Satoh, T.; Fujii, H. *Science.* **1998**, *280*, 560.
69. *APEX 2, Crystallography software package*; Bruker AXS: Madison, WI, 2005.
70. *SAINT, Data Reduction Software*; Bruker AXS: Madison, WI, 1999.

71. Sheldrick, G. M. *SADABS v.2.01, Area Detector Absorption Correction Program*; Bruker AXS: Madison, WI, 2006.
72. Nonius (1998). *COLLECT*. Nonius BV, Delft, The Netherlands.
73. Otwinowski, Z.; Minor, W. *Methods in Enzymology*. 1997, Vol. 276, *Macromolecular Crystallography, Part A*, edited by C. W. Carter Jr & R. M. Sweet, p 307-326. New York: Academic Press.
74. Sheldrick, G. M. *SHELXS, program for solution of crystal structures*. *Acta Cryst. A* **64**, 2008, 112-122.
75. Sheldrick, G. M. *SHELXL, program for refinement of crystal structures*. *Acta Crystallogr., Section A*. **2008**, 64, 112-122.

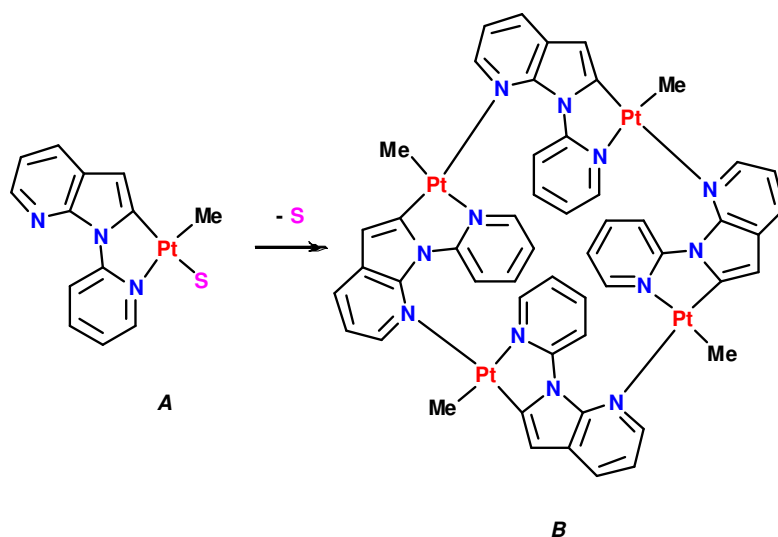
CHAPTER 3

Self-assembly of Isomeric Clamshell Dimers of Platinum(II)

A version of this chapter has been published: McCready, M.S.; Puddephatt, R.J. *Dalton Trans.*, **2012**, 41: 12378-12385.

3.1 Introduction

The use of self-assembly techniques for the synthesis of complex structures continues to be an active field of research [1-8]. Of specific interest is the use of this powerful strategy towards the synthesis of many discrete two-dimensional and three-dimensional metallo-supramolecular architectures [9-21]. Recently, many of these highly complex metallo-supramolecular architectures have been shown to perform functions ranging from the encapsulation of substrates to catalyzing reactions within their cavities [22-30]. Through the incorporation of organometallic precursor complexes, highly specified structures have been prepared. Rationally designed organometallic precursor complexes can arrange through self-association of monomer units, yielding highly specified metallosupramolecular complexes. These architectures typically arrange through the utilization of highly selective self-sorting methods [1-3,31,32]. In the self-association of coordination complexes, the method typically relies on the reversible formation and cleavage of labile metal-ligand bonds. This reversibility of formation consequently allows for self-sorting and error correction to occur, promoting the formation of the thermodynamically favoured isomer selectively [1-3,33,34]. For example, the monomer fragment **A** shown in scheme 3.1 selectively forms a macrocyclic tetramer **B** [35].



Scheme 3.1. Selective formation of a macrocycle. "S" indicates a weakly associated solvent molecule.

This method of self-sorting predominantly allows for the preparation of the

thermodynamically favoured isomer of a complex. This in turn yields very few examples in the literature where less stable isomers, (kinetic mistakes), can be isolated [1-3,33,34]. More typically, one observes the formation of the kinetically favoured isomers as intermediates during the isomerization process on route to the formation of the thermodynamically favoured isomer [36-40]. For example, the reaction of dithiols with AsCl_3 occurs through intermediate steps to give macrocycles such as the mixture of *syn*- and *anti-C* (Figure 3.1), of which the *syn* isomer was structurally characterized. However, in this case the self-association of both isomers cannot be accomplished selectively [33].

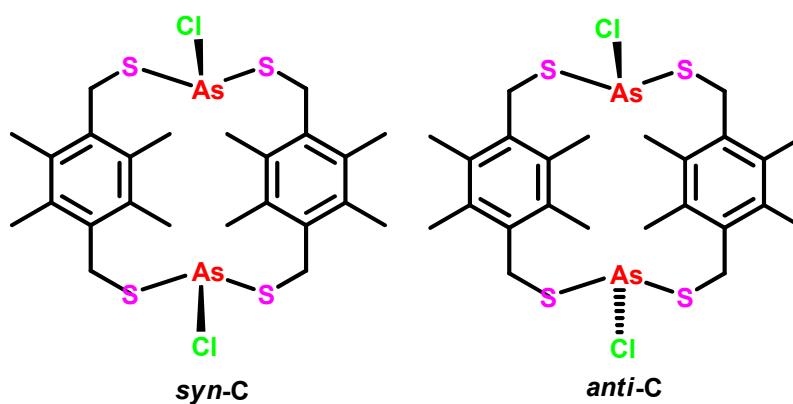


Figure 3.1. Isomers formed by self-assembly.

Square planar platinum(II) complexes have long been known to undergo ligand substitution with retention of stereochemistry, the selectivity of which is often determined by the *trans*-effect [41-43]. Through the application of the principles of the *trans*-effect, many simple isomeric complexes of platinum(II) have been synthesized [44-47]. Specifically this technique is highly useful in medicine as the products of these processes are typically inert to *cis-trans* isomerization [48]. Figure 3.2 gives examples *D* and *E* of binuclear platinum(II) complexes which exhibit isomerism [46,47].

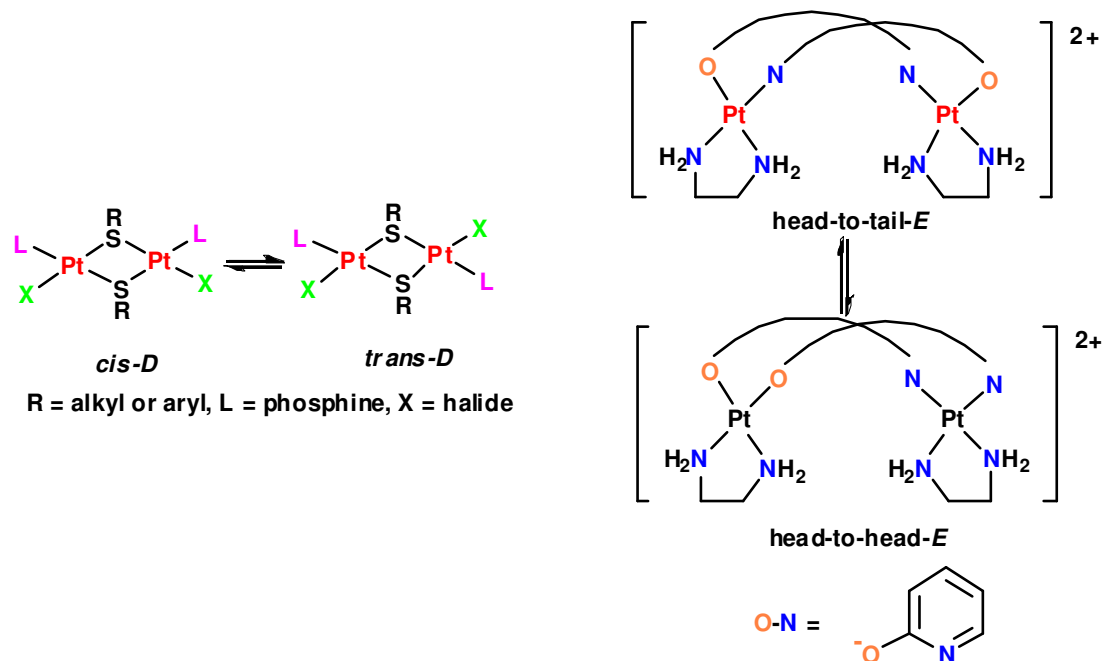


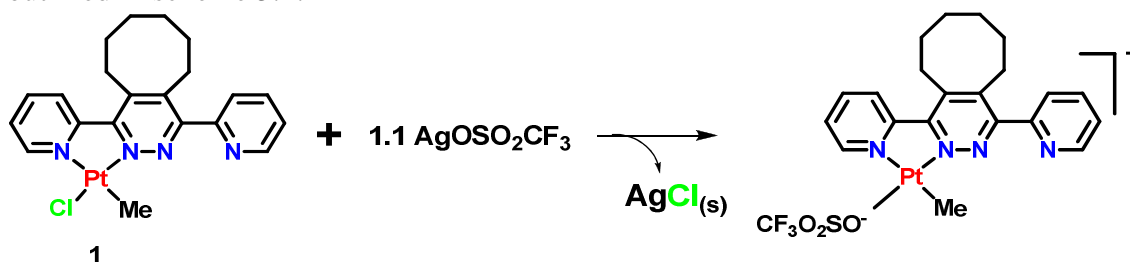
Figure 3.2. Isomeric diplatinum(II) complexes.

A synthetic methodology based on *cis-trans* isomerism at platinum(II) should be applicable in the field of self-assembly. We postulate that the utilization of this isomerization at platinum(II) should provide an avenue by which highly-selective metallosupramolecular architectures could be designed rationally, however we are not aware of any examples of complex isomeric structures being obtained in this way [1-3,35-40,44-47]. This chapter outlines the synthesis, isolation and structural characterization of an isomeric pair of binuclear organoplatinum “clamshell” complexes. These complexes are prepared in a logical way from simple platinum(II) precursor complexes **1** and **2**. The formation of both isomeric complexes is monitored by multinuclear NMR spectroscopy, and the dimeric structures have been characterized crystallographically. Through the characterization of reaction intermediates, a general mechanism of the isomerization process and formation of the dimer complexes is presented. The reversibility of formation of the dimeric “clamshell” complexes is also evaluated. These dimeric platinum(II) complexes are prepared in a logical and rational way and so establish a useful synthetic protocol for self-assembly of isomeric self-assembled molecular materials.

3.2 Synthesis of the clamshell dimers

3.2.1 Synthesis of *endo,endo*-[Pt₂Me₂(μ₂-κ³-6-dppd)₂](OTf)₂

In an effort to explore the ability of these platinum complexes of **6-dppd** to activate C-H bonds, a monomethylplatinum(II) complex with a weakly coordinating ligand needed to be synthesized. This would in turn allow for a vacant coordination site to become available at the platinum(II) center leading to the potential of activating C-H bonds in a similar manner to that reported in the literature [49-53]. In the case of complex **1**, this would require the abstraction of the chloride ligand, in turn generating the vacant coordination site which would be occupied by the weakly coordinating species, as outlined in scheme 3.2.



Scheme 3.2. Proposed reaction scheme for the formation of a monomethylplatinum(II) complex with a weakly coordinating ligand from complex **1**.

To accomplish this, a 10% excess of silver trifluoromethanesulfonate was added to an acetone-*d*₆ solution of complex **1** and the mixture was allowed to stir for 10 minutes. The originally orange solution gradually turned yellow with presence of the silver chloride precipitate forming. After filtering the silver chloride out of the solution, ¹H NMR spectroscopy was utilized to characterize the product of the reaction. The ¹H NMR spectrum, figure 3.3, indicated the presence of a single methylplatinum resonance at 1.54 ppm with ²J(PtH) = 75 Hz which was consistent with the formation of monomethylplatinum(II) product. The aromatic region of the spectrum contained eight distinct resonances arising from the pyridyl protons, which supports the formation of an unsymmetrical product. The presence of ¹⁹⁵Pt satellites on both resonances associated with the *ortho* hydrogens would suggest that a complex, in which both pyridyl groups are bonded to a platinum center is formed. The values associated with the couplings are

significantly different, $^3J(\text{PtH}) = 34 \text{ Hz}$ for the resonance furthest downfield at 9.05 ppm and $^3J(\text{PtH}) = 20 \text{ Hz}$ for the resonance slightly more upfield at 8.59 ppm. The values of the couplings would suggest that each pyridyl ring is positioned *trans* to a different group. The ^1H NMR spectrum also possessed three sharp multiplet resonances in the methylene region which had not been observed for either complex **1** or **2**.

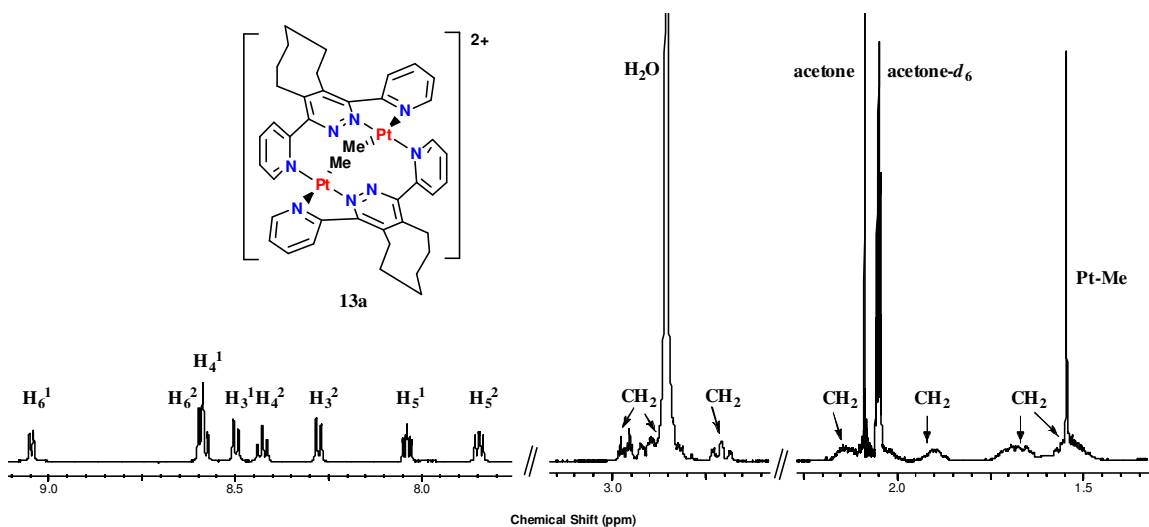
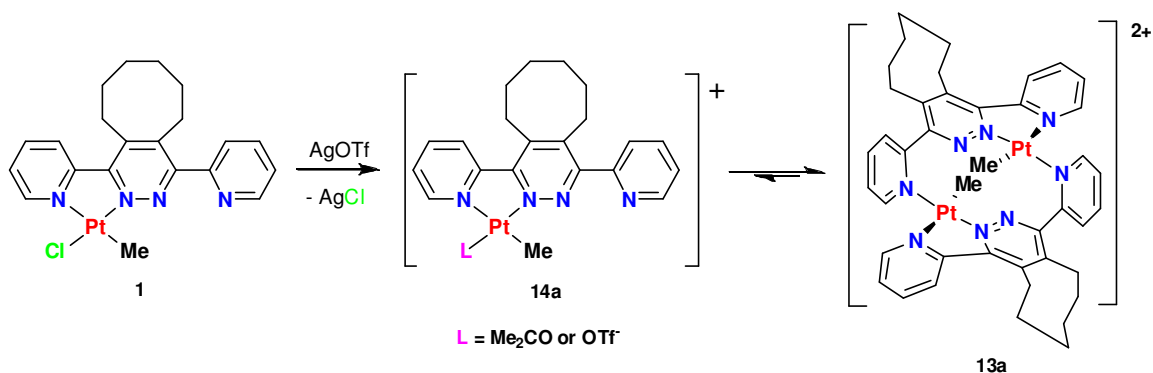


Figure 3.3. ^1H NMR spectrum of complex **13a**, *endo,endo*- $[\text{Pt}_2\text{Me}_2(\mu_2\text{-}\kappa^3\text{-6-dppd})_2](\text{OTf})_2$ in acetone- d_6 . Conventional labelling schemes are utilized for pyridyl rings. CH_2 represents the protons of the cyclooctyl ring. Residual solvent signals for moist acetone are labelled.

It was not until crystals suitable for single crystal X-ray analysis were discovered within the NMR tube, that the identity of the product was able to be determined. It was found that upon abstraction of the chloride anion by the silver trifluoromethanesulfonate, rather than the trifluoromethanesulfonate anion occupying the vacant coordination site, the dangling pyridyl group of a second equivalent of the $[\text{PtMe}(6\text{-dppd})]^+$ generated *in situ* ligates the platinum center. This allows for the formation of a dimeric clam-shell like complex, $[\text{Pt}_2\text{Me}_2(6\text{-dppd})_2]^{2+}[\text{OSO}_2\text{CF}_3]_2^-$ **13a**, as depicted in scheme 3.3. The solid state structure of complex **13a**, figure 3.4, aids in the complete assignment of the ^1H NMR spectrum, specifically portraying the cause of the *ortho*-pyridyl resonances both possessing ^{195}Pt satellites. In order to facilitate coordination of the monomer units, it appears as though the dangling pyridyl group coordinates to the platinum center of the

second monomer in a manner resulting in a $75.8(3)^\circ$ rotation of the pyridyl group away from the planar orientation expected for the conjugated ligand system.



Scheme 3.3. Synthesis of *endo,endo*- $[\text{Pt}_2\text{Me}_2(\mu_2\text{-}\kappa^3\text{-6-dppd})_2](\text{OTf})_2$, **13a**, through the self-assembly of two equivalents of the monomer **14a**.

The molecular structure of complex **13a** allows one to conclude that the dimer exhibits significant steric constraint. Specifically, the methyl groups being coordinated in the inward directed position at the platinum(II) center leads to a distortion of the typically square planar arrangement of Pt1 and Pt1A. This arrangement attributes to the methyl group deviating from the expected square planar geometry by 9.4° above the plane as a consequence of the strain placed on the platinum center by the dangling pyridyl group of the second $[\text{PtMe}(6\text{-dppd})]^+$ monomer. The positioning of the methyl group also leads to a somewhat stacked arrangement of the two monomer units, further resulting in both methyl groups being directed into the same void opposite the bulky cyclooctene ring. This arrangement prevents the ability of the clam-shell structure to open at a wider angle in an effort to alleviate a significant amount of the steric constraint. It appears that, upon ligation of the dangling pyridyl group to the adjacent platinum center, the pyridyl group bends the platinum atom away from the plane of the chelate. This functions to introduce a twisting of the conformation of the pyridyl and pyridazine rings of the five-membered chelate. Complex **1** and **2** both illustrate that the pyridyl and pyridazine rings, which contribute to the five-membered chelate formed upon ligation to the platinum center, exist in a coplanar arrangement with minor twisting of either ring relative to the other. In the case of **13a**, there is a loss of planarity which is evidenced by a distortion of the

pyridyl group from coplanarity with the pyridazine group by 26.4° . This distortion, along with the steric restriction imposed upon complex **13a**, results in a narrow and congested clam-shell type structure with a distance of 3.004 \AA between monomer units as measured from Pt1 to C9A, the pyridazine carbon directly across from the platinum center, and an α angle of 31.6° between planes.

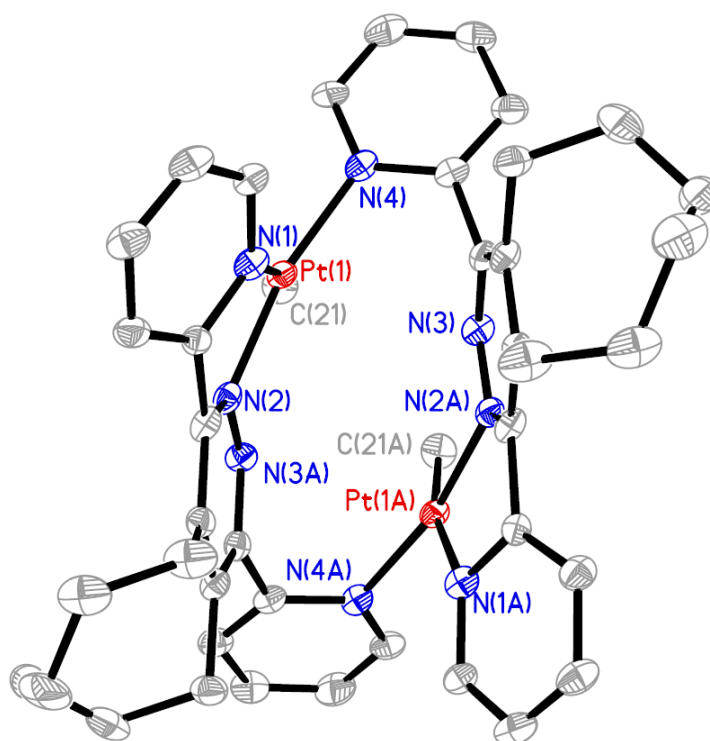


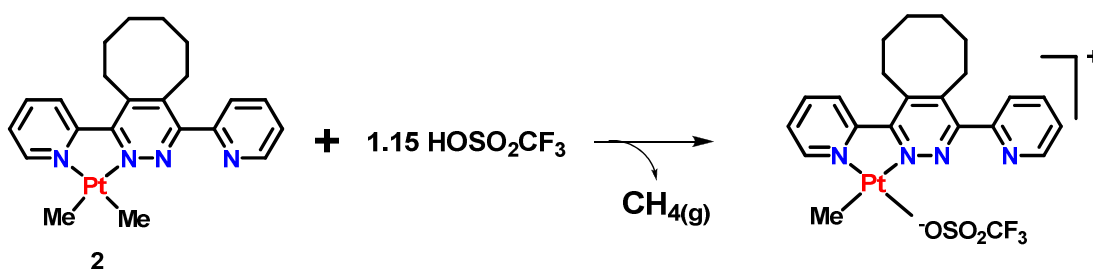
Figure 3.4. Molecular structure of complex **13a**, with an atomic numbering scheme (hydrogen atoms, acetone molecules and trifluoromethanesulfonate anions are omitted for clarity).

Table 3.1: Bond lengths [Å] and angles [°] for *endo,endo*-[Pt₂Me₂(μ₂-κ³-6-dppd)₂](OTf)₂, 13a.

Pt(1)-N(1)	2.102(9)	Pt(1)-N(2)	2.005(9)
Pt(1)-N(4)	2.028(9)	Pt(1)-C(21)	2.023(13)
N(1)-Pt(1)-N(2)	78.4(4)	N(1)-Pt(1)-N(4)	102.5(4)
N(1)-Pt(1)-C(21)	167.4(4)	N(2)-Pt(1)-N(4)	167.8(3)
N(2)-Pt(1)-C(21)	96.1(4)	N(4)-Pt(1)-C(21)	85.3(4)
N(1)-C(5)-C(6)-N(2)	26.4(13)	N(3)-C(9)-C(10)-N(4)	75.8(12)

3.2.2 Synthesis of *exo,exo*-[Pt₂Me₂(μ₂-κ³-6-dppd)₂](OTf)₂

Following the same research motivation employed in the reaction of complex **1** with silver trifluoromethanesulfonate, (scheme 3.2), again the synthesis of a monomethylplatinum(II) complex containing a weakly coordinating ligand was attempted. To accomplish this, an acetone solution of complex **2** was treated with 1.15 equivalents of trifluoromethanesulfonic acid at 0°C, with rapid stirring for 5 minutes, after which an obvious colour change from red to yellow was observed. This reaction is outlined in scheme 3.4.



Scheme 3.4. Proposed reaction scheme for the formation of a monomethylplatinum(II) complex with a weakly coordinating ligand from complex **2**.

The reaction was allowed to stir for an additional two hours before the volume was reduced *in vacuo* yielding a yellow oil. This oil was dissolved in minimal acetone and layered with 1 mL of pentane leading to the precipitation of a yellow solid which was isolated by Hirsch filtration and washed with 1 mL of pentane. The product was then characterized by ^1H NMR spectroscopy, figure 3.5, which confirmed the presence of a single methylplatinum resonance at 1.20 ppm with $^2J(\text{PtH}) = 74$ Hz. The aromatic region of the spectrum again contained eight resonances arising from the pyridyl protons. Similar to the spectrum of complex **13a**, the resonances associated with the *ortho* hydrogens on both pyridyl rings exhibit the presence of ^{195}Pt satellites. The values of the couplings are significantly different, $^3J(\text{PtH}) = 34$ Hz for the resonance furthest downfield at 9.06 ppm and $^3J(\text{PtH}) = 21$ Hz for the resonance slightly more upfield at 8.88 ppm. The values of the couplings would suggest that each pyridyl ring is positioned *trans* to a different group. The ^1H NMR spectrum indicated that the proposed methylplatinum(II) species with a weakly coordinating ligand was not the product of the reaction, rather a complex in which both pyridyl groups were bonded to a platinum center was again formed. Again the presence of sharp multiplets in the methylene region was observed, leading one to believe that a dimeric species similar to complex **13a** was formed. Single crystals of the product suitable for X-ray diffraction analysis were produced by various solvent combinations resulting in three different molecular structures of the product.

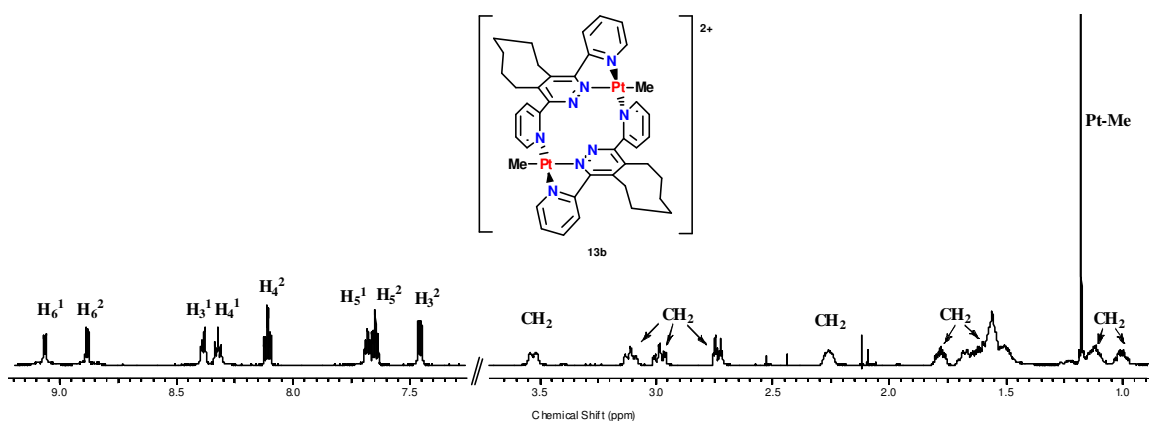
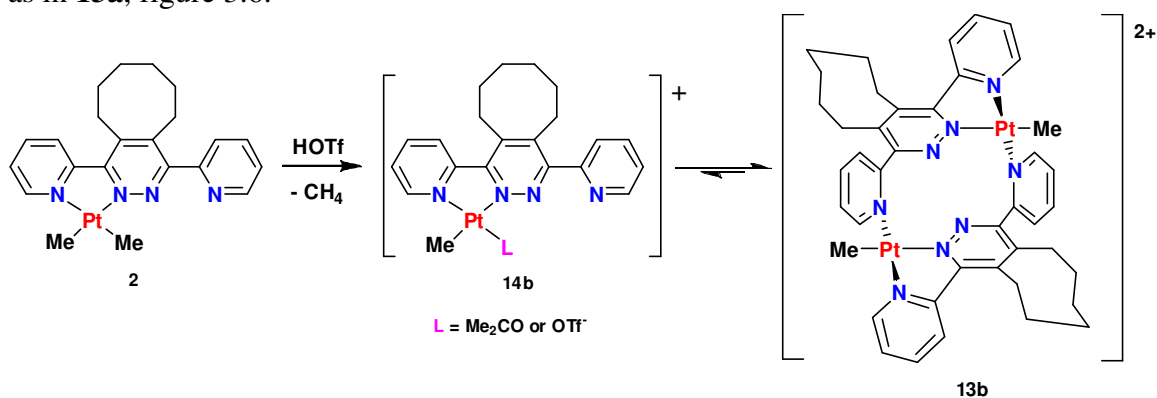


Figure 3.5. ^1H NMR spectrum of complex **13b**, *exo,exo*- $[\text{Pt}_2\text{Me}_2(\mu_2\text{-}\kappa^3\text{-6-dppd})_2](\text{OTf})_2$ in CD_2Cl_2 . Conventional labelling schemes are utilized for pyridyl rings. CH_2 represents the protons of the cyclooctyl ring.

The single crystal X-ray diffraction analysis of the product supported the previous assumption and confirmed the formation of a dimeric species in which 2 equivalents of $[\text{PtMe}(\text{6-dppd})]^+$ combined to form the complex $[\text{Pt}_2\text{Me}_2(\text{6-dppd})_2]^{2+}[\text{OSO}_2\text{CF}_3]_2^-$, complex **13b**. Depicted in figures 3.6 through 3.8 are the solid state structures of the various solvates of **13b**. The obvious difference between the three structures; **13b**• $2(\text{C}_3\text{H}_6\text{O})\cdot(\text{H}_2\text{O})$, **3b**• $2(\text{C}_3\text{H}_6\text{O})$, and **13b**• (CH_2Cl_2) , is the incorporation of solvent molecules into the unit cell and within the interior void of the clamshell structure. The confirmation of the structure of **13b** supports the findings of the ^1H NMR in which both pyridyl groups are coordinated to a platinum center. Again, the dangling pyridyl group which is initially not coordinating to the platinum center in the $[\text{PtMe}(\text{6-dppd})]^+$ monomer, coordinates to the platinum(II) center by presumably displacing the weakly coordinating trifluoromethanesulfonate group. This dimeric species thus forms in an analogous manner to that of complex **13a** as is depicted in scheme 3.5. A significant difference is noted upon inspection of the stereochemistry at the platinum center. It becomes evident that in complex **13b**, the methyl group occupies the outward directed coordination site of the square planar platinum(II) center rather than the inward position as in **13a**, figure 3.6.



Scheme 3.5. Synthesis of *exo,exo*- $[\text{Pt}_2\text{Me}_2(\mu_2\text{-}\kappa^3\text{-6-dppd})_2](\text{OTf})_2$, **13b**, through the self-assembly of two equivalents of the monomer **14b**.

The different stereochemistry at platinum suggests the formation of two isomers of $[\text{Pt}_2\text{Me}_2(\text{6-dppd})_2]^{2+}$, complexes **13a** and **13b**. The coordination mode exhibited by complex **13b**, appears to produce a dimer of $[\text{PtMe}(\text{6-dppd})]^+$ monomers which is significantly less hindered and constrained than complex **13a**. Further observation of the structure of **13b** shows that both of the methyl groups are positioned on opposite sides of

the dimer and are oriented outward, presumably in an effort to alleviate some of the steric constraint on the system. The position of these methyl groups allows the dangling pyridyl group to ligate the platinum center in a much more favourable manner. This pyridyl group coordinates to the platinum center of the second monomer unit in a mode that results in a $74.0(8)^\circ$ rotation away from the planar orientation expected for the conjugated system in the acetone solvate. ^1H - ^1H NOESY NMR analysis confirmed that the methyl group is directed outward in solution and is not simply a consequence of crystallizing in the solid state. As can be observed from the solid state structure of complex **13b**, there is significantly less steric constraint placed on the system compared to that for **13a**. This is best observed by looking again at the geometry of the platinum centers. Both platinum centers in the acetone solvate exhibit a nearly ideal square planar geometry, with only a 1.2° distortion of the nitrogen atom of the dangling pyridyl group from planarity. This value is significantly less than the distortion observed for complex **13a**. In complex **13b**, the methyl groups are directed outward, away from the center of the dimeric compound. In this conformation, the monomer units coordinate in a manner which alleviates significant steric strain leading to a larger α angle of 50.1° and an increased separation between monomer units with a Pt2 and C30 distance of 3.174 \AA .

Upon closer comparison of the molecular structures of **13b**• $2(\text{C}_3\text{H}_6\text{O})$ • (H_2O) , **13b**• $2(\text{C}_3\text{H}_6\text{O})$, and **13b**• (CH_2Cl_2) , figures 3.6, 3.7 and 3.8 respectively, it becomes apparent as to why these structures possess different unit cells. The most significant and obvious difference between the three structures of **13b** is the incorporation of different solvent molecules and solvent mixtures. The two most similar structures, **13b**• $2(\text{C}_3\text{H}_6\text{O})$ • (H_2O) and **13b**• $2(\text{C}_3\text{H}_6\text{O})$, differ only by the incorporation of an additional water molecule which forms hydrogen bonding interactions with the trifluoromethanesulfonate anions. The bond parameters associated with the platinum(II) centers in each structure of **13b** are all very similar, as well each structure maintains a nearly square planar arrangement at the platinum center. The various parameters associated with the structures of **13b** are outlined in table 3.5 for comparison.

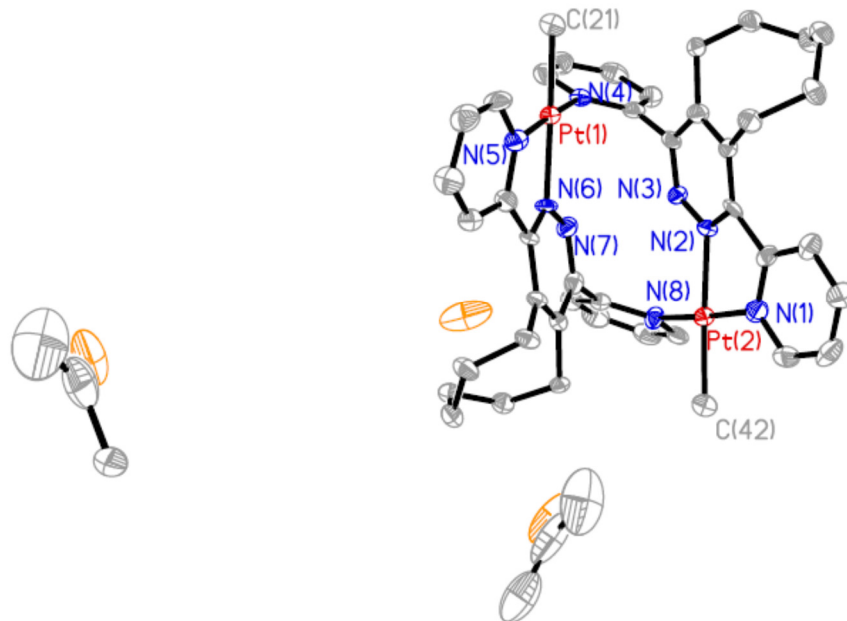


Figure 3.6. Molecular structure of complex **13b**•2(C₃H₆O)•(H₂O), (hydrogen atoms, and trifluoromethanesulfonate anions are omitted for clarity). Acetone solvent molecules are depicted as is the H₂O solvent molecule as an isolated oxygen atom.

Table 3.2: Bond lengths [Å] and angles [°] for *exo,exo*-[Pt₂Me₂(μ₂-κ³-6-dppd)₂](OTf)₂•2(C₃H₆O)•(H₂O), **13b•2(C₃H₆O)•(H₂O).**

Pt(1)-N(1)	2.014(4)	Pt(2)-N(5)	2.002(5)
Pt(1)-N(2)	2.091(4)	Pt(2)-N(4)	2.024(4)
Pt(1)-N(8)	2.031(4)	Pt(2)-N(6)	2.070(4)
Pt(1)-C(21)	2.047(5)	Pt(2)-C(42)	2.042(6)
N(1)-Pt(1)-N(8)	176.75(17)	N(5)-Pt(2)-N(4)	178.35(17)
N(1)-Pt(1)-N(2)	78.32(17)	N(5)-Pt(2)-N(6)	78.28(17)
N(8)-Pt(1)-N(2)	99.65(17)	N(4)-Pt(2)-C(N6)	100.22(17)
N(1)-Pt(1)-C(21)	95.9(2)	N(5)-Pt(2)-C(42)	96.0(2)
N(2)-Pt(1)-C(21)	173.4(2)	N(6)-Pt(2)-C(42)	174.1(2)
N(8)-Pt(1)-C(21)	86.3(2)	N(4)-Pt(2)-C(42)	85.5(2)
N(5)-C(26)-C(27)-N(6)	0.3(6)	N(3)-C(9)-C(10)-N(4)	-99.5(6)
N(1)-C(5)-C(6)-N(2)	18.0(6)	N(7)-C(30)-C(31)-N(8)	86.9(6)

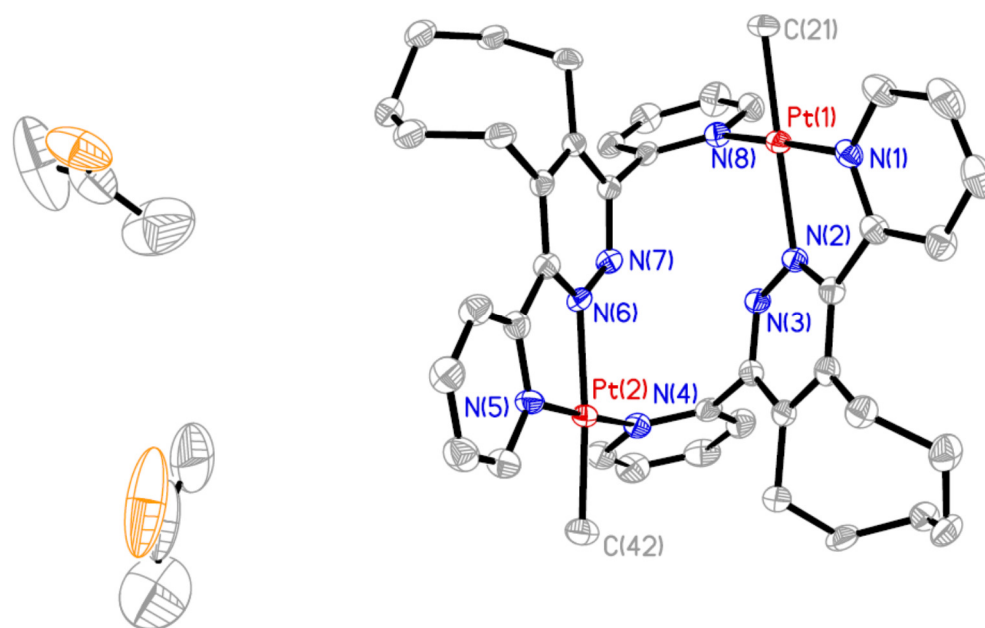


Figure 3.7. Molecular structure of complex **13b•2(C₃H₆O)**, (hydrogen atoms, and trifluoromethanesulfonate anions are omitted for clarity). Acetone solvent molecules are depicted.

Table 3.3: Bond lengths [Å] and angles [°] for *exo,exo*-[Pt₂Me₂(μ₂-κ³-6-dppd)₂](OTf)₂•2(C₃H₆O), **13b•2(C₃H₆O).**

Pt(1)-N(5)	2.0208(15)	Pt(2)-N(1)	1.9958(15)
Pt(1)-N(4)	2.0390(15)	Pt(2)-N(2)	2.1023(15)
Pt(1)-N(6)	2.0904(15)	Pt(2)-N(8)	2.0275(15)
Pt(1)-C(21)	2.091(9)	Pt(2)-C(42)	2.078(9)
N(5)-Pt(1)-N(4)	175.6(6)	N(1)-Pt(2)-N(8)	176.7(3)
N(5)-Pt(1)-N(6)	78.2(6)	N(1)-Pt(2)-C(42)	96.1(3)
N(4)-Pt(1)-N(6)	97.7(6)	N(8)-Pt(2)-C(42)	87.1(3)
N(5)-Pt(1)-C(21)	96.7(3)	N(1)-Pt(2)-N(2)	77.9(3)
N(4)-Pt(1)-C(21)	87.4(3)	N(8)-Pt(2)-N(2)	99.0(3)
N(6)-Pt(1)-C(21)	174.9(3)	C(42)-Pt(2)-N(2)	173.7(3)
N(5)-C(26)-C(27)-N(6)	12.8(1)	N(3)-C(9)-C(10)-N(4)	104.7(7)
N(1)-C(5)-C(6)-N(2)	10.2(9)	N(7)-C(30)-C(31)-N(8)	106.0(8)

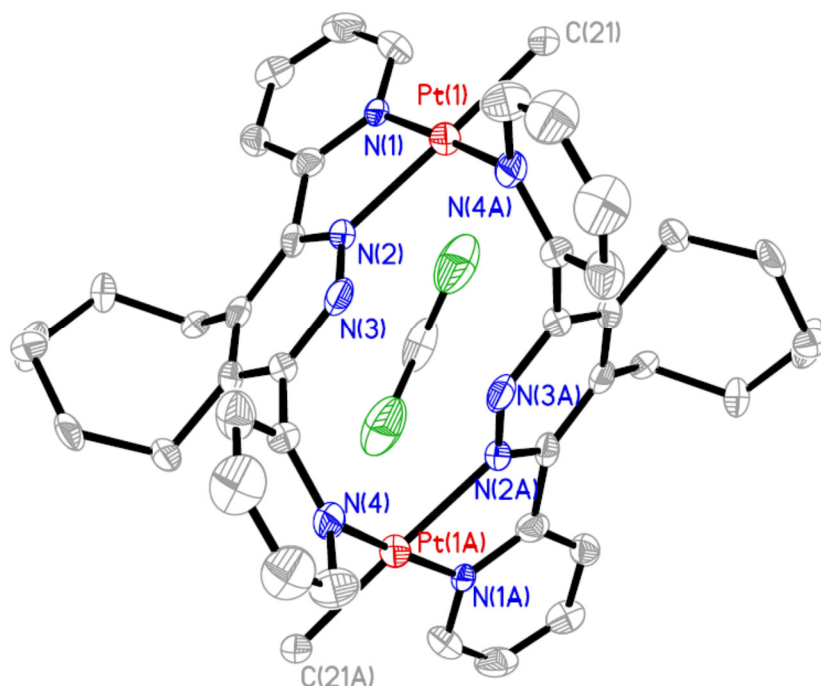


Figure 3.8. Molecular structure of complex **13b**·CH₂Cl₂, (hydrogen atoms, and trifluoromethanesulfonate anions are omitted for clarity). The dichloromethane solvent molecule is depicted.

Table 3.4: Bond lengths [Å] and angles [°] for *exo,exo*-[Pt₂Me₂(μ₂-κ³-6-dppd)₂](OTf)₂·CH₂Cl₂, **13b·CH₂Cl₂**

Pt(1)-N(1)	2.010(7)	Pt(1)-N(2)	2.076(6)
Pt(1)-N(4)	2.020(7)	Pt(1)-C(21)	2.073(7)
N(1)-Pt(1)-N(2)	78.3(3)	N(1)-Pt(1)-N(4)	175.7(2)
N(1)-Pt(1)-C(21)	96.7(3)	N(2)-Pt(1)-N(4)	98.5(3)
N(2)-Pt(1)-C(21)	174.9(3)	N(4)-Pt(1)-C(21)	86.5(3)
N(1)-C(5)-C(6)-N(2)	13.9(9)	N(3)-C(9)-C(10)-N(4)	-106.8(8)

Table 3.5: Selected parameters for comparison of $13b \cdot 2(C_3H_6O) \cdot (H_2O)$, $13b \cdot 2(C_3H_6O)$, and $13b \cdot CH_2Cl_2$.

	$13b \cdot 2(C_3H_6O) \cdot (H_2O)$	$13b \cdot 2(C_3H_6O)$	$13b \cdot (CH_2Cl_2)$
Deviation from square planar geometry ($^{\circ}$)	1.2	2.3	1.4
α Angle ($^{\circ}$)	50.1	57.1	57.1
Distance of Solvent from platinum(II) centers (\AA)	Pt1-O7A = 4.385 Pt2-O7A = 4.255	Pt1-O8A = 4.226 Pt2-O8A = 4.028	Pt1-Cl1 = 4.202

Another striking similarity is the incorporation of a solvent molecule within the open pocket of the clam-shell structures. This is best depicted in figure 3.9, which shows both the incorporation of the solvent molecules within the clam-shell structure, as well as the degree to which each structure is required to open in order to accommodate this molecule. Specifically in the case of the structures of $13b \cdot 2(C_3H_6O) \cdot (H_2O)$ and $13b \cdot 2(C_3H_6O)$, an acetone molecule resides within the pocket of each structure. In the case of $13b \cdot 2(C_3H_6O)$, the acetone molecule is found significantly closer to the platinum centers, deep within the pocket of the clam-shell, leading to a wider opening angle and some distortion of the backbone structure. This acetone molecule is positioned roughly 0.2 \AA closer to the platinum centers in $13b \cdot 2(C_3H_6O)$ than in the structure of $13b \cdot 2(C_3H_6O) \cdot (H_2O)$. This proximity of the solvent molecule to the platinum centers effects a skewing of the pyridyl group of the chelate from planarity by 22.3° relative to the pyridazine ring, presumably in an effort to relieve steric congestion provided by the acetone molecule. This also leads to an increase in the α angle of the clam-shell configuration by 7° .

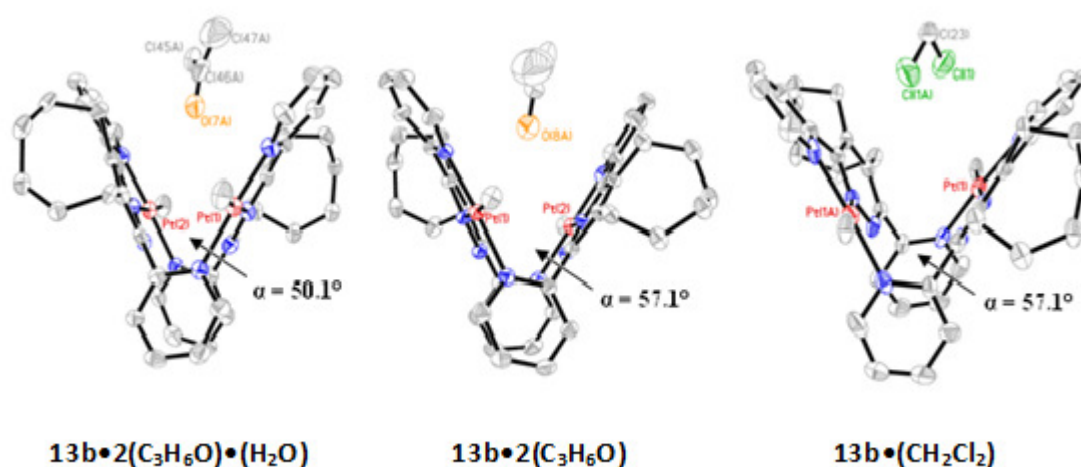


Figure 3.9. Comparison of the solvent inclusions and α angles of the three analogous clam-shell structures of **13b**. Hydrogen atoms, trifluoromethanesulfonate anions and some solvent molecules omitted for clarity.

In the case of **13b**•(CH_2Cl_2), the dichloromethane solvent molecule resides within the open pocket of the clam-shell structure. The chlorine atoms are positioned roughly 4.2 Å from the platinum centers which is an intermediate value compared to the other structures of **13b**. The larger chlorine atoms do however impose a larger steric effect on the structure and leads to an α angle of the clam-shell structure of 57.1° while maintaining planarity of the chelate as well as the geometry at the platinum centers.

3.3 Studies of the Mechanism and Selectivity

In an effort to understand how the dimeric complexes **13a** and **13b** were being formed, variable temperature NMR experiments were performed. To an acetone- d_6 solution of complex **2**, was added a slight stoichiometric excess of trifluoromethanesulfonic acid at -80°C. A series of the variable temperature ^1H NMR spectra are depicted in figure 3.10. Upon addition of the acid, one immediately observes the formation of CH_4 at 0.12 ppm as well as the loss of both of the methylplatinum(II) resonances from the complex **2** starting material. One also observes the formation of two new resonances in the methyl region at 0.89 ppm and 0.92 ppm which become better resolved as the reaction mixture is gradually warmed in increments of 20°C. At -40°C,

(spectrum (b)), these two methyl resonances are completely resolved and ^{195}Pt satellites begin to become observable providing evidence for the formation of a new methylplatinum containing complex. At $+20^\circ\text{C}$, (spectrum (c)), the coupling constant and relative integration values can be determined for each methylplatinum resonance. It was determined that the resonance originally at 0.89 ppm now had a chemical shift of 0.99 ppm with $^2J(\text{PtH}) = 75$ Hz and the resonance originally at 0.92 ppm now had a chemical shift of 1.04 ppm with a $^2J(\text{PtH}) = 80$ Hz. These two resonances were present in a 3:1 relative integration ratio of the most upfield methylplatinum resonance relative to the most downfield. This provided reason to assume that the formation of two methylplatinum containing species were being formed, which were believed to be the monomethylplatinum(II) species **14a** and **14b**, originally proposed with a weakly coordinating ligand, (scheme 3.6). The formation of two monomethylplatinum(II) products arises due to the possibility that either methyl group of complex **2** may be reductively eliminated along with a hydride, producing CH_4 and the corresponding monomethylplatinum(II) species, **14a** and **14b**, as further outlined in scheme 3.6. The resonances that are attributed to the methylene protons of the cyclooctene ring are significantly broadened at -80°C indicating that there is some exchange process occurring, but become completely resolved at 0°C . The six methylene resonances in the spectra were determined to be the result of both sets of cyclooctene ring proton resonances of the two monomethyl species overlapping, which was supported by the relative integration ratios. The pyridyl resonances observed at $+20^\circ\text{C}$ also supports the formation of two species by the presence of 16 resonances, albeit some are overlapping, but overall possesses a consistent relative integration ratio with the proposed reaction in scheme 3.6. Two broad and overlapping resonances at 11.00 ppm and 11.60 ppm appear in the spectrum at -80°C and gradually resolve as a single broad resonance at 11.00 ppm as the temperature is increased incrementally to $+20^\circ\text{C}$. These resonances at -80°C are presumed to be the result of a proton exchanging from free trifluoromethanesulfonic acid to the nitrogen atom of the non-coordinating pyridyl ring. The resultant single broad resonance observed at $+20^\circ\text{C}$ is portraying the average of the two original resonances of the exchange process.

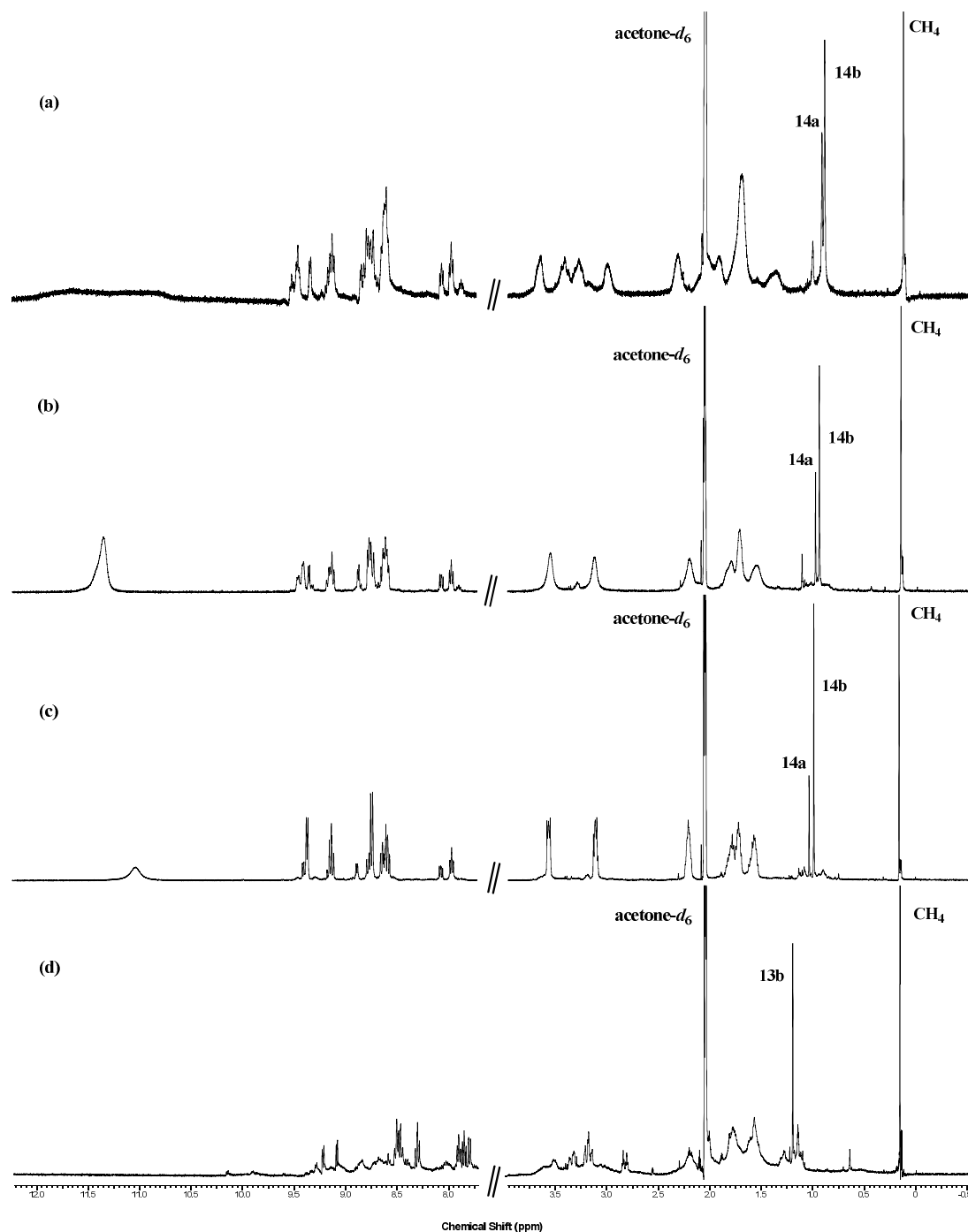
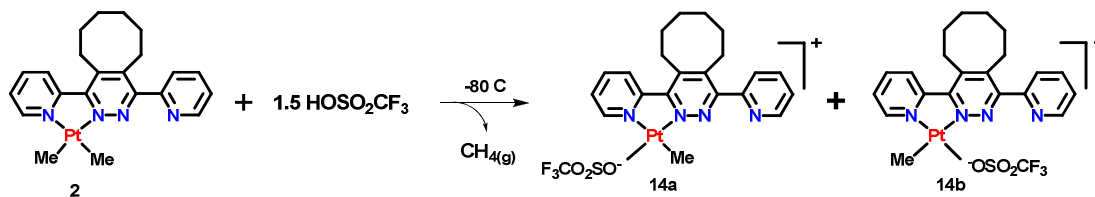


Figure 3.10. Variable temperature ^1H NMR spectra of the protonolysis of complex **2** yielding complexes **14a/14b** on route to the formation of complex **13b**. Methylplatinum resonances are labelled based on their corresponding complex. Spectrum (a) was collected at -80°C , spectrum (b) at -40°C , spectrum (c) at $+20^\circ\text{C}$ and spectrum (d) at $+25^\circ\text{C}$ 72 hours after the initial addition of trifluoromethanesulfonic acid.



Scheme 3.6. Proposed reaction scheme for the formation of both isomers of a monomethylplatinum(II) complex with a weakly coordinating ligand from complex **2**.

After 72 hours, a ^1H NMR spectroscopic experiment was again performed on the reaction mixture of complex **2** and trifluoromethanesulfonic acid to observe if there was a preference for the formation of one monomethylplatinum(II) species over the other, spectrum (d) in Figure 3.10. The spectrum obtained provided no evidence of either **14a** or **14b**, rather it contained a single methylplatinum resonance at 1.20 ppm with a $^2J(\text{PtH}) = 74$ Hz. This resonance was consistent with the formation of the dimeric species **13b** and indeed the other characteristic resonances for complex **13b** were present with identical chemical shifts and coupling values. This indicates that the formation of complexes **13a** and **13b** likely occurs via the formation of a monomethylplatinum(II) species with a weakly coordinating ligand on route to the formation of the dimeric species.

In order to prove this theory, the variable temperature NMR experiment was repeated using acetonitrile- d_3 as the solvent. The thought was that the use of acetonitrile should aid in stabilizing the formation of the monomethylplatinum(II) species due to the stronger donating ability of acetonitrile than acetone, and therefore will resist the formation of the dimeric species. Upon addition of trifluoromethanesulfonic acid at -40°C , the evolution of CH_4 was again observed by the appearance of a singlet resonance at 0.18 ppm, figure 3.11.

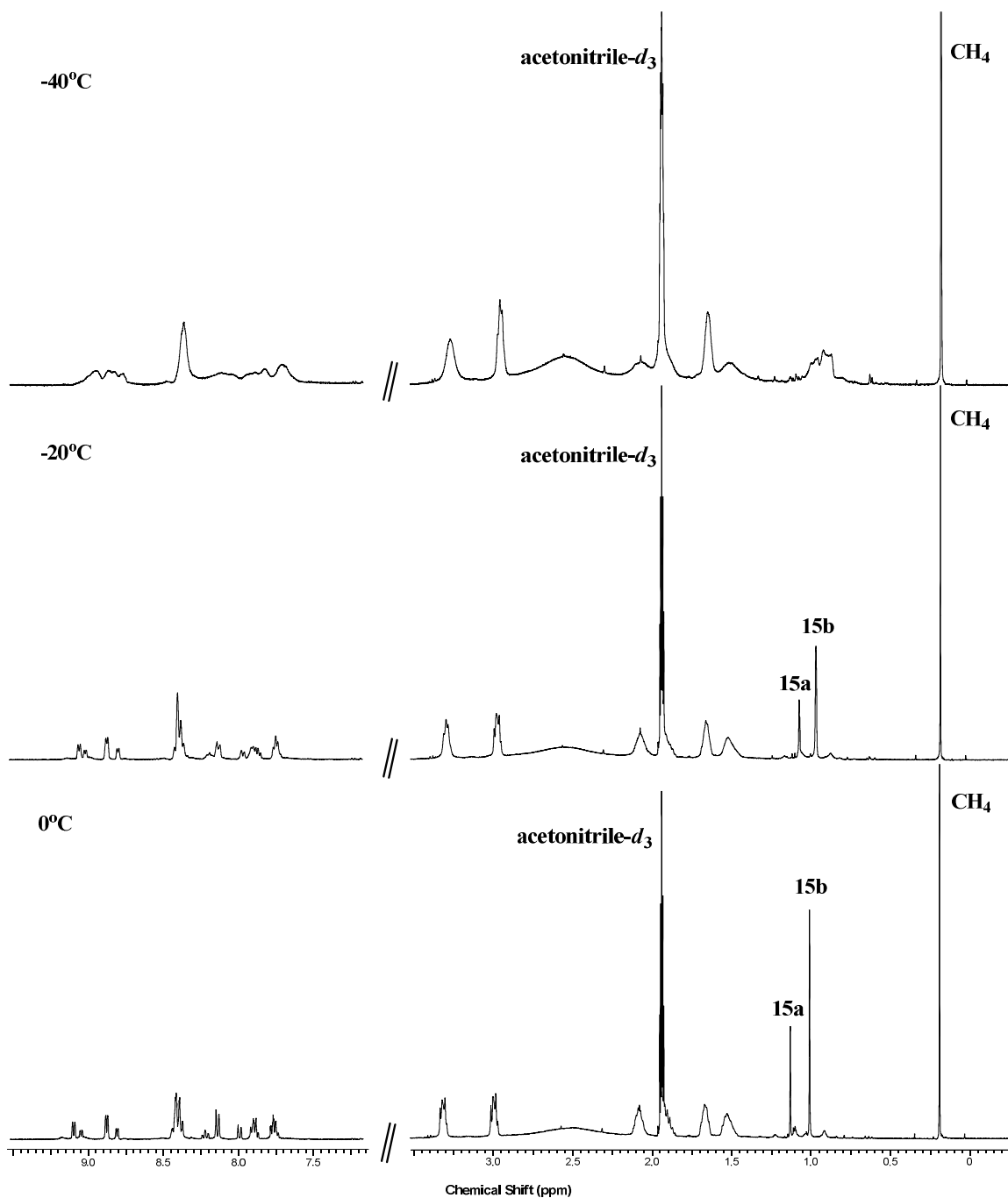
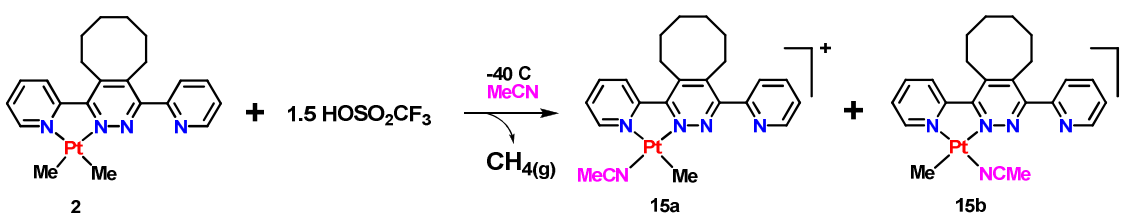


Figure 3.11. Variable temperature ¹H NMR spectra of the protonolysis of complex **2** yielding complexes **15a/15b**, the acetonitrile adducts of **14a/14b**. Methylplatinum resonances are labelled based on their corresponding complex.

The methylplatinum resonances of complex **2** were no longer observable and it was not until the reaction mixture was warmed to -30°C that any resonances could be observed that could be attributed to methylplatinum species' **15a** and **15b**, the acetonitrile adducts of **14a** and **14b**. These resonances were fully resolved at 0°C and were assigned again as being a result of the formation of the monomethylplatinum(II) complexes **15a** and **15b** as depicted in scheme 3.7. The singlet resonance at 1.01 ppm with $^2J(\text{PtH}) = 75$ Hz was found to have an integration ratio of 2:1 relative to the second methylplatinum resonance. The second more downfield methylplatinum resonance was observed at 1.13 ppm with $^2J(\text{PtH}) = 75$ Hz. The remainder of the spectrum was also fully resolved at this point and supported the formation of two acetonitrile adducts of the monomethylplatinum(II) complexes **15a** and **15b** from scheme 3.7.



Scheme 3.7. Formation of the two isomers of an acetonitrile adduct of the monomethylplatinum(II) monomer species.

Further evidence for the formation of the acetonitrile adducts was provided by the addition of trifluoromethanesulfonic acid, and a small amount of acetonitrile, to an acetone- d_6 solution of complex **2** at 0°C . It was found that upon addition of the acid, CH_4 was evolved and the acetonitrile adducts of the monomethylplatinum(II) complexes were again formed. This postulation can be supported by the presence of ^{195}Pt satellites on the resonances associated with the acetonitrile protons, figure 3.13. The resonance at 2.77 ppm possessed $^4J(\text{PtH}) = 8$ Hz and correlated through integration values to the methylplatinum resonance at 1.02 ppm. The second acetonitrile proton resonance was observed at 2.89 ppm with $^4J(\text{PtH}) = 15$ Hz and correlated to the methylplatinum resonance at 1.21 ppm. The two isomers of the monomethylplatinum species **15b** and **15a** were present in a 2:1 ratio respectively. To determine if there was a thermodynamic

preference for the formation of one isomer over the other, NMR spectra of the reaction mixture were acquired over time. The spectra acquired 3 hours after the initial addition of the acid indicated that the isomer in which the methylplatinum resonance was furthest downfield, **15a**, was slowly isomerizing to the second isomer, **15b**. The ratio of these two isomers in solution was determined to be 2.5:1. Concurrent to the isomerization, was the formation of a new methylplatinum containing complex with a methylplatinum resonance at 1.20 ppm and a $^2J(\text{PtH}) = 75$ Hz. This resonance was determined to be arising from the gradual formation of complex **13b** through the use of previous spectra as a fingerprint. After 24 hours, the ratio of complex **13b** to isomer **15b** and isomer **15a** was found to be 4:2:1 respectively, and after 48 hours the ratio was determined to be 4:1:0.3. It seems likely that the two isomers of the acetonitrile adduct gradually isomerize from isomer **15a** in which the methyl group is directed inward to **15b** in which the methyl group is directed outward. This would allow for two units of isomer **15b** to come together and form complex **13b** by displacing the weakly coordinating acetonitrile ligands and coordinating through the dangling pyridyl groups. This theory is supported by the fact that the alternative isomer of complex **13b** was not formed in this reaction. Scheme 3.8 depicts this proposed method of isomerization.

Computational studies were performed in order to further validate the conclusions drawn from the ^1H NMR experiment, figure 3.12. DFT calculations performed using the parent ligand dppd as a model for 6-dppd indicate that there is very little energetic difference between isomers **15a** and **15b**, with **15b** being more stable than **15a** by 1 kJ mol^{-1} . The fact that the *endo* and *exo* isomers of $[\text{PtMe}(\text{NCMe})(\text{dppd})]^+$ have almost equivalent energies is consistent with the observation that the compounds exist in equilibrium and exhibit a very gradual isomerization towards the *exo* isomer.

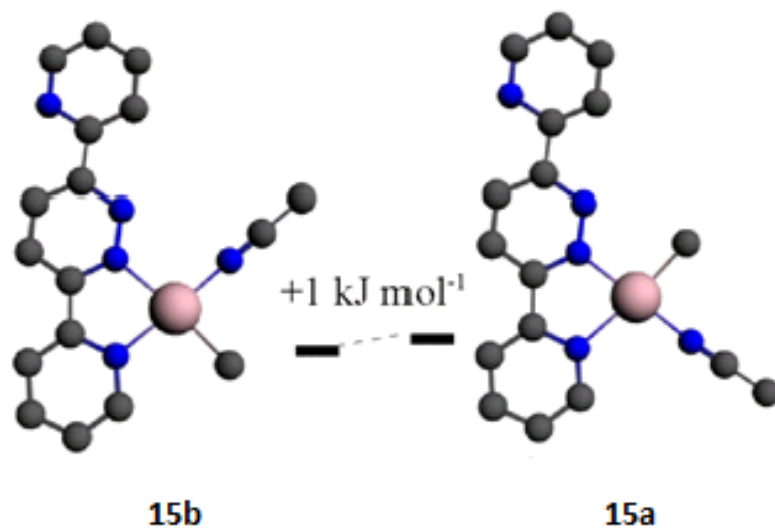
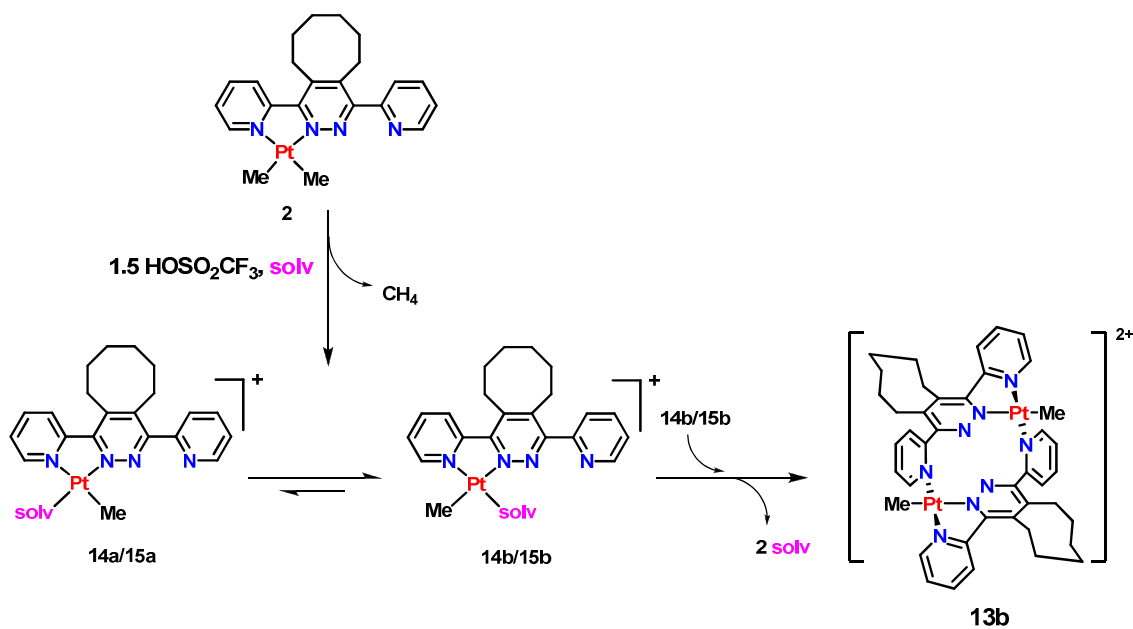


Figure 3.12. Calculated structures and relative energies for the isomers of the model complex $[\text{PtMe}(\text{NCMe})(\text{dppd})]^+$.



Scheme 3.8. Formation and subsequent isomerism of **14a/15a** and **14b/15b** on route to form complex **13b**, where “solv” may be acetone, **14**, or acetonitrile, **15**.

Trifluoromethanesulfonate counter anions were omitted for clarity.

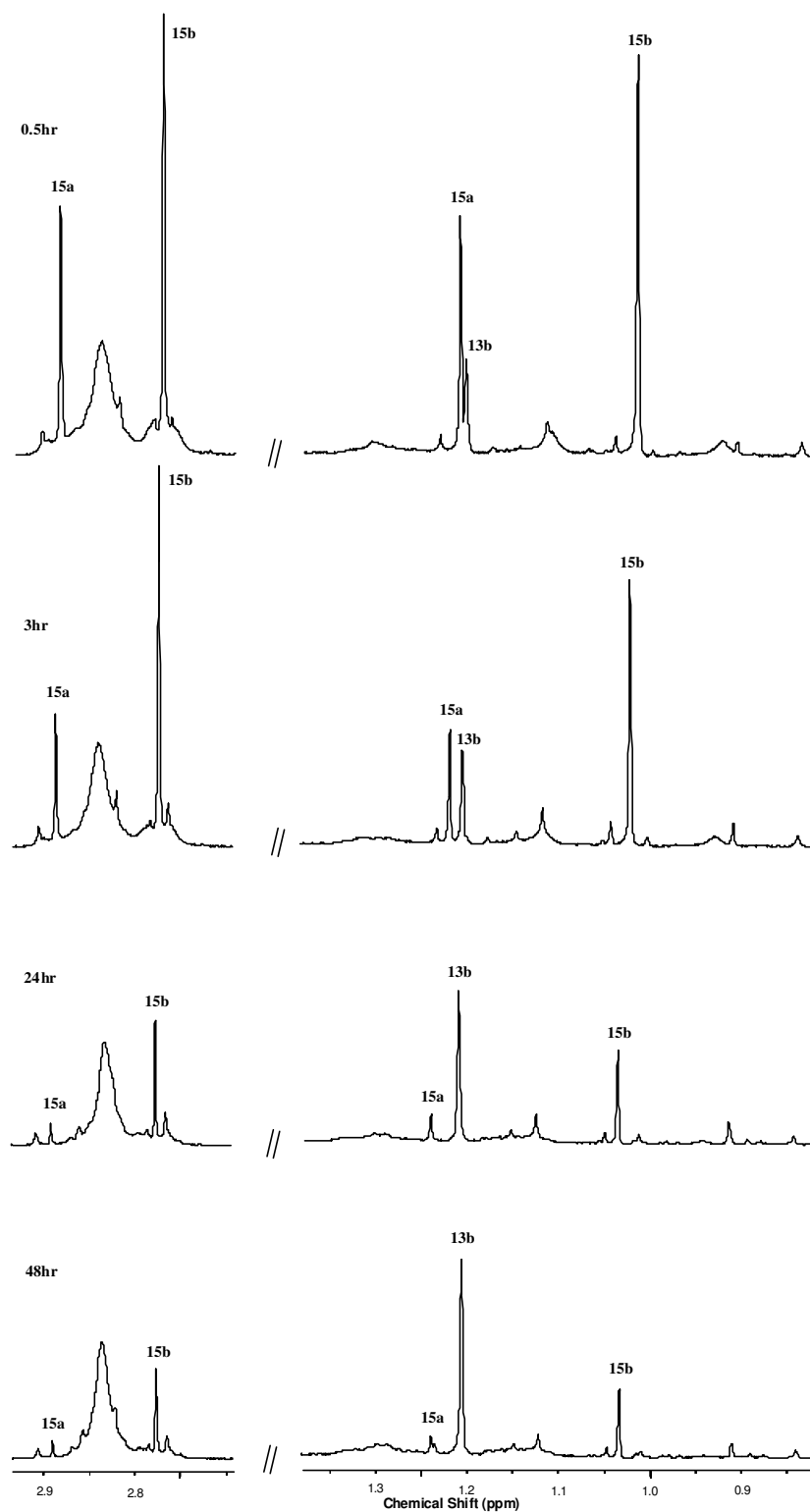


Figure 3.13. ^1H NMR spectra, (acetone- d_6), monitoring the formation of complexes **15a/15b** and the concurrent isomerization to **13b**. Methylplatinum and acetonitrile resonances are labelled based on their corresponding complexes.

The formation of only complex **13b** from the mixture of isomers **15a** and **15b** leads one to believe that there is a thermodynamic preference to the formation of complex **13b** over **13a**. This theory was tested by adding trifluoromethanesulfonic acid to an acetone-*d*₆ solution of complex **2** at -40°C. This reaction mixture was allowed to stir for 5 minutes and then allowed to warm to room temperature over the course of 20 minutes. The ¹H NMR spectra obtained 30 minutes after the addition of the acid showed evidence for the formation of both isomeric forms of the dimeric clam-shell complex, **13a** and **13b** in a 1:1 ratio. This was confirmed by using the previously attained spectra for each complex as a fingerprint. This reaction was monitored over time to determine whether complex **13a** or **13b** was preferred thermodynamically. It was found that after 48 hours, isomer **13b** was present in a 2:1 ratio versus **13a**, and after 6 days **13b** was observed to be the only product present in the NMR spectrum, figure 3.15. This experiment indicates that there is a thermodynamic preference for the formation of isomer **13b** over **13a**. This also supports the finding in which the monomethylplatinum(II) isomer **15a** gradually converted to isomer **15b** on route to the dimerization, forming **13b**. This in turn insinuates that **13a** is the kinetic isomer which is formed in higher amounts early in the reaction and subsequently isomerizes to form **13b** as the thermodynamic sink. The observation of **13b** being more stable than **13a** is further supported by DFT calculations, figure 3.14. These computational studies, based on the parent ligand dppd as a model for 6-dppd, indicate that the isomer **13b** is more stable than the isomer **13a** by 43 kJ mol⁻¹. This is fully consistent with the observation that **13b** is the only isomer present under equilibrium conditions. The isomerism from **13a** to **13b** is proposed to follow the process outlined in scheme 3.9. This isomerism follows the premise that two identical monomer units associate to form the corresponding dimeric complex. Therefore the isomerism from **13a** to **13b** is not occurring through an intramolecular rearrangement of the clam-shell structure. A complete cleavage of the dimer structure **13a** to its respective monomers is required as depicted in the first step. Upon the regeneration of the monomer units **14a/15a**, a rearrangement occurs at the tri-coordinated platinum center to form **14b/15b** in solution, (step 2). Amalgamation of two equivalents of **14b/15b** occurs through the coordination of the dangling pyridyl groups to the adjacent platinum center through the loss of the weakly coordinated ligand molecule, (step 3).

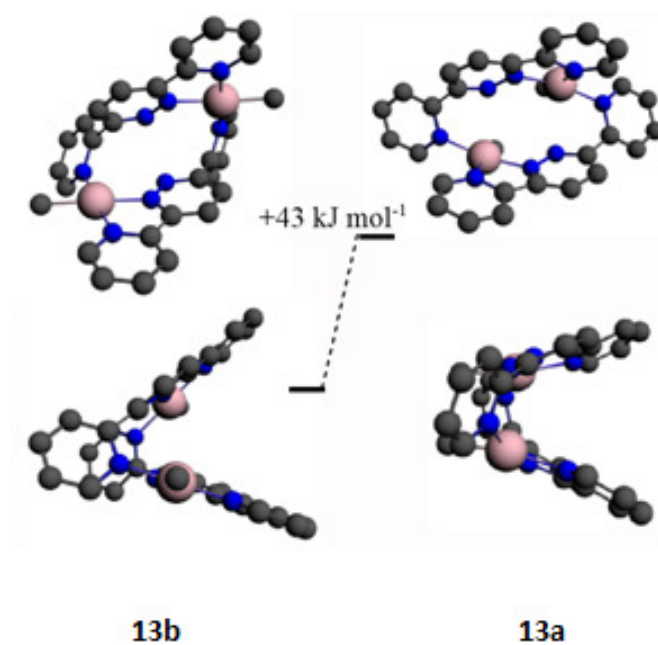


Figure 3.14. Calculated structures and relative energies for the models of the dimer complexes **13a** and **13b**.

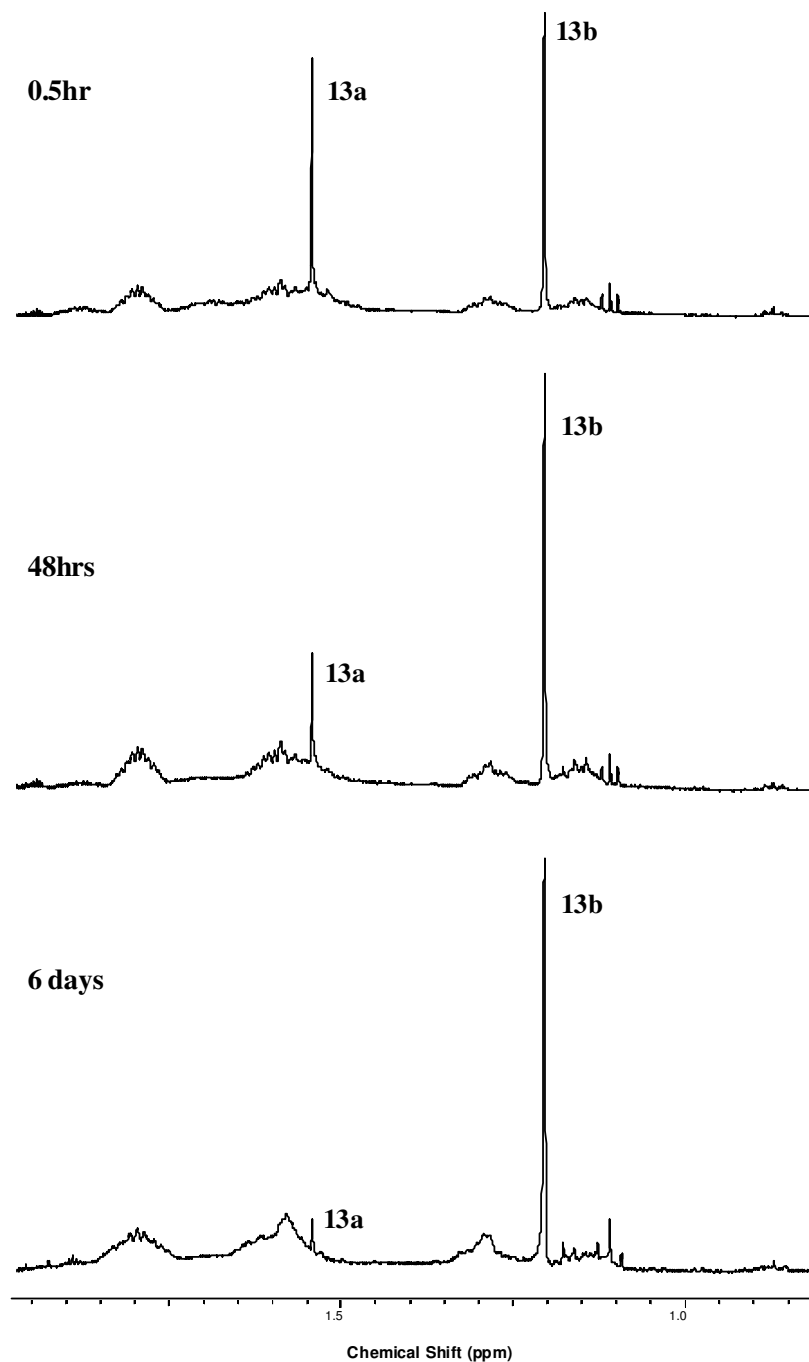
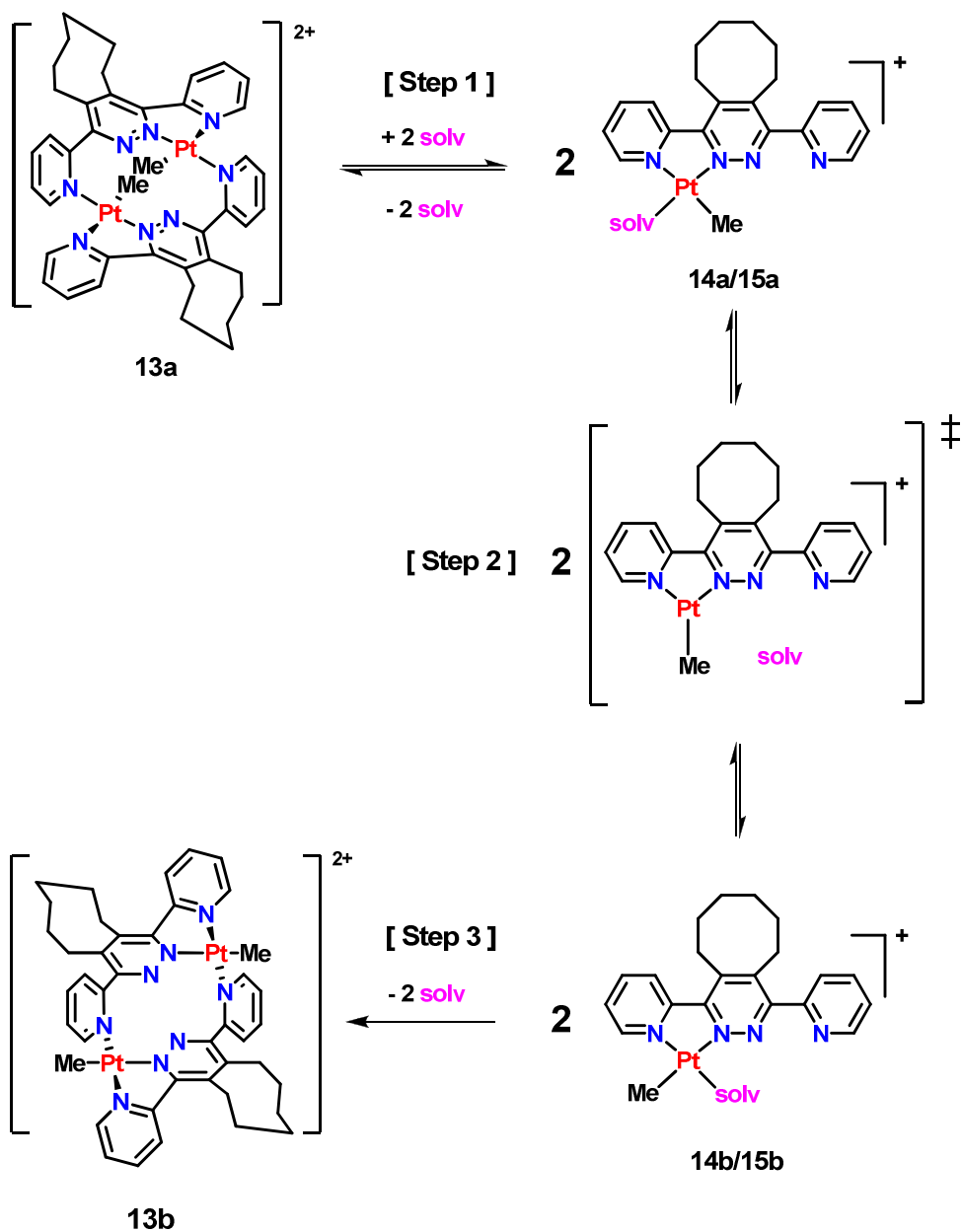


Figure 3.15. ^1H NMR spectra, (acetone- d_6), monitoring the protonolysis of complex **2** yielding complexes **13a** and **13b** and the subsequent isomerization from **13a** to **13b** over the course of 6 days. Methylplatinum resonances are labelled based on their corresponding complexes.

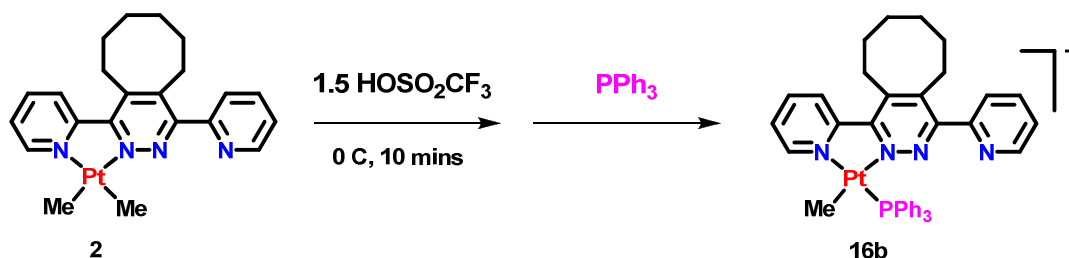


Scheme 3.9. Proposed 3-step isomerism pathway for the isomerism of **13a** to **13b** in solution, where “solv” represents an acetone or acetonitrile molecule. Trifluoromethanesulfonate counter anions are omitted for clarity. Step 1 depicts the initial cleavage of **13a** into its monomer units, **14a/15a**. Step 2 represents the rearrangement step in which **14a/15a** converts to **14b/15b** gradually in solution via a three-coordinate platinum(II) intermediate. Step 3 consists of the coordination of 2 units of **14b/15b** to form **13b** irreversibly.

3.4 Reversibility of Formation of the Clamshell Dimers

In an effort to better understand the nature of the monomethylplatinum(II) monomer complexes **14a/15a** and **14b/15b**, an isolable product was required. Various attempts to crystallize the acetonitrile monomer complexes were found to be unsuccessful as **13b** formed continuously as the thermodynamic sink for the isomerization even at 0°C. It was thought that it may be possible to cleave complex **13b** into its monomer units by refluxing a suspension of **13b** in acetonitrile, but again **13b** was found to resist cleavage. It was postulated that if the donor strength of the solvent was increased, the monomer complexes would be stabilized and resist the dimerization step. Using this concept, trifluoromethanesulfonic acid was added to a pyridine solution of complex **2**. The ¹H NMR spectrum of the product of this addition was determined again to be complex **13b**. The gentle reflux of a suspension of **13b** in pyridine also failed to disrupt the stable clamshell structure of **13b**. In a final effort to capture the monomer species, triphenylphosphine was utilized as the coordinating ligand. The significantly increased donor ability of the phosphine was thought to be able to form the monomers favourably, and the incorporation of the bulky aryl groups would aid in the ability to isolate the monomers. To an acetonitrile solution of complex **2** was added a slight excess of trifluoromethanesulfonic acid at 0°C. After allowing the reaction mixture to stir for 10 minutes, an acetone solution of one equivalent of PPh₃ was added at which point the reaction mixture was stirred for 3 hours before the red-orange reaction mixture was allowed to warm to room temperature. Upon isolation of the red-orange product, ¹H NMR spectra were acquired of an acetone-*d*₆ solution of the product. The ¹H NMR spectrum, figure 3.16, contained an apparent doublet resonance at 0.85 ppm which possessed ¹⁹⁵Pt satellites with a ²*J*(PtH) = 71 Hz. This doublet was thought to arise due to the methylplatinum protons coupling with the ³¹P atom of the coordinated PPh₃ ligand, and possessed a coupling value of ³*J*(PH) = 3 Hz. Further evidence for the coordination of the PPh₃ ligand was provided by the coupling pattern of the *ortho* proton resonance of the coordinated pyridyl group. This resonance at 9.35 ppm, which is typically observed as a doublet with ¹⁹⁵Pt satellites, is observed to possess both ¹⁹⁵Pt and ³¹P couplings of 33 Hz and 4 Hz respectively. The integration values of both the resonances known to be due to methylplatinum containing complexes of **6-dppd** and of PPh₃ were consistent with the

formation of the complex $[\text{PtMe}(\text{PPh}_3)(6\text{-dppd})]^+$, **16b** scheme 3.10. A doublet resonance of peculiar chemical shift was observed at 6.24 ppm which was not consistent with either PPh_3 or typical resonances of the platinum(II) complexes of **6-dppd**. gCOSY NMR analysis allowed for this resonance to be assigned to H_3 of the non-coordinating pyridyl ring. This indicates that this proton is significantly shielded, likely by one of the phenyl rings of PPh_3 leading to an upfield shift by roughly 2 ppm relative to complex **2**. ^1H - ^1H NOESY NMR analysis was also utilized to confirm the overall stereochemistry about the platinum(II) center. It was determined that the PPh_3 ligand was directed towards the interior part of the monomer as evidence of a coupling interaction found between the methyl group and the *ortho* proton of the coordinated pyridyl ring. This leads to the overall stereochemical determination of complex **16b** as depicted in scheme 3.10. The formation of complex **16b** was further supported by the $^{31}\text{P}\{^1\text{H}\}$ NMR, figure 3.17, in which a singlet was observed at 19.37 ppm with ^{195}Pt satellites which possessed a coupling value $^1J(\text{PtP}) = 4360$ Hz, indicating that the PPh_3 ligand was directly bonded to the platinum(II) center. Throughout this investigation, no evidence of the formation of the second isomer, **16a**, with the PPh_3 directed outward was observed. This proposed formation of **16b** and its *exo* geometry was further supported by computational studies, figure 3.18, in which the *exo* isomer of the model complex $[\text{PtMe}(\text{PPh}_3)(\text{dppd})]^+$ was found to be more stable than the *endo* isomer by 7 kJ mol^{-1} .



Scheme 3.10. Formation of complex **16b**, $[\text{PtMe}(\text{PPh}_3)(6\text{-dppd})]^+[\text{OSO}_2\text{CF}_3]^-$.

Trifluoromethanesulfonate counter anion omitted for clarity.

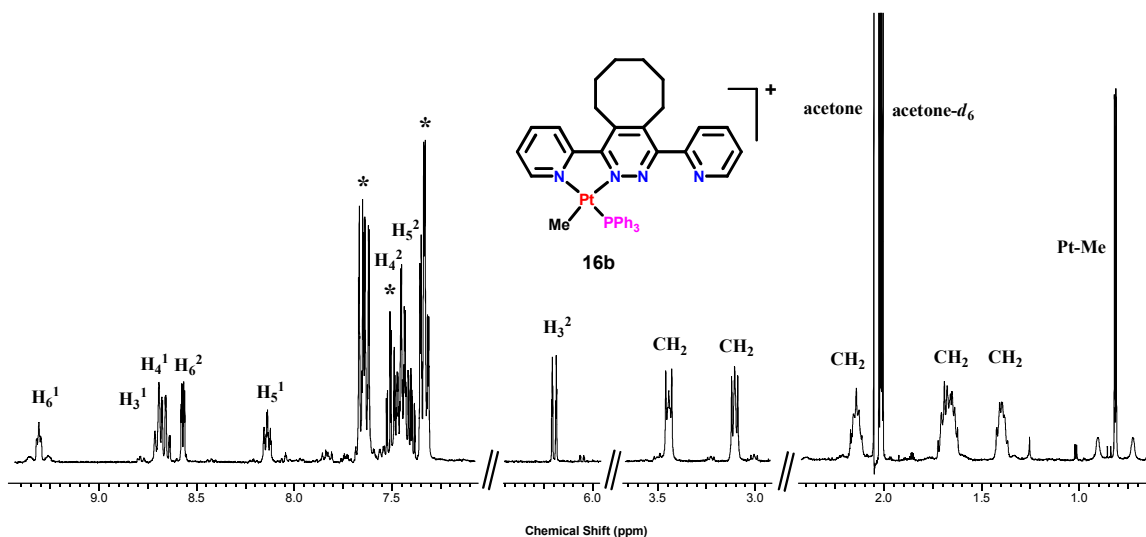


Figure 3.16. ^1H NMR spectrum of complex **16b**, $[\text{PtMe}(\text{PPh}_3)(6\text{-dppd})](\text{OTf})$ in acetone- d_6 . Conventional labelling schemes are utilized for pyridyl rings. CH_2 represents the protons of the cyclooctyl ring. Residual solvent signal for acetone is labelled. * represents the protons of the phenyl rings on the PPh_3 ligand.

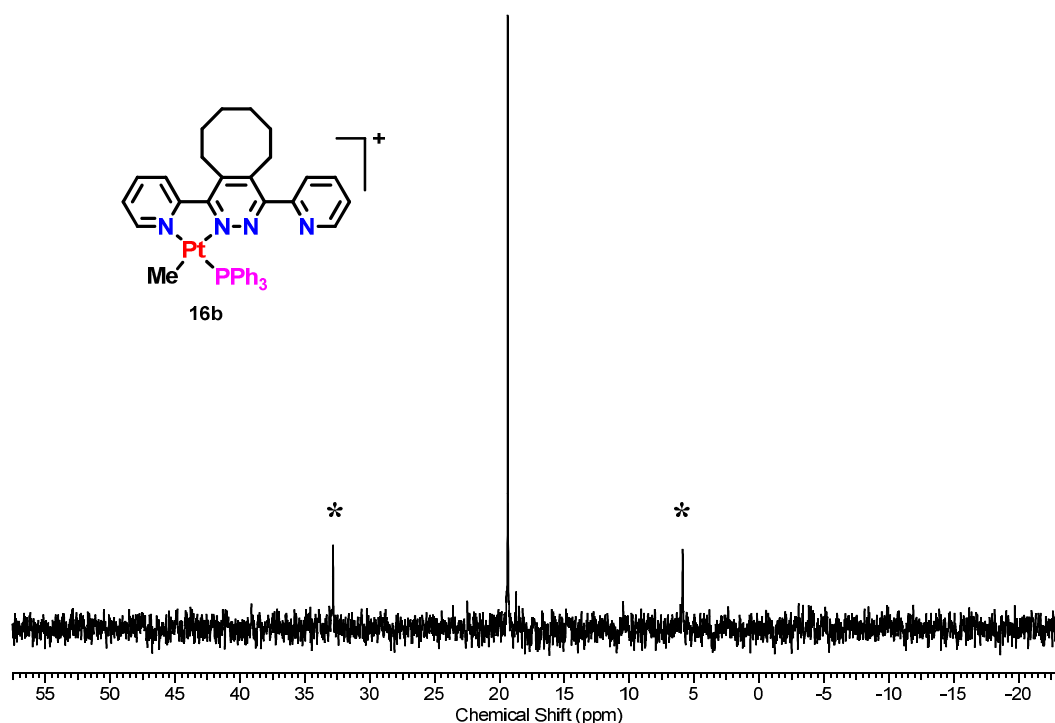


Figure 3.17. $^{31}\text{P}\{^1\text{H}\}$ NMR spectrum of complex **16b**, $[\text{PtMe}(\text{PPh}_3)(6\text{-dppd})](\text{OTf})$ in acetone- d_6 . * indicates the presence of ^{195}Pt satellites from the coupling of the PPh_3 ligand to the platinum center.

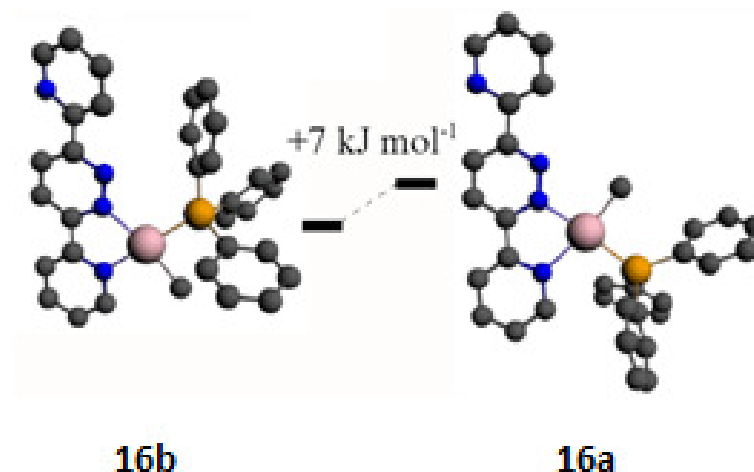
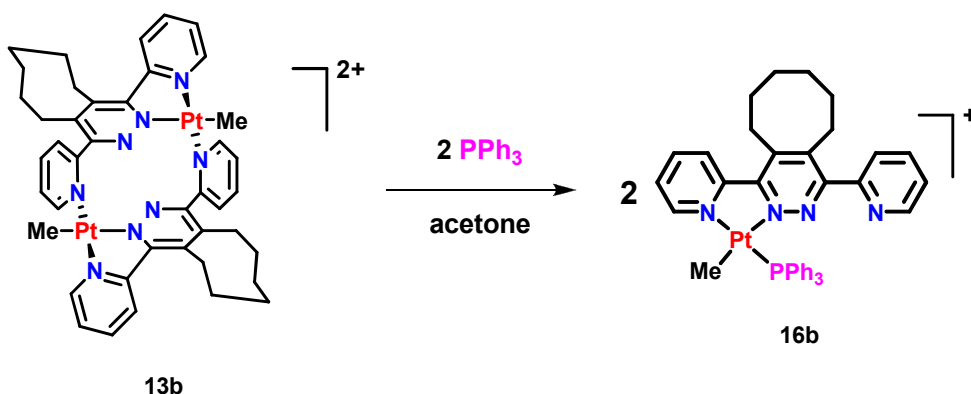


Figure 3.18. Calculated structures and relative energies for the isomers of the model complex $[\text{PtMe}(\text{PPh}_3)(\text{dppd})]^+$.

This proposed stereochemistry was confirmed through X-ray crystallographic analysis of a single crystal of complex **16b**. Figure 3.19 depicts the solid state structure of complex **16b**. The formation of complex **16b** was also observed when PPh_3 was added to an acetone suspension of **13b** as depicted in scheme 3.11. This indicates that the formation of **16b** is thermodynamically favoured over **13b**, leading to the disruption of the stable dimeric clam-shell structure and formation of the monomeric species. This finding provides some intrigue into the use of phosphine based ligands or their analogs such as benzyldiphenylphosphine for *ortho*-metallation type chemistry in which a C-H bond activation step would likely be observed.



Scheme 3.11. Formation of complex **16b** from **13b** via the cleavage of the clam-shell structure into 2 equivalents of complex **16b**. Trifluoromethanesulfonate counter anions omitted for clarity.

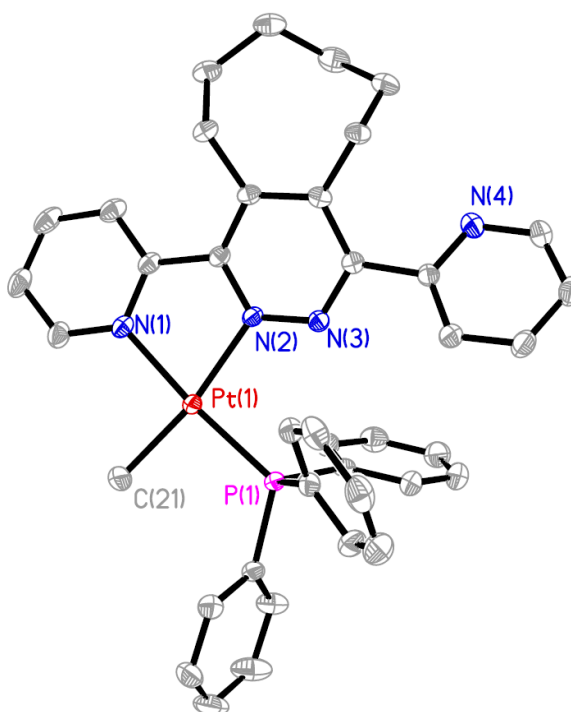


Figure 3.19. Molecular structure of complex **16b**, (hydrogen atoms and trifluoromethanesulfonate anions are omitted for clarity).

Table 3.6: Bond lengths [Å] and angles [°] for *exo*-[PtMe(PPh₃)(6-dppd)](OTf), **16b**

Pt(1)-N(1)	2.0905(16)	Pt(1)-N(2)	2.0934(15)
Pt(1)-C(21)	2.047(2)	Pt(1)-P(1)	2.2339(5)
N(1)-Pt(1)-N(2)	77.91(6)	N(1)-Pt(1)-P(1)	174.88(5)
N(1)-Pt(1)-C(21)	92.78(8)	N(2)-Pt(1)-P(1)	96.98(4)
N(2)-Pt(1)-C(21)	170.39(8)	P(1)-Pt(1)-C(21)	92.33(7)
N(1)-C(5)-C(6)-N(2)	18.0(2)	N(3)-C(9)-C(10)-N(4)	145.26(17)

3.5 Conclusions

The synthesis and characterization of two isomeric clamshell dimers of platinum(II) was examined and each distinct isomer could be formed in a logical way. Through the addition of silver trifluoromethanesulfonate to an acetone solution of complex **1**, *endo*-[PtClMe(6-dppd)], the chloride anion can be abstracted leading to the formation of exclusively **13a**, *endo,endo*-[Pt₂Me₂(μ₂-κ³-6-dppd)₂][OTf]₂ a dimeric platinum(II) complex. This process allows for the synthesis of a dimeric structure in which the stereochemistry at the platinum center was retained and hence the methyl groups were directed inwards leading to a sterically hindered conformation. Alternatively, through the addition of trifluoromethanesulfonic acid to an acetone solution of complex **2**, [PtMe₂(6-dppd)], a protonolysis reaction is performed resulting in the generation of methane gas and the concomitant formation of **13a** and its isomer **13b**, *exo,exo*-[Pt₂Me₂(μ₂-κ³-6-dppd)₂][OTf]₂. Isomer **13b**, was observed to direct the methyl groups away from the interior of the clamshell dimer thus alleviating some of the steric strain observed in **13a** which is supported by the observation of a much large hinge angle of α = 50.1° versus 31.6° for that of **13a**. The protonolysis reaction of complex **2** with trifluoromethanesulfonic acid was observed to produce both isomers of **13** in solution due to the presence of two methyl groups at the platinum(II) center. Both **13a** and **13b** were completely characterized and three distinct unit cells of **13b** were observed, each containing a solvent molecule in the open 'mouth' of the clam-shell structure. Variable temperature ¹H NMR experiments indicated that the resultant formation of the dimeric complexes **13a** and **13b** via the protonolysis approach relied on the initial generation of monomethylplatinum(II) intermediates **14a**, (*endo*-[Pt(C₃H₆O)(Me)(6-dppd)]⁺ and **14b**, *exo*-[PtMe(C₃H₆O)(6-dppd)]⁺. These monomer species would then combine selectively to form **13a** through the incorporation of two units of **14a**, or **13b** through the incorporation of two units of **14b**. This dimerization occurs solely through self-recognition and as such allows for the formation of the *exo,exo* dimer **13b** or the *endo,endo* dimer **13a**. Molecular models show that the *endo,exo* dimer is highly strained so that no assembly by self-discrimination can occur. The lifetimes of the monomers was observed to be rather short-lived in acetone, but could be vastly prolonged through increase in the donor strength of the solvent. Through employing acetonitrile as a

solvent, longer lived intermediates **15a**, *endo*-[Pt(NCMe)Me(6-dppd)]⁺ and **15b**, *exo*-[PtMe(NCMe)(6-dppd)]⁺ could be observed and completely characterized in solution. Increasing the lifetime of the intermediates allowed for the study of the mechanism by which the dimers were formed under protonolysis conditions. It was concluded that isomerism from **14a/15a** to **14b/15b** occurred in solution, leading to the determination that complex **13a** was the kinetically preferred isomer of **13** and gradually, through dissociation, isomerization and association would lead to the formation of **13b**. The less stable dimer **13a** slowly converts to **13b** in solution, presumably by reversible dissociation to **14a**, isomerisation to **15a** and dimerization, so the self-sorting process eventually yields complex **13b** selectively. Thus, the self-assembly with complexes that are relatively inert towards *cis-trans* isomerisation can occur selectively to yield isomeric products. The formation of the monomer species was supported by the observation of complex **16b** which trapped the monomer species during the aggregation process. complex **16b** was also found to be prepared through the cleavage of the dimeric clamshell structure **13b**, proving the strength of the donor molecule dictates the formation of either the monomer or dimer species. These isomeric clamshell dimer complexes were prepared in a logical way and so establish a useful synthetic protocol for self-assembly of isomeric self-assembled molecular materials. The method clearly has potential in forming more complex structures.

3.6 Experimental

Reagents and General Procedures. All reactions were carried out in an inert atmosphere of dry nitrogen using standard Schlenk techniques, unless otherwise specified. All solvents used for air and moisture sensitive materials were purified using an Innovative Technology Inc. *PURE SOLV* solvent purification system (SPS). The complexes **1** and **2** were prepared following the procedures noted in Chapter 2. NMR spectra were recorded at ambient temperature, unless otherwise noted (ca. 25°C), on Varian Mercury 400 or Varian Inova 400 or 600 spectrometers. Chemical shifts are reported relative to TMS (^1H), 85% H_3PO_4 (^{31}P), and trifluorotoluene, (^{19}F). Complete assignment of each compound was aided by the use of ^1H - ^1H NOESY, ^1H - $^{13}\text{C}\{^1\text{H}\}$ -HSQC and ^1H - ^1H gCOSY experiments. Commonly practiced labeling schemes for pyridyl rings are utilized when labeling signals in NMR spectroscopic analysis. Elemental analyses were performed by either Guelph Chemical Laboratories or Laboratoire d'Analyse Élémentaire de l'Université de Montréal. Mass spectrometric analysis was carried out using an electrospray PE-Sciex Mass Spectrometer (ESI-MS) coupled with a TOF detector. DFT calculations were carried out by Dr. R.J. Puddephatt by using the 2011 Amsterdam Density Functional Program based on the BLYP functional, with frozen core potential, first-order scalar relativistic corrections (ZORA, SAPA) and the double zeta (DZP) basis set.

X-ray Crystallography. A suitable crystal of each compound was coated in Paratone oil and mounted on a glass fiber loop. X-ray data for compounds **13a**, **13b•2(C₃H₆O)**, **13b•CH₂Cl₂** and **16b** were collected at 150K with ω and φ scans on a Bruker Smart Apex II diffractometer using graphite-monochromated $\text{MoK}\alpha$ radiation ($\lambda = 0.71073 \text{ \AA}$) and Bruker SMART software [54]. Unit cell parameters were calculated and refined from the full data set. Cell refinement and data reduction were performed using the Bruker APEX2 and SAINT programs respectively [55]. Reflections were scaled and corrected for absorption effects using SADABS [56]. X-ray data for and compound **13b•2(C₃H₆O)•H₂O** were collected at 150K with ω and φ scans on a Nonius Kappa-CCD diffractometer using graphite-monochromated $\text{MoK}\alpha$ radiation ($\lambda = 0.71073 \text{ \AA}$) and COLLECT software [57]. Unit cell parameters were calculated and refined from the full

data set. Cell refinement and data reduction were performed using the DENZO-SMN software programs [58]. Reflections were scaled and corrected for absorption effects using DENZO-SMN [58]. All structures were solved by either Patterson or direct methods with SHELXS [59] and refined by full-matrix least-squares techniques against F^2 using SHELXL [60]. All non-hydrogen atoms were refined anisotropically. The hydrogen atoms were placed in calculated positions and refined using the riding model. No special considerations were required for the refinement of complexes, **13b**•**2(C₃H₆O)**, and **16b**. The unit cell of compound **13a** contained a disordered trifluoromethanesulfonate molecule which was refined isotropically in order to properly model the disorder. Also, the methyl group of this molecule was refined isotropically as when refined anisotropically it would produce a non-positive definite. The unit cell of compound **13b**•**2(C₃H₆O)**•**(H₂O)** contains a water molecule modeled as an isolated oxygen atom. The hydrogen atoms of the water molecule could not be located or positions calculated using the riding atom procedure, so the water molecule was treated as an oxygen atom only. The unit cell of **13b**•**(CH₂Cl₂)** contained a heavily disordered solvent molecule, for which no suitable model could be found. The electron density related to this molecule was removed from the reflection data using SQUEEZE (PLATON) [61], leaving a void of about 214 Å³.

endo,endo-[Pt₂Me₂(6-dppd)₂]²⁺ [OSO₂CF₃]₂⁻, Complex 13a. To a 1mL acetone-d⁶ solution of [PtMeCl(6-dppd)] Complex **1**, (0.010g, 0.01781mmol) was added a 10% excess of silver trifluoromethanesulfonate (0.005g, 0.01959mmol) at room temperature. After stirring for 15 minutes an obvious colour change from orange to yellow was observed, as well as the precipitation of silver chloride. Upon gravity filtration of the silver chloride precipitate, the resultant yellow solution was studied by NMR spectroscopy. Crystals suitable for single crystal X-ray diffraction studies were produced by the crystallization of complex **13a** from the acetone-*d*₆ NMR sample after 48hours. Yield 81%, (0.0097g). **¹H NMR in acetone-*d*₆:** δ 1.52 (m, 1H, CH₂^C), 1.54 (s, 3H, CH₃, ²J(Pt-H)=75Hz), 1.68 (m, 1H, CH₂^E), 1.90 (m, 4H, CH₂^D, CH₂^D, CH₂^B, CH₂^C), 2.14 (m, 1H, CH₂^F), 2.71 (td, 1H, CH₂^B), 2.91 (m, 1H, CH₂^F), 2.98 (dt, 1H, CH₂^E), 7.85 (t, 1H, H^{5'}, ³J(H^{5'}H^{6'})=6Hz, ³J(H^{5'}H^{4'})=8Hz), 8.04 (td, 1H, H⁵, ³J(H⁵H⁶)=6Hz, ³J(H⁵H⁴)=8Hz), 8.28 (d, 1H, H^{3'}, ³J(H^{3'}H^{4'})=8Hz), 8.43 (t, 1H, H^{4'}, ³J(H^{4'}H^{5'})=8Hz, ³J(H^{4'}H^{3'})=8Hz), 8.50 (d,

1H, H³, ³J(H³H⁴)=8Hz, 8.59 (t, 1H, H⁴, ³J(H⁴H⁵)=8Hz, ³J(H⁴H³)=8Hz), 8.59 (d, 1H, H⁶, ³J(H⁶H⁵)=6Hz, ³J(Pt-H⁶)=20Hz), 9.05 (d, 1H, H⁶, ³J(H⁶H⁵)=6Hz, ³J(Pt-H⁶)=34Hz). ¹³C NMR in acetone-*d*₆: δ -4.41 (s, CH₃, Pt-CH₃), 25.43 (s, cyclic CH₂), 25.69 (s, cyclic CH₂), 27.34 (s, cyclic CH₂), 29.03 (s, cyclic CH₂), 30.06 (s, cyclic CH₂), 30.16 (s, cyclic CH₂), 127.40 (s, aromatic C), 128.18 (s, aromatic C), 128.46 (s, aromatic C), 128.87 (s, aromatic C), 139.37 (s, aromatic C), 139.76 (s, aromatic C), 140.88 (s, aromatic C), 141.72 (s, aromatic C), 143.07 (s, aromatic C), 147.15 (s, aromatic C), 148.48 (s, aromatic C), 153.64 (s, aromatic C), 154.94 (s, aromatic C), 161.67 (s, aromatic C). ¹⁹F NMR in acetone-*d*₆: δ -78.80 (s, free trifluoromethanesulfonate). ESI-MS(TOF): [[C₄₂H₄₆N₈Pt₂]²⁺ Calculated m/z = 526.16g/mol; Determined m/z = 526.2g/mol; where z = 2. Elemental Analysis: Anal. Calc'd. [C₄₂H₄₆N₈Pt₂]²⁺[O₃SCF₃]₂⁻• 2CH₂Cl₂ (%): C, 36.32; H, 3.31; N, 7.37; S, 4.22. Found: C, 36.36; H, 3.56; N, 7.55; S, 4.74.

***exo,exo*-[Pt₂Me₂(6-dppd)₂]²⁺ [OSO₂CF₃]₂⁻, Complex 13b.** To an acetone solution of [PtMe₂(6-dppd)] **2**, (0.010g, 0.01848mmol) was added trifluoromethanesulfonic acid, (1.9μL, 0.0215mmol) at 0°C. After stirring for 5 minutes an obvious colour change from red to yellow was observed. After 2 hours the yellow solution was reduced in *vacuo* to afford a yellow oil. Upon addition of 1mL of acetone and layering with 1mL of pentane, a yellow powder began to precipitate out of solution. The resultant yellow solid was isolated by Hirsch filtration and washed with 1mL of pentane. After isolation and removing residual solvent *in vacuo*, the product was dissolved in acetone-*d*₆ for NMR spectroscopic analysis. Crystals suitable for single crystal X-ray diffraction studies were produced by various methods and solvent combinations. Yield 92%, (0.0121g). ¹H NMR in acetone-*d*₆: δ 1.00 (m, 1H, CH₂^C), 1.12 (m, 1H, CH₂^E), 1.20 (s, 3H, CH₃, ²J(Pt-H)=74Hz), 1.56 (m, 4H, CH₂^D, CH₂^D, CH₂^B, CH₂^C), 1.78 (m, 1H, CH₂^F), 2.26 (m, 1H, CH₂^B), 2.73 (dt, 1H, CH₂^F), 2.98 (td, 1H, CH₂^E), 3.11 (t, 1H, CH₂^A), 3.52 (d, 1H, CH₂^A), 7.45 (d, 1H, H³, ³J(H³H⁴)=7Hz), 7.65 (td, 1H, H⁵, ³J(H⁵H⁶)=6Hz, ³J(H⁵H⁴)=8Hz), 7.68 (t, 1H, H⁵, ³J(H⁵H⁶)=6Hz, ³J(H⁵H⁴)=8Hz), 8.11 (td, 1H, H⁴, ³J(H⁴H⁵)=8Hz, ³J(H⁴H³)=8Hz), 8.32 (t, 1H, H⁴, ³J(H⁴H⁵)=8Hz, ³J(H⁴H³)=8Hz), 8.38 (d, 1H, H³, ³J(H³H⁴)=8Hz), 8.88 (d, 1H, H⁶, ³J(H⁶H⁵)=6Hz, ³J(Pt-H⁶)=21Hz), 9.06 (d, 1H, H⁶, ³J(H⁶H⁵)=6Hz, ³J(Pt-H⁶)=34Hz). ¹³C NMR in acetone-*d*₆: δ -6.22 (s, CH₃, Pt-CH₃), 25.63 (s, cyclic CH₂), 26.47 (s, cyclic CH₂), 28.07 (s, cyclic CH₂), 28.25 (s, cyclic CH₂),

29.63 (s, cyclic CH₂), 29.82 (s, cyclic CH₂), 127.19 (s, aromatic C), 128.19 (s, aromatic C), 128.26 (s, aromatic C), 129.10 (s, aromatic C), 139.95 (s, aromatic C), 141.02 (s, aromatic C), 146.12 (s, aromatic C), 146.54 (s, aromatic C), 151.00 (s, aromatic C), 154.30 (s, aromatic C), 155.86 (s, aromatic C), 156.48 (s, aromatic C). **¹⁹F NMR in acetone-*d*₆**: δ -78.82 (s, free trifluoromethanesulfonate). **ESI-MS(TOF)**:

[[C₄₂H₄₆N₈Pt₂]²⁺ Calculated m/z = 526.16g/mol; Determined m/z = 526.2g/mol; where z = 2. **Elemental Analysis**: Anal. Calc'd. [C₄₂H₄₆N₈Pt₂]²⁺[O₃SCF₃]₂⁻•CH₂Cl₂ (%): C, 37.64; H, 3.37; N, 7.94; S, 4.47. Found: C, 37.85; H, 3.76; N, 7.54; S, 4.28.

***endo*-[PtMe(C₃H₆O)(6-dppd)]⁺ [OSO₂CF₃]⁻, Complex 14a.** To an acetone-*d*₆ solution of [PtMe₂(6-dppd)] **2**, (0.010g, 0.01848mmol) was added trifluoromethanesulfonic acid, (1.9μL, 0.0215mmol) at -80°C in an NMR tube. ¹H NMR spectra were attained at varying temperature allowing for the characterization of **14a** formed *in situ*. **¹H NMR in acetone-*d*₆**: δ 1.02 (s, 3H, CH₃, ²J(PtH)=75Hz), 1.54 (m, 2H, CH₂), 1.72 (s, 2H, CH₂), 1.76 (m, 2H, CH₂), 2.20 (m, 2H, CH₂), 3.12 (m, 2H, CH₂), 3.56 (m, 2H, CH₂), 8.06 (dd, 1H, ³J(HH)=6Hz, ³J(HH)=8Hz), 8.56 (dd, 1H, ³J(HH)=6Hz, ³J(HH)=8Hz), 8.64 (t, 1H, ³J(HH)=8Hz), 8.77 (d, 1H, ³J(HH)=8Hz, ³J(HH)=8Hz), 8.86 (d, 1H, ³J(HH)=8Hz), 9.14 (t, 1H, ³J(HH)=8Hz, ³J(HH)=8Hz), 9.36 (d, 1H, ³J(HH)=6Hz), 9.41 (d, 1H, ³J(HH)=6Hz, ³J(PtH)=26Hz).

***exo*-[PtMe(C₃H₆O)(6-dppd)]⁺ [OSO₂CF₃]⁻, Complex 14b.** To an acetone-*d*₆ solution of [PtMe₂(6-dppd)] **2**, (0.010g, 0.01848mmol) was added trifluoromethanesulfonic acid, (1.9μL, 0.0215mmol) at -80°C in an NMR tube. ¹H NMR spectra were attained at varying temperature allowing for the characterization of **14b** formed *in situ*. **¹H NMR in acetone-*d*₆**: δ 0.98 (s, 3H, CH₃, ²J(PtH)=75Hz), 1.54 (m, 2H, CH₂), 1.72 (s, 2H, CH₂), 1.76 (m, 2H, CH₂), 2.20 (m, 2H, CH₂), 3.12 (m, 2H, CH₂), 3.56 (m, 2H, CH₂), 7.94 (dd, 1H, ³J(HH)=6Hz, ³J(HH)=8Hz), 8.57 (dd, 1H, ³J(HH)=6Hz, ³J(HH)=8Hz), 8.62 (t, 1H, ³J(HH)=8Hz), 8.74 (d, 1H, ³J(HH)=8Hz, ³J(HH)=8Hz), 8.75 (d, 1H, ³J(HH)=8Hz), 9.12 (t, 1H, ³J(HH)=8Hz, ³J(HH)=8Hz), 9.36 (d, 1H, ³J(HH)=6Hz), 9.40 (d, 1H, ³J(HH)=6Hz, ³J(PtH)=24Hz).

endo-[PtMe(NCMe)(6-dppd)]⁺ [OSO₂CF₃]⁻, Complex 15a. To an acetone-*d*₆ solution of [PtMe₂(6-dppd)] **2**, (0.010g, 0.01848mmol) was added trifluoromethanesulfonic acid, (1.9μL, 0.0215mmol) and acetonitrile at 0°C in an NMR tube. ¹H NMR spectra were attained at varying temperature allowing for the characterization of **15a** formed *in situ*. **¹H NMR in acetone-*d*₆:** δ 1.21 (s, 3H, CH₃, ²*J*(PtH)=76Hz), 1.59 (m, 2H, CH₂), 1.73 (s, 2H, CH₂), 2.10 (m, 2H, CH₂), 2.20 (m, 2H, CH₂), 2.89 (s, 3H, NCMe, ⁴*J*(PtH)=15Hz), 3.19 (m, 2H, CH₂), 3.50 (m, 2H, CH₂), 7.75 (dd, 1H, ³*J*(HH)=6Hz, ³*J*(HH)=8Hz), 7.88 (dd, 1H, ³*J*(HH)=6Hz, ³*J*(HH)=8Hz), 8.01 (t, 1H, ³*J*(HH)=8Hz), 8.25 (d, 1H, ³*J*(HH)=8Hz, ³*J*(HH)=8Hz), 8.39 (d, 1H, ³*J*(HH)=8Hz), 8.46 (t, 1H, ³*J*(HH)=8Hz, ³*J*(HH)=8Hz), 8.81 (d, 1H, ³*J*(HH)=6Hz), 9.31 (d, 1H, ³*J*(HH)=6Hz, ³*J*(PtH)=20Hz).

exo-[PtMe(NCMe)(6-dppd)]⁺ [OSO₂CF₃]⁻, Complex 15b. To an acetone-*d*₆ solution of [PtMe₂(6-dppd)] **2**, (0.010g, 0.01848mmol) was added trifluoromethanesulfonic acid, (1.9μL, 0.0215mmol) and acetonitrile at 0°C in an NMR tube. ¹H NMR spectra were attained at varying temperature allowing for the characterization of **15b** formed *in situ*. **¹H NMR in acetone-*d*₆:** δ 1.02 (s, 3H, CH₃, ²*J*(PtH)=75Hz), 1.59 (m, 2H, CH₂), 1.73 (s, 2H, CH₂), 2.10 (m, 2H, CH₂), 2.20 (m, 2H, CH₂), 2.72 (s, 3H, NCMe, ⁴*J*(PtH)=12Hz), 3.19 (m, 2H, CH₂), 3.50 (m, 2H, CH₂), 7.78 (dd, 1H, ³*J*(HH)=6Hz, ³*J*(HH)=8Hz), 7.91 (dd, 1H, ³*J*(HH)=6Hz, ³*J*(HH)=8Hz), 8.15 (t, 1H, ³*J*(HH)=8Hz), 8.39 (d, 1H, ³*J*(HH)=8Hz, ³*J*(HH)=8Hz), 8.41 (d, 1H, ³*J*(HH)=8Hz), 8.44 (t, 1H, ³*J*(HH)=8Hz, ³*J*(HH)=8Hz), 8.88 (d, 1H, ³*J*(HH)=6Hz), 9.25 (d, 1H, ³*J*(HH)=6Hz, ³*J*(PtH)=20Hz).

exo-[PtMe(PPh₃)(6-dppd)]⁺[OSO₂CF₃]⁻, Complex 16b. To (10mg, 0.01848mmol) of [PtMe₂(6-dppd)] **2**, dissolved in 1mL of acetonitrile, was added ~40μL of a 0.538M solution of trifluoromethanesulfonic acid in acetonitrile at 0°C. Upon addition the originally red solution became an orange-yellow colour. After stirring for ten minutes at 0°C, an acetonitrile solution of triphenylphosphine, (4.84mg, 0.01848mmol) was added at which time the reaction mixture was allowed to gradually warm to room temperature. After 3 hours of stirring, the red-orange solution was removed *in vacuo* to afford a red-orange solid. After successive washings with 2mL of diethyl ether, the red-orange product was dissolved in acetone-*d*₆. A single crystal suitable for X-ray diffraction studies was produced by slow diffusion of pentane into an acetone solution of the

product. Yield 73%. **¹H NMR in acetone-*d*₆**: δ 0.85 (d, 3H, CH₃, ²*J*(Pt-H)=71Hz, ³*J*(P-H)= 3Hz), 1.43 (m, 2H, CH₂^D), 1.68 (m, 2H, CH₂^C), 1.73 (m, 2H, CH₂^B), 2.18 (m, 2H, CH₂^E), 3.14 (t, 2H, CH₂^A), 3.47 (t, 2H, CH₂^F), 6.24 (d, 1H, H^{3'}, ³*J*(H^{3'}H^{4'})=8Hz), 7.37 (td, 6H, H^m, ³*J*(H^mH^o)=7Hz, ³*J*(H^mH^p)=7Hz, ⁴*J*(P-H^m)=2Hz), 7.43 (td, 1H, H^{5'}, ³*J*(H^{5'}H^{6'})=5Hz, ³*J*(H^{5'}H^{4'})=8Hz), 7.49 (t, 3H, H^p, ³*J*(H^{m1}H^p)=7Hz, ³*J*(H^{m2}H^p)=7Hz, ⁵*J*(P-H^p)=2Hz), 7.54 (t, 1H, H^{4'}, ³*J*(H^{4'}H^{3'})=8Hz, ³*J*(H^{4'}H^{5'})=8Hz), 7.68 (td, 6H, H^o, ³*J*(H^oH^m)=7Hz, ³*J*(P-H^o)=12Hz), 8.17 (t, 1H, H⁵, ³*J*(H⁵H⁶)=5Hz, ³*J*(H⁵H⁴)=7Hz), 8.60 (d, 1H, H^{6'}, ³*J*(H^{6'}H^{5'})=5Hz), 8.69 (td, 1H, H⁴, ³*J*(H⁴H⁵)=7Hz, ³*J*(H⁴H³)=8Hz), 8.21 (d, 1H, H³, ³*J*(H³H⁴)=8Hz), 9.35 (dd, 1H, H⁶, ³*J*(H⁶H⁵)=5Hz, ³*J*(Pt-H⁶)=33Hz, ⁴*J*(P-H⁶)=4Hz).

¹³C NMR in acetone-*d*₆: δ -5.27 (s, CH₃, Pt-CH₃), 22.03 (s, cyclic CH₂), 25.15 (s, cyclic CH₂), 26.38 (s, cyclic CH₂), 28.03 (s, cyclic CH₂), 29.49 (s, cyclic CH₂), 30.25 (s, cyclic CH₂), 124.07 (s, aromatic C), 124.64 (s, aromatic C), 128.27 (d, aromatic C of PPh₃, ²*J*(P-C) = 11Hz), 128.27 (s, aromatic C of PPh₃, overlap), 128.96 (s, aromatic C), 129.72 (s, aromatic C), 130.88 (d, aromatic C of PPh₃, ³*J*(P-C) = 3Hz), 132.57 (s, aromatic C), 134.23 (s, aromatic C), 134.28 (d, aromatic C of PPh₃, ¹*J*(P-C) = 11Hz), 136.54 (s, aromatic C), 141.37 (s, aromatic C), 144.58 (s, aromatic C), 146.46 (s, aromatic C), 148.51 (s, aromatic C), 149.10 (s, aromatic C), 151.75 (s, aromatic C), 153.55 (s, aromatic C).

³¹P NMR in acetone-*d*₆: δ 19.37 (s, ¹*J*(Pt-P)=4360Hz). **¹⁹F NMR in acetone-*d*₆**: δ -78.82 (s, free trifluoromethanesulfonate). **ESI-MS(TOF)**: ([C₃₉H₃₈N₄PPt]⁺) Calculated precise mass = 788.250g/mol; Determined Precise Mass = 788.248g/mol. **Elemental Analysis**: Anal. Calc'd. [C₄₀H₃₈N₄PPt]⁺[OSO₂CF₃]⁻• 1.5(C₃H₆O) (%): C, 52.14; H, 4.62; N, 5.47. Found: C, 52.60; H, 4.98; N, 6.02.

Table 3.7: Crystallographic data for *endo,endo*-[Pt₂Me₂(μ₂-κ³-6-dppd)₂](OTf)₂, **13a**.

<i>endo,endo</i>-[Pt₂Me₂(μ₂-κ³-6-dppd)₂](OTf)₂ • C₃H₆O	
Empirical Formula	C ₄₇ H ₅₂ N ₈ O ₇ S ₂ F ₆ Pt ₂
Formula Weight	1409.26
Wavelength	0.71073 Å
Crystal System	Monoclinic
Space Group	P 2/n
Unit Cell Dimensions	a = 10.6068(11) Å α = 90° b = 8.7983(9) Å β = 90.805(2)° c = 26.434(3) Å γ = 90°
Volume	2466.6(4) Å ³
Z	2
Density (calculated)	1.897 Mg/m ³
Absorption Coefficient (μ)	5.832 mm ⁻¹
Crystal Size	0.07x 0.05 x 0.02 mm ³
Refinement Method	Full-matrix least-squares on F ²
Goodness of fit on F ²	1.251
Final R indices [I > 2σ(I)]	R1 = 0.0652, wR2 = 0.1169
R indices (all data)	R1 = 0.0956, wR2 = 0.1257

Table 3.8: Crystallographic data for *exo,exo*-[Pt₂Me₂(μ₂-κ³-6-dppd)₂](OTf)₂,
13b•2(C₃H₆O)•H₂O

<i>exo,exo</i>-[Pt₂Me₂(μ₂-κ³-6-dppd)₂](OTf)₂•2(C₃H₆O)•H₂O	
Empirical Formula	C ₅₀ H ₅₈ N ₈ O ₉ S ₂ F ₆ Pt ₂
Formula Weight	1483.34
Wavelength	0.71073 Å
Crystal System	Triclinic
Space Group	P -1
Unit Cell Dimensions	a = 12.493(3) Å α = 77.96(3)° b = 14.767(3) Å β = 76.62(3)° c = 15.879(3) Å γ = 76.14(3)°
Volume	2730.4(10) Å ³
Z	2
Density (calculated)	1.804 Mg/m ³
Absorption Coefficient (μ)	5.276 mm ⁻¹
Crystal Size	0.14 x 0.10 x 0.07 mm ³
Refinement Method	Full-matrix least-squares on F ²
Goodness of fit on F ²	1.118
Final R indices [I > 2σ(I)]	R1 = 0.0487, wR2 = 0.1352
R indices (all data)	R1 = 0.0834, wR2 = 0.1763

Table 3.9: Crystallographic data for *exo,exo*-[Pt₂Me₂(μ₂-κ³-6-dppd)₂](OTf)₂,
13b•2(C₃H₆O)

<i>exo,exo</i>-[Pt₂Me₂(μ₂-κ³-6-dppd)₂](OTf)₂ • 2(C₃H₆O)	
Empirical Formula	C ₅₀ H ₅₈ N ₈ O ₈ S ₂ F ₆ Pt ₂
Formula Weight	1467.34
Wavelength	0.71073 Å
Crystal System	Triclinic
Space Group	P -1
Unit Cell Dimensions	a = 12.7063(3) Å α = 82.069(1)° b = 14.4106(4) Å β = 81.589(1)° c = 15.2200(4) Å γ = 77.840(1)°
Volume	2678.4(1) Å ³
Z	2
Density (calculated)	1.819 Mg/m ³
Absorption Coefficient (μ)	5.376 mm ⁻¹
Crystal Size	0.23 x 0.09 x 0.06 mm ³
Refinement Method	Full-matrix least-squares on F ²
Goodness of fit on F ²	1.075
Final R indices [I > 2σ(I)]	R1 = 0.0356, wR2 = 0.0825
R indices (all data)	R1 = 0.0554, wR2 = 0.0907

Table 3.10: Crystallographic data for *exo,exo*-[Pt₂Me₂(μ₂-κ³-6-dppd)₂](OTf)₂,
13b•CH₂Cl₂

<i>exo,exo</i>-[Pt₂Me₂(μ₂-κ³-6-dppd)₂](OTf)₂•CH₂Cl₂	
Empirical Formula	C ₄₅ H ₄₈ N ₈ O ₆ S ₂ F ₆ Cl ₂ Pt ₂
Formula Weight	1436.11
Wavelength	0.71073 Å
Crystal System	Orthorhombic
Space Group	Pbcn
Unit Cell Dimensions	a = 12.6348(8) Å α = 90° b = 22.0849(13) Å β = 90° c = 19.8889(12) Å γ = 90°
Volume	5549.8(6) Å ³
Z	4
Density (calculated)	1.719 Mg/m ³
Absorption Coefficient (μ)	5.278 mm ⁻¹
Crystal Size	0.20 x 0.07 x 0.07 mm ³
Refinement Method	Full-matrix least-squares on F ²
Goodness of fit on F ²	1.042
Final R indices [I > 2σ(I)]	R ₁ = 0.0570, wR ₂ = 0.1190
R indices (all data)	R ₁ = 0.1051, wR ₂ = 0.1309

Table 3.11: Crystallographic data for *exo*-[PtMe(PPh₃)(6-dppd)](OTf), **16b**

<i>exo</i>-[PtMe(PPh₃)(6-dppd)](OTf)	
Empirical Formula	C ₄₀ H ₃₈ N ₄ O ₃ S F ₃ P ₁ Pt ₁
Formula Weight	937.86
Wavelength	0.71073 Å
Crystal System	Triclinic
Space Group	P -1
Unit Cell Dimensions	a = 9.8817(2) Å α = 83.127(1)° b = 11.1700(2) Å β = 78.985(1)° c = 18.5352(3) Å γ = 66.785(1)°
Volume	1843.4(1) Å ³
Z	2
Density (calculated)	1.690 Mg/m ³
Absorption Coefficient (μ)	3.966 mm ⁻¹
Crystal Size	0.261 x 0.162 x 0.129 mm ³
Refinement Method	Full-matrix least-squares on F ²
Goodness of fit on F ²	1.030
Final R indices [I>2σ(I)]	R1 = 0.0212, wR2 = 0.0459
R indices (all data)	R1 = 0.0264, wR2 = 0.0472

3.7 References

1. Safont-Sempere, M. M.; Fernández, G.; Würthner, F. *Chem. Rev.* **2011**, *111*, 5784–5814.
2. Chakrabarty, R.; Mukherjee, P. S.; Stang, P. J. *Chem. Rev.* **2011**, *111*, 6810–6918.
3. Lippert, B.; Sanz Miguel, P. J. *Chem. Soc. Rev.* **2011**, *40*, 4475–4487.
4. Lu, X.; Li, X.; Guo, K.; Xie, T-Z.; Moorefield, C. N.; Wesdemiotis, C.; Newkome, G. R. *J. Am. Chem. Soc.* **2014**, *136*, 18149–18155.
5. Xu, L.; Wang, Y.-X.; Yang, H-B. *Dalton Trans.* **2015**, *44*, 867–890.
6. Zheng, Y-R.; Suntharalingam, K.; Johnstone, T. C.; Lippard, S. J. *Chem. Sci.* **2014**. DOI: 10.1039/c4sc01892c
7. Cook, T. R.; Vajpayee, V.; Lee, M.; Stang, P. J.; Chi, K. *Acc. Chem. Rev.* **2013**, *46*, 2464–2474.
8. Smulders, M.; Riddell, I. A; Browne, C.; Nitschke, J. R. *Chem. Soc. Rev.* **2013**, *42*, 1728–1754.
9. Nakamura, T.; Ube, H.; Shionoya, M. *Chem. Lett.* **2013**, *42*, 328-334.
10. Whittell, G. R.; Hager, M. D.; Schubert, U. S.; Manners, I. *Nat. Mater.* **2011**, *10*, 176–188.
11. King, P. J. *Annu. Rep. Prog. Chem., Sect. A.* **2008**, *104*, 325–342.
12. Lusby, P. J. *Annu. Rep. Prog. Chem., Sect. A.* **2008**, *104*, 297–324.
13. Han, Y-F.; Li, H.; Weng, L-H.; Jin, G-X. *Chem. Commun.* **2010**, *46*, 3556–3558.
14. Brusilowskij, B.; Dzyuba, E.V; Troff, R.W.; Schalley, C. A. *Dalton. Trans.* **2011**, *40*, 12089–12096.
15. Miyake, R.; Tashiro, S.; Shiro, M.; Tanaka, K.; Shionoya, M. *J. Am. Chem. Soc.* **2008**, *130*, 5646–5647.

16. Gutie, A.; Engeser, M.; Lorenz, Y.; Schilling, R.; Go, P.; Mart, A. *Organometallics*. **2012**, *31*, 1533–1545.
17. Chmielewski, M. J.; Buhler, E.; Candau, J.; Lehn, J-M. *Chem. Eur. J.* **2014**, *20*, 6960–6977.
18. Aridomi, T.; Takamura, K.; Igashira-Kamiyama, A.; Kawamoto, T.; Konno, T. *Chem. Eur. J.* **2008**, *14*, 7752–7755.
19. Martínez-Calvo, M.; Romero, M. J.; Pedrido, R.; González-Noya, A. M.; Zaragoza, G.; Bermejo, M. R. *Dalton Trans.* **2012**, *41*, 13395–13404.
20. Zhang, J.; Su, C-Y. *Coord. Chem. Rev.* **2013**, *257*, 1373–1408.
21. Lai, S.; Chan, M. C.; Peng, S.; Che, C. *Angew. Chem. Int. Ed.* **1999**, *38*, 669–671.
22. Yamanaka, M.; Kawaharada, M.; Nito, Y.; Takaya, H.; Kobayashi, K. *J. Am. Chem. Soc.* **2011**, *133*, 16650–16656.
23. Pariya, C.; Sparrow, C. R.; Back, C-K.; Sandí, G.; Fronczek, F. R.; Maverick, A. W. *Angew. Chem. Int. Ed.* **2007**, *46*, 6305–6308.
24. Kusukawa, T.; Fujita, M. *J. Am. Chem. Soc.* **2002**, *124*, 13576–13582.
25. Bruns, C. J.; Fujita, D.; Hoshino, M.; Sato, S.; Stoddart, J. F.; Fujita, M. *J. Am. Chem. Soc.* **2014**, *136*, 12027–12034.
26. Leenders, S.H.A.M.; Gramage-Doria, R.; de Bruin, B.; Reek, J.N.H. *Chem. Soc. Rev.* **2015**, *44*, 433–448.
27. Rebilly, J-N.; Colasson, B.; Bistri, O.; Over, D.; Reinaud, O. *Chem. Soc. Rev.* **2015**, *44*, 467–489.
28. Ronson, T.K.; Giri, C.; Beyeh, N.K.; Minkkinen, A.; Topić, F.; Holstein, J.J.; Rissanen, K.; Nitschke, J.R. *Chem. Eur. J.* **2013**, *19*, 3374–3382.
29. Hall, B.R.; Manck, L.E.; Tidmarsh, I.S.; Stephenson, A.; Taylor, B.F.; Blaikie, E.J.; Vander Griend, D.A.; Ward, M.D. *Dalton. Trans.* **2011**, *40*, 12132–12145.
30. Kawano, M.; Kobayashi, Y.; Ozeki, T.; Fujita, M. *J. Am. Chem. Soc.* **2006**, *128*, 6558–6559.

31. Northrop, B. H.; Zheng, Y.-R.; Chi, K.-W.; Stang, P. J. *Acc. Chem. Res.* **2009**, *42*, 1554–1563.
32. Zheng, Y.-R.; Yang, H.-B.; Ghosh, K.; Zhao, L.; Stang, P. J. *Chem. Eur. J.* **2009**, *15*, 7203–7214.
33. Cangelosi, V. M.; Carter, T. G.; Zakharov, L. N.; Johnson, D. W. *Chem. Commun.* **2009**, 5606–5608.
34. Albrecht, M.; Dehn, S.; Frohlich, R. *Angew. Chem., Int. Ed.* **2006**, *45*, 2792.
35. Zhao, S.-B.; Wang, R.-Y.; Wang, S. *J. Am. Chem. Soc.* **2007**, *129*, 3092–3093.
36. Annibale, V.T.; Lund, L.M.; Song, D. *Chem. Commun.* **2010**, *46*, 8261.
37. Frischmann, P.D.; Guieu, S.; Tabeshi, R.; MacLachlan, M.L. *J. Am. Chem. Soc.* **2010**, *132*, 7668.
38. Chi, K.W.; Addicott, C.; Arif, A.A.; Stang, P.J. *J. Am. Chem. Soc.* **2004**, *126*, 16569.
39. Pirondini, L.; Bertolini, F.; Cantadori, B.; Uggozoli, F.; Massera, C.; Dalcanale, E. *Proc. Natl. Acad. Sci. U.S.A.* **2002**, *99*, 4911.
40. Qin, Z.; Jennings, M.C.; Puddephatt, R.J. *Chem. Commun.* **2001**, 2676.
41. Chernyaev, I.I. *Ann. Inst. Platine SSSR.* **1926**, *4*, 261.
42. Grinberg, A.A. *Ann. Inst. Platine SSSR.* **1927**, *5*, 109.
43. Langford, C.H.; Gray, H.B. "Ligand Substitution Processes." Wiley, New York, 1965.
44. Jain, V.K.; Jain, L. *Coord. Chem. Rev.* **2005**, *249*, 3075.
45. Nedelec, N.; Rochon, F.D. *Inorg. Chem.* **2001**, *40*, 5236.
46. Matsumoto, K.; Moriyama, H.; Suzuki, K. *Inorg. Chem.* **1990**, *29*, 2096.
47. Chatt, J.; Hart, F.A. *J. Chem. Soc.* **1960**, 2807.
48. Reedijk, J. *Proc. Natl. Acad. U.S.A.* **2003**, *100*, 3611.
49. Bonnington, K. J.; Zhang, F.; Moustafa, M. M. A. R.; Cooper, B. F. T.; Jennings, M. C.; Puddephatt, R. J. *Organometallics* **2012**, *31*, 306–317.

50. Heyduk, A. F.; Driver, T. G.; Labinger, J. A.; Bercaw, J. E. *J. Am. Chem. Soc.* **2004**, *126*, 15034–15035.
51. Karshtedt, D.; Mcbee, J. L.; Bell, A. T.; Tilley, T. D. *Organometallics* **2006**, *25*, 1801–1811.
52. Zhao, S-B.; Gang, W.; Wang, S. *Organometallics* **2006**, *25*, 5979–5989.
53. Zhang, F.; Kirby, C. W.; Hairsine, D. W.; Jennings, M. C.; Puddephatt, R. J. *J. Am. Chem. Soc.* **2005**, *127*, 14196–14197.
54. *APEX 2, Crystallography software package*; Bruker AXS: Madison, WI, 2005.
55. *SAINTE, Data Reduction Software*; Bruker AXS: Madison, WI, 1999.
56. Sheldrick, G. M. *SADABS v.2.01, Area Detector Absorption Correction Program*; Bruker AXS: Madison, WI, 2006.
57. Nonius (1998). *COLLECT*. Nonius BV, Delft, The Netherlands.
58. Otwinowski, Z.; Minor, W. *Methods in Enzymology*. 1997, Vol. 276, *Macromolecular Crystallography, Part A*, edited by C. W. Carter Jr & R. M. Sweet, p 307-326. New York: Academic Press.
59. Sheldrick, G. M. *SHELXS, program for solution of crystal structures. Acta Cryst.* **A64**, 2008, 112-122.
60. Sheldrick, G. M. *SHELXL, program for refinement of crystal structures. Acta Crystallogr., Section A.* **2008**, *64*, 112-122.
61. Spek, A.L. *Acta Cryst.* **2009**, *D65*, 148-155.

CHAPTER 4

Supramolecular Organoplatinum(IV) Chemistry: Complexes with a Pendent Hydrogen Bond Acceptor

4.1 Introduction

The field of supramolecular chemistry is heavily dependent on the ability of molecules to form strong yet reversible hydrogen bonds in both an intermolecular and intramolecular manner [1-3]. Hydrogen bonds are relatively facile to introduce and form in a directional manner allowing the chemist to design self-assembled architectures in a logical manner [3,4]. Another significant benefit of hydrogen bonds is that they are easily reversible due to the relatively weak manner of their bonding [2-4]. These properties often allow for the selective preparation of a desired compound through the formation and dissociation of hydrogen bonds. These interactions are critical for the self-assembly of molecules into supramolecular architectures and functional materials [1,2,5-7].

Although these principles are often utilized in organic and inorganic chemistry, the self-assembly of complex structures is often less employed in organometallic chemistry due to the incompatibility of the functional groups typically involved in hydrogen bonds with the metal-carbon bonds. The metal-carbon bonds are often cleaved by these functional groups through protonolysis of the metal-carbon bond [1-3,8-20]. Alkylplatinum(IV) complexes however have shown to overcome this detrimental property due to the stability of the Pt-C bonds towards protonolysis and as such these alkylplatinum(IV) complexes have given rise to an extensive variety of supramolecular chemistry [9,13,19-31]. Despite the potential of alkylplatinum(IV) complexes, their self-assembly has been slow to develop due to the inherently slow manner in which ligands substitute at both platinum(II) and platinum(IV) complexes relative to its other congeners [32,33]. However, it has been shown previously that the slow ligand substitution can be utilized advantageously in the design of specific isomeric forms of platinum complexes [34-36].

As of late, there has been an increased amount of interest in the use of dimethylplatinum(II) complexes containing nitrogen donor ligands in supramolecular chemistry, due in part to the variety of ligand derivatives available [9,26,31]. By derivatizing the ligand one can affect both the properties of the ligand as well as the supramolecular architectures formed by the resultant complex through the promotion or inhibition of secondary bonding. For example, 4,4'-di-*tert*-butyl-2,2'-bipyridine *A* shown

in figure 4.1, is a common derivative of the generic ligand 2,2'-bipyridine utilized mainly due to its enhanced solubility in common organic solvents [9, 37-40]. Other derivatives such as **B** are used to anchor transition metal catalysts to oxide supports [31]. By incorporating functional groups such as amides and esters, one can introduce secondary bonding properties into the ligand as shown in **C** [26]. By incorporating these functional groups, the self-assembly of their corresponding organoplatinum(IV) complexes can be facilitated by both hydrogen bonding and π -stacking.

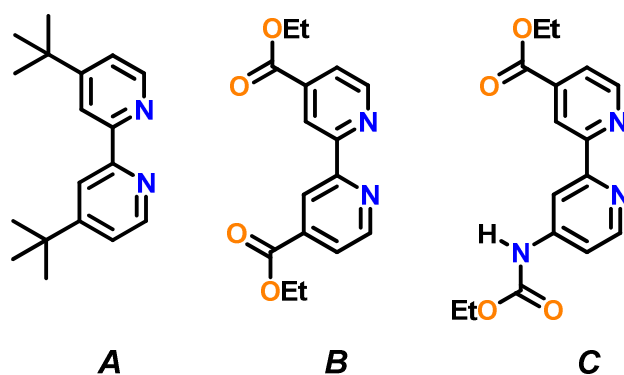
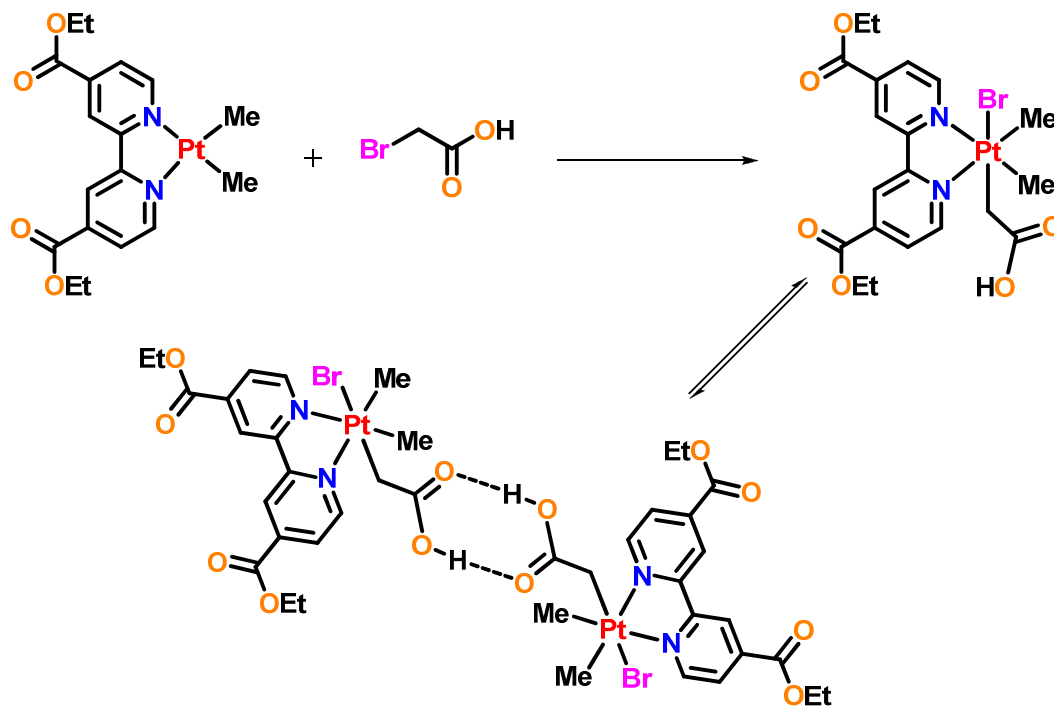


Figure 4.1. Various ligands derived on 2,2'-bipyridine used for crystal engineering and supramolecular organometallic chemistry.

Another mechanism by which one can introduce functional groups capable of being hydrogen bond donors or acceptors is by installing them at platinum(II) complexes via oxidative addition. This is typically done through the reaction of an organoplatinum(II) precursor complex and an equivalent of an alkyl bromide substrate containing hydrogen bond donors [9,21,22,26,29,31,37,38,40]. This results in the corresponding organoplatinum(IV) complex which is then capable of forming supramolecular structures. As an example, carboxylic acid groups have been installed via the oxidative addition of the RCH_2-Br bond in the substrate yielding the corresponding organoplatinum(IV) complex. These complexes commonly self-assemble to form dimers through hydrogen bonding as shown in scheme 4.1. Following this approach, carboxylic acids, amides, alcohols and boronic acids have been successfully installed at platinum(II) resulting in a platinum(IV) complexes capable of forming a wide array of supramolecular structures such as oligomers, polymers, and sheets.



Scheme 4.1. Representative oxidative addition reaction of a substrate containing hydrogen bonding functionality yielding an organoplatinum(IV) complex capable of forming a self-assembled dimer.

Previous work in the Puddephatt group using ligand *D* and its corresponding dimethylplatinum(II) complex *E*, in figure 4.2, has shown the ability to form a variety of supramolecular structures through the presence of the hydrogen bond acceptor nitrogen and oxygen atoms in the ligand [41-43]. Organoplatinum(IV) derivatives containing both the ligand *E* and carboxylic acid functional groups have been shown to form supramolecular polymers through hydrogen bonding between the carboxylic acid and both the nitrogen and oxygen hydrogen bond acceptor atoms. When boronic acid groups are present in the organoplatinum(IV) species', sheet like structures are observed through secondary bonding between the donor boronic acids and acceptor bromide atoms [41]. It is with this motivation that the supramolecular chemistry of organoplatinum(IV) complexes based on complex **2**, figure 4.2, has been explored. The free pyridyl group in **2**

is non-coordinating in most circumstances, but should be sufficiently nucleophilic to entertain intermolecular and intramolecular hydrogen bonding [35,44,45].

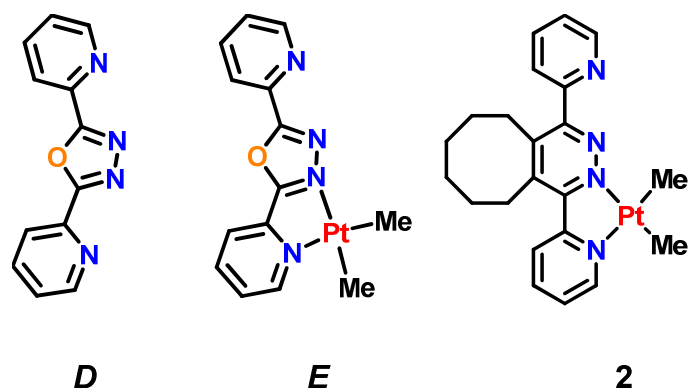
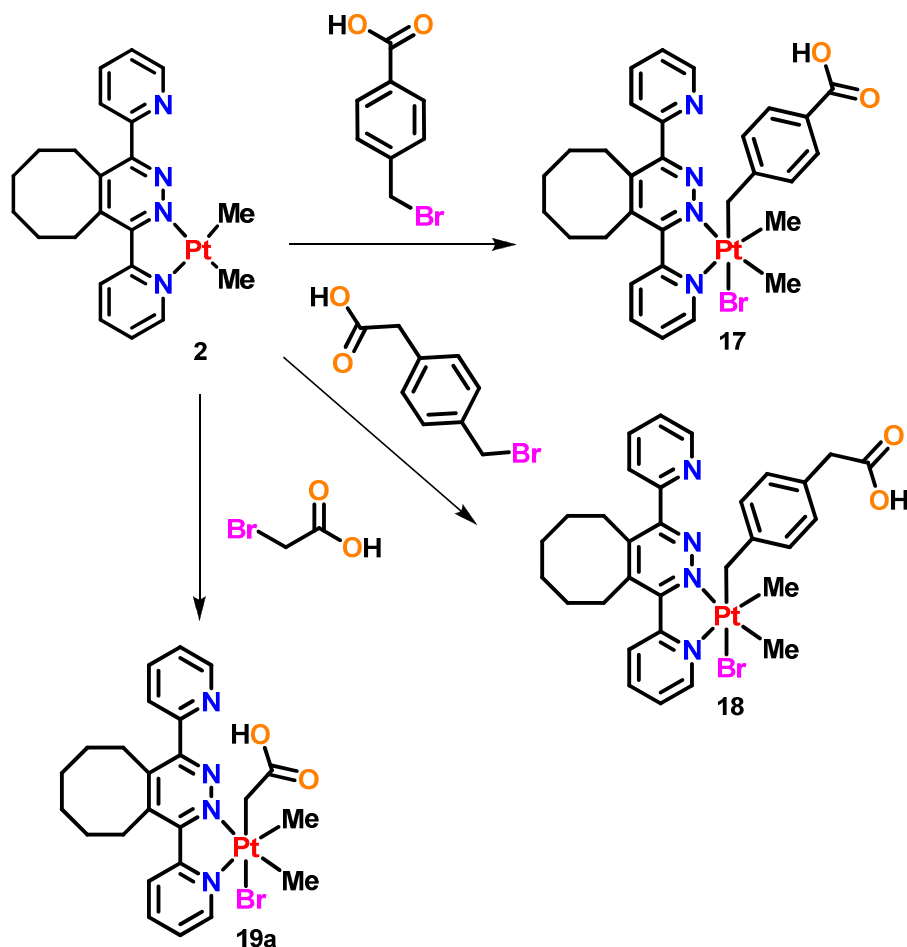


Figure 4.2. Ligands and platinum(II) complexes possessing hydrogen bond acceptor atoms built into the ligand backbone.

This chapter describes the reactivity of complex **2** towards the oxidative addition of substrates capable of forming hydrogen bonding interactions. The reaction of **2** with carboxylic acid, alcohol and boronic acid containing substrates yields air stable organoplatinum(IV) complexes containing hydrogen bond donors. The supramolecular chemistry of these complexes is explored and the effect of incorporating a hydrogen bonding acceptor group in the ligand is investigated. This chapter further describes the varying supramolecular structures of the organoplatinum(IV) complexes and their dependence on not only the presence of the hydrogen bond acceptor in the ligand, but the type and substitution of the hydrogen bond donor.

4.2 Reaction of 2 with Carboxylic Acid Derivatives

Substrates containing carboxylic acid functional groups were installed at complex **2** through oxidative addition of a Br-CH₂ bond. The substrates α -bromo-4-toluic acid, 4-(bromomethyl)phenylacetic acid, and bromoacetic acid, all reacted at room temperature in acetone to give the corresponding platinum(IV) complexes in accordance with scheme 4.2. In all of the above cases, the oxidative addition of the substrates yielded only the *trans* isomers which were isolated as air-stable yellow solids. The formation of products of *trans* oxidative addition solely is supported in the literature, although similar reactions with dimethylplatinum(II) complexes have been shown to produce mixtures of both *cis* and *trans* isomers, [9,26,31,41].



Scheme 4.2. Oxidative addition of carbon-bromine bonds to yield **17**, **18** and **19a**.

The reaction of **2** with α -bromo-4-toluic acid in acetone yielded a bright yellow solid, complex **17**, *trans*-[PtBrMe₂(CH₂-4-C₆H₄CO₂H)(6-dppd)], in high yield, scheme 4.2. The formation of complex **17** was proposed based on the ¹H NMR spectrum of the solid, figure 4.3, in which two distinct methylplatinum resonances were observed at a chemical shifts of $\delta = 1.42$ and $\delta = 1.75$ ppm and coupling constants ²J_{PtH} = 70 Hz and 71 Hz respectively. Two distinct methylplatinum resonances arise due to the lack of symmetry in complex **17**. These values of chemical shift are consistent with those typically observed for platinum(IV) complexes formed via the *trans* oxidative addition of substrates [26,31,41]. The coupling constant values of 70 Hz and 71 Hz are indicative of a platinum(IV) complex being formed in which the methyl groups are positioned *trans* to nitrogen [26,31,41]. Further support for the formation of complex **17** was provided by the presence of Pt-195 satellites present on the resonances diagnostic for the methylene group of the substrate. The unsymmetrical nature of complex **17** results in the methylene proton resonances appearing as an AB spin system with chemical shifts of $\delta = 2.84$ ppm and 2.89 ppm and coupling constant values of ²J_{PtH} = 92 Hz and ²J_{PtH} = 83 Hz respectively. This chemical shift and coupling constant values is consistent with similar compounds previously synthesized which further supports the formation of complex **17** via *trans* oxidative addition. The aromatic region of the ¹H NMR spectrum of complex **17** possesses eight resonances resulting from the pyridyl protons of the ligand backbone and two resonances which arise due to phenyl protons on the 4-toluic acid group. A resonance at $\delta = 9.07$ ppm was observed to possess Pt-195 satellites with a coupling constant value of ³J_{PtH} = 19Hz. This resonance was attributed to the *ortho* proton resonance of the pyridyl ring of the ligand which coordinates to the platinum center. Using a gCOSY NMR spectrum and this *ortho* pyridyl proton resonance as a reference, the remainder of the pyridyl resonances can be assigned. Pt-195 satellites were also observed around the doublet resonance at $\delta = 6.43$ ppm with a coupling constant value of ⁴J_{PtH} = 19Hz. The possession of satellites allows for the assignment of this resonance to the protons *ortho* to the methylene group on the phenyl ring of the 4-toluic acid group. An additional doublet at $\delta = 7.27$ ppm was shown to have a correlation in the gCOSY spectrum with the doublet at $\delta = 6.43$ ppm and therefore is assigned to the remaining protons positioned *meta* to the methylene group of the 4-toluic acid group.

Single crystals of complex **17** were able to be grown from the slow diffusion of pentane into an acetone solution of **17**. The molecular structure of **17** is shown in figure 4.4. The structure confirms that the platinum(IV) adopts an octahedral geometry resultant from the *trans* oxidative addition of α -bromo-4-toluic acid. Selected bond distances and angles of complex **17** are given in table 4.1. It is noticed that the toluic acid ligand adopts an orientation directly above the pyridazine ring due to favourable π - π interactions between the aromatic groups. This is very common for these types of compounds and is reported previously in the literature [35,45]. The non-coordinating pyridyl group is observed to deviate from the plane of the pyridazine ring to presumably alleviate unfavourable steric strain. The carboxylic acid group on the toluic acid ligand take part in self-assembly via $\text{OH}\cdots\text{BrPt}$ hydrogen bonding to give supramolecular polymers, with $\text{O}(1)\cdots\text{Br}(1\text{A}) = 3.19 \text{ \AA}$. In similar complexes, the carboxylic acids are observed to form head-to-tail dimer structures and as such this polymeric structure is somewhat unexpected [31,43]. Similar polymers formed from hydrogen bonding to BrPt units are observed however, in the case of amides and boronic acids acting as the hydrogen bond donors [11,12,31,37,40,46-48]. In this case hydrogen bonding to the BrPt group is evidently preferred over interactions with the pendent hydrogen bond acceptor pyridyl group or the formation of head to tail dimers. Figure 4.5 shows the supramolecular polymeric structure of complex **17**.

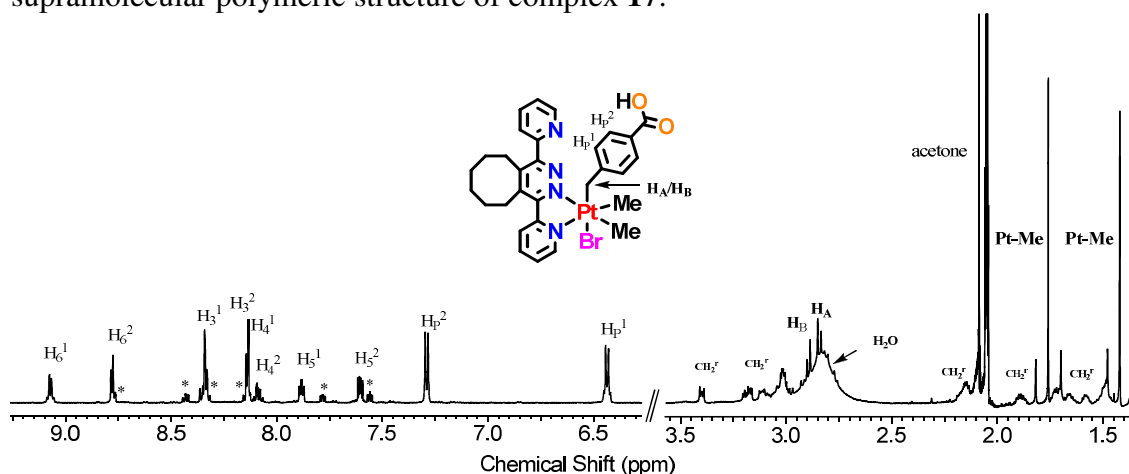


Figure 4.3. ^1H NMR spectrum of complex **17**, $[\text{PtBrMe}_2(\text{CH}_2\text{-4-C}_6\text{H}_4\text{CO}_2\text{H})(6\text{-dppd})]$, in acetone- d_6 . * indicates trace amounts of starting material complex **2**. CH_2^f indicates the proton resonances due to the cyclooctyl ring.

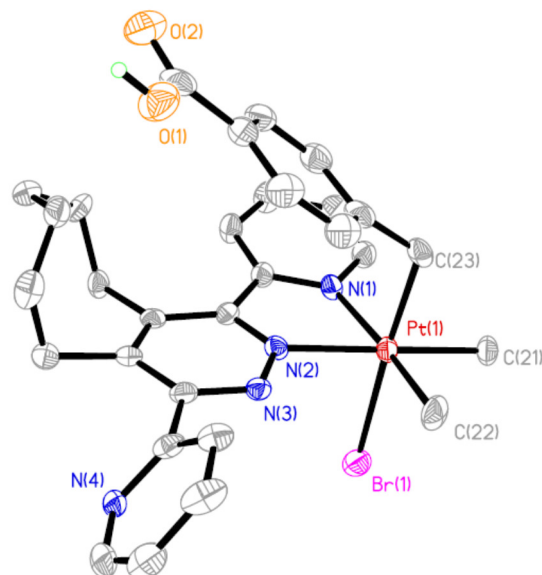


Figure 4.4. Molecular structure of complex **17**, with an atomic numbering scheme (hydrogen atoms excluded for clarity).

Table 4.1: Bond lengths [Å] and angles [°] for [PtBrMe₂(CH₂-4-(C₆H₄CO₂H)(6-dppd)], **17.**

Pt(1)-N(1)	2.144(6)	Pt(1)-N(2)	2.127(5)
Pt(1)-C(21)	2.091(6)	Pt(1)-C(22)	2.050(7)
Pt(1)-Br(1)	2.5830(8)	Pt(1)-C(23)	2.098(7)
N(1)-Pt(1)-N(2)	74.9(2)	C(21)-Pt(1)-C(22)	86.5(3)
N(2)-Pt(1)-C(21)	174.0(2)	N(2)-Pt(1)-C(23)	95.8(2)
N(2)-Pt(1)-C(22)	98.7(3)	N(1)-Pt(1)-C(21)	100.0(2)
C(21)-Pt(1)-C(23)	87.1(3)	C(22)-Pt(1)-C(23)	89.7(3)
N(1)-Pt(1)-C(22)	173.3(3)	N(1)-Pt(1)-C(23)	88.9(2)
N(2)-Pt(1)-Br(1)	87.82(15)	C(22)-Pt(1)-Br(1)	89.5(2)
N(1)-Pt(1)-Br(1)	92.37(15)	C(21)-Pt(1)-Br(1)	89.4(2)
C(23)-Pt(1)-Br(1)	176.41(19)	Pt(1)-C(23)-C(24)	114.4(4)

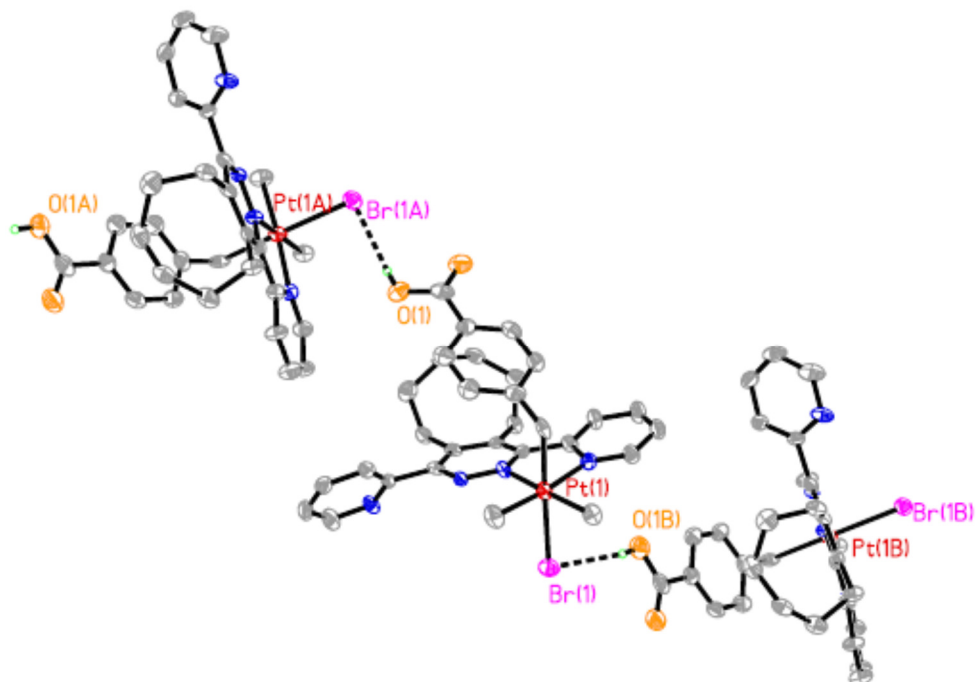


Figure 4.5. A view of the supramolecular polymeric structure of complex **17**.

In a manner similar to that for the preparation of complex **17**, the oxidative addition reaction of **2** with 4-(bromomethyl)phenylacetic acid was performed. This reaction again occurred via a *trans* oxidative addition yielding complex **18**, *trans*-[PtBrMe₂(CH₂-4-C₆H₄CH₂CO₂H)(6-dppd)], as depicted previously in scheme 4.2. Complex **18** is again an air stable bright yellow solid, produced in high yield and soluble in organic solvents. The ¹H NMR spectrum of complex **18** again contains two methylplatinum resonances at $\delta = 1.42$ and 1.68 ppm with coupling constants $^2J_{\text{PtH}} = 70$ Hz for both resonances, figure 4.6. These chemical shifts and coupling constants are similar to those observed for complex **17** and are diagnostic of a dimethylplatinum(IV) complex in which the methyl groups are positioned *trans* the nitrogen donor atoms of the ligand. The methylene protons of the CH₂ linker give rise again to an AB spin system at $\delta = 2.78$ and 2.81 ppm with $^2J_{\text{PtH}} = 90$ Hz and 88 Hz respectively. These values support the formation of the *trans* product of oxidative addition as the methylene group being positioned *trans* to bromine would explain the coupling constant values observed. Further downfield, two doublet resonances are observed for the phenyl ring protons at $\delta = 6.25$ and $\delta = 6.48$ ppm. The resonance at $\delta = 6.25$ ppm is observed to possess Pt-195

satellites with a coupling constant value ${}^4J_{\text{PtH}} = 19$ Hz, which supports the assignment of the resonance being that of the phenyl proton in the *ortho* position relative to the methylene group coordinated to the platinum center. Also further downfield, eight resonances are observed similarly to the of complex **17** which can be attributed to the pyridyl protons of the ligand, the furthest downfield of which possessing Pt-195 satellites with a coupling constant value of ${}^3J_{\text{PtH}} = 19$ Hz.

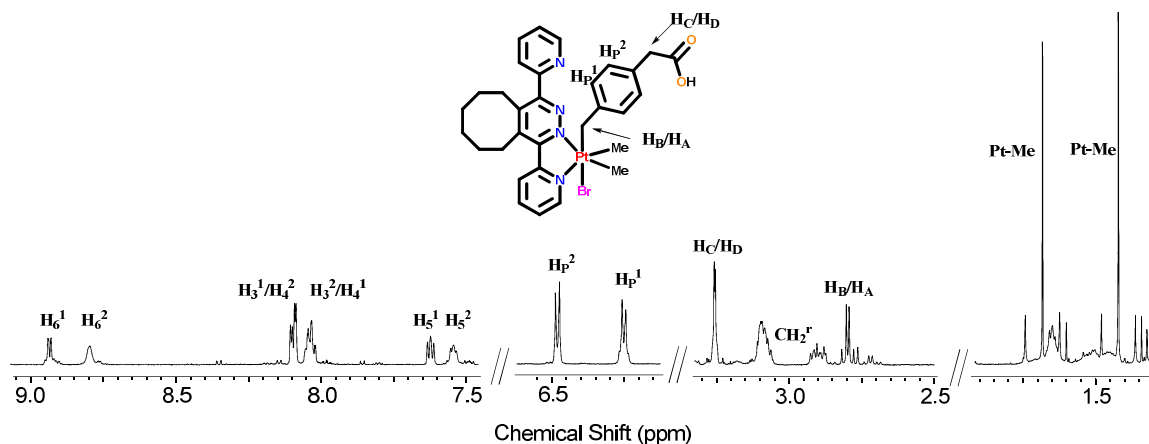


Figure 4.6. ${}^1\text{H}$ NMR spectrum of complex **18**, $[\text{PtBrMe}_2(\text{CH}_2\text{-4-C}_6\text{H}_4\text{CH}_2\text{CO}_2\text{H})(6\text{-dppd})]$, in CD_2Cl_2 . CH_2^r indicates the proton resonances due to the cyclooctyl ring.

The formation of the *trans* product was further confirmed through X-ray diffraction analysis of single crystals of **18** which were grown through the slow vapour diffusion of pentane into a concentrated dichloromethane solution of complex **18**. The solid state structure of **18**, figure 4.7, confirms the predicted *trans* stereochemistry inferred from the ${}^1\text{H}$ NMR spectrum. Similar to **17**, the benzyl group is positioned above the plane of the pyridazine ring as a result of π - π stacking interactions. Important bond lengths and angles for **18** can be found in table 4.2.

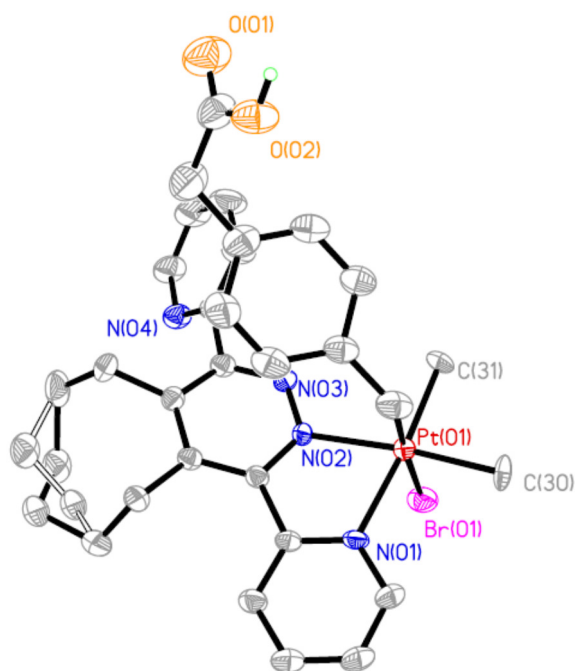


Figure 4.7. Molecular structure of complex **18**, with an atomic numbering scheme (hydrogen atoms and solvent molecules excluded for clarity).

Table 4.2: Bond lengths [Å] and angles [°] for [PtBrMe₂(CH₂-4-(C₆H₄CH₂CO₂H)(6-dppd)], **18.**

Pt(01)-N(01)	2.153(4)	Pt(01)-N(02)	2.140(4)
Pt(01)-C(21)	2.103(6)	Pt(01)-C(30)	2.068(6)
Pt(01)-Br(01)	2.5826(9)	Pt(01)-C(31)	2.062(5)
N(01)-Pt(01)-N(02)	75.29(16)	C(21)-Pt(01)-C(30)	86.4(3)
N(02)-Pt(01)-C(21)	92.1(2)	N(02)-Pt(01)-C(31)	99.0(2)
N(02)-Pt(01)-C(30)	173.6(2)	N(01)-Pt(01)-C(21)	90.8(2)
C(21)-Pt(01)-C(31)	89.9(3)	C(30)-Pt(01)-C(31)	87.3(3)
N(01)-Pt(01)-C(30)	98.5(2)	N(01)-Pt(01)-C(31)	174.2(2)
N(02)-Pt(01)-Br(01)	91.48(11)	C(30)-Pt(01)-Br(01)	90.0(2)
N(01)-Pt(01)-Br(01)	89.57(12)	C(21)-Pt(01)-Br(01)	176.39(18)
C(31)-Pt(01)-Br(01)	90.2(2)	Pt(01)-C(21)-C(22)	116.4(4)

Propagation of the structure of **18** in the solid state gives the supramolecular linear polymeric structure as depicted in figure 4.8. This indicates that the polymeric structure is a result of the self-assembly of monomer units via a hydrogen bonding interaction. Unlike **17**, the hydrogen bonding interaction in **18** is observed between the carboxylic acid group of one monomer unit and the nitrogen acceptor atom of the non-coordinating pyridyl group of an adjacent monomer unit. The hydrogen bonding interaction has an N(04)•••O(02B) distance of 2.749 Å, which is a shorter distance than that of an analogous organoplatinum(IV) complex indicating the presence of a strong interaction [43]. Presumably the flexibility provided by the methylene group between the benzyl group and carboxylic acid allows for **18** to adopt an orientation that promotes the observed polymerization through the N•••HO hydrogen bonding rather than PtBr•••HO hydrogen bonding as observed in the less flexible complex **17**.

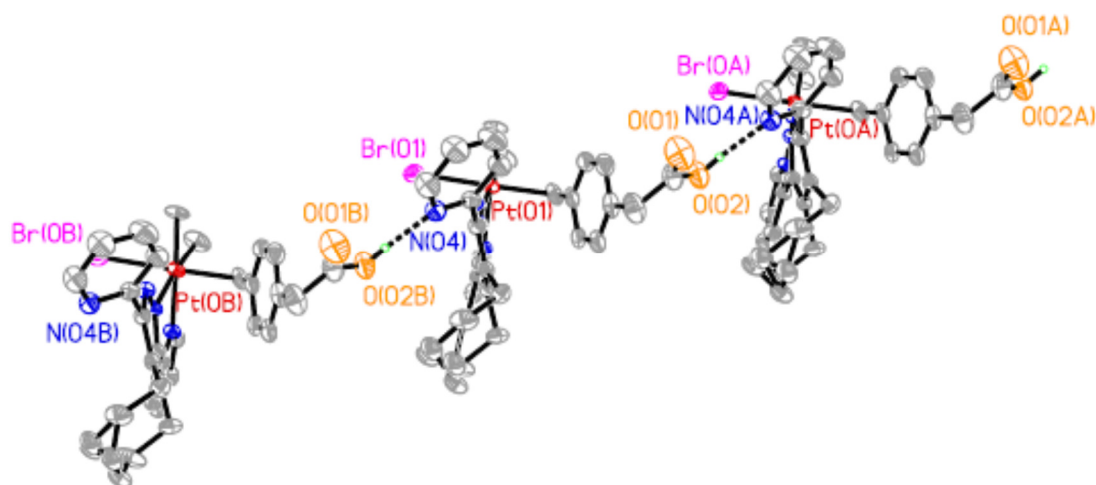


Figure 4.8. A view of the supramolecular polymeric structure of complex **18**.

The two benzyl derivatives, complexes **17** and **18**, were shown to be the products of the *trans* oxidative addition of their corresponding substrates. Comparatively, an equivalent of bromoacetic acid was added to an acetone solution of complex **2**, in order to determine if the aliphatic substrates reacted in a similar manner to the benzylic substrates producing *trans*-[PtBrMe₂(CH₂CO₂H)(6-dppd)], complex **19a**, as in scheme 4.2. To investigate this, an NMR scale reaction was performed in which an equimolar amount of bromoacetic was added to an NMR tube charged with an acetone-*d*₆ solution of complex **2**. After addition of bromoacetic acid, the NMR tube was shaken to facilitate mixing of the reagents and a ¹H NMR spectrum was acquired within ten minutes. The ¹H NMR spectrum acquired of the reaction mixture provided evidence for the formation of three distinct complexes as is interpreted by the presence of six methylplatinum signals. Figure 4.9 depicts the methylplatinum region of the ¹H NMR spectrum for the reaction between complex **2** and bromoacetic acid. A similar spectrum had been observed previously in the formation of [PtI₂Me₂(6-dppd)], complex **7**, where two *cis* and one *trans* isomer of the complex were observed. Using the spectra of complex **7** as a reference, the ¹H NMR spectrum of the reaction mixture can be interpreted. The spectrum contains two methyl platinum resonances of higher intensity at $\delta = 0.73$ ppm and $\delta = 1.49$ ppm with coupling constants of $^2J_{\text{PtH}} = 73$ Hz and 69 Hz respectively. These resonances can be attributed to the formation of complex **19b**, one of the *cis* isomers of the addition of bromoacetic acid to complex **2**. A set of methylplatinum resonances attributed to the second *cis* isomer, **19c**, are observed, albeit at a significant lesser intensity, at $\delta = 0.75$ ppm and $\delta = 1.76$ ppm with coupling constants of $^2J_{\text{PtH}} = 74$ Hz and 70 Hz respectively. The upfield methylplatinum resonances at 0.73 and 0.75 ppm for complexes **19b** and **19c** are consistent with a methyl group being positioned *trans* to a bromine atom as the bromine atoms have a lower *trans* influence relative to the nitrogen atoms of the pyridyl ring. Complex **19b** is determined to be the *cis* isomer of complex **19** in which the equatorial methyl group is *exo* directed and the acetic acid group is *endo* directed due to a ¹H-¹H NOESY correlation between the methylplatinum resonance at $\delta = 1.49$ ppm and the *ortho* proton resonance on the pyridyl ring of **19b** at $\delta = 9.15$ ppm. Therefore **19c** is the *cis* isomer with the *endo* directed methyl group. The remaining two methylplatinum resonances at $\delta = 1.46$ ppm and $\delta = 1.65$ ppm with coupling constant values of $^2J_{\text{PtH}} = 70$

Hz for both resonances are attributed to the formation of the *trans* isomer **19a**. The chemical shift and coupling constants are diagnostic of methyl groups being positioned *trans* to the nitrogen donor atoms of the ligand and are consistent with observed values for complexes **17** and **18**. Through the use of gCOSY ^1H - ^1H NMR spectra and the 1D ^1H NMR spectrum, the complete sets of pyridyl resonances and methylene resonances can be assigned for all isomers of **19**.

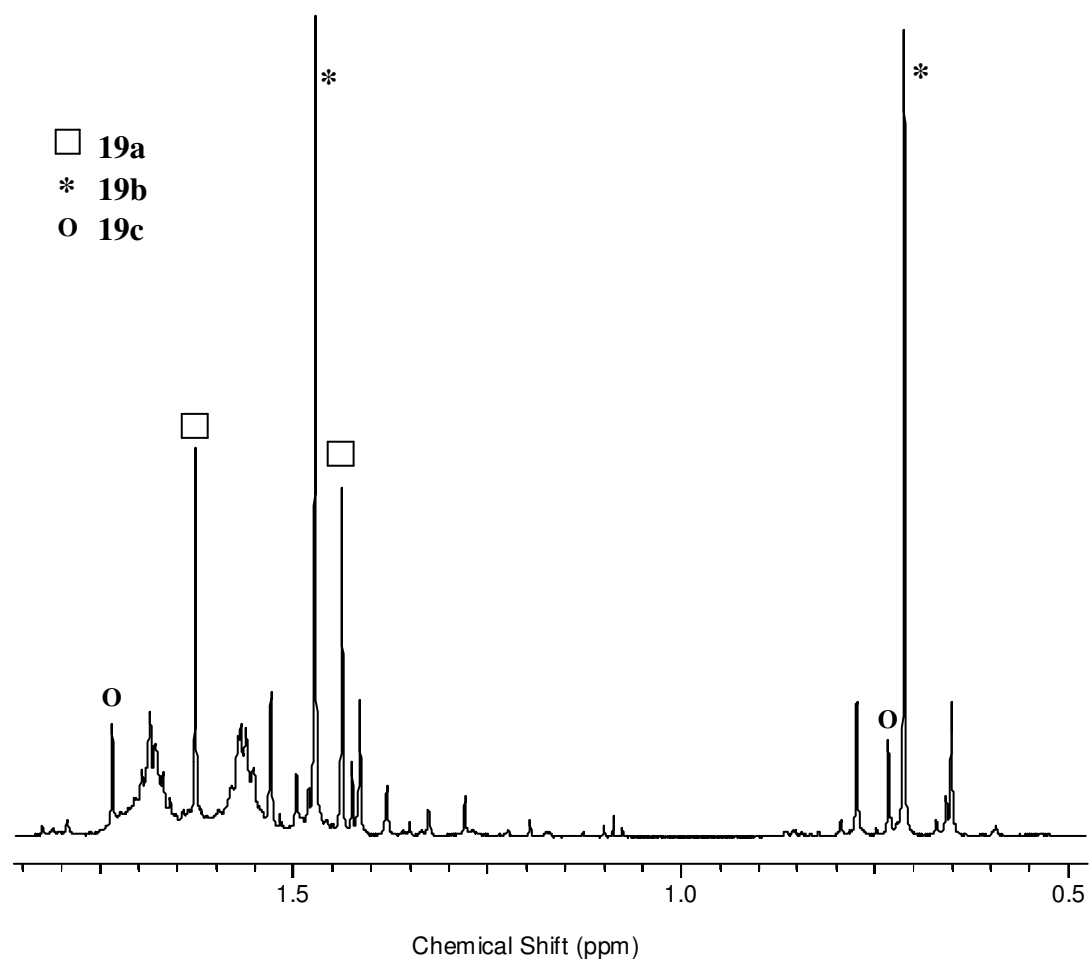
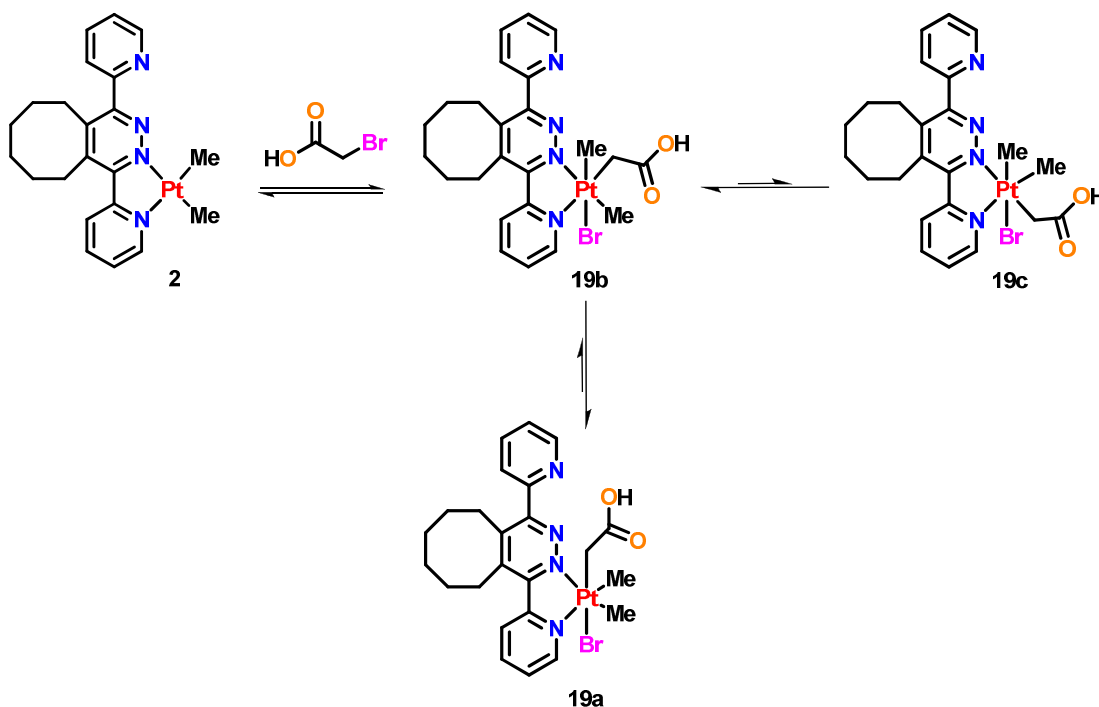


Figure 4.9. ^1H NMR spectrum of the methylplatinum region for the oxidative addition of bromoacetic acid at complex **2** giving **19a**, **19b**, and **19c**.

Complexes **19a**, **19b**, and **19c** are observed to be initially formed in a ratio of 3:6:1. Figure 4.10 shows how the proportions of each complex changes over time. It can be seen that after 24 hours from initial mixing of reagents, the ratio of isomers drastically changes. Isomerization from the *cis* to *trans* isomers must occur readily in solution leading to a isomer ratio of **19a**:**19b**:**19c** of 3:1:1 after 24 hours and 6:1:1 after 48 hours. The spectrum acquired 72hours after initial mixing of reagents shows only a trace amount of the *cis* isomers present indicating that the isomerization to the *trans* isomer is complete after 72 hours yielding solely complex **19a**. The time series spectra support the conclusion that the complex **19b** is the kinetic isomer and is formed in higher proportion initially before isomerizing to complex **19a** the thermodynamic isomer. This proposed isomerism is depicted in scheme 4.3.



Scheme 4.3. Oxidative addition of bromoacetic acid at complex **2** and subsequent isomerizations to form complexes **19a**, **19b** and **19c**.

By adding bromoacetic acid to an acetone solution of complex **2** and allowing the mixture to stir for 72hours, complex **19a** can be prepared as an air stable bright yellow solid in high yield. A portion of this solid is then dissolved in minimal dichloromethane

and pentane is allowed to slowly diffuse into the solution yielding the formation of single crystal suitable for X-ray diffraction analysis. Complex **19a** was confirmed crystallographically to be the product of *trans* oxidative addition as shown in figure 4.11. Important bond lengths and angles are listed in table 4.3. The carboxylic acid group in the acetic acid ligand takes part in hydrogen bonding as an acceptor and donor pair forming a supramolecular dimer as depicted in figure 4.12. This type of head to tail hydrogen bonding is expected for carboxylic acids leading to the formation of complementary supramolecular dimers rather than the polymers formed for complexes **17** and **18** [31]. The graph set description of the hydrogen bonded dimer system is $R_2^2(8)$, which is usual for acid groups [49]. The carboxylic acid groups are oriented in a manner to form intermolecular $\text{OH}\cdots\text{O}=\text{C}$ hydrogen bonds, with an $\text{O}\cdots\text{O}$ distance of 2.626 Å. This distance is diagnostic of a very strong hydrogen bonding interaction.

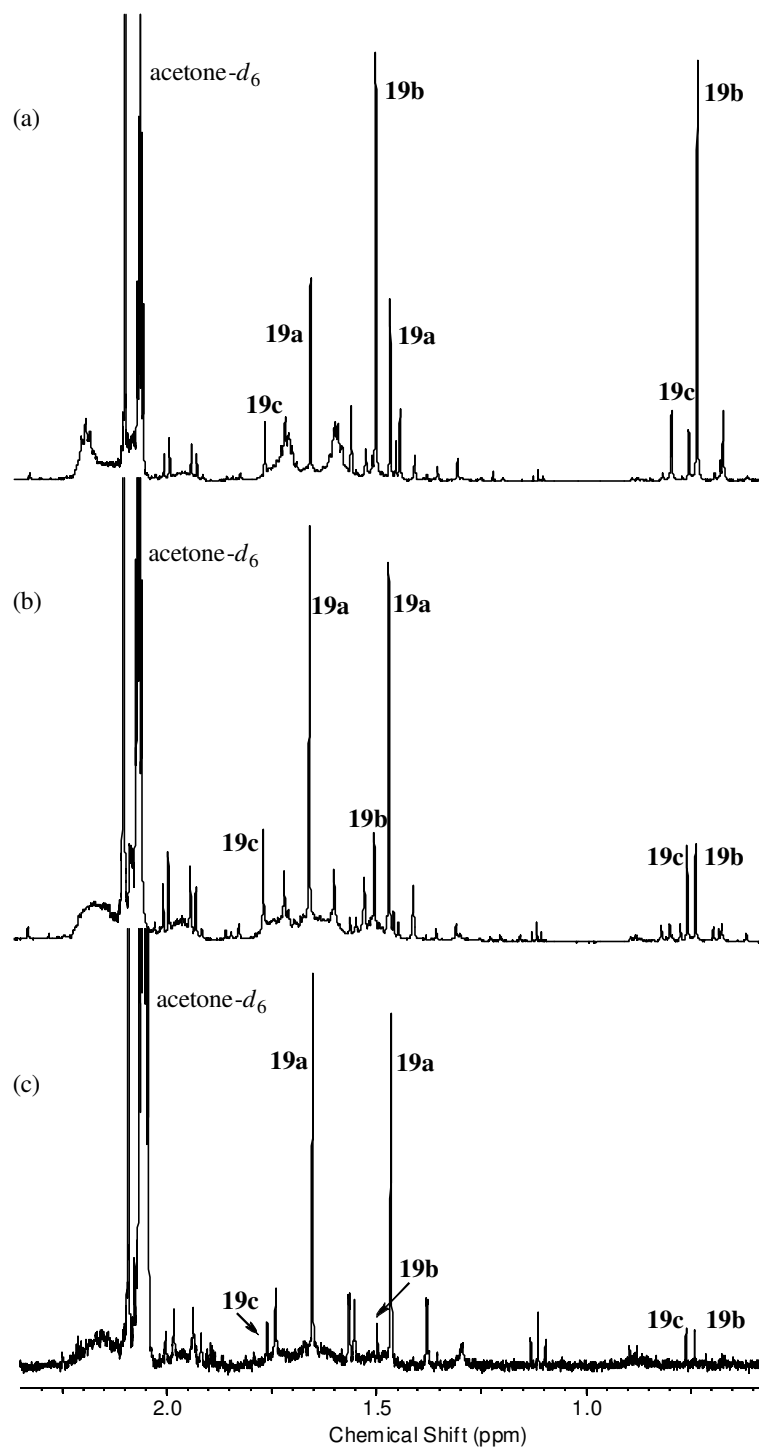


Figure 4.10. Methylplatinum regions of the ^1H NMR spectra, (acetone- d_6), monitoring the formation and isomerization between complexes **19a**, **19b**, and **19c** over time. Spectrum (a) was collected 10 minutes after initial mixing of reagents, spectrum (b) after 24 hours and spectrum (c) after 48 hours.

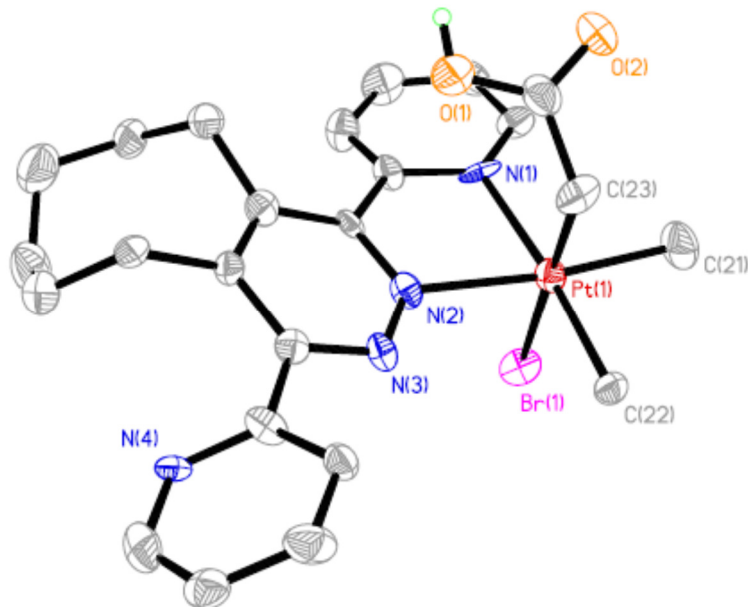


Figure 4.11. Molecular structure of complex **19a**, with an atomic numbering scheme (hydrogen atoms and solvent molecules excluded for clarity).

Table 4.3: Bond lengths [Å] and angles [°] for [PtBrMe₂(CH₂CO₂H)(6-dppd)], **19a.**

Pt(1)-N(1)	2.154(10)	Pt(1)-N(2)	2.168(10)
Pt(1)-C(21)	2.057(13)	Pt(1)-C(22)	2.077(12)
Pt(1)-Br(01)	2.5496(15)	Pt(1)-C(23)	2.098(12)
N(1)-Pt(1)-N(2)	76.3(4)	C(21)-Pt(1)-C(22)	87.1(6)
N(2)-Pt(1)-C(21)	173.2(5)	N(2)-Pt(1)-C(23)	87.6(5)
N(2)-Pt(1)-C(22)	98.6(5)	N(1)-Pt(1)-C(21)	98.1(6)
C(21)-Pt(1)-C(23)	89.3(6)	C(22)-Pt(1)-C(23)	85.1(5)
N(1)-Pt(1)-C(22)	174.7(5)	N(1)-Pt(1)-C(23)	96.1(4)
N(2)-Pt(1)-Br(1)	91.7(3)	C(22)-Pt(1)-Br(1)	92.7(4)
N(1)-Pt(1)-Br(1)	86.0(3)	C(21)-Pt(1)-Br(1)	91.7(5)
C(23)-Pt(1)-Br(1)	177.6(4)	Pt(1)-C(23)-C(24)	109.1(8)

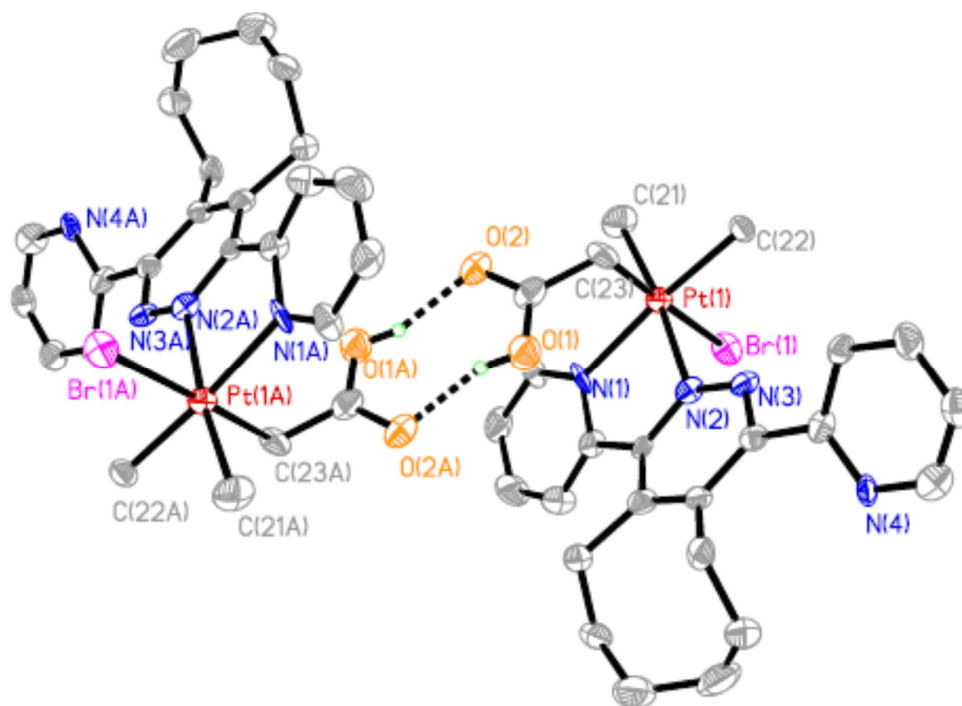
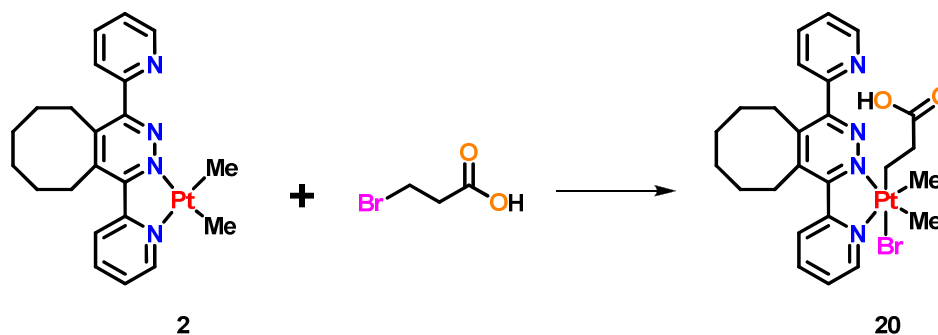


Figure 4.12. A view of the supramolecular dimer structure of complex **19a**.

To further investigate the oxidative addition of aliphatic carboxylic acids at complex **2**, 3-bromopropionic acid was added to an acetone solution of complex **2** and allowed to stir for 24 hours, scheme 4.4. After workup, the reaction yielded a bright orange solid which was isolated in moderate yield. This solid was proposed to be the product of *trans* oxidative addition, *trans*-[PtBrMe₂(CH₂CH₂CO₂H)(6-dppd)], complex **20**.



Scheme 4.4. Proposed oxidative addition of 3-bromopropionic acid at complex **2** yielding the product of *trans* addition, [PtBrMe₂(CH₂CH₂CO₂H)(6-dppd)], **20**.

The ^1H NMR spectrum of the solid in dichloromethane- d_2 contained evidence of the formation of two independent compounds, figure 4.13. The major complex produced in this reaction possessed only a single methylplatinum resonance at $\delta = 1.44$ ppm with coupling constant values of $^2J_{\text{PtH}} = 80$ Hz. The values of the coupling constant indicate that the major product formed is likely an organoplatinum(II) species and not the proposed organoplatinum(IV) complex, **20**. The presence of only a single methylplatinum resonance in the ^1H NMR spectrum can be attributed to the reaction of 3-bromopropionic acid with complex **2** producing a dimethylplatinum(II) complex which possesses only a single methyl group. The aromatic region of the spectrum possessed eight distinct pyridyl resonances which is diagnostic of the complex remaining unsymmetrical and the integration values of these resonances in comparison with the methylplatinum resonance support the formation of a monomethylplatinum(II) complex. The values of chemical shift and coupling constant for this complex, complex **21**, are similar to those observed for complex **1**, [PtClMe(6-dppd)]. It has been shown in the literature that the reaction of dimethylplatinum(II) complexes can react with 3-bromopropionic acid to form bromomethylplatinum(II) products [43,50]. We propose that the formation of complex **21**, [PtBrMe(6-dppd)], involves a β -elimination from an intermediate [PtMe₂(CH₂CH₂CO₂H)(6-dppd)]⁺, complex **A**, followed by a concomitant loss of methane from the resultant intermediate **B** as shown in scheme 4.5.

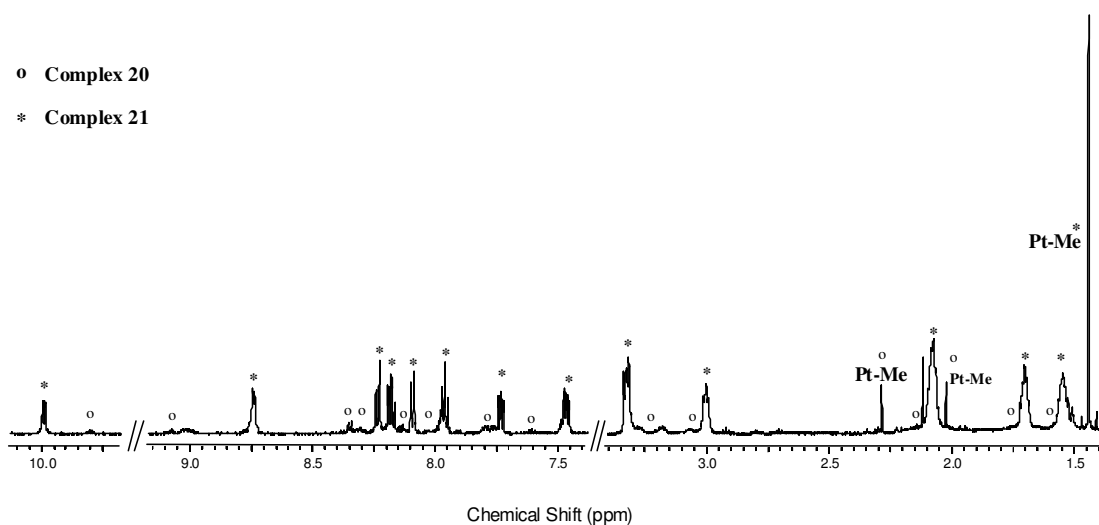
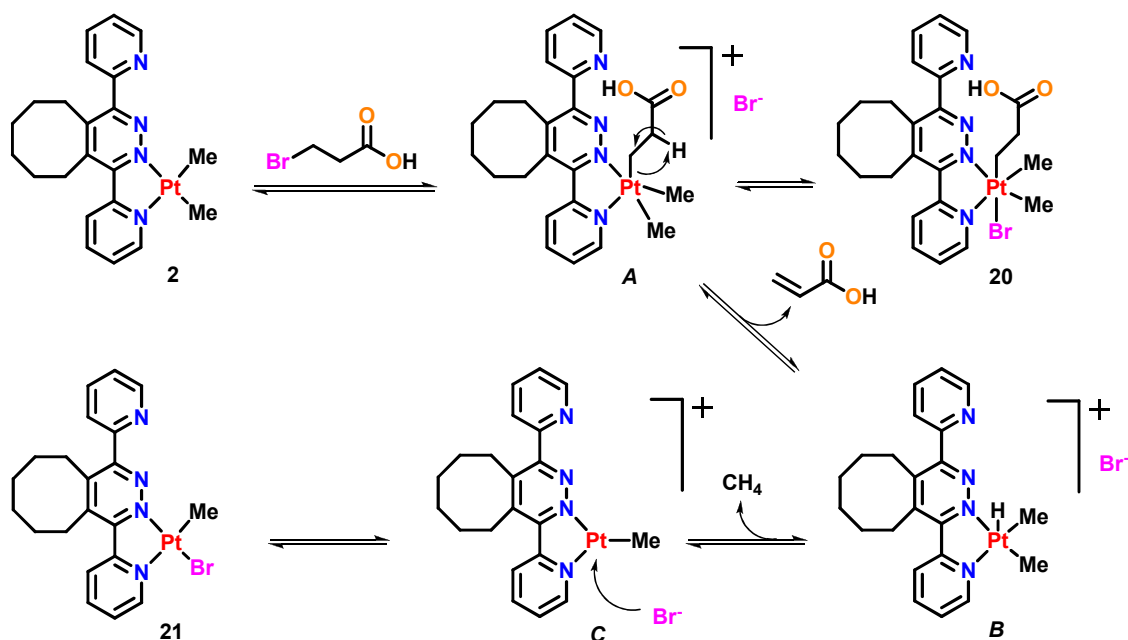


Figure 4.13. ^1H NMR spectrum of the reaction between **2** and 3-bromopropionic acid in CD_2Cl_2 , yielding both complexes **20** and **21** as products.



Scheme 4.5. Proposed mechanism for the formation of complexes **20** and **21** through the reaction of 3-bromopropionic acid with complex **2**.

Evidence for the trace formation of an organoplatinum(IV) complex can be observed in the same ^1H NMR spectrum as complex **21**. Methylplatinum resonances $\delta = 2.03$ ppm and 2.29 ppm with coupling constants $^2J_{(\text{PtH})} = 70$ Hz and 71 Hz respectively are observed although in a significantly lesser amount than **21** as determined by an integration ratio comparison of 6:1. These values are diagnostic of organoplatinum(IV) complexes with methyl groups being positioned *trans* to nitrogen atoms. The aromatic region of the ^1H NMR spectrum contained evidence of additional proton resonances although they could not be readily assigned due to their poor intensity. The minor complex present in the ^1H NMR spectrum of the reaction between **2** and 3-bromopropionic acid is proposed to be that of the *trans* oxidative addition, complex **20**.

Single crystals grown from a dichloromethane solution of the reaction mixture were found to be suitable for single crystal X-ray diffraction analysis. The X-ray analysis of these crystals confirmed the actual structure of this compound was $[\text{PtBrMe}(6\text{-dppd})]$, complex **21** as depicted in figure 4.14. Important bond parameters are listed in table 4.4.

It was found that similar to complex **1**, the methyl group present was again directed inward to make the *endo* complex [35]. This preference to form the *endo* platinum(II) square planar complex is likely due to the formation of favourable secondary bonding interactions of the manner NCH...Br and PtCH₃...N [43].

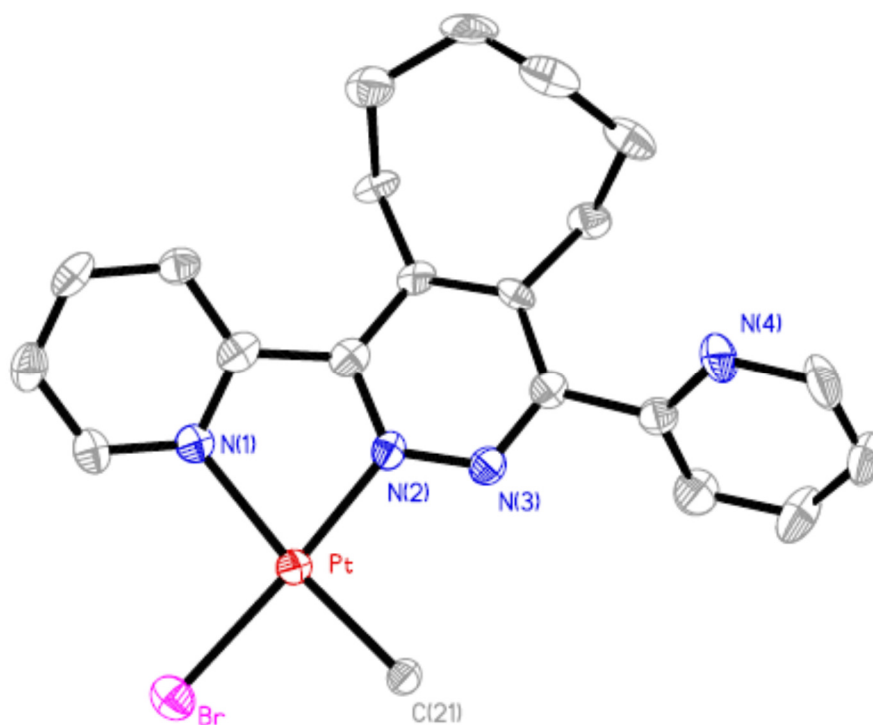


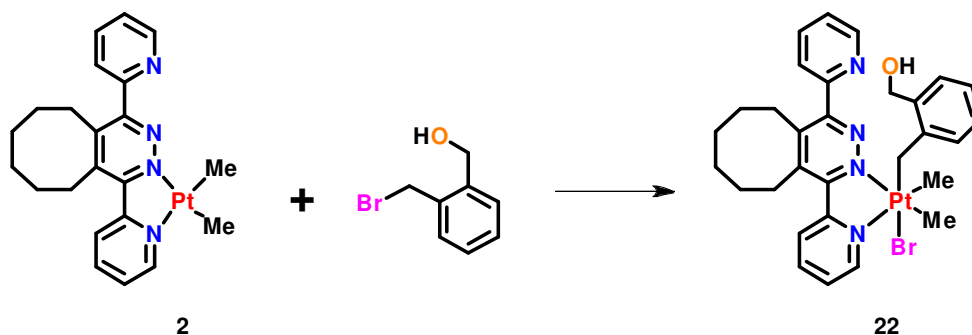
Figure 4.14. Molecular structure of complex **21**, with an atomic numbering scheme (hydrogen atoms excluded for clarity).

Table 4.4: Bond lengths [Å] and angles [°] for [PtBrMe(6-dppd)], **21.**

Pt-N(1)	2.101(7)	Pt-N(2)	1.987(7)
Pt-C(21)	2.050(8)	Pt-Br	2.4172(11)
N(1)-Pt-C(21)	173.3(3)	N(1)-Pt-Br	97.7(2)
N(1)-Pt-N(2)	78.5(3)	N(2)-Pt-C(21)	95.0(3)
N(2)-Pt-Br	174.4(2)	C(21)-Pt-Br	88.9(3)

4.3 Reaction of Complex 2 with an alcohol as a hydrogen bond donor

Following the findings that *para* substituted benzyl carboxylic acid derivatives were capable of forming hydrogen bonding networks between adjacent molecular units using both their hydrogen bond donor and acceptor abilities. It is interesting to note that in the previously discussed complexes, there is no hydrogen bonding interaction with the non-coordinating pyridyl nitrogen atom of the **6-dppd** backbone. It has been shown previously that the free pyridyl nitrogen donor atom in complex **2** is not significantly nucleophilic to coordinate additional equivalents of metal atoms [35,45], however under the correct conditions has been shown to be able to coordinate to adjacent equivalents of **2** intermolecularly. It is with that motivation that the oxidative addition of a substrate with a pendent hydrogen bond donor group positioned in a manner to interact with this free nitrogen donor atom was investigated. Through analysis of the X-ray structures of the carboxylic acid derivatives discussed in the previous section, it was determined that the incorporation of the hydrogen bond donor in the *ortho* position relative to the methylene bridge would be the best candidate to induce an intramolecular hydrogen bond interaction. Therefore the substrate 2-(bromomethyl)benzyl alcohol was selected as it met all of the desired properties to potential facilitate the formation of an intramolecular hydrogen bonding interaction depending on whether the *ortho* alcohol group directed inwards towards the **6-dppd** ligand or outwards. The reaction of 2-(bromomethyl)benzyl alcohol with complex **2** was predicted to occur through *trans* oxidative addition yielding complex **22**, *trans*-[PtBrMe₂(CH₂-2-C₆H₄-CH₂OH)(6-dppd)], as depicted in scheme 4.6.



Scheme 4.6. Proposed oxidative addition of 2-(bromomethyl)benzyl alcohol at complex **2** yielding the product of *trans* addition, [PtBrMe₂(CH₂-2-C₆H₄-CH₂OH)(6-dppd)], **22**.

In the manner depicted in scheme 4.6, equimolar amounts of complex **2** and 2-(bromomethyl)benzyl alcohol were dissolved in minimal acetone and allowed to stir for 2 hours at room temperature. After purification, a bright yellow solid was isolated in high yield. The ^1H NMR spectrum of the product in CD_2Cl_2 , figure 4.15, indicates that a mixture of products are formed in this reaction. The major product, which is present in a significantly larger quantity as can be determined through comparative integration, is presumed to be the product of the *trans* oxidative addition of 2-(bromomethyl)benzyl alcohol, complex **22**. This postulation is supported by the presence of two methylplatinum resonances at $\delta = 1.40$ ppm and 1.77 ppm with coupling constants $^2J_{(\text{PtH})} = 70$ Hz for both resonances. These coupling constants and chemical shifts are typical of dimethylplatinum(IV) complexes in which the methyl groups are oriented *trans* to the nitrogen donor atoms of the ligand. Methylene proton resonances are observed as an AB spin system with Pt-195 satellites at $\delta = 2.67$ ppm and 2.85 ppm with coupling constants of $^2J_{(\text{PtH})} = 87$ Hz and 106 Hz respectively, indicating that indeed the benzyl alcohol ligand was coordinated at the platinum center. This is further supported by the presence of Pt-195 satellites on the *ortho* resonance of the benzyl group at $\delta = 5.86$ ppm with $^4J_{(\text{PtH})} = 18$ Hz. Three additional benzyl proton resonances were observed as well as eight distinct pyridyl resonances all with integration values supporting the formation of complex **22** and all able to be absolutely assigned using ^1H - ^1H gCOSY NMR spectra. The minor products are assumed to be the products of *cis* oxidative addition. These products appear in the spectrum with an abundance of less than 5%, which can be extracted through comparing related integration values, and as such are found to be unresolvable.

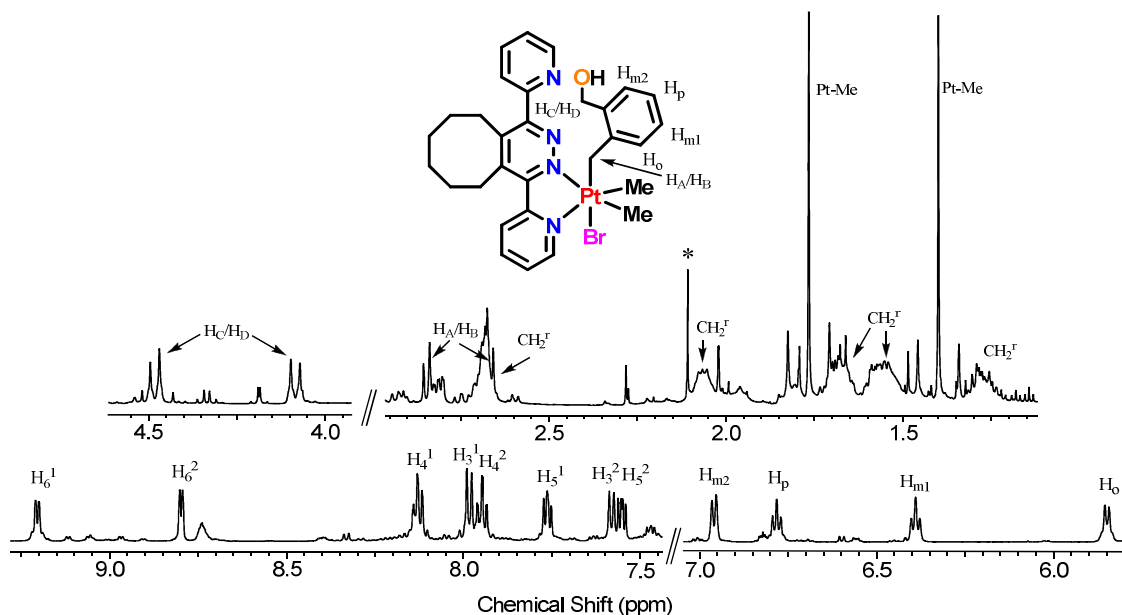


Figure 4.15. ^1H NMR spectrum of complex **22** in CD_2Cl_2 . CH_2^f represents the methylene protons of the cyclooctyl ring and the * indicates the presence of residual acetone. Minor complex present is unresolvable but presumed to be a *cis* addition product.

Single crystals of complex **22** suitable for X-ray diffraction analysis were grown from a methylene chloride and chloroform mixture. The solid state structure of **22**, shown in figure 4.16, confirms the proposed *trans* addition of 2-bromomethylbenzyl alcohol. Important bond distances and angles are listed in table 4.5. The *trans* geometry is likely favoured by weak π -stacking interactions as can be observed by the orientation of the benzylic group directly above the pyridazine ring of the ligand 6-dppd. Unlike analogous compounds to **22**, intramolecular hydrogen bonding is observed in this complex between the nitrogen atom of the non-coordinating pyridyl ring and hydroxyl hydrogen atom. The flexibility of the benzylic alcohol allows for the alcohol and pyridyl groups being able to orient themselves in a manner to promote intramolecular hydrogen bonding. The $\text{N}\cdots\text{O}$ distance of 2.794 Å supports the conclusion that an intramolecular hydrogen bond is formed in complex **22**.

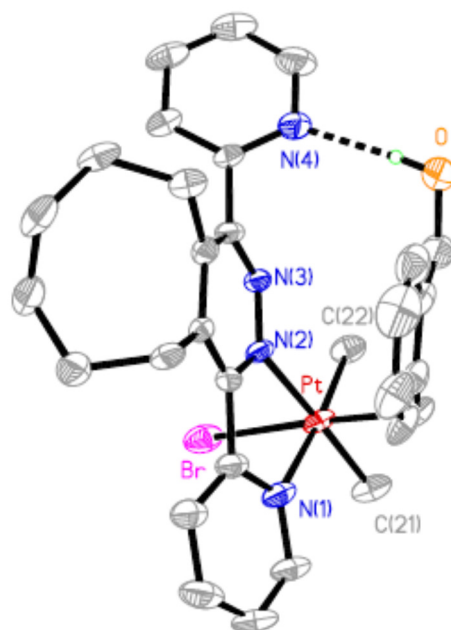


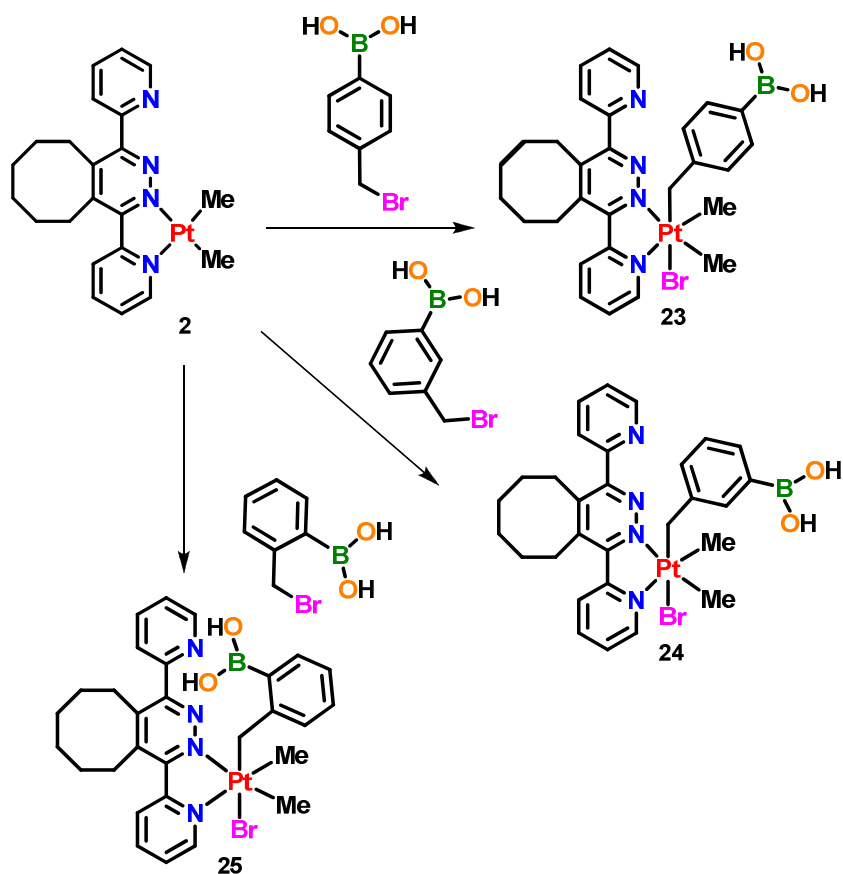
Figure 4.16. Molecular structure of complex **22**, with an atomic numbering scheme (hydrogen atoms and solvent molecules excluded for clarity).

Table 4.5: Bond lengths [Å] and angles [°] for [PtBrMe₂(CH₂-2-C₆H₄-CH₂OH)(6-dppd)], **22.**

Pt-N(1)	2.137(6)	Pt-N(2)	2.133(5)
Pt-C(21)	2.060(7)	Pt-C(22)	2.042(6)
Pt-Br	2.5991(8)	Pt-C(23)	2.089(7)
N(1)-Pt-N(2)	75.6(2)	C(21)-Pt-C(22)	83.9(3)
N(2)-Pt-C(21)	177.4(2)	N(2)-Pt-C(23)	94.5(2)
N(2)-Pt-C(22)	98.7(2)	N(1)-Pt-C(21)	101.9(2)
C(21)-Pt-C(23)	85.5(3)	C(22)-Pt-C(23)	92.0(3)
N(1)-Pt-C(22)	174.2(2)	N(1)-Pt-C(23)	89.5(2)
N(2)-Pt-Br	87.31(14)	C(22)-Pt-Br	90.2(2)
N(1)-Pt-Br	88.54(15)	C(21)-Pt-Br	92.5(2)
C(23)-Pt-Br	176.86(19)	Pt-C(23)-C(24)	114.0(4)

4.4 Reaction of Complex 2 with boronic acid derivatives as hydrogen bond donors

Supramolecular chemists readily utilize the secondary interactions of aryl-boronic acids when trying to design cyclic hydrogen bonded dimers due to the tendency of these substrates to form said structures [51,52]. Recently these types of interactions have been influential in the field of molecular recognition and the formation of self-assembled networks [53]. Aryl-boronic acids have been previously installed at platinum(II) complexes through the oxidative addition reaction of a variety of (bromomethyl)phenylboronic acids and have shown the ability to undergo self-assembly in the solid state [41]. Interestingly it was found that not all organoplatinum(IV) complexes with arylboronic acid groups gave the expected complementary self-association products and interactions between the boronic acid groups and halogens was also observed. Previous work has shown that even in the presence of free oxygen and nitrogen donors which could participate in hydrogen bonding, the arylboronic acids still show preference to hydrogen bond with the PtBr groups. There is potential to design more complex structures utilizing the self-assembly of arylboronic acids however a greater understanding of the design features is required. Rational and predicted design of these organoplatinum(IV) complexes possessing arylboronic acids could have a direct impact on organometallic synthesis through C-C bond forming reactions [54], as well as allowing for the design of boronic acids of other metals which have applications in neutron capture therapy and photonic materials [54-56]. It is with this motivation that the reaction of complex **2** with three phenyl boronic acids is explored and the supramolecular chemistry of the complexes is evaluated. The reaction of complex **2** with equimolar amounts of the *ortho*, *meta*, and *para* substituted (bromomethyl)phenyl boronic acids was observed to proceed rapidly in acetone to yield a yellow solution after one hour. The resultant yellow solids were proposed to be the respective organoplatinum(IV) complexes as depicted in scheme 4.7.



Scheme 4.7. Oxidative addition reactions of the carbon bromine bonds in three (bromomethyl)phenyl boronic acids giving complexes **23**, **24**, and **25**.

The oxidative addition of the Br-CH₂ bond in *para*-(bromomethyl)phenyl boronic acid at complex **2** yielded a bright yellow solid product proposed to be that of the *trans* oxidative addition, **23**, as shown in scheme 4.7. The ¹H NMR spectrum of **23** in acetone-*d*₆, figure 4.17, supports the formation of the *trans* addition product through the presence of only eight distinct pyridyl resonances as well as the presence of methylplatinum resonances at $\delta = 1.39$ ppm and 1.75 ppm with coupling constants $^2J_{\text{PtH}} = 70$ Hz and 71 Hz respectively. Further evidence for the incorporation of the phenyl boronic acid substituent is provided by the presence of Pt-195 satellites on the methylene proton resonances at $\delta = 2.78$ ppm with $^2J_{\text{PtH}} = 92$ Hz, and 2.84 ppm with $^2J_{\text{PtH}} = 93$ Hz. One set of phenyl resonances were also observed as two doublets with the phenyl *ortho* resonance being the most upfield and is observed to possess Pt-195 satellites with a coupling constant value $^4J_{\text{PtH}} = 18$ Hz. Numerous attempts at growing single crystals of

23 were made but the subsequent X-ray analysis never provided quality data for a solid state structure.

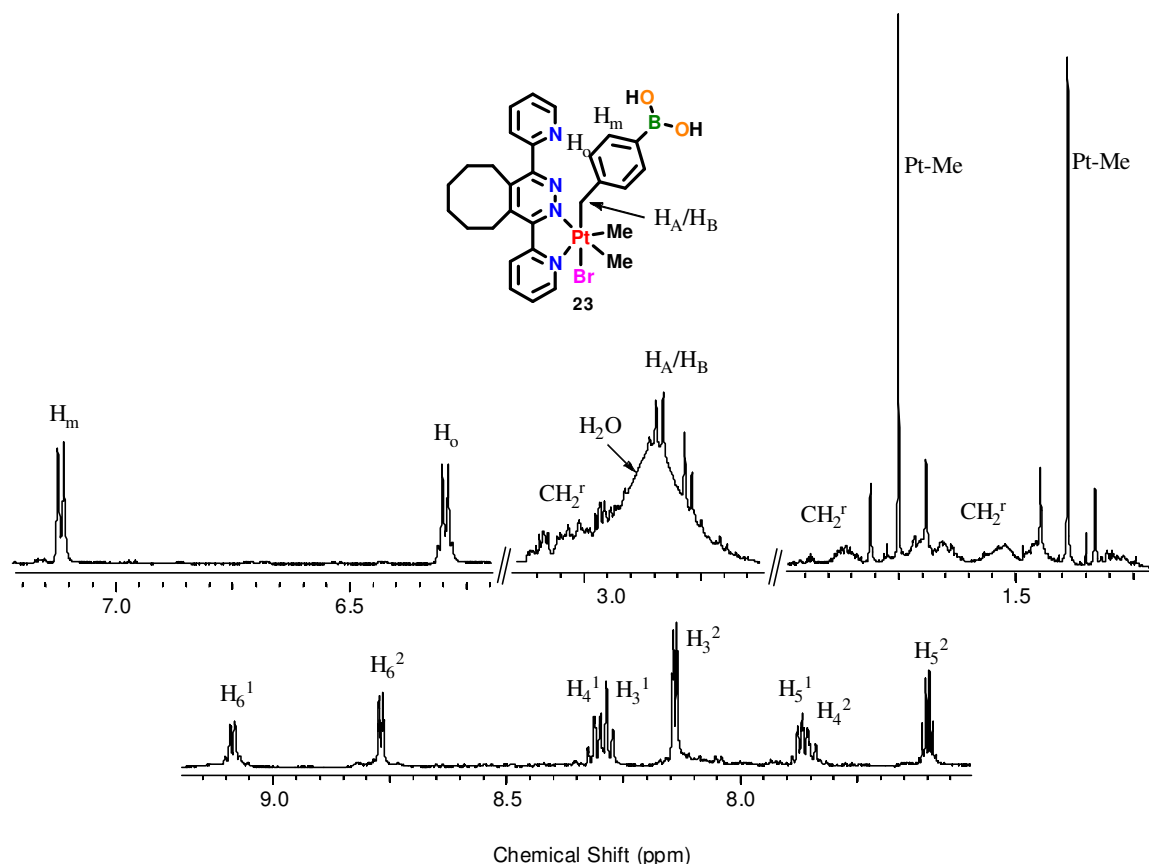


Figure 4.17. ^1H NMR of complex **23** in acetone- d_6 . CH_2^f represents the methylene protons of the cyclooctyl ring.

In a manner similar to that in the preparation of **23**, an acetone mixture of complex **2** and *meta*-(bromomethyl)phenyl boronic acid was allowed to stir for an hour and after working up the reaction, a bright yellow solid believed to be complex **24**, $[\text{PtBrMe}_2(\text{CH}_2\text{-3-C}_6\text{H}_4\text{-B(OH)}_2)(6\text{-dppd})]$, was isolated. The ^1H NMR spectrum again provided evidence for the formation of the *trans* oxidative addition product. Two methylplatinum resonances at $\delta = 1.40$ ppm and 1.72 ppm with coupling constants $^2J_{(\text{PtH})} = 70$ Hz and 71 Hz respectively were observed again representative of methyl groups being positioned *trans* to the nitrogen donor atoms of the ligand. This would mean that the methylene group of the phenyl boronic acid ligand would be positioned *trans* to bromine which is supported by the methylene resonances being observed at $\delta = 2.77$ ppm and 2.86 ppm with coupling

constants ${}^2J_{(\text{PtH})} = 91$ Hz and 96 Hz respectively. These chemical shifts and coupling constants are diagnostic of a carbon atom (CH_2) being positioned *trans* to a bromine atom. A single set of eight pyridyl resonances are again observed highlighted by the *ortho* pyridyl proton at $\delta = 9.04$ ppm possessing Pt-195 satellites with coupling constants ${}^3J_{(\text{PtH})} = 18$ Hz. Four phenyl protons are observed in the spectrum, with the protons positioned *ortho* to the methylene group both possessing Pt-195 satellites with coupling constants ${}^4J_{(\text{PtH})} = 18$ Hz and 11 Hz for protons $\text{H}_{\text{o}1}$ and $\text{H}_{\text{o}2}$ respectively as labelled in figure 4.18. Single crystals of **24**, as the acetone solvate, suitable for X-ray analysis were able to be grown from acetone confirming the overall *trans* oxidative addition of *meta*-(bromomethyl)phenyl boronic acid at **2**. The solid state structure of **24** is shown in figure 4.19, and selected bond parameters presented in Table 4.6.

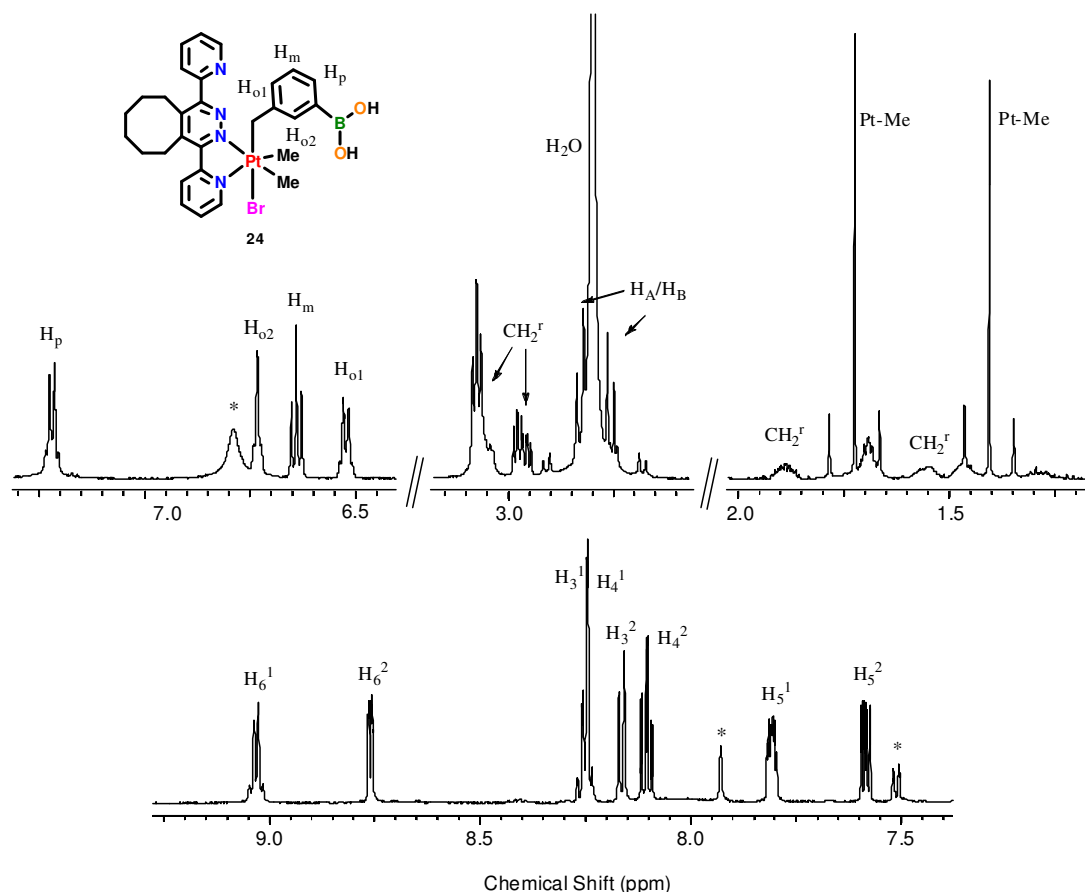


Figure 4.18. ${}^1\text{H}$ NMR of complex **24** in $\text{acetone-}d_6$. CH_2^r represents the methylene protons of the cyclooctyl ring and * represents residual unreacted *meta*-(bromomethyl)phenyl boronic acid.

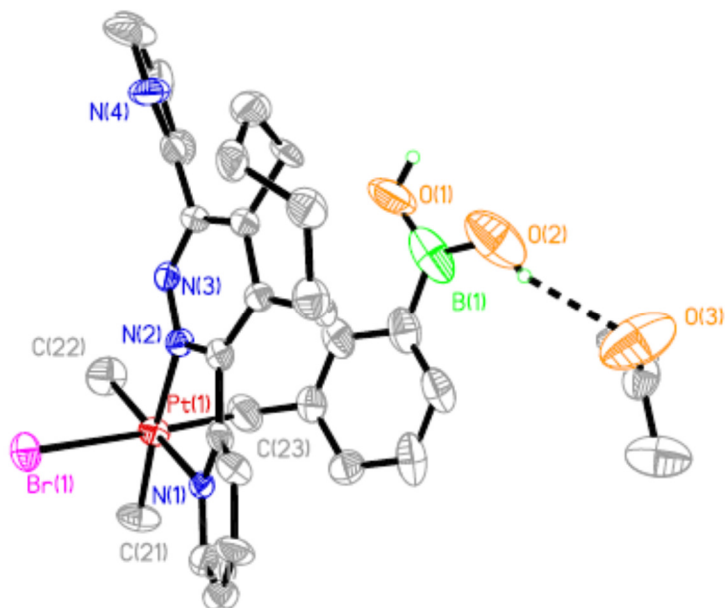


Figure 4.19. Molecular structure of complex **24**, with an atomic numbering scheme (hydrogen atoms excluded for clarity).

Table 4.6: Bond lengths [Å] and angles [°] for [PtBrMe₂(CH₂-3-C₆H₄-B(OH)₂)(6-dppd)], **24.**

Pt(1)-N(1)	2.167(7)	Pt(1)-N(2)	2.135(6)
Pt(1)-C(21)	2.055(8)	Pt(1)-C(22)	2.047(9)
Pt(1)-Br(1)	2.6201(10)	Pt(1)-C(23)	2.045(10)
N(1)-Pt(1)-N(2)	75.8(2)	C(21)-Pt(1)-C(22)	86.6(4)
N(2)-Pt(1)-C(21)	174.9(4)	N(2)-Pt(1)-C(23)	89.2(3)
N(2)-Pt(1)-C(22)	97.9(4)	N(1)-Pt(1)-C(21)	99.9(3)
C(21)-Pt(1)-C(23)	88.5(4)	C(22)-Pt(1)-C(23)	86.9(5)
N(1)-Pt(1)-C(22)	172.2(3)	N(1)-Pt(1)-C(23)	97.6(4)
N(2)-Pt(1)-Br(1)	90.90(18)	C(22)-Pt(1)-Br(1)	89.7(3)
N(1)-Pt(1)-Br(1)	85.72(17)	C(21)-Pt(1)-Br(1)	91.6(3)
C(23)-Pt(1)-Br(1)	176.6(3)	Pt(1)-C(23)-C(24)	117.0(7)

The molecular structure of **24** exhibits a hydrogen bonding interaction between the boronic acid group hydrogen atom and an adjacent acetone solvent molecule. This hydrogen bond has an OH...O=C bond distance of 3.204 Å indicating that the interaction is weak in nature. It is also observed that the non-coordinating pyridyl group is directed away from the boronic acid group preventing any intramolecular hydrogen bonding to occur between these groups. Complex **24** self-assembled in the solid state to give a supramolecular polymer facilitated by hydrogen bonding interactions between the boronic acid group and the PtBr unit of an adjacent molecule. This type of polymeric structure was observed previously in the supramolecular structure of complex **17** and is not without precedent in the supramolecular chemistry of organoplatinum(IV) boronic acids [41]. The hydrogen bonding interaction is between one BOH group and the PtBr group of a neighbouring molecule with a O(1)...Br(1A) bond distance of 3.372 Å. Again this bond distance lies within a region considered as weak hydrogen, but in any case gives rise to the supramolecular polymer depicted in figure 4.20.

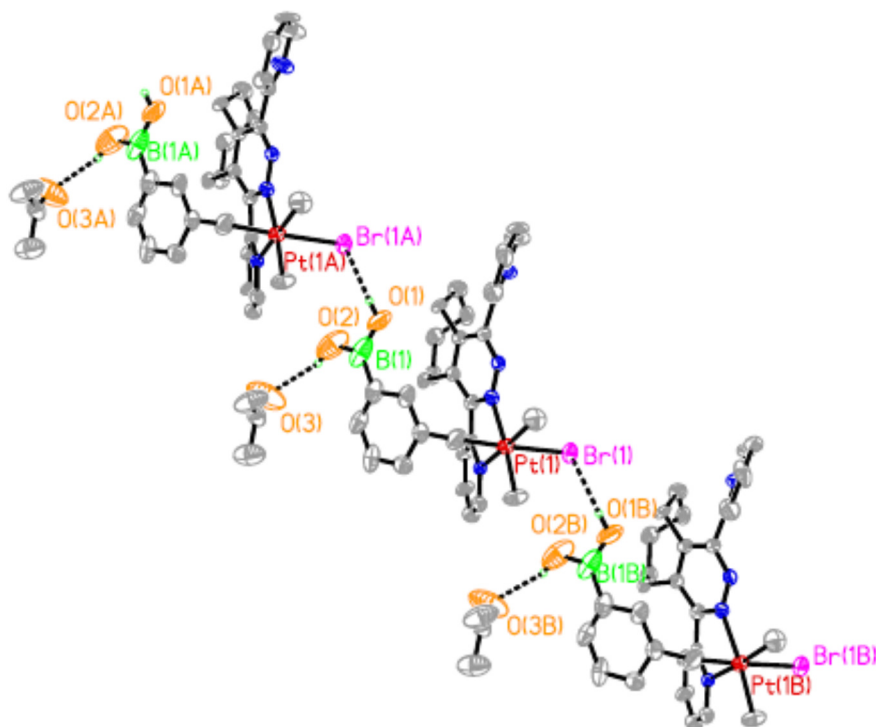


Figure 4.20. A view of the supramolecular polymer structure of complex **24**.

The final derivative of the phenyl boronic acids, *ortho*-(bromomethyl)phenyl boronic acid was reacted with complex **2** in a similar manner to that of the *para* and *meta* derivatives, scheme 4.7. After allowing the two reagents to stir at room temperature for 2 hours, a yellow solid was isolated. The solid was expected to be the product of *trans* oxidative addition, *trans*-[PtBrMe₂(CH₂-2-C₆H₄-B(OH)₂)(6-dppd)], **25**. The ¹H NMR spectrum of **25**, figure 4.21, contained two methyl platinum resonances at δ = 1.40 ppm and 1.69 ppm with coupling constants ²J_(PtH) = 70 Hz and 71 Hz respectively which is consistent with the previous complexes **23** and **24** in which *trans* oxidative addition was observed. The methylene resonances were observed at δ = 3.01 ppm and 3.46 ppm and again possessing Pt-195 satellites with coupling constants ²J_(PtH) = 104 Hz and 89 Hz respectively. The four phenyl proton resonances of the phenyl boronic ligand were observed in the aromatic region of the spectrum, with the resonance positioned *ortho* to the methylene group possessing Pt-195 satellites with a coupling constant of ⁴J_(PtH) = 18Hz. These observations coupled with the presence of only eight pyridyl resonances is indicative of *trans* oxidative addition of *ortho*-(bromomethyl)phenyl boronic acid occurring to yield **25**.

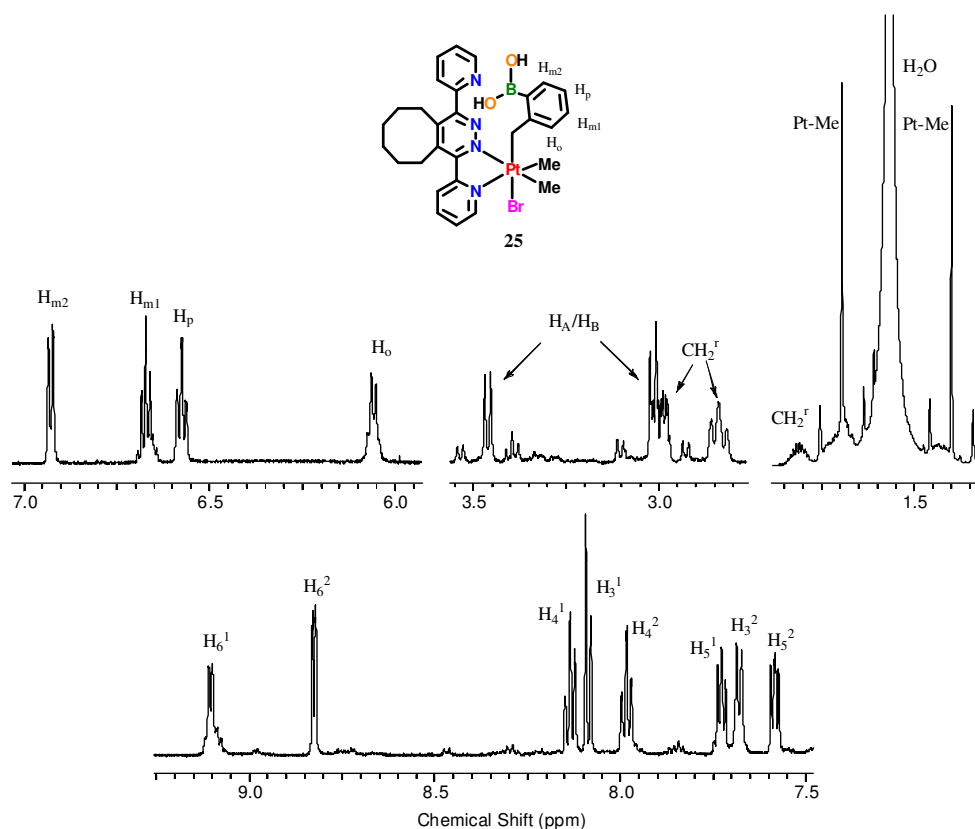


Figure 4.21. ^1H NMR of complex **25** in CD_2Cl_2 . CH_2^r represents the methylene protons of the cyclooctyl ring

The proposed geometry of complex **25** was confirmed by the solid state structure, figure 4.22. The benzyl group is observed to be oriented *trans* to the bromine atom as expected and in a manner similar to **24**, the benzyl group is positioned directly over the pyridazine ring due to favourable π - π stacking. Again the non-coordinating pyridyl group does not participate in hydrogen bonding with the hydroxyl groups of the boronic acid, rather a hydrogen bonding interaction between the hydroxyl group and solvent tetrahydrofuran is observed with a distance of $\text{O}(2)\cdots\text{O}(4) = 2.642 \text{ \AA}$. This bond distance is consistent with a strong hydrogen bonding interaction between **25** and the solvent molecule. Complex **25** self-assembles to form a supramolecular dimer structure in which two adjacent molecules of **25** form a complementary hydrogen bonding pair, figure 4.23. Similar structures are observed in analogous organoplatinum(IV) boronic acids. The hydrogen bond pairs are described using graph set notation as $\text{R}_2^2(8)$ similar to complex **19a**, and share a hydrogen bonding interaction with a distance $\text{O}(1)\cdots\text{O}(2\text{A}) = 2.743 \text{ \AA}$. Again this distance is representative of a strong hydrogen bond and the values are

consistent with other head-to-tail hydrogen bonded organoplatinum(IV) boronic acids. The dimer structure is supported by the hydrogen bonds between the remaining hydroxyl group and the tetrahydrofuran solvent molecules as observed in the molecular structure.

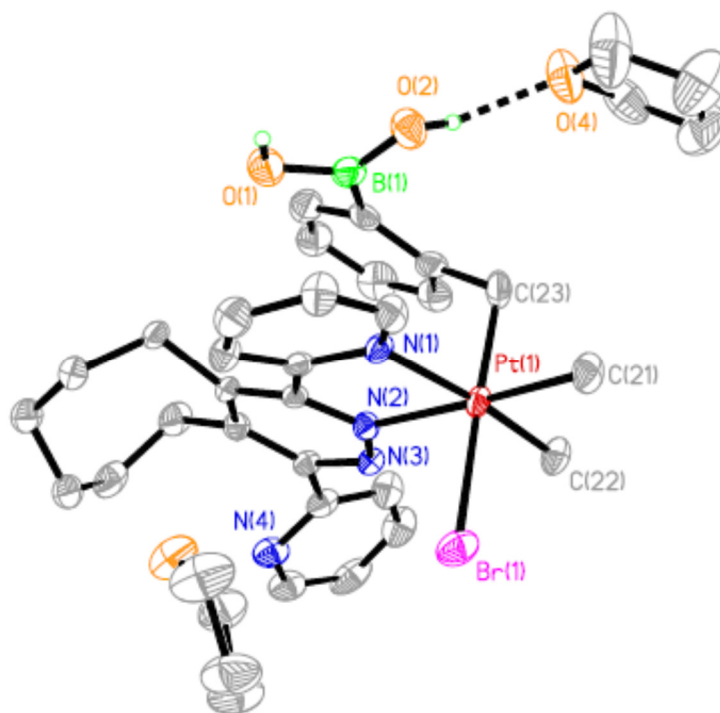


Figure 4.22. Molecular structure of complex **25**, with an atomic numbering scheme (hydrogen atoms excluded for clarity).

Table 4.7: Bond lengths [Å] and angles [°] for [PtBrMe₂(CH₂-2-C₆H₄-B(OH)₂)(6-dppd)], 25.

Pt(1)-N(1)	2.163(4)	Pt(1)-N(2)	2.134(4)
Pt(1)-C(21)	2.061(5)	Pt(1)-C(22)	2.040(6)
Pt(1)-Br(1)	2.5721(7)	Pt(1)-C(23)	2.079(6)
N(1)-Pt(1)-N(2)	75.86(17)	C(21)-Pt(1)-C(22)	86.4(2)
N(2)-Pt(1)-C(21)	175.5(2)	N(2)-Pt(1)-C(23)	95.3(2)
N(2)-Pt(1)-C(22)	98.0(2)	N(1)-Pt(1)-C(21)	99.7(2)
C(21)-Pt(1)-C(23)	85.3(3)	C(22)-Pt(1)-C(23)	90.1(3)
N(1)-Pt(1)-C(22)	173.6(2)	N(1)-Pt(1)-C(23)	92.2(2)
N(2)-Pt(1)-Br(1)	87.29(12)	C(22)-Pt(1)-Br(1)	90.01(19)
N(1)-Pt(1)-Br(1)	87.88(12)	C(21)-Pt(1)-Br(1)	92.1(2)
C(23)-Pt(1)-Br(1)	177.38(17)	Pt(1)-C(23)-C(24)	114.8(4)

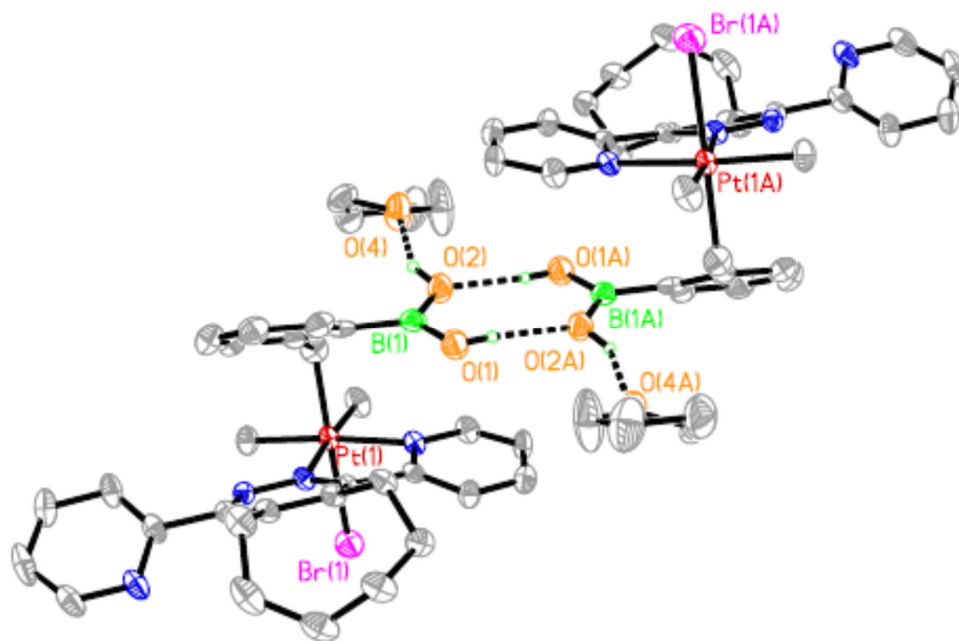


Figure 4.23. A view of the supramolecular dimer structure of complex 25.

4.5 Conclusions

The dimethylplatinum(II) complex, **2**, undergoes oxidative addition reactions of alkyl and benzyl bromide substrates to yield the corresponding organoplatinum(IV) complexes. When hydrogen bonding functionality is incorporated into these substrates, the resultant complexes are observed to self-assemble into a variety of architectures ranging from monomeric, dimeric and even polymeric structures. The supramolecular structure that the organoplatinum(IV) complexes form shows a dependence on the type of hydrogen bonding group employed, the orientation of the hydrogen bonding group and the proximity of this group to non-coordinated pyridyl ring of the **6-dppd** ligand backbone.

The oxidative addition of alkyl and benzyl bromide substrates possessing carboxylic acid functional groups led to the formation of stable organoplatinum(IV) complexes in most cases. The one exception was the oxidative addition of 3-bromopropionic acid which through a proposed β -elimination and loss of methane yielded the platinum(II) complex, **21** [PtBrMe(6-dppd)]. In all other cases, the organoplatinum(IV) carboxylic acids self-assemble into polymers in the case of benzyl bromide derivatives, and dimers in the case of bromoacetic acid. The polymers propagate through either intermolecular N \cdots HO interactions between the pyridyl group and the carboxylic acid, **18**, or weak PtBr \cdots HO secondary interactions, **17**. The acetic acid derivative, **19a** was shown to self-assemble into a head-to-tail dimer structure through intermolecular C=O \cdots HO interactions.

Introduction of an alcohol group as a hydrogen bond donor resulted in the only case of an intramolecular hydrogen bonding interaction between the pyridyl group and the alcohol, **22**. The N \cdots HO interaction is facilitated in part by the proximity and directionality of the benzyl alcohol group and its inherent flexibility.

Finally, the oxidative addition of *ortho*, *meta*, and *para* (bromomethyl)phenyl boronic acids resulted in the formation of stable organoplatinum(IV) boronic acids. The *meta* derivative, **24**, was observed to self-assemble in the solid state to form a polymeric structure propagated by weak PtBr \cdots HO intermolecular interactions between adjacent

monomers. The *ortho* derivative on the other hand, **25**, self-assembled in the solid state to form a complementary head-to-tail dimer structure. This supramolecular structure is formed through complementary OH...OB hydrogen bonding and supported by additional hydrogen bonding to tetrahydrofuran solvent molecules.

The vast array of supramolecular architectures formed via the self-assembly of organoplatinum(IV) complexes possessing hydrogen bonding functionality exemplifies their significance to the field of supramolecular chemistry. Couple the variety of structures with the ease of synthesis and this oxidative addition protocol could be a useful method to design monomeric units capable of tailored supramolecular chemistry with direct applications to crystal engineering and molecular materials.

4.6 Experimental

Reagents and General Procedures. All reactions were carried out in an inert atmosphere of dry nitrogen using standard Schlenk techniques, unless otherwise specified. All solvents used for air and moisture sensitive materials were purified using an Innovative Technology Inc. *PURE SOLV* solvent purification system (SPS). Complex **2** was prepared as previously reported in chapter 2. NMR spectra were recorded at ambient temperature, unless otherwise noted (ca. 25°C), on Varian Mercury 400 or Varian Inova 400 or 600 spectrometers. ¹H chemical shifts are reported relative to TMS (¹H). Complete assignment of each compound was aided by the use of ¹H-¹H NOESY, ¹H-¹³C{¹H}-HSQC and ¹H-¹H gCOSY experiments as required. The standard labeling schemes for pyridyl rings are utilized when labeling signals in NMR spectroscopic analysis. Elemental analyses were performed by either Guelph Chemical Laboratories or Laboratoire d'Analyse Élémentaire de l'Université de Montréal. Mass spectrometric analysis was carried out using an electrospray PE-Sciex Mass Spectrometer (ESI-MS) coupled with a TOF detector.

X-ray Crystallography. A suitable crystal of each compound was coated in Paratone oil and mounted on a glass fiber loop. X-ray data for compounds **17**, **19a**, **21**, **22**, **24**, and **25** were collected at 150K with ω and φ scans on a Bruker Smart Apex II diffractometer using graphite-monochromated MoK α radiation ($\lambda = 0.71073 \text{ \AA}$) and Bruker SMART software [57]. Unit cell parameters were calculated and refined from the full data set. Cell refinement and data reduction were performed using the Bruker APEX2 and SAINT programs respectively [58]. Reflections were scaled and corrected for absorption effects using SADABS [59]. X-ray data for compounds **18** was collected at 150K with ω and φ scans on a Nonius Kappa-CCD diffractometer using graphite-monochromated MoK α radiation ($\lambda = 0.71073 \text{ \AA}$) and COLLECT software [60]. Unit cell parameters were calculated and refined from the full data set. Cell refinement and data reduction were performed using the DENZO-SMN software programs [61]. Reflections were scaled and corrected for absorption effects using DENZO-SMN [61]. All structures were solved by either Patterson or direct methods with SHELXS [62] and refined by full-matrix least-squares techniques against F^2 using SHELXL [63]. All non-hydrogen atoms were

refined anisotropically. The hydrogen atoms were placed in calculated positions and refined using the riding model.

[PtBrMe₂(CH₂-4-C₆H₄CO₂H)(6-dppd)], complex 17. To an acetone solution of complex **2** (0.010g, 0.0184mmol) is added one equivalent (0.004g, 0.0184mmol) of α -bromo-4-toluic acid. An immediate colour change was observed as the originally deep red solution became a bright yellow solution following the addition of the α -bromo-4-toluic acid. After letting the reaction mixture stir for 90mins, the yellow solid product was collected via Hirsch filtration, washed with pentane (3 x 2mL) and then dried under high vacuum. Yield 94%. Crystals of the product were grown by dissolving the yellow powdered solid in acetone and allowing excess pentane to migrate into the vial. **¹H NMR in acetone-d₆:** δ 1.42 (s, 3H, $^2J(\text{PtH}) = 70$ Hz, CH₃), 1.75 (s, 3H, $^2J(\text{PtH}) = 71$ Hz, CH₃), 1.45 - 3.50 (12H, 6 x CH₂ on ring unresolvable), 2.84 (d, 1H, $^2J(\text{HH}) = 9$ Hz, $^2J(\text{PtH}) = 92$ Hz, CH₂^A), 2.89 (d, 1H, $^2J(\text{HH}) = 9$ Hz, $^3J(\text{PtH}) = 83$ Hz, CH₂^B), 6.43 (d, 2H, $^3J(\text{HH}) = 8$ Hz, $^4J(\text{PtH}) = 19$ Hz, H_P¹), 7.27 (d, 2H, $^3J(\text{HH}) = 8$ Hz, H_P²), 7.60 (m, 1H, H₅²), 7.87 (m, 1H, H₅¹), 8.01 (dd, 1H, H₄²), 8.13 (m, 2H, H₄¹/H₃²), 8.34 (d, 1H, H₃¹), 8.77 (d, 1H, H₆²), 9.07 (d, 1H, $^3J(\text{PtH}) = 19$ Hz, H₆¹). **Elemental Analysis:** Anal. Calc'd. [C₃₀H₃₃BrN₄O₂Pt]•0.25(C₃H₆O) (%): C, 47.90; H, 4.51; N, 7.27. Found: C, 47.90; H, 4.00; N, 7.13.

[PtBrMe₂(CH₂-4-C₆H₄CH₂CO₂H)(6-dppd)], complex 18. To an acetone solution of complex **2** (0.010g, 0.0184mmol) is added one equivalent (0.0042g, 0.0184mmol) of 4-(bromomethyl)phenylacetic acid. An immediate colour change was observed as the originally deep red solution became a bright yellow solution following the addition of the 4-(bromomethyl)phenylacetic acid. After letting the reaction mixture stir for 60mins, the yellow solid product was collected via Hirsch filtration, washed with pentane (3 x 2mL) and then dried under high vacuum. Yield 87%. Crystals of the product were grown by dissolving the yellow powdered solid in acetone and allowing excess pentane to migrate into the vial. **¹H NMR in CD₂Cl₂:** δ 1.42 (s, 3H, $^2J(\text{PtH}) = 70$ Hz, CH₃), 1.68 (s, 3H, $^2J(\text{PtH}) = 70$ Hz, CH₃), 1.45 - 2.10 (8H, 4 x CH₂ on ring unresolvable), 2.78 (d, 1H, $^2J(\text{HH}) = 9$ Hz, $^2J(\text{PtH}) = 90$ Hz, CH₂^A), 2.81 (d, 1H, $^2J(\text{HH}) = 9$ Hz, $^3J(\text{PtH}) = 88$ Hz, CH₂^B), 2.90 (m, 2H, CH₂ ring), 3.09 (m, 2H, CH₂ ring), 3.25 (d, 2H, CH₂^{C/D}), 6.25 (d,

2H, $^3J(\text{HH}) = 8 \text{ Hz}$, $^4J(\text{PtH}) = 19 \text{ Hz}$, H_A), 6.48 (d, 2H, $^3J(\text{HH}) = 8 \text{ Hz}$, H_B), 7.54 (m, 1H, H_5^1), 7.62 (m, 1H, H_5^2), 8.05 (dd, 2H, $\text{H}_4^2/\text{H}_4^1$), 8.09 (d, 2H, $\text{H}_3^1/\text{H}_3^2$), 8.78 (d, 1H, H_6^2), 8.96 (d, 1H, $^3J(\text{PtH}) = 20 \text{ Hz}$, H_6^1). **ESI-MS(TOF):** $[\text{C}_{31}\text{H}_{35}\text{BrN}_4\text{O}_2\text{PtNa}]^+$ Calculated precise mass = 793.147g/mol; Determined Precise Mass = 793.1454g/mol. **Elemental Analysis:** Anal. Calc'd. $[\text{C}_{31}\text{H}_{35}\text{BrN}_4\text{O}_2\text{Pt}] \cdot 0.5(\text{C}_3\text{H}_6\text{O}) \cdot \text{H}_2\text{O}$ (%): C, 47.74; H, 4.93; N, 6.85. Found: C, 47.94; H, 4.23; N, 6.95.

[PtBrMe₂(CH₂CO₂H)(6-dppd)], complex 19 (19a, 19b, 19c). To an acetone solution of complex **2** (0.010g, 0.0184mmol) was added an equimolar amount of bromoacetic acid. An immediate colour change from red to bright yellow was observed. After removing the acetone under reduced pressure, excess bromoacetic acid was washed away with diethyl ether. The complex was dried under vacuum and then dissolved in acetone-*d*₆ for ¹H NMR analysis. Yield 89%. ¹H NMR analysis indicated that there was a mixture of three complexes **19a**, **19b** and **19c**. **¹H NMR in acetone-*d*₆: (19a):** δ 1.46 (s, 3H, $^2J(\text{PtH}) = 70 \text{ Hz}$, CH₃), 1.65 (s, 3H, $^2J(\text{PtH}) = 70 \text{ Hz}$, CH₃), 1.28 - 3.45 (12H, 6 x CH₂ on ring unresolvable), 1.93 (d, 1H, $^2J(\text{HH}) = 10 \text{ Hz}$, $^2J(\text{PtH}) = 95 \text{ Hz}$, CH₂^A), 1.99 (d, 1H, $^2J(\text{HH}) = 10\text{Hz}$, $^3J(\text{PtH}) = 91 \text{ Hz}$, CH₂^B), 7.60 (m, 1H, H_5^1), 7.88 (m, 1H, H_5^2), 8.11 (m, 2H, $\text{H}_4^2/\text{H}_3^1$), 8.35 (dd, 1H, H_4^1), 8.55 (d, 1H, H_3^2), 8.79 (d, 1H, H_6^2), 8.99 (d, 1H, $^3J(\text{PtH}) = 17 \text{ Hz}$, H_6^1). **(19b)** δ 0.73 (s, 3H, $^2J(\text{PtH}) = 73 \text{ Hz}$, CH₃), 1.49 (s, 3H, $^2J(\text{PtH}) = 69 \text{ Hz}$, CH₃), 1.28 - 3.45 (12H, 6 x CH₂ on ring unresolvable), 3.21 (d, 1H, $^2J(\text{HH}) = 10 \text{ Hz}$, $^2J(\text{PtH}) = 93 \text{ Hz}$, CH₂^A), 3.24 (d, 1H, $^2J(\text{HH}) = 10\text{Hz}$, $^3J(\text{PtH}) = 91 \text{ Hz}$, CH₂^B), 7.61 (m, 1H, H_5^1), 8.02 (m, 1H, H_5^2), 8.09 (m, 1H, H_4^2), 8.27 (d, 1H, H_3^2), 8.49 (dd, 1H, H_4^1), 8.70 (d, 1H, H_3^1), 8.81 (d, 1H, H_6^2), 9.16 (d, 1H, $^3J(\text{PtH}) = 22 \text{ Hz}$, H_6^1). **(19c)** δ 0.75 (s, 3H, $^2J(\text{PtH}) = 73 \text{ Hz}$, CH₃), 1.75 (s, 3H, $^2J(\text{PtH}) = 69 \text{ Hz}$, CH₃), 1.28 - 3.45 (12H, 6 x CH₂ on ring unresolvable), 2.87 (d, 1H, $^2J(\text{HH}) = 10 \text{ Hz}$, $^2J(\text{PtH}) = 97 \text{ Hz}$, CH₂^A), 3.10 (d, 1H, $^2J(\text{HH}) = 10\text{Hz}$, $^3J(\text{PtH}) = 92 \text{ Hz}$, CH₂^B), 7.61 (m, 1H, H_5^1), 7.99 (m, 1H, H_5^2), 8.06 (m, 1H, H_4^2), 8.14 (d, 1H, H_3^2), 8.44 (dd, 1H, H_4^1), 8.65 (d, 1H, H_3^1), 8.79 (d, 1H, H_6^2), 9.45 (d, 1H, $^3J(\text{PtH}) = 17 \text{ Hz}$, H_6^1). **Elemental Analysis:** Anal. Calc'd for $[\text{C}_{24}\text{H}_{29}\text{BrN}_4\text{O}_2\text{Pt}] \cdot (\text{C}_3\text{H}_6\text{O}) \cdot (\text{H}_2\text{O})$ (%): C, 42.86; H, 4.93; N, 7.41. Found: C, 42.68; H, 4.45; N, 7.74.

[PtBrMe₂(CH₂CH₂CO₂H)(6-dppd)], complex 20. To an acetone solution of complex **2** (0.010g, 0.0184mmol) was added an equimolar amount of 3-bromopropionic acid. An immediate colour change from red to bright yellow was observed. After removing the acetone under reduced pressure, excess 3-bromopropionic acid was washed away with diethyl ether. The complex was dried under vacuum and then dissolved in CD₂Cl₂ for ¹H NMR analysis. ¹H NMR analysis indicated that there was a mixture of two complexes **20** and **21**. **¹H NMR in CD₂Cl₂ for 20:** δ 2.03 (s, 3H, ²J(PtH) = 70 Hz, CH₃), 2.29 (s, 3H, ²J(PtH) = 70 Hz, CH₃), 1.28 - 3.45 (12H, 6 x CH₂ on ring unresolvable), 1.90 - 3.10 (2 x CH₂ methylene protons unresolvable), 7.60 (m, 1H, H₅¹), 7.78 (m, 1H, H₅²), 8.03 (d, 1H, H₃¹), 8.15 (m, 1H, H₄²), 8.30 (dd, 1H, H₄¹), 8.35 (d, 1H, H₃²), 9.03 (d, 1H, H₆²), 9.80 (d, 1H, H₆¹).

[PtBrMe(6-dppd)], complex 21. To an acetone solution of complex **2** (0.010g, 0.0184mmol) was added an equimolar amount of 3-bromopropionic acid. An immediate colour change from red to bright yellow was observed. After removing the acetone under reduced pressure, excess 3-bromopropionic acid was washed away with diethyl ether. The complex was dried under vacuum and then dissolved in CD₂Cl₂ for ¹H NMR analysis. Yield 78%. ¹H NMR analysis indicated that there was a mixture of two complexes **20** and **21**. **¹H NMR in CD₂Cl₂ for 21:** δ 1.44 (s, 3H, ²J(PtH) = 80 Hz, CH₃), 1.55 (m, 2H, CH₂), 1.70 (m, 2H, CH₂), 2.08 (m, 2H, CH₂), 3.00 (m, 2H, CH₂), 3.33 (m, 2H, CH₂), 7.46 (m, 1H, H₅¹), 7.73(m, 1H, H₅²), 7.96 (d, 1H, H₄²), 8.10 (d, 1H, H₃²), 8.18 (dd, 1H, H₄¹), 8.23 (d, 1H, H₃¹), 8.74 (d, 1H, H₆²), 10.00 (d, 1H, ³J_{PtH} = 24Hz, H₆¹).
Elemental Analysis: Anal. Calc'd for [C₂₁H₂₃BrN₄Pt]•0.5(C₃H₆O) (%): C, 42.53; H, 4.12; N, 8.82. Found: C, 42.59; H, 3.90; N, 8.64.

[PtBrMe₂(CH₂-2-C₆H₄-CH₂OH)(6-dppd)], complex 22. Acetone solutions of complex **2**, (0.010 g, 0.0184 mmol) and 2-(bromomethyl)benzyl alcohol (0.0037g, 0.0184 mmol) were added together and allowed to stir for two hours. The then yellow acetone mixture was layered with pentane and allowed to stand in the refrigerator for 12 hours to induce precipitation. The yellow precipitate was then collected via Hirsch filtration and washed with pentane 2 x 2mL. Yield 81%. **¹H NMR in CD₂Cl₂:** δ 1.40 (s, 3H, ²J(PtH) = 70 Hz, CH₃), 1.77 (s, 3H, ²J(PtH) = 70 Hz, CH₃), 1.20 - 3.10 (12H, 6 x CH₂ on ring

unresolvable), 2.67 (d, 1H, $^2J(\text{HH}) = 9 \text{ Hz}$, $^2J(\text{PtH}) = 87 \text{ Hz}$, CH_2^{A}), 2.85 (d, 1H, $^2J(\text{HH}) = 9 \text{ Hz}$, $^3J(\text{PtH}) = 106 \text{ Hz}$, CH_2^{B}), 2.67 (d, 1H, $^2J(\text{HH}) = 15 \text{ Hz}$, CH_2^{C}), 4.48 (d, 1H, $^2J(\text{HH}) = 15 \text{ Hz}$, CH_2^{D}), 5.86 (d, 1H, $^3J(\text{HH}) = 7 \text{ Hz}$, $^4J(\text{PtH}) = 18 \text{ Hz}$, H_o), 6.39 (t, 1H, $^3J(\text{HH}) = 7 \text{ Hz}$, $^3J(\text{HH}) = 7 \text{ Hz}$, H_{m1}), 6.78 (t, 1H, $^3J(\text{HH}) = 7 \text{ Hz}$, $^3J(\text{HH}) = 7 \text{ Hz}$, H_p), 6.96 (d, 1H, $^3J(\text{HH}) = 7 \text{ Hz}$, H_{m2}), 7.56 (m, 1H, H_5^1), 7.59 (d, 1H, H_3^2), 7.76 (m, 1H, H_5^2), 7.95 (dd, 1H, H_4^2), 7.99 (d, 1H, H_3^1), 8.13 (dd, 1H, H_4^1), 8.80 (d, 1H, H_6^2), 9.21 (d, 1H, $^3J(\text{PtH}) = 17 \text{ Hz}$, H_6^1). **Elemental Analysis:** Anal. Calc'd for $[\text{C}_{30}\text{H}_{35}\text{BrN}_4\text{OPt}]\cdot(\text{H}_2\text{O})$ (%): C, 47.37; H, 4.90; N, 7.37. Found: C, 47.34; H, 4.56; N, 7.13.

[PtBrMe₂(CH₂-4-C₆H₄-CH₂-B(OH)₂)(6-dppd)], complex 23. To an acetone solution of complex **2**, (0.010g, 0.0184mmol) was added an equimolar acetone solution of *para*-(bromomethyl)phenyl boronic acid, (0.0040g, 0.0184mmol). After allowing the reaction mixture to stir for one hour, the yellow solution was layered with pentane and a yellow solid precipitated out over time. This solid was then collected via Hirsch filtration and washed with pentane 2 x 1mL. After drying under high vacuum, the yellow solid was massed and a yield of 75% was determined. **¹H NMR in acetone-*d*₆:** δ 1.39 (s, 3H, $^2J(\text{PtH}) = 70 \text{ Hz}$, CH_3), 1.75 (s, 3H, $^2J(\text{PtH}) = 71 \text{ Hz}$, CH_3), 1.25 - 3.15 (12H, 6 x CH_2 on ring unresolvable), 2.78 (d, 1H, $^2J(\text{HH}) = 9 \text{ Hz}$, $^2J(\text{PtH}) = 91 \text{ Hz}$, CH_2^{A}), 2.86 (d, 1H, $^2J(\text{HH}) = 9 \text{ Hz}$, $^3J(\text{PtH}) = 93 \text{ Hz}$, CH_2^{B}), 6.30 (d, 2H, $^3J(\text{HH}) = 8 \text{ Hz}$, $^4J(\text{PtH}) = 18 \text{ Hz}$, H_o), 7.13 (d, 2H, $^3J(\text{HH}) = 8 \text{ Hz}$, H_m), 7.60 (dd, 1H, H_5^2), 7.87 (m, 2H, $\text{H}_5^1/\text{H}_4^2$), 8.15 (d, 1H, H_3^2), 8.30 (m, 2H, $\text{H}_4^1/\text{H}_3^1$), 8.78 (d, 1H, H_6^2), 9.10 (d, 1H, $^3J(\text{PtH}) = 19 \text{ Hz}$, H_6^1). **Elemental Analysis:** Anal. Calc'd for $[\text{C}_{29}\text{H}_{34}\text{BrN}_4\text{O}_2\text{BPt}]\cdot 1.5(\text{H}_2\text{O})$ (%): C, 44.46; H, 4.76; N, 7.15. Found: C, 44.25; H, 4.35; N, 7.02.

[PtBrMe₂(CH₂-3-C₆H₄-CH₂-B(OH)₂)(6-dppd)], complex 24. To an acetone solution of complex **2**, (0.010g, 0.0184mmol) was added an equimolar acetone solution of *meta*-(bromomethyl)phenyl boronic acid, (0.0040g, 0.0184mmol). After allowing the reaction mixture to stir for one hour, the yellow solution was layered with pentane and a yellow solid precipitated out over time. This solid was then collected via Hirsch filtration and washed with pentane 2 x 1mL. After drying under high vacuum, the yellow solid was massed and a yield of 68% was determined. **¹H NMR in acetone-*d*₆:** δ 1.40 (s, 3H, $^2J(\text{PtH}) = 70 \text{ Hz}$, CH_3), 1.72 (s, 3H, $^2J(\text{PtH}) = 71 \text{ Hz}$, CH_3), 1.25 - 3.12 (12H, 6 x CH_2 on

ring unresolvable), 2.77 (d, 1H, $^2J(\text{HH}) = 9 \text{ Hz}$, $^2J(\text{PtH}) = 91 \text{ Hz}$, CH_2^{A}), 2.86 (d, 1H, $^2J(\text{HH}) = 9\text{Hz}$, $^3J(\text{PtH}) = 96 \text{ Hz}$, CH_2^{B}), 6.53 (d, 1H, $^3J(\text{HH}) = 9 \text{ Hz}$, $^4J(\text{PtH}) = 18 \text{ Hz}$, $\text{H}_{\text{O}1}$), 6.64 (dd, 1H, $^3J(\text{HH}) = 9 \text{ Hz}$, $^3J(\text{HH}) = 9 \text{ Hz}$, H_{m}), 6.73 (s, 1H, $^4J(\text{PtH}) = 11 \text{ Hz}$, $\text{H}_{\text{O}2}$), 7.22 (d, 1H, $^3J(\text{HH}) = 8 \text{ Hz}$, H_{p}), 7.58 (dd, 1H, H_{S^2}), 7.81 (m, 1H, H_{S^1}), 8.10 (dd, 1H, H_{A^2}), 8.17 (d, 1H, H_{S^2}), 8.25 (m, 2H, $\text{H}_{\text{S}^1}/\text{H}_{\text{A}^1}$), 8.76 (d, 1H, H_{S^2}), 9.04 (d, 1H, $^3J(\text{PtH}) = 18 \text{ Hz}$, H_{S^1}). **Elemental Analysis:** Anal. Calc'd for $[\text{C}_{29}\text{H}_{34}\text{BrN}_4\text{O}_2\text{BPt}]$ (%): C, 46.05; H, 4.53; N, 7.41. Found: C, 46.25; H, 4.56; N, 6.89.

[PtBrMe₂(CH₂-2-C₆H₄-CH₂-B(OH)₂)(6-dppd)], complex 25. To an acetone solution of complex **2**, (0.010g, 0.0184mmol) was added an equimolar acetone solution of *ortho*-(bromomethyl)phenyl boronic acid, (0.0040g, 0.0184mmol). After allowing the reaction mixture to stir for one hour, the yellow solution was layered with pentane and a yellow solid precipitated out over time. This solid was then collected via Hirsch filtration and washed with pentane 2 x 1mL. After drying under high vacuum, the yellow solid was massed and a yield of 83% was determined. **¹H NMR in CD₂Cl₂:** δ 1.40 (s, 3H, $^2J(\text{PtH}) = 70 \text{ Hz}$, CH_3), 1.69 (s, 3H, $^2J(\text{PtH}) = 71 \text{ Hz}$, CH_3), 1.25 - 3.12 (12H, 6 x CH_2 on ring unresolvable), 3.01 (d, 1H, $^2J(\text{HH}) = 9 \text{ Hz}$, $^2J(\text{PtH}) = 104 \text{ Hz}$, CH_2^{A}), 3.46 (d, 1H, $^2J(\text{HH}) = 9\text{Hz}$, $^3J(\text{PtH}) = 89 \text{ Hz}$, CH_2^{B}), 6.05 (d, 1H, $^3J(\text{HH}) = 7 \text{ Hz}$, $^4J(\text{PtH}) = 18 \text{ Hz}$, H_{O}), 6.57 (dd, 1H, $^3J(\text{HH}) = 7 \text{ Hz}$, $^3J(\text{HH}) = 7 \text{ Hz}$, H_{p}), 6.67 (dd, 1H, $^3J(\text{HH}) = 7 \text{ Hz}$, $^3J(\text{HH}) = 7 \text{ Hz}$, H_{m}), 6.92 (d, 1H, $^3J(\text{HH}) = 7 \text{ Hz}$, $\text{H}_{\text{m}2}$), 7.58 (dd, 1H, H_{S^2}), 7.68 (d, 1H, H_{S^2}), 7.73 (dd, 1H, H_{S^1}), 7.98 (dd, 1H, H_{A^2}), 8.08 (d, 1H, H_{S^1}), 8.13 (dd, 1H, H_{A^1}), 8.82 (d, 1H, H_{S^2}), 9.09 (d, 1H, $^3J(\text{PtH}) = 19 \text{ Hz}$, H_{S^1}). **Elemental Analysis:** Anal. Calc'd for $[\text{C}_{29}\text{H}_{34}\text{BrN}_4\text{O}_2\text{BPt}] \cdot 1(\text{H}_2\text{O})$ (%): C, 44.98; H, 4.69; N, 7.23. Found: C, 45.23; H, 4.52; N, 6.87.

Table 4.8: Crystallographic data for [PtBrMe₂(CH₂-4-C₆H₄CO₂H)(6-dppd)], 17.

[PtBrMe₂(CH₂-4-C₆H₄CO₂H)(6-dppd)]

Empirical Formula	C ₃₀ H ₃₃ Br N ₄ O ₂ Pt
Formula Weight	756.60
Wavelength	0.71073 Å
Crystal System	Monoclinic
Space Group	P 2 ₁ /c
Unit Cell Dimensions	a = 9.0266(5) Å α = 90° b = 20.4300(9) Å β = 94.271(4)° c = 14.7440(6) Å γ = 90°
Volume	2711.4(2) Å ³
Z	4
Density (calculated)	1.853 Mg/m ³
Absorption Coefficient (μ)	6.684 mm ⁻¹
Crystal Size	0.06 x 0.04 x 0.03 mm ³
Refinement Method	Full-matrix least-squares on F ²
Goodness of fit on F ²	1.005
Final R indices [I > 2σ(I)]	R1 = 0.0463, wR2 = 0.0860
R indices (all data)	R1 = 0.0893, wR2 = 0.1000

Table 4.9: Crystallographic data for [PtBrMe₂(CH₂-4-C₆H₄CH₂CO₂H)(6-dppd)], **18.**

[PtBrMe₂(CH₂-4-C₆H₄CH₂CO₂H)(6-dppd)]·CH₂Cl₂	
Empirical Formula	C ₃₂ H ₃₅ Br Cl ₂ N ₄ O ₂ Pt
Formula Weight	855.56
Wavelength	0.71073 Å
Crystal System	Triclinic
Space Group	P -1
Unit Cell Dimensions	a = 10.258(2) Å α = 80.57(3) ° b = 10.484(2) Å β = 80.05(3) ° c = 16.122(3) Å γ = 72.63(3) °
Volume	1618.2(6) Å ³
Z	2
Density (calculated)	1.756 Mg/m ³
Absorption Coefficient (μ)	5.771 mm ⁻¹
Crystal Size	0.40 x 0.35 x 0.15 mm ³
Refinement Method	Full-matrix least-squares on F ²
Goodness of fit on F ²	1.097
Final R indices [I > 2σ(I)]	R1 = 0.0389, wR2 = 0.1045
R indices (all data)	R1 = 0.0453, wR2 = 0.1209

Table 4.10: Crystallographic data for [PtBrMe₂(CH₂CO₂H)(6-dppd)], **19a**.

[PtBrMe₂(CH₂CO₂H)(6-dppd)]·0.5(CH₂Cl₂)

Empirical Formula	C _{24.50} H ₃₀ Br Cl N ₄ O ₂ Pt
Formula Weight	722.97
Wavelength	0.71073 Å
Crystal System	Orthorhombic
Space Group	P bcn
Unit Cell Dimensions	a = 11.0835(16) Å α = 90° b = 15.125(2) Å β = 90° c = 28.8870(4) Å γ = 90°
Volume	5157.1(12) Å ³
Z	8
Density (calculated)	1.862 Mg/m ³
Absorption Coefficient (μ)	7.124 mm ⁻¹
Crystal Size	0.05 x 0.03 x 0.01 mm ³
Refinement Method	Full-matrix least-squares on F ²
Goodness of fit on F ²	1.081
Final R indices [I > 2σ(I)]	R1 = 0.0637, wR2 = 0.1439
R indices (all data)	R1 = 0.1171, wR2 = 0.1692

Table 4.11: Crystallographic data for [PtBrMe(6-dppd)], **21**.

[PtBrMe(6-dppd)]	
Empirical Formula	C ₂₁ H ₂₃ Br N ₄ Pt
Formula Weight	606.43
Wavelength	0.71073 Å
Crystal System	Monoclinic
Space Group	P 2 ₁ /c
Unit Cell Dimensions	a = 18.083(3) Å α = 90° b = 12.964(2) Å β = 92.263(4)° c = 8.3848(14) Å γ = 90°
Volume	1964.0(6) Å ³
Z	4
Density (calculated)	2.051 Mg/m ³
Absorption Coefficient (μ)	9.192 mm ⁻¹
Crystal Size	0.05 x 0.03 x 0.02 mm ³
Refinement Method	Full-matrix least-squares on F ²
Goodness of fit on F ²	1.018
Final R indices [I > 2σ(I)]	R1 = 0.0454, wR2 = 0.0890
R indices (all data)	R1 = 0.0873, wR2 = 0.1036

Table 4.12: Crystallographic data for [PtBrMe₂(CH₂-2-C₆H₄-CH₂OH)(6-dppd)],
22.

[PtBrMe₂(CH₂-2-C₆H₄-CH₂OH)(6-dppd)]·CH₂Cl₂·CHCl₃	
Empirical Formula	C ₃₂ H ₃₇ Br Cl ₅ N ₄ O ₂ Pt
Formula Weight	961.91
Wavelength	0.71073 Å
Crystal System	Monoclinic
Space Group	P 2 ₁ /n
Unit Cell Dimensions	a = 9.7737(5) Å α = 90° b = 10.0964(5) Å β = 97.239(2)° c = 36.9181(2) Å γ = 90°
Volume	3614.0(3) Å ³
Z	4
Density (calculated)	1.768 Mg/m ³
Absorption Coefficient (μ)	5.393 mm ⁻¹
Crystal Size	0.08 x 0.05 x 0.02 mm ³
Refinement Method	Full-matrix least-squares on F ²
Goodness of fit on F ²	1.041
Final R indices [I > 2σ(I)]	R1 = 0.0479, wR2 = 0.1028
R indices (all data)	R1 = 0.0793, wR2 = 0.1199

Table 4.13: Crystallographic data for [PtBrMe₂(CH₂-3-C₆H₄-B(OH)₂)(6-dppd)], **24**.

[PtBrMe₂(CH₂-3-C₆H₄-B(OH)₂)(6-dppd)]·C₃H₆O	
Empirical Formula	C ₃₂ H ₄₀ B Br N ₄ O ₃ Pt
Formula Weight	814.49
Wavelength	0.71073 Å
Crystal System	Triclinic
Space Group	P -1
Unit Cell Dimensions	a = 8.8735(6) Å α = 94.577(4)° b = 10.9710(6) Å β = 93.652(4)° c = 17.8017(11) Å γ = 113.547(4)°
Volume	1574.96(17) Å ³
Z	2
Density (calculated)	1.717 Mg/m ³
Absorption Coefficient (μ)	5.762 mm ⁻¹
Crystal Size	0.06 x 0.05 x 0.02 mm ³
Refinement Method	Full-matrix least-squares on F ²
Goodness of fit on F ²	1.056
Final R indices [I>2σ(I)]	R1 = 0.0592, wR2 = 0.1169
R indices (all data)	R1 = 0.0972, wR2 = 0.1330

Table 4.14: Crystallographic data for [PtBrMe₂(CH₂-2-C₆H₄B(OH)₂)(6-dppd)], 25.**[PtBrMe₂(CH₂-2-C₆H₄-B(OH)₂)(6-dppd)]·2(C₄H₈O)**

Empirical Formula	C ₃₇ H ₅₀ B Br N ₄ O ₄ Pt
Formula Weight	900.62
Wavelength	0.71073 Å
Crystal System	Monoclinic
Space Group	P 2 ₁ /c
Unit Cell Dimensions	a = 9.8253(3) Å α = 103.365(2)° b = 9.9194(3) Å β = 95.890(2)° c = 19.4252(6) Å γ = 99.558(2)°
Volume	1796.63(10) Å ³
Z	2
Density (calculated)	1.665 Mg/m ³
Absorption Coefficient (μ)	5.062 mm ⁻¹
Crystal Size	0.05 x 0.04 x 0.01 mm ³
Refinement Method	Full-matrix least-squares on F ²
Goodness of fit on F ²	1.042
Final R indices [I > 2σ(I)]	R1 = 0.0449, wR2 = 0.0834
R indices (all data)	R1 = 0.0893, wR2 = 0.0926

4.7 References

1. Haiduc, I.; Edelman, F.T. *Supramolecular Organometallic Chemistry*; Wiley-VCH: Weinheim, Germany, **1999**.
2. Atwood, J.L.; Steed, J.W. *Encyclopedia of Supramolecular Chemistry*, Marcel Dekker: New York, **2004**.
3. Jeffrey, G.A. *An Introduction to Hydrogen Bonding*. Oxford University Press: New York, **1997**.
4. Desiraju, G.M.; Steiner, T. *The Weak Hydrogen Bond in Structural Chemistry and Biology*, Oxford University Press: New York, **1999**.
5. Oh, M.; Carpenter G.B.; Sweigart, D.A. *Acc. Chem. Res.* **2004**, *37*, 1.
6. Son, S.U.; Reingold, J.A.; Carpenter, G.B.; Czech, P.T.; Sweigart, D.A. *Organometallics*. **2006**, *25*, 5276.
7. Puddephatt, R.J. *Chem. Soc. Rev.* **2008**, *37*, 2012.
8. Addicott, C.; Das, N.; Stang, P.J. *Inorg. Chem.* **2004**, *43*, 5335.
9. Au, R.H.; Jennings, M.C.; Puddephatt, R.J. *Organometallics*. **2009**, *28*, 3754.
10. Zheng, Y.R.; Yang, H.B.; Northrop, B.H.; Ghosh, K.; Stang, P.J. *Inorg. Chem.* **2008**, *47*, 4706.
11. Burchell, T.J.; Eisler, D.J.; Jennings, M.C.; Puddephatt, R.J. *Chem. Commun.* **2003**, 2228.
12. Burchell, T.J.; Puddephatt, R.J. *Inorg. Chem.* **2005**, *44*, 3718.

13. Tiekink, E.R.T.; Vittal, J.J. *Frontiers of Crystal Engineering*, Wiley: Chichester, **2006**.
14. Robin, A.Y.; Fromm, K.M. *Coord. Chem. Rev.* **2006**, 250, 2127.
15. Tabei, E.S.; Samouei, H.; Rashidi, M. *Dalton Trans.* **2011**, 40, 1138.
16. Braga, D.; Grepioni, F. *Coord. Chem. Rev.* **1999**, 183, 19.
17. Marque Rivas, J.C.; Brammer, L. *Coord. Chem. Rev.* **1999**, 183, 43.
18. Gianneschi, N.C.; Tiekink, E.R.T.; Rendina, L.M. *J. Am. Chem. Soc.* **2000**, 122, 8474.
19. Rashidi, M.; Jennings, M.C.; Puddephatt, R.J. *Cryst. Eng. Commun.* **2003**, 5, 65.
20. Zhang, F. Jennings, M.C.; Puddephatt, R.J. *Chem. Commun.* **2007**, 1496.
21. Fraser, C.S.; Jenkins, H.A.; Jennings, M.C.; Puddephatt, R.J. *Organometallics.* **2000**, 19, 1635.
22. Fraser, C.S.; Jennings, M.C.; Puddephatt, R.J. *Chem. Commun.* **2001**, 1310.
23. Fraser, C.S.; Jennings, M.C.; Puddephatt, R.J. *Chem. Commun.* **2002**, 1224.
24. Fraser, C.S.; Eisler, D.J.; Puddephatt, R.J. *Polyhedron.* **2005**, 25, 266.
25. Monaghan, P.K.; Puddephatt, R.J. *Dalton Trans.* **1988**, 595.
26. Au, R.H.; Jennings, M.C.; Puddephatt, R.J. *Organometallics.* **2009**, 28, 5052.

27. Au, R.H.; Jennings, M.C.; Puddephatt, R.J. *Dalton Trans.* **2009**, 3519.
28. Djuran, M.I.; Milinkovic, S.U.; Habtemariam, A; Parsons, S.; Sadler, P.J. *J. Inorg. Biochem.* **2002**, 88, 268.
29. Au, R.H. ; Fraser, C.S.; Eisler, D.J.; Jennings, M.C.; Puddephatt, R.J. *Organometallics.* **2009**, 28, 1719.
30. Au, R.H.; Findlay-Shirras, L.J.; Woody, N.M.; Jennings, M.C.; Puddephatt, R.J. *Can. J. Chem.* **2009**, 87, 904.
31. Safa, M.A.; Puddephatt, R.J. *J. Organomet. Chem.* **2013**, 724, 7.
32. Sauvage, J-P.; Hosseini, M.W. *Comprehensive Supramolecular Chemistry* ; Pergamon Press: Oxford, **1996**.
33. Suzuki, K.; Tominaga, M.; Kawano, M.; Fujita, M. *Chem. Commun.* **2009**, 1638.
34. Langford, C.H.; Gray, H.B. *Ligand Substitution Processes.* Wiley, New York, **1965**.
35. McCready, M.S.; Puddephatt, R.J. *Dalton Trans.* **2012**, 41, 12378.
36. Zhao, S-B.; Wang, R-Y.; Wang, S. *J. Am. Chem. Soc.* **2007**, 129, 3092.
37. Scott, J.D.; Puddephatt, R.J. *Organometallics.* **1983**, 2, 1643.
38. Achar, S.; Scott, J.D.; Vittal, J.J.; Puddephatt, R.J. *Organometallics.* **1993**, 12, 4592.

39. Hill, G.S.; Manojlovic-Muir, L.J.; Muir, K.W.; Puddephatt, R.J. *Organometallics*. **1997**, *16*, 525.
40. Achar, S.; Catalano, V.J. *Polyhedron*. **1997**, *16*, 1555.
41. Safa, M.A.; Abo-Amer, A.; Borecki, A.; Cooper, B.F.T.; Puddephatt, R.J. *Organometallics*. **2012**, *31*, 2675.
42. Abo-Amer, A.; Boyle, P.D.; Puddephatt, R.J. *J. Organomet. Chem.* **2014**, *770*, 79.
43. Abo-Amer, A.; Puddephatt, R.J. *J. Inorg. Organomet. Polym.* **2014**, *24*, 114.
44. Abo-Amer, A.; McCready, M.S.; Zhang, F.; Puddephatt, R.J. *Can. J. Chem.* **2012**, *90*, 46.
45. McCready, M.S.; Puddephatt, R.J. *Organometallics*. **2015**, doi: 10.1021/om501023r.
46. Bohm, H.J.; Klebe, G.; Brode, S.; Hesse, U. *Chem. Eur. J.* **1996**, *2*, 1509.
47. Gleitsman, K.R.; Lester, H.A.; Dougherty, D.A. *Chem. Bio. Chem.* **2009**, *10*, 1385.
48. Burchell, T.J.; Eisler, D.J.; Puddephatt, R.J. *Inorg. Chem.* **2004**, *43*, 5550.
49. Bernstein, J.; Davis, R.E.; Shimoni, L.; Chang, N.L. *Angew. Chem. Int. Ed.* **1995**, *34*, 1555.
50. Puddephatt, R.J. *Angew. Chem. Int. Ed.* **2002**, *41*, 261.

51. Nishiyabu, R.; Kubo, Y.; James, T.D.; Fossey, J.S. *Chem. Commun.* **2011**, 47, 1106.
52. Maly, K.E.; Malek, N.; Fournier, J.H.; Rodriguez-Cuamatzi, P.; Maris, T.; Wuest, J.D. *Pure Appl. Chem.* **2006**, 78, 1305.
53. Takeuchi, M.; Ikeda, M.; Sugaski, A.; Shinkai, S. *Acc. Chem. Res.* **2001**, 34, 865.
54. Miayura, N.; Suzuki, A. *Chem. Rev.* **1995**, 95, 2457.
55. Hosseini, S.S.; Bhadbhade, M.; Clarke, R.J.; Rutledge, P.J.; Rendina, L. *Dalton Trans.* **2011**, 40, 506.
56. Wu, Y.B.; Guo, H.M.; Zhang, X.; James, T.D.; Zhao, J.Z. *Chem. Eur. J.* **2011**, 17, 7632.
57. *APEX 2, Crystallography software package*; Bruker AXS: Madison, WI, 2005.
58. *SAINT, Data Reduction Software*; Bruker AXS: Madison, WI, 1999.
59. Sheldrick, G. M. *SADABS v.2.01, Area Detector Absorption Correction Program*; Bruker AXS: Madison, WI, 2006.
60. Nonius (1998). *COLLECT*. Nonius BV, Delft, The Netherlands.
61. Otwinowski, Z.; Minor, W. *Methods in Enzymology*. 1997, Vol. 276, *Macromolecular Crystallography, Part A*, edited by C. W. Carter Jr & R. M. Sweet, p 307-326. New York: Academic Press.

62. Sheldrick, G. M. *SHELXS, program for solution of crystal structures. Acta Cryst. A* **64**, 2008, 112-122.
63. Sheldrick, G. M. *SHELXL, program for refinement of crystal structures. Acta Crystallogr., Section A.* **2008**, 64, 112-122.

CHAPTER 5

Design, Synthesis and Reactivity of Bimetallic Platinum(II) Complexes Based on Ditopic Ligand Designs

5.1 Introduction

The use of transition metal catalysts in modern day synthesis has become a very valuable tool to affect challenging transformations and convert raw materials into value added products [1-5]. Taking motivation from nature, where highly selective catalysts that possess two or more metal centers have been developed, scientists aim to imitate these biocatalysts through polymetallic catalyst designs [6-8]. By mimicking the designs of bio-inspired catalysts there is potential to harness some of the unique reactivity and selectivity that is observed in nature. It is with that motivation that the design and development of bimetallic transition metal catalysts has garnered significant interest in recent years. Specifically, bimetallic complexes have shown to be highly efficient catalysts in affecting complex chemical transformations [1,2,9-13]. This is due in part to the cooperative interactions that can be displayed by proximal metal centers. This cooperativity that is accessed in bimetallic complexes allows the chemist to access reactivity and selectivity that is not often available in monometallic systems. The key to accessing the cooperative reactivity lies in the design of the ditopic ligand scaffold. By designing the ligand to position the metal centers in close proximity to one another, the cooperative reactivity can be encouraged [14,15]. Feringa *et al.* report that in order to maximize the cooperativity between metal centers they should be positioned within 3.5 to 6.0 Å [16]. This will allow that even in the absence of a direct metal-metal bond, the two metal centers are sufficiently close to allow for the interaction of a substrate with both metal centers. The work of Marks *et al.* has shown that the use of a strained bimetallic catalyst, leads to a 4-fold rate increase in the incorporation of ethylene into alkene copolymerization reaction relative to the monometallic species [17]. They attribute the rate increase to the ability of the second metal center to stabilize the substrate during alkene activation. The Messerle group have also reported on the pronounced influence that the scaffold design imparts on the promotion of the dehydroalkoxylation of alkyne diols by bimetallic rhodium(I) catalysts [18,19]. They noted a distinct enhancement in the catalytic rate of the bimetallic complexes, (i) in figure 5.1 as compared to the corresponding monometallic complexes as well as a dependence on the ligand design itself for the bimetallic complexes. They observed greater rates of catalysis for complexes with a more rigid ligand scaffold design similar to (i) in figure 5.1 versus

those with a more semi rigid design, (ii) in figure 5.1. Therefore to enhance the reactivity and cooperative effects the two metal centers can impart, a rigid ligand design should be employed making anthracene an ideal candidate as a ditopic ligand scaffold [11,16,20]. If anthracene is functionalized in the 1,8 positions, the metal centers are held sufficiently close to elicit the desired cooperative effect.

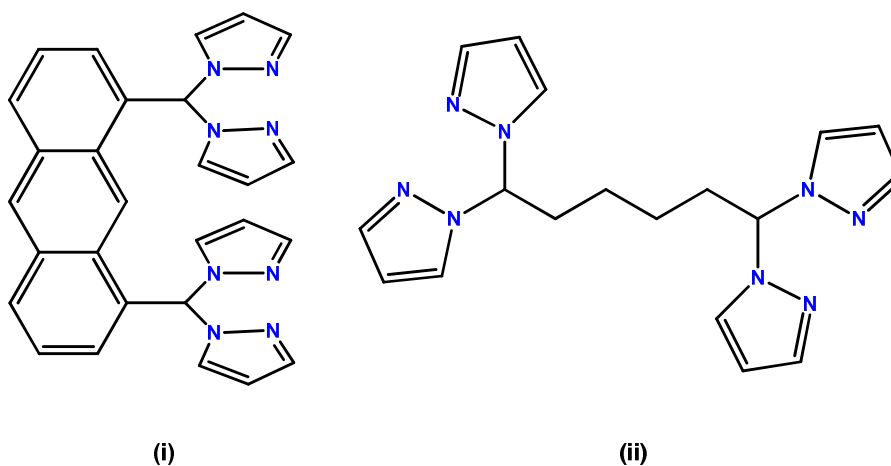


Figure 5.1. Examples of ditopic ligands which allow for cooperative effects in bimetallic complexes.

Similar to anthracene derived ligands, xanthene derived ligands have been shown to offer a desirable scaffold to affect cooperative chemistry. By replacing the rigidity of the anthracene backbone with slight flexibility imparted by the CH₂ and O atom linker, the backbone is capable of puckering to slightly modify the internuclear distances between adjacent metal centers [21-23]. Another distinct advantage of xanthene derived ligands is the ease of synthesis relative to the anthracene derivatives as well as the enhanced solubility [24]. In addition, the incorporation of the oxygen atom also imparts an electronic difference in the backbone and could allow for both an electron donating interaction to a ligand or metal center as well as a possible hydrogen bond accepting atom. To this end, substituted xanthenes have been used on multiple occasions as linker groups for potentially bimetallic transition metal complexes. If substituted in the 4,5 position, the ligand provides an ideal distance between adjacent metal centers to elicit cooperative reactivity. The work by Shishido *et. al.* illustrates this effect nicely as their ligand design and corresponding dipalladium(II) complex, (i) in figure 5.2, has been

shown to promote to copolymerization of ethylene with acrylate [25]. Panunzi *et. al.* also illustrate the ability of these xanthene derivatives to function as excellent scaffolds in the formation of bimetallic complexes of platinum(II), (ii) in figure 5.2 [24].

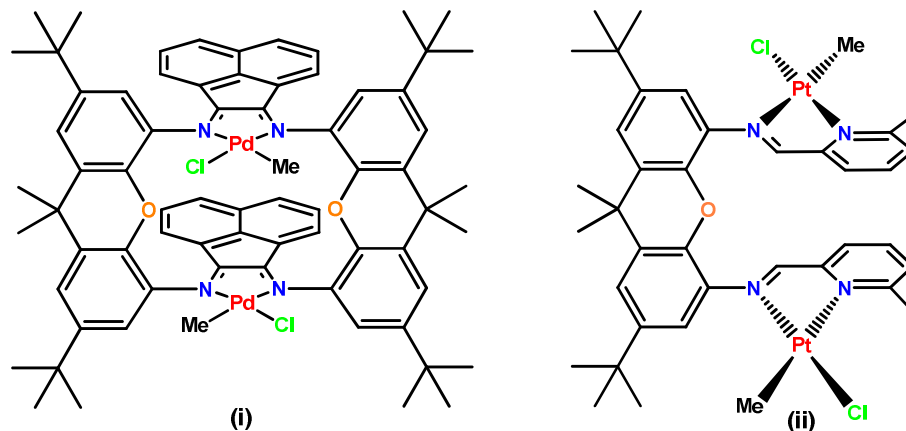
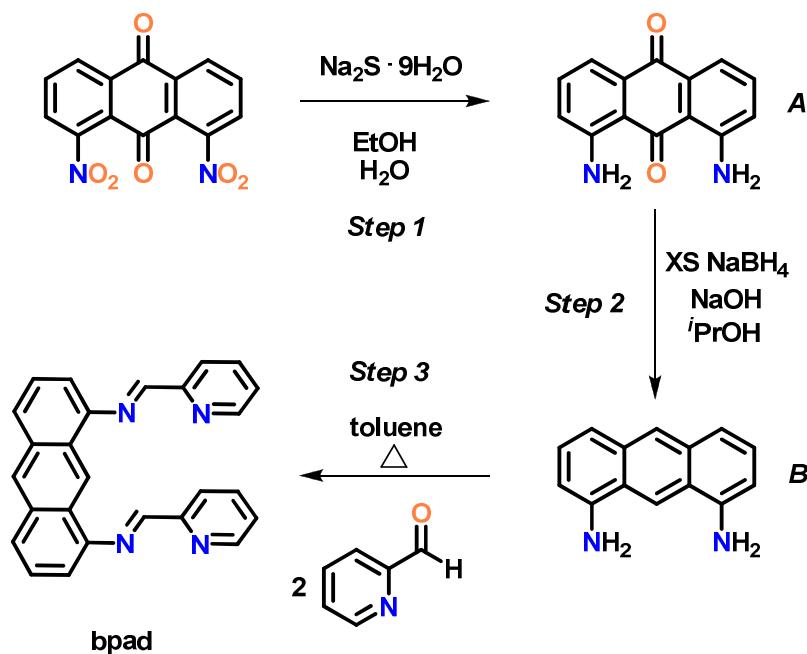


Figure 5.2. Bimetallic complexes based on a xanthene ligand scaffold.

The reactivity of platinum(II) complexes towards oxidative addition has been investigated thoroughly and has shown to be very useful in preparing specific and rationally designed platinum(IV) complexes [26-46]. Although the use of platinum complexes in industry is not as desirable as its congeners, platinum complexes allow for easier elucidation of mechanisms throughout the reaction pathways due to its slower kinetics. With this in mind, the design of bimetallic complexes of platinum(II) should allow for the investigation of the cooperativity between metal centers when complexed by ditopic ligands. With its propensity for the oxidative addition reaction and the consequent stability of the resultant platinum(IV) species, diplatinum(II) complexes should allow for the study of the cooperativity of the two metal centers towards substrate activation. It is with this motivation that the design and synthesis of four ditopic ligands based on anthracene and xanthene scaffolds are outlined in the following chapter. The ability of these ligands to form bimetallic platinum(II) complexes is explored and the reactivity of these complexes towards the oxidative addition of substrates is investigated.

5.2 Ligand Synthesis

The new ligand **bpad**, N^1, N^8 -bis(pyridin-2-ylmethylene)anthracene-1,8-diamine, was synthesized in three steps from 1,8-dinitroanthraquinone as outlined in scheme 5.1.



Scheme 5.1. Synthetic steps on route to the preparation of the ligand **bpad**.

Initially 1,8-dinitroquinone was reduced using sodium sulfide nonahydrate to give 1,8-diaminoanthraquinone, **A**, in high yield and purity. The ^1H NMR spectrum contained three broad signals of equivalent integration in the aromatic region arising due to the three distinct aromatic protons. The amine protons give rise to a broad resonance at $\delta = 7.86$ ppm which has an integration value twice that of the aromatic protons. These resonances coupled with the mass spectral information give diagnostic evidence of the formation of **A**. Then by modifying a procedure by Love *et al.*, this compound was further reduced using sodium borohydride to afford the deep purple 1,8-diaminoanthracene, **B** in scheme 5.1 in a nearly quantitative yield [47]. It was important to carry out this reaction in the absence of light in order to prevent undesired side reactions from occurring. The formation of **B** was confirmed through ^1H NMR spectroscopy by the presence of four aromatic proton resonances. The two singlets furthest downfield possess relative integration values that are half the value of the

remaining aromatic resonances. This indicates that these resonances arise due to the presence of the protons which result from the reduction of the ketones in **A**. The remaining aromatic resonances were assigned using ^1H - ^1H gCOSY NMR spectroscopy as well as considering the differing multiplicities. The two doublet resonances overlap at $\delta = 7.18$ ppm and as such give rise to a signal with a relative integration value four times that of the singlet resonances and shows correlation to the triplet resonance slightly upfield. The amine proton resonances in **B** are shifted significantly upfield relative to their chemical shift observed in **A**, and are observed to integrate to four.

In the final step, a toluene solution of **B** was stirred under refluxing conditions in the presence of two equivalents of 2-pyridinecarboxaldehyde. The reaction mixture was stirred under reflux for 12 hours with the use of a Dean-Stark trap allowing for the removal of water diazeotropically. After removing all of the solvent toluene, the resultant brown oil was dissolved in minimal acetone and layered with hexane to affect the precipitation of a brown solid which was collected by Hirsch filtration in moderate yield. After drying the brown solid, it was then characterized by ^1H , and ^{13}C NMR spectroscopy as well as electrospray ionization mass spectrometry. This reaction is outlined in step 3 of scheme 5.1. The formation of the ligand **bpad** was confirmed by the presence of additional resonances in the ^1H NMR spectrum arising due to the incorporation of the pyridyl groups into the anthracene backbone. A resonance diagnostic of the imine proton, H_i , is observed at $\delta = 8.79$ ppm as a singlet which can be differentiated from the singlets of the ligand backbone through comparing integration values. The imine proton resonance integrates to twice the value of the remaining singlet resonances attributed to the anthracene backbone, which confirms the incorporation of two pyridyl groups into the **bpad** ligand. Indirect evidence of the incorporation of the pyridyl groups is also provided by the disappearance of proton resonances that arise due to the amine protons. The remaining pyridyl and anthracene backbone proton resonances are assigned through two-dimensional NMR spectra and are annotated in figure 5.3.

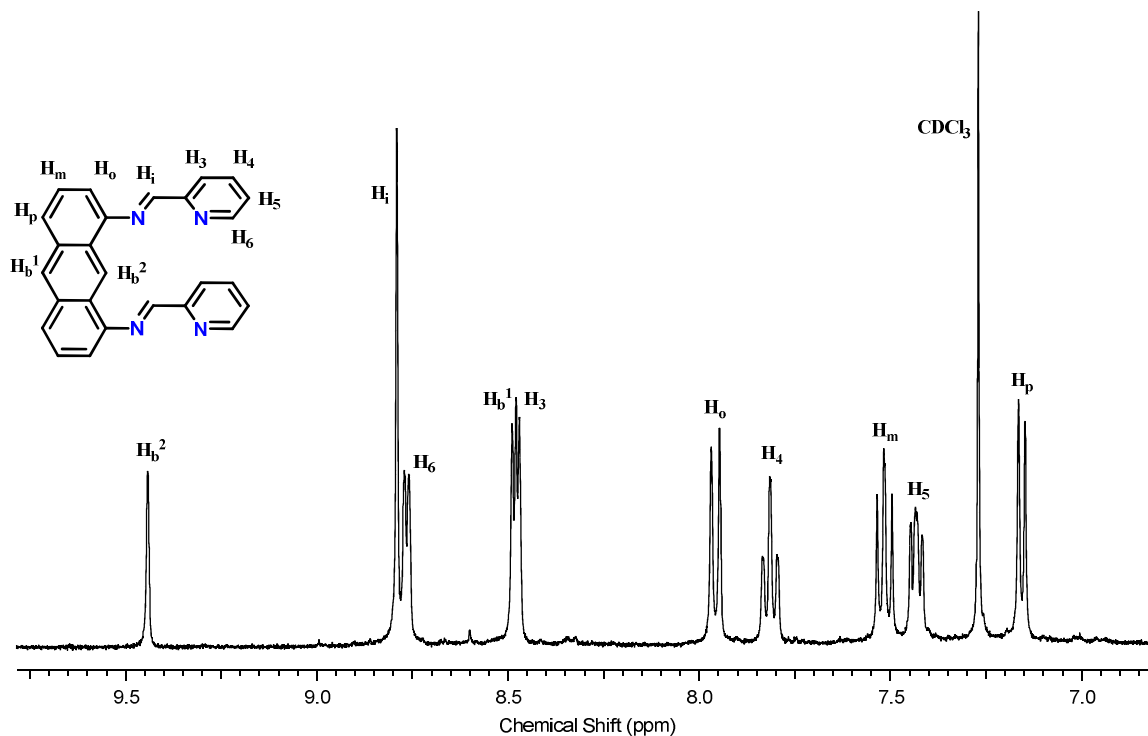


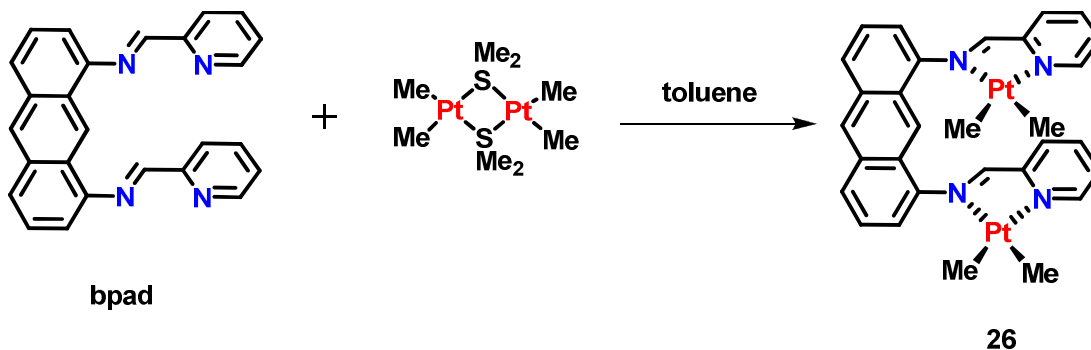
Figure 5.3. ^1H NMR spectrum of the ligand **bpad** in CDCl_3 .

By looking at the image of **bpad** in scheme 5.1, it becomes evident that the pyridyl arms of the ligand could exist in orientations in which the pyridyl groups directly align or are positioned *anti* to one another. Regardless of the orientation of the pyridyl arms, both isomers would be symmetric possessing either a mirror plane or a C_2 rotation axis. Due to rapid rotation of the arms, there is only evidence of a single set of resonances in the ^1H NMR spectrum.

5.3 Synthesis of a dimethylplatinum(II) complex of **bpad**

The dimethylplatinum(II) complex of the ligand **bpad**, was prepared through the complexation of two equivalents of the metal center by **bpad**, scheme 5.2. This was achieved through the addition of a dry toluene solution of $[\text{Pt}_2\text{Me}_4(\mu\text{-SMe}_2)_2]$ to a dry toluene solution of **bpad** under an inert atmosphere and in an equimolar ratio [48]. Upon addition of the reagents, the reaction mixture began to take on a violet purple colour which is indicative of a complexation reaction occurring between the ligand and the

metal center. The reaction mixture was allowed to stir at room temperature for 3 hours before the solvent toluene was removed under reduced pressure. The resultant deep purple oil was dissolved in minimal acetone and layered with pentane to affect the precipitation of a purple solid overnight at 5°C. After vacuum filtration, a bright purple solid was collected and subsequently washed with pentane to afford complex **26**, [Pt₂Me₄(bpad)] in an 81% yield.



Scheme 5.2. Synthesis of complex **26**, [Pt₂Me₄(bpad)].

The ¹H NMR spectrum of **26**, figure 5.4, provided confirmation that a dimethylplatinum(II) center was indeed ligated at both coordination sites through the continued presence of symmetry in the molecule. A single set of resonances that are attributed to the pyridyl arms were observed in the spectrum. This is concluded based on the presence of platinum-195 satellites on both the imine proton, δ = 9.76 ppm, and the *ortho* pyridyl proton, δ = 9.05 ppm, with coupling constant values of ³J(PtH) = 33 Hz and ³J(PtH) = 25 Hz respectively. These values are consistent with those typically observed for dimethylplatinum(II) complexes with diimine ligands [46,49]. Full assignment of the resonances in the aromatic region of the spectrum was aided by ¹H-¹H gCOSY NMR spectroscopy and are annotated in figure 5.4. In addition to the platinum-195 satellites present on the imine and *ortho* pyridyl resonances of the ligand, two resonances resultant from the presence of the methyl groups on the platinum centers were observed. These singlet resonances possessed platinum-195 satellites and were observed at δ = 0.36 ppm and δ = 0.95 ppm with coupling constants of ²J(PtH) = 88 Hz and ²J(PtH) = 86 Hz respectively. These chemical shift values are diagnostic of the formation of a dimethylplatinum(II) complex. The unsymmetrical nature of the diimine coordination

environment leads to the presence of two inequivalent methylplatinum resonances. These resonances can be differentiated and as such ^1H - ^1H NOESY NMR spectroscopy allows for the absolute assignment of these resonances as the *exo* directed methyl group, Me_A , shows a correlation to the *ortho* proton resonance of the ligand. This allows for the assignment of the most upfield methylplatinum resonance being attributed to the *endo* directed methyl group, Me_B , and the more downfield resonance being attributed to the *exo* methyl group. The formation of **26** was further supported by both ESI-MS as well as elemental analysis.

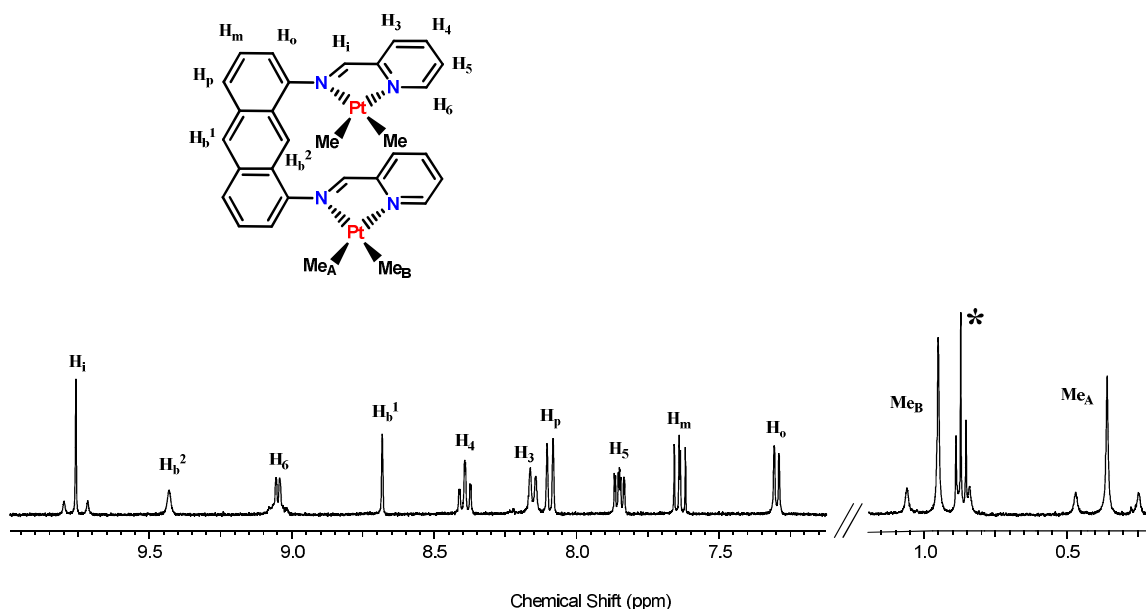


Figure 5.4. ^1H NMR spectrum of complex **26**, $[\text{Pt}_2\text{Me}_4(\text{bpad})]$, in acetone- d_6 . * indicates the presence of residual pentane.

Numerous attempts to grow single crystals suitable for X-ray diffraction were performed however in each instance the originally red-purple solution of **26** would result in the formation of a black solid. This solid was not appreciably soluble in any NMR solvent and therefore it could not be identified. To investigate this, a sample of complex **26** was left stirring in acetone at room temperature. After 24 hours it was observed that the originally deep red-purple colour of complex **26** had dissipated and now a black solid was observed to be suspended in solution. Again this solid was not soluble in any

solvents including dimethylsulfoxide. We believed that perhaps the proximity of the dimethylplatinum(II) centers to the anthracene backbone was leading to an initial C-H activation of the anthracene backbone and in turn lead to the formation and concomitant loss of methane gas en route to a decomposition of **26**. To test this, a toluene-*d*₈ solution of complex **26** was heated in an NMR tube and various spectra were acquired over time. The time series ¹H NMR spectra are depicted in figure 5.5. Prior to heating, the acquired spectra clearly displays the aromatic proton resonances of **26** as well as two equally intense methylplatinum resonances at $\delta = 1.22$ ppm and $\delta = 1.66$ ppm, spectrum (a). The NMR tube charged with the toluene-*d*₈ solution of **26** was then heated at 80°C for 3 hours in an oil bath and a second spectrum was acquired, spectrum (b). The spectrum acquired after 3 hours of heating shows the resonances of **26** still present however they appear in a significantly lower intensity. To that end there also appears to be some new broad resonances present in the baseline of the spectrum at $\delta = 0.95$ ppm and $\delta = 1.35$ ppm. Spectrum (c), acquired after a total of 18 hours of heating **26** shows no evidence of any aromatic protons being present. The spectrum also lacks the initial methylplatinum resonances of **26**, however no new resonances of any appreciable intensity are present in the spectrum. The originally purple solution of **26** also was now observed to be black after the 18 hours of heating leading to the determination that decomposition again had occurred. After removing the toluene-*d*₈ solvent and dissolving the reaction mixture in dms-*d*₆, a black solid remained in the NMR tube and there still remained no appreciable proton signals in the ¹H NMR spectrum. This experiment indicated that the bimetallic platinum(II) complex, **26**, was not stable for extended periods of time in any type of solvent and would therefore need to be oxidized to platinum(IV) complexes quickly upon isolation. This was further supported by the purple solid **26** becoming a black solid over the course of two days being kept at room temperature in a vial. This black solid again was insoluble.

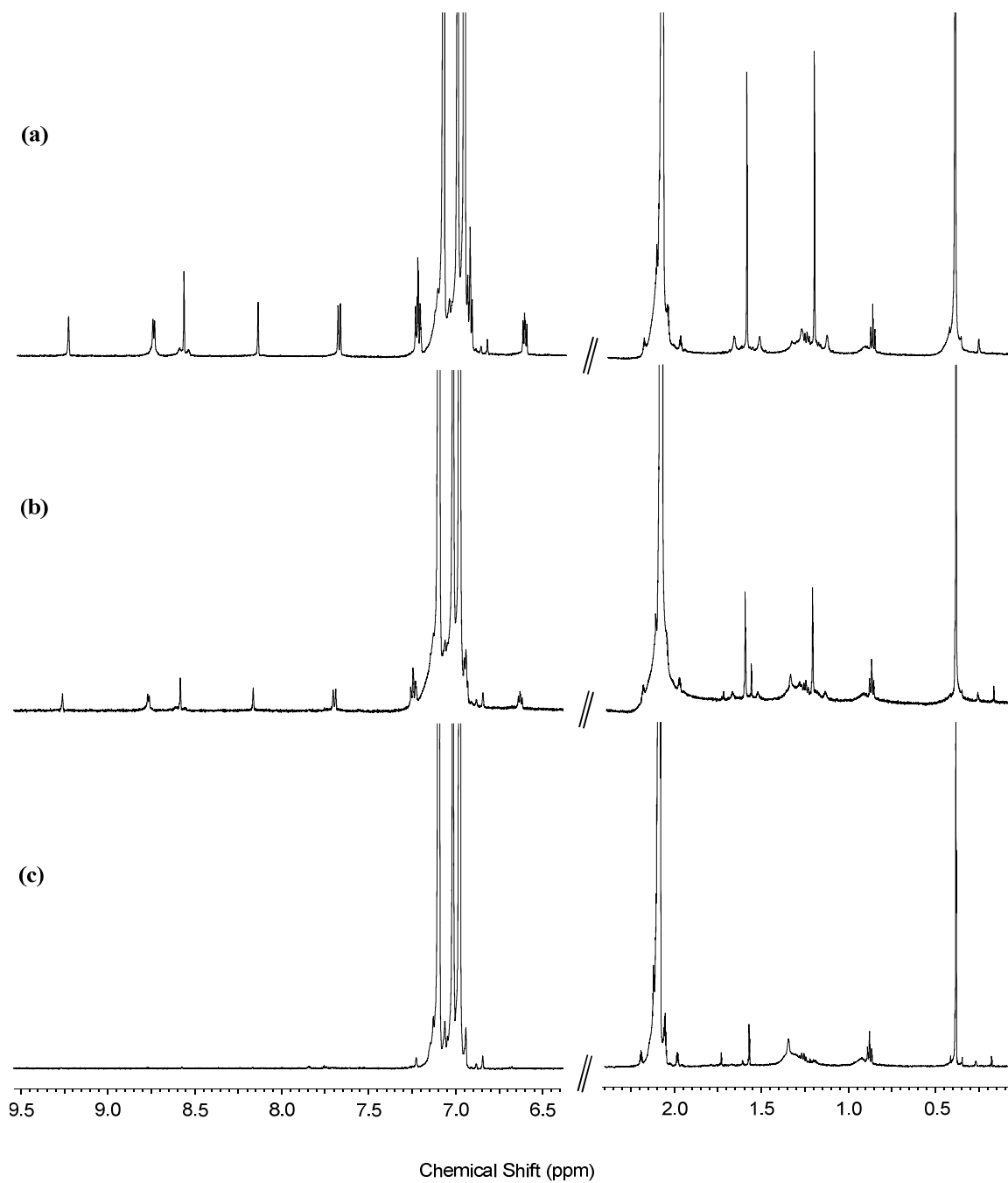
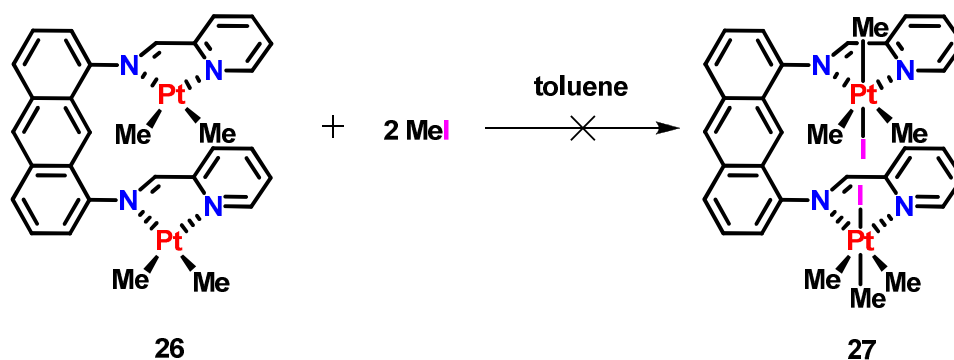


Figure 5.5. ^1H NMR spectrum of **26** in toluene- d_8 acquired over a period of 18 hours while heating. (a) initial spectrum, (b) 3 hours after initial heating, (c) 18 hours after initial heating.

5.4 Reactivity of complex **26** towards oxidative addition.

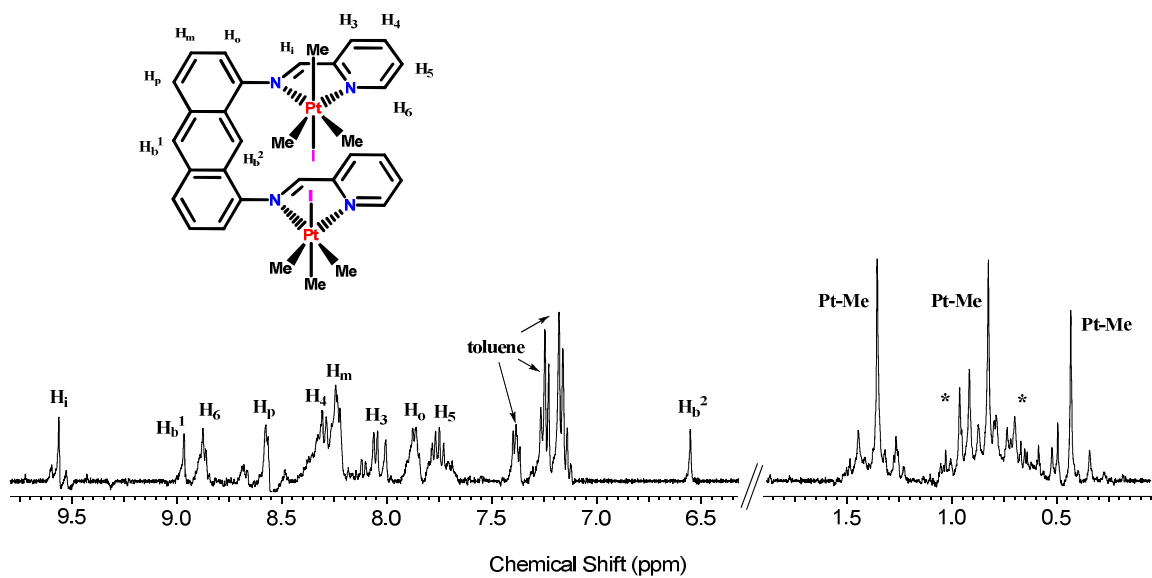
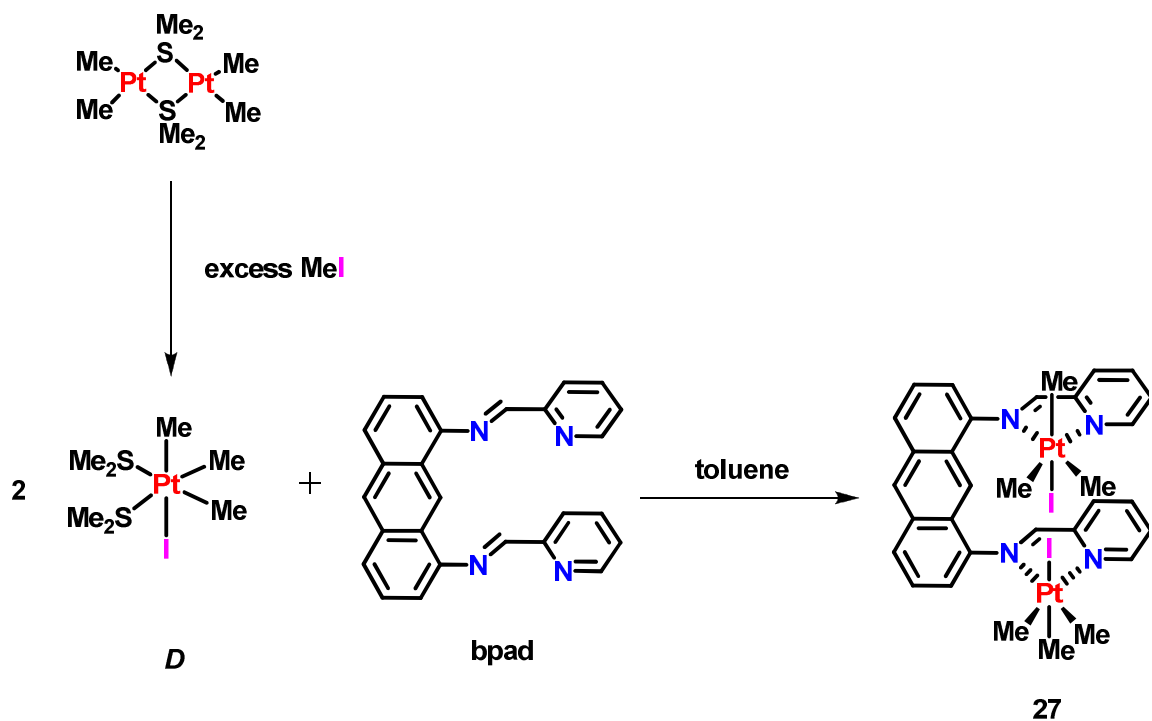
As complex **26** was found to be unstable under ambient or inert conditions for extended periods of time before decomposing to a black unidentified and insoluble solid, reactions with **26** needed to be performed directly after its isolation. As such, the ability of complex **26** to undergo oxidative addition to yield a potentially more stable bimetallic platinum(IV) product was examined. Initially two equivalents of methyl iodide were added to a solution of **26** in dry toluene solvent, scheme 5.3. An immediate colour change from deep purple to brown was observed. After allowing to stir for three hours at room temperature the toluene mixture was allowed to sit for 5 minutes at which time the mixture was observed to separate into a clear colourless solution with a black solid suspension. Again the black solid was found to be insoluble and was presumed to be the degradation product observed previously. It appears that in the process of oxidative addition the bimetallic platinum(II) precursor degrades to give an insoluble black solid again presumed to be due to the metalation of the anthracene backbone.



Scheme 5.3. Proposed oxidative addition of methyl iodide at **26**.

In an effort to avoid this proposed metalation event in the preparation of a bimetallic platinum(IV) complex of **bpad**, the oxidation of the platinum(II) dimer was performed prior to the coordination of the ligand as shown in scheme 5.4. This was achieved by stirring an acetone solution of the platinum(II) dimer complex with excess methyl iodide. After allowing the two reactants to stir for 2 hours, the acetone solvent was removed and any excess methyl iodide was washed away with diethyl ether. The resultant oil was the iodotrimethylplatinum(IV) species, **D** in scheme 5.4, which was

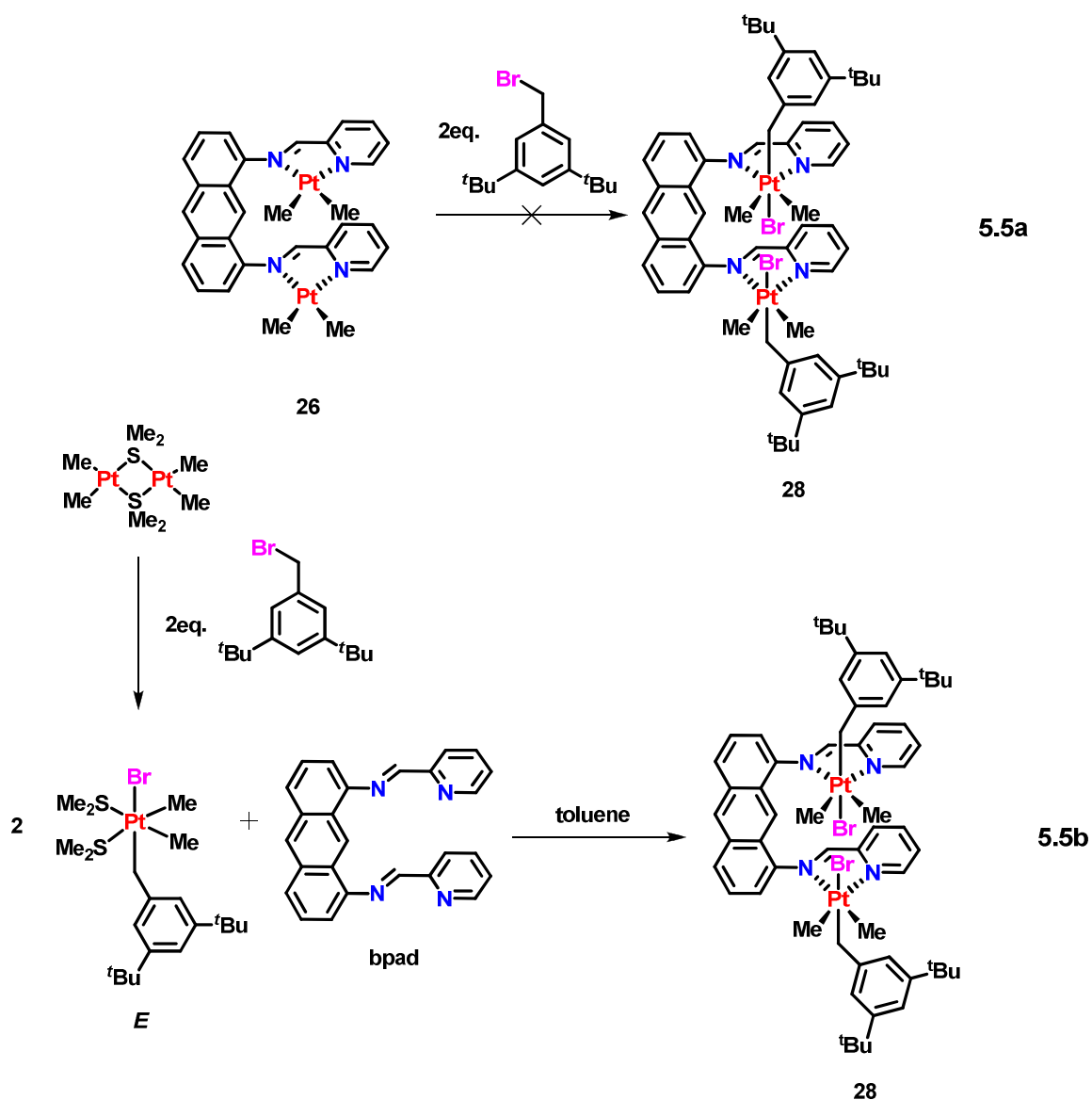
dissolved in minimal toluene and added to an equimolar amount of **bpad** dissolved in toluene. After stirring for 1 hour a yellow solution was obtained with slight evidence of a black solid forming in the reaction vial. Immediately the reaction mixture was filtered to remove the black solid and then the solvent toluene was removed under reduced pressure leaving a yellow oil. The yellow oil was found to be sparingly soluble in most solvents, however the oil was most soluble in dmsO. As such a ^1H NMR spectrum of the yellow oil was obtained in $\text{dmsO-}d_6$, figure 5.6. The spectrum contained three distinct methylplatinum resonances at $\delta = 0.42$ ppm, $\delta = 0.81$ ppm and $\delta = 1.34$ ppm with coupling constants of $^2J(\text{PtH}) = 72$ Hz, 71 Hz and 71 Hz respectively. As is typical with all iodotrimethylplatinum(IV) complexes, the most upfield resonance is a result of the axial methyl group which is positioned *trans* to the higher *trans* influence ligand iodine. The other two resonances result from the methyl groups positioned *trans* to the nitrogen atoms of the diimine ligand. In the aromatic region of the spectrum, 10 resonances were observed although due to the limited solubility of the complex in $\text{dmsO-}d_6$ their intensity was relatively weak. Complete assignment of these resonances was aided by $^1\text{H-}^1\text{H}$ gCOSY NMR analysis. Notably the resonance at $\delta = 9.55$ ppm, the imine proton resonance, was observed to have platinum-195 satellites with $^3J(\text{PtH}) = 28$ Hz. This value is diagnostic of the metal center being platinum(IV) and therefore provides further support for the oxidative addition of methyl iodide. Also of significance is the upfield shift of a singlet resonance to $\delta = 6.54$ ppm. This resonance is a result of the proton, H_b^2 , which is on the anthracene backbone and directed inward towards the metal centers, being significantly shielded in the now platinum(IV) complex relative to **26**. The yellow oil was also submitted for mass spectrometric analysis where a mass representing the ionic complex $[\text{Pt}_2\text{IME}_6(\text{bpad})]^+$ was observed at $m/z = 993.13$. This complex would be the result of the loss of I^- from the product of the oxidative addition of methyl iodide at both platinum centers, $[\text{Pt}_2\text{I}_2\text{Me}_6(\text{bpad})]$, **27**. These results support the formation of **27** via the incorporation of the platinum(IV) precursors at both coordination sites of the ligand as proposed in scheme 5.4.



Attempts to grow single crystals of complex **27** from a variety of solvents were unsuccessful due to the limited solubility of the complex in most solvents. In some cases, the formation of the insoluble black solid was observed during crystallization attempts.

In an effort to increase the solubility of the bimetallic organoplatinum(IV) species formed by oxidative addition of a substrate at **26**, the reactivity of this complex towards 3,5-di-*tert*-butylbenzyl bromide was explored. Two equivalents of the substituted benzyl bromide were added to a toluene solution of **26** while stirring as outlined in scheme 5.5a. Similar to the oxidative addition of methyl iodide at **26**, the addition of 3,5-di-*tert*-butylbenzyl bromide to a solution of **26** led to the formation of an insoluble black solid. To avoid this unwanted reaction, a similar strategy as depicted in scheme 5.4 was utilized, whereby an acetone solution of the platinum(II) dimer complex was oxidized in the presence of excess of the substituted benzyl bromide to give the complex **E**. This platinum(IV) species was then added to a toluene solution of **bpad** in order to allow for complexation as depicted in scheme 5.5b.

The resultant yellow oil was found to be sparingly soluble in acetone which allowed for ^1H NMR and mass spectrometric analysis to be performed. The ^1H NMR spectrum confirmed that the complexation reaction had occurred. The observation of platinum-195 satellites on both the imine proton resonance at $\delta = 9.68$ ppm with a coupling constant of $^3J(\text{PtH}) = 30$ Hz and the *ortho* proton resonance of the pyridyl group at $\delta = 8.48$ ppm with $^3J(\text{PtH}) = 19$ Hz provide evidence that the **bpad** ligand complexed the platinum centers. Two methylplatinum resonances at $\delta = 1.10$ ppm and $\delta = 1.32$ ppm with $^2J(\text{PtH}) = 70$ Hz also supports that the platinum centers are platinum(IV) indicating that the oxidative addition reaction had occurred. The mass spectrum of **28** indicated the presence of complex $[\text{Pt}_2\text{BrMe}_4(\text{CH}_2\text{-}3,5\text{-}^t\text{Bu}(\text{C}_6\text{H}_3))_2(\text{bpad})]^+$, $m/z = 1321.45$, which would arise due to the loss of a bromide anion from **28**. The ^1H NMR and mass spectrometric data are consistent and support the formation of **28** as proposed in scheme 5.4b. An acetone solution of **28** was allowed to sit undisturbed while pentane vapour slowly diffused in over the course of 7 days. After 7 days the formation of a brown oil and black solid was observed in the vial. The brown oil was washed to again give **28** by ^1H NMR spectroscopy but the black solid was again insoluble.



Scheme 5.5a illustrates the attempted oxidative addition of 3,5-di-*tert*-butylbenzyl bromide at **26**. **5.5b** depicts the synthetic route towards the preparation of **28**, $[\text{Pt}_2\text{Br}_2\text{Me}_4(\text{CH}_2\text{-3,5-}^t\text{Bu}(\text{C}_6\text{H}_3))_2(\text{bpad})]$.

The ligand **bpad** provided numerous obstacles towards fully elucidating the bimetallic platinum complexes that were formed. The formation of a black solid upon the synthesis of both platinum(II) and platinum(IV) complexes of **bpad** did not allow for the full analysis of the bimetallic complexes synthesized. In turn the reactivity of the bimetallic complexes could not be investigated as the products often degraded before

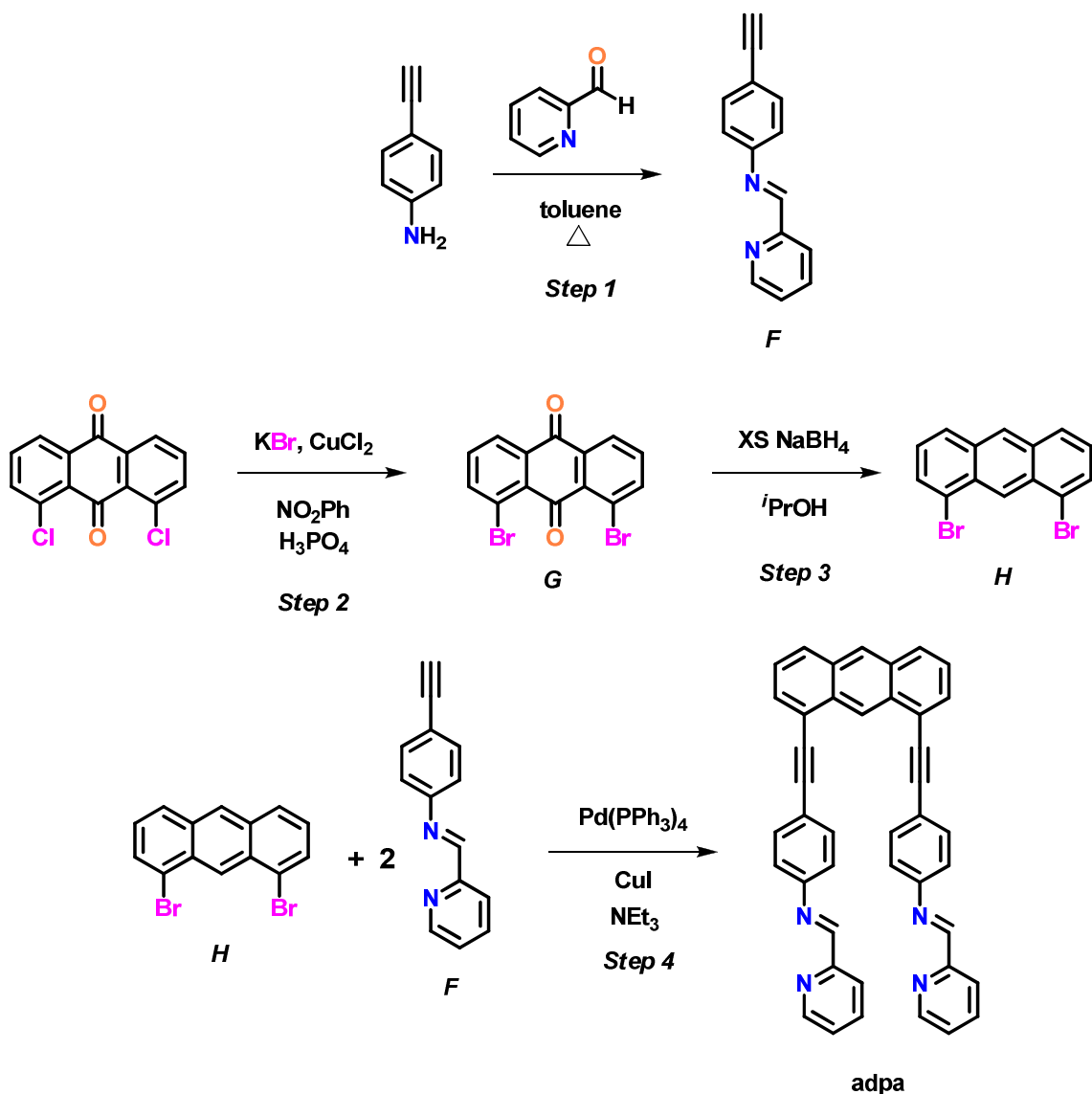
reacting fully. The detrimental formation of the black solid we proposed to be due to an interaction between the platinum centers and the backbone of the anthracene ligand as a result of its proximity. By moving the platinum centers further from the anthracene backbone it would eliminate the deleterious side reaction. To address this and further evaluate the use of an anthracene backbone to support bimetallic complexes of platinum(II), a new ligand system needed to be designed.

5.5 Ligand Synthesis

To address the concern of the decomposition of complex **26**, an anthracene based ligand system in which the platinum centers are held further from the backbone needed to be designed. The group of Datong Song has previously designed an anthracene based ligand which adopts a U-shape [50]. The ligand keeps the metal centers at a sufficient distance from the anthracene backbone while the length of the arms also provides some flexibility for cooperation between both metal centers. Using the Song group's design as a template, the new ligand **adpa**, (*N,N*)-4,4'-(anthracene-1,8-diylbis(ethyne-2,1-diyl))-bis(*N*-(pyridin-2-ylmethylene)aniline), was prepared by the Sonagashira coupling of two equivalents of the alkynyl based arms and dibromoanthracene as shown in step 4 of scheme 5.6. The alkynyl derived arms for the ligand synthesis were prepared by the condensation of 4-ethynylaniline with 2-pyridinecarboxaldehyde. The two reagents were refluxed in toluene with a Dean-Stark trap overnight, and after workup afforded the brown solid product **F**, step 1 scheme 5.6, in nearly quantitative yield. Evidence for the formation of the compound is provided by the appearance of the imine proton resonance at $\delta = 8.59$ ppm. The presence of this signal indicates that the condensation reaction indeed occurred.

The anthracene backbone was prepared in two steps, steps 2 and 3 in scheme 5.6. First a nitrobenzene solution of 1,8-dichloroanthraquinone was heated to 200°C in the presence of CuCl₂ and excess KBr. After working up the reaction mixture the bright yellow green 1,8-dibromoanthraquinone, **G**, was collected in a 55% yield. This was subsequently reduced to 1,8-dibromoanthracene, **H**, using excess sodium borohydride.

With the dibromoanthracene and alkynyl moiety in hand, the coupling reaction could be performed, step 4 scheme 5.6. 1,8-dibromoanthracene and two equivalents of the alkyne were added to a reaction flask and were then dissolved in dry triethylamine. To this mixture was then added catalytic amounts of copper iodide and tetrakis(triphenylphosphine)palladium(0). The reaction mixture was heated to reflux and allowed to stir under nitrogen for 24 hours. After purification by column chromatography, the ligand **adpa** was obtained in a 68% yield.



Scheme 5.6. Synthetic procedure for the preparation of the ditopic ligand **adpa**.

The formation of **adpa** was supported by both mass spectrometric and ^1H NMR analysis. The ^1H NMR spectrum of **adpa**, figure 5.7, shows the incorporation of two equivalents of the alkynyl moiety onto the anthracene backbone. This is confirmed through comparative integration values between peaks known to be of the anthracene backbone, H_b^2 at $\delta = 8.51$ ppm and integration value of 1, versus that of the alkynyl arm, H_i at $\delta = 8.58$ ppm and integration value of 2. The ^1H NMR spectrum of **adpa** was completely assigned through the use of gCOSY NMR analysis.

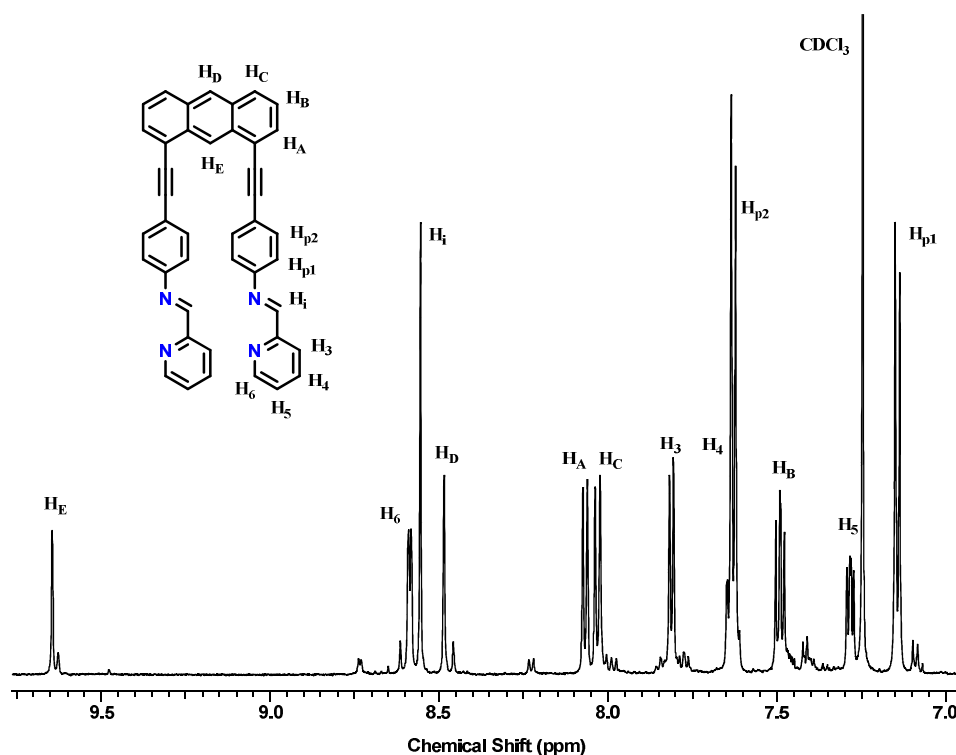
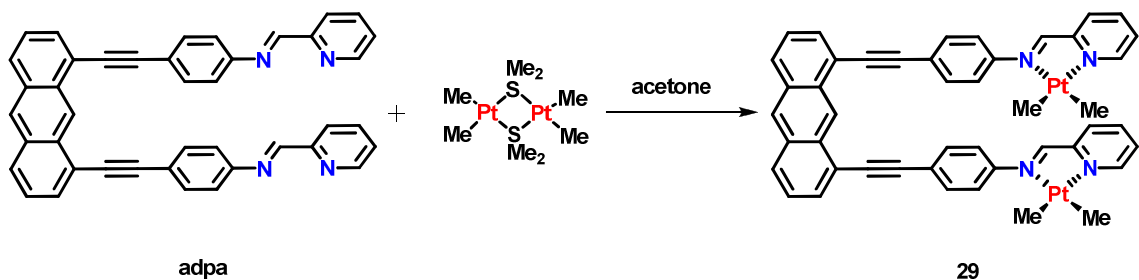


Figure 5.7. ^1H NMR spectrum of the ligand **adpa** in CDCl_3 .

5.6 Synthesis of a dimethylplatinum(II) complex of adpa

The dimethylplatinum(II) complex of the ligand **adpa**, was prepared through the complexation of two equivalents of the metal center by **adpa**, scheme 5.7. This was achieved through the equimolar portions of $[\text{Pt}_2\text{Me}_4(\mu\text{-SMe}_2)_2]$ and **adpa** in acetone. Upon addition of the reagents, the reaction mixture began to take on a reddish brown colour which is typical for complexation reactions occurring between the ligand and the metal center. The reaction mixture was allowed to stir at room temperature for 3 hours

before the solvent acetone was reduced in *vacuo*. The resultant deep red solution was then layered with pentane to effect the precipitation of a red solid overnight at 5°C. After vacuum filtration, a bright red solid was collected and subsequently washed with pentane to afford complex **29**, [Pt₂Me₄(adpa)] in an 88% yield.



Scheme 5.7. Synthesis of complex **29**, [Pt₂Me₄(adpa)].

The ¹H NMR spectrum of **29**, figure 5.8, provided confirmation that a dimethylplatinum(II) center was indeed ligated at both coordination sites through the continued presence of symmetry in the molecule. A single set of resonances that are attributed to the alkynyl arms were observed in the spectrum. This is concluded based on the presence of platinum-195 satellites on both the imine proton, $\delta = 9.29$ ppm, and the *ortho* pyridyl proton, $\delta = 8.85$ ppm, with coupling constant values of $^3J(\text{PtH}) = 28$ Hz and $^3J(\text{PtH}) = 20$ Hz respectively. These values are consistent with those typically observed for dimethylplatinum(II) complexes with diimine ligands [46,49]. Full assignment of the resonances in the aromatic region of the spectrum was aided by ¹H-¹H gCOSY NMR spectroscopy and are annotated in figure 5.8. In addition to the platinum-195 satellites present on the imine and *ortho* pyridyl resonances of the ligand, two resonances resultant from the presence of the methyl groups on the platinum centers were observed. These singlet resonances possessed platinum-195 satellites and were observed at $\delta = 1.08$ ppm and $\delta = 1.19$ ppm with coupling constants of $^2J(\text{PtH}) = 84$ Hz and $^2J(\text{PtH}) = 86$ Hz respectively. These chemical shift values are diagnostic of the formation of a dimethylplatinum(II) complex. The formation of **29** was further supported by ESI-MS as the sodium adduct [Pt₂Me₄(adpa)Na]⁺ with $m/z = 1057.22474$ amu.

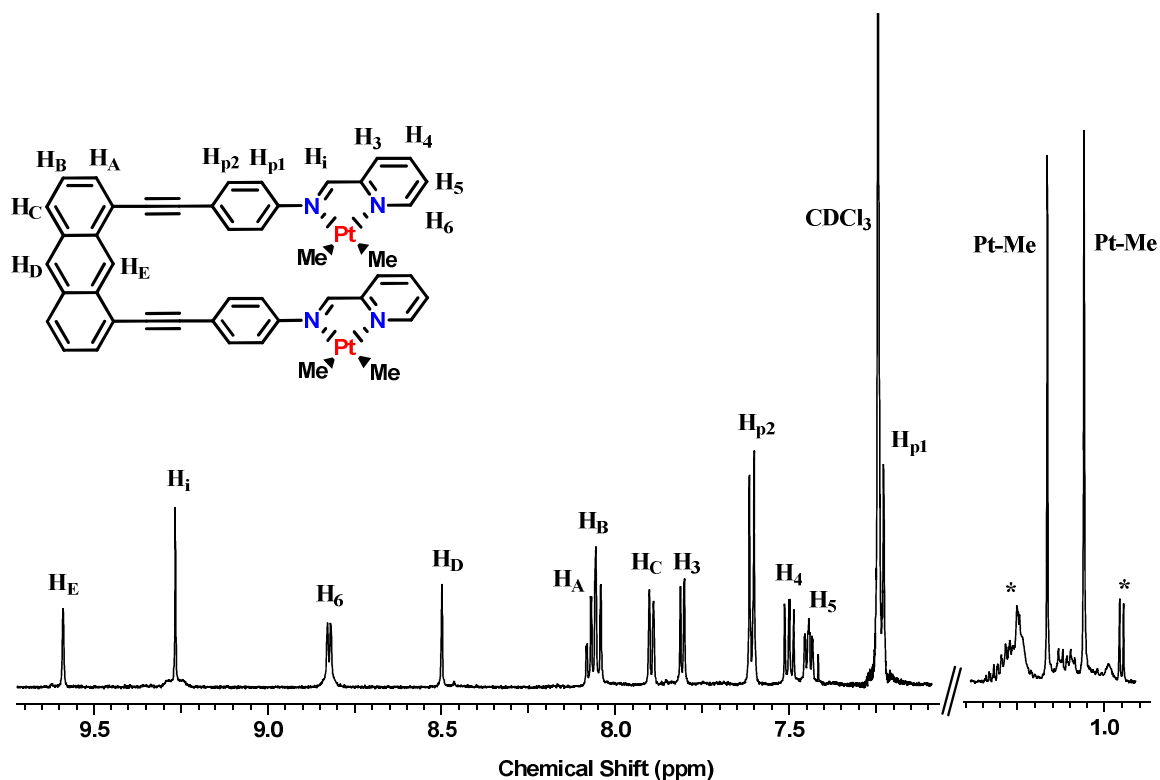
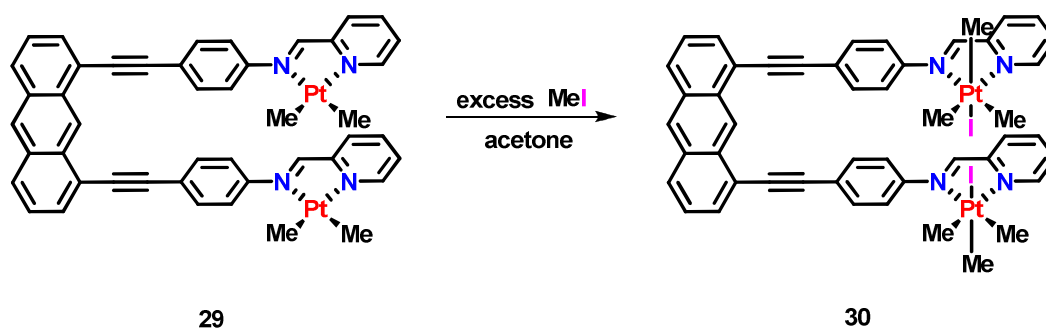


Figure 5.8. ^1H NMR spectrum of **29** in CDCl_3 . * indicates trace hexane solvent.

Numerous attempts to grow single crystals suitable for X-ray diffraction analysis were made but no suitable crystals could be grown. Unlike the previous system, no degradation products were observed.

5.7 Reactivity of Complex **29** towards Oxidative Addition

Unlike complex **26**, complex **29** was proposed to perform oxidative addition reactions giving the resultant platinum(IV) complexes without the requirement of oxidizing the platinum center prior to complexation with the ligand. With that motivation an acetone solution of **29** was charged with a slight excess of methyl iodide and allowed to stir for three hours, scheme 5.8. The initially red solution became bright yellow over time and after concentrating the solution and layering with pentane afforded a bright yellow solid.



Scheme 5.8. Preparation of **30** via the oxidative addition of methyl iodide at **29**,

The ^1H NMR spectrum, figure 5.9, supports the formation of the product of the *trans* oxidative addition of methyl iodide at both platinum centers. This is evidenced through the appearance of an additional methylplatinum resonance in the ^1H NMR spectrum at $\delta = 0.56$ ppm with a $^3J(\text{PtH})$ coupling constant value of 73 Hz. This shift and coupling constant value is consistent with a methyl group being positioned *trans* to an iodine ligand. The additional two methylplatinum resonances at $\delta = 1.10$ ppm and $\delta = 1.48$ ppm both with $^3J(\text{PtH}) = 70$ Hz arise due to the two equatorial methyl groups which are positioned *trans* to the nitrogen atoms of the **adpa** ligand. The newly synthesized complex, $[\text{Pt}_2\text{I}_2\text{Me}_6(\text{adpa})]$ complex **30**, maintains a similar symmetric nature as its starting platinum(II) complex as evidenced by the same number of aromatic resonances in the spectrum. Of note, the imine proton resonance at $\delta = 9.53$ ppm possesses platinum-195 satellites with $^3J(\text{PtH}) = 27$ Hz and the *ortho* pyridyl resonance also possesses satellites with $^3J(\text{PtH}) = 18$ Hz. Both of these values are diagnostic of the platinum(II) complex **29** being oxidized to a platinum(IV) species proposed to be that of complex **30**. Additional evidence to support the formation of **30** was provided by ESI-MS analysis which identified the molecular ion $[\text{Pt}_2\text{I}_2\text{Me}_6(\text{adpa})\text{Na}]^+$ with $m/z = 1341.08063$. Portions of **30** were then dissolved in a variety of solvents in an attempt to grow crystals for single crystal X-ray diffraction analysis. Despite the method, conditions, or solvent combinations employed; single crystals suitable for analysis could not be prepared.

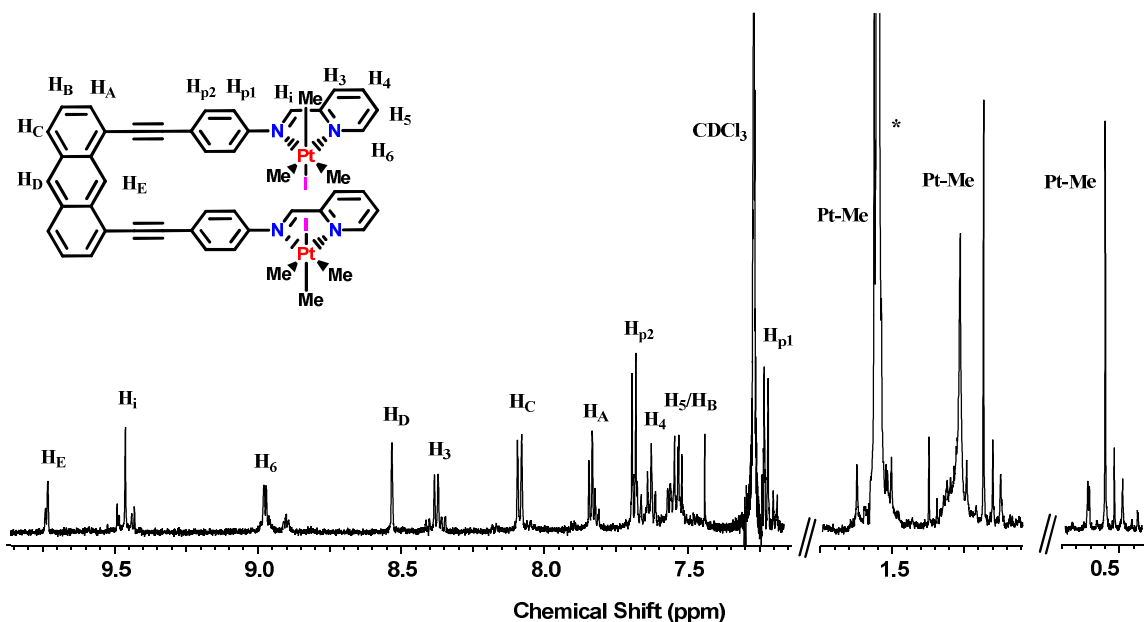
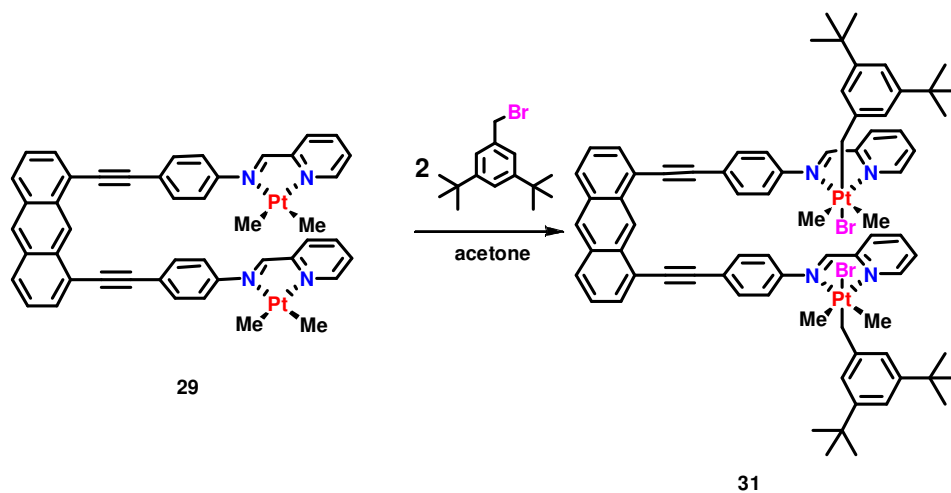


Figure 5.9. ^1H NMR spectrum, CDCl_3 , of **30**. * indicates the presence of water.

In an effort to increase the solubility and grow single crystals of a bimetallic platinum(IV) complex with the ligand **adpa**, the oxidative addition reaction of 3,5-di-*tert*-butylbenzyl bromide at complex **29** was performed as outlined in scheme 5.9.

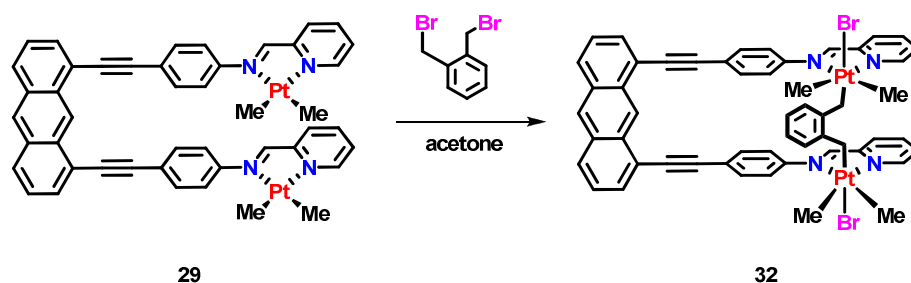


Scheme 5.9. The oxidative addition of 3,5-di-*tert*-butylbenzyl bromide at **29** to give the resultant platinum(IV) complex **31**.

The addition of two equivalents of 3,5-di-*tert*-butylbenzyl bromide to an acetone solution of **29** afforded a bright yellow solution after three hours of stirring. After work

up a yellow oil was obtained. The ^1H NMR spectrum provided evidence for the formation of the *trans* oxidative addition product **31** through the presence of two methyl platinum resonances at $\delta = 1.12$ ppm and 1.47 ppm both with $^3J(\text{PtH}) = 70$ Hz. This along with the presence of platinum-195 satellites on the methylene protons of the benzyl group support the oxidative addition of the substrate at **29**. Attempts to crystallize the platinum(IV) complex **31** were unsuccessful as yellow oils were consistently produced. In the absence of a solid state structure the *trans* oxidative addition cannot be confirmed, however the ^1H NMR data for **31** is consistent with chemical shifts and coupling constant values observed for platinum(IV) species with benzyl groups present [51].

The ability of the platinum(II) centers of **29** to react cooperatively was investigated through the reaction of **29** with a bifunctional substrate. Dibromoxylenes have previously shown the ability to react with two separate platinum(II) centers to form bimetallic complexes. It was proposed that the reaction of one equivalent of 1,2-dibromoxylene should therefore allow for the oxidative addition of the substrate at each platinum center and would give rise to a xylene-bridged complex, **32** $[\text{Pt}_2\text{Br}_2\text{Me}_4(1,2\text{-CH}_2(\text{C}_6\text{H}_4)\text{CH}_2)(\text{adpa})]$ in scheme 5.10. To investigate this, to an acetone solution of **29** was added drop wise a half equivalent of 1,2-dibromoxylene dissolved in acetone. After the addition was complete the reaction mixture was allowed to stir for 3 hours before the solvent volume was reduced *in vacuo*. After layering the now orange acetone solution with pentane, an orange solid was produced. This oil had limited solubility but was found to be sparingly soluble in acetone. A portion of this solid was dissolved in acetone- d_6 and analyzed by ^1H NMR spectroscopy.



Scheme 5.10. The cooperative reactivity of **29** towards a bifunctional substrate giving **32**.

The ^1H NMR spectrum, figure 5.10, contained two methylplatinum resonances of equal integration at $\delta = 1.07$ ppm and 1.44 ppm both with coupling constants of $^3J(\text{PtH}) = 70$ Hz. These values would suggest that the methyl groups are positioned *trans* to the nitrogen atoms of the ligand and would support a *trans* oxidative addition reaction. The presence of a single AB doublet at $\delta = 2.56$ ppm and 2.63 ppm with $^2J(\text{PtH}) = 96$ Hz and 104 Hz respectively would support the oxidative addition of the *ortho*-xylene at each platinum center and suggest that **32** is overall symmetric. Broad resonances at $\delta = 6.33$ ppm and 6.44 ppm are determined by ^1H - ^1H gCOSY NMR analysis to be a result of the aromatic protons on the xylene ligand. The appearance of only two resonances further supports the symmetric nature of complex **32**. Additional support for the formation of a complex which incorporates an equivalent of 1,2-dibromoxylene at complex **29** comes from the ESI-MS which identifies the molecular ion $[\text{Pt}_2\text{BrMe}_4(1,2\text{-CH}_2(\text{C}_6\text{H}_4)\text{CH}_2)(\text{adpa})]^+$ at $m/z = 1217.21591$ amu. In a similar manner to all complexes prepared based on the anthracene ligand design, single crystals of **32** could not be grown and therefore the structure as proposed in scheme 5.10 is not confirmed.

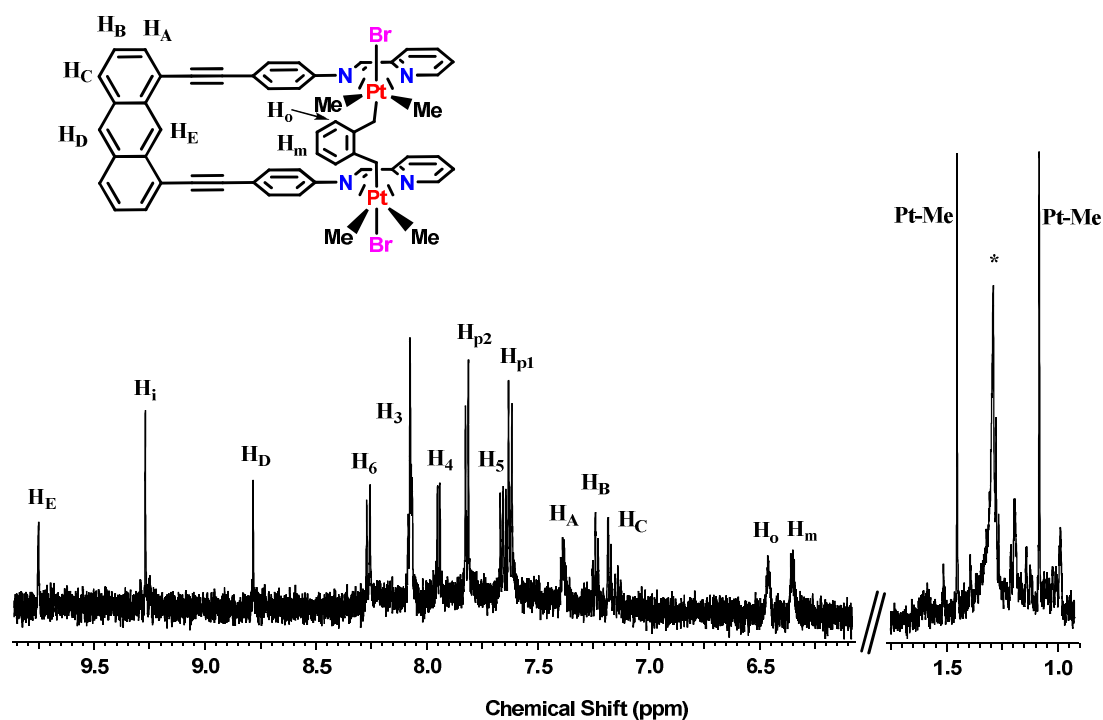
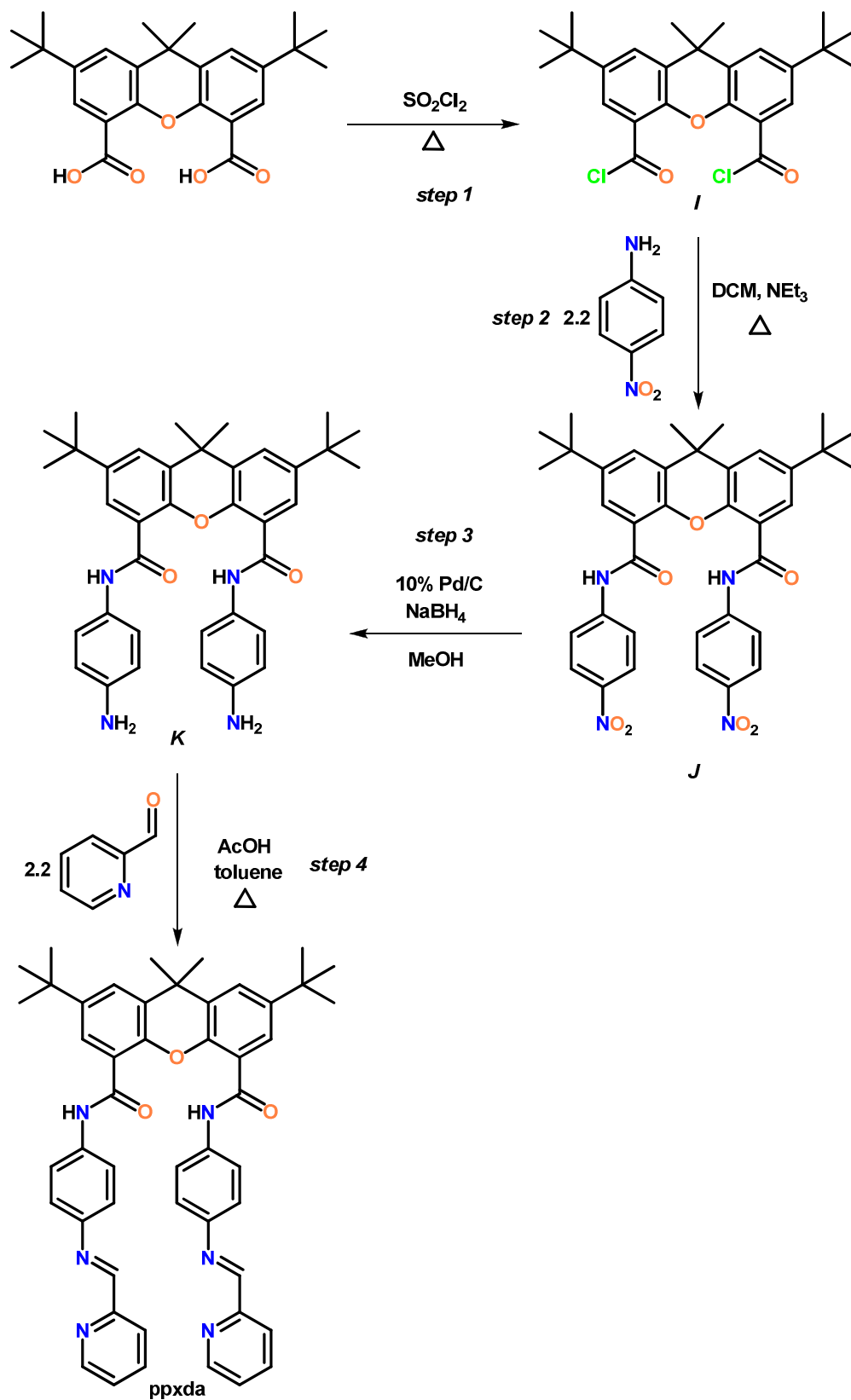


Figure 5.10. ^1H NMR spectrum of complex **32** in acetone- d_6 . * indicates the presence of residual pentane solvent.

5.8 Ligand Synthesis

Previous work with an anthracene ligand scaffold showed detrimental effects if the metal centers were located proximal to the backbone. Although there are obvious differences between anthracene and xanthene, both in atomic configuration and flexibility, positioning the metal centers further from the backbone was decided to be the best avenue to take. In order to do so, long linker groups needed to be incorporated between the xanthene scaffold and the coordination site. These groups needed to be somewhat flexible in order for slight modifications in intermetallic distances to be made to elicit maximum cooperative effect but at the same time maintain some rigidity to fix both metal centers in a proper orientation. Considering these factors, the novel ligand 2,7-di-*tert*-butyl-9,9-dimethyl- N^4, N^5 -bis(4-(pyridin-2-ylmethyleneamino)phenyl)-xanthene-4,5-dicarboxamide, **ppxda**, was prepared as outlined in scheme 5.11. The installation of the *tert*-butyl and methyl groups in the backbone are intended to enhance the solubility of the complexes as was a problem previously observed in the anthracene systems. In addition the presence of the oxygen atom in the backbone should not only prevent a metalation event from occurring, but also provide a polar interaction that could aid in crystallizations and packing.

Initially, the reactivity of 2,7-di-*tert*-butyl-9,9-dimethyl-9*H*-xanthene-4,5-dicarboxylic acid was enhanced by converting it to the corresponding diacid dichloride, **I**, by refluxing the white solid in thionyl chloride for three hours, step 1 in scheme 5.11. After reflux, the excess thionyl chloride was removed to afford the diacid dichloride **I** in quantitative yield. The diacid dichloride was then dissolved in dry dichloromethane to which a dichloromethane solution of a slight excess of *para*-nitroaniline was added, step 2 scheme 5.11. After adding triethylamine to the reaction mixture, it was stirred at room temperature for 12 hours before being heated at reflux for an additional three hours. After reflux, the dichloromethane mixture was washed with water and extracted against dichloromethane. After drying with magnesium sulfate and evaporating the solvent in *vacuo*, a white solid identified as **J**, 2,7-di-*tert*-butyl-9,9-dimethyl- N^4, N^5 -bis(4-nitrophenyl)xanthene-4,5-dicarboxamide, was isolated in moderate yield.



Scheme 5.11. Synthetic route to the preparation of ppxda.

Compound **J** was then reduced using 10% Pd/C and sodium borohydride to afford **K**, *N*⁴,*N*⁵-bis(4-aminophenyl)-2,7-di-*tert*-butyl-9,9-dimethyl-xanthene-4,5-dicarboxamide, in a nearly quantitative yield, step 3 in scheme 6.1. The final step of the synthesis of **ppxda**, step 4 scheme 5.11, involved the condensation of the diamine **K** with 2-pyridinecarboxaldehyde. To a toluene solution of the two reagents was 2 drops of acetic acid prior to stirring the mixture under reflux with a Dean-Stark trap attached. After heating overnight, the toluene solvent was removed and the resultant tan solid was washed with pentane to remove residual 2-pyridinecarboxaldehyde. The tan solid was confirmed to be the ditopic xanthene based ligand **ppxda** by ¹H NMR and EI-MS analysis.

The ¹H NMR spectrum of **ppxda** shown in figure 5.11 provides evidence for the formation of the product through the appearance of four resonances arising from the incorporation of the pyridyl rings. Further evidence is provided by the observation of a singlet resonance at $\delta = 8.56$ ppm with a relative integration value of 2. This resonance is attributed to the imine protons present in the ligand and confirm that the condensation reaction had occurred. Indirect evidence provided by the absence of an amine proton resonance observed previously in **C**, further supports the successful synthesis of **ppxda**. The molecular ion observed in the EI-MS spectrum also supports the formation of **ppxda** with a $m/z = 768.37948$ amu.

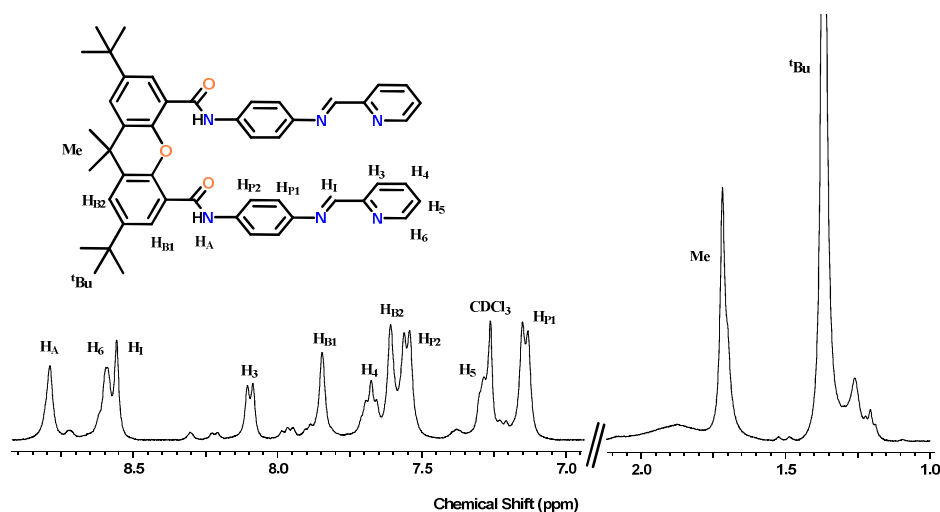
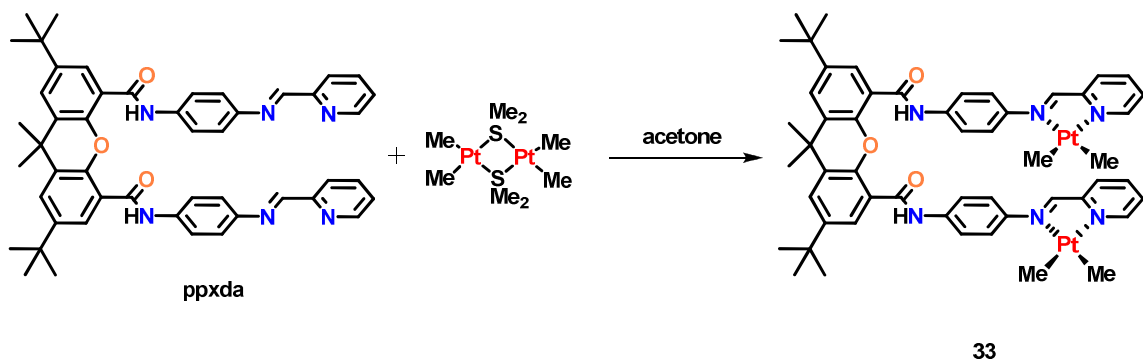


Figure 5.11. ¹H NMR spectrum of the ligand **ppxda** in CDCl₃.

5.9 Synthesis of a bimetallic dimethylplatinum(II) complex of ppxda

The bimetallic dimethylplatinum(II) complex of the ligand **ppxda**, was prepared through the complexation of two equivalents of the metal center by **ppxda**, scheme 5.12. The complexation of two equivalents of dimethylplatinum(II) by the ditopic diamide ligand **ppxda** was achieved through the reaction of equimolar portions of $[\text{Pt}_2\text{Me}_4(\mu\text{-SMe}_2)_2]$ and **ppxda** in acetone [48]. Upon addition of the reagents, the initially tan solution began to take on a red colour which is typical for complexation reactions occurring between the ligand and the metal center. The reaction mixture was allowed to stir at room temperature for an hour before the solvent acetone was reduced in *vacuo*. The resultant deep red oil was then dissolved in minimal acetone layered with pentane to affect the precipitation of a red solid overnight at 5°C. After vacuum filtration, a bright red solid was collected and subsequently washed with pentane to afford complex **33**, $[\text{Pt}_2\text{Me}_4(\text{ppxda})]$ in an 85% yield.



Scheme 5.12. Complexation of two dimethylplatinum(II) centers by **ppxda** giving the bimetallic complex **33**.

A portion of complex **33** was then dissolved in acetone- d_6 and a ^1H NMR spectrum was acquired, figure 5.12. Two methylplatinum resonances were observed in the spectrum each with a relative integration value of 6 protons. These resonances were observed at $\delta = 0.95$ ppm and 1.14 ppm with coupling constant values of $^2J(\text{PtH}) = 84$ Hz and 87 Hz respectively. The presence of only two resonances suggests that complex **33** is symmetric as an asymmetric complex would give rise to additional methylplatinum signals. This does not however provide evidence for the pyridyl groups being positioned

directly above one another as depicted in scheme 5.12 or the other isomer in which the pyridyl groups are positioned *anti*. The presence of platinum-195 satellites on the imine proton resonance at $\delta = 9.58$ ppm with a coupling constant value of $^3J(\text{PtH}) = 30$ Hz provides further evidence for not only the complexation of two dimethylplatinum(II) units by the ligand **ppxda** but also that the resultant complex **33** is symmetric. The remaining resonances were assigned completely using gCOSY NMR spectroscopic analysis and are annotated in figure 5.12. The successful formation of **33** was confirmed via ESI-MS analysis where the molecular ion observed was that of $[\text{Pt}_2\text{Me}_4(\text{ppxda})\text{Na}]^+$, the cation produced by the incorporation of a sodium ion within **33** at $m/z = 1239.38779$.

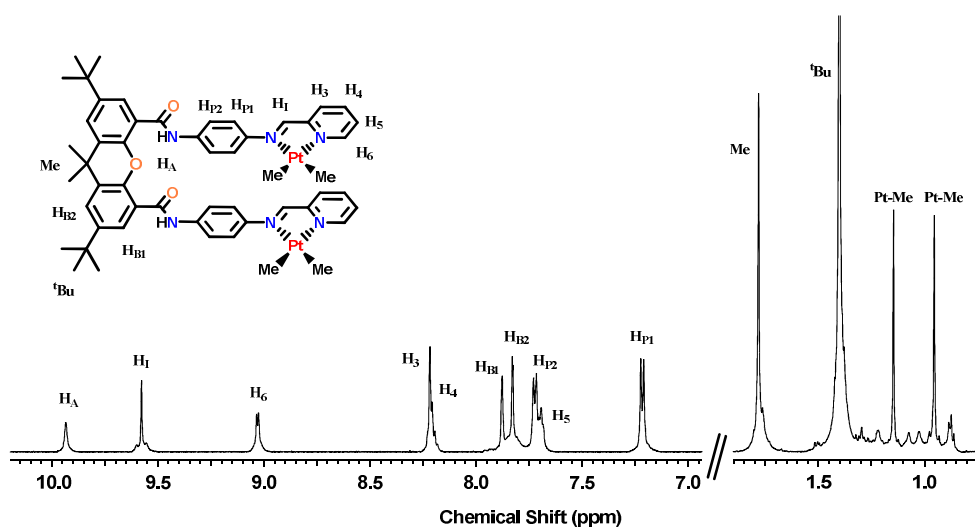


Figure 5.12. ^1H NMR spectrum of complex **33**, $[\text{Pt}_2\text{Me}_4(\text{ppxda})]$, in acetone- d_6 .

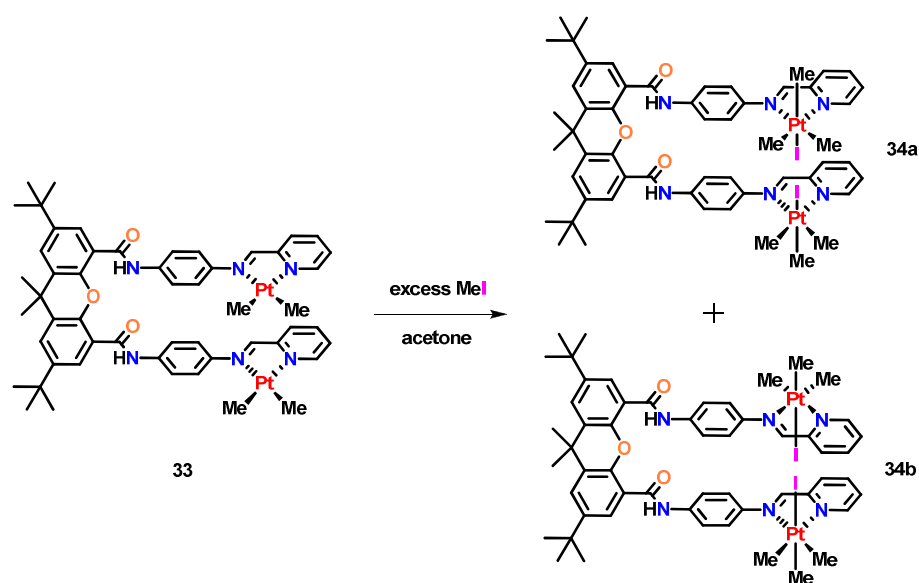
5.10 Reactivity of Complex **33** Towards Oxidative Addition

With complex **33** synthesized and characterized by ^1H NMR spectroscopy and ESI-MS analysis, the reactivity that it exhibited towards the oxidative addition reaction was investigated. Initially, an NMR tube was charged with an acetone- d_6 sample of complex **33**. To the red solution was then added a slight excess of methyl iodide. A ^1H NMR spectrum was acquired 10 minutes after the addition of methyl iodide and is depicted in figure 5.13. The spectrum of the now dull yellow solution indicates the formation of two distinct complexes after 10 minutes in a nearly equivalent amount. This

is concluded by the presence of five methylplatinum resonances in the spectrum. The two most upfield methylplatinum resonances at $\delta = 0.44$ ppm and 0.61 ppm both with coupling constant values of ${}^2J(\text{PtH}) = 72$ Hz, are likely a result of two axial methyl groups which would be positioned *trans* to the iodide ligand after oxidative addition. Both the chemical shift and coupling constants for these resonances are consistent with that assignment. Additional methylplatinum resonances are observed at $\delta = 1.13$, 1.22 and 1.46 ppm with coupling constant values of ${}^2J(\text{PtH}) = 70$ Hz for each. These values are typical of those observed for the equatorial methyl groups which are positioned *trans* to the nitrogen atoms in the ligand framework. The resonance at 1.46 ppm integrates to twice the value of all of the other methylplatinum resonances and as such it is likely that two methylplatinum resonances are coincident giving a total of six methylplatinum resonances. The coupling constant values do not support an assignment in which two methyl groups are positioned *trans* to one another, so the likelihood of one of the products being a *cis* addition product is rather low. It appears more likely that due to ease by which the amide arms of the ligand **ppxda** could rotate, that the two sets of methylplatinum resonances could be due to the presence of two isomers in solution of the complex *trans*-[Pt₂I₂Me₆(ppxda)]. These isomers, **34a** and **34b** as depicted in scheme 5.13, arise due to the ability of the pyridyl groups to be positioned directly above one another, **34a**, or in an *anti* manner **34b**. Both of these isomers should be present in solution initially, but one would suspect that isomerization should occur between the two over time and a preference for one isomer should be observed. In the aromatic region of the ¹H NMR spectrum two sets of resonances are again observed. The two imine proton signals at $\delta = 9.29$ and 9.43 ppm both possess platinum-195 satellites with coupling constant values of ${}^3J(\text{PtH}) = 27$ Hz and 28 Hz. Similar values of the coupling constant are observed in analogous complexes and support that complex **33** was indeed oxidized to a platinum(IV) species **34a** and **34b**. The resonances attributed to each isomer can be determined through the use of gCOSY NMR spectra and the relative integration values and are labelled as R1 and R2 for simplicity until their assignment as **34a** and **34b** can be absolutely determined.

An additional ¹H spectrum acquired one hour after the initial addition of methyl iodide to an acetone-*d*₆ solution of **33** shows no change in relative amounts of **34a** and

34b, figure 5.14b. However in a spectrum acquired twenty-four hours after the initial addition of methyl iodide, figure 5.14c, a drastic change in the relative amounts of both isomers is observed. The most upfield resonance at $\delta = 0.44$ ppm attributed to the axial methyl group of one of the isomers was now observed to be two times the relative integration value in comparison to the resonance at 0.61 ppm for the axial methyl group of the second isomer. The same observations can be made of all of the resonances in the spectrum and based on the relative integration values and gCOSY NMR spectra, the resonances are assigned completely and attributed to being of a distinct isomer as denoted in figure 5.14. In a ^1H NMR spectrum acquired after 48 hours, the relative ratio of the presence of both isomers increases to 2.5:1, figure 5.14d.



Scheme 5.13. Oxidative addition of MeI at **33** giving **34a** and **34b**, isomers of *trans*- $[\text{Pt}_2\text{I}_2\text{Me}_6(\text{ppxda})]$.

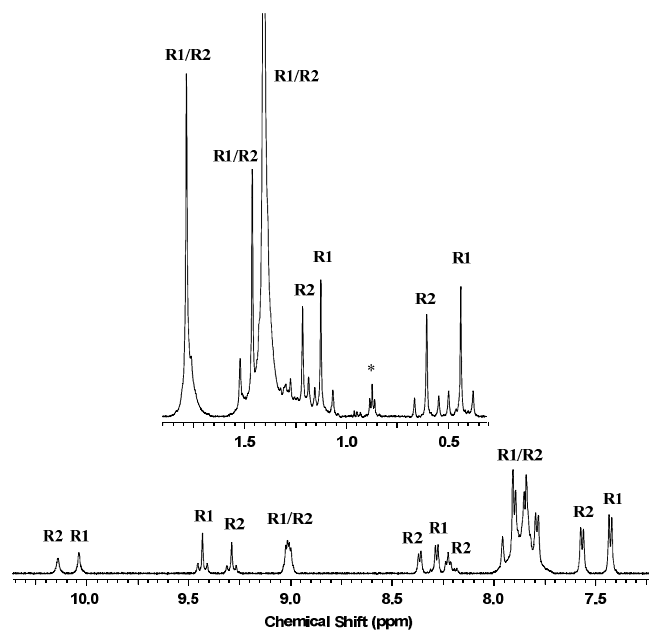


Figure 5.13. ^1H NMR spectrum of the product mixture from the oxidative addition of MeI at **33**. The resonances of the two isomers of the product complex **34**, *trans*- $[\text{Pt}_2\text{I}_2\text{Me}_6(\text{ppxda})]$, have been assigned and labelled as R1 or R2 where possible.

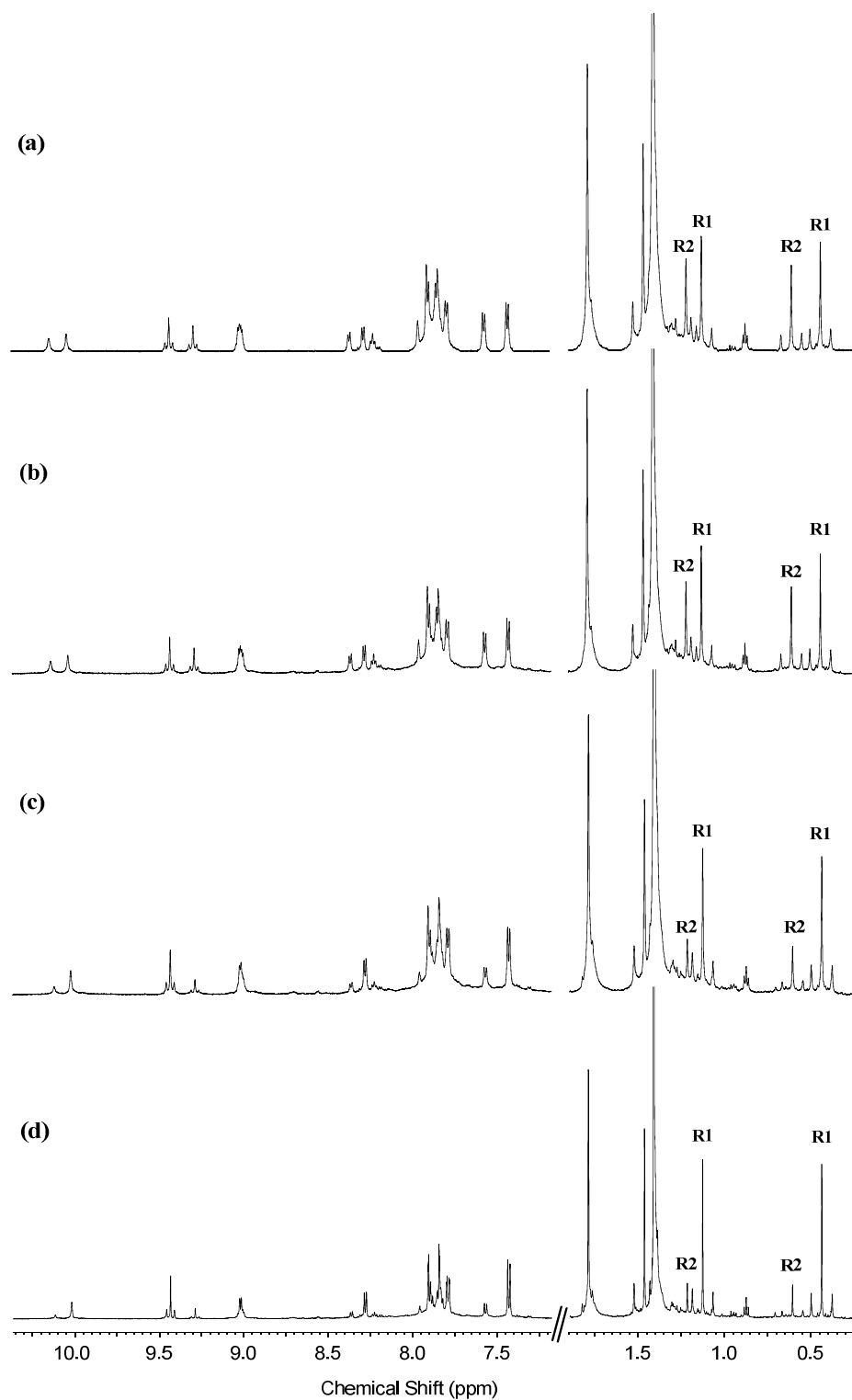


Figure 5.14. Time series ^1H NMR spectra of the isomerization between isomers of **34**, denoted R1 and R2. Spectrum (a) is taken 10 minutes, (b) 1 hour, (c) 24 hours and (d) 48 hours after initial addition of MeI.

After concentrating the acetone solution of **34a/34b**, the mixture was layered with pentane to affect the precipitation of a yellow solid. This yellow solid was dissolved in minimal acetone and pentane solvent vapour was allowed to diffuse into the acetone solution of **34a/34b**. This yielded the formation of yellow prism shaped single crystal which were suitable for X-ray diffraction analysis. The solid state structure depicted in figure 5.15, supports the formation of the trimethyliodide complex via the oxidative addition of methyl iodide at both platinum centers in **33**. For simplicity, figure 5.16 depicts a single equivalent of **34b**. The solid state structure of **34** adopts the *anti* orientation which is attributed to isomer **34b**. The methyl groups adopt a *fac* geometry at the platinum centers as a result of the *trans* oxidative addition of methyl iodide. The axial methyl groups have consistent bond lengths of Pt(1)-C(2A) = 2.063(4) Å and Pt(2)-C(5A) = 2.062(5) Å which are typical values for methyl groups oriented *trans* to iodide. The equatorial methyl groups show little difference in bond lengths ranging from Pt(1)-C(1A) = 2.049(4) Å to Pt(1)-C(3A) = 2.057(4) Å indicating minimal difference in the donor ability of the pyridine and imine nitrogen atoms. The xanthene backbone exhibits flexibility at the bridging CH₂ and O groups leading to a puckering of the backbone at an angle of 12°. This flexibility in the backbone allows the two amide arms to orient themselves in a manner that allows for some proximity between the arms. The two arms do not lie completely coplanar but the slight deviation from planarity allows for a distance of 3.312 Å between the imine carbon atoms on adjacent arms and 3.588 Å between adjacent pyridyl rings. Due to the *anti* orientation observed in the structure of **34b**, the platinum center Pt(1) is 6.753 Å away from the iodide atom I(2) of the second arm. This distance would presumably decrease if the *syn* isomer, **34a** was adopted. Pertinent bond parameters for **34b** are outlined in table 5.1.

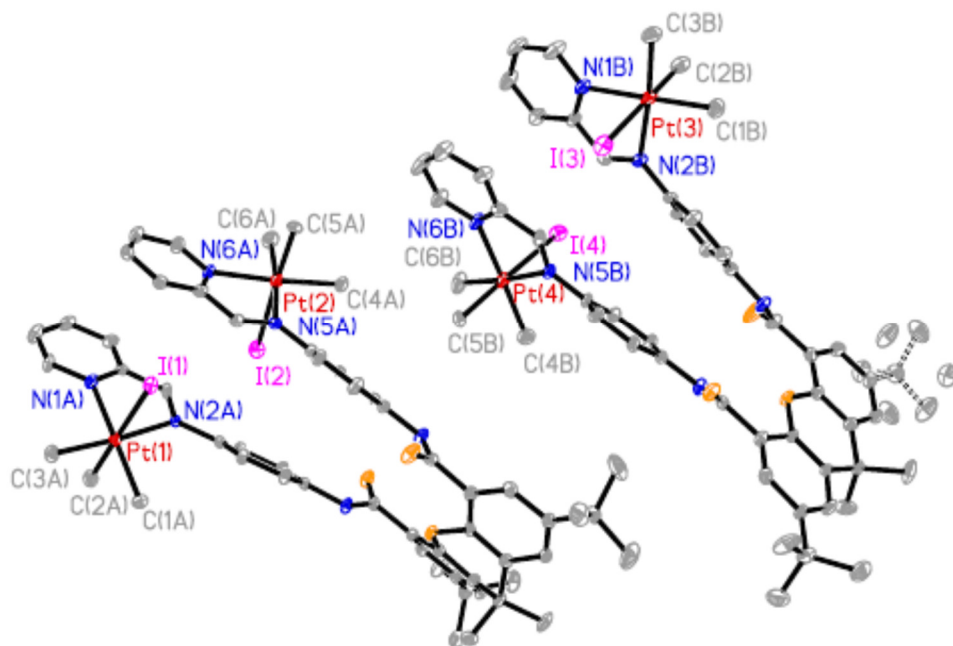


Figure 5.15. Molecular structure of complex **34b**, with an atomic numbering scheme. Hydrogen atoms, and solvent molecules are excluded for clarity.

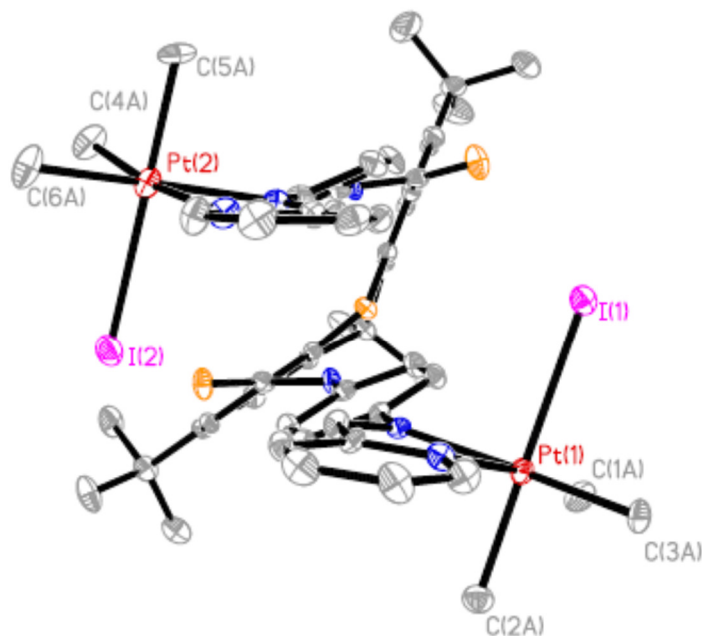


Figure 5.16. Molecular structure of complex **34b** depicting the puckering of the xanthene backbone. Hydrogen atoms, and solvent molecules are excluded for clarity.

Table 5.1: Bond lengths [Å] and angles [°] for [Pt₂Me₆(ppxda)], 34b.

Pt(1)-C(1A)	2.049(4)	Pt(2)-C(4A)	2.052(4)
Pt(1)-C(2A)	2.063(4)	Pt(2)-C(5A)	2.062(5)
Pt(1)-C(3A)	2.057(4)	Pt(2)-C(6A)	2.057(4)
Pt(1)-N(1A)	2.168(3)	Pt(2)-N(6A)	2.166(3)
Pt(1)-N(2A)	2.168(3)	Pt(2)-N(5A)	2.192(3)
Pt(1)-I(1)	2.7952(6)	Pt(2)-I(2)	2.7779(7)
C(1A)-Pt(1)-C(3A)	86.04(16)	C(4A)-Pt(2)-C(6A)	86.32(17)
C(1A)-Pt(1)-C(2A)	87.49(17)	C(4A)-Pt(2)-C(5A)	85.81(18)
C(3A)-Pt(1)-C(2A)	88.55(17)	C(6A)-Pt(2)-C(5A)	90.3(2)
C(1A)-Pt(1)-N(1A)	171.50(15)	C(4A)-Pt(2)-N(6A)	172.45(16)
C(3A)-Pt(1)-N(1A)	97.97(14)	C(6A)-Pt(2)-N(6A)	96.46(15)
C(2A)-Pt(1)-N(1A)	85.13(15)	C(5A)-Pt(2)-N(6A)	87.15(15)
C(1A)-Pt(1)-N(2A)	99.22(14)	C(4A)-Pt(2)-N(5A)	100.64(15)
C(3A)-Pt(1)-N(2A)	174.43(13)	C(6A)-Pt(2)-N(5A)	172.87(14)
C(2A)-Pt(1)-N(2A)	89.82(15)	C(5A)-Pt(2)-N(5A)	88.68(16)
N(1A)-Pt(1)-N(2A)	76.58(12)	N(6A)-Pt(2)-N(5A)	76.44(12)
C(1A)-Pt(1)-I(1)	91.79(13)	C(4A)-Pt(2)-I(2)	91.82(13)
C(3A)-Pt(1)-I(1)	91.16(12)	C(6A)-Pt(2)-I(2)	90.74(14)
C(2A)-Pt(1)-I(1)	179.24(13)	C(5A)-Pt(2)-I(2)	177.34(12)
N(1A)-Pt(1)-I(1)	95.61(9)	N(6A)-Pt(2)-I(2)	95.15(9)
N(2A)-Pt(1)-I(1)	90.53(9)	N(5A)-Pt(2)-I(2)	90.58(9)

The crystals used in the X-ray diffraction analysis were then dissolved in acetone- d_6 in order to determine which resonances in the spectrum were resultant of complex **34b**. The ^1H NMR spectrum shown in figure 5.17 indicates that the resonances of **34b** are those that are observed to be from the more abundant thermodynamically favoured isomer from spectrum 5.14. This would indicate that although both isomer **34a** and **34b** are formed initially, there is a thermodynamic preference for **34b**. Therefore the kinetically preferred *syn* isomer **34a** slowly isomerizes to the thermodynamically favoured *anti* isomer **34b** in solution. This process is depicted in scheme 5.14.

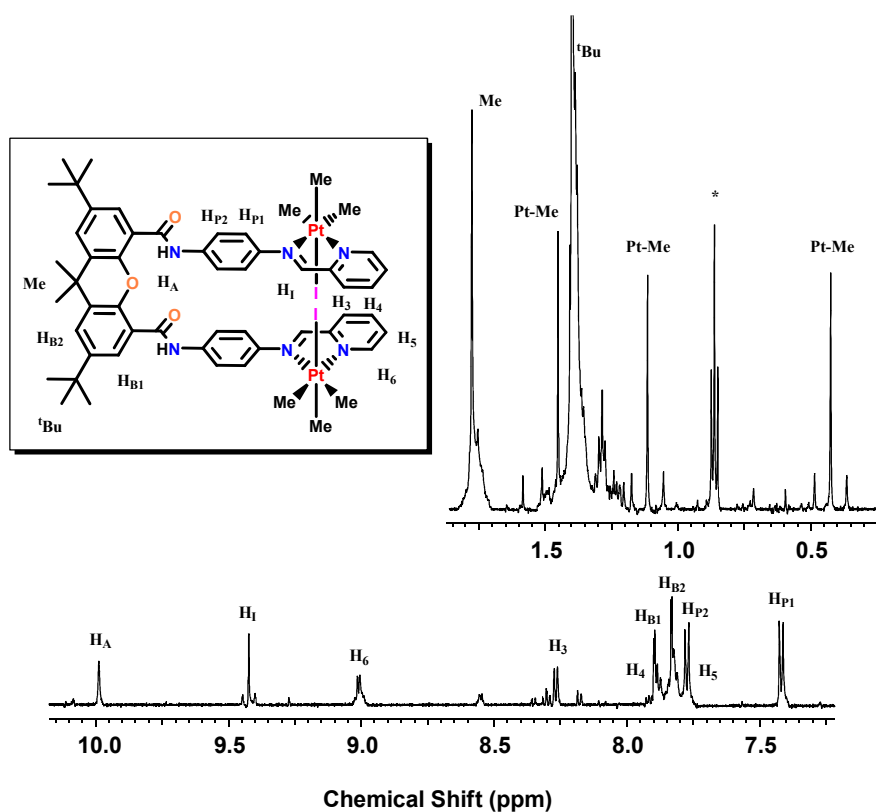
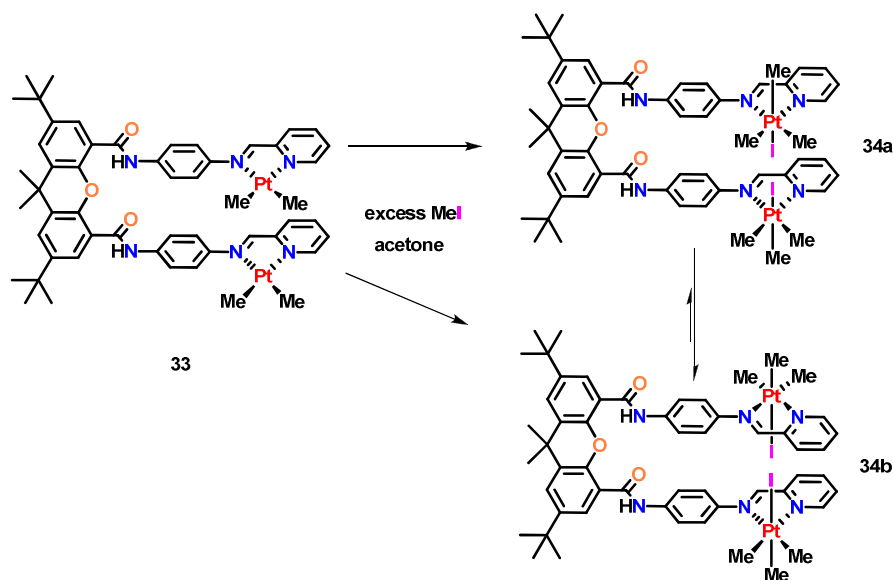
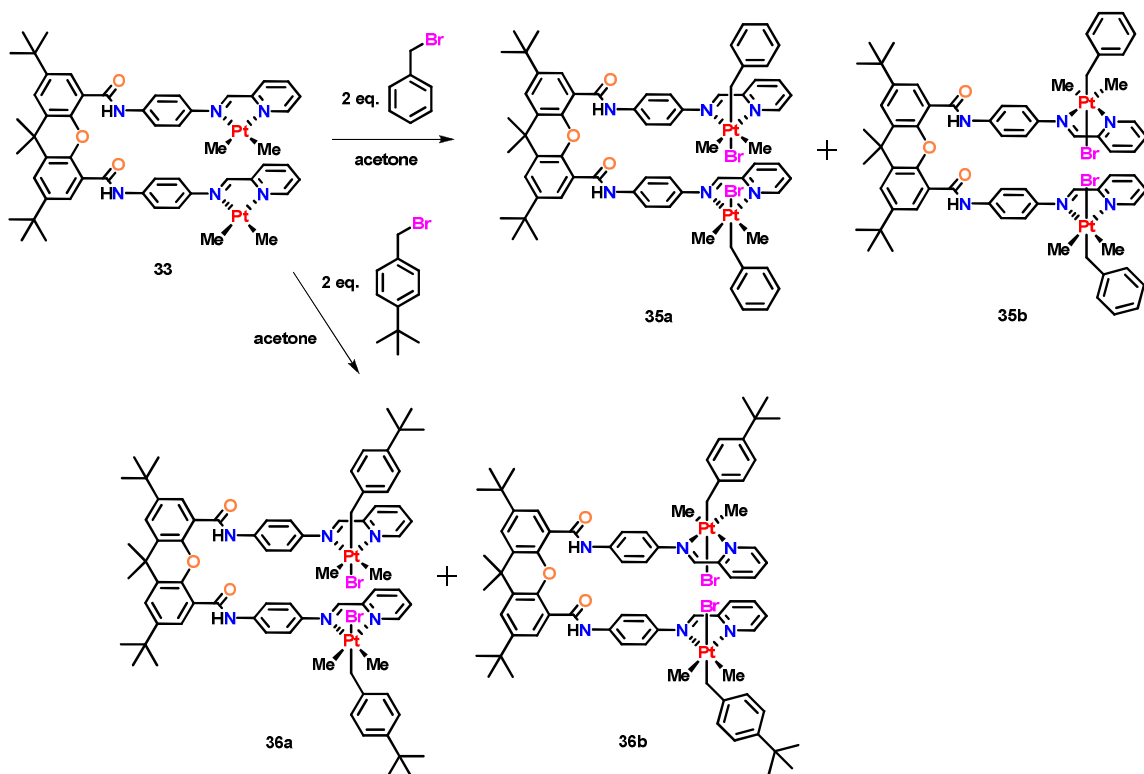


Figure 5.17. ^1H NMR spectrum of **34b** in acetone- d_6 . * indicates residual pentane. Minor complex is **34a** resultant from isomerization in solution.



Scheme 5.14. The oxidative addition of MeI at **33** to give **34a** and **34b** followed by the subsequent isomerization from isomer **34a** to **34b** in solution.

The reactivity of complex **33** towards the oxidative addition was investigated further by adding two equivalents of bromomethylbenzyl derivatives to **33** as shown in scheme 5.15. First, a slight excess of benzyl bromide was added to an acetone- d_6 solution of **33**. The ^1H NMR spectrum acquired showed evidence again for the formation of both isomers of the complex $\text{trans}[\text{Pt}_2\text{Br}_2\text{Me}_4(\text{CH}_2\text{-C}_6\text{H}_5)_2(\text{ppxda})]$, **35a/35b**. Four distinct methylplatinum resonances were observed in the spectrum, the chemical shifts and coupling constants of which provide evidence for the formation of two dimethylplatinum(IV) complexes. Further evidence for the addition of benzyl bromide at complex **33** was provided by the observation of platinum-195 satellites on the CH_2 resonances of the benzyl group, $\delta = 2.45$ ppm and 2.52 ppm and $^2J(\text{PtH}) = 92$ Hz and 99 Hz respectively. There is no preference observed for one of the isomers over the other as evidenced by the equivalent relative integration values observed even after an extended reaction time. Although there is evidence for both isomers in solution, their respective identities remains undetermined due to the inability to crystallize this complex in the solid state, presumably due to the lack of preference between isomers.

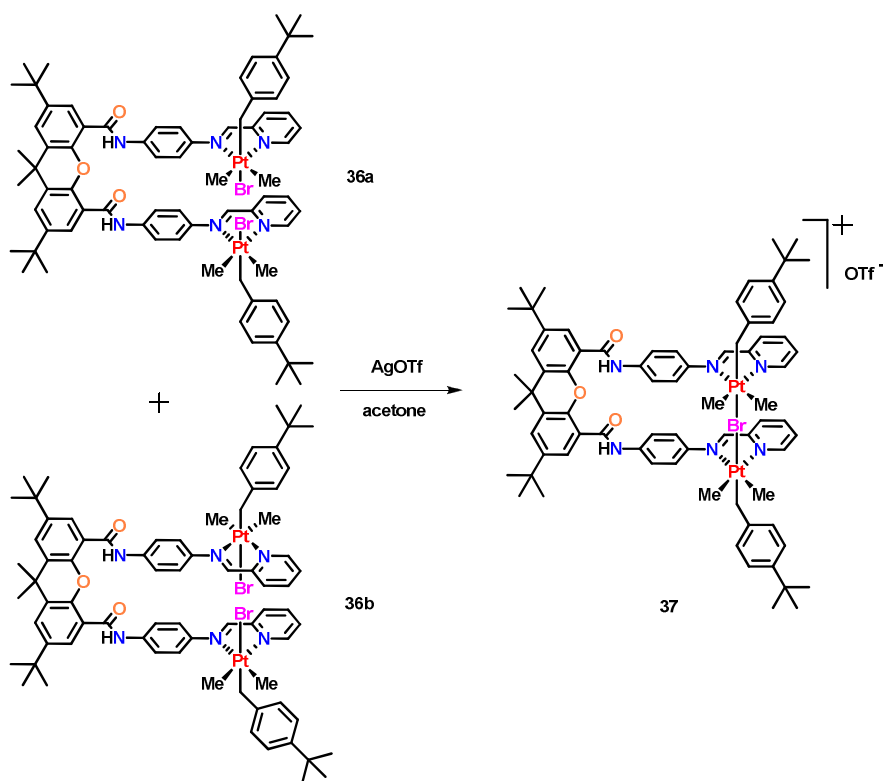


Scheme 5.15. Oxidative addition of bromomethylbenzyl bromide derivatives at **33** to give **35a/35b** and **36a/36b**.

In an analogous manner to the preparation of **35a/35b**, a slight excess of 4-*tert*-butylbenzyl bromide was added to an acetone- d_6 solution of **33**. The bright yellow solution that resulted from the addition was proposed to be *trans*-[Pt₂Br₂Me₄(4-CH₂-C₆H₄-C(CH₃)₃)], complex **36**. Similar to **35a/35b**, the ¹H NMR spectrum of the reaction mixture provided evidence for the formation of two isomers, **36a/36b**. However unlike the case of **35a/35b**, there is a preference in the relative amounts of each isomer formed. The resonances of the preferred isomer possess relative integration values two times greater than the minor isomer, which is a similar ratio that is observed in the case of **34a/34b**. In the absence of solid state structures, it is presumed that the *anti* isomer **36b** is the more predominant isomer in the mixture based on the results of the methyl iodide system.

The tendency of complex **33** to form isomers upon oxidation to organoplatinum(IV) complexes should not be unexpected based on the design of the

ligand. However the preference observed towards the formation of the *anti* isomer in the above cases yields diplatinum(IV) complexes in which the two platinum centers are separated by a large distance which would hinder the ability of cooperative interactions. By removing one or more equivalents of the halide ligands in the diplatinum(IV) complexes one could access a potentially bridged bimetallic complex of the ligand **ppxda** in which the pyridyl groups would need to be positioned *syn* with respect to each other to accommodate the bridging ligand. It is with this motivation that an acetone solution of complex **36a/36b**, formed from the oxidative addition of 4-*tert*-butylbenzyl bromide at **33**, was treated with one equivalent of silver trifluoromethanesulfonate and allowed to stir for one hour, scheme 5.16. It was proposed that the abstraction of one of the bromide ligands would lead to the formation of a complex possessing a bridged bromide ligand between two platinum centers, **37** in scheme 5.16. In order to form this complex the ligand arms would have to adopt the *syn* orientation in order to accommodate both the linearity and distance requirements.



Scheme 5.16. Proposed synthesis of a bridged diplatinum(IV) complex, **37**, through a halide abstraction from **36a/36b**.

After stirring for one hour, the yellow solution was filtered to remove the silver bromide that precipitated from solution. The solvent acetone was then removed in *vacuo* and the resultant yellow oil was then dissolved in acetone- d_6 in order for a ^1H NMR spectrum to be acquired, figure 5.18. Based on the ^1H NMR spectrum, the reaction appeared to produce one major product. This product gave rise to two methylplatinum resonances at $\delta = 1.05$ ppm and 1.31 ppm, both with coupling constant values of $^2J(\text{PtH}) = 69$ Hz. These values are typical for platinum(IV) species' in which the methyl groups are positioned *trans* to nitrogen atoms of the ligand backbone. The methylene protons of the *tert*-butylbenzyl fragments were both observed to possess platinum-195 satellites with coupling constants $^2J(\text{PtH}) = 96$ Hz, diagnostic of the CH_2 groups being positioned *trans* to a halide ligand. The aromatic region of the spectrum possessed resonances arising due to both the incorporation of the benzyl group as well as the ligand. The number of resonances supports the formation of a symmetric complex and through the use of gCOSY NMR spectra can be assigned and is annotated as such in figure 5.18. The presence of starting material resonances as the minor complex indicates that less than one equivalent of silver trifluoromethanesulfonate was added. The ^1H NMR spectrum supports the formation of a complex as proposed in scheme 5.16, however this assignment is only tentative in the absence of a solid state structure.

In an effort to crystallize an analogous complex, a similar reaction was carried out using **34b** as the starting diplatinum complex. By treating an acetone solution of **34b** with two equivalents of silver trifluoromethanesulfonate, both iodide ligands could be abstracted leaving two vacant coordination sites which could be occupied by a solvent molecule or trifluoromethanesulfonate anion, **38** scheme 5.17. After the addition of the silver salt and two hours of stirring the reaction mixture, the resultant yellow solution was filtered to remove silver iodide and the acetone solvent volume was then reduced. A yellow solid was obtained by layering the acetone solution with pentane, which was subsequently collected via vacuum filtration and washed with pentane and water. A sample of the yellow solid was then dissolved in acetone- d_6 and a ^1H NMR spectrum was acquired.

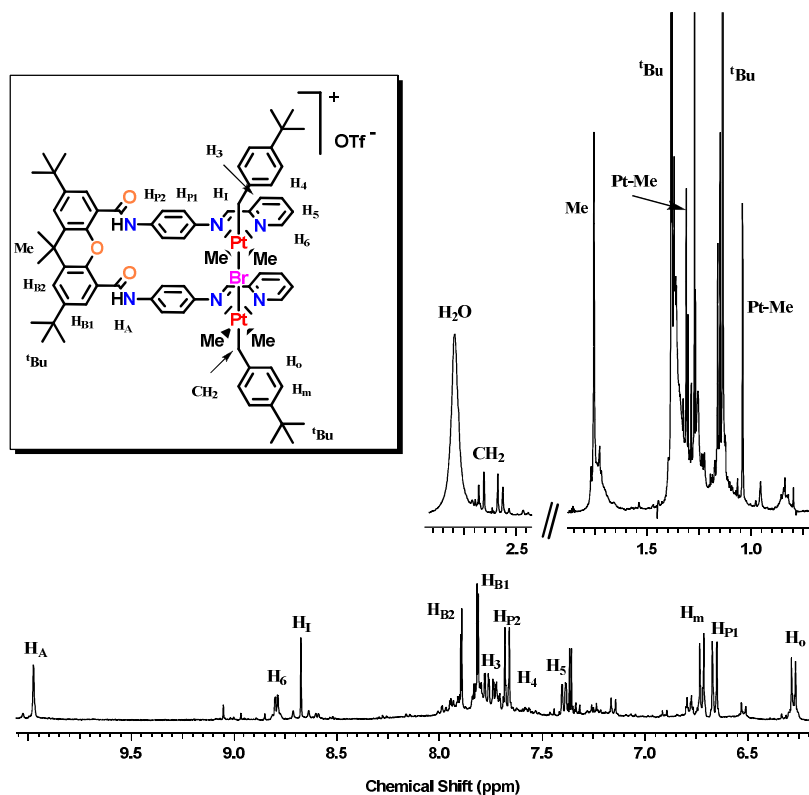
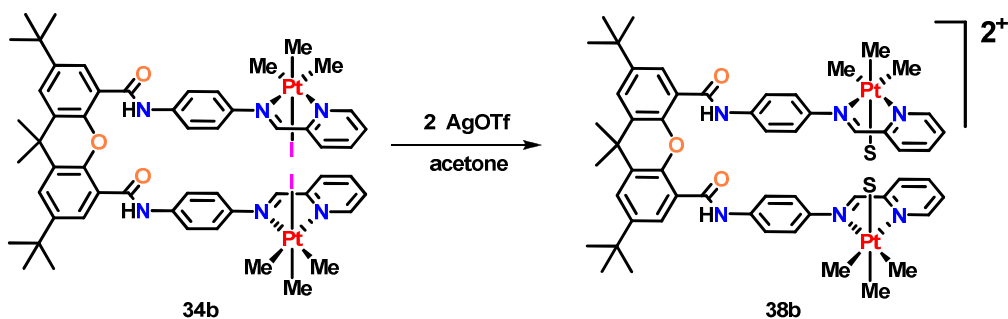


Figure 5.18. ^1H NMR spectrum of a potentially bromide-bridged diplatinum complex, **37**. Trace minor complex in the spectrum is unreacted starting material **36a/36b**.

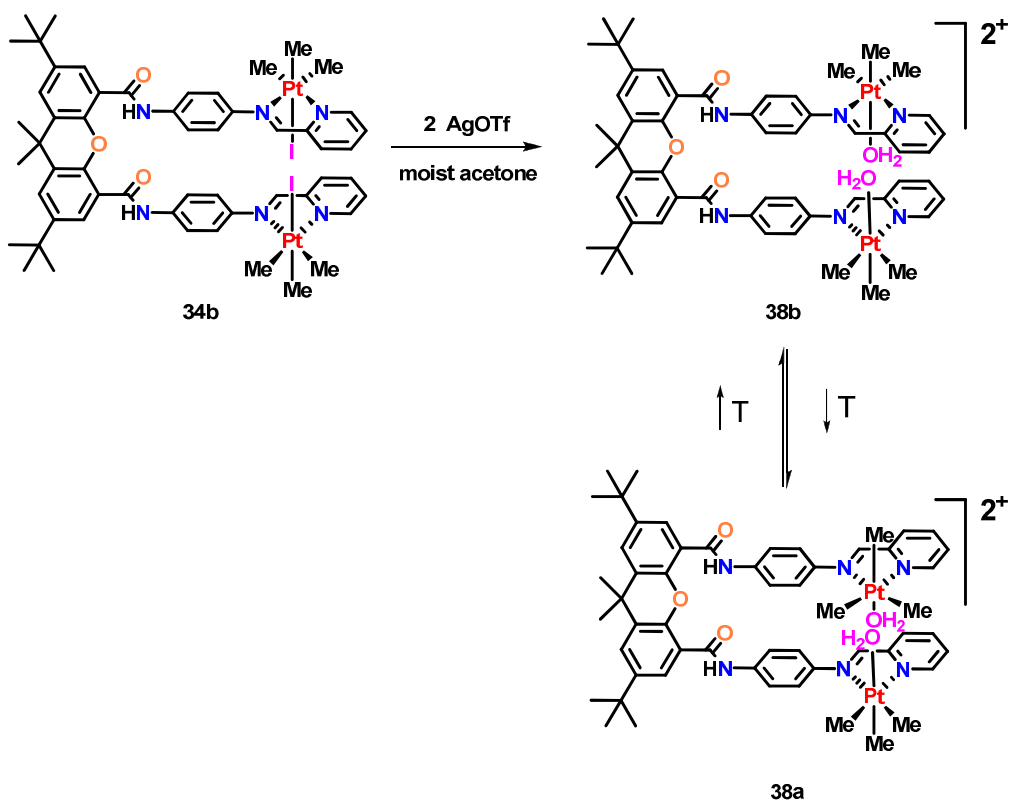


Scheme 5.17. Halide abstraction from **34b** yielding a diplatinum(IV) complex with two vacant coordination sites. “S” indicates solvent water, acetone or trifluoromethanesulfonate.

The ^1H NMR spectrum of the yellow solid indicated that there was only one trimethylplatinum(IV) species present in solution at 25°C . The most upfield methylplatinum resonance initially observed in **34b**, was significantly broadened out and indicated that an exchange process may be occurring at the axial methyl group. The two equatorial methylplatinum resonances were somewhat broadened out, however not to the extent of the axial group. The chemical shift and coupling constant values of these resonances, $\delta = 1.00$ and 1.24 ppm both with $^2J(\text{PtH}) = 68$ Hz, are consistent with methyl groups positioned *trans* to nitrogen atoms and very similar to values observed in **34b**. The aromatic proton resonances also exhibited broadening and as such indicated perhaps an exchange process was occurring that may be temperature dependent. A new broad singlet resonance was observed in the aromatic region of the spectrum at $\delta = 6.14$ ppm with a relative integration value of 4. It was proposed that this resonance could be due to the coordination of water molecules at the vacant coordination sites created by the abstraction of the iodide ligand. This would therefore mean that the complex produced in this reaction would **38** where $\text{S} = \text{H}_2\text{O}$. Based on the broadness of the resonances and the possibility of an exchange process occurring, a variable temperature NMR experiment needed to be carried out. As such NMR spectra were recorded at 10°C intervals between 20°C and -30°C , some of which are depicted and labelled in figure 5.19. The spectrum acquired at 10°C indicates that the broad methylplatinum resonance furthest upfield at $\delta = 0.67$ ppm is actually two methylplatinum resonances as this signal begins to split into two distinct signals. This becomes further pronounced at 0°C where two individual resonances are clearly observed at $\delta = 0.61$ and 0.65 ppm each with coupling constants of approximately $^2J(\text{PtH}) = 80$ Hz. The methylplatinum resonance at $\delta = 1.21$ ppm is also observed to be splitting into two resonances. These observations would suggest that at lower temperature the two isomers, **38a** and **38b**, scheme 5.18, can be resolved but at room temperature the exchange process occurs rapidly. At -30°C , the six methylplatinum resonances are resolved and the aromatic region of the spectrum is completely resolved as well. Using comparative integration values and gCOSY NMR spectra, the resonances attributed to each isomer were assigned as annotated in figure 5.19. Based on the ^1H NMR spectra the coalescence temperature was observed to be 25°C and can be used to calculate the free energy requirement of the exchange process using equation 5.1. The

calculated value was determined to be 63 kJ/mol, where h is Planck's constant in $\text{J}\cdot\text{s}$, N_A is Avagadro's number in mol^{-1} , R is the value for the gas constant in $\text{J}\cdot\text{K}^{-1}\cdot\text{mol}^{-1}$, T_C is the coalescence temperature in K , and $\nu_a-\nu_b$ is the frequency difference in Hz between the two observed resonances. ESI-MS spectral data also confirms the formation of the diaqua complex $[\text{Pt}_2\text{Me}_6(\text{OH}_2)_2(\text{ppxda})][\text{OTf}]_2$.

$$\Delta G_{calc}^\ddagger = RT_C \ln \left[\frac{RT_C \sqrt{2}}{\pi N_A h |\nu_a - \nu_b|} \right] \quad \text{equation 5.1}$$



Scheme 5.18. Synthesis of **38b** from the coordination of water after halide abstraction and the temperature dependence between **38b** and **38a**. Counteranions omitted for clarity.

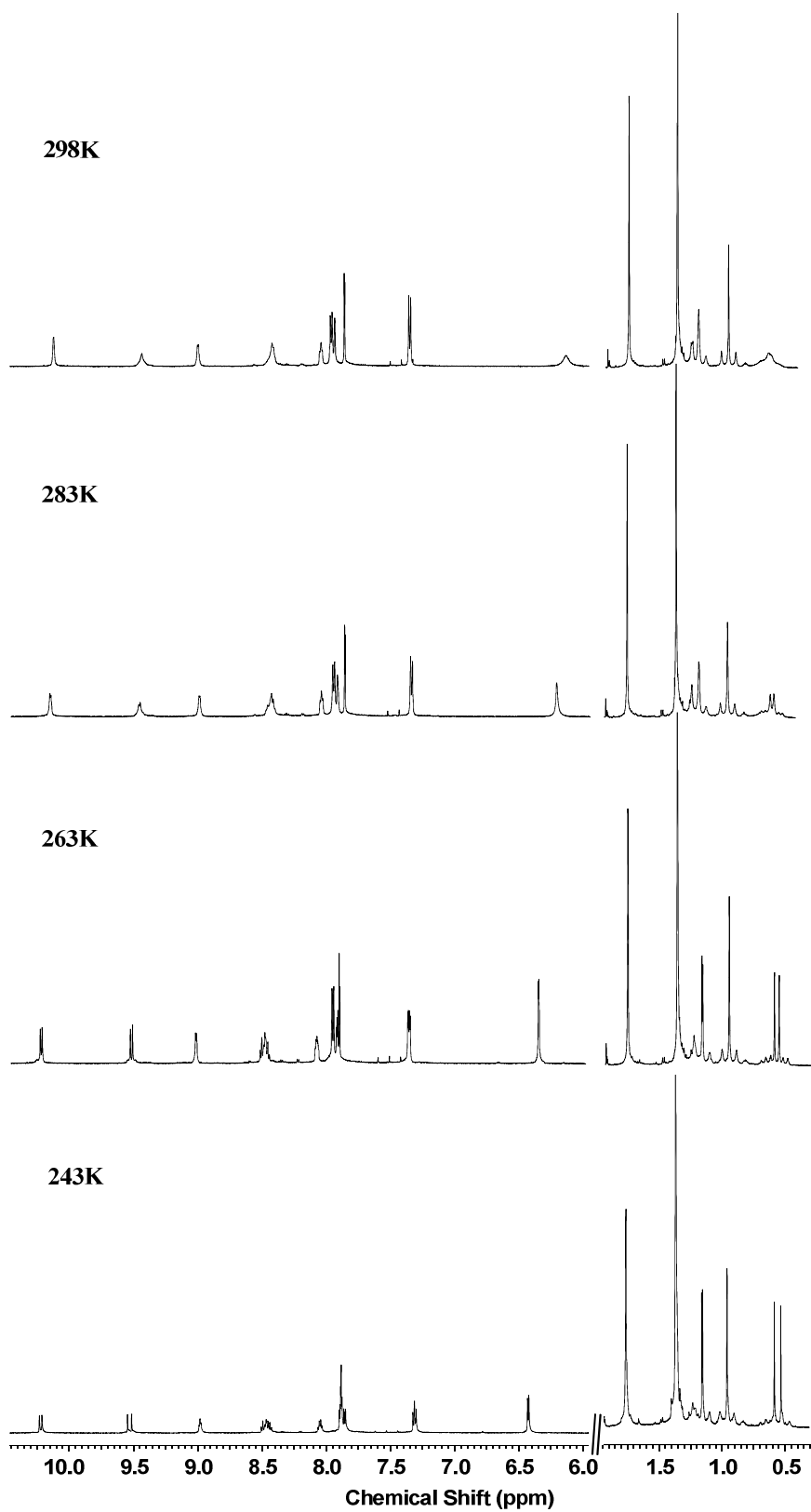
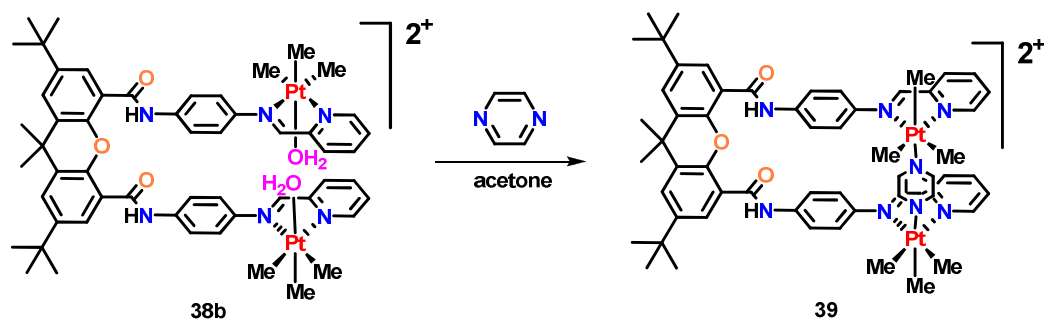


Figure 5.19. Variable temperature ^1H NMR spectra, (acetone- d_6), of complex **38a/38b**.

In an effort to have both amide arms of a diplatinum(IV) complex be positioned directly above one another so that the platinum centers are more proximal, the incorporation of a bridging group was proposed. It was thought that by adding an equivalent of pyrazine to the diaqua complex **38a/38b**, one could force the resultant complex to adopt a *syn* arrangement in which the platinum centers are aligned more linearly and bridged by the pyrazine ligand, scheme 5.19. To test this, a half equivalent of pyrazine was added to a sample of **38a/38b** in acetone-*d*₆. After allowing the two reagents to mix a ¹H NMR spectrum was acquired of the yellow solution.



Scheme 5.19. Formation of the pyrazine bridged diplatinum(IV) complex, **39**.
Counteranions omitted for clarity.

Unlike the spectrum acquired at 25°C for **38a/38b**, the spectrum of the pyrazine bridged complex **39**, [Pt₂Me₆(C₄H₄N₂)(ppxda)][OTf]₂, possessed sharp resonances attributed to the methylplatinum groups, figure 5.20. These resonances observed at $\delta = 0.85, 1.06, \text{ and } 1.30$ ppm with coupling constant values of ${}^2J(\text{PtH}) = 72$ Hz, 68 Hz and 68 Hz respectively, are diagnostic of a trimethylplatinum(IV) complex in which the methyl groups are positioned *trans* to imine nitrogen donors. The aromatic region of the spectrum contained the typically observed resonances of the **ppxda** ligand with platinum satellites observed on the imine proton resonance at $\delta = 9.40$ ppm with coupling constant values ${}^3J(\text{PtH}) = 27$ Hz; and on the *ortho* pyridyl resonance at $\delta = 9.09$ ppm with ${}^3J(\text{PtH}) = 18$ Hz. These are typically observed values of organoplatinum(IV) complexes. The diagnostic evidence of the incorporation of the bridging pyrazine group is provided by a broad singlet resonance observed at $\delta = 8.54$ ppm with a relative integration value of 4. This indicates that overall symmetric nature of **39** as all pyrazine protons are observed to

be equivalent at ambient temperature. The observation of pyrazine being incorporated into **39** supports an orientation in which both amide arms are positioned directly over top of one another rendering the platinum centers in a more linear arrangement. This increases the proximity of the metal centers which could enhance the cooperativity between them.

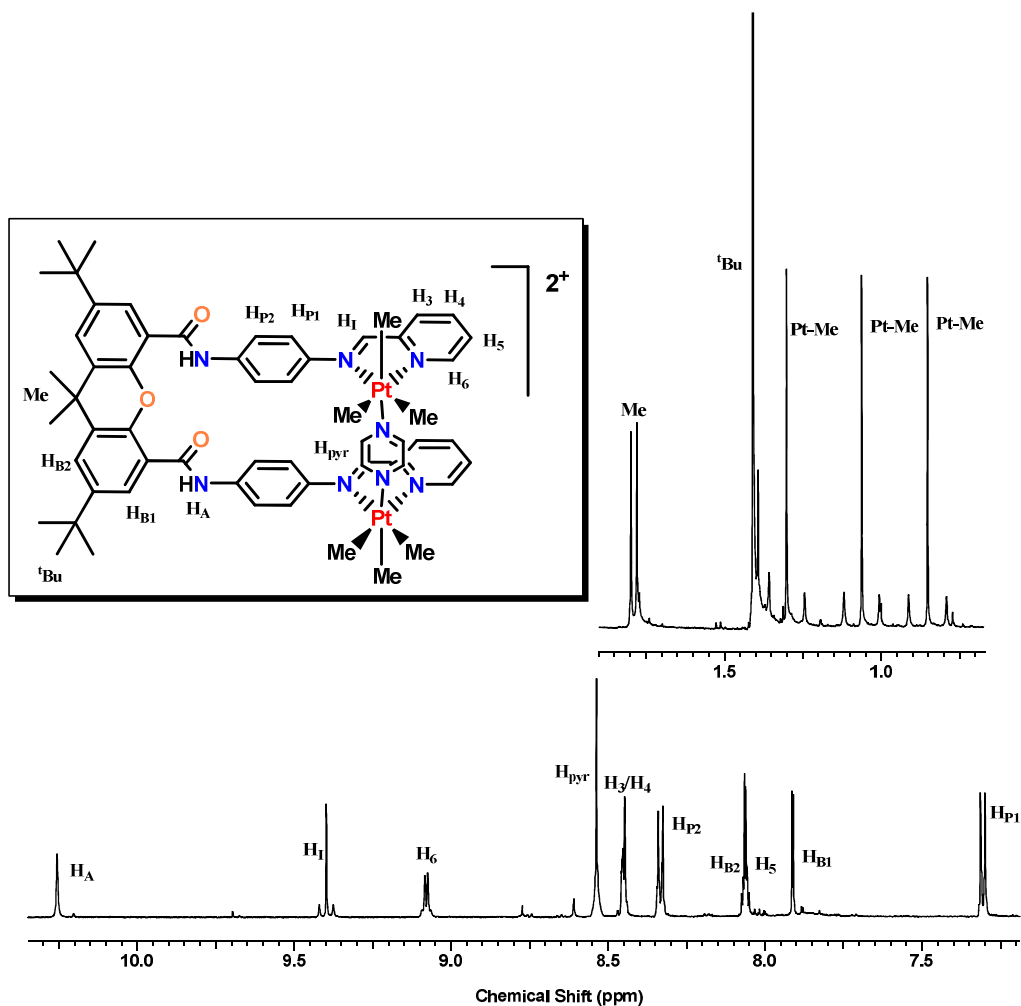


Figure 5.20. ^1H NMR of **39** in acetone- d_6 .

Unfortunately solid state structures of these complexes were not obtained due to the inability to them crystallize effectively. Presumably the increased amount of rotational freedom imparted by the ligand design could be a reason for some of this inability. Unlike the anthracene based systems derived on **bpad**, which saw detrimental effects when positioning the platinum(II) centers close to the anthracene backbone, the

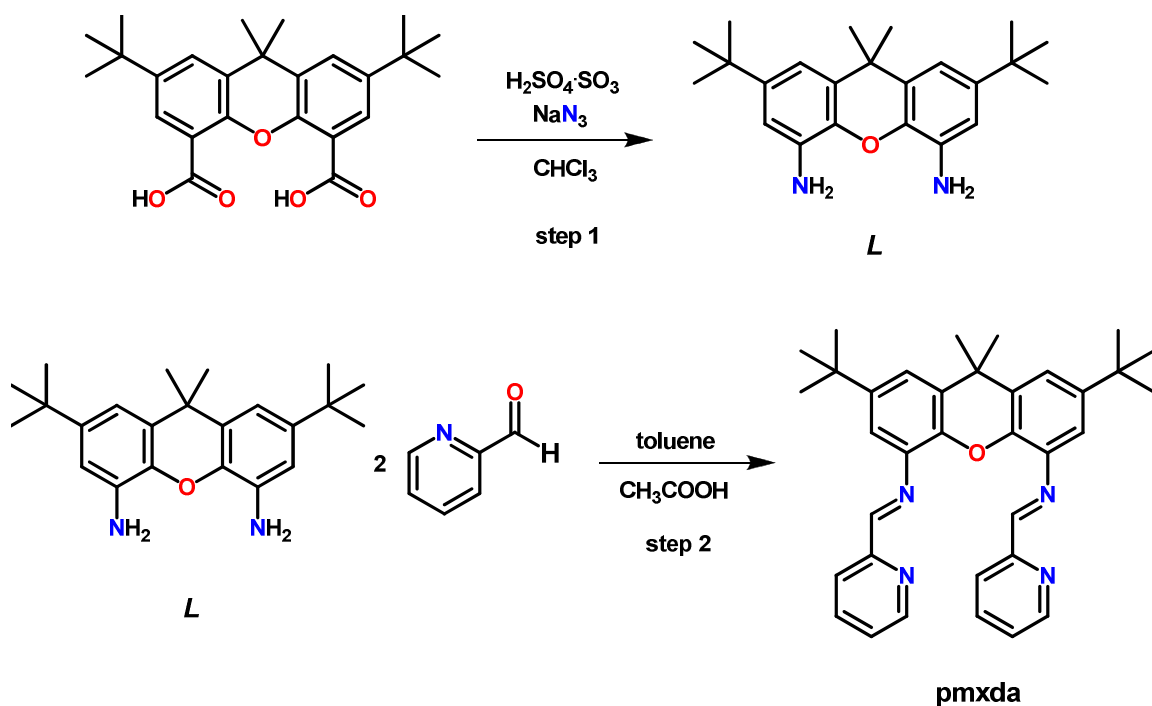
xanthene derived ligands should not suffer the same restrictions. The presence of a bridging oxygen atom present in the backbone of the xanthene derived ligands would eliminate the metalation event we propose to occur in the anthracene ligand. By designing a ligand which would coordinate the metal centers closer to the backbone, the need for the long linker groups between the backbone and chelating sites would be removed and this could eliminate some of the rotational isomer issues observed in the case for **ppxda** derived complexes. With that motivation, a new ligand design was proposed, synthesized and investigated.

5.11 Ligand Synthesis

Considering the issues and limitations imposed on **ppxda** as a result of its multiple degrees of rotational freedom, a ligand which is structurally more rigid appeared to be ideal. By removing the long linker groups between the backbone and coordination sites one would remove a lot of the rotational freedom while still maintaining a close distance between coordination sites. With this in mind, the new ligand 2,7-di-*tert*-butyl-9,9-dimethyl-bis(pyridine-2-ylmethylene)-9*H*-xanthene-4,5-diamine, **pmxda**, was prepared in two steps as outlined in scheme 5.20. Rather than the long diamide linker used in **ppxda**, the spacer between the xanthene backbone and coordination sites is a one atom bridge. This maintains a close proximity between the coordination sites and the backbone but still maintains proximity between the coordinations sites on each arm of the ligand.

Initially, a chloroform solution of 2,7-di-*tert*-butyl-9,9-dimethyl-9*H*-xanthene-4,5-dicarboxylic acid was cooled while stirring before fuming sulfuric acid was carefully added to the reaction mixture dropwise. To the now yellow solution was added an excess of NaN_3 gradually in portions over a period of 20 minutes with stirring. After the final addition the reaction mixture was stirred at 0°C for one hour and then heated at 50°C for one hour before being neutralized and then made basic with a KOH solution. After a quick workup a white solid was afforded in good yield. This solid was found by ^1H NMR and ESI-MS to be 2,7-di-*tert*-butyl-9,9-dimethyl-9*H*-xanthene-4,5-diamine, **L**, step 1 in scheme 5.20.

With compound **L** was dissolved in toluene and to this solution was added a slight excess of 2-pyridinecarboxaldehyde and a drop of acetic acid, (step 2 in scheme 5.20). A Dean-Stark trap was attached to the flask and the reaction mixture was then heated at reflux while stirring for 3 hours. The toluene solvent was removed under reduced pressure to afford a yellow solid product. This solid was washed with pentane and collected by Hirsch filtration in excellent yield. The yellow solid, **pmxda**, was found to be soluble in organic solvents, although use of CHCl_3 has shown to lead to the acid promoted cleavage of the imine bonds, and as such a ^1H NMR spectrum was acquired in CD_2Cl_2 , figure 5.21.



Scheme 5.20. Synthesis of the new xanthene based ligand **pmxda**.

The ^1H NMR spectrum of **pmxda** contains the expected *tert*-butyl and methyl resonances of the xanthene backbone as was observed in the case of **ppxda**. Evidence for the formation of **pmxda** was provided by the presence of four resonances corresponding to the aromatic protons of the pyridine ring as well as a distinct imine proton resonance at $\delta = 8.65$ ppm. The absence of amine protons provides indirect evidence for the formation of **pmxda** from **L**. The single set of aromatic protons from the pyridyl ring as well as the

xanthene backbone implies that the ligand possesses symmetry. This could be a result of a mirror plane in the case where the pyridyl rings are oriented *syn* to one another, I in figure 5.22; or the more likely *anti* orientation of the pyridyl rings, II in figure 5.22 which would contain a C_2 rotation axis. Work by Panunzi *et al.* supports the formation of the *anti* isomer in a similar complex as is determined by the solid state structure [24]. Previous work with complexes of **ppxda** did indicate a thermodynamic preference for the *anti* orientation.

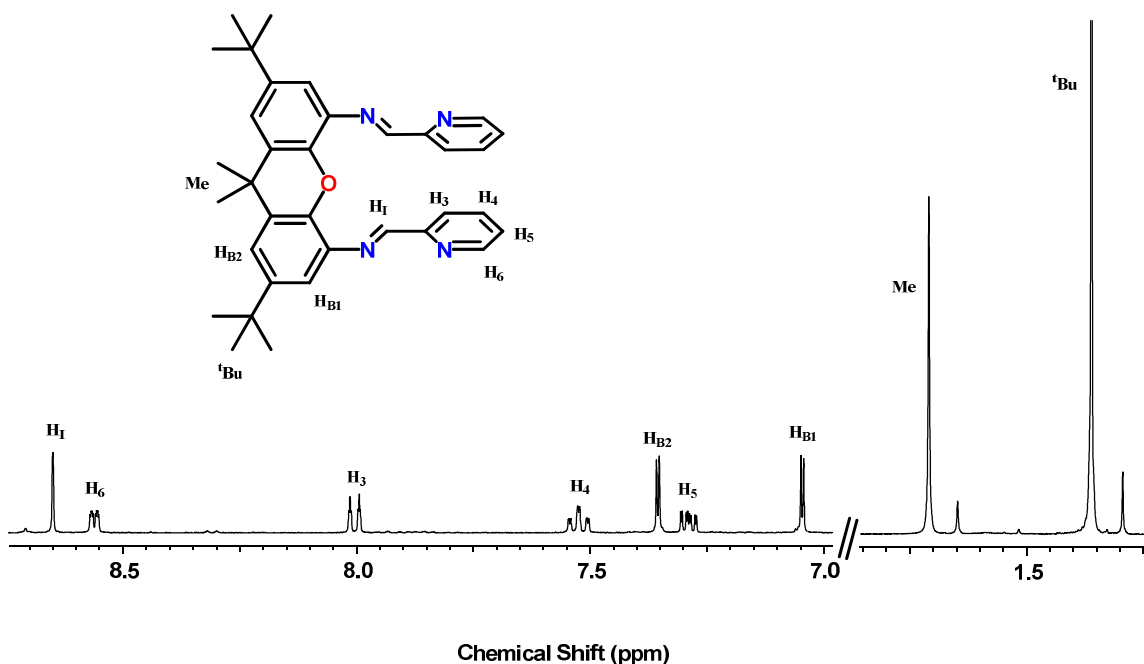


Figure 5.21. ^1H NMR spectrum of the ligand **pmxda** in CD_2Cl_2 .

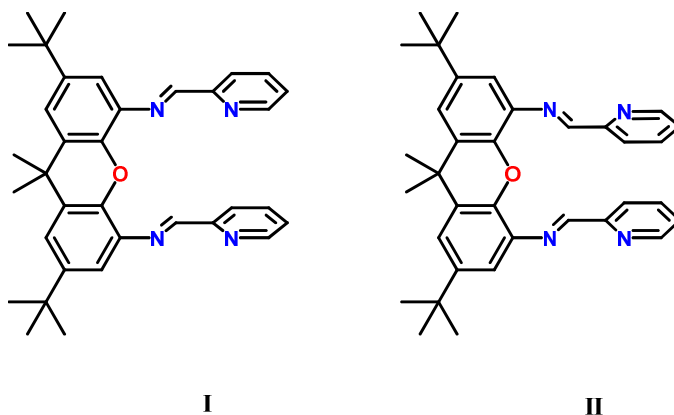
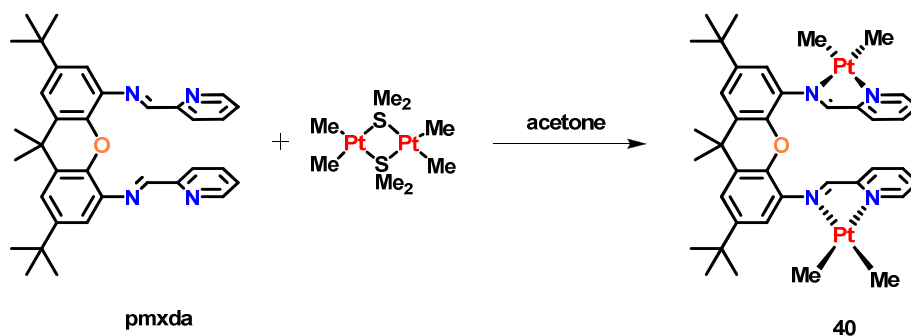


Figure 5.22. Possible rotational conformations of **pmxda**.

5.12 Synthesis of a bimetallic dimethylplatinum(II) complex of **pmxda**

The bimetallic dimethylplatinum(II) complex of the ligand **pmxda**, was prepared through the complexation of two equivalents of the metal center by **pmxda**, scheme 5.21. The preparation of complex **40**, [Pt₂Me₄(**pmxda**)], was achieved through the addition of equimolar portions of [Pt₂Me₄(μ-SMe₂)₂] and **pmxda** in acetone [43]. Upon the addition of the reagents, the initially yellow solution began to take on a purple colour which is typical for complexation reactions occurring between the ligand and the metal center. The reaction mixture was allowed to stir at room temperature for three hours before the solvent acetone was removed in *vacuo*. The resultant purple solid was then suspended in pentane and collected by Hirsch filtration. The bright purple solid, complex **40**, was prepared in a 92% yield.



Scheme 5.21. Complexation of two dimethylplatinum(II) centers by **pmxda** giving the bimetallic complex **40**.

A portion of complex **40** was then dissolved in acetone-*d*₆ and a ¹H NMR spectrum was acquired, figure 5.23. Two methylplatinum resonances were observed in the spectrum each with a relative integration value of 6 protons. These resonances were observed at δ = 0.74 ppm and 1.15 ppm with coupling constant values of ²J(PtH) = 87 Hz and 88 Hz respectively. The presence of only two resonances suggests that complex **40** maintains symmetry, and based on the previous findings we would propose an *anti* geometry as depicted in scheme 5.21. The presence of platinum-195 satellites on the imine proton resonance at δ = 9.62 ppm with a coupling constant value of ³J(PtH) = 34Hz provides further evidence for the complexation of two dimethylplatinum(II) units by the

ligand **pmxda**. The remaining resonances were assigned completely using gCOSY NMR spectroscopic analysis and are annotated in figure 5.23. The successful formation of **40** was confirmed via ESI-MS analysis where the molecular ion observed was that of $[\text{Pt}_2\text{Me}_4(\text{pmxda})\text{Na}]^+$, the cation produced by the incorporation of a sodium ion within **40** at $m/z = 1003.31978$.

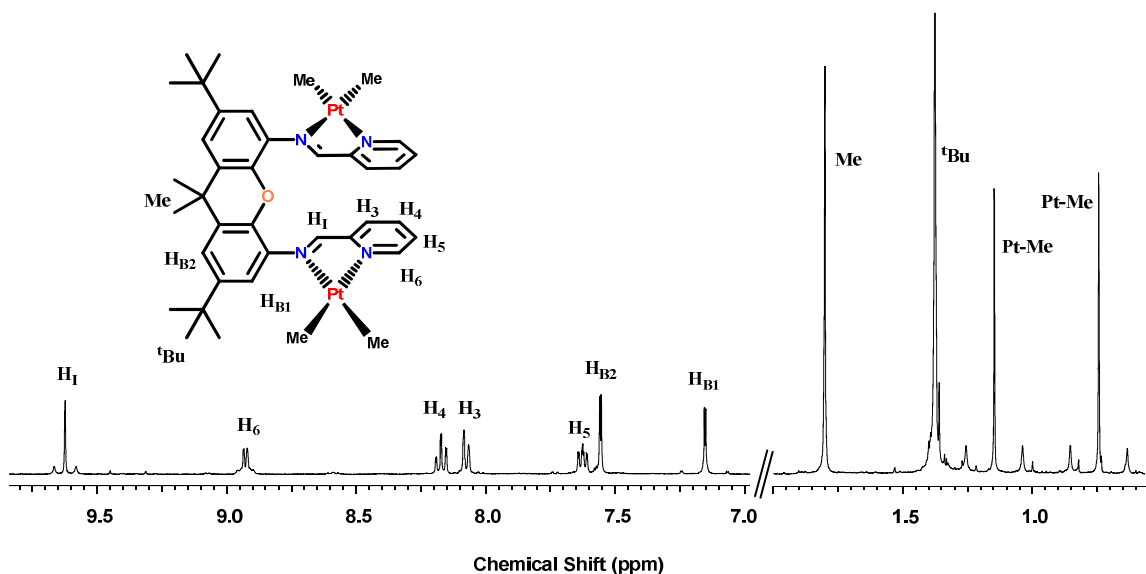
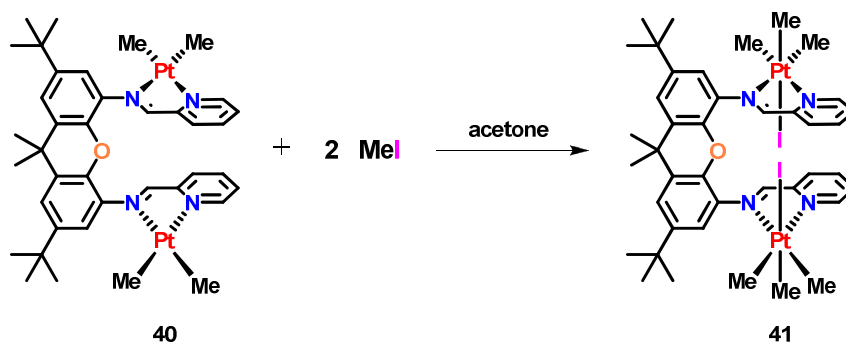


Figure 5.23. ^1H NMR spectrum of complex **40**, $[\text{Pt}_2\text{Me}_4(\text{ppxda})]$, in acetone- d_6 .

5.13 Reactivity of Complex **40** Towards Oxidative Addition

The reactivity of the bimetallic dimethylplatinum(II) complex **40**, towards the oxidative addition reaction with various substrates was investigated. Similar to the study of **33**, the analogous complex to **40**, an NMR tube was charged with an acetone- d_6 sample of complex **40**. A slight excess of methyl iodide was added to the purple solution of **40**, which immediately became bright yellow upon addition. A ^1H NMR spectrum was acquired 10 minutes after the addition of methyl iodide and is depicted in figure 5.24. The disappearance of resonances attributed to complex **40** from the spectrum provided evidence that a reaction had occurred yielding a new trimethylplatinum(IV) species, **41** as outlined in scheme 5.22.



Scheme 5.22. The oxidative addition of methyl iodide at **40** to give *trans*-[Pt₂I₂Me₆(pmxda)], **41**.

The ¹H NMR spectrum acquired in acetone-*d*₆ displayed two distinct and resolved methylplatinum resonances. The most upfield resonance at δ = 0.82 ppm with a coupling constant value ²J(PtH) = 73 Hz is diagnostic of an axial methyl group being positioned *trans* to the iodide ligand. This supports the formation of the *fac* isomer of the trimethyliodideplatinum(IV) complex of **pmxda**. The additional resolved methylplatinum resonance at δ = 1.51 ppm with ²J(PtH) = 71 Hz is typical for an equatorial methyl group being positioned *trans* to a nitrogen donor atom of the **pmxda** ligand. Slightly upfield of this resonance at δ = 1.20 ppm, a broad resonance is observed. The extremely broadened appearance indicates an exchange process is occurring. This could presumably be due to an isomerism event between the two possible isomer arrangements of **41**. Additional broad resonances were observed in the aromatic region of the ¹H NMR spectrum which prevents the ultimate assignment of **41**.

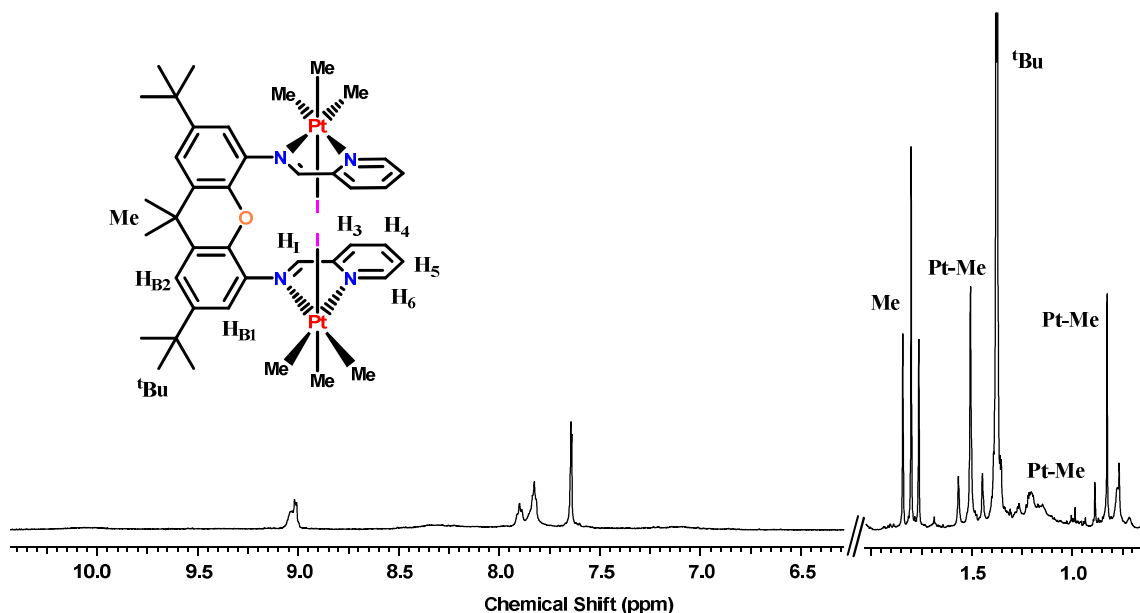


Figure 5.24. ^1H NMR spectrum of **41** acquired at 298K in acetone- d_6 . Aromatic resonance remain unassigned as many are broadened out due to an exchange process and are observed in the baseline.

The broadness of the resonances being a result of an exchange process indicates that a variable temperature NMR experiment could be of value in determining the true composition of **41**. After removing the acetone- d_6 solvent under reduced pressure, the bright yellow oil was dissolved in CD_2Cl_2 for the low temperature experiment. ^1H NMR and ^1H - ^1H gCOSY NMR spectra were acquired at temperature increments of 10°C over a range from $+25^\circ\text{C}$ to -40°C . The initial spectrum acquired at 25°C , (a) in figure 5.25, contained similar methylplatinum resonances as were observed in the spectrum originally acquired in acetone- d_6 however a significant increase in the resolution of the signals was observed. The decreased amount of broadening would suggest that the exchange process is slower in dichloromethane than in acetone. The resonances in the aromatic region however still remain very broad. The spectrum acquired at 0°C , (b) figure 5.25 indicates a drastic sharpening of the resonances in the aromatic region of the spectrum to the point where absolute assignment can be made and platinum-195 satellites can be observed. The imine resonance at $\delta = 9.92$ ppm is observed to possess platinum-195 satellites with $^3J(\text{PtH}) = 24$ Hz. This value indicates that indeed a platinum(IV) species was produced in the formation of **41** and further supports the assignment of this complex as *trans*-

[Pt₂I₂Me₆(pmxda)]. Also at this temperature all three methylplatinum resonances are fully resolved, the previously unassigned resonance at $\delta = 1.23$ ppm being observed to have platinum-195 satellites with $^2J(\text{PtH}) = 70$ Hz which supports the assignment of the resonance arising due to the methyl group being positioned *trans* to a nitrogen atom of the ligand backbone. The best resolution is observed at the lowest temperature, -40°C (d) in figure 5.25, and the identity of **41** can be confidently assigned. The assignment of **41** as [Pt₂I₂Me₆(pmxda)] is supported in addition by ESI-MS data which identify the molecular ion as [Pt₂IME₆(pmxda)]⁺ with a $m/z = 1137.27777$ amu.

After concentrating the dichloromethane solution of **41**, it was layered with pentane to affect the precipitation of a yellow solid. This yellow solid was dissolved in minimal dichloromethane and pentane solvent vapour was allowed to diffuse into the solution of **41** gradually. This yielded the formation of yellow prism shaped single crystal which were suitable for X-ray diffraction analysis. The solid state structure depicted in figure 5.26, supports the formation of the trimethyliodide diplatinum(IV) complex via the oxidative addition of methyl iodide at both platinum centers in **40**. The solid state structure of **41** confirms the assumed *anti* orientation which was tentatively assigned based on previous findings. The methyl groups adopt a *fac* geometry at the platinum centers as a result of the *trans* oxidative addition of methyl iodide. The axial methyl groups have consistent bond lengths of Pt(1)-C(2A) = 2.065(1) Å and Pt(2)-C(5A) = 2.058(5) Å which are typical values for methyl groups oriented *trans* to iodide. The equatorial methyl groups show little difference in bond lengths ranging from Pt(1)-C(1A) = 2.042(4) Å to Pt(1)-C(3A) = 2.048(4) Å indicating minimal difference in the donor ability of the pyridine and imine nitrogen atoms. Unlike **34b**, the complex **41** does not exhibit a puckering of the backbone and maintains a nearly planar structure. The two arms lie nearly coplanar but the slight deviation from planarity allows for a distance of 3.597 Å between adjacent pyridyl rings. Due to the *anti* orientation observed in the structure of **41**, the platinum center Pt(1) is 7.750 Å away from Pt(2) which is distal in terms of cooperative reactivity potential. This could be presumably overcome if the *syn* isomer became accessible. Pertinent bond parameters for **41** are outlined in table 5.2.

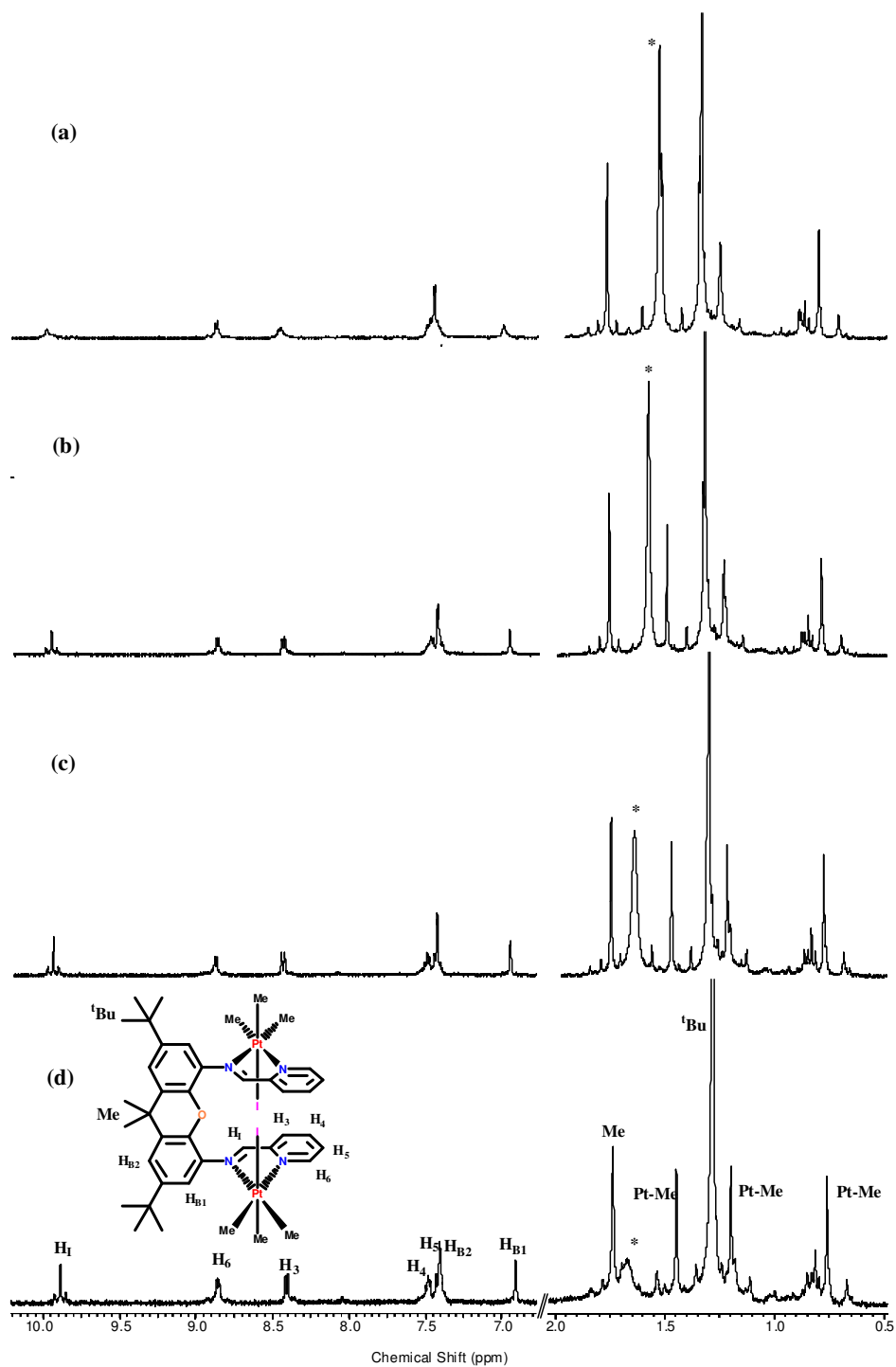


Figure 5.25. Variable temperature NMR spectra of **41** in CD_2Cl_2 . Spectra are acquired at (a) 298K, (b) 273K, (c) 253K, (d) 233K. * indicates the presence of water.

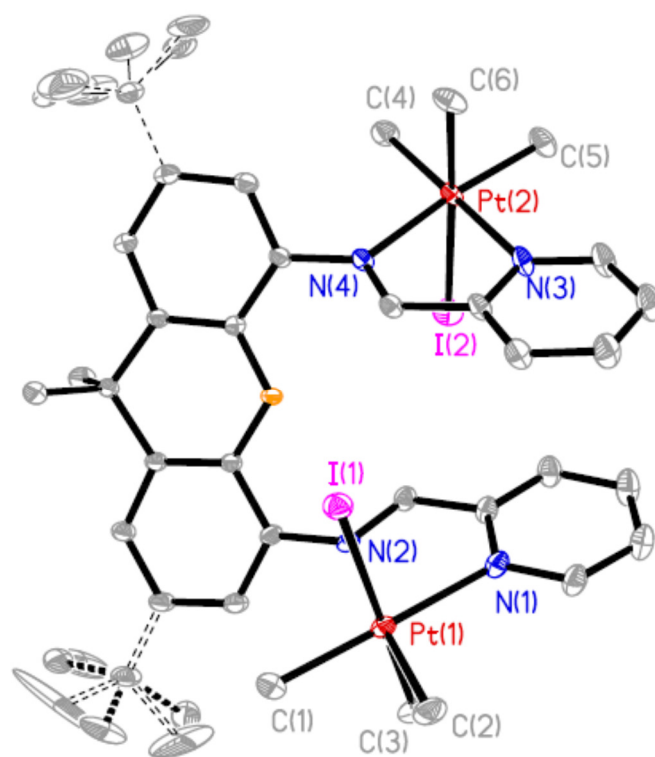
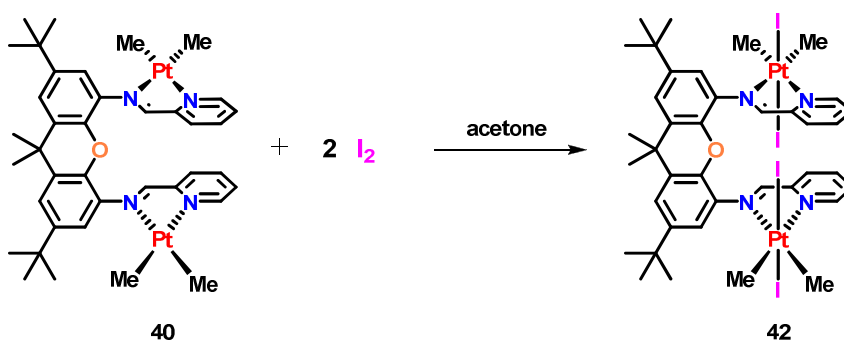


Figure 5.26. Molecular structure of complex **41**, with an atomic numbering scheme. Hydrogen atoms and solvent molecules are omitted for clarity.

Table 5.2: Bond lengths [Å] and angles [°] for [Pt₂I₂Me₆(pmxda)], 41.

Pt(1)-C(2)	2.042(2)	Pt(2)-C(5)	2.041(3)
Pt(1)-C(1)	2.048(3)	Pt(2)-C(4)	2.047(3)
Pt(1)-C(3)	2.065(3)	Pt(2)-C(6)	2.058(3)
Pt(1)-N(1)	2.169(2)	Pt(2)-N(3)	2.144(2)
Pt(1)-N(2)	2.1785(18)	Pt(2)-N(4)	2.1874(19)
Pt(1)-I(1)	2.7748(4)	Pt(2)-I(2)	2.7623(4)
C(2)-Pt(1)-C(1)	84.55(12)	C(5)-Pt(2)-C(4)	86.06(12)
C(2)-Pt(1)-C(3)	88.08(12)	C(5)-Pt(2)-C(6)	88.55(12)
C(1)-Pt(1)-C(3)	91.25(12)	C(4)-Pt(2)-C(6)	90.44(12)
C(2)-Pt(1)-N(1)	98.99(10)	C(5)-Pt(2)-N(3)	95.47(10)
C(1)-Pt(1)-N(1)	175.77(10)	C(4)-Pt(2)-N(3)	177.83(10)
C(3)-Pt(1)-N(1)	86.57(11)	C(6)-Pt(2)-N(3)	88.05(11)
C(2)-Pt(1)-N(2)	175.25(10)	C(5)-Pt(2)-N(4)	171.85(10)
C(1)-Pt(1)-N(2)	99.98(10)	C(4)-Pt(2)-N(4)	102.04(9)
C(3)-Pt(1)-N(2)	90.40(9)	C(6)-Pt(2)-N(4)	90.48(10)
N(1)-Pt(1)-N(2)	76.42(7)	N(3)-Pt(2)-N(4)	76.42(7)
C(2)-Pt(1)-I(1)	91.51(9)	C(5)-Pt(2)-I(2)	93.68(9)
C(1)-Pt(1)-I(1)	88.45(8)	C(4)-Pt(2)-I(2)	88.91(8)
C(3)-Pt(1)-I(1)	179.52(8)	C(6)-Pt(2)-I(2)	177.62(9)
N(1)-Pt(1)-I(1)	93.75(6)	N(3)-Pt(2)-I(2)	92.54(6)
N(2)-Pt(1)-I(1)	90.03(5)	N(4)-Pt(2)-I(2)	87.43(5)

In a similar experiment, an acetone solution of **40** was allowed to stir at room temperature while two equivalents of iodine dissolved in acetone were added gradually over 10 minutes. The originally deep purple solution gradually changed to a bright vibrant yellow colour as the iodine was added. Upon concentrating the acetone solvent under reduced pressure, a yellow oil was afforded upon layering the acetone solution with pentane. This oil, presumed to be *trans*-[Pt₂I₄Me₄(pmxda)], complex **42**, was proposed to be formed by the *trans* oxidative addition of iodine at **40**, scheme 5.23.



Scheme 5.23. The oxidative addition of iodine at **40** to give *trans*-[Pt₂I₄Me₄(pmxda)], complex **42**.

The ¹H NMR spectrum of complex **42** contained two distinct methylplatinum resonances which are observed to be shifted downfield relative to the equatorial methyl resonances of **41**. This is a typical observation in diiododimethylplatinum(IV) complexes as is observed in the case observed in chapter 2 for complex **7a** [52]. The methylplatinum resonances observed at $\delta = 2.11$ and 2.45 ppm each possessed platinum-195 satellites with coupling constant values of $^2J(\text{PtH}) = 74$ Hz. The aromatic region of the spectrum possessed seven resonances which is expected for the *trans* addition product and are assigned and annotated in figure 5.27. The product maintains the symmetry expected of a complex which adopts the *anti* orientation due to the presence of C₂ rotation axis. The proposal of the formation of **42** is further supported by the ESI-MS spectrum in which a molecular ion associated with [Pt₂I₃Me₄(pmxda)]⁺ is observed with $m/z = 1361.04447$ amu.

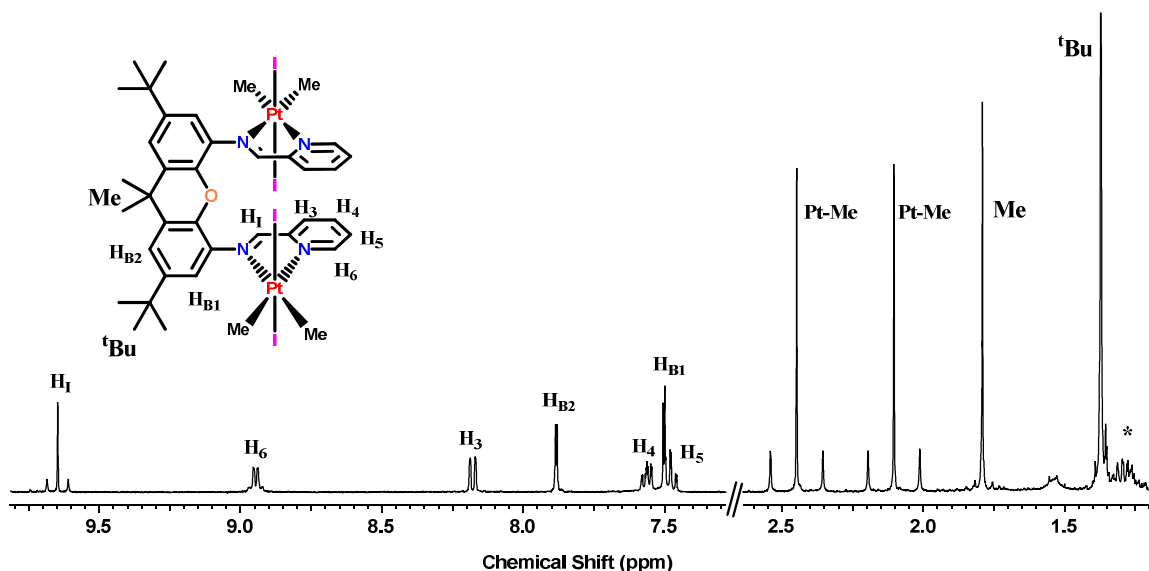


Figure 5.27. ^1H NMR spectrum of **42**, $\text{trans-}[\text{Pt}_2\text{L}_4\text{Me}_4(\text{pmxda})]$, acquired in CD_2Cl_2 . * indicates trace amounts of pentane.

Data was collected on the crystal grown from the vapour diffusion of pentane into a concentrated solution of **42**, by single crystal X-ray diffraction analysis and a solid state structure was defined as observed in figure 5.28. This figure illustrates the structure and connectivity of **42** however the data set could not be refined and as such bond parameters will not be reported. The solid state structure clearly confirms the assignment of **42** being the result of the *trans* oxidative addition of iodine at **40**. It also confirms the proposed *anti* orientation of the metal centers to create an increased platinum-platinum distance which is not favourable for cooperative reactivity. The Pt-I bond lengths range from, 2.62 Å to 2.65 Å, in the molecule which are consistent with those reported previously [52]. Unlike the methyl iodide complex **34b**, the xanthene backbone in **42** does not pucker and maintains a planar rigidity. Rotation of the diimine arms allows for a minimized energy structure to occur which limits the steric interactions between iodide ligands on adjacent metal centers. This rotation also leads to an observed π - π stacking interaction between pyridyl groups with a 3.66 Å separation between adjacent planes. The intermetallic distance is observed to be 7.78 Å which is similar to the distance of **41** and would presumably decrease in the *syn* alignment.

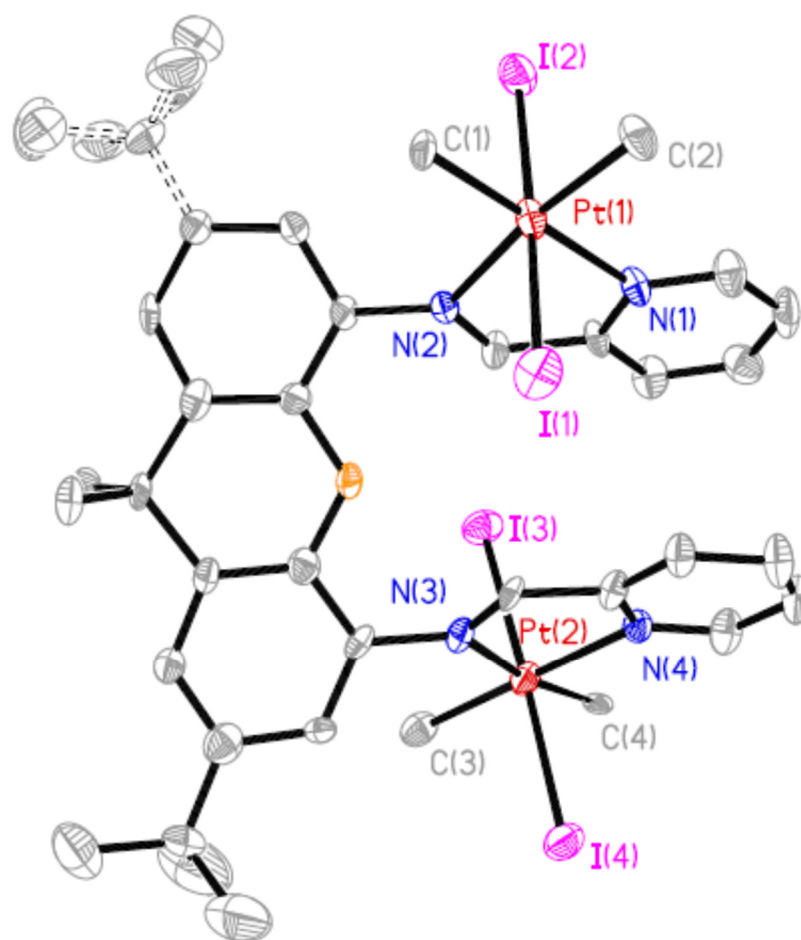
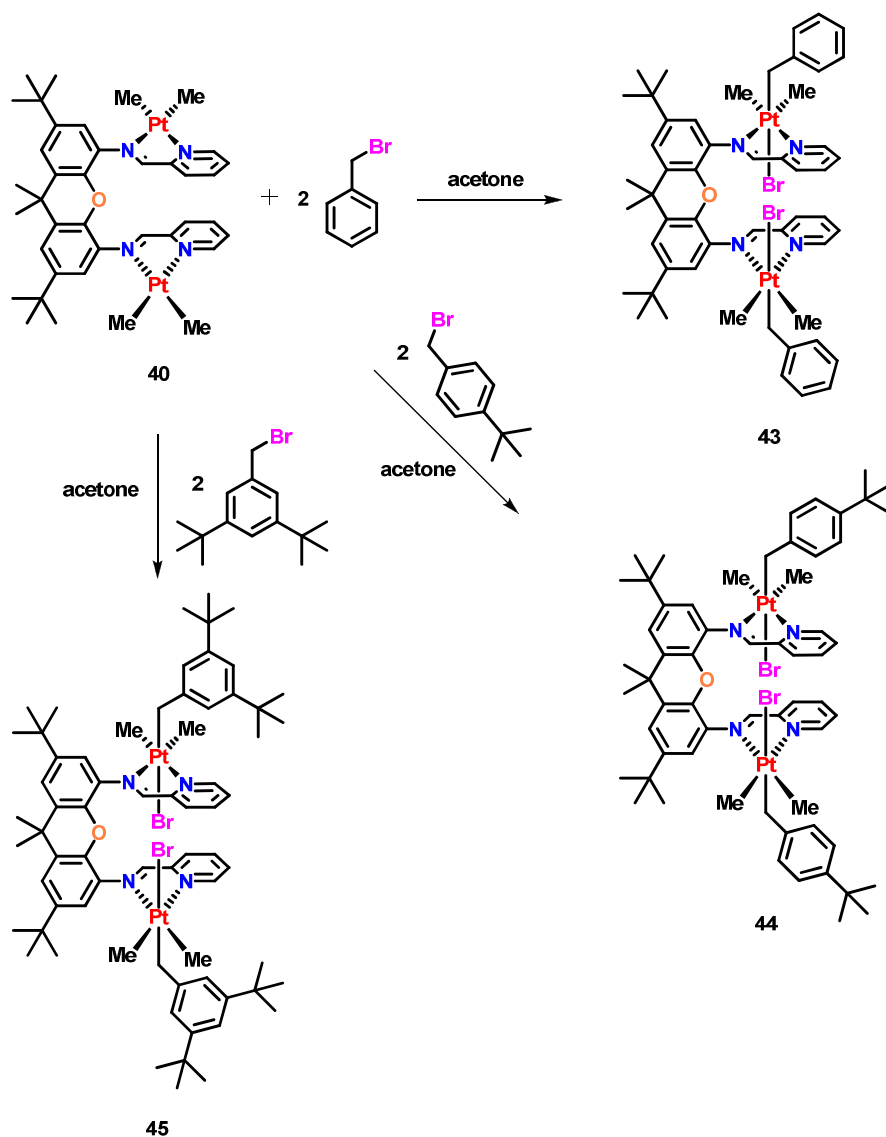


Figure 5.28. Molecular structure of complex **42**, with an atomic numbering scheme. Hydrogen atoms and solvent molecules are omitted for clarity.

It has been shown previously that benzyl bromide derivatives react with dimethylplatinum(II) complexes by *trans* oxidative addition to give the corresponding dimethylplatinum(IV) complexes [51]. By introducing two equivalents of these substrates to complex **40** the oxidative addition reaction should occur at each platinum center giving a bimetallic platinum(IV) complex. With that motivation, the reactivity of **40** towards the oxidative addition of benzyl bromide derivatives is explored as outlined in scheme 5.24.



Scheme 5.24. The formation of complexes **43**, **44**, and **45** via the *trans* oxidative addition of the corresponding benzyl bromides at **40**.

The reaction of **40** with benzyl bromide occurred rapidly to afford $[\text{Pt}_2\text{Br}_2\text{Me}_4(\text{CH}_2\text{-C}_6\text{H}_5)_2(\text{pmda})]$, complex **43** in high yield as a yellow oil. The complex was readily characterized by its ^1H NMR spectrum, figure 5.29, which contained two methylplatinum resonances at $\delta = 1.10$ ppm and $\delta = 1.53$ ppm with coupling constant values of $^2J(\text{PtH}) = 70$ Hz and $^2J(\text{PtH}) = 71$ Hz respectively. These values indicate that the two methyl groups are positioned *trans* to the nitrogen donor atoms of the ligand and support the formation of the *trans* oxidative addition product as proposed. In addition,

two doublet resonances were observed at $\delta = 2.77$ and 3.35 ppm which possessed platinum-195 satellites with coupling constant values of ${}^2J(\text{PtH}) = 80$ Hz and 106 Hz respectively. This AB doublet resonance represents the inequivalent protons that reside on the CH_2 bridge of the benzyl ligand. The aromatic region of the spectrum possessed the typical resonances observed for the ligand **pmxda**, but also contained additional resonances for the aromatic protons of the benzyl ligand. The ${}^1\text{H}$ NMR spectrum provides string evidence for the formation of the *trans* product of oxidative addition and indicates that **43** is also symmetric, which is consistent with the *anti* orientation that is believed to be the most stable isomer of these types of complexes.

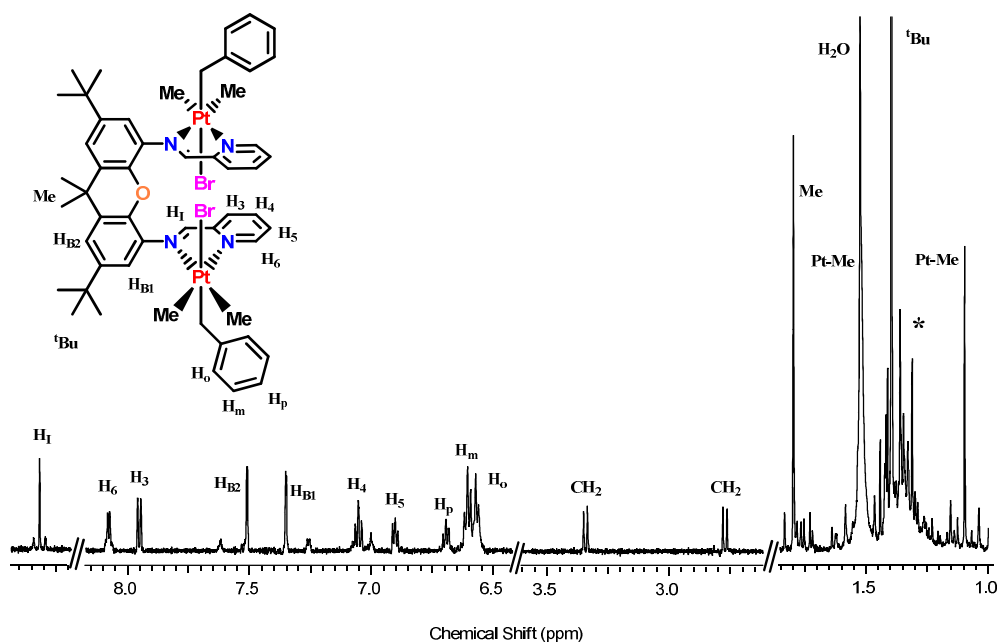


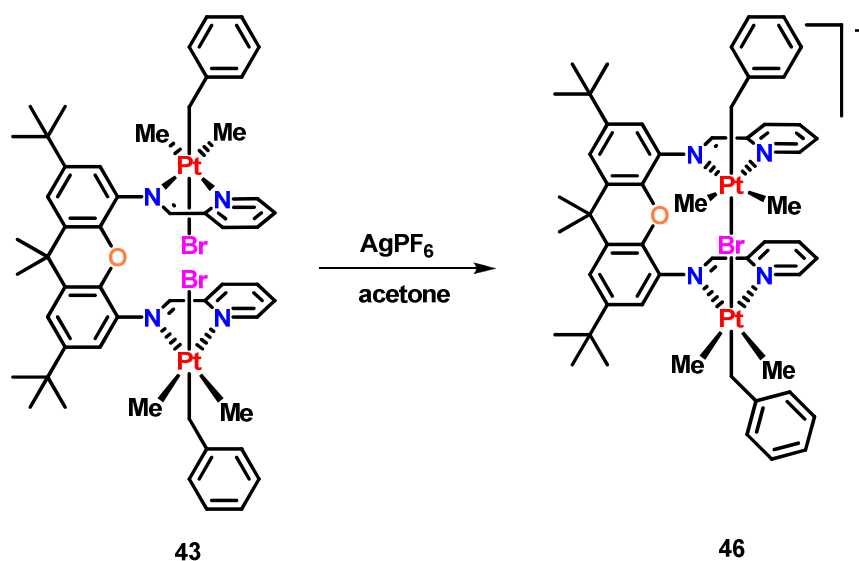
Figure 5.29. ${}^1\text{H}$ NMR spectrum of **43** in CD_2Cl_2 . * indicates trace amounts of pentane in the spectrum.

In a manner similar to the one employed for the synthesis of **43**, two equivalents of 4-*tert*-butylbenzyl bromide were added to an acetone solution of **40** with stirring, affording a bright yellow oil after workup. This oil, complex **44**, was characterized by ${}^1\text{H}$ NMR spectroscopy as the *trans* oxidative addition product, $[\text{Pt}_2\text{Br}_2\text{Me}_4(4\text{-CH}_2\text{-C}_6\text{H}_4\text{-C}(\text{CH}_3)_3)_2(\text{pmxda})]$. The observation of two methylplatinum resonances, $\delta = 1.07$ ppm, ${}^2J(\text{PtH}) = 69$ Hz and $\delta = 1.54$ ppm, ${}^2J(\text{PtH}) = 71$ Hz, is consistent with the formation of a product in which both methyl groups are *trans* to the nitrogen atoms of the ligand. A

similar AB doublet is observed due to the presence of the CH₂ bridge of the *tert*-butylbenzyl group and as well the aromatic protons of this ligand are observed in the spectrum. The formation of this complex, **44**, was further supported via ESI-MS spectral analysis which identified the molecular ion as [Pt₂BrMe₄(4-CH₂-C₆H₄-C(CH₃)₃)₂-(pmxda)]⁺ through the loss of a bromide ligand, m/z = 1353.47682 amu.

The formation of **45**, [Pt₂Br₂Me₄(3,5-CH₂-C₆H₃-(C(CH₃)₃)₂)₂(pmxda)], was also confirmed by ¹H NMR and ESI-MS spectra, after two equivalents of 3,5-di-*tert*-butylbenzyl bromide was added to an acetone solution of **40**. The ¹H NMR spectrum possessed again two methylplatinum resonances with chemical shifts and coupling constants consistent with those observed in the case of **43** and **44**. The data for **45** would suggest that product is again formed via the *trans* oxidative addition of the substrate at **40** as outlined in scheme 5.24. Unfortunately, no solid state structural analysis was able to be performed on these complexes as single crystals could not be grown. Despite this, the ¹H NMR and ESI-MS data provided diagnostic evidence that the complexes **43**, **44**, and **45** adopt the *trans* geometry as proposed and is also consistent with the literature [51].

The preference observed towards the formation of the *anti* isomer in the above cases yields diplatinum(IV) complexes in which the two platinum centers are separated by a large distance which would hinder the ability of cooperative interactions. By removing one or more equivalents of the halide ligands in the diplatinum(IV) complexes one could access a potentially bridged bimetallic complex of the ligand **pmxda** in which the pyridyl groups would need to be positioned *syn* with respect to each other to accommodate the bridging ligand. It is with this motivation that an acetone solution of complex **43**, formed from the oxidative addition of benzyl bromide at **40**, was treated with one equivalent of silver hexafluorophosphate and allowed to stir for one hour, scheme 5.25. It was proposed that the abstraction of one of the bromide ligands would lead to the formation of a complex possessing a bridging bromide between two platinum centers, **46** in scheme 5.25. In order to form this complex the ligand arms would have to adopt the *syn* orientation in order to accommodate both the linearity and distance requirements.



Scheme 5.25. Proposed synthesis of a bridged diplatinum(IV) complex, **46**, through a halide abstraction from **43**.

After stirring for one hour, the yellow solution was filtered to remove the silver bromide that precipitated from solution. The solvent acetone was then removed in *vacuo* and the resultant yellow oil was then dissolved in acetone-*d*₆ in order for a ¹H NMR spectrum to be acquired, figure 5.30. Based on the ¹H NMR spectrum, the reaction appeared to produce one major product. This product gave rise to two methylplatinum resonances at $\delta = 1.09$ ppm and 1.52 ppm, with coupling constant values of $^2J(\text{PtH}) = 70$ Hz and 72 Hz respectively. These values are typical for platinum(IV) species' in which the methyl groups are positioned *trans* to nitrogen atoms of the ligand backbone and are different than those observed for the parent complex, **43**. The methylene protons of the benzyl fragments were both observed to possess platinum-195 satellites with coupling constants $^2J(\text{PtH}) = 82$ Hz and $^2J(\text{PtH}) = 107$ Hz, diagnostic of the CH₂ groups being positioned *trans* to a halide ligand. The aromatic region of the spectrum possessed resonances arising due to both the incorporation of the benzyl group as well as the ligand. The number of resonances supports the formation of a symmetric complex and through the use of gCOSY NMR spectra can be assigned and is annotated as such in figure 5.30. The presence of the hexafluorophosphate counter anion was observed in ³¹P and ¹⁹F

NMR spectra acquired. The ^1H NMR spectrum supports the formation of a complex as proposed in scheme 5.25, however this assignment is only tentative in the absence of a solid state structure.

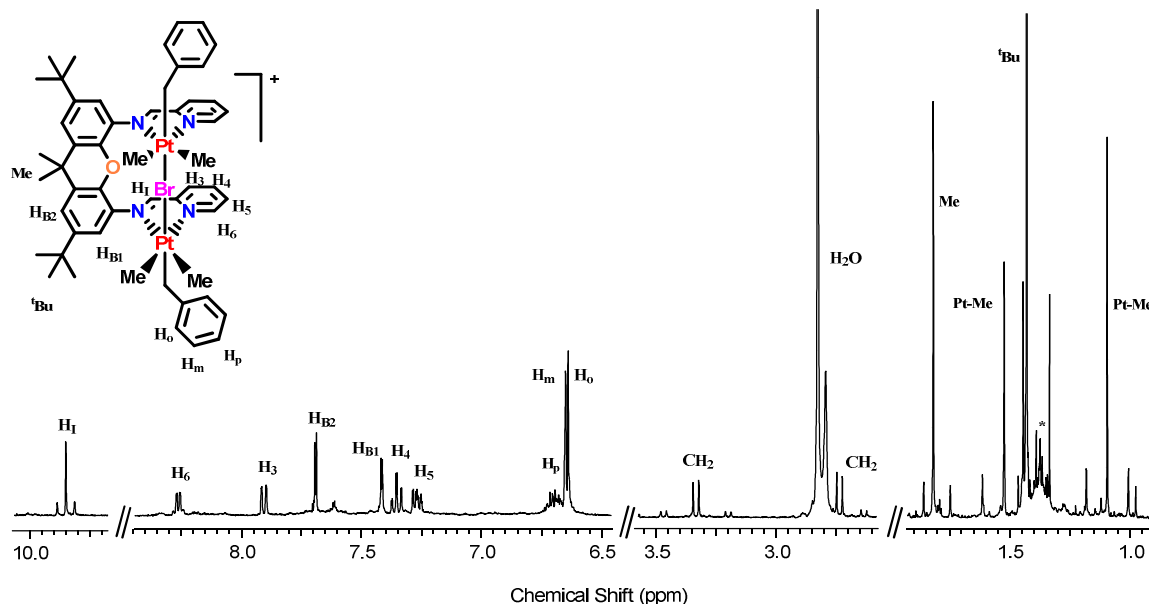


Figure 5.30. ^1H NMR spectrum of a potentially bromide-bridged diplatinum complex, **46**. * indicates the presence of residual pentane solvent.

In order to determine the viability of a diplatinum(IV) complex in which the pyridyl rings are oriented in a *syn* manner and therefore the metal centers are aligned more linearly, an experiment by which a bridging ligand is introduced was explored. The idea being that by introducing two equivalents of silver triflate to complex **41**, a vacant coordination site would be made available at each platinum center. Work with the **ppxda** ligand system indicated the formation of an initial diaqua complex **38a/38b**, in which the aqua ligands can be displaced by a better donor ligand. If the ligand utilized is pyrazine, or something with two donor atoms, the possibility of forming a bridged bimetallic platinum(IV) complex is possible. To that end, two equivalents of silver triflate were added to an acetone solution of **41**. After stirring the reaction mixture for an hour, the yellow solution was filtered to remove the silver iodide formed. After a quick workup, a yellow solid was isolated and a ^1H NMR spectrum was acquired, figure 5.31. Similar to that of **38a/38b** the spectrum exhibited broadened methylplatinum and aromatic

resonances. The two methylplatinum resonances furthest upfield are observed to overlap as a broad signal at $\delta = 0.88$ ppm and slightly downfield of that the third methylplatinum resonance was observed at $\delta = 1.30$ ppm. An additional new broad resonance is observed at $\delta = 6.36$ ppm and has a relative integration value of four. This resonance is attributed to the presence of two aqua ligands to indicate the formation of complex **47**, scheme 5.26, the analogous species to **38a/38b** observed previously. This determination was supported by the ESI-MS analysis which identifies **47**, $[\text{Pt}_2\text{Me}_4(\text{OH}_2)_2(\text{pmxda})][\text{O}_3\text{SCF}_3]_2$, as the molecular ion with $m/z = 1027.3750$ amu.

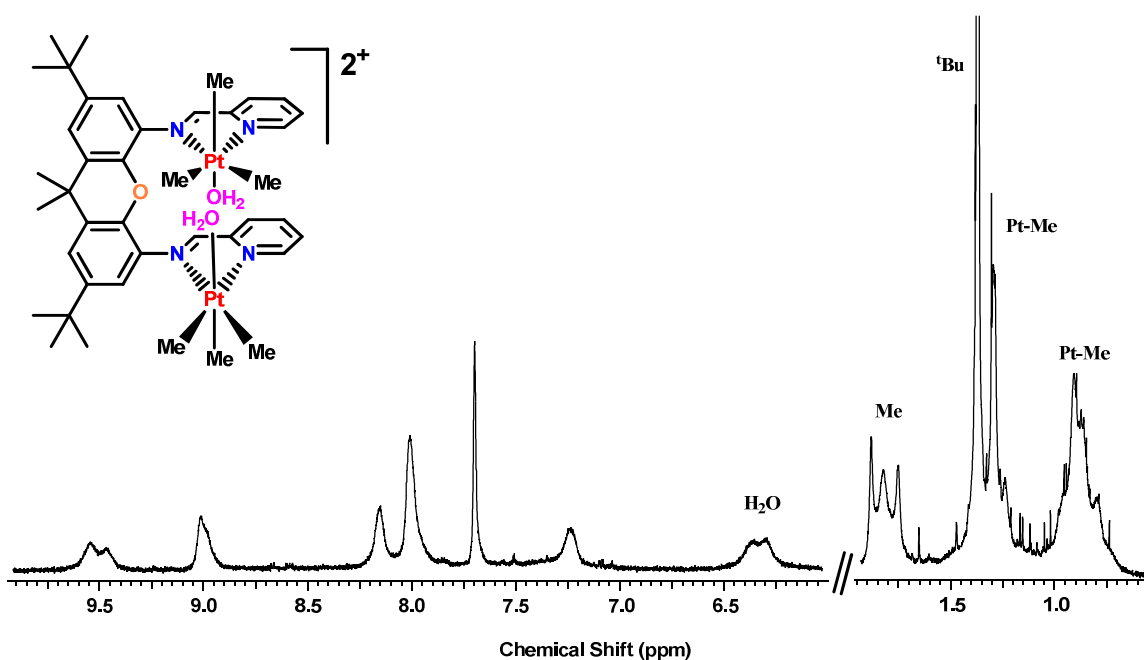
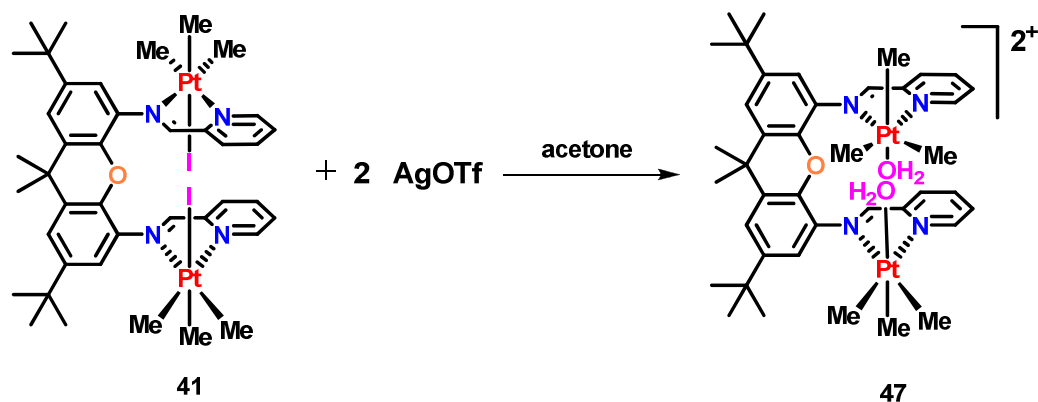


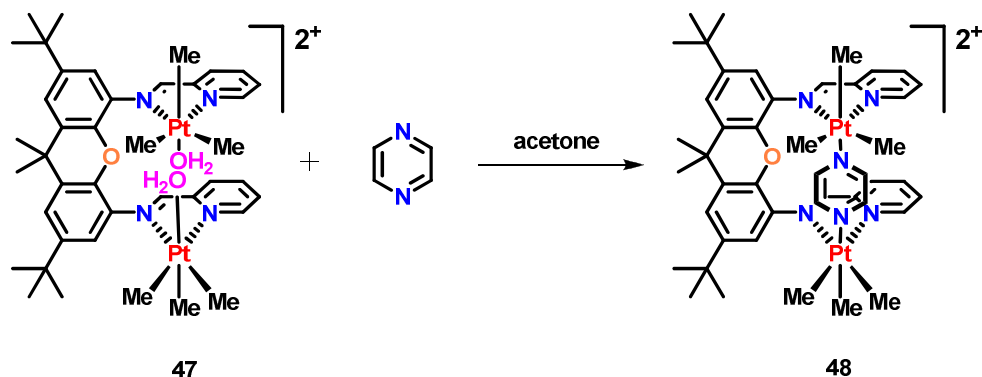
Figure 5.31. ^1H NMR spectrum of **47** acquired in acetone- d_6 .



Scheme 5.26. The preparation of the diaqua complex **47** via a halide abstraction of **41**. Trifluoromethanesulfonate counteranions omitted for clarity.

With the diaqua complex **47** in hand, a half equivalent of pyrazine was added to a dichloromethane- d_2 solution, scheme 5.27. The ^1H NMR spectrum, figure 5.32, of the bright yellow solution indicated the increased resolution of all resonances as the bridged pyrazine complex, **48** $[\text{Pt}_2\text{Me}_4(\text{C}_4\text{H}_4\text{N}_2)(\text{pmxda})][\text{O}_3\text{SCF}_3]_2$, was formed *in situ*. The furthest upfield methylplatinum resonance at $\delta = 1.01$ ppm is observed to have platinum-195 satellites with coupling constant value $^2J(\text{PtH}) = 72$ Hz whereas the remaining two resonances slightly downfield at $\delta = 1.27$ and 1.48 ppm have values of 70 Hz. This would suggest the most upfield resonance be a result of the methyl group in the axial position *trans* to the pyrazine nitrogen atom. The aromatic region of the spectrum possesses the seven resonances expected as a result of the ligand, but also two new resonances each with a relative integration value of two. These broad singlet resonances at $\delta = 8.20$ and 8.75 ppm are a result of the incorporation of pyrazine, and indicate that the protons of this ring are not in equivalent environments. It seem plausible that two protons would be directed inward towards the xanthene ligand core and as such experience different electronic and steric effects making them magnetically and chemically inequivalent from the two outward directed protons. Pentane solvent vapour was then allowed to diffuse into the yellow dichloromethane solution of **48** which led to the formation of yellow prismatic single crystals. Data was collected on the crystals by single crystal X-ray diffraction analysis, and a solid state structure was defined as observed in figure 5.33. This figure illustrates the structure and connectivity of **48**.

However, the data set could not be refined and as such bond parameters will not be reported. The solid state structure of **48** clearly depicts the more linear arrangement of the platinum centers as they are bridged by the pyrazine ligand. This proves the proposed *syn* arrangement of **48** in scheme 5.27. The platinum-nitrogen distances of 2.13 Å and 2.23 Å are typical lengths for this type of interaction. The diimine arms are observed to bow away from the pyrazine to accommodate its size within the pocket of the **pmxda** ligand. This flexibility allows for a deviation from linearity in terms of the C(3)-Pt(1)-N(5)-N(6)-Pt(2)-C(6) linker away from an expected 180° angle to accommodate the pyrazine bridge. The two pyridyl rings bow away from each other giving an interplanar spacing of 3.78 Å as measured from centroid to centroid. The two platinum centers are separated by 6.73 Å as a result of this bowing which would presumably be shortened by the incorporation of a shorter single atom bridge. Even at this distance, the complex shows distinct promise in the ability to undergo cooperative reactivity as the metal center separation is well with the established distance requirements.



Scheme 5.27. Formation of the pyrazine bridged diplatinum(IV) complex, **48**.
Counteranions omitted for clarity.

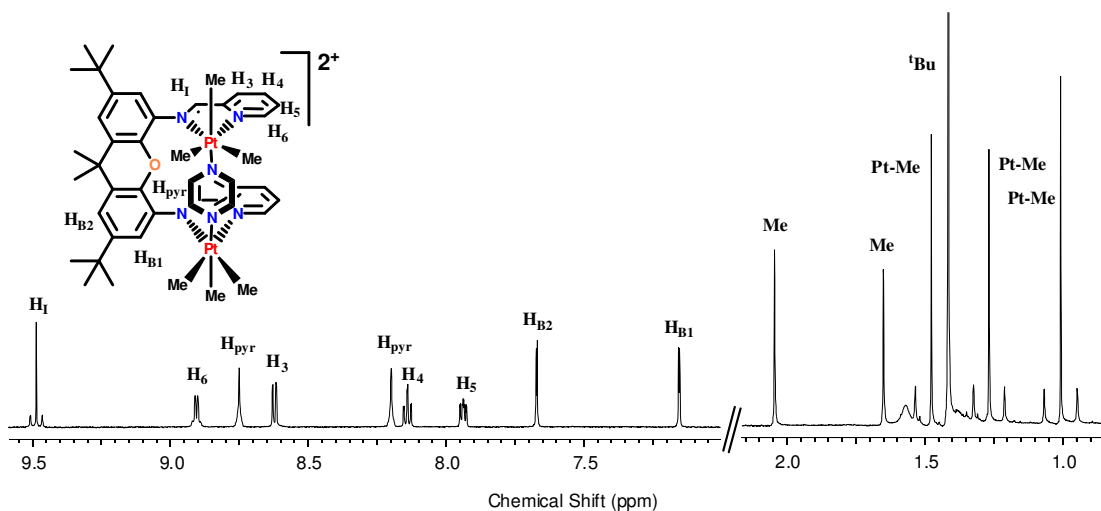


Figure 5.32. ^1H NMR spectrum of the pyrazine bridged diplatinum(IV) complex **48** in CD_2Cl_2 .

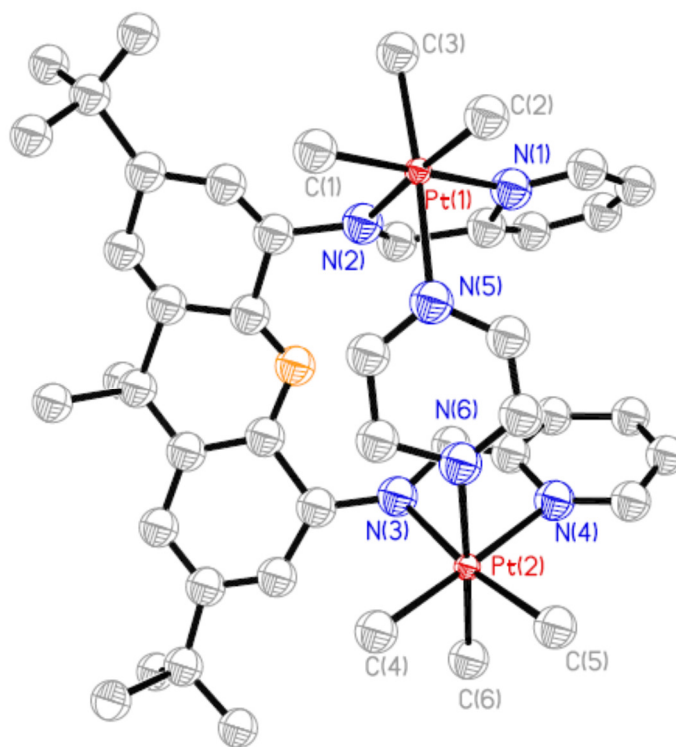
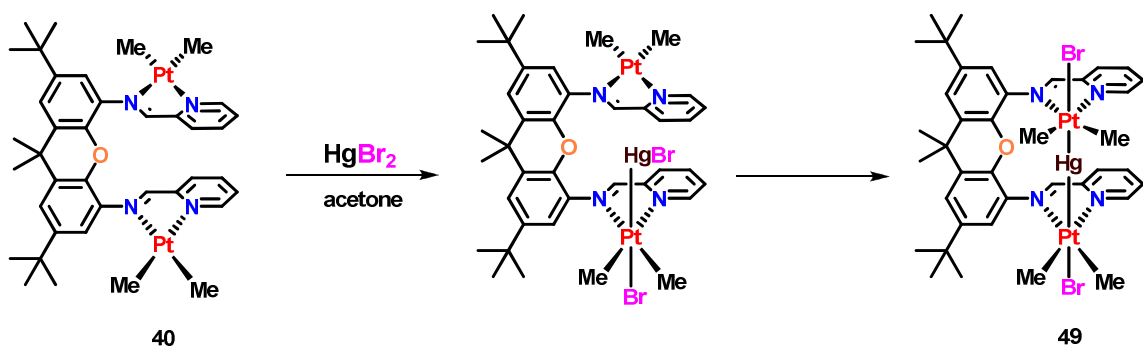


Figure 5.33. Molecular structure of complex **48**, with an atomic numbering scheme. Hydrogen atoms, solvent molecules and trifluoromethanesulfonate counteranions omitted for clarity.

As the bimetallic platinum complexes of the ligand **pmxda** are observed to be able to easily accommodate the *syn* orientation, as evidenced by the structure of **48**, the cooperative reactivity of **40** was investigated. It was proposed that by introducing a bifunctional substrate which would interact at both platinum centers, the *syn* orientation would be adopted and each metal center would be involved in the reactivity. To that end, mercury(II) halide complexes have been observed to undergo oxidative addition in a *trans* manner at platinum(II) complexes giving a linear X-Pt-Hg-X arrangement. By oxidatively adding one equivalent of a mercuric halide at one of the platinum(II) centers, the second Hg-X bond could be positioned effectively for a second oxidative addition event and lead to the formation of a linear X-Pt-Hg-Pt-X arrangement as proposed in scheme 5.28.



Scheme 5.28. The oxidative addition of mercuric bromide giving **49**, the potentially mercury bridged diplatinum complex.

With that motivation, an acetone solution of **40** was treated with half an equivalent of mercuric bromide. The originally purple solution became a bright red colour and gradually a vibrant orange solid precipitated from solution. This solid was sparingly soluble in acetone and after filtering the solid and washing with pentane, a portion was dissolved in acetone- d_6 and a ^1H NMR spectrum was acquired. The ^1H NMR spectrum, figure 5.34, indicated that the two dimethylplatinum(II) centers had indeed been oxidized yielding two dimethylplatinum(IV) groups with resonances arising at $\delta = 1.01$ and 1.51 ppm. Both of these resonances possessed the expected platinum-195 satellites both with coupling constant values of $^2J(\text{PtH}) = 62$ Hz which is typical for platinum(IV) complexes containing mercury as a ligand. Also additional satellites due to

mercury-199 are observed on the methylplatinum resonances with $^3J(\text{HgH}) = 12 \text{ Hz}$ for both which indicates that the Pt-Hg moiety is indeed bonded rather than a donor-acceptor interaction occurring. The aromatic region of the spectrum possessed the seven resonances typically observed for platinum(IV) complexes of the **pmxda** ligand supporting the formation of a symmetric species. In order for this complex to maintain symmetry, oxidative addition across both Hg-Br bonds must have occurred at each platinum center giving a *syn* arrangement of the pyridyl groups. If the oxidative addition event occurred only at one platinum center, the complex would be unsymmetrical and one platinum center would be platinum(IV) and the other platinum(II), giving two sets of methylplatinum resonances in the NMR spectrum with very different coupling constant values. The other possible way in which a symmetric complex could form would be through the oxidative addition of an equivalent of HgBr₂ at each platinum center. This is not supported by ESI-MS which indicated that the molecular contained only a single mercury atom as is true for the case of **49**. The molecular ion was observed to be [C₃₉H₅₀HgN₄OPt₂Br]⁺ formed by the loss of a bromide ligand with $m/z = 1261.21478$ amu. This observation along with the ¹H NMR spectrum supports the formation of **49** through the oxidative addition of an Hg-Br bond at each platinum center.

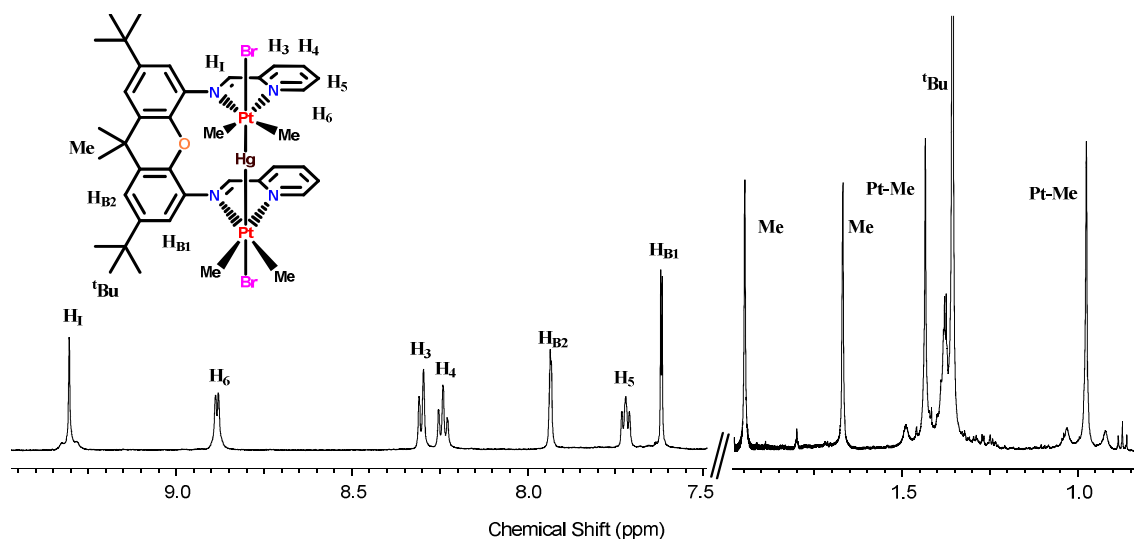


Figure 5.34. ¹H NMR spectrum of **49** acquired in acetone-*d*₆.

5.14 Conclusions

The design, synthesis and characterization of two ligands based on an anthracene backbone were outlined in this chapter. The first ligand, **bpad**, was prepared by the condensation reaction between 2-pyridinecarboxaldehyde and 1,8-diamionanthracene. This ligand was shown to complex two equivalents of dimethylplatinum(II) centers to give a bimetallic complex, complex **26**. This complex was shown to decompose over time at room temperature in both atmospheric and inert environments. Although the manner of decomposition was not identified as the product could not be characterized, it is believed that the proximity of the platinum center to the anthracene backbone leads to its decomposition through a metalation event. The reactivity of **26** towards the oxidative addition of methyl iodide was explored. Upon initial oxidation of **26** by methyl iodide, the formation of the decomposition product was immediately observed. By oxidizing the platinum center to platinum(IV) prior to coordination of the ligand, a bimetallic platinum(IV) complex of the ligand **bpad** was afforded, complex **27**. This complex could be characterized by ^1H NMR analysis but was again shown to decompose overtime. Similar reactivity was also observed for the oxidative addition of 3,5-di-*tert*-butylbenzyl bromide at **26** giving the product of decomposition. The pre-oxidation of the platinum(II) center prior to coordination of the ligand gave the resultant diplatinum(IV) complex **28**. The degradation of these complexes and relative instability did not allow for structure determination or full reactivity study.

The installation of coordinating sites more distal from the anthracene backbone was proposed to address the decomposition event. As such the ligand **adpa** was prepared via the Sonagashira coupling of an alkynyl moiety and 1,8-dibromoanthracene. The ligand **adpa** was shown to coordinate two equivalents of a platinum(II) center giving rise to the bimetallic platinum complex, **29**. Complex **29** was shown to be stable for prolonged periods of time and no evidence of a degradation product was observed. This supports the proposal of the proximity of the platinum centers in **26** to the anthracene backbone leading to the decomposition. Complex **29** was shown to react rapidly with both methyl iodide and 3,5-di-*tert*-butylbenzyl bromide giving rise to the bimetallic organoplatinum(IV) complexes **30** and **31**. These bimetallic organoplatinum(IV)

complexes were unable to be characterized by X-ray crystallography and as such their formation as the product of *trans* oxidative addition is proposed by ^1H NMR and mass spectrometric analysis only.

The ability of the metal centers in **29** to react cooperatively was examined by the reaction of **29** with half an equivalent of a bifunctional substrate, 1,2-dibromoxylene. The product, complex **32**, was proposed to be the result of an oxidative addition event occurring at each platinum(II) center. This would give rise to a bimetallic organoplatinum(IV) complex with a xylene bridge between the two platinum centers. The formation of this complex is supported by ^1H NMR analysis but no solid state structural analysis was able to be performed on this complex.

The use of anthracene as a backbone provides the opportunity to design ligands capable of complexing two platinum centers within a close proximity such that they may react cooperatively. Although the separation between metal centers is sufficient, a more flexible ligand backbone which is functionalized in a facile way would be more advantageous.

The functionalized and somewhat flexible xanthene backbone was used in the design of the second generation ligands. The first xanthene derived ligand, **ppxda**, was prepared in high yield after four steps. This ligand was shown to complex two equivalents of a dimethylplatinum(II) center to give the bimetallic complex, complex **33**. Complex **33** was shown to be able to adopt two isomeric forms, one in which the pyridyl resonances are positioned directly atop one another in a *syn* manner and the other the more thermodynamically preferred *anti* isomer. As such the reactivity towards oxidative addition yielded products which were also isomeric. The oxidative addition of methyl iodide gave a mixture of isomers at room temperature, both **34a** and **34b**. Variable temperature NMR experiments were used to determine the identity of each isomer. It was also found that the *anti* arrangement observed in **34b** was preferred. The structure was confirmed in the solid state by single crystal X-ray diffraction analysis showing the overall *trans* oxidative addition product. Similar oxidative addition reactions were

performed with benzyl bromide derivatives to give complexes **35a/35b** and **36a/36b** in isomeric mixtures.

The ability to form bimetallic complexes in which the ligand adopted the *syn* conformation was investigated by first exposing **36a/36b** to a halide abstraction event. This in turn gave rise to **37**, the bromide bridged analogue of **36a/b**, in which the two platinum centers were arranged linearly and joined together via a bromide ion bridge. This arrangement would provide the most proximal orientation of the platinum centers and would be beneficial to cooperative reactivity. This was then further investigated by forming the diaqua complex **38** through two halide abstractions at complex **34b**. This diaqua complex was shown to react in a facile manner with pyrazine giving the pyrazine bridged diplatinum complex **39** in which a nitrogen donor atom on pyrazine bonded directly to both platinum centers.

The high amount of rotational freedom allowed by **ppxda** was removed in the design of the second xanthene derived ligand **pmxda**. This ligand, prepared in two steps, was shown to easily coordinate two equivalents of a dimethylplatinum(II) center, **40**, in a proposed *anti* arrangement. Similar to its long linker analogue, **40** was shown to oxidatively add two equivalents of both iodine and methyl iodide giving rise to both **42** and **41** respectively. Both complexes were confirmed as the products of the *trans* oxidative addition of the respective substrates, and were observed to adopt the thermodynamically preferred *anti* orientation. Complex **40** underwent simple oxidative addition chemistry with benzyl bromide and its derivatives to give the corresponding dimethylplatinum(IV) complexes in high yield. Complex **43** formed by the oxidative addition of benzyl bromide was observed to give the bridged bromide complex **46** upon halide atom abstraction. This ability to form the *syn* orientation of a complex was then proven in the solid state after complex **41** was treated with two equivalents of silver trifluoromethanesulfonate to give the diaqua complex **47**. This complex again reacted rapidly with pyrazine to give **48**, in which the pyrazine ligand bonded to both platinum centers and was observed in the solid state to form the bimetallic bridged complex in the *syn* orientation. Finally the cooperative reactivity of **40** was examined when it was treated with half an equivalent of the bifunctional substrate, HgBr₂. ¹H NMR and ESI-

MS data both support the formation of the mercury bridged diplatinum(IV) complex, **49**. This complex is proposed to be formed by two oxidative addition events occurring using the same mercuric bromide molecule as a substrate. Unfortunately the structure of **49** was not confirmed in the solid state.

Both anthracene and xanthene based scaffolds were found to be sufficient backbones for the design of diplatinum complexes. The ability to functionalize and tailor the xanthenes, along with their ease of synthesis and enhanced solubility make them better candidates than the anthracene systems. Complexes of this type should be excellent candidates for bimetallic catalysis and as such their cooperative reactivity should be investigated further.

5.15 Experimental:

Reagents and General Procedures. All reactions were carried out in an inert atmosphere of dry nitrogen using standard Schlenk techniques, unless otherwise specified. All solvents used for air and moisture sensitive materials were purified using an Innovative Technology Inc. *PURE SOLV* solvent purification system (SPS). The complexes *cis/trans*-[PtCl₂(SMe₂)₂] and [Pt₂Me₄(μ-SMe₂)₂] were prepared from K₂[PtCl₄] according to the literature [48]. NMR spectra were recorded at ambient temperature, unless otherwise noted (ca. 25°C), on Varian Mercury 400 or Varian Inova 400 or 600 spectrometers. ¹H chemical shifts are reported relative to TMS (¹H). Complete assignment of each compound was aided by the use of ¹H-¹H NOESY, ¹H-¹³C{¹H}-HSQC and ¹H-¹H gCOSY experiments. The standard labeling schemes for pyridyl rings are utilized when labeling signals in NMR spectroscopic analysis. Mass spectrometric analysis was carried out using an electrospray PE-Sciex Mass Spectrometer (ESI-MS) coupled with a TOF detector.

X-ray Crystallography. The crystallography for this chapter was performed by Dr. Paul D. Boyle. A suitable crystal of each compound was coated in Paratone oil and mounted on a glass fiber loop. X-ray data for compounds **34b**, **41**, **42**, and **48** were collected at 150K with ω and φ scans on a Bruker Smart Apex II diffractometer using graphite-monochromated MoK α radiation ($\lambda = 0.71073 \text{ \AA}$) and Bruker SMART software [53]. Unit cell parameters were calculated and refined from the full data set. Cell refinement and data reduction were performed using the Bruker APEX2 and SAINT programs respectively [54]. Reflections were scaled and corrected for absorption effects using SADABS [55]. All structures were solved by direct methods with SHELXS [56] and refined by full-matrix least-squares techniques against F^2 using SHELXL [57]. All non-hydrogen atoms were refined anisotropically. The hydrogen atoms were placed in calculated positions and refined using the riding model.

1,8-diaminoanthracene-9,10(4aH,9aH)-dione, (A). The synthesis follows a procedure similar to that of Gozin [58]. In a round bottomed flask was added 16.0g, (66.67mol) of Na₂S.9H₂O and subsequently dissolved in 300mL of H₂O. To this was added 5.0g, (16.766mol) of dinitroanthraquinone dissolved in 100mL of ethanol. The mixture was

subsequently refluxed for 12hr with stirring, cooled to room temperature and then poured into 300mL of ice/water. The deep red-purple product was then collected via vacuum filtration and washed with water and then dried *in vacuo*. The product can be recrystallized from ethanol affording a 98% yield. **¹H NMR in dmsO-d₆**: δ 7.16 (br. s, 2H), 7.35 (br. s, 2H), 7.45 (br. s, 2H), 7.86 (br. S, 4H). **EI-MS** [C₁₄H₁₀N₂O₂]⁺: calculated m/z = 238; determined m/z = 238.1.

1,8-diaminoanthracene, (B). The synthesis is derived from procedures similar of Gozin *et. al.*¹ and Love *et. al.*² [42,58]. A major modification is that the reaction should be performed in the absence of light to avoid an undesired intramolecular reaction of the product. In a round bottomed flask under an N₂ atmosphere was added diaminoanthraquinone (3.66g, 0.0154mol), NaOH (0.133g, 0.0033mol) and isopropanol, 150mL. To this was added carefully and portion wise sodium borohydride (6.33g, 0.1673mol). The mixture was then heated to reflux for 60 hours and subsequently poured into an ice/water mixture (300mL). The precipitate was then collected by vacuum filtration, washed with water and dried *in vacuo*. The crude product was purified by flask column chromatography (9:1 chloroform to methanol) affording 1,8-diaminoanthracene as a red-brown solid in 95% yield. **¹H NMR in dmsO-d₆**: δ 5.84 (br. s, 4H), 6.55 (t, ³J = 4Hz, 2H), 7.18 (d, ³J = 4Hz, 4H), 8.16 (s, 1H), 8.79 (s, 1H). **EI-MS** [C₁₄H₁₂N₂]⁺: calculated m/z = 207.1; determined m/z = 208.1.

(N¹E, N⁸E)-N¹,N⁸-bis(pyridin-2-ylmethylene)anthracene-1,8-diamine, (bpad). In a round bottom flask was added a toluene solution of 1,8-diaminoanthracene, (0.500g, 2.392mmol). To this solution with stirring was added two equivalents of 2-pyridinecarboxaldehyde, (0.455mL, 4.785mmol). The mixture was then heated to reflux and using a Dean-Stark apparatus the resultant water produced during the imine condensation reaction was collected and removed from the system. After heating the mixture for 12 hours, the volume of the brown solution was reduced *in vacuo*, dissolved in acetone and concentrated on vacuum before addition of pentane lead to the precipitation of the product in moderate yield, 72%. **¹H NMR in CDCl₃**: δ 7.16 (d, ³J = 7Hz, 2H), 7.45 (dd, ³J = 5Hz, ³J = 7Hz, 2H), 7.52 (dd, ³J = 7Hz, ³J = 9Hz, 2H), 7.81 (dd, ³J = 7Hz, ³J = 7Hz, 2H), 7.97 (d, ³J = 9Hz, 2H), 8.48 (d, ³J = 7Hz, 2H), 8.48 (s, 1H), 8.76

(d, $^3J = 5\text{Hz}$, 2H), 8.79 (s, 2H), 9.44 (s, 1H). **ESI-MS(TOF):** $[\text{C}_{26}\text{H}_{18}\text{N}_4]^+$ Calculated $m/z = 386$; determined $m/z = 386.3$. **Elemental Analysis:** Anal. Calc'd. $\text{C}_{26}\text{H}_{18}\text{N}_4 \cdot 0.5 \text{CH}_2\text{Cl}_2(\%)$: C, 74.46; H, 4.48; N: 12.94%. Found: C, 74.21; H, 4.46; N, 13.06%.

[Pt₂Me₄(bpad)], complex 26. A dry toluene solution of the Pt(II) dimer, $[\text{Pt}_2\text{Me}_4(\mu\text{-SMe}_2)_2]$, (0.100g, 0.174mmol), was charged with an equivalent of **bpad** dissolved in toluene, (0.067g, 0.174mmol). The mixture was stirred and immediately turned deep purple in colour and was subsequently stirred for 3hr. The solvent volume of the resultant suspension was then removed in *vacuo*, after which the product was dissolved in minimal acetone and layered with pentane to affect the precipitation of a purple solid which was collected using vacuum filtration and washed with pentane, yielding complex **26** as a purple solid in 81% yield. **¹H NMR in acetone-*d*₆:** δ 0.36 (s, $^2J(\text{PtH}) = 88\text{Hz}$, 6H, Pt-Me), 0.95 (s, $^2J(\text{PtH}) = 86\text{Hz}$, 6H, Pt-Me), 7.30 (d, $^3J = 7\text{Hz}$, 2H, H_o), 7.64 (dd, $^3J = 7\text{Hz}$, $^3J = 9\text{Hz}$, 2H, H_m), 7.85 (dd, $^3J = 6\text{Hz}$, $^3J = 8\text{Hz}$, 2H, H₅), 8.09 (d, $^3J = 9\text{Hz}$, 2H, H_p), 8.15 (d, $^3J = 8\text{Hz}$, 2H, H₃), 8.39 (dd, $^3J = 8\text{Hz}$, $^3J = 8\text{Hz}$, 2H, H₄), 8.68 (s, 1H, H_b¹), 9.05 (d, $^3J = 5\text{Hz}$, $^3J(\text{PtH}) = 25\text{Hz}$, 2H, H₅), 9.43 (s, 1H, H_b²), 9.76 (s, $^3J = 33\text{Hz}$, 2H, H_i). **ESI-MS(TOF):** $[\text{C}_{30}\text{H}_{30}\text{N}_4\text{Pt}_2\text{Na}]^+$ Calculated $m/z = 859.2$; determined $m/z = 859.16525$.

[Pt₂I₂Me₆(bpad)], complex 27. To an acetone solution of $[\text{Pt}_2\text{Me}_4(\mu\text{-SMe}_2)_2]$, (0.010g, 0.0174mmol), was added an excess of methyl iodide, (500 μL). After stirring for two hours to afford $[\text{PtIME}_3(\text{SMe}_2)_2]$, **D**, the acetone solvent was removed and the resultant oil was washed with diethyl ether to remove any excess methyl iodide. Complex **D** was then dissolved in dry toluene and charged with a half equivalent of **bpad** dissolved in toluene, (0.0034g, 0.0087mmol). The mixture was stirred for one hour over which time the solution became a yellow colour with some slight formation of a black precipitate. After gravity filtering off the black precipitate, the toluene solvent was removed under reduced pressure affording a yellow oil. This oil was found to be sparingly soluble in dmso and was determined to be produce in a 78% yield. **¹H NMR in dmso-*d*₆:** δ 0.44 (s, $^2J(\text{PtH}) = 72\text{Hz}$, 6H), 0.83 (s, $^2J(\text{PtH}) = 71\text{Hz}$, 6H), 1.36 (s, $^2J(\text{PtH}) = 71\text{Hz}$, 6H), 6.56 (s, 1H, H_b²), 7.75 (dd, $^3J = 7\text{Hz}$, $^3J = 5\text{Hz}$, 2H, H₅), 7.87 (d, $^3J = 9\text{Hz}$, 2H, H_o), 8.05 (d, $^3J = 7\text{Hz}$, 2H, H₃), 8.25 (dd, $^3J = 9\text{Hz}$, $^3J = 9\text{Hz}$, 2H, H_m), 8.31 (dd, $^3J = 7\text{Hz}$, $^3J = 7\text{Hz}$, 2H, H₄), 8.58 (d, $^3J = 9\text{Hz}$, 2H, H_p), 8.88 (d, $^3J = 5\text{Hz}$, $^3J(\text{PtH}) = 19\text{Hz}$, 2H, H₆), 8.97 (s, 1H,

H_b¹), 9.57 (s, ³J = 30Hz, 2H, H_i). **ESI-MS(TOF):** [C₃₂H₃₆IN₄Pt₂]⁺ Calculated m/z = 993.13; determined m/z = 993.12694.

[Pt₂Br₂Me₄(CH₂-3,5-di-^tBu(C₆H₃))₂(bpad)], complex 28. To an acetone solution of [Pt₂Me₄(μ-SMe₂)₂], (0.010g, 0.0174mmol), was added a slight excess of 3,5-di-*tert*-butylbenzyl bromide, (0.01016g). After stirring for three hours to afford [PtBrMe₂(CH₂-3,5-^tBu-(C₆H₃))(SMe₂)₂], *E*, the acetone solvent was removed and the resultant oil was washed with diethyl ether to remove any excess methyl iodide. Complex *E* was then dissolved in dry toluene and charged with a half equivalent of **bpad** dissolved in toluene, (0.0034g, 0.0087mmol). The mixture was stirred for two hours over which time the solution became a yellow colour with some slight formation of a black precipitate. After gravity filtering off the black precipitate, the toluene solvent was removed under reduced pressure affording a yellow oil. This oil was found to be sparingly soluble in acetone and was determined to be produce in a 61% yield. **¹H NMR in acetone-*d*₆:** δ 1.10 (s, ²J(PtH) = 70Hz, 6H), 1.31 (s, ²J(PtH) = 70Hz, 6H), 1.32 (s, 36H, ^tBu), 2.80 (d, ²J = 9Hz, ²J(PtH) = 73 Hz, 2H, H_A), 3.34 (d, ²J = 9Hz, ²J(PtH) = 101 Hz, 2H, H_B), 6.71 (s, ⁴J(PtH) = 10Hz, 4H, H_{po}) 6.92 (s, 2H, H_{pp}), 7.53 (dd, 2H, H₅), 7.55 (d, 2H, H_o), 7.62 (dd, 2H, H₄), 7.73 (dd, 2H, H_m), 7.80 (d, 2H, H_p), 7.98 (d, 2H, H₃), 8.18 (d, ³J(PtH) = 18Hz, 2H), 8.73 (s, 1H, H_b¹), 8.75 (s, 1H, H_b²), 9.68 (s, ³J = 30Hz, 2H, H_i). **ESI-MS(TOF):** [C₆₀H₇₆BrN₄Pt₂]⁺ Calculated m/z = 1321.5; determined m/z = 1321.45834.

4-ethynyl-*N*-(pyridine-2-ylmethylene)aniline, (*F*). To a toluene solution of 4-ethynylaniline, (1.0g, 8.547mmol), is added a slight excess of 2-pyridinecarboxaldehyde, (0.92g, 8.75mmol). A drop of glacial acetic acid is added to catalyze the reaction. The toluene solution is heated at reflux with a Dean Stark trap for 24 hours. The solvent is then removed from the reaction mixture. The brown oil is then washed with hexane to afford a yellowish-brown solid. The solid is collected via Buchner filtration, washed with hexane and allowed to dry. Yield 94%. **¹H NMR in CDCl₃:** δ 4.32 (s, 1H, sp-H), 7.24 (d, 2H, H_{p2}), 7.39 (m, 1H, H₅), 7.55 (d, 2H, H_{p1}), 7.83 (t, 1H, H₄), 8.20 (d, 1H, H₃), 8.59 (s, 1H, H_i), 8.73 (d, 1H, H₆). **EI-MS** [C₁₄H₁₀N₂]⁺: calculated m/z = 206.2; determined m/z = 206.0842.

1,8-dibromoanthraquinone, (G). A round-bottomed flask is charged with 5.0g, 18.05mmol, of 1,8-dichloroanthraquinone dissolved in 55mL of nitrobenzene [58]. To this is added 10.0g of KBr and 0.25g of CuCl₂. 10mL of H₃PO₄ is then added to the reaction mixture which is subsequently heated to 200°C while stirring. After boiling off any water a reflux condenser is placed on the flask and the mixture is refluxed for 48 hours. After refluxing, methanol is added to the reaction mixture to affect the precipitation of a green solid. The solid is then collected by filtration and dissolved in dichloromethane and extracted against water. After drying with magnesium sulfate, the dichloromethane solution is filtered and subsequently evaporated to yield **G**, in a 68% yield. ¹H NMR in CDCl₃: δ 7.56 (dd, 2H), 8.04 (d, 2H), 8.26 (d, 2H). EI-MS [C₁₄H₆Br₂O₂]⁺: calculated m/z = 365.9; determined m/z = 365.4973.

1,8-dibromoanthracene, (H). A round-bottomed flask is charged with 2.0g, 5.46mmol, of 1,8-dibromoanthraquinone dissolved in 100mL of isopropanol. To this is added 1.03g, 27.1mmol, of NaBH₄ gradually with stirring over the course of three hours. After the final addition, the reaction mixture is stirred for an additional hour at room temperature after which point 15mL of HCl is added to the mixture and heated at reflux for an hour. After one hour, a yellow-green solid forms, which is then collected by filtration and washed with water. After recrystallizing from toluene and drying, **H** was collected by filtration in a 85% yield. ¹H NMR in CDCl₃: δ 7.34 (dd, 2H, H_B), 7.85 (d, 2H, H_C), 7.98 (d, 2H, H_A), 8.44, (s, 1H, H_D), 9.20 (s, 1H, H_E). ESI-MS [C₁₄H₈Br₂]⁺: calculated m/z = 335.5; determined m/z = 334.8923.

(NE,N'E)-4,4'-(anthracene-1,8-diylbis(ethyne-2,1-diyl))-bis(N-(pyridin-2-ylmethylene)aniline), adpa. A round-bottomed flask is charged with 0.250g, (0.745mmol), of 1,8-dibromoanthracene (**H**) and 0.328g, (1.59mmol), of 4-ethynyl-N-(pyridine-2-ylmethylene)aniline (**F**). To this 91mg of Pd(PPh₃)₄ and 15mg of CuI were added and the reaction flask was subsequently flushed with nitrogen. After purging the reaction flask, 20mL of dry triethylamine was added and the reaction mixture was subsequently heated at reflux for 24hours. After refluxing for 24 hours the solvent was removed in *vacuo* and the resultant brown solid was dissolved in dichloromethane and extracted against water. After drying the dichloromethane solution with magnesium

sulfate, the dichloromethane solvent was removed under reduced pressure. The resultant solid was adhered to silica and subjected to silica gel column chromatography using ethyl acetate/hexanes (20%) as eluent to yield a yellow solid in 68% yield. **¹H NMR in CDCl₃**: δ 7.17 (d, 4H, H_{P1}), 7.31 (dd, 2H, H₅), 7.52 (t, 2H, H_B), 7.66 (d, 4H, H_{P2}), 7.67 (t, 2H, H₄), 7.84 (d, 2H, H₃), 8.06 (d, 2H, H_C), 8.10 (d, 2H, H_A), 8.51 (s, 1H, H_D), 8.58 (s, 2H, H_i), 8.61 (d, 2H, H₆), 9.67 (s, 1H, H_E). **ESI-MS** [C₄₂H₂₆N₄]⁺: calculated m/z = 586.2; determined m/z = 586.21726.

[Pt₂Me₄(adpa)], complex 29. A dry toluene solution of the Pt(II) dimer, [Pt₂Me₄(SMe₂)₂], (0.100g, 0.174mmol), was charged with an equivalent of **adpa** dissolved in toluene, (0.102g, 0.174mmol). The mixture was stirred and immediately turned deep red in colour and was subsequently stirred for 3hr. The solvent volume of the resultant suspension was then reduced in *vacuo* and then placed in an ice bath to affect the precipitation of a red solid which was collected using vacuum filtration and washed with pentane. The resultant red solid, complex **29**, was collected in an 88% yield. **¹H NMR in CDCl₃**: δ 1.08 (s, ²J(PtH) = 84Hz, 6H), 1.19 (s, ²J(PtH) = 86Hz, 6H), 7.25 (d, ³J = 8 Hz, 4H, H_{P1}), 7.47 (dd, ³J = 7Hz, ³J = 5Hz, 2H, H₅), 7.52 (dd, ³J = 7Hz, ³J = 7Hz, 2H, H₄), 7.25 (d, ³J = 8 Hz, 4H, H_{P2}), 7.84 (d, ³J = 7 Hz, 2H, H₃), 7.92 (d, ³J = 8 Hz, 2H, H_C), 8.08 (d, ³J = 8Hz, 2H, H_A), 8.10 (t, ³J = 8Hz, 2H, H_B), 8.52 (s, 1H, H_D), 8.85 (d, ³J = 5Hz, ³J(PtH) = 20Hz, 2H, H₆), 9.29 (s, ³J = 28Hz, 2H, H_i), 9.61 (s, 1H, H_E). **ESI-MS(TOF)**: [C₄₆H₃₈N₄Pt₂Na]⁺ Calculated m/z = 1057.23; determined m/z = 1057.22474.

[Pt₂I₂Me₆(adpa)], complex 30. To an acetone solution of complex **29**, (0.010g, 0.00965mmol), was added a slight excess of methyl iodide, 1.5μL, (0.0195mmol). The acetone mixture was then stirred for three hours over which time the originally red solution became yellow in colour. After stirring for three hours the solvent volume was reduced in *vacuo* and then the solution was layered with pentane to affect the precipitation of a yellow solid. After isolating and washing with cold pentane, the yellow solid, **30**, was collected in an 85% yield. **¹H NMR in CDCl₃**: δ 1.08 (s, ²J(PtH) = 84Hz, 6H), 1.19 (s, ²J(PtH) = 86Hz, 6H), 7.25 (d, ³J = 8 Hz, 4H, H_{P1}), 7.47 (dd, ³J = 7Hz, ³J = 5Hz, 2H, H₅), 7.52 (dd, ³J = 7Hz, ³J = 7Hz, 2H, H₄), 7.25 (d, ³J = 8 Hz, 4H, H_{P2}), 7.84 (d, ³J = 7 Hz, 2H, H₃), 7.92 (d, ³J = 8 Hz, 2H, H_C), 8.08 (d, ³J = 8Hz, 2H, H_A), 8.10 (t, ³J =

8Hz, 2H, H_B), 8.52 (s, 1H, H_D), 8.85 (d, ³J = 5Hz, ³J(PtH) = 20Hz, 2H, H₆), 9.29 (s, ³J = 28Hz, 2H, H_i), 9.61 (s, 1H, H_E). **ESI-MS(TOF):** [C₄₈H₄₄N₄Pt₂I₂Na]⁺ Calculated m/z = 1341.08; determined m/z = 1341.08063.

[Pt₂Br₂Me₄(CH₂-3,5-di-*t*-Bu(C₆H₃))₂(adpa)], complex 31. Complex **31** was prepared in a manner analogous to **30**. Rather than methyl iodide, 0.0054g (0.0193mmol), of 3,5-di-*tert*-butylbenzyl bromide was added to an acetone solution of **29**. Yield 77%. **¹H NMR in acetone-*d*₆:** δ 1.14 (s, ²J(PtH) = 70Hz, 6H), 1.40 (s, 18H), 1.48 (s, ²J(PtH) = 70Hz, 6H), 2.57 (d, ²J(HH) = 8Hz, ²J(PtH) = 91 Hz, 2H), 2.67 (d, ²J(HH) = 8Hz, ²J(PtH) = 109 Hz, 2H), 6.17 (s, 4H, H_o), 7.65 (t, ³J = 8 Hz, 2H, H_B), 7.77 (d, ³J = 8Hz, 4H, H_{p1}), 7.92 (d, ³J = 8 Hz, 4H, H_{p2}), 7.99 (dd, ³J = 7Hz, ³J = 5Hz, 2H, H₅), 8.00 (s, 2H, H_p), 8.01 (d, ³J = 7 Hz, 2H, H_C), 8.25 (d, ³J = 8 Hz, 2H, H_A), 8.29 (d, ³J = 7Hz, 2H, H₃), 8.37 (t, ³J = 7Hz, 2H, H₄), 8.78 (s, 1H, H_D), 9.01 (s, ³J = 25 Hz, 2H, H_i), 9.09 (d, ³J = 5Hz, ³J(PtH) = 21Hz, 2H, H₆), 9.64 (s, 1H, H_E).

[Pt₂Br₂Me₄(CH₂-1,2-(C₆H₄)-CH₂)(adpa)], complex 32. Complex **32** was prepared in a manner analogous to **30**. Rather than methyl iodide, 0.0026g (0.00965mmol), of 1,2-dibromoxylene was added to an acetone solution of **29**. Yield 81%. **¹H NMR in acetone-*d*₆:** δ 1.08 (s, ²J(PtH) = 70Hz, 6H), 1.46 (s, ²J(PtH) = 70Hz, 6H), 2.56 (d, ²J(HH) = 9Hz, ²J(PtH) = 96 Hz, 2H), 2.63 (d, ²J(HH) = 9Hz, ²J(PtH) = 104 Hz, 2H), 6.34 (t, ³J = 8Hz, 2H, H_m), 6.47 (d, ³J = 8Hz, 2H, H_o), 7.17 (d, ³J = 8 Hz, 2H, H_C), 7.22 (t, ³J = 8Hz, 2H, H_B), 7.38 (d, ³J = 8Hz, 2H, H_A), 7.62 (d, ³J = 8 Hz, 4H, H_{p1}), 7.65 (dd, ³J = 5 Hz, ³J = 7 Hz, 2H, H₅), 7.81 (d, ³J = 8 Hz, 4H, H_{p2}), 7.94 (t, ³J = 8 Hz, 2H, H₄), 8.09 (d, ³J = 8Hz, 2H, H₃), 8.27 (d, ³J = 5Hz, ³J(PtH) = 18Hz, 2H, H₆), 8.78 (s, 1H, H_D), 9.27 (s, ³J = 21Hz, 2H, H_i), 9.75 (s, 1H, H_E). **ESI-MS(TOF):** [C₅₄H₄₆N₄Pt₂Br]⁺ Calculated m/z = 1217.22; determined m/z = 1217.21591.

2,7-di-*tert*-butyl-9,9-dimethyl-9H-xanthene-4,5-dicarbonyl dichloride, I. 0.500g, (1.218mmol), of 2,7-di-*tert*-butyl-9,9-dimethyl-9H-xanthene-4,5-dicarboxylic acid was dissolved in 50mL of SO₂Cl₂. The reaction mixture was stirred for 3 hours with heating at reflux. After 3 hours the excess SO₂Cl₂ was removed by flushing a stream of N₂ into the round-bottomed flask. The resultant off-white solid was then isolated in quantitative

yield, 0.544g. $^1\text{H NMR}$ in CDCl_3 : δ 1.37 (s, 18H, ^tBu), 1.67 (s, 6H, Me), 7.67 (d, $^4J(\text{HH}) = 2\text{Hz}$, 2H, H_B), 7.90 (d, $^4J(\text{HH}) = 2\text{Hz}$, 2H, H_A).

2,7-di-*tert*-butyl-9,9-dimethyl- N^4,N^5 -bis(4-nitrophenyl)xanthene-4,5-dicarboxamide, *J*. 0.544g, (1.218mmol), of 2,7-di-*tert*-butyl-9,9-dimethylxanthene-4,5-dicarbonyl dichloride was combined with 2.2 equivalents of *p*-nitroaniline, (0.370g, 2.680mmol), in a round-bottomed flask and removed of air and moisture using Schlenk techniques. To this inert flask was added 40mL of dry dichloromethane and NEt_3 (0.34g, 3.35mmol). The reaction mixture was allowed to stir overnight at room temperature under N_2 . After 12 hours of stirring at room temperature the reaction mixture was heated at reflux for 3 hours. This dichloromethane solution was then washed with 15mL of distilled water and extracted against dichloromethane. The organic fractions were collected and dried over MgSO_4 , filtered and subsequently the solvent was removed *in vacuo*. The resultant off-white solid was washed with a 9:1 diethyl ether/dichloromethane solvent mixture to dissolve residual *p*-nitroaniline. The remaining white solid product was collected via Hirsch filtration and washed with diethyl ether and pentane. Yield 51%. $^1\text{H NMR}$ in **acetone- d_6** : δ 1.39 (s, 18H, ^tBu), 1.77 (s, 6H, Me), 7.78 (d, $^4J(\text{HH}) = 2\text{Hz}$, 2H, H_B), 7.83 (d, $^3J(\text{HH}) = 9\text{Hz}$, 4H, H_{P1}), 7.85 (d, $^4J(\text{HH}) = 2\text{Hz}$, 2H, H_A), 7.98 (d, $^3J(\text{HH}) = 9\text{Hz}$, 4H, H_{P2}), 10.10 (s, 2H, NH). **EI-MS** [$\text{C}_{37}\text{H}_{38}\text{N}_4\text{O}_7$] $^+$: calculated $m/z = 650.72$; determined $m/z = 650.27540$.

N^4,N^5 -bis(4-aminophenyl)-2,7-di-*tert*-butyl-9,9-dimethyl-xanthene-4,5-dicarboxamide, *K*. 0.3095g, (0.4756mmol), of ***B*** was suspended in 50mL of MeOH at 0°C . To this was added 0.020g of 10% Pd/C and the mixture was then stirred. To this stirred solution was added gradually over 15 minutes 0.180g of NaBH_4 . The reaction mixture was allowed to stir for 6 hours and gradually warmed to room temperature. Once the starting material was completely consumed as confirmed by TLC, (33% EtOAc/Hex), the reaction mixture was filtered to remove any solids. The methanol solvent was then removed under reduced pressure and the resultant off-white oil was washed with 20mL of water. This aqueous solution was extracted with dichloromethane and the organic fractions were then dried over MgSO_4 . The dichloromethane solvent was removed *in vacuo*, and an off-white solid product was precipitated from a concentrated

dichloromethane solution with pentane, collected via Hirsch filtration and washed with cold pentane. Yield 98%. **¹H NMR in CDCl₃**: δ 1.37 (s, 18H, ^tBu), 1.70 (s, 6H, Me), 1.83 (s (br.), 4H, NH₂) 6.54 (d, ³J(HH) = 9Hz, 4H, H_{P1}), 7.26 (d, ³J(HH) = 9Hz, 4H, H_{P2}), 7.58 (d, ⁴J(HH) = 2Hz, 2H, H_B), 7.82 (d, ⁴J(HH) = 2Hz, 2H, H_A), 8.57 (s, 2H, NH). **EI-MS** [C₃₇H₄₂N₄O₃]⁺: calculated m/z = 590.72; determined m/z = 590.32427.

2,7-di-*tert*-butyl-9,9-dimethyl-*N*⁴,*N*⁵-bis(4-((*E*)-pyridin-2-ylmethyleneamino)phenyl)-xanthene-4,5-dicarboxamide, ppxda. To a toluene solution of **C**, (0.2803g, 0.4756mmol), was added 2.2 equivalents of 2-pyridinecarboxaldehyde, (0.100mL, 1.044mmol). To this solution was added 2 drops of acetic acid, and a dean-stark condenser was attached to the flask. The mixture was refluxed overnight after which time the solvent toluene was removed *in vacuo*. The resultant brown solid was washed with pentane, collected via Hirsch filtration, and subsequently washed again with pentane and diethyl ether to remove excess 2-pyridine carboxaldehyde. The product was isolated as a tan solid in 88% yield. **¹H NMR in CDCl₃**: δ 1.37 (s, 18H, ^tBu), 1.72 (s, 6H, Me), 7.13 (d, ³J(HH) = 7Hz, 4H, H_{P1}), 7.29 (dd, ³J(HH) = 7Hz, ³J(HH) = 5Hz, 2H, H₅), 7.55 (d, ³J(HH) = 7Hz, 4H, H_{P2}), 7.61 (s, 2H, H_B), 7.67 (dd, ³J(HH) = 7Hz, ³J(HH) = 7Hz, 2H, H₄), 7.85 (s, 2H, H_A), 8.09 (d, ³J(HH) = 7Hz, 2H, H₃), 8.56 (s, 2H, H_i), 8.59 (d, ³J(HH) = 5Hz, 2H, H₆), 8.79 (s, 2H, NH). **EI-MS** [C₄₉H₄₈N₆O₃]⁺ calculated m/z = 767.96; determined m/z = 768.37948.

[Pt₂Me₄(ppxda)], Complex 33. To an acetone solution of the platinum dimer, (0.020g, 0.0348mmol), was added dropwise an acetone solution of 2,7-di-*tert*-butyl-9,9-dimethyl-*N*⁴,*N*⁵-bis(4-((*E*)-pyridin-2-ylmethyleneamino)phenyl)-xanthene-4,5-dicarboxamide, (0.028g, 0.0348mmol). The acetone solution was allowed to stir and the originally tan solution gradually became a deep red solution. After stirring for 1hr, the solvent was removed *in vacuo*, and the resultant red oil was dissolved in acetone and layered with pentane, leading to the precipitation of a red solid. This solid was collected by Hirsch filtration and washed with cold pentane. Yield 0.036g, 85%. **¹H NMR in acetone-*d*₆**: δ 0.95 (s, ²J(PtH) = 84Hz, 6H, Pt-Me), 1.14 (s, ²J(PtH) = 87Hz, 6H, Pt-Me), 1.40 (s, 18H, ^tBu), 1.78 (s, 6H, Me), 7.22 (d, ³J(HH) = 9Hz, 4H, H_{P1}), 7.70 (dd, ³J(HH) = 8Hz, ³J(HH) = 5Hz, 2H, H₅), 7.72 (d, ³J(HH) = 9Hz, 4H, H_{P2}), 7.83 (s, 2H, H_{B1}), 7.87 (s, 2H, H_{B2}),

8.21 (dd, $^3J(\text{HH}) = 8\text{Hz}$, $^3J(\text{HH}) = 8\text{Hz}$, 2H, H₄), 8.22 (d, $^3J(\text{HH}) = 8\text{Hz}$, 2H, H₃), 9.03 (d, $^3J(\text{HH}) = 5\text{Hz}$, $^3J(\text{PtH}) = 25\text{ Hz}$, 2H, H₆), 9.58 (s, $^3J(\text{PtH}) = 30\text{ Hz}$, 2H, H_i), 9.92 (s, 2H, NH). **ESI-MS** [C₅₃H₆₀N₆O₃Pt₂Na]⁺ calculated m/z = 1239.39; determined m/z = 1239.38779.

[Pt₂I₂Me₆(ppxda)], Complex 34a/34b. To an acetone-*d*₆ solution of **33**, (0.010g, 0.0082mmol) was added 1.2μL, (0.0164mmol) of iodomethane. Immediately the bright red colour of the mixture became a dull yellow colour. The reaction mixture was stirred and ¹H NMR spectra were collected after 10mins, 1hr, 24hr, 48hr to monitor the progress of the reaction. ¹H NMR analysis of the time series indicates the formation of two isomers in solution, **34a** the *syn* isomer and **34b** the *anti* isomer. Upon layering the acetone solution with pentane, a yellow solid was afforded and collected via Hirsch filtration. Yield 74%. Single crystals of **34b** were grown by the vapour diffusion of pentane into a concentrated acetone solution of a mixture of **34a/34b**. The crystals produced were that of **34b** and ¹H NMR analysis on them allowed for the complete assignment of both isomers. **¹H NMR in acetone-*d*₆: 34a:** δ 0.61 (s, $^2J(\text{PtH}) = 72\text{Hz}$, 6H, Pt-Me_{ax}), 1.21 (s, $^2J(\text{PtH}) = 70\text{Hz}$, 6H, Pt-Me_{eq}), 1.41 (s, 18H, ¹Bu), 1.46 (s, $^2J(\text{PtH}) = 70\text{Hz}$, 6H, Pt-Me_{eq}), 1.79 (s, 6H, Me), 7.56 (d, $^3J(\text{HH}) = 9\text{Hz}$, 4H, H_{P1}), 7.83 (d, $^3J(\text{HH}) = 9\text{Hz}$, 4H, H_{P2}), 7.83 (dd, $^3J(\text{HH}) = 8\text{Hz}$, $^3J(\text{HH}) = 5\text{Hz}$, 2H, H₅), 7.88 (s, 2H, H_{B1}), 7.96 (s, 2H, H_{B2}), 8.23 (dd, $^3J(\text{HH}) = 8\text{Hz}$, $^3J(\text{HH}) = 8\text{Hz}$, 2H, H₄), 8.37 (d, $^3J(\text{HH}) = 8\text{Hz}$, 2H, H₃), 9.01 (d, $^3J(\text{HH}) = 5\text{Hz}$, $^3J(\text{PtH}) = 17\text{ Hz}$, 2H, H₆), 9.31 (s, $^3J(\text{PtH}) = 27\text{ Hz}$, 2H, H_i), 10.12 (s, 2H, NH). **34b:** δ 0.44 (s, $^2J(\text{PtH}) = 72\text{Hz}$, 6H, Pt-Me_{ax}), 1.13 (s, $^2J(\text{PtH}) = 70\text{Hz}$, 6H, Pt-Me_{eq}), 1.41 (s, 18H, ¹Bu), 1.46 (s, $^2J(\text{PtH}) = 70\text{Hz}$, 6H, Pt-Me_{eq}), 1.79 (s, 6H, Me), 7.43 (d, $^3J(\text{HH}) = 9\text{Hz}$, 4H, H_{P1}), 7.80 (d, $^3J(\text{HH}) = 9\text{Hz}$, 4H, H_{P2}), 7.83 (dd, $^3J(\text{HH}) = 8\text{Hz}$, $^3J(\text{HH}) = 5\text{Hz}$, 2H, H₅), 7.84 (s, 2H, H_{B1}), 7.87 (dd, $^3J(\text{HH}) = 8\text{Hz}$, $^3J(\text{HH}) = 8\text{Hz}$, 2H, H₄), 7.91 (s, 2H, H_{B2}), 8.27 (d, $^3J(\text{HH}) = 8\text{Hz}$, 2H, H₃), 9.02 (d, $^3J(\text{HH}) = 5\text{Hz}$, $^3J(\text{PtH}) = 17\text{ Hz}$, 2H, H₆), 9.43 (s, $^3J(\text{PtH}) = 27\text{ Hz}$, 2H, H_i), 10.02 (s, 2H, NH). **ESI-MS** [C₅₅H₆₆N₆O₃IPt₂]⁺ calculated m/z = 1375.35; determined m/z = 1375.35714.

[Pt₂Br₂Me₄(CH₂(C₆H₅))₂(ppxda)], Complex 35a/35b. To an acetone-*d*₆ solution of **33**, (0.010g, 0.0082mmol) was added 1.95μL, (0.0164mmol) of benzyl bromide. Immediately the bright red colour of the mixture became a bright yellow colour. ¹H

NMR analysis of the reaction mixture indicated the formation of two isomers in solution, **35a** the *syn* isomer and **35b** the *anti* isomer. The identities of the isomers can not be determined and therefore the assignment is not absolute but inferences were made based upon similar resonances of the *tert*-butyl derivative. Upon layering the acetone solution with pentane, a yellow solid was afforded and collected via Hirsch filtration. Yield 81%.

¹H NMR in acetone-*d*₆: 35a: δ 1.18 (s, ²*J*(PtH) = 70Hz, 6H, Pt-Me), 1.40 (s, 18H, ^tBu), 1.46 (s, ²*J*(PtH) = 70Hz, 6H, Pt-Me), 1.78 (s, 6H, Me), 2.49 (d, ²*J*(HH) = 9Hz, ²*J*(PtH) = 88Hz, 2H, CH₂^a), 2.56 (d, ²*J*(HH) = 9Hz, ²*J*(PtH) = 106Hz, 2H, CH₂^b), 6.56 (d, ³*J*(HH) = 8Hz, 4H, H_o), 6.71, (t, ³*J*(HH) = 8Hz, 4H, H_m), 6.85 (t, ³*J*(HH) = 8Hz, 2H, H_p), 7.41 (d, ³*J*(HH) = 9Hz, 4H, H_{P1}), 7.55 (dd, ³*J*(HH) = 7Hz, ³*J*(HH) = 5Hz, 2H, H₅), 7.65 (d, ³*J*(HH) = 9Hz, 4H, H_{P2}), 7.84 (s, 2H, H_{B1}), 7.87 (s, 2H, H_{B2}), 8.00 (dd, ³*J*(HH) = 8Hz, ³*J*(HH) = 8Hz, 2H, H₄), 8.17 (d, ³*J*(HH) = 8Hz, 2H, H₃), 8.52 (d, ³*J*(HH) = 5Hz, ³*J*(PtH) = 18 Hz, 2H, H₆), 9.32 (s, ³*J*(PtH) = 27 Hz, 2H, H_i), 10.06 (s, 2H, NH). **35b:** δ 1.14 (s, ²*J*(PtH) = 70Hz, 6H, Pt-Me), 1.40 (s, 18H, ^tBu), 1.44 (s, ²*J*(PtH) = 70Hz, 6H, Pt-Me), 1.78 (s, 6H, Me), 2.45 (d, ²*J*(HH) = 9Hz, ²*J*(PtH) = 92Hz, 2H, CH₂^a), 2.51 (d, ²*J*(HH) = 9Hz, ²*J*(PtH) = 96Hz, 2H, CH₂^b), 6.35 (d, ³*J*(HH) = 8Hz, 4H, H_o), 6.70, (t, ³*J*(HH) = 8Hz, 4H, H_m), 6.83 (t, ³*J*(HH) = 8Hz, 2H, H_p), 7.00 (d, ³*J*(HH) = 9Hz, 4H, H_{P1}), 7.56 (dd, ³*J*(HH) = 7Hz, ³*J*(HH) = 5Hz, 2H, H₅), 7.83 (d, ³*J*(HH) = 9Hz, 4H, H_{P2}), 7.84 (s, 2H, H_{B1}), 7.87 (s, 2H, H_{B2}), 7.92 (d, ³*J*(HH) = 8Hz, 2H, H₃), 8.10 (dd, ³*J*(HH) = 8Hz, ³*J*(HH) = 8Hz, 2H, H₄), 8.61 (d, ³*J*(HH) = 5Hz, ³*J*(PtH) = 18 Hz, 2H, H₆), 9.18 (s, ³*J*(PtH) = 25 Hz, 2H, H_i), 9.92 (s, 2H, NH). **ESI-MS** [C₆₇H₇₄BrN₆O₃Pt₂]⁺ calculated m/z = 1476.45; determined m/z = 1476.16742.

[Pt₂Br₂Me₄(4-CH₂-(C₆H₄)-C(CH₃)₃)₂(ppxda)], Complex 36a/36b. To an acetone-*d*₆ solution of **33**, (0.010g, 0.0082mmol) was added 2.3μL, (0.0164mmol) of 4-*tert*-butylbenzyl bromide. Immediately the bright red colour of the mixture became a dull yellow colour. ¹H NMR analysis of the reaction mixture indicated the formation of two isomers in solution, **36a** the *syn* isomer and **36b** the *anti* isomer. The resonances of each isomer were assigned based on the assumption that the *anti* isomer would again be the most thermodynamically preferred as is the case for **34a/34b**. Upon layering the acetone solution with pentane, a yellow solid was afforded and collected via Hirsch filtration. Yield 71%. **¹H NMR in acetone-*d*₆: 36a:** δ 1.11 (s, 18H, ^tBu), 1.16 (s, ²*J*(PtH) = 70Hz,

6H, Pt-Me), 1.39 (s, 18H, ^tBu), 1.45 (s, ²J(PtH) = 70Hz, 6H, Pt-Me), 1.74 (s, 6H, Me), 2.55 (d, ²J(HH) = 9Hz, ²J(PtH) = 80Hz, 2H, CH₂^a), 2.72 (d, ²J(HH) = 9Hz, ²J(PtH) = 97Hz, 2H, CH₂^b), 6.45 (d, ³J(HH) = 8Hz, 4H, H_o), 6.73 (d, ³J(HH) = 8Hz, 4H, H_m), 7.02 (d, ³J(HH) = 9Hz, 4H, H_{p1}), 7.15 (dd, ³J(HH) = 7Hz, ³J(HH) = 5Hz, 2H, H₅), 7.29 (d, ³J(HH) = 9Hz, 4H, H_{p2}), 7.57 (dd, ³J(HH) = 8Hz, ³J(HH) = 8Hz, 2H, H₄), 7.66 (s, 2H, H_{B1}), 7.76 (d, ³J(HH) = 8Hz, 2H, H₃), 7.88 (s, 2H, H_{B2}), 8.41 (d, ³J(HH) = 5Hz, ³J(PtH) = 18 Hz, 2H, H₆), 8.92 (s, ³J(PtH) = 25 Hz, 2H, H_i), 9.02 (s, 2H, NH). **36b**: δ 1.11 (s, 18H, ^tBu), 1.15 (s, ²J(PtH) = 70Hz, 6H, Pt-Me), 1.34 (s, ²J(PtH) = 70Hz, 6H, Pt-Me), 1.39 (s, 18H, ^tBu), 1.74 (s, 6H, Me), 2.44 (d, ²J(HH) = 9Hz, ²J(PtH) = 84Hz, 2H, CH₂^a), 2.52 (d, ²J(HH) = 9Hz, ²J(PtH) = 97Hz, 2H, CH₂^b), 6.26 (d, ³J(HH) = 8Hz, 4H, H_o), 6.68 (d, ³J(HH) = 8Hz, 4H, H_m), 6.97 (d, ³J(HH) = 9Hz, 4H, H_{p1}), 7.25 (dd, ³J(HH) = 7Hz, ³J(HH) = 5Hz, 2H, H₅), 7.51 (d, ³J(HH) = 9Hz, 4H, H_{p2}), 7.57 (dd, ³J(HH) = 8Hz, ³J(HH) = 8Hz, 2H, H₄), 7.67 (s, 2H, H_{B1}), 7.84 (d, ³J(HH) = 8Hz, 2H, H₃), 7.88 (s, 2H, H_{B2}), 8.43 (d, ³J(HH) = 5Hz, ³J(PtH) = 19 Hz, 2H, H₆), 8.70 (s, 2H, NH), 9.06 (s, ³J(PtH) = 29 Hz, 2H, H_i). **ESI-MS** [C₇₅H₉₀BrN₆O₃Pt₂]⁺ calculated m/z = 1588.57; determined m/z = 1588.49802.

[Pt₂(μ₂-Br)Me₂(4-CH₂-(C₆H₄)-C(CH₃)₃)₂(ppxda)][O₃SCF₃], Complex 37. To an acetone solution of **36a/36b**, (0.027g, 0.0164mmol) was added one equivalent of silver trifluoromethanesulfonate, (0.0021g, 0.0082mmol). After the yellow solution was stirred for one hour, an off-white precipitate was observed. This precipitate, silver bromide, was removed by filtration and the yellow solution was then concentrated and layered with pentane to affect the precipitation of a yellow solid. Yield 61%. **¹H NMR in acetone-*d*₆**: δ 1.04 (s, ²J(PtH) = 70Hz, 6H, Pt-Me), 1.14 (s, 18H, ^tBu), 1.31 (s, ²J(PtH) = 70Hz, 6H, Pt-Me), 1.39 (s, 18H, ^tBu), 1.75 (s, 6H, Me), 2.57 (d, ²J(HH) = 9Hz, ²J(PtH) = 97Hz, 2H, CH₂^a), 2.67 (d, ²J(HH) = 9Hz, ²J(PtH) = 98Hz, 2H, CH₂^b), 6.28 (d, ³J(HH) = 8Hz, 4H, H_o), 6.66 (d, ³J(HH) = 9Hz, 4H, H_{p1}), 6.72 (d, ³J(HH) = 8Hz, 4H, H_m), 7.40 (d, ³J(HH) = 8Hz, 2H, H₃), 7.51 (d, ³J(HH) = 9Hz, 4H, H_{p2}), 7.73 (dd, ³J(HH) = 7Hz, ³J(HH) = 5Hz, 2H, H₅), 7.78 (dd, ³J(HH) = 8Hz, ³J(HH) = 8Hz, 2H, H₄), 7.81 (s, 2H, H_{B1}), 7.90 (s, 2H, H_{B2}), 8.67 (s, ³J(PtH) = 30 Hz, 2H, H_i), 8.80 (d, ³J(HH) = 5Hz, ³J(PtH) = 19 Hz, 2H, H₆), 9.97 (s, 2H, NH). **ESI-MS** [C₇₅H₉₀BrN₆O₃Pt₂]⁺ calculated m/z = 1588.57; determined m/z = 1588.48975.

[Pt₂Me₆(OH₂)₂(ppxda)][O₃SCF₃]₂, Complex 38a/38b. To an acetone-*d*₆ solution of **34b**, (0.012g, 0.0082mmol) was added two equivalents, (0.0042g, 0.0164mmol) of silver trifluoromethanesulfonate. After stirring for one hour, the bright yellow solid was filtered to remove the silver iodide precipitate and then the acetone solvent was removed under reduced pressure. The yellow oil was dissolved in acetone-*d*₆ and a ¹H NMR spectrum was acquired. A variable temperature NMR experiment was also performed in which spectra were acquired at 25°C, 20°C, 10°C, 0°C, -10°C, -20°C and -30°C. ¹H NMR analysis of the temperature series indicates the formation of two isomers in solution, **38a** the *syn* isomer and **38b** the *anti* isomer. Upon layering the acetone-*d*₆ solution with pentane, a yellow solid was afforded and collected via Hirsch filtration. Yield 91%. **¹H NMR in acetone-*d*₆ at 253K: 38a:** δ 0.61 (s, ²*J*(PtH) = 80Hz, 6H, Pt-Me_{ax}), 0.97 (s, ²*J*(PtH) = 68Hz, 6H, Pt-Me_{eq}), 1.18 (s, ²*J*(PtH) = 68Hz, 6H, Pt-Me_{eq}), 1.38 (s, 18H, ¹Bu), 1.77 (s, 6H, Me), 6.39 (s, 4H, OH₂), 7.34 (d, ³*J*(HH) = 9Hz, 4H, H_{P1}), 7.89 (s, 2H, H_{B1}), 7.91 (d, ³*J*(HH) = 9Hz, 4H, H_{P2}), 7.93 (s, 2H, H_{B2}), 8.05 (dd, ³*J*(HH) = 8Hz, ³*J*(HH) = 5Hz, 2H, H₅), 8.47 (m, 4H, H₄/H₃), 8.99 (d, ³*J*(HH) = 5Hz, ³*J*(PtH) = 17 Hz, 2H, H₆), 9.53 (s, ³*J*(PtH) = 26 Hz, 2H, H_i), 10.22 (s, 2H, NH). **38b:** δ 0.57 (s, ²*J*(PtH) = 80Hz, 6H, Pt-Me_{ax}), 0.98 (s, ²*J*(PtH) = 68Hz, 6H, Pt-Me_{eq}), 1.18 (s, ²*J*(PtH) = 68Hz, 6H, Pt-Me_{eq}), 1.38 (s, 18H, ¹Bu), 1.77 (s, 6H, Me), 6.38 (s, 4H, OH₂), 7.33 (d, ³*J*(HH) = 9Hz, 4H, H_{P1}), 7.89 (s, 2H, H_{B1}), 7.91 (d, ³*J*(HH) = 9Hz, 4H, H_{P2}), 7.93 (s, 2H, H_{B2}), 8.05 (dd, ³*J*(HH) = 8Hz, ³*J*(HH) = 5Hz, 2H, H₅), 8.47 (m, 4H, H₄/H₃), 8.99 (d, ³*J*(HH) = 5Hz, ³*J*(PtH) = 17 Hz, 2H, H₆), 9.51 (s, ³*J*(PtH) = 26 Hz, 2H, H_i), 10.21 (s, 2H, NH). **ESI-MS** [C₅₅H₇₀N₆O₅Pt₂]⁺ calculated m/z = 1284.47; determined m/z = 1284.46965.

[Pt₂Me₆(C₄H₄N₂)(ppxda)][O₃SCF₃]₂, Complex 39. To an acetone-*d*₆ solution of **38a/38b**, was added one equivalent, (0.0064g, 0.0082mmol) of pyrazine. After allowing the reagents to mix in the NMR tube, a ¹H NMR spectrum was acquired. Upon layering the acetone-*d*₆ solution with pentane, a yellow solid was afforded and collected via Hirsch filtration. Yield 92%. **¹H NMR in acetone-*d*₆:** δ 0.86 (s, ²*J*(PtH) = 72Hz, 6H, Pt-Me_{ax}), 1.06 (s, ²*J*(PtH) = 68Hz, 6H, Pt-Me_{eq}), 1.31 (s, ²*J*(PtH) = 68Hz, 6H, Pt-Me_{eq}), 1.41 (s, 18H, ¹Bu), 1.78 (s, 3H, Me), 1.80 (s, 3H, Me), 7.31 (d, ³*J*(HH) = 9Hz, 4H, H_{P1}), 7.91 (s, 2H, H_{B1}), 8.07 (s, 2H, H_{B2}), 8.07 (dd, ³*J*(HH) = 8Hz, ³*J*(HH) = 5Hz, 2H, H₅), 8.33 (d,

$^3J(\text{HH}) = 9\text{Hz}$, 4H, $\text{H}_{\text{P}2}$), 8.46 (m, 4H, H_4/H_3), 8.54 (s, 4H, H_{pyr}), 9.09 (d, $^3J(\text{HH}) = 5\text{Hz}$, $^3J(\text{PtH}) = 18\text{ Hz}$, 2H, H_6), 9.40 (s, $^3J(\text{PtH}) = 27\text{ Hz}$, 2H, H_i), 10.26 (s, 2H, NH).

2,7-di-*tert*-butyl-9,9-dimethyl-9H-xanthene-4,5-diamine, L. A chloroform solution of xanthene dicarboxylic acid, (0.60g, 1.4mmol in 20mL of CHCl_3), was allowed to stir while cooling in an ice bath to 0°C . Once cooled, 0.100mL of fuming sulfuric acid was added carefully in a drop-wise manner to the reaction mixture. Upon addition of the fuming sulfuric acid, the solution changed from an off-white to a yellow colour. To this mixture was then gradually added (0.34 g, 5.8mmol) of NaN_3 while stirring. The mixture was then allowed to stir at 0°C for one hour before being heated at 50°C for one hour while stirring. After cooling the reaction mixture to room temperature for an hour, the solution was treated with $\text{KOH}/\text{H}_2\text{O}$ until the pH stabilized at $\text{pH} = 12$. The organic layer was extracted with CHCl_3 and CH_2Cl_2 and then washed with water and brine. Solvent was then removed under reduced pressure yielding an off-white solid powder. Yield 84%. $^1\text{H NMR}$ in CDCl_3 : $\delta = 1.31$ (s, 18H, ^tBu); 1.62 (s, 6H, Me); 3.17 (*br. s*, 4H, NH_2); 6.71 (d, $^4J(\text{HH}) = 2\text{Hz}$, 2H, $\text{H}_{\text{B}1}$); 6.85 (d, $^4J(\text{HH}) = 2\text{Hz}$, 2H, $\text{H}_{\text{B}2}$). **EI-MS** [$\text{C}_{23}\text{H}_{33}\text{N}_2\text{O}$] $^+$: calculated $m/z = 353.25$; determined $m/z = 353.21475$.

2,7-di-*tert*-butyl-9,9-dimethyl-bis(pyridine-2-ylmethylene)-9H-xanthene-4,5-diamine, pmxda. To a toluene solution of the xanthene diamine, (0.514g, 1.46mmol), was added two equivalents of 2-pyridinecarboxaldehyde (0.278mL, 2.92mmol) with a catalytic amount of acetic acid. To the round bottomed flask was added a Dean-Stark condenser and the reaction mixture was subsequently heated at reflux for 3 hours. After 3 hours the solvent volume was removed under reduced pressure and the yellow solid product was washed with pentane and collected via hirsch filtration. Yield 91%. $^1\text{H NMR}$ analysis using CDCl_3 as a solvent yielded the product of acid catalyzed hydrolysis and the product was found to be insoluble in acetone. $^1\text{H NMR}$ in CD_2Cl_2 : $\delta 1.36$ (s, 18H, ^tBu); 1.71 (s, 6H, Me); 7.05 (d, $^4J(\text{HH}) = 2\text{Hz}$, 2H, $\text{H}_{\text{B}1}$); 7.29 (dd, $^3J(\text{HH}) = 5\text{Hz}$, $^3J(\text{HH}) = 7\text{Hz}$, 2H, H_5); 7.36 (d, $^4J(\text{HH}) = 2\text{Hz}$, 2H, $\text{H}_{\text{B}2}$); 7.53 (td, $^3J(\text{HH}) = 8\text{Hz}$, $^3J(\text{HH}) = 7\text{Hz}$, 2H, H_4); 8.01 (d, $^3J(\text{HH}) = 8\text{Hz}$, 2H, H_3); 8.57 (d, $^3J(\text{HH}) = 5\text{Hz}$, 2H, H_6); 8.65 (s, 2H, H_1). **ESI-MS** [$\text{C}_{35}\text{H}_{39}\text{N}_4\text{O}$] $^+$: calculated $m/z = 531.31$; determined $m/z = 531.31239$. [$\text{C}_{35}\text{H}_{38}\text{N}_4\text{ONa}$] $^+$: calculated $m/z = 553.29$; determined $m/z = 553.28953$.

[Pt₂Me₄(pmxda)], Complex 40. To an acetone solution of **pmxda**, (0.0923g, 0.174mmol), was added dropwise an acetone solution of [Pt₂Me₄(μ-SMe₂)₂] (0.100g, 0.174mmol). The reaction mixture was then allowed to stir for 3 hours yielding a bright purple solution. After removing the solvent under reduced pressure the product was collected via Hirsch filtration from a pentane solution. A yield of 92% of the bright purple solid was collected. **¹H NMR in acetone-*d*₆**: δ ; 0.74 (s, ²J(PtH) = 88Hz, 6H, Pt-Me); 1.15 (s, ²J(PtH) = 87Hz, 6H, Pt-Me); 1.38 (s, 18H, ^tBu); 1.80 (s, 6H, Me); 7.16 (d, ⁴J(HH) = 2Hz, 2H, H_{B1}); 7.56 (d, ⁴J(HH) = 2Hz, 2H, H_{B2}); 7.62 (dd, ³J(HH) = 5Hz, ³J(HH) = 7Hz, 2H, H₅); 8.08 (d, ³J(HH) = 8Hz, 2H, H₃); 8.17 (dd, ³J(HH) = 8Hz, ³J(HH) = 7Hz, 2H, H₄); 8.93 (d, ³J(HH) = 5Hz, ³J(PtH) = 23Hz, 2H, H₅); 9.62 (s, ³J(PtH) = 34Hz, 2H, H_I). **ESI-MS** [C₃₉H₅₀N₄OPt₂Na]⁺: calculated m/z = 1003.32; determined m/z = 1003.31978.

[Pt₂I₂Me₆(pmxda)], Complex 41. To a purple-red acetone solution of Pt₂XL2 (0.020g, 0.0204mmol) was added two equivalents (2.6μL, 0.0408mmol) of methyl iodide. The reaction mixture was allowed to proceed for 3 hours while stirring after which point the acetone solvent was removed *in vacuo*. The resultant yellow solid was dissolved in minimal dichloromethane and precipitated with pentane. The solid was subsequently collected via Hirsch filtration and washed with pentane (3x2mL). Yield 89%. **¹H NMR in CD₂Cl₂ at 253K**: δ 0.77 (s, ²J(PtH) = 72Hz, 6H, Pt-Me), 1.21 (s, ²J(PtH) = 70Hz, 6H, Pt-Me), 1.30 (s, 18H, ^tBu), 1.47 (s, ²J(PtH) = 71Hz, 6H, Pt-Me), 1.74 (s, 6H, Me), 6.94 (d, ⁴J(HH) = 2Hz, 2H, H_{B1}), 7.42 (d, ⁴J(HH) = 2Hz, 2H, H_{B2}); 7.44 (dd, ³J(HH) = 5Hz, ³J(HH) = 7Hz, 2H, H₅), 7.48 (dd, ³J(HH) = 8Hz, ³J(HH) = 7Hz, 2H, H₄), 8.44 (d, ³J(HH) = 8Hz, 2H, H₃), 8.87 (d, ³J(HH) = 5Hz, ³J(PtH) = 16Hz, 2H, H₆), 9.92 (s, ³J(PtH) = 27Hz, 2H, H_I). **ESI-MS** [C₄₁H₅₆I₂N₄OPt₂]⁺: calculated m/z = 1137.28; determined m/z = 1137.27777.

[Pt₂I₄Me₄(pmxda)], Complex 42. To a purple-red acetone solution of **40** (0.020g, 0.0204mmol) was added two equivalents (0.0103g, 0.0408mmol) of iodine. The orange-yellow reaction mixture was allowed to proceed for 3 hours while stirring after which point the acetone solvent was removed *in vacuo*. The resultant off-yellow oil was dissolved in minimal dichloromethane and precipitated with pentane. The solid was

subsequently collected via Hirsch filtration and washed with pentane (3x2mL). Yield 77%. **¹H NMR in CD₂Cl₂**: δ 1.37 (s, 18H, ^tBu), 1.79 (s, 6H, Me), 2.11 (s, ²J(PtH) = 73Hz, 6H, Pt-Me), 2.45 (s, ²J(PtH) = 75Hz, 6H, Pt-Me), 7.48 (dd, ³J(HH) = 7Hz, ³J(HH) = 8Hz, 2H, H₅), 7.50 (d, ⁴J(HH) = 2Hz, 2H, H_{B1}), 7.56 (dd, ³J(HH) = 7Hz, ³J(HH) = 8Hz, 2H, H₄), 7.89 (d, ⁴J(HH) = 2Hz, 2H, H_{B2}), 8.18 (d, ³J(HH) = 8Hz, 2H, H₃), 8.95 (d, ³J(HH) = 5Hz, ³J(PtH) = 19Hz, 2H, H₆), 9.65 (s, ³J(PtH) = 30Hz, 2H, H₁). **ESI-MS** [C₃₉H₅₀I₃N₄OPt₂]⁺: calculated m/z = 1361.04; determined m/z = 1361.04447.

[Pt₂Br₂Me₄(CH₂C₆H₅)₂(pmxda)], Complex 43. To a purple-red acetone solution of **40** (0.020g, 0.0204mmol) was added two equivalents (4.8μL, 0.0408mmol) of benzyl bromide. The reaction mixture was allowed to stir for 3 hours while stirring after which point the acetone solvent was removed *in vacuo*. The resultant yellow oil was dissolved in minimal dichloromethane and washed with pentane. The dichloromethane solution was then concentrated giving a yellow oil which was subsequently massed and a ¹H NMR spectrum was collected. Yield 92%. **¹H NMR in CD₂Cl₂**: δ 1.10 (s, ²J(PtH) = 70Hz, 6H, Pt-Me), 1.40 (s, 18H, ^tBu), 1.53 (s, ²J(PtH) = 71Hz, 6H, Pt-Me), 1.80 (s, 6H, Me), 2.77 (d, ²J(HH) = 9.5Hz, ²J(PtH) = 102Hz, 2H, CH₂^A), 3.34 (d, ²J(HH) = 9.5Hz, ²J(PtH) = 96Hz, 2H, CH₂^B), 6.57 (d, ³J(HH) = 7Hz, 4H, H_o), 6.61 (t, ³J(HH) = 7Hz, 4H, H_m), 6.70 (t, ³J(HH) = 7Hz, 2H, H_p), 6.91 (dd, ³J(HH) = 5Hz, ³J(HH) = 7Hz, 2H, H₅), 7.06 (dd, ³J(HH) = 8Hz, ³J(HH) = 7Hz, 2H, H₄), 7.35 (d, ⁴J(HH) = 2Hz, 2H, H_{B1}), 7.51 (d, ⁴J(HH) = 2Hz, 2H, H_{B2}), 7.96 (d, ³J(HH) = 8Hz, 2H, H₃), 8.08 (d, ³J(HH) = 5Hz, ³J(PtH) = 15Hz, 2H, H₆), 9.83 (s, ³J(PtH) = 27Hz, 2H, H₁). **ESI-MS** [C₅₃H₆₄BrN₄OPt₂]⁺: calculated m/z = 1241.36; determined m/z = 1241.34801.

[Pt₂Br₂Me₄(4-CH₂-C₆H₄-C(CH₃)₃)₂(pmxda)], Complex 44. To a purple-red acetone solution of **40** (0.020g, 0.0204mmol) was added two equivalents (7.5μL, 0.0408mmol) of 4-*tert*-butylbenzyl bromide. The reaction mixture was allowed to proceed for 3 hours while stirring after which point the acetone solvent was removed *in vacuo*. The resultant yellow solid was dissolved in minimal dichloromethane and precipitated with pentane. The solid was subsequently collected via Hirsch filtration and washed with pentane (3x2mL). Yield 94%. **¹H NMR in CD₂Cl₂**: δ 1.04 (s, 18H, ^tBu), 1.07 (s, ²J(PtH) = 69Hz, 6H, Pt-Me), 1.40 (s, 18H, ^tBu), 1.54 (s, ²J(PtH) = 71Hz, 6H, Pt-Me), 1.80 (s, 6H,

Me), 2.72 (d, $^2J(\text{HH}) = 9 \text{ Hz}$, $^2J(\text{PtH}) = 98\text{Hz}$, 2H, CH_2^{A}), 3.33 (d, $^2J(\text{HH}) = 9\text{Hz}$, $^2J(\text{PtH}) = 98\text{Hz}$, 2H, CH_2^{B}), 6.53 (d, $^3J(\text{HH}) = 8\text{Hz}$, 4H, H_o), 6.61 (d, $^3J(\text{HH}) = 8\text{Hz}$, 4H, H_m), 6.85 (dd, $^3J(\text{HH}) = 5\text{Hz}$, $^3J(\text{HH}) = 7\text{Hz}$, 2H, H_5), 7.00 (dd, $^3J(\text{HH}) = 7\text{Hz}$, $^3J(\text{HH}) = 7\text{Hz}$, 2H, H_4), 7.39 (d, $^4J(\text{HH}) = 2\text{Hz}$, 2H, $\text{H}_{\text{B}1}$), 7.52 (d, $^4J(\text{HH}) = 2\text{Hz}$, 2H, $\text{H}_{\text{B}2}$), 7.91 (d, $^3J(\text{HH}) = 7\text{Hz}$, 2H, H_3), 8.07 (d, $^3J(\text{HH}) = 5\text{Hz}$, $^3J(\text{PtH}) = 21\text{Hz}$, 2H, H_6), 9.82 (s, $^3J(\text{PtH}) = 29\text{Hz}$, 2H, H_i). **ESI-MS** [$\text{C}_{61}\text{H}_{80}\text{BrN}_4\text{OPt}_2$] $^+$: calculated $m/z = 1353.48$; determined $m/z = 1353.47682$.

[Pt₂Br₂Me₄(3,5-CH₂-C₆H₃-(C(CH₃)₃)₂)₂(pmxda)], Complex 45. To a purple-red acetone solution of Pt₂XL2 (0.020g, 0.0204mmol) was added two equivalents (0.0115g, 0.0408mmol) of 3,5-di-*tert*butylbenzyl bromide. The reaction mixture was allowed to proceed for 3 hours while stirring after which point the acetone solvent was removed *in vacuo*. The resultant yellow solid was dissolved in minimal dichloromethane and precipitated with pentane. The solid was subsequently collected via Hirsch filtration and washed with pentane (3x2mL). Yield 83%. **¹H NMR in CD₂Cl₂**: δ 1.02 (s, 36H, ^tBu), 1.09 (s, $^2J(\text{PtH}) = 70\text{Hz}$, 6H, Pt-Me), 1.41 (s, 18H, ^tBu), 1.57 (s, $^2J(\text{PtH}) = 72\text{Hz}$, 6H, Pt-Me), 1.83 (s, 6H, Me), 2.81 (d, $^2J(\text{HH}) = 9\text{Hz}$, $^2J(\text{PtH}) = 78\text{Hz}$, 2H, CH_2^{A}), 3.36 (d, $^2J(\text{HH}) = 9\text{Hz}$, $^2J(\text{PtH}) = 98\text{Hz}$, 2H, CH_2^{B}), 6.50 (s, 4H, H_o), 6.77 (s, 2H, H_p), 6.89 (dd, $^3J(\text{HH}) = 5\text{Hz}$, $^3J(\text{HH}) = 7\text{Hz}$, 2H, H_5), 6.98 (dd, $^3J(\text{HH}) = 7\text{Hz}$, $^3J(\text{HH}) = 7\text{Hz}$, 2H, H_4), 7.52 (d, $^4J(\text{HH}) = 2\text{Hz}$, 2H, $\text{H}_{\text{B}1}$), 7.55 (d, $^4J(\text{HH}) = 2\text{Hz}$, 2H, $\text{H}_{\text{B}2}$), 7.94 (d, $^3J(\text{HH}) = 7\text{Hz}$, 2H, H_3), 8.16 (d, $^3J(\text{HH}) = 5\text{Hz}$, $^3J(\text{PtH}) = 15\text{Hz}$, 2H, H_6), 9.80 (s, $^3J(\text{PtH}) = 29\text{Hz}$, 2H, H_i). **ESI-MS** [$\text{C}_{69}\text{H}_{96}\text{BrN}_4\text{OPt}_2$] $^+$: calculated $m/z = 1465.61$; determined $m/z = 1465.60559$.

[Pt₂(μ_2 -Br)Me₄(CH₂-C₆H₅)₂(pmxda)][PF₆], Complex 46. By taking an acetone solution of **43** (0.005g) and adding to it with stirring an equivalent of silver hexafluorophosphate, (0.002g), a yellow solution with an offwhite precipitate is afforded. After stirring the mixture for one hour, the solvent was removed under reduced pressure and the resultant yellow oil was extracted with dichloromethane and washed vigorously with water. After drying the dichloromethane solution over anhydrous MgSO₄, the solvent was removed under reduced pressure and ¹H, ¹⁹F, and ³¹P NMR spectra were acquired from a CD₂Cl₂ solution. Yield 90%. **¹H NMR in CD₂Cl₂**: δ 1.10 (s, $^2J(\text{PtH}) =$

70Hz, 6H, Pt-Me), 1.40 (s, 18H, ^tBu), 1.53 (s, ²J(PtH) = 71Hz, 6H, Pt-Me), 1.80 (s, 6H, Me), 2.77 (d, ²J(HH) = 9.5Hz, ²J(PtH) = 102Hz, 2H, CH₂^A), 3.34 (d, ²J(HH) = 9.5Hz, ²J(PtH) = 96Hz, 2H, CH₂^B), 6.57 (d, ³J(HH) = 7Hz, 4H, H_o), 6.61 (t, ³J(HH) = 7Hz, 4H, H_m), 6.70 (t, ³J(HH) = 7Hz, 2H, H_P), 6.91 (dd, ³J(HH) = 5Hz, ³J(HH) = 7Hz, 2H, H₅), 7.06 (dd, ³J(HH) = 8Hz, ³J(HH) = 7Hz, 2H, H₄), 7.35 (d, ⁴J(HH) = 2Hz, 2H, H_{B1}), 7.51 (d, ⁴J(HH) = 2Hz, 2H, H_{B2}), 7.96 (d, ³J(HH) = 8Hz, 2H, H₃), 8.08 (d, ³J(HH) = 5Hz, ³J(PtH) = 15Hz, 2H, H₆), 9.83 (s, ³J(PtH) = 27Hz, 2H, H₁). **¹⁹F NMR in CD₂Cl₂:** δ = -71.30 (d, ¹J(PF) = 711.2Hz). **³¹P NMR in CD₂Cl₂:** δ = -144.38 (sept, ¹J(PF) = 711.2Hz). **ESI-MS [C₅₃H₆₄BrN₄OPt₂]⁺:** calculated m/z = 1241.36; determined m/z = 1241.34801.

[Pt₂Me₄(OH₂)₂(pmda)][O₃SCF₃], Complex 47. To an acetone solution of **41** (0.010g, 0.0088mmol), was added with stirring 2 equivalents of silver trifluoromethanesulfonate, (0.0044g, 0.0176mmol) in an effort to abstract all of the iodide and replace it with the bulky non-coordinating anion triflate. After removing the acetone solvent under reduced pressure, the remaining yellow solid was washed with 5mL of water and extracted with methylene chloride, 3x10mL, and dried over anhydrous magnesium sulfate. After removing the methylene chloride solvent under reduced pressure, the yellow oil was dissolved in methylene chloride-*d*₂ and a ¹H NMR spectrum acquired. Yield 92%. **¹H NMR in CD₂Cl₂:** δ 0.90 (s(br.), 12H, Pt-Me), 1.31 (s, 6H, Pt-Me), 1.39 (s, 18H, ^tBu), 1.82 (s, 6H, Me), 6.29 (s, 4H, H₂O), 7.23 (s, 2H), 7.70 (s, 2H), 8.01 (s, 4H), 8.15 (s, 2H), 9.01 (s, 2H), 9.54 (s, 2H). **ESI-MS [C₄₁H₅₇N₄O₂Pt₂]⁺:** calculated m/z = 1027.38; determined m/z = 1027.37590.

[Pt₂Me₄(C₄H₄N₂)(pmda)][O₃SCF₃]₂, Complex 48. To an acetone solution of **47** (0.010g, 0.0088mmol), was added with stirring a half equivalent of pyrazine, (0.0008g, 0.0044mmol). After removing the acetone solvent under reduced pressure, the remaining yellow solid was washed with pentane. The solid was dissolved in methylene chloride-*d*₂ and a ¹H NMR spectrum acquired. Yield 84%. **¹H NMR in CD₂Cl₂:** δ 1.01 (s, ²J(PtH) = 72Hz, 6H, Pt-Me), 1.27 (s, ²J(PtH) = 68Hz, 6H, Pt-Me), 1.42 (s, 18H, ^tBu), 1.48 (s, ²J(PtH) = 70Hz, 6H, Pt-Me), 1.65 (s, 3H, Me), 2.04 (s, 3H, Me), 7.15 (d, ⁴J(HH) = 2Hz, 2H, H_{B1}), 7.67 (d, ⁴J(HH) = 2Hz, 2H, H_{B2}), 7.94 (dd, ³J(HH) = 7Hz, ³J(HH) = 5Hz, 2H, H₅), 8.14 (dd, ³J(HH) = 8Hz, ³J(HH) = 7Hz, 2H, H₄), 8.20 (s, 2H, H_{pyr}), 8.63 (d, ³J(HH) =

8Hz, 2H, H₃), 8.75 (s, 2H, H_{pyr}), 8.91 (d, ³J(HH) = 5Hz, ³J(PtH) = 18Hz, 2H, H₆), 9.49 (s, ³J(PtH) = 26Hz, 2H, H₁). **ESI-MS** [C₄₅H₆₀N₆OPt₂]⁺: calculated m/z = 1113.40; determined m/z = 1113.40980.

[Pt₂Br₂(μ₂-Hg)Me₄(pmxda)], Complex 49. To a purple-red acetone-*d*₆ solution of **40**, (0.010g, 0.0102mmol) was added an equivalent (0.0037g, 0.0102mmol) of mercuric bromide. The vibrant orange solution was placed in an NMR tube and sonicated for 15minutes prior to the collection of a ¹H NMR spectrum. A vibrant orange solid was noticed in the tube and was subsequently collected via Hirsch filtration and washed with pentane (3x2mL). The solid was dissolved in methylene chloride-*d*₂ and a ¹H NMR spectrum was collected and found to be similar to that of the solution. Yield 81%. ¹H NMR in CD₂Cl₂: δ 1.01 (s, ²J(PtH) = 62Hz, ³J(HgH) = 12Hz, 6H, Pt-Me), 1.37 (m, 18H, ^tBu), 1.51 (s, ²J(PtH) = 62Hz, ³J(HgH) = 12Hz, 6H, Pt-Me), 1.78 (s, 3H, Me), 1.88 (s, 3H, Me), 7.59 (d, ⁴J(HH) = 2Hz, 2H, H_{B1}), 7.62 (d, ⁴J(HH) = 2Hz, 2H, H_{B2}), 7.72 (dd, ³J(HH) = 7Hz, ³J(HH) = 5Hz, 2H, H₅), 8.10 (d, ³J(HH) = 7Hz, 2H, H₃), 8.19 (dd, ³J(HH) = 7Hz, ³J(HH) = 7Hz, 2H, H₄), 8.90 (d, ³J(HH) = 5Hz, ³J(PtH) = 18Hz, 2H, H₆), 9.25 (s, ³J(PtH) = 26Hz, 2H, H₁). **ESI-MS** [C₃₉H₅₁BrN₄OHgPt₂]⁺: calculated m/z = 1261.22; determined m/z = 1261.21478.

Table 5.3: Crystallographic data for [Pt₂I₂Me₆(ppxda)], **34b**.

[Pt₂I₂Me₆(ppxda)]·1.5(C₃H₆O)	
Empirical Formula	C _{59.5} H ₇₅ I ₂ N ₆ O _{4.5} Pt ₂
Formula Weight	1591.11
Wavelength	0.71073 Å
Crystal System	Triclinic
Space Group	P -1
Unit Cell Dimensions	a = 13.496(4) Å α = 79.514(12) ° b = 18.389(4) Å β = 80.015(10) ° c = 26.472(7) Å γ = 70.173(9) °
Volume	6033(3) Å ³
Z	4
Density (calculated)	1.752 Mg/m ³
Absorption Coefficient (μ)	5.710 mm ⁻¹
Crystal Size	0.14 x 0.08 x 0.07 mm ³
Refinement Method	Full-matrix least-squares on F ²
Goodness of fit on F ²	0.998
Final R indices [I>2σ(I)]	R1 = 0.0477, wR2 = 0.0698
R indices (all data)	R1 = 0.1055, wR2 = 0.0832

Table 5.4: Crystallographic data for [Pt₂I₂Me₆(pmxda)], **41**.

[Pt₂I₂Me₆(pmxda)]·CH₂Cl₂	
Empirical Formula	C ₄₁ H ₅₈ I ₂ Cl ₂ N ₄ O Pt ₂
Formula Weight	1355.12
Wavelength	0.71073 Å
Crystal System	Monoclinic
Space Group	P 2 ₁ /c
Unit Cell Dimensions	a = 14.045(3) Å α = 90° b = 29.203(6) Å β = 96.662(9) ° c = 11.3466(19) Å γ = 90 °
Volume	4622.5(16) Å ³
Z	4
Density (calculated)	1.947 Mg/m ³
Absorption Coefficient (μ)	7.564 mm ⁻¹
Crystal Size	0.19 x 0.18 x 0.14 mm ³
Refinement Method	Full-matrix least-squares on F ²
Goodness of fit on F ²	1.057
Final R indices [I>2σ(I)]	R1 = 0.0446, wR2 = 0.0862
R indices (all data)	R1 = 0.0792, wR2 = 0.0953

5.16 References

1. Johnson, B.F.G. *Appl. Organomet. Chem.* **2000**, *14*, 129.
2. Suess-Fink, G.; Meister, G. *Adv. Organomet. Chem.* **1993**, *35*, 41.
3. Trost, B.M. *Angew. Chem. Int. Ed.* **1995**, *34*, 259.
4. Sheldon, R.A. *J. Mol. Catal. A: Chem.* **1996**, *107*, 75.
5. Sheldon, R.A. *Pure Appl. Chem.* **2000**, *72*, 1233.
6. Strater, N.; Lipscomb, W.N.; Klabunde, T.; Krebs, B. *Angew. Chem. Int. Ed.* **1996**, *35*, 2024.
7. van der Vlugt, J.I. *Eur. J. Inorg. Chem.* **2012**, 363.
8. Park, J.; Hong, S. *Chem. Soc. Rev.* **2012**, *41*, 6931.
9. Stephan, D.W. *Coord. Chem. Rev.* **1989**, *95*, 41.
10. Lemke, F.R.; Szalda, D.J.; Bullock, R.M. *J. Am. Chem. Soc.* **1991**, *113*, 8466.
11. Wei, L.; Bell, A.; Ahn, K.H.; Holl, M.M.; Warner, S.; Williams, I.D.; Lippard, S.J. *Inorg. Chem.* **1990**, *29*, 825.
12. Moss, J.R.; Scott, L.G. *Coord. Chem. Rev.* **1984**, *60*, 171.
13. Casey, C.P.; Audett, J.D. *Chem. Rev.* **1986**, *86*, 339.
14. Bratko, I.; Gomez, M. *Dalton Trans.* **2013**, *42*, 10664.
15. Gavrilova, A.L.; Bosnich, B. *Chem. Rev.* **2004**, *104*, 349.
16. van den Beuken, E.K.; Feringa, B.L. *Tetrahedron.* **1998**, *54*, 12985.
17. Delferro, M.; Marks, T.J. *Chem. Rev.* **2011**, *111*, 2450.
18. Ho, J.H.H.; Choy, S.W.S.; Macgregor, S.A.; Messerle, B.A. *Organometallics*, **2011**, *30*, 5978.

19. Timerbulatova, M.G.; Gatus, M.R.D.; Vuong, K.Q.; Bhadbhade, M.; Algarra, A.G.; Macgregor, S.A.; Messerle, B.A. *Organometallics*. **2013**, *32*, 5071.
20. Shibasaki, M.; Kanai, M.; Matsunaga, S.; Kumagai, N. *Acc. Chem. Res.* **2009**, *42*, 1117.
21. Gavrilova, A.L.; Bosnich, B. *Chem. Rev.* **2004**, *104*, 349.
22. McNevin, M.J.; Hagadorn, J.R. *Inorg. Chem.* **2004**, *43*, 1159.
23. Haack, P.; Limberg, C.; Tietz, T.; Metzinger, R. *Chem. Commun.* **2011**, *47*, 6374.
24. Panunzi, A.; Giordano, F.; Orabana, I.; Ruffo, F. *Inorg. Chim. Acta.* **2005**, *358*, 1217.
25. Takani, S.; Takeuchi, D.; Osakada, K.; Akamatsu, N.; Shishido, A. *Angew. Chem. Int. Ed.* **2014**, *53*, 9246.
26. Monaghan, P. K.; Puddephatt, R. J. *Organometallics* **1984**, *3*, 444–449.
27. Monaghan, P. K.; Puddephatt, R. J. *Dalt. Trans.* **1988**, *1*, 595–599.
28. Rendina, L. M.; Puddephatt, R. J. *Chem. Rev.* **1997**, *97*, 1735–1754.
29. Rostovtsev, V. V.; Henling, L. M.; Labinger, J. A.; Bercaw, J. E. *Inorg. Chem.* **2002**, *41*, 3608–3619.
30. Zhang, F.; Broczkowski, M. E.; Jennings, M. C.; Puddephatt, R. J. *Can. J. Chem.* **2005**, *83*, 595–605.
31. Bonnington, K. J.; Jennings, M. C.; Puddephatt, R. J. *Organometallics* **2008**, *27*, 6521–6530.
32. McKeown, B. a; Gonzalez, H. E.; Friedfeld, M. R.; Gunnoe, T. B.; Cundari, T. R.; Sabat, M. *J. Am. Chem. Soc.* **2011**, *133*, 19131–19152.
33. Hoseini, S. J.; Nasrabadi, H.; Nabavizadeh, S. M.; Rashidi, M.; Puddephatt, R. J. *Organometallics* **2012**, *31*, 2357–2366.
34. Pellarin, K. R.; McCready, M. S.; Sutherland, T. I.; Puddephatt, R. J. *Organometallics* **2012**, *31*, 8291–8300.
35. Pellarin, K. R.; McCready, M. S.; Puddephatt, R. J. *Organometallics* **2012**, *31*, 6388–6394.
36. Calvet, T.; Crespo, M.; Font-Bardía, M.; Jansat, S.; Martínez, M. *Organometallics* **2012**, *31*, 4367–4373.

37. Momeni, B. Z.; Rashidi, M.; Jafari, M. M.; Patrick, B. O.; Abd-El-Aziz, A. S. *J. Organomet. Chem.* **2012**, *700*, 83–92.
38. Pellarin, K. R.; McCready, M. S.; Puddephatt, R. J. *Dalton Trans.* **2013**, *42*, 10444–10453.
39. Pellarin, K. R.; Puddephatt, R. J. *Organometallics* **2013**, *32*, 3604–3610.
40. Safa, M.; Puddephatt, R. J. *J. Organomet. Chem.* **2013**, *724*, 7–16.
41. Fraser, C. S.; Jenkins, H.; Jennings, M. C.; Puddephatt, R. J. *Organometallics* **2000**, *19*, 1635–1642.
42. Safa, M. A.; Abo-Amer, A.; Borecki, A.; Cooper, B. F. T.; Puddephatt, R. J. *Organometallics* **2012**, *31*, 2675–2681.
43. Au, R. H. W.; Fraser, C. S. a.; Eisler, D. J.; Jennings, M. C.; Puddephatt, R. J. *Organometallics* **2009**, *28*, 1719–1729.
44. Abo-Amer, A.; Puddephatt, R.J. *J. Inorg. Organomet. Polym.* **2014**, *24*, 114-120.
45. Moustafa, M. E.; McCready, M. S.; Puddephatt, R. J. *Organometallics* **2013**, *32*, 2552–2557.
46. McCready, M.S.; Puddephatt, R.J. *Organometallics*. **2015**, doi: 10.1021/om501023r
47. Askarizadeh, E.; Devoille, A.M.J.; Bozhai, D.M.; Slawin, A.M.Z.; Love, J.B. *Inorg. Chem.* **2009**, *48*, 7491.
48. Hill, G.; Irwin, M. J.; Levy, C. J.; Rendina, L. M.; Puddephatt, R. J. *Inorg. Synth.* **1998**, *32*, 149-153.
49. McCready, M. S.; Puddephatt, R. J. *Dalton Trans.* **2012**, *41*, 12378–12385.
50. Tan, R.; Wang, Z-B.; Li, Y.; Kozera, D.J.; Lu, Z-H.; Song, D. *Inorg. Chem.* **2012**, *51*, 7039.
51. Aseman, M. D.; Rashidi, M.; Nabavizadeh, S. M.; Puddephatt, R. J. *Organometallics* **2013**, *32*, 2593–2598.
52. Nabavizadeh, S.M.; Amini, H.; Rashidi, M.; Pellarin, K.R.; McCready, M.S.; Cooper, B.F.T.; Puddephatt, R.J. *J. Organomet. Chem.* **2012**, *713*, 60-67.
53. *APEX 2, Crystallography software package*; Bruker AXS: Madison, WI, 2005.
54. *SAINT, Data Reduction Software*; Bruker AXS: Madison, WI, 1999.

55. Sheldrick, G.M. *SADABS v.2.01, Area Detector Absorption Correction Program*; Bruker AXS: Madison, WI, 2006.
56. Sheldrick, G.M. *SHELXS, program for solution of crystal structures. Acta Cryst. A64. 2008*, 112-122.
57. Sheldrick, G.M. *SHELXL, program for refinement of crystal structures. Acta Crystallogr., Section A. 2008*, 64, 112-122.
58. Dahan, A.; Ashkenazi, T.; Kuznetsov, V.; Makievski, S.; Drug, E.; Fadeev, L.; Bramson, M.; Schokoroy, S.; Rozenshine-Kemelmakher, E.; Gozin, M. *J. Org. Chem. 2007*, 72, 2289.
59. Perez-Trujillo, M.; Maestre, I.; Jaime, C.; Alvarez-Larena, A.; Piniella, J.F.; Virgili, A. *Tetrahedron. 2005*, 16, 3084.

CHAPTER 6

General Conclusions

6.1 General Conclusions

In this work, new monometallic and bimetallic organoplatinum complexes possessing ditopic bidentate nitrogen donor ligands have been synthesized. These novel complexes were characterized by $^1\text{H-NMR}$, $^{13}\text{C-NMR}$, $^{19}\text{F-NMR}$, $^{31}\text{P-NMR}$, mass spectrometry and elemental analysis. The solid state structures of many of the complexes were determined by single crystal X-ray diffraction analysis. The reaction pathways, methods of isomerization, and exchange processes in a few instances were investigated through the use of variable temperature $^1\text{H NMR}$ spectroscopy.

To facilitate the study of the reactivity of bimetallic dimethylplatinum(II) complexes, novel ditopic ligands based on diimine donors were synthesized. These fully characterized ligands were designed to coordinate two metal centers in either a side-by-side coordination mode or a cofacial arrangement of metal centers to elicit maximum cooperative effects. Three different principle ligand scaffolds were utilized with varying degrees of intermetallic distances and also varying amounts of backbone rigidity. The coordination chemistry of each ligand was investigated in depth through numerous attempts to prepare bimetallic diplatinum complexes or heterobimetallic complexes of the ligands.

Several novel monometallic and bimetallic dimethylplatinum(II) complexes were prepared based on the ditopic ligand designs. These complexes were observed to undergo the facile oxidative addition of a variety of substrates. The oxidative addition reaction is an essential reaction to organometallic chemistry and as such it is utilized in many catalytic processes. The ability to undergo oxidative addition reactions at two proximal metal centers provides insight into the role of bimetallic complexes in catalysis, particularly processes which require two bond activation events or the activation and functionalization of a substrate by two adjacent metal centers. Therefore, the results of our work should provide an increase in the understanding of the factors affecting the design, synthesis and reactivity of monometallic and bimetallic organoplatinum complexes based on ditopic ligand scaffolds. This contribution should demonstrate the importance of the rational design of ditopic ligands in order to elicit the optimal cooperative effects between metal centers.

Initially, the use of a ditopic ligand which could coordinate two dimethylplatinum(II) centers in a side-by-side manner was thought to be an ideal arrangement. To this end, the ligand **6-dppd**, 1,4-di(2-pyridyl)-5,6,7,8,9,10-hexahydrocycloocta[d]pyridazine, was prepared through the inverse electron demand Diels-Alder reaction of cyclooctyne and 3,6-pyridyl-1,2,4,5-tetrazine. The ligand **6-dppd** possessed two potential diimine bidentate coordination sites positioned adjacent to one another in a side-by-side arrangement. This ligand was shown to coordinate only a single equivalent of a dimethylplatinum(II) center and numerous attempts at preparing diplatinum complexes via bridging interactions were observed to be unsuccessful. The complex [PtMe₂(6-dppd)], was presumed to be incapable of coordinating a second platinum center due to a steric clash between the free pyridyl group and the cyclooctyl backbone as well as the projection of the *exo* directed methyl group towards the second coordination site. Attempts to prepare heterobimetallic complexes of **6-dppd** using zinc and copper proved to be unsuccessful. The attempted preparation of a bimetallic complex of [PtMe₂(6-dppd)] using mercuric halides was observed to give the product of oxidative addition of the mercuric halide at the platinum center [PtXMe₂(HgX)(6-dppd)], where X = Cl, Br, OAc, rather than the complex [PtMe₂HgX₂(6-dppd)]. This indicated that the platinum(II) center in the complex was a much better nucleophile than the free pyridyl nitrogen atom in the ligand. As such the oxidative addition of various substrates at [PtMe₂(6-dppd)] was shown to occur rapidly at room temperature to give the corresponding platinum(IV) complexes. The dimethylplatinum(II) complex was shown to react with methyl iodide, bromine and benzyl bromide derivatives to give the *trans* oxidative addition products. When treated with an equivalent of iodine however, [PtMe₂(6-dppd)] was observed to give a variety of complexes. The oxidative addition of iodine was observed to give first a mixture of the *trans* and *cis* addition complexes of [PtI₂Me₂(6-dppd)]. After an initial *trans* oxidative addition, an isomerization event led to the formation of both *cis* isomers in solution. At this point an equivalent of [PtMe₂(6-dppd)] reacted with an equivalent of *cis*-[PtI₂Me₂(6-dppd)] to give the platinum(II) complex [PtIME(6-dppd)] and the trimethylplatinum(IV) complex [PtMe₃(6-dppd)]⁺. The oxidative addition of iodine at the platinum(II) complex and coordination of an iodide ligand at the platinum(IV) complex gave both [PtI₃Me(6-dppd)] and [PtIME₃(6-

dppd)] respectively. The highly reactive [PtMe₂(6-dppd)] was also observed to oxidatively add a dichloromethane solvent molecule giving a variety of isomers of the platinum(IV) complex [PtClMe₂(CH₂Cl)(6-dppd)]. This oxidative addition was observed to be enhanced photolytically and is proposed to occur via a free radical chain mechanism. [PtMe₂(6-dppd)] exhibited the ability to incorporate deuterium into reductively eliminated methane after being subjected to deuteriolysis via CH bond activation events. This was observed through the reaction of DCl yielding [PtClDMe₂(6-dppd)] at low temperatures and subsequent reductive elimination of methane. The H/D exchange was evident due to the formation of all possible isotopomers of methane. These results demonstrate the ability of this relatively simple system to undergo C-H bond activation events.

The design, synthesis and characterization of two isomeric clamshell dimer complexes of platinum(II) was carried out in chapter 3. When a platinum(II) complex, *endo*-[PtClMe(6-dppd)], was treated with an equivalent of silver trifluoromethanesulfonate, a bimetallic dimer complex of platinum(II), *endo,endo*-[Pt₂Me₂(μ₂-κ³-6-dppd)₂][O₃SCF₃]₂ was prepared exclusively. By undergoing a halide abstraction event, the stereochemistry at the platinum center was retained and the desired isomer was formed exclusively in a logical way. When the dimethylplatinum(II) complex [PtMe₂(6-dppd)] was treated with trifluoromethanesulfonic acid, the protonolysis led to the formation of methane gas and the concomitant formation of both the *endo,endo* and *exo,exo* isomers of [Pt₂Me₂(μ₂-κ³-6-dppd)₂][O₃SCF₃]₂ in solution. Variable temperature ¹H NMR experiments indicated that the protonolysis led to the initial formation of a solvent coordinated complexes *endo* or *exo* [PtMe(S)(6-dppd)]⁺, where S = acetone or acetonitrile. These complexes could then form their respective dimeric complexes through self recognition. The *exo,exo* isomer was observed both experimentally and computationally to be the thermodynamically preferred isomer and as such the *endo,endo* isomer was observed to convert gradually in solution to the *exo,exo* species through reversible dissociation, isomerization and subsequent dimerization. This self-sorting process would give rise to the *exo,exo* isomer selectively over time. By increasing the donor strength of the ligand from acetonitrile to triphenylphosphine, the dimerization process was observed to be inhibited. The increased donor strength of the

phosphine was also observed open the clamshell dimer structure to give two equivalents of the monomer species *exo*-[PtMe(PPh₃)(6-dppd)][O₃SCF₃]. These isomeric clamshell dimer complexes were prepared in a logical manner and establish a useful synthetic protocol for the self-assembly of isomeric molecular materials.

The reactivity of [PtMe₂(6-dppd)] with benzyl bromide derivatives giving thermodynamically stable organoplatinum(IV) complexes provides an excellent avenue to prepare highly functionalized platinum(IV) species. Therefore the oxidative addition of alkyl bromide derivatives containing hydrogen bonding functionality was investigated in order to prepare and study platinum(IV) complexes capable of participating in supramolecular chemistry. Of specific interest was the role that the non-coordinating pyridyl group present on the ligand backbone would play in the formation of supramolecular complexes. The oxidative addition of alkyl and benzyl bromide substrates possessing carboxylic acid functional groups led to the formation of stable organoplatinum(IV) complexes in most cases. The reaction of 3-bromopropionic acid with [PtMe₂(6-dppd)] led to a β-elimination event occurring after the initial oxidative addition. When organoplatinum(IV) complexes were prepared incorporating benzyl bromide derivatives with carboxylic acids, self-assembled polymer structures were observed, propagated by N•••HO interactions between the pyridyl group and the carboxylic acid or weak PtBr•••HO secondary interactions. The addition of bromoacetic acid led to the formation of head-to-tail dimeric structures via self-assembly. Introduction of an alcohol group as a hydrogen bond donor resulted in the only case of an intramolecular hydrogen bonding interaction between the pyridyl group and the alcohol. The oxidative addition of *ortho*, *meta*, and *para* (bromomethyl)phenyl boronic acids resulted in the formation of stable organoplatinum(IV) boronic acids. The platinum(IV) complexes containing boronic acids self-assembled in the solid state to give supramolecular polymer and dimeric structures. The formation of a variety of supramolecular organoplatinum complexes propagated by numerous hydrogen bonding and secondary interactions shows promise in the ability to form supramolecular architectures based on organometallic precursors. The method of using oxidative addition to install the hydrogen bonding groups shows to be very useful and preparing

these precursors and as such should be employed to design highly specific monomers which can be tailored to form desired supramolecular structures via self-assembly.

Two novel ligands based on an anthracene scaffold were designed and synthesized. The generation one design of the anthracene ligand, **bpad** = N¹,N⁸-bis(pyridin-2-ylmethylene)anthracene-1,8-diamine, was shown to complex two equivalents of a dimethylplatinum(II) center to give the cofacial bimetallic complex [Pt₂Me₄(bpad)]. This complex was shown to decompose over time at room temperature in both atmospheric and inert environments. Although the manner of decomposition was not identified as the product could not be characterized, it is believed that the proximity of the platinum center to the anthracene backbone leads to its decomposition through a potential metalation event. [Pt₂Me₄(bpad)] was shown to decompose upon the oxidative addition of a variety of substrates as well making the study of its reactivity impossible. Diplatinum(IV) complexes of **bpad** were investigated through the coordination of two platinum(IV) centers by **bpad**. The degradation of these complexes facilitated by the proximity of the platinum centers to the anthracene backbone was addressed in the second generation design of the anthracene based ligand. The ligand **adpa**, **adpa** = (N,N)-4,4'-(anthracene-1,8-diylbis(ethyne-2,1-diyl))-bis(N-(pyridin-2-ylmethylene)aniline), possessed long alkynyl arms which position the metal centers further from the anthracene backbone whilst still maintaining the cofacial arrangement of the metal centers. The ligand **adpa** was shown to complex two equivalents of a dimethylplatinum(II) center giving the bimetallic complex [Pt₂Me₄(adpa)]. The bimetallic diplatinum complex was shown to be stable for long periods of time with no degradation observed. [Pt₂Me₄(adpa)] reacted rapidly with both methyl iodide and 3,5-di-*tert*-butylbenzyl bromide yielding the thermodynamically stable corresponding diplatinum(IV) complexes through the *trans* oxidative addition. The ability of [Pt₂Me₄(adpa)] to react cooperatively was examined by reacting it with half an equivalent of a bifunctional substrate, 1,2-dibromoxylene. The product was proposed to be the result of an oxidative addition event occurring at each platinum(II) center. This gives rise to a bimetallic organoplatinum(IV) complex with a xylene bridge between the two platinum centers. Complexes derived from the ligand **adpa** should provide beneficial cooperative reactivity when they possess two metal centers. Despite this, their

challenging synthesis and poor solubility may make the use of these types of ligand prohibitive.

Two novel ligands based on a xanthene derived scaffold were designed, synthesized and their corresponding coordination chemistry was explored. The ligand **ppxda**, **ppxda** = 2,7-di-*tert*-butyl-9,9-dimethyl-*N*⁴,*N*⁵-bis(4-(pyridin-2-ylmethyleneamino)phenyl)-xanthene-4,5-dicarboxamide, was shown to easily complex two equivalents of a dimethylplatinum(II) center giving rise to the stable bimetallic platinum(II) complex [Pt₂Me₄(ppxda)]. This complex was shown to be able to adopt two isomeric forms, one in which the pyridyl resonances are positioned directly atop one another in a *syn* manner and the other the more thermodynamically preferred *anti* oriented isomer. As such the reactivity towards oxidative addition yielded products which were also isomeric. The oxidative addition of methyl iodide gave a mixture of isomers at room temperature. Variable temperature NMR experiments were used to determine that the *anti* isomer was thermodynamically preferred. The chirality of this structure was confirmed in the solid state by single crystal X-ray diffraction analysis showing the overall *trans* oxidative addition product. Similar oxidative addition reactions were performed with benzyl bromide derivatives to give the corresponding bimetallic cofacial organoplatinum(IV) complexes again in isomeric mixtures. The *syn* orientation of a diplatinum complex of **ppxda** was prepared by a halide abstraction event from [Pt₂Br₂Me₄(CH₂-4-(C₆H₄)-C(CH₃)₃)₂(ppxda)] to give the bromide bridged analog. In this complex the two platinum centers were arranged linearly in a cofacial manner and joined together via a bromide ion bridge. An additional diplatinum(IV) complex with *syn* arrangement was prepared in which a pyrazine ligand with two nitrogen donor sites was observed to bridge the two platinum centers and lock them into the *syn* arrangement.

The high amount of rotational freedom allowed by **ppxda** was removed in the design of the second xanthene derived ligand **pmxda**, **pmxda** = 2,7-di-*tert*-butyl-9,9-dimethyl-bis(pyridine-2-ylmethylene)-9H-xanthene-4,5-diamine. This ligand was shown to easily coordinate two equivalents of a dimethylplatinum(II) center giving [Pt₂Me₄(pmxda)], in a proposed *anti* arrangement. Similar to its long linker analog, [Pt₂Me₄(ppxda)] was shown to oxidatively add two equivalents of both iodine and

methyl iodide giving rise to diplatinum(IV) complexes through *trans* oxidative addition. Both complexes were observed to adopt the thermodynamically preferred *anti* orientation in the solid state. Bromide and pyrazine bridged structures similar to those observed in the ppxda system were prepared easily using analogous methods. In this case a solid state structural determination of the pyrazine bridged species illustrated the linear arrangement of the platinum centers adopted through the *syn* arrangement. Finally the cooperative reactivity of [Pt₂Me₄(pmxda)] was examined by treating it with half an equivalent of the bifunctional substrate, HgBr₂. ¹H NMR and ESI-MS data both support the formation of the mercury bridged diplatinum(IV) complex, **49**. This complex is proposed to be formed by two oxidative addition events occurring using the same mercuric bromide molecule as a substrate. The xanthene based scaffolds were found to be sufficient backbones for the design of diplatinum complexes and as such complexes of this type should be excellent candidates for bimetallic catalysis and their cooperative reactivity should be investigated further.

6.2 Future Work

Future work surrounding the reactivity of bimetallic complexes of dimethylplatinum(II) should focus on the use of face-to-face ligand scaffold designs such as those presented in this thesis. Specifically, the xanthene derived ligands **ppxda** and **pmxda** show promise for eliciting cooperative reactivity between adjacent metal centers. The ability of these complexes to catalyze chemical transformations would be of particular interest. By activating a C-H bond of a substrate molecule at one metal centre and an oxidant such as oxygen or a peroxide at the second, one could then force a cooperative reductive elimination event to occur. This would yield a functionalized derivative as the product. As such, exploring the reactivity of complexes based on **pmxda** and their reactivity towards oxidants such as dioxygen and peroxides should be explored. Modifications of both sterics and electronics of the ligand designs may also afford intriguing new chemistry surrounding bimetallic dimethylplatinum(II) complexes and could be explored. The application of these bimetallic complexes towards fundamental catalysis will provide significant insight into the cooperative reactivity and viability of these catalysts in modern synthesis.

CURRICULUM VITAE

- Name:** Matthew Scott McCready
- Post-secondary Education and Degrees:** University of Western Ontario
London, Ontario, Canada
2006-2010 B.Sc. Hons. Sp.
- The University of Western Ontario
London, Ontario, Canada
2010-2015 Ph.D.
- Honours and Awards:** Ontario Graduate Scholarship (OGS)
Doctoral Scholarship
2011-2013
- Natural Science and Engineering Research Council (NSERC)
Doctoral Fellowship - PGS D2
2013-2015
- Related Work Experience**
- Teaching Assistant
The University of Western Ontario
2010-2014
- Research Assistant
The University of Western Ontario
2010-2015
- Publications:**
- McCready, M.S. and Puddephatt R. J. *Inorg. Chem. Commun.* **2010**, 14, 210-212.
- McCready, M.S. and Puddephatt, R. J. *Acta Cryst.* **2011**, E67: m604-m605.
- Abo-Amer, A.; McCready, M.S.; Zhang, F. and Puddephatt, R.J. *Can. J. Chem.* **2012**, 90, 1, 46-54.
- Nabavizadeh, S.M.; Amini, H.; Rashidi, M.; Pellarin, K.R.; McCready, M.S.; Cooper, B.F.T.; Puddephatt, R.J. *J. Organomet. Chem.* **2012**. 713: 60-67.
- Pellarin, K.R.; McCready, M.S.; Puddephatt, R.J. *Organometallics*. **2012**, 31, 17: 6388-6394.
- Moustafa, M.E.; McCready, M.S.; Puddephatt, R.J. *Organometallics*. **2012**, 31, 17: 6262-6269.

- McCready, M.S. and Puddephatt, R.J. *Dalton Trans.* **2012**, 41: 12378-12385.
- Pellarin, K.R.; McCready, M.S.; Sutherland, T.I.; Puddephatt, R.J. *Organometallics.* **2012**, 31(23): 8291-8300.
- Moustafa, M.E.; McCready, M.S.; Puddephatt, R.J. *Organometallics.* **2013**, 32(9): 2552-2557.
- Kim, S.; Boyle, P.D.; McCready, M.S.; Pellarin, K.R.; Puddephatt, R.J. *Chem. Commun.* **2013**, 49(57): 6421-6423.
- Pellarin, K.R.; McCready, M.S.; Puddephatt, R.J. *Dalton Trans.* **2013**, 42(29): 10444-10453.
- Hazlehurst, R.J.; Pellarin, K.R.; McCready, M.S.; Puddephatt, R.J. *Can. J. Chem.* **2015**, 93(1), 74-81.
- McCready, M.S.; Puddephatt, R.J. *Organometallics.* **2015**, ASAP. doi: 10.1021/om501023r.

Presentations:

- McCready, M.S.; Puddephatt, R.J. *A 3,6-bis(2-pyridyl)pyridazine complex of dimethylplatinum(II): An attempt at bimetallic C-H bond activation*, Canadian Society of Chemistry Conference and Exhibition, **2011**.
- McCready, M.S.; Puddephatt, R.J. *A 3,6-bis(2-pyridyl)pyridazine complex of dimethylplatinum(II): An attempt at bimetallic C-H bond activation*, Inorganic Discussion Weekend, **2011**.
- McCready, M.S.; Puddephatt, R.J. *Self-assembly of isomeric clamshell dimers of platinum(II)*, Inorganic Discussion Weekend, **2012**.